

5-8-2004

Secondary Clarifier Modeling: A Multi-Process Approach

Alonso Griborio
University of New Orleans

Follow this and additional works at: <https://scholarworks.uno.edu/td>

Recommended Citation

Griborio, Alonso, "Secondary Clarifier Modeling: A Multi-Process Approach" (2004). *University of New Orleans Theses and Dissertations*. 173.
<https://scholarworks.uno.edu/td/173>

This Dissertation is protected by copyright and/or related rights. It has been brought to you by ScholarWorks@UNO with permission from the rights-holder(s). You are free to use this Dissertation in any way that is permitted by the copyright and related rights legislation that applies to your use. For other uses you need to obtain permission from the rights-holder(s) directly, unless additional rights are indicated by a Creative Commons license in the record and/or on the work itself.

This Dissertation has been accepted for inclusion in University of New Orleans Theses and Dissertations by an authorized administrator of ScholarWorks@UNO. For more information, please contact scholarworks@uno.edu.

SECONDARY CLARIFIER MODELING: A MULTI-PROCESS APPROACH

A Dissertation

**Submitted to the Graduate Faculty of the
University of New Orleans
in partial fulfillment of the
requirements for the degree of**

**Doctor of Philosophy
in
The Engineering and Applied Sciences Program**

by

Alonso G. Griborio

**B.S. University Rafael Urdaneta, 1994
M.S. University of Zulia, 2001**

August 2004

Copyright 2004, Alonso G. Griborio
All Rights Reserved

To Andres, Samantha and Alonso
If I am somebody, I am somebody for you

ACKNOWLEDGMENTS

I want to express my deepest gratitude to my adviser, Dr. John Alex McCorquodale, not only for his guidance and support during the development of this dissertation, but also for his patience, his encouragement, and his great ability to transmit ideas. The level of knowledge and expertise that Dr. McCorquodale has showed me during my studies, really impresses me.

I would like to express my special appreciation to Dr. Enrique La Motta, who has been involved in the collection and evaluation of the field data. Thanks for your collaboration.

I would like to thank the rest of my dissertation committee, Dr. Donald Barbe, Dr. Curtis Outlaw and Dr. Dale Easley. The comments and corrections provided by the committee in different chapters of this dissertation are greatly appreciated.

I wish to express my gratitude to Dr. Ioannis Georgiou for his guidance in the elaboration of the TECPLOT files, and his comments in different chapters of the dissertation. Similarly I wish to express my thanks to the people that have been involved in the maintenance of aerobic units at the Marrero Experimental Pilot Plant, Jose Jimenez, Adriana Bustillos, Jackie Luque, and Jose Rojas.

I would like to thank the people that participated at the Clarifier Workshop at Brown and Caldwell's Walnut Creek office, in special to Dr. Denis Parker and Dr. Eric Wahlberg, for the valuable suggestions in ways to improve the model, and for sharing part of their experience in clarifier design and optimization.

Especially I want to acknowledge to my parents, Alonso and Yudit Griborio, for their incommensurable support, without them, I would not have accomplished this goal.

Finally, I am grateful to my beloved wife, Shirley Poliszuk, for her love, patience and support.

TABLE OF CONTENTS

LIST OF FIGURES	xi
LIST OF TABLES	xviii
LIST OF ABBREVIATIONS AND SYMBOLS	xxii
ABSTRACT	xxix
CHAPTER 1	
1 INTRODUCTION	1
1.1 Background and Problem Definition	1
1.2 Scope and Objectives	8
1.3 Dissertation Organization	9
CHAPTER 2	
2 LITERATURE REVIEW	11
2.1 Historical Review of 2-D Modeling of Settling Tanks	11
2.2 Processes in Settling Tanks	20
2.2.1 Flow in Settling Tanks	20
2.2.1.1 Modeling Equations	23
2.2.2 Settling Properties of the Sludge	27
2.2.3 Turbulence Model	33
2.2.4 Sludge Rheology in Settling Tanks	37
2.2.5 Flocculation Process in Settling Tanks	41
2.2.6 Temperature Effects on Settling Tanks	56

CHAPTER 3

3 RESEARCH ON SETTLING PROPERTIES. DEVELOPMENT OF A COMPOUND SETTLING MODEL	59
3.1 Research on Settling Properties	59
3.1.1 Study on Wall Effects and Effects of the Stirring Mechanism	60
3.1.2 Study on Discrete Settling	61
3.1.2.1 Measurement of Discrete Settling Velocities	63
3.1.2.2 Calculation of the Discrete Settling Fractions	66
3.1.3 Study on Compression Settling.....	68
3.2 Development of the Settling Model.....	70
3.3 Effects of Temperature on Settling Velocities.....	71

CHAPTER 4

4 SETTLING TANK MODEL DEVELOPMENT.....	76
4.1 Development of Quasi 3D (Q3D) Settling Tank Model.....	76
4.1.1 Governing Equations	76
4.1.2 Turbulence Model and Rheology of the Sludge	81
4.1.3 Settling Model.....	85
4.1.4 Flocculation Sub-Model.....	86
4.1.4.1 Shear Induced Flocculation.....	87
4.1.4.1 Differential Settling Flocculation	88
4.1.4.2 Transfer of Primary Particles to Flocs in the Flocculation Sub-Model.....	89
4.1.5 Temperature Sub-Model	90

4.1.5.1 Influent Wastewater Temperature and Transport	91
4.1.5.2 Surface Heat Exchange	92
4.1.6 Scraper Sub-Model	99
4.2 Numerical Methods	103
4.3 Boundary Conditions	109
4.3.1 Stream Function Boundary Conditions	109
4.3.2 Vorticity Boundary Conditions	110
4.3.3 Solids Boundary Conditions	111
4.3.4 Thermal Boundary Conditions	112
4.3.5 Swirl Boundary Conditions	113
4.3.6 Turbulence Model Boundary Conditions	114
CHAPTER 5	
5 MODEL CALIBRATION, TESTING AND VALIDATION	115
5.1 Calibration of the model. Case Study: Marrero WWTP	116
5.1.1 Calibration of the Settling Sub-Model	118
5.1.1.1 Discrete Settling	119
5.1.1.2 Zone and Compression Settling	123
5.1.2 Calibration of the Flocculation Sub-Model	127
5.1.3 MLSS, ESS, Flow Rates and RAS	130
5.1.4 Model Simulation	131
5.2 Testing: Grid Dependency Test	137
5.3 Validation of the Model	142
5.3.1 Marrero WWTP	142

5.3.1.1 Marrero WWTP – Early Validation.....	146
5.3.2 Oxley Creek WWTP	148
5.3.3 Darvill WWTP New SSTs.....	154
CHAPTER 6	
6 MODEL APPLICATIONS AND RESULTS	162
6.1 Influence of the Flocculation State on the Secondary Settling Tank Performance	162
6.2 Flocculation in Secondary Settling Tanks	164
6.3 Effects of Center Well on Flocculation and Hydrodynamics	165
6.4 Optimum Dimensions for the Center Well	169
6.5 Effects of SLR (Constant SOR) on the Optimum Dimensions of the Center Well.....	174
6.6 Effects of SOR (Constant MLSS, Variable SLR) on the Optimum Dimensions of the Center Well.....	176
6.7 Solids Flux Limiting Analysis for the Marrero WWTP - Maximum SLR	178
6.7.1 1D Solids Flux Analysis	178
6.7.2 Q3D Solids Flux Analysis	181
6.8 Effect of the SOR on the Performance of the SST – Marrero Case	185
6.9 Effect of the SOR and the MLSS on the Performance of the SST for a Constant SLR – Marrero Case	189
6.10 Evaluation of the Different Component of the Flocculation Sub-Model. ...	193
6.11 Effect of Sludge Withdrawal Systems on the Settler Performance	195

6.12 Comparison between Gravity and Rake Induced Flows. Effectiveness of the Scraper	199
6.13 Effect of Swirl Components on the Settler Performance	201
6.14 Effect of Temperature and Seasonal Variation on Clarifier Performance ...	204
6.14.1 Effect of temperature on settling velocity due to change of viscosity	204
6.14.2 Effect of Influent Temperature Variation and Heat Exchange on the Hydrodynamics and Performance of Clarifiers	206
6.15 Stability Criteria Analysis	216
CHAPTER 7	
7 CONCLUSIONS AND RECOMMENDATIONS	218
7.1 General Conclusions	218
7.2 Specific Conclusions	220
7.3 Recommendations	224
REFERENCES	229
APPENDIX A	
MARRERO WASTEWATER TREATMENT PLANT	250
APPENDIX B	
LABORATORY PROCEDURES	251
APPENDIX C	
EXPERIMENTAL PILOT PLANT	252
APPENDIX D	
DISCRETE FRACTIONS AND DISCRETE SETTLING VELOCITIES	254

APPENDIX E

RESEARCH ON ZONE SETTLING AND COMPRESSION RATE

PROPERTIES	264
------------------	-----

APPENDIX F

RESEARCH ON TEMPERATURE EFFECTS ON ZONE SETTLING	280
--	-----

APPENDIX G

DATA COLLECTED DURING THE VALIDATION OF THE MODEL	288
---	-----

APPENDIX H

DEVELOPMENT OF THE DIFFERENTIAL SETTLING FLOCCULATION

EQUATION	293
----------------	-----

APPENDIX I

1DFT ANALYSES	297
---------------------	-----

APPENDIX J

FORTRAN SOURCE CODE FOR THE Q3D CLARIFIER MODEL	307
---	-----

APPENDIX K

INPUT FILES FOR RUNNING THE Q3D CLARIFIER FORTRAN CODE ...	435
--	-----

VITA	440
------------	-----

LIST OF FIGURES

Figure 2.1	Flow Processes in a Rectangular Clarifier.....	21
Figure 2.2	Flow Processes in a Circular Clarifier.....	23
Figure 2.3	Effective kinematic viscosity of activated sludge	39
Figure 2.4	Effect of HRT on the SSS removal	49
Figure 3.1	Solid Liquid Interface Depth vs. Time Using 3 Different Apparatus for a MLSS = 3800 mg/L	61
Figure 3.2	Sketch of Settling Column.....	65
Figure 3.3	Settling Velocities for Hindered and Compression Zone.....	69
Figure 3.4	Ratios V_{sT_1} / V_{sT_2} and μ_{T_2} / μ_{T_1} for Different TSS Concentrations.....	74
Figure 3.5	Effect of Temperature on Zone Settling Velocity	75
Figure 4.1	The Processes Composing the Surface Heat Exchange	92
Figure 4.2	Declination Angle, Sine and Cosine of the Declination Angle	94
Figure 4.3	Local Latitude.....	94
Figure 4.4	Cosine of the Sun's Hour Angle.....	95
Figure 4.5	Albedo of the Water	96
Figure 4.6	Scheme of Circular Settling Tank for Scraper Definition	100
Figure 4.7	Scheme of Scraper, Tangential and Radial Velocity.....	101
Figure 4.8	Scheme of Scraper Effect in the θ - direction.....	103
Figure 4.9	Scalar Control Volume Used for Discretisation Schemes.....	105
Figure 4.10	Stream Function Boundary Conditions	109
Figure 4.11	Vorticity Boundary Conditions	110
Figure 4.12	Solids Boundary Conditions.....	111

Figure 4.13	Heat Exchange Boundary Conditions	112
Figure 4.14	Swirl Boundary Conditions	113
Figure 4.15	Boundary Conditions for the Simplified Turbulence Model.....	114
Figure 5.1	Geometry Capabilities of the Model	116
Figure 5.2	Solids-Liquid Interface vs. Time in a Batch Settling Test	124
Figure 5.3	Field data and Fitted Exponential Equations for Zone Settling and Compression Rate	126
Figure 5.4	Supernatant SS versus Flocculation Time in a Batch Test.....	129
Figure 5.5	RAS SS and ESS Concentration Predicted by the Model	133
Figure 5.6a	Concentration Contours at 540 minutes of simulation time for the MarreroWWTP Test Case using a 60x20 grid.....	134
Figure 5.6b	Stream Function and Velocity Vectors at 540 minutes of Simulation Time for the Marrero WWTP Test Case using a 60x20 grid	135
Figure 5.6c	Trajectory Paths and Zones for the 60x20 grid. Marrero WWTP.	135
Figure 5.7	RAS and ESS Concentrations for Different Grid Sizes	138
Figure 5.8	Concentration Contours for 3 Different Grids Used in the Marrero Test Case.....	140
Figure 5.9	Stream Function Contours and Velocity Vectors for 3 Different Grids Used in the Marrero Test Case.....	141
Figure 5.10	RAS SS and ESS Concentration Predicted by the Model During the Validation.....	144
Figure 5.11	Concentration Contours at 540 minutes of simulation time for the Validation - Marrero WWTP Test Case using a 60x20 grid	145

Figure 5.12	Measured and Predicted Concentration Profiles at 8.8 m Radial Distance for the Marrero SST	146
Figure 5.13	Early Validation of the ESS Simulated by the Model	147
Figure 5.14	Flow Rates and Inlet Solids Concentration During at The Oxley Creek WWTP SST	150
Figure 5.15	Concentration Contours at 420 minutes of simulation time for the Oxley WWTP Validation Case using a 40x20 grid	151
Figure 5.16	Measured and Predicted Concentration Profiles at Different Radial Distances for the SST of the Oxley Creek WWTP	152
Figure 5.17	ESS, RAS SS and SLR for the Unsteady Simulation of the Oxley Creek WWTP SST	153
Figure 5.18	ESS and RAS SS Predicted by the Q3D Model for the Stress Test on the Darvill WWTP New SSTs	158
Figure 5.19	Suspended Solids Contours and Velocity Vector for the Four Stress Test on the Darvill WWTP New SSTs	159
Figure 6.1	ESS for Three Study Cases with Different Initial Discrete Settling Fractions.....	163
Figure 6.2	ESS for 4 Study Cases in Center Well Effects	166
Figure 6.3	Concentration Contours and Velocity Vectors for the Marrero SST with and without Center Well	167
Figure 6.4	Mean Square Velocity Gradient for Marrero SST with and without Center Well.....	168

Figure 6.5	Effect of Center Well Radius on Clarifier Performance (Baffle Depth = 2.6m, SOR = 1 m/h, SLR= 4.20 kg/m ³ , RAS = 50%)	169
Figure 6.6	Effect of Center Well Radius on the Clarifier's Flow Pattern (Baffle Depth = 2.6m, SOR = 1 m/h, SLR= 4.20 kg/m ³ , RAS = 50%)	170
Figure 6.7	Effect of Center Well Depth on the ESS (Baffle Radius = 5.0 m, SOR = 1 m/h, SLR= 4.20 kg/m ³ , RAS = 50%)	171
Figure 6.8	Effect of Center Well Depth on the Clarifier's Flow Pattern (Baffle Radius = 5.0 m, SOR = 1 m/h, SLR= 4.20 kg/m ³ , RAS = 50%)	172
Figure 6.9	Comparison of Two Different Center Well Depths under Extreme Loading Conditions (Baffle Radius = 4.5 m, SOR = 2.5 m/h, MLSS = 2. kg/m ³ , RAS = 50%)	173
Figure 6.10	Flow Pattern and SS Contours for Two Different Center Well Depths under Extreme Loading Conditions (Baffle Radius = 4.5 m, SOR = 2.5 m/h, MLSS = 2.8 kg/m ³ , RAS = 50%)	174
Figure 6.11	Effect of SLR on Optimum Position of the Center Well (Baffle Depth = 2.6m, SOR = 1 m/h, SLR= Variable; RAS = 50%)	175
Figure 6.12	Effect of SOR on Optimum Position of the Center Well (Baffle Depth = 2.6m, MLSS = 2.8 Kg/m ³ , SLR= Variable, RAS = 50%)	176
Figure 6.13	Optimum Center Well Radius versus SOR (Baffle Depth = 2.6m, MLSS = 2.8 Kg/m ³ , SLR= Variable, RAS = 50%)	177
Figure 6.14	Flow Pattern and SS Contours for a Large Center Well under Different SOR Loadings (CW Radius = 6.5 m, CW Depth = 2.6 m, MLSS = 2.8 kg/m ³ , RAS = 50%)	178

Figure 6.15A	1D Solids Flux Analysis for the Marrero WWTP using the Zone Settling Properties	179
Figure 6.15B	1D Solids Flux Analysis for the Marrero WWTP using the Zone Settling and Compression Rate Properties ($V_o = 10.54$ m/h, $K_I = 0.40$ L/g, $V_c = 3.20$ m/h, $K_c = 0.184$ L/g)	180
Figure 6.16	ESS vs SLR. Limiting Solids Flux Analysis (SOR= 1 m/h, UFR= 0.5 m/h, MLSS= Variable, RAS =50%)	182
Figure 6.17	Sludge Blanket Position for Limiting and Failing SLRs (SOR= 1 m/h, UFR= 0.5 m/h, MLSS= Variable, RAS = 50%)	184
Figure 6.18	ESS vs SOR. Limiting Solids Flux Analysis (SOR= Variable, UFR= $0.5 \times \text{SOR}$, MLSS= 2.8 Kg/m^3)	186
Figure 6.19	Influence of SOR in the Flow Pattern and the Position of the Sludge Blanket (SOR= Variable, UFR= $0.5 \times \text{SOR}$, MLSS= 2.8 Kg/m^3)	188
Figure 6.20	Performance of the SST for a Constant SLR and Variables SOR and MLSS (SOR= Variable, UFR= $0.5 \times \text{SOR}$, MLSS= Variable, SLR= $4.20 \text{ Kg/m}^2 \cdot \text{h}$)	190
Figure 6.21	Effects of the MLSS and SOR with a Constant SLR on the SST Suspended Solids Contours (SOR= Variable, UFR= $0.5 \times \text{SOR}$, MLSS= Variable, SLR= $4.20 \text{ Kg/m}^2 \cdot \text{h}$)	191
Figure 6.22	Evaluations of the Flocculation Processes at Different MLSS (SOR= 2.0 m/h)	194
Figure 6.23A	Flat Bed Clarifier with Suction Withdrawal System (Depth = 5.0m, SOR= 1.0 m/h, UFR= 0.5 m/h, MLSS= 2800 mg/L)	197

Figure 6.23B	Flat Bed Clarifier with Suction Withdrawal System – Lower RAS Ratio (Depth = 5.0m, SOR= 1.0 m/h, UFR= 0.3 m/h, MLSS= 2800mg/L).....	197
Figure 6.24	Oscillation Presented in the RAS SS and ESS Concentration with the Simulation of the Rake Type Scraper	198
Figure 6.25	Horizontal Velocities in a Gravity Flow for a Sloping Bed Circular Clarifier (Bottom Slope= 8.33).....	199
Figure 6.26	Horizontal Velocities in a Gravity Flow for a Sloping Bed Circular Clarifier and Comparison with the Radial Velocities of the Scraper (Bottom Slope= 8.33%, Scraper Velocity= 0.033 rpm, Blade Angle= 45°)..	201
Figure 6.27	Simulated Velocity Gradients with and without Inlet Deflector (SOR= 1.0 m/h)	203
Figure 6.28	Predicted ESS and RAS SS Concentrations with Settling Properties Corrected for Different Temperatures due to Change of Viscosity	206
Figure 6.29	Effect of Influent Temperature Variation on the ESS Concentration (SOR= 1.0 m/h, MLSS= 2800 mg/L)	208
Figure 6.30	Effect of Influent Temperature Variation on the Suspended Solids Contours ($\Delta T = +1^{\circ}\text{C}$, SOR= 1.0 m/h, MLSS= 2800 mg/L)	209
Figure 6.31	Effect of Influent Temperature Variation on the Internal Temperature Distribution ($\Delta T = +1^{\circ}\text{C}$, SOR= 1.0 m/h, MLSS= 2800 mg/L).....	210
Figure 6.32	Effect of Influent Temperature Variation on the Internal Temperature Distribution for a Low incoming MLSS ($\Delta T = +1^{\circ}\text{C}$, SOR= 1.0 m/h, MLSS= 300 mg/L).....	212

Figure 6.33	Effect of Seasonal Variation on the Performance of the SST (SOR= 1.0 m/h, MLSS= 2800 mg/L).....	213
Figure 6.34	Effect of Surface Cooling on the Suspended Solids Contours	214
Figure 6.35	Temperature Stratification under the Effect of a Surface Cooling Process for an Influent Temperature Equal to 26.5°C.....	215
Figure 6.36	Temperature Stratification under the Effect of a Surface Cooling Process for an Influent Temperature Equal to 16.0°C.....	215
Figure 7.1	Recommended Coupled System.....	226

LIST OF TABLES

Table 3.1	Settling Regions Based on the TSS Concentration.....	70
Table 3.2	Settling Velocities and Dynamic Viscosities for Samples at Normal and Cooled Temperature.....	73
Table 3.3	Ratios V_{sT_1} / V_{sT_2} and μ_{T_2} / μ_{T_1} for Different Samples.....	74
Table 4.1	Settling Velocities and Cross Sectional Diameters for Different Particle ..	89
Table 5.1	Dimensions and Operating Characteristics of the SST at the Marrero WWTP	117
Table 5.2	MLSS, RAS and Threshold Concentration.....	118
Table 5.3	Discrete Settling Velocities of Large Flocs	119
Table 5.4	Discrete Settling Velocities of Medium Flocs	120
Table 5.5	Data for the Calculation of the Discrete Settling Velocity of Small Flocs.....	121
Table 5.6	Data for the Calculation of the Discrete Settling Fractions	122
Table 5.7	Discrete Settling Velocities and Fractions.....	123
Table 5.8	Field Data for the Determination of the Settling Parameter of the Zone Settling and Compression Rate Exponential Equations.....	125
Table 5.9	Calibrated Settling Parameter of the Hindered and Compression Settling Equations.....	126
Table 5.10	Kinetic Constant for the Flocculation Sub-Model	129
Table 5.11	Suspended Solids Concentrations Measured During the Calibration Period	130
Table 5.12	Flow Rates, SOR and RAS During the Calibration Period	130

Table 5.13	Input Data for the Clarifier Model Simulation	132
Table 5.14	Comparison between Measured and Predicted Values for Calibrated Model	133
Table 5.15	Grid Sizes Evaluated in the Dependency Test.....	137
Table 5.16	ESS and RAS SS Concentrations at Equilibrium Conditions for 3 Grid Sizes	139
Table 5.17	Suspended Solids Concentrations Measured at the Marrero WWTP During the Validation Period	142
Table 5.18	General Data for the Validation of the Q3D Model – Marrero WWTP ...	143
Table 5.19	Comparison between Measured and Predicted Values During the Validation of the Q3D Model	144
Table 5.20	Settling Properties (Takacs’ Model) for the Oxley Creek WWTP	148
Table 5.21	Summary of Oxley Creek WWTP SST Characteristics	149
Table 5.22	Predicted and Measured ESS and RAS SS Concentration Under Steady State Conditions for the Oxley Creek WWTP SST Simulation	151
Table 5.23	Geometry of Darvill WWTP New SSTs.....	155
Table 5.24	Summary of the Four SLR Stress Test Done on the Darvill WWTP New SSTs	155
Table 5.25	1 DFT Predicted Maximum SOR	156
Table 5.26	Darvill WWTP New SST Stress Test Results	156
Table 5.27	Sludge Settleability Parameters for the Darvill WWTP	157
Table 5.28	Summary of the Q3D Model Simulation Results for the Stress Test 1 to 4 on the Darvill WWTP New SSTs. Comparison with the Actual Stress	

	Tests and with SettlerCAD Simulations	160
Table 6.1	Discrete Settling Fractions for Three Study Cases	162
Table 6.2	ESS and RAS SS for Three Study Cases with Different Discrete Settling Fractions.....	163
Table 6.3	ESS and RAS SS for a Study Case with and without Simulation of the ..	164
Table 6.4	ESS and RAS SS for Three Study Cases in Center Well's Effects	165
Table 6.5	Settling Properties used in the Solids Flux Analysis	180
Table 6.6	Simulated Data and Predicted ESS and RAS SS in the Solids Flux Analysis of the Marrero WWTP SST (RAS = 50%)	182
Table 6.7	Simulated Data and Predicted ESS and RAS SS in the Study of the Effect of the SOR on the Performance of the Marrero SST	186
Table 6.8	Simulated Data and Predicted ESS and RAS SS in the Study of the Effect of the SOR and MLSS with Constant SLR on the Performance of the SST	189
Table 6.9	Evaluations of the Flocculation Processes on SST at High SOR	193
Table 6.10	Settling Properties Used in the Evaluation of the Sludge Withdrawal Systems	195
Table 6.11	Effect of the Sludge Withdrawal Systems on the SST Performance	196
Table 6.12	Scraper and Gravity Flow Velocities.....	200
Table 6.13	Predicted ESS and RAS SS Concentrations with and without an Inlet Deflector for Good and Poor Settling	202
Table 6.14	Comparison between Settling Properties at 26.5 and 15.0 °C. Correction Based on the Change of Viscosity	205

Table 6.15	Predicted ESS values for Different Temperature Variations.....	207
Table 6.16	Heat Exchange Parameters Summer and Winter Conditions	207

LIST OF ABBREVIATIONS AND SYMBOLS

Abbreviations

1D, 2D, 3D	One-, two- and three dimensional
ADI	Alternating direction implicit
AS	Activated sludge
CCOD	Colloidal COD
CFD	Computational fluid dynamics
CFSTR	Continuous flow stirred tank reactor
COD	Chemical oxygen demand
CRTC	Clarifier research technical committee
DCOD	Dissolved COD
DO	Dissolved oxygen
DSS	Dispersed suspended solids
EESS	Excess effluent suspended solids
EPS	Extracellular polymeric substance
ESS	Effluent suspended solids
FCW	Flocculation center well
FDM	Finite difference method
FEM	Finite element method
FSS	Flocculated suspended solids
FTC	Flow-through curves
FVM	Finite volume method
FW	Flocculation well
HLP	Hybrid linear-parabolic and oscillation-free convection scheme
HRT	Hydraulic retention time
ISS	Influent suspended solids
KE	Kinetic energy
MLSS	Mixed liquor suspended solids
PCOD	Particulate COD

PDE	Partial differentials equation
PE	Potential energy
PST	Primary settling tank
Q3D	Quasi 3-dimensional clarifier model
QUICK	Quadratic upstream interpolation for convective kinematics
RAS	Return activated sludge, recycle ratio
SIM	Strip integral method
SLR	Solids loading rate
SOR	Surface overflow rate
SRT	Sludge retention time
SS	Suspended solids
SSS	Supernatant suspended solids
SST	Secondary settling tank
ST	Settling tank
SVD	Settling velocity distribution
TCOD	Total COD
TDS	Total dissolved solids
TF/SC	Trickling filter-solids contact processes
TSS	Total suspended solids
UFR	underflow rate
WWTP	Wastewater treatment plant
ZSV	Zone settling velocity

Symbols

English

A	area Albedo, Equation 4.29
A_s	clarifier superficial area
a	residual concentration of particles

B	settling parameter for Equation 2.17
	opening height, Equation 2.51
b	fitting parameter, Equation 2.16
C	concentration of unflocculated particles
C_D	drag coefficient
C_p	specific heat
C_o	initial concentration of influent particles
c	fitting parameter, Equation 2.16
d	fitting parameter, Equation 2.16
D	fractal dimension
	diameter of the inlet, Equation 2.50
d_a	size of the aggregate
dp	diameter of the particle
E	porosity
$E a$	atmospheric emissivity
e	air vapour pressure
F	force
f	discrete settling fraction
	partition function, Equation 3.1
G	means square velocity gradient
g	vertical component of the gravitational acceleration
h	vertical distance
Hb	height of the blade on the scraper submodel
I_o	insolation at outer limit of earth's atmosphere
k	settling parameter
J_{she}	total surface heat flux
J_{sn}	net solar shortwave radiation

J_{an}	atmospheric longwave radiation
J_{br}	water longwave radiation
J_{cc}	heat transfer due to conduction and convection
J_{ec}	heat transfer due to evaporation and condensation
K	settling parameter
k	turbulence kinetic energy
k_c	settling parameters for the compression settling model
k_l	settling parameters for the zone settling settling parameters of the hindered settling zone for the Takacs model
k_2	settling parameter for the low solids concentration region
k_f	flocculation constant, Equation 2.39
K_A	floc aggregation coefficient
K_B	floc breakup rate coefficient
L_f	longest dimension of the floc
l_m	mixing length
M	mass
m	settling constant for Cho model coefficient for cylindrical or Cartesian coordinates in Equations 2.1 to 2.6 stress growth exponent, Equation 2.34 floc break up rate exponent, Equation 2.35 relative thickness of air mass, Equation 4.27
N	number of arm in the scraper submodel Fraction of the sky obscured by clouds, Equation 4.28
n	primary particle number concentration
n	settling constant for Cho model (Chapter 2) non-Newtonian exponent (Chapter 2) turbidity factor of the air, Equation 4.27
N_R	Reynolds number
p	hydrostatic pressure
P	total energy loss or power imparted to the water
Pe	Peclet number

P_o	empirical coefficient, Equation 2.22
Q	air-flow rate
Q_e, Q_{eff}	effluent flow rate
Q_i	influent flow rate
q	fitting parameter, Equation 2.16
r	radius
S_o	specific surface area
S_s	particle specific gravity
T	temperature
T_d	dew point temperature
T_{sw}	water surface temperature
U_w	wind speed
u	velocity along r- and x- coordinate
v	velocity along y- coordinate
V	reactor volume
V_{br}	velocity of the blade in the radial direction
V_o	settling parameter
V_c	compression rate parameter
V_s	particle settling velocity
V_{sp}	terminal settling velocity of the primary particle
V_t	tangential velocity solids
W_{bo}	solar constant
X	concentration of suspended solids
X_d	threshold for discrete settling
X_h	threshold for hindered settling
X_c	threshold for compression settling
X_{min}	minimum attainable settling concentration
z	cloud base-altitude, Equation 4.28

Greek

ν_{sy}	eddy diffusivity of suspended solids in the y-direction
------------	---

ν_{sr}	eddy diffusivity of suspended solids in the r-(x) direction
ν_t	eddy viscosity
σ	Stefan-Boltzmann constant
σ_{sr}	Schmidt number in the r-(x) direction
σ_{sy}	Schmidt number in the y-direction
μ	fluid dynamic viscosity
ν	kinematic viscosity
Θ	settling parameter, Equation 2.17
Γ	settling parameter, Equation 2.17
Γ_r	effective diffusion coefficient in the r- direction
Γ_y	effective diffusion coefficient in the y- direction
ε	the rate of energy dissipation
	emissivity of water, Equation 4.31
λ	Kolmogorov microscale
	overall primary particle removal rate, Equation 2.38
	molecular diffusivity, Equation 2.58
ϕ	solids fraction
ρ_f	floc density
ϕ_g	gel solids fraction
ρ_p	particle density
ρ, ρ_l	fluid density
ρ_r	reference density
τ	shear stress
τ_o	yield stress
τ	sun's hour angle
η_p	plastic viscosity
γ^*	magnitude of the strain rate
α	equilibrium primary particle number concentration
	recycle ratio

	angle of the radiation with the horizon
β	removed primary particle concentration, Equation 2.38
$\beta(a,p)$	collision frequency function between the aggregate and small particles
κ	permeability of the aggregate
v_θ	velocity components in the θ - directions respectively
ν_{eff}	effective viscosity
ω	vorticity
ψ	stream function
Ω	scraper angular velocity
α	equilibrium primary particle number concentration
	recycle ratio
	angle of the radiation with the horizon
λ	Kolmogorov microscale
	overall primary particle removal rate, Equation 2.38
	molecular diffusivity, Equation 2.58
δ	declination angle
Φ	local latitude

ABSTRACT

The performance of settling tanks depends on several interrelated processes and factors that include: hydrodynamics, settling, turbulence, sludge rheology, flocculation, temperature changes and heat exchange, geometry, loading, the nature of the floc, the atmospheric conditions and the total dissolved solids concentration. A Quasi-3D (Q3D) clarifier model has been developed to include the following factors: axisymmetric hydrodynamics (including the swirl component), five types of settling (nonsettleable particles, unflocculated discrete settling, flocculated discrete settling, hindered settling and compression), turbulence, sludge rheology, flocculation with four classes of particles, temperature changes and surface heat exchange with the atmosphere, various external and internal geometry configurations, unsteady solids and hydraulic loading, the nature of the floc settling/interaction. The model includes: shear flocculation, differential settling flocculation and sweep flocculation. The Q3D model reproduces the major features of the hydrodynamic processes and solids distribution on secondary clarifiers. When the model is executed with the field derived settling characteristics, it can accurately predict the effluent and recirculation suspended solids concentrations. The model has been formulated to conserve fluid, tracer and solids mass.

The model has been developed and tested using field data from the UNO Pilot Plant and the Jefferson Parish Waste Water Treatment Plant located at Marrero, Louisiana. A field testing procedure is presented that addresses all of the settling regimes that are encountered in a Secondary Settling Tank.

Results obtained with the Q3D model indicate that the flocculation process plays a major role in the effluent suspended solids (ESS) on secondary clarifiers. The extent of actual flocculation depends on the design of the center well and on the concentration of the incoming mixed liquor suspended solids (MLSS). The center well promotes flocculation, but its most important benefit is the improvement on the tank hydrodynamics. The changes in temperature on secondary clarifiers play an important role on the performance of secondary settling tanks. The gravity induced radial velocities in the sludge blanket are

higher than the radial velocities of the scraper in the region near the hopper, therefore the blades are not highly effective in conveying the solids in this region.

CHAPTER 1

1 INTRODUCTION

1.1 Background and Problem Definition

“The bottle neck limiting the capacity of the wastewater treatment plant” (Ekama and Marais, 2002), “the most sensitive and complicated process in an activated sludge treatment plant” (Ji et al., 1996), “almost invariably the reason for poor performance of an activated sludge system” (Wahlberg et al., 1995); these are just a few examples of expressions emphasizing the role of the secondary clarifier in the overall performance of the activated sludge system. Already critical in conventional biological treatment systems; the new treatment tendencies based on pollutant size distribution [e.g. role of bioflocculation on COD removal, La Motta et al. (2004a)] further stress the importance of secondary settling tanks (SST). In suspended growth systems, such as conventional activated sludge (AS), dissolved, colloidal and even a portion of particulate contaminants have been converted (i.e., oxidize in the biological-aeration tank) into suspended microbial mass, water and biogases. The SST has the responsibility of the physical separation of the microbial mass and remaining settleable particles from the liquid (i.e., clarification function).

In high rate-flocculation systems, only the dissolved and a portion of the colloidal contaminants are oxidized; a portion of the remaining colloidal portion and the particulate contaminants are aggregated into flocs that have to be removed by sedimentation. In this type of systems the secondary clarifiers not only have to account for clarification, but also guarantee the floc structure (i.e., avoid floc break up) and promote the aggregation of remaining dispersed particles and flocs that have been broken up in the conveyance devices (i.e., flocculation function). Obviously, the success of the treatment depends on the clarifier performance. In addition, both conventional AS and flocculation systems require the maintenance of an appropriate biomass concentration; it is the function of the SST to produce a thickened underflow sludge, which is removed in the return sludge flow

and transported to the biological reactor (i.e., thickening function). A fourth, usually overlooked, function should be added: storage. The SST has to allow for accumulation of sludge during peak flows, but also for accumulation of sludge due to system operation (e.g., when the wasted sludge is less than the biomass produced daily, solids accumulation will occur in the biological reactor, in the SST or in both). Although it is commonly assumed that the sludge purged from the system is equal to the produced biomass, La Motta et al. (2004b) found that sludge accumulation is very likely to occur under typical operating conditions.

The performance of SST depends on several interrelated processes; for simplicity, these processes have been divided into six groups: (A) hydrodynamics, (B) settling, (C) turbulence, (E) sludge rheology, (F) flocculation, and (G) heat exchange and temperature changes. At the same time, these processes depend on numerous, also interrelated factors, that include: (1) the geometry of the tank, including inlet and outlet configurations, sludge withdrawal mechanisms, internal baffles and bottom slope; (2) loading, including solids and hydraulic loading, and time variations; (3) the nature of the floc in the mixed liquor suspended solids (MLSS), including the settling properties and the tendency to aggregation and break up; (4) the variations in the total dissolved solids (TDS); (5) the atmospheric conditions, including ambient and water temperature, shortwave and longwave radiations, and wind. Naturally, the weight of these processes and factors is variable, and therefore neglecting assumptions can be made. However, a complete model for SST must include sub-models for the six aforementioned groups, allowing for the representation of the interrelated factors. Obviously this is not an easy task, and so far it has not been completed (to the knowledge of the author).

Being three dimensional in nature, the modeling of the clarifier processes should also be done in 3D. However, by neglecting wind shear and assuming an axisymmetric flow, this can be done accurately in 2D. Nevertheless the most common way of designing secondary settling tanks is the 1D flux theory (1DFT). According to Ekama et al. (1997) this is done in two stages: firstly, zone settling and thickening considerations are applied, which lead to the determination of the surface area and depth; secondly, internal features

are included in the tank, which should optimize the clarification efficiency. This second stage is usually done following some semi-empirical rules (e.g., twenty minutes retention time in the flocculator center-well) and strongly relies on the engineer's experience. Ekama et al. (1997) concluded that the predicted maximum permissible solids loading rate, using the 1DFT, over-predicts the permissible solids loading rate (SLR) by about 25%. However, there was no convincing evidence that an 80% reduction in the predicted SLR needed to be applied for all SST (Ekama and Marais, 2002). Definitely, different tank geometries and configurations might give different correction factors.

1D models do not account for the major features in tank hydrodynamics and internal configurations; this has to be done at least in a 2D layout. Several 2D models of various complexities have been developed for simulating circular and rectangular, primary and secondary settling tanks. A detailed historical review will be presented in Chapter 2 but a state of the art review in 2D modeling will now be presented.

The first 2D clarifier model was presented by Larsen (1977). His model, developed for rectangular clarifiers, was based on the equations of motion, continuity and an exponential equation relating settling velocity to concentration. He introduced the concept of stream function and vorticity, and the generation of vorticity by internal density gradients and shear along solid boundaries. Diffusivity was assumed equal to eddy viscosity, which was computed on the basis of the Prandtl mixing length theory.

Schamber and Larock (1981) introduced the $k-\epsilon$ turbulence into a finite element model to simulate neutral density flow in the settling zone of a rectangular tank. Imam et al. (1983) developed and tested a numerical model to simulate the settling of discrete particles in rectangular clarifiers operating under neutral density conditions. A two-step alternating direction implicit (ADI), weighted upwind-centered finite difference scheme was used to solve the 2D sediment transport and vorticity-transport stream function equations. Abdel-Gawad and McCorquodale (1984b) applied a strip integral method (SIM) to a primary circular settling tank in order to simulate the flow pattern and dispersion characteristics of the flow under steady conditions. The authors expanded their work (Abdel-Gawad and

McCorquodale, 1985b) coupling the hydrodynamics with a transport model to simulate the transport and settling of primary particles in circular settling tanks; the model was restricted to the neutral density case. Celik et al. (1985) presented a numerical finite-volume method (FVM) using the k - ϵ turbulence model for predicting the hydrodynamics and mixing characteristics of rectangular settling tanks. Devantier and Larock (1986, 1987) introduced a Galerkin finite element method to model a steady two-dimensional flow in a circular SST. They modelled the sediment-induced density current in the circular clarifier but did not model the inlet region.

McCorquodale et al. (1991) introduced a numerical model for unsteady flow in a circular clarifier. The model included a description of density currents in the settling zone only. The authors introduced the double-exponential settling velocity formula of Takacs et al. (1991), which allows for a lower settling velocity in a low-solids concentration region. Although this equation was developed for one-dimensional settling tank modelling, it has been widely used in 2D modelling since then.

Zhou and McCorquodale (1992a, 1992c,) presented a numerical and computer model for unsteady flow in a center-fed secondary circular clarifier that included simulation of the inlet zone. At that time, they (McCorquodale and Zhou, 1994a) concluded that numerical models were sufficiently well advanced so that they could be used as a tool in the selection of critical tank dimensions such as depth, diameter, launder locations, bottom slope and skirt dimensions.

Lately, Zhou et al. (1994) used a numerical model to investigate the unsteady flow regime and the temperature mixing in temperature-stratified primary rectangular settling tanks. They introduced an equation of state for the local fluid density as a function of temperature, and a convection-diffusion equation to determine the temperature field in the tank.

Krebs (1991) used the computational fluid dynamic (CFD) computer code PHOENICS to model velocity and the volume fraction field in rectangular clarifiers in steady state. Lyn

et al. (1992) developed a 2D steady state model to simulate the settling of discrete particles in rectangular tanks with a settling velocity distribution (SVD). The model, which accounted for the effects of sediment-induced density currents, included a simple approach to describe flocculation. The flocculation model assumed only turbulent shear-induced flocculation. Szalai et al. (1994) included swirl effects into a circular tank. The calculations were restricted to steady state and neutrally buoyant case. Dahl et al. (1994) presented a steady state model that took into account the rheology of the activated sludge; it included the Bingham plastic characteristic of activated sludge suspensions.

Ji et al. (1996) coupled a 2D clarifier model to an aerobic biological reactor. The coupling arrangement was used to simulate the response of the system to the change of the return activated sludge ratio (RAS) under steady-state influent and investigate the possible remedial actions for peak wet weather flow conditions for a dynamic influent. Vitasovic et al. (1997) used data, collected by Wahlberg et al. (1993) through application of the Clarifier Research Technical Committee (CRTC) protocol, to perform simulations of the Denver secondary clarifier. They tested different loadings and settling properties, and introduced modifications in the tank geometry (decreased the size of the flocculation center well and added a Crosby baffle) that improved the hydrodynamics and tank performance.

Lakehal et al. (1999) and Armbruster et al. (2001) presented a model for unsteady simulation of circular clarifiers that included the sludge blanket in the computation domain. A rheology function was included that accounted for the increased viscosity of highly concentrated sludge mixtures. Stamou et al. (2000) applied a 2D mathematical model to the design of double-deck secondary clarifier. They modelled each tank independently adjusting the boundary conditions for the independent cases.

Ekama and Marais (2002) applied the 2D hydrodynamic model SettlerCAD (Zhou et al., 1998) to simulate full scale circular SSTs with the main goal of evaluating the applicability of the one-dimensional idealized flux theory for the design of SST. The

results of the 1D and 2D approaches were compared with full-scale stress tests. Settler-CAD accurately predicted the results of 12 of 15 selected tests.

In recent years, CFD commercial programs have become fast and user-friendly and have been widely used by engineers in many fields. Two of the most common CFD packages are PHOENICS and FLUENT. Examples of PHOENICS applications can be found in Krebs (1991), Dahl et al. (1994), Krebs et al. (1995), De Cock et al. (1999) and Brouckaert and Buckley (1999). Laine et al. (1999), De Clercq (2003), and Jayanti and Narayanan (2004) used FLUENT for their simulation of the 2D hydrodynamics of settling tanks. De Clercq presented an extensive study in SSTs that included calibration and validation with both lab-scale and full-scale investigations. He implemented submodels that account for the rheology of the sludge, the Takacs solids settling velocity and the scraper mechanism.

Despite its well advanced state, several gaps and shortcomings have been identified in current 2D models. Krebs (1995) discussed that 2D models had not become relevant for application since they are very complex and require a lot of understanding. Krebs (1995), Krebs et al. (1996), Mazzolani et al. (1998), Lakehal et al. (1999) and Ekama and Marais (2002) all expressed their concern about the way the settling properties are treated in current settling tank models. They were basically describing the shortcomings in the use of the Takacs model. As Ekama and Marais (2002) pointed out: “While the description of the hydrodynamics of the SSTs has progressed dramatically with the advent of 2D and 3D hydrodynamic models, description of the sludge settling behavior in these models has not progressed very much beyond that in the 1D flux theory models and remains the major weakness in the models.” In this respect, Lakehal et al. (1999) found that the Takacs equation underestimates the value of the settling velocities in the sludge blanket. Other limitations in current models were identified by McCorquodale (2004) who indicated that present SST models lack a realistic, physically based flocculation submodel, thermal and TDS density simulation. Further, De Clercq (2003) indicated that the simulation of swirl effects induced by rotating scrapers and inlet vanes is relevant for the accurate simulation of the flow field, something that is not currently included in SST

models. Even though very little information about 3D models has been published, the limitations presented in this paragraph about 2D models extend to 3D models, with the exception of swirl effect simulation.

The discussion presented so far is summarized as follows:

- Secondary clarifiers play a major role in the overall wastewater treatment plant performance. SST should be designed at least with the same level of detail and expertise as is used to design the biological process.
- Although a very complex problem, SSTs are designed with many simplifications. The most common way of designing a SST is the 1DFT model, which seems to over-predict the permissible solids loading and does not account for the major hydrodynamic features of the tanks. Internal geometry, which may control the clarification efficiency of the clarifier, can not be evaluated using 1D models. The internal features are usually added following semi-empirical rules and are based on engineering experience.
- 2D and 3D models account for hydrodynamic and internal geometry configurations. However, these models are not fully developed, and their use is not widespread. The major limitations of current SST models seem to be: a simplistic simulation of the settling velocities that is too dependent on the calibration of the model and does not account for the settling velocities of the entire range of suspended solids concentration usually encountered in SST; the lack of flocculation submodels, so far flocculation has been only incorporated in primary clarifier models; the lack of heat exchange, thermal and TDS density simulation. In addition, current 2D models do not include swirl effects. Another important disadvantage of 2D and 3D models is that they are not fully available to design engineers and plant operators.

It can be concluded from the discussion that the current ways in which SSTs are designed and modified could and should be improved. Providing a tool that might lead to clarifier optimization, as well as understanding, quantifying and visualizing the major processes dominating the tank performance, are the main goals of this research.

1.2 Scope and Objectives

This research focuses on the development of a Quasi-3D model (Q3D model) that can be used as an aid in the design, operation and modification of secondary clarifiers. This model represents in a 2D scheme the major physical processes occurring in SSTs. However, swirl effects due to rotating scrapers and inlet vanes are also included, hence the Quasi-3D definition. Obviously, such a model can be a powerful tool; it might lead to clarifier optimization, developing cost-effective solutions for new sedimentation and flocculation projects and helping existent clarifiers to reach new-more demanding standards with less expensive modifications. An important benefit is that the model may increase the understanding of the internal processes in clarifiers and their interactions, e.g., clarifying the role of flocculation on the tank performance. A major goal is to present a model that can be available to the professionals involved in operation, modification and design of clarifiers; in this respect, the model was developed following two premises: first; a non-commercial code for the solver was developed, i.e., no commercial CFD program was used to avoid the high cost of this type of software; second, the recalibration of the model for the application to specific cases was designed to be as straightforward as possible, i.e., whenever possible the theory with the simplest calibration parameters was used. The specific objectives of this research include:

- Develop a mathematical model for secondary clarifiers in 2D; this model will include a momentum equation for the calculation of the velocities in the theta direction, which will account for swirl effects. The rheology of the sludge and turbulence effects will also be modelled.

- Develop an appropriate relationship for the simulation of the settling velocities on the entire curve of suspended solids usually encountered in SST.
- Introduce a flocculation submodel in the general SST model, including surface heat exchange.
- Introduce a temperature submodel in the general SST model.
- Develop a model calibration procedure, including the calibration of the settling properties and flocculation submodels.
- Evaluate the grid and time dependency of the model solution.
- Evaluate the role of the different submodels (e.g. settling properties, flocculation, temperature, and rheology) in the SST prediction.

1.3 Dissertation Organization

This document is organized into six chapters:

Chapter 1 introduces the topic, presents a short description about clarifier modeling, and discusses the problem, the dissertation scope and objectives, and the organization of the document.

Chapter 2 presents a literature review on the topics related to the dissertation. 2D clarifier modeling, hydrodynamics of settling tank, settling properties of the sludge, turbulence modeling, sludge rheology, flocculation, and temperature effects are the major topics discussed in this chapter.

Chapter 3 presents the research on settling properties that led to the development of a compound settling model. A study about the effects of temperature on the settling properties is also presented in this chapter.

Chapter 4 demonstrates the development of the Quasi 3D mathematical model. This chapter introduces the governing equations, the turbulence and rheology submodels, and the scraper submodel that are used in the model. Chapter 3 presents a short review in numerical methods and a discussion about the methods used in this research to discretise and solve the differential equations.

Chapter 5 discusses the calibration of the model, including the calculation of all the parameters needed for the calibration. This chapter also includes a grid dependency test and the validation of the model with three different test cases.

Chapter 6 presents several applications of the model. The results of these applications are discussed in this chapter.

Chapter 7 states the general and specific conclusions of the research. Recommendations for improving the model and future research are also presented in this chapter.

Eleven appendices provide background, general and detail information, and most of the data collected during the development of this research.

CHAPTER 2

2 LITERATURE REVIEW

2.1 Historical Review of 2-D Modeling of Settling Tanks

The clarifier modeling field has its beginning in 1904 when Hazen introduced the overflow rate concept, a design concept which has been widely used and still is a major criterion in settling tank design. Hazen's theory states that the hydraulic retention time should be equal to the time needed for a particle to settle from the top to the bottom of the tank; in this way all the particles with settling velocities higher than that of the design particle will be removed. Hazen's theory has many assumptions that make its application unrealistic for secondary settling tanks: (1) Hazen assumes a uniform horizontal velocity field where turbulence is not considered; in reality, the flow field in SST is turbulent and heterogeneous in nature, and the high solids loading and low hydraulic loading lead to density-dominated flows. The relationship between hydraulic efficiency and removal of suspended solids cannot be clearly understood unless the influences of density differences on the hydrodynamics are considered (Zhou and McCorquodale, 1992a). (2) Hazen assumes that the settling rate of the particle is constant and is independent of the flow; this can be true for discrete particles settling, but in SST the flocculent, hindered and compression settling usually dominate the process, and these are influenced by the concentration of suspended solids and the biological nature of the flocs. Also, flow and sedimentation strongly interact via density effects and flocculation or floc break up (Ekama et al., 1997). In large grit chambers and primary settling tanks Hazen's assumptions can be approximately valid and useful to represent the process.

Anderson (1945) recognized that the flow in secondary clarifiers is not uniform and is affected by the existence of density currents due to density stratification. He examined the effect of the density currents upon the design factors and on the general performance of the clarifier.

Dobbins (1944) and Camp (1945, 1952) introduced analytical solutions that allowed vertical mixing to be included in a Hazen type model. The analysis presented by Dobbins was based on the concept of overflow rate using a plug flow assumption and accounted for the effects of wall-generated turbulence on sedimentation. Camp approximated the effect of turbulence in retarding settling. In general, their theories expanded the knowledge of the sedimentation process, but their simple approaches fail to account for many of the hydraulic characteristics of real clarifiers that could only be presented in good detail in 2D models.

The pioneering work in 2D clarifier modeling was presented by Larsen (1977). Larsen, who based his work in rectangular clarifiers, presented an extensive research. His work was supported by experimental and field measurements, which provided valuable information on the various hydrodynamics processes in clarifiers (Zhou and McCorquodale, 1992a). His work in energy fluxes, density of suspension and density currents was remarkable, as was his work in inlet considerations, jets, energy dissipation and G values.

Larsen also presented a 2D mathematical model for rectangular clarifiers. The model was based on the equations of motion, continuity and an exponential equation relating settling velocity to concentration. He introduced the concept of stream function and vorticity, and the generation of vorticity by internal density gradients and shear along solids boundaries. Diffusivity was assumed equal to eddy viscosity, which was computed on the basis of the Prandtl mixing length theory proportional to the local velocity gradient and a mixing length squared. Larsen set the baseline for future researches that have improved his work, but many of his developments are still valid and useful.

Schamber and Larock (1981) presented a finite element model to predict flow patterns in rectangular basins. They introduced the k- ϵ turbulence model to simulate neutral density flow in the settling zone of the tank.

Imam et al. (1983) developed and tested a numerical model to simulate the settling of discrete particles in rectangular clarifiers operating under neutral density conditions. A two-step alternating direction implicit (ADI), weighted upwind-centered finite difference scheme was used to solve the 2D sediment transport and vorticity-transport stream function equations. A constant eddy viscosity, obtained with the aid of a physical model, was used. As an interesting result of the research, the removal predicted by the numerical model was consistently less than predicted by the Camp-Dobbins approach.

Abdel-Gawad and McCorquodale (1984a) applied a strip integral method to a primary rectangular settling tank in order to simulate the flow pattern and dispersion characteristics of the flow. They used a modified Prandtl mixing length as a turbulent model, which was reported to give reasonable results. When compared with previous models (Imam et al., 1983; Schamber and Larock, 1981) the model was considerably more efficient both in computational time and storage. The authors expanded their work (Abdel-Gawad and McCorquodale, 1985a) coupling the hydrodynamics with a transport model to simulate the transport and settling of primary particles in rectangular settling tanks; the model was restricted to the neutral density case. They classified the influent solids in several fractions of solids with a settling velocity for each class, including a non-settleable class. The authors (Abdel-Gawad and McCorquodale, 1984b), also applied the SIM to simulate the flow pattern and dispersion characteristic in a circular primary clarifier. A modified mixing length model was applied, and proved to give reasonable results when comparing with experimental data. They included a transport equation (Abdel-Gawad and McCorquodale, 1985b) to allow the simulation of particle concentration distribution in primary circular clarifiers.

Celik et al. (1985) presented a numerical finite-volume method using the $k-\epsilon$ turbulence model for predicting the hydrodynamics and mixing characteristics of rectangular settling tanks. They used the hybrid scheme to predict the flow field and were quite successful in predicting the major hydrodynamic features of the physical model studied by Imam et al. (1983).

Devantier and Larock (1986, 1987) introduced a Galerkin finite element method to model a steady two-dimensional flow in a circular SST. They modelled the sediment-induced density current in the circular clarifier but didn't model the inlet region. They used a modified k - ϵ turbulence model, which was reported to require a significant computational effort but with good turbulence predictions. They were able to simulate only low solids loading rates; the influent suspended solids (ISS) concentration was limited to 1,400 mg/L, apparently due to instabilities that could have been solved by grid refinement, but the grid had already created the largest computer central-core storage requirement that could be supplied by their computer.

Stamou et al. (1989) presented a 2D numerical model to simulate the flow and settling performance of primary rectangular clarifiers. The approach of the model was similar to the previous model of Abdel-Gawad and McCorquodale (1985a), but they applied the more sophisticated k - ϵ turbulence model. Both models predicted about the same removal efficiency when applied to similar cases; however, the computational time seemed to be importantly larger for Stamou's model.

Adams and Rodi (1990) compared the performance of the model of Celik et al. (1985) with that of another version based on the same model equations but using an improved numerical scheme. They used a second order finite volume technique known as QUICK (Quadratic Upstream Interpolation for Convective Kinematics) to simulate the dye transport in two different rectangular clarifier configurations (the influences of particle settling, density differences and flocculation were not modelled). They concluded that the predictions based on the hybrid scheme (Celik et al., 1985) were significantly influenced by numerical diffusion; the scheme constantly under predicted the peaks of the FTC. The numerically more accurate QUICK scheme, however, over predicted the peaks of the flow-through curves (FTC) in all cases compared with experimental values. They reported that apparently too little mixing was generated by the k - ϵ model.

McCorquodale et al (1991) introduced a numerical model for unsteady flow in a circular center-fed clarifier. Two cases were modelled: (a) diurnal variation in flow at a constant

mixed liquor suspended solids (MLSS) concentration; and (b) a sudden increase in the MLSS. The model included a description of density currents in the settling zone only. The ordinary differential equations were solved using the Runge-Kutta-Verner fifth order method. The authors introduced the double-exponential settling velocity formula of Takacs et al. (1991), which allows for a lower settling velocity in a low-solids concentration region. Although this equation was developed for one-dimensional settling tank modelling, it has been widely used in 2D modelling since then.

Zhou and McCorquodale (1992a, 1992c,) presented a numerical and computer model for unsteady flow in a center-fed secondary circular clarifier that included simulation of the inlet zone. The authors used the hybrid finite difference procedure of Patankar and Spalding (1972) to solve the partial differential equations. They modelled and confirmed by physical tests some important phenomena, e.g. the density waterfall in the inlet zone, the influence of the waterfall on the bottom density current, flow entrainment, recirculation eddies and the influence of skirt radius on the clarifier performance. An explanation was given by the effect of inlet densimetric Froude number on effluent solids concentration, however only low densimetric Froude numbers were modelled. The turbulent stresses were calculated by the use of the eddy viscosity and the $k-\epsilon$ model. Zhou and McCorquodale (1992b) also presented a similar model for rectangular clarifiers; the model was verified by application to three field investigations. They reported that the removal efficiency was strongly related to settling properties of the sludge and that the settling velocity formula should account for the effect of nonuniform particle sizes; the calibration with the Takacs' formula satisfied this requirement.

Zhou et al. (1992) and McCorquodale and Zhou (1993, 1994a, 1994b) expanded their work in clarifier modelling. They modelled different hydraulic and solids loading and tested different clarifiers configurations including sloping bottom, different depths and different return activated sludge ratio (RAS). They found that the upward velocities in the withdrawal zone increase with decreasing densimetric Froude number, mostly due to the entrainment into the density waterfall. At that time, they (McCorquodale and Zhou, 1994a) concluded that numerical models were sufficiently well advanced so that they

could be used as a tool in the selection of critical tank dimensions such as depth, diameter, launder locations, bottom slope and skirt dimensions.

Lately, Zhou et al. (1994) used a numerical model to investigate the unsteady flow regime and the temperature mixing in temperature-stratified primary rectangular settling tanks. They introduced an equation of state for the local fluid density as a function of temperature, and a convection-diffusion equation to determine the temperature field in the tank.

Krebs (1991), Krebs et al. (1992), Samstag et al. (1992), Lyn et al. (1992), Szalai et al. (1994) and Dahl et al. (1994) are other important examples of 2D clarifier modelling in the early and mid-nineties. Krebs (1991) used the CFD computer code PHOENICS to model velocity and the volume fraction field in rectangular clarifiers in steady state. The turbulent flow was approximated with a constant turbulent viscosity. Krebs found positive effects in the hydrodynamic of the tank when a dividing wall was added. Krebs et al. (1992) used the same commercial CFD program and the same features presented by Krebs (1991) to model the effect of a porous wall in the inlet region of a rectangular clarifier. They reported that the rise in the sludge level before the wall reduced the buoyancy energy at the inlet; this resulted in a more uniform velocity distribution before the wall. After the wall the flow field was defined by the difference in sludge height on both side of the porous wall. Samstag et al. (1992) studied the influence of different underflow geometries in clarifier performance, using an extension of the model presented by McCorquodale et al. (1991). Lyn et al. (1992) developed a 2D steady state model to simulate the settling of discrete particles in rectangular tanks with a settling velocity distribution (SVD), using the k - ε turbulent model. The model, which accounted for the effects of sediment-induced density currents, included a simple approach to describe flocculation. The flocculation model assumed only turbulent shear-induced flocculation. The authors concluded that the effect of the shear-induced flocculation on the concentration field and the removal efficiency might be of secondary importance; opposite to importance of the SVD, they concluded that the correct modelling of the SVD was critical in obtaining a reliable prediction of the suspended solids field and removal

rates. Szalai et al. (1994) extended the work of Lyn and Zhang by taking into consideration the swirl effect. Instead of the HYBRID scheme they applied a low numerical diffusion technique known as HLP (hybrid linear-parabolic and oscillation-free convection scheme). The calculations were restricted to steady state and neutrally buoyant case, and their results were verified with the experiments of McCorquodale (1976). The implementation of swirl induced by rotating scrapers and inlet swirl vanes showed good agreement with the experimental FTC. Dahl et al. (1994) presented a steady state model that took into account the rheology of the activated sludge; it included the Bingham plastic characteristic of activated sludge suspensions. The model, applied to a rectangular tank, was calibrated using a single free and hindered settling velocity.

In the years that followed several attempts were made to demonstrate the application and validation of available models, applying them to existing clarifiers and using them for analysis of specific practical aspects in clarifier design, e.g. Krebs et al. (1995) presented the optimization of inlet-structure design for PST and SST. Krebs et al. (1996) studied the influence of inlet and outlet configuration on the flow in secondary rectangular clarifiers. Ji et al. (1996) coupled a 2D clarifier model to an aerobic biological reactor. The coupling arrangement was used to simulate the response of the system to the change of RAS under steady-state influent and investigate the possible remedial actions for peak wet weather flow conditions for a dynamic influent. Vitasovic et al. (1997) used data, collected by Wahlberg et al. (1993) through application of the Clarifier Research Technical Committee protocol, to perform simulations of the Denver secondary clarifier. They tested different loadings and settling properties, and introduced modifications in the tank geometry (decreased the size of the flocculation center well and added a Crosby baffle) that improved the hydrodynamic and tank performance. An important feature of their model is that it simulated the unsteady sludge blanket development caused by solids accumulation and compression.

Chebbo et al. (1998) and Wells and LaLiberte (1998a) presented a different approach to the widely used convection-diffusion equation for suspended solids transport. Chebbo et al. modelled the particle trajectories as a stochastic diffusion process. This approach was

used to calculate the removal efficiency in a primary rectangular tank using a SVD that included a nonsettleable portion. Well and LaLiberte simplified the process by modelling the steady state condition of a two-layer flow. The model, even though very simple, predicted interface height with and without suspended solids and temperature effects.

Mazzolani et al. (1998) presented a steady-state model for rectangular clarifiers. Their major contribution was the use of a generalized settling model that accounts for both discrete settling conditions in low concentration regions and hindered settling conditions in high concentration regions of the tank.

Lakehal et al. (1999) and Armbruster et al. (2001) presented a model for unsteady simulation of circular clarifiers that included the sludge blanket in the computation domain. A rheology function was included that accounted for the increased viscosity of highly concentrated sludge mixtures.

Stamou et al. (2000) applied a 2D mathematical model to the design of double-deck secondary clarifier. They modelled each tank independently adjusting the boundary conditions for the independent cases. The modelled flow fields in both tanks were similar, however the upper tank was in general more efficient in SS removal. Rheology conditions were not modelled.

Ekama and Marais (2002) applied the 2D hydrodynamic model SettlerCAD (Zhou et al., 1998) to simulate full scale circular SSTs with the main goal of evaluating the applicability of the one-dimensional idealized flux theory for the design of SSTs. The results of the 1D and 2D approaches were compared with full-scale stress tests. SettlerCAD accurately predicted the results of 12 of 15 selected tests. Kleine and Reddy (2002) developed a FEM model that when applied to the same cases, yields similar results to SettlerCAD.

In recent years, CFD commercial programs have become fast and user-friendly and have been widely used by engineers in many fields. Probably the two more common CFD

packages, among sanitary engineers, are PHOENICS and FLUENT; these have been used in simulation for diagnosis and evaluation of geometry modifications and/or operating conditions in PSTs and SSTs. Examples of PHOENICS applications can be found in Krebs (1991), Dahl et al. (1994), Krebs et al. (1995) and Brouckaert and Buckley (1999), who used the program for improving the design and operation of water and wastewater treatment plants. De Cock et al. (1999) also used PHOENICS to study the feasibility of flocculation in a storage sedimentation basin. They estimated the effect of coagulation-flocculation on the efficiency of the storage basin modifying the PHOENICS code with the introduction of a flow growth and break-up model. Laine et al. (1999), De Clercq (2003), and Jayanti and Narayanan (2004) used FLUENT for their simulation of the 2D hydrodynamics of settling tanks. Laine et al. and Jayanti and Narayanan presented studies in primary type settling tanks. De Clercq presented an extensive study in SSTs that included calibration and validation with both lab-scale and full-scale investigations. He implemented submodels that account for the rheology of the sludge, the Takacs solids settling velocity and the scraper mechanism; however, the validation was conducted without applying the scraper submodel (they concluded that its inclusion resulted in unrealistic solids blanket, probably due to the absence of swirl and other 3D effects on the model). A detailed explanation of the advantages and disadvantages of commercial CFD programs is presented in McCorquodale (2004).

2.2 Processes in Settling Tanks

2.2.1 Flow in Settling Tanks

Since the initial theory of settling in an ideal basin presented by Hazen (1904), many researchers have made contributions to a better understanding of the flow processes in a settling tank. Camp (1945) identified that the hydrodynamic presented in a real tank deviates from the ideal presented by Hazen due to four major reasons: (1) flocculation process in the clarifier, (2) retarding in settling due to turbulence, (3) the fact that some of the fluid passes through the tank in less time than the residence time (short-circuiting), and (4) the existence of density currents in the clarifier. Camp (1945) stated that “short-circuiting” is exhibited by all tanks and is due to differences in the velocities and lengths of stream paths and it is accentuated by density currents. Camp defined density currents as a flow of fluid into a relatively quiet fluid having a different density, and identified that the differences in density may be caused by differences in temperature, salt content, or suspended matter content.

Larsen (1977) divided the settling tank into four zones and identified some of the processes occurring in each one of these: (1) the inlet zone, a part of the tank in which the flow pattern and solids distribution is directly influenced by the energy of the influent. Mixing and entrainment are important features in this zone. (2) The settling zone, in which Larsen described two currents, a bottom current and a return current separated by a nearly horizontal interface. (3) The sludge zone, located at the bottom of the tank containing settled material which moves horizontally. (4) The effluent zone, which is the part of the settling tank in which the flow is governed by the effluent weirs. Figure 2.1 shows the zones and the flow pattern suggested by Larsen (1977) for rectangular settling tanks.

Larsen also identified that the flow in settling tanks is maintained and affected by major energy fluxes:

- 1) Kinetic energy (KE) associated with the inlet flow.
- 2) Potential energy (PE) associated with influent suspension having a higher density than the ambient suspension.
- 3) Wind shear at the free surface transferring energy to the basin.
- 4) Surface heat exchange that in the case of atmospheric cooling may produce water with higher density and therefore supply a source of potential energy.
- 5) Energy flux associated with water surface slope.
- 6) Energy losses due to internal friction and settling.

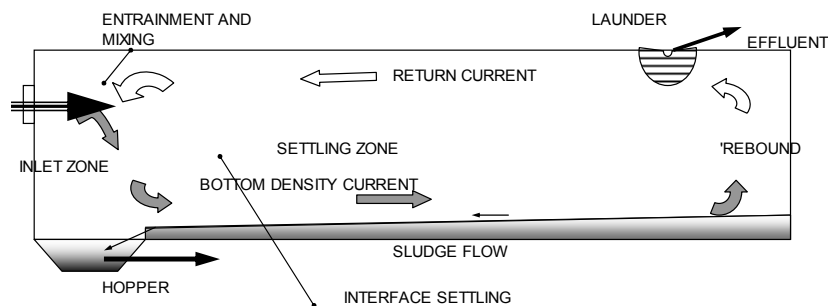


Figure 2.1 Flow Processes in a Rectangular Clarifier
(after Larsen, 1997)

In the matter of energy fluxes affecting the flow in settling tanks, Larsen presented the following conclusions: (1) The KE is mainly dissipated in the inlet zone, and in addition

to defining the flow pattern in this zone, the influent is diluted by entrainment. (2) The PE of SS is partly dissipated at the inlet and partly converted to KE through the density current which forms a flow along the bottom of the basin. The flow rate of the bottom currents is higher than the inlet flow rate due to the additional flow supply by a counter-flow in the upper layer (caused by the density current). (3) Gravity adds a small amount of energy to this flow. (4) The energy leaving the system, kinetic energy of the outflow and potential energy of the SS leaving the tank, is negligible as a component of the settling tank. (5) Wind shear and heat exchange may be of significance. These energy contributions affect mainly the upper layers where turbulence mixing may be enhanced. (6) All the energy inputs cause turbulence, which greatly affect the flow field and concentration distributions in the settling tank. Thus, the amount of SS in the effluent may depend on these energy inputs.

The effects of density differences, between the influent flow and the ambient liquid, in the flow pattern in circular and rectangular clarifiers have been largely studied and documented. Density waterfall, entrainment of clarified liquid into the density waterfall increasing the total flow, formation of the bottom density current, rebound at the end wall, recirculation of excess flow, possible short circuiting from the inlet zone to the RAS withdrawal and other associated effects have been identified in field measurements (e.g. Larsen, 1977; Lumley et al., 1988; Samstag et al., 1992; Deininger et al., 1996), as well as in hydraulic model tests (e.g. McCorquodale, 1976, 1977, 1987; McCorquodale et al., 1991; Zhou and McCorquodale, 1992a; Zhou et al., 1992, 1994; van Marle and Kranenburg, 1994; Moursi et al., 1995; Baumer et al., 1996, Krebs et al., 1998), and numerical models (e.g. Krebs, 1991; McCorquodale et al., 1991; Zhou and McCorquodale, 1992a, 1992b; Zhou et al., 1992, 1994; Lyn et al., 1992; Krebs et al., 1996). Figure 2.2 shows some of the density associated effects in circular clarifiers.

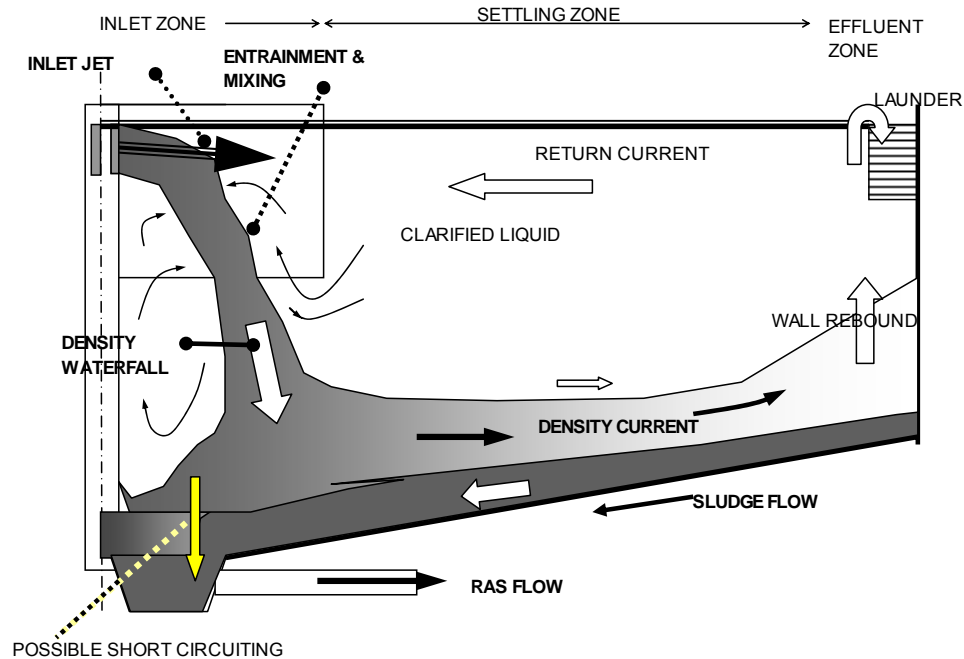


Figure 2.2 Flow Processes in a Circular Clarifier (after McCorquodale, 2004)

2.2.1.1 Modeling Equations

The hydrodynamic and solids stratification of settling tanks have been successfully described by application of the following governing equations and conservation laws:

- a) Continuity equation (conservation of fluid mass).
- b) Fluid momentum equations (conservation of momentum).
- c) Mass transport equation, including the modeling of the settling behavior of the particles (conservation of particulate mass).
- d) Energy equations (conservation of energy).
- e) Turbulence modeling equations.

Continuity, momentum and mass transport equations have been used in all 2D and 3D models to describe the flow pattern in clarifiers. Few modifications have been introduced in these equations since the original work of Larsen (1977), except in the treatment of the settling velocities [major modifications in the differential equations are presented in the work of Chebbo et al. (1998) and Wells and LaLiberte (1998a)]. On the other hand, different turbulence models have been proposed and used with different levels of success (see section 2.2.3, turbulence models), and few models have included energy considerations (see section 2.2.6, temperature effects).

The following conservation equations can be used to describe two-dimensional, unsteady, turbulent, and density stratified flow in a settling tank using either rectangular or cylindrical co-ordinates (Ekama et al., 1997; McCorquodale, 2004):

Continuity Equation:

$$\frac{\partial r^m u}{\partial r} + \frac{\partial r^m v}{\partial y} = 0 \dots\dots\dots (2.1)$$

Conservation of Momentum in the Radial Direction (r or x):

$$\frac{\partial u}{\partial t} + u \frac{\partial u}{\partial r} + v \frac{\partial u}{\partial y} = -\frac{1}{\rho} \frac{\partial p}{\partial r} + \frac{1}{r^m} \frac{\partial}{\partial r} (r^m \nu_t \frac{\partial u}{\partial r}) + \frac{1}{r^m} \frac{\partial}{\partial y} (r^m \nu_t \frac{\partial u}{\partial y}) + S_u \dots\dots\dots (2.2)$$

Conservation of Momentum in the Vertical Direction (y):

$$\frac{\partial v}{\partial t} + u \frac{\partial v}{\partial r} + v \frac{\partial v}{\partial y} = -\frac{1}{\rho} \frac{\partial p}{\partial y} + \frac{1}{r^m} \frac{\partial}{\partial r} (r^m \nu_t \frac{\partial v}{\partial r}) + \frac{1}{r^m} \frac{\partial}{\partial y} (r^m \nu_t \frac{\partial v}{\partial y}) + g \frac{\rho - \rho_r}{\rho} + S_v \dots\dots\dots (2.3)$$

where,

$$S_u = \frac{1}{r^m} \frac{\partial}{\partial r} (r^m \nu_t \frac{\partial u}{\partial r}) + \frac{1}{r^m} \frac{\partial}{\partial y} (r^m \nu_t \frac{\partial v}{\partial r}) - 2 \frac{\nu_t}{r^2} u m \dots\dots\dots (2.4)$$

$$S_v = \frac{1}{r^m} \frac{\partial}{\partial r} (r^m \nu_t \frac{\partial u}{\partial y}) + \frac{1}{r^m} \frac{\partial}{\partial y} (r^m \nu_t \frac{\partial v}{\partial y}) \dots\dots\dots (2.5)$$

in Equations 2.1 to 2.5; $m = 1$ yields the Cylindrical coordinates, and $m = 0$ with $r = x$ gives the Cartesian coordinates. The variables u and v are temporal mean velocity components in the r (x) and y directions respectively; p is the general pressure less the hydrostatic pressure at reference density ρ_r ; ρ is the fluid density; g is the component of gravitational acceleration in the vertical direction and ν_t is eddy viscosity. Equations 2.2 and 2.3 are derived from the Navier- Stokes equations for incompressible fluids, extended with the inclusion of a density gradients term ($g \frac{\rho - \rho_r}{\rho}$) for the simulation of buoyancy effects.

Conservation of Particulate Mass (Solids Transport) or Concentration Equation:

$$\frac{\partial X}{\partial t} + u \frac{\partial X}{\partial r} + v \frac{\partial X}{\partial y} = \frac{1}{r^m} \frac{\partial}{\partial r} (r^m \nu_{sr} \frac{\partial X}{\partial r}) + \frac{1}{r^m} \frac{\partial}{\partial y} (r^m \nu_{sy} \frac{\partial X}{\partial y} + r^m V_s X) \dots\dots (2.6)$$

where X is concentration of SS; ν_{sr} is the eddy diffusivity of suspended solids in the r -(x) direction; ν_{sy} is eddy diffusivity of suspended solids in the y -direction; and V_s is particle settling velocity. By using the Reynolds analogy between mass transport and momentum transport, the sediment eddy diffusivity can be related to the eddy viscosity ν_t by the formula (Zhou and McCorquodale, 1992a; Ekama et al., 1997):

$$\nu_{sr} = \frac{\nu_t}{\sigma_{sr}} \dots\dots\dots (2.7)$$

$$v_{sy} = \frac{v_t}{\sigma_{sy}} \dots\dots\dots (2.8)$$

where σ_{sr} and σ_{sy} are the Schmidt numbers in the r-(x) direction and the y-direction respectively. Typical values of the Schmidt number are in the range 0.5 to 1.3 (e.g. Celik and Rodi, 1988; Adams and Rodi, 1990; Zhou and McCorquodale, 1992a, 1992b; Szalai et al., 1994; Krebs et al., 1996; Lakehal et al., 1999).

Using the single-phase flow assumption (which implies that the volume occupied by the solids is negligible), the equations described above can be considered as the theoretical model to represent the major physical processes of solids movement (McCorquodale, 2004). Equations 2.2 and 2.3 (momentum) and Equation 2.6 (mass transfer equation) can be described as a combination of an unsteady term (variation of the property with respect to time), two advective transport terms (describing the fluid-mass transfer process due to convection or flow movement in the plane), two terms related to the eddy diffusion (mixing processes due to turbulent diffusion in two directions) and a source term (which usually extends the ‘pure water’ equation for the simulation of ‘dirty water’). For example, Equation 2.3 includes a source term for the simulation of buoyancy effects and Equation 2.6 a term for the simulation of the particle settling process. Moreover, source terms are also used for the simulation of additional physical and biological process, like flocculation or biological decay processes. In addition to the aforementioned terms, the momentum equations include a pressure gradient term as a flow driving force.

In the case of 3D modeling the convection and diffusion terms are increased to 3 to indicate the space variation of the variables. The buoyancy and the particle settling terms are not affected by the third dimension.

As mentioned before, the discussed equations are used in conjunction with equations modeling the settling properties, the turbulence nature and the rheology of the sludge. Due to the importance of these associated processes, their modelling will be further discussed in the next sections.

2.2.2 Settling Properties of the Sludge

Settling particles can settle according to four different regimes, basically depending on the concentration and relative tendency of the particle to interact: 1) discrete particle, 2) flocculent particles, 2) hindered or zone, and 4) compression. In PST the settling process is dominated by regimes 1) and 2), but in SST the four settling regimes occur at some locations and times. A description of the four classes is presented elsewhere (e.g. Takacs et al, 1991; Ekama et al., 1997; Tchobanoglous et al., 2003) and won't be repeated here. This review focuses on the equations that have been previously presented to model one or more of the four regimes.

Models Based on Discrete Particles Settling

The settling of discrete particles, assuming no interaction with the neighboring particles, can be found by means of the classic laws of sedimentation of Newton and Stokes. Equating Newton's law for drag force to the gravitational force moving the particle, we get Equation 2.9.

$$V_{sp} = \sqrt{\frac{4}{3} \frac{g}{C_D} \frac{(\rho_p - \rho_l)}{\rho_l} d_p} \dots\dots\dots (2.9)$$

where V_{sp} is the terminal settling velocity of the primary particle; C_D is the drag coefficient; g is the acceleration due to gravity; ρ_p and ρ_l are the particle and liquid density respectively; and d_p is the diameter of the particle. The drag coefficient is a function of the Reynolds number (N_R) and the particle shape. For settling particles N_R is defined as:

$$N_R = \frac{V_{sp} d_p}{\nu} \dots\dots\dots (2.10)$$

In Laminar flow ($N_R < 1$) the drag Coefficient C_D for spherical particles is equal to $24/N_R$, which yields Stokes' law for settling velocity:

$$V_{sp} = \frac{g(S_s - 1)d_p^2}{18\nu} \dots\dots\dots (2.11)$$

where S_s is the particle specific gravity.

Beyond the theoretical description of Equations 2.10 and 2.11, great efforts have been made in quantifying the actual settling velocity of discrete flocs and particle aggregates and relating it to the particles characteristics (e.g. Li and Ganczarczyk, 1987, 1992; Namer and Ganczarczyk, 1993; Hilligardt and Hoffmann, 1997; Gorczyca and Ganczarczyk, 2002; Kinnear, 2002). Li and Ganczarczyk (1987) presented equations relating the settling velocity (measured in mm/s) of activated sludge flocs to the cross sectional diameter (dp , measured in mm) and longest dimension (L_f , mm):

$$V_{sp} = 0.35 + 1.77 dp \dots\dots\dots (2.12)$$

$$V_{sp} = 0.33 + 1.28 L_f \dots\dots\dots (2.13)$$

As shown in Equations 2.12 and 2.13, Li and Ganczarczyk (1987) found that the individual floc settling velocity is better correlated to the first power of the floc size than the second power as proposed by Stokes' law. This fact may be attributed to different floc densities and irregular shapes of the flocs.

Models Based on Zone Settling

In the activated sludge field the settling velocity of relative high concentration (in which particles settle as a unit at the same velocity independent of size) is usually measured in a batch test where the velocity of the sludge interface is measured directly. This value is commonly referred to as the Zone Settling Velocity (ZSV). As presented lately, the ZSV is influenced by several factors, but the most important is the initial sludge concentration.

According to Catunda and van Haandel (1992) the best known models to describe the relationship are those by Vesilind (1968) and Dick (1972). Vesilind (Equation 2.14) and Dick (Equation 2.15) are also referred to as the exponential and power models, respectively.

$$ZSV = V_o e^{-kX} \dots\dots\dots (2.14)$$

$$ZSV = V_o (X)^{-K} \dots\dots\dots (2.15)$$

In Equations 2.14 and 2.15; X is the sludge concentration, and V_o , k and K are settling constants. Smollen and Ekama (1984) analyzed extensive data and found that the Vesilind model gave the best prediction.

Model Based on Flocculent Settling

Some attempts have been made to include the effect of flocculation on the settling velocity. For example, Malcherek (1994) modified the power model including the average velocity gradient (G), while Rasmussen and Larsen (1996) used a similar approach but using the exponential model. Malcherek (1994) proposed:

$$V_s = qX^b \frac{1+cG}{1+dG^2} \dots\dots\dots (2.16)$$

Where V_s is the settling velocity at concentration X and q , b , c , and d are fitted parameters. Rasmussen and Larsen proposed:

$$V_s = V_o e^{(BX+\Theta G)} + \Gamma \dots\dots\dots (2.17)$$

where V_o is the maximal settling velocity, B and Θ are empirical constants, and Γ is the minimal settling/compression velocity. Rasmussen and Larsen discussed that the turbulence effects seen in Equation 2.17 cannot be directly compared to the turbulence

effects on flocculation. Equation 2.17 predicts that the settling velocity increases as the velocity gradient decreases, with a higher value of V_s at $G=0$, while flocculation theory suggests that should exist an optimum G -value higher than zero.

Models Based on Compression Settling

Generally in solids flux analysis the compression settling zone has been treated as an extension of Vesilind's equation (van Haandel, 1992; Ekama et al., 1997). Rasmussen and Larsen (1996) treated it as a constant settling velocity, while Bhargava and Rajagopal (1993) expressed the falling rate of the interface in the compression zone as first-order rate reaction [Bhargava and Rajagopal cited that Coulson and Richardson (1955) and Weber (1972) showed a similar expression]. Other approaches to model the compression zone have been based on the Carman-Kozeny equation or in Darcy's law for flow through porous media (e.g. Cho et al., 1993; Islam and Karamisheva, 1998; Karl and Wells, 1999; Zheng and Bagley, 1999; Kinnear, 2002). A good explanation of the analogy between the filtration and the sedimentation processes is presented in Islam and Karamisheva (1998).

Combined Models

Takacs et al. (1991) introduced a correction factor in Vesilind's equation to account for the settling of smaller slow-settling particles always presented at diluted concentrations in settling tanks. They also included a concentration of non-settleable particles as the minimum attainable concentration in the clarifier. Their generalized model is:

$$V_s = V_o \left[e^{-k_1(X-X_{min})} - e^{-k_2(X-X_{min})} \right] \dots\dots\dots (2.18)$$

where V_s is the settling velocity at sludge concentration X ; V_o is the theoretical maximum settling velocity of the particles; X_{min} is the minimum attainable settling concentration (non-settleable portion of the influent concentration); k_1 and k_2 are settling parameters, characteristics of the hindered settling zone and low solids concentration, respectively.

The first term of Equation 2.18 is similar to Vesilind's equation for the simulation of the zone settling velocity, and the second term tries to simulate the effect of discrete particle settling at dilute concentrations. For high concentration (e.g. typically found in sludge blankets) Equation 2.18 is basically reduced to Vesilind's equation.

Since its introduction by McCorquodale et al. (1991) the Takacs model for settling velocity has been the favorite model among researches involved in SST modeling (e.g. Zhou and McCorquodale, 1992a, 1992b, 1992c; McCorquodale and Zhou, 1993, 1994b; Samstag et al., 1992; Krebs et al., 1996; Ji et al., 1996; Vitasovic et al., 1997; Zhou et al., 1998; Lakehal et al., 1999; Armbruster et al., 2001; Stamou et al., 2000; Kleine and Reddy, 2002; De Clercq, 2003). Grijnspeerdt et al. (1995) compared the Takacs model with another five models (namely Laikari, 1989; Otterpohl and Freund, 1992; Dupont and Henze, 1992; Hamilton et al., 1992 and a combination of Takacs and Otterpohl) and found that Takacs was the most reliable to fit the data.

Other modifications to the Vesilind and Takacs models have been presented by Dupont and Dahl (1995), Vanrolleghem et al. (1996) and Vanderhasselt et al. (1999). These modifications usually include another fitting parameter that makes harder the identification of the settling properties.

Models Based on the Analogy between Filtration and Sedimentation Processes

Several authors have proposed models based on the Karman-Kozeny equation, which describes the flow through porous media. Usually, the resulting settling velocity equations have been presented in the form:

$$V_s = k \frac{(1 - nX)^m}{X} \dots\dots\dots (2.19)$$

where k , n and m are settling constants. Steinour (1944), Scott (1966) and Islam and Karamisheva (1998) derived an expression with $m = 3$, while Cho et al. (1993) got $m = 4$. Cho et al. (1993) presented a general four-parameter equation (Equation 2.20), and

obtained Equation 2.19 assuming constant what they called the viscosity term, and Equation 2.21 neglecting the volume fraction with respect to 1.

$$V_S = k \frac{(1 - n_1 X)^4}{X} e^{-n_2 X} \dots\dots\dots (2.20)$$

$$V_S = k \frac{e^{-nX}}{X} \dots\dots\dots (2.21)$$

Cho et al. (1993) reported that the exponential model presented in Equation 2.21 gave the best prediction of the experimental data when compared with Equation 2.14, 2.15 and 2.19 (for $m = 3$ or $m = 4$).

Recently, Kinnear (2002) used the Karman-Kozeny equation to derive Equation 2.22,

$$V_S = \frac{(\rho_l - \rho_f)gE^3}{5S_0^2(1-E)\mu} \quad \text{for } \phi < \phi_g \quad (2.22)$$

$$V_S = \frac{\left[(1-E)(\rho_l - \rho_f)g + Po \left[\frac{(1-E)}{(1-E_g)} \right]^m \frac{\partial E}{\partial z} \right] E^3}{5S_0^2(1-E)^2 \mu} \quad \text{for } \phi \geq \phi_g$$

where ρ_l and ρ_f are the liquid and floc densities, E is the porosity, $S_o = 6/dp$ is the specific surface area, dp is the particle diameter, μ is the fluid dynamic viscosity, Po is an empirical coefficient, and ϕ and ϕ_g are the solids and gel solid fraction respectively. Kinnear (2002) defined the gel concentration as the solids fraction at which flocs at a lower elevation provide mechanical support to flocs at a higher elevation.

The Equations derived from filtration equations (2.19 to 2.22) seem to correctly predict the hindered and compression settling regimes (good correlations have been reported by

their developers) but it seems obvious that such equations will tend to overestimate the settling velocities when applied to dilute concentrations.

2.2.3 Turbulence Model

Kleine and Reddy (2002) gave a simple but precise definition of turbulence: “turbulence is an eddying motion, which has a wide spectrum of eddy sizes. The eddies can be considered as vortex elements, which stretch each other, thereby passing energy on to smaller and smaller eddies until viscous forces become active and dissipate the energy. When buoyancy forces are present, there is also an exchange between potential energy of the mean flow and turbulent kinetic energy.” The length scale of the eddy where the energy is dissipated by viscous forces is called the Kolmogorov microscale, which is defined as:

$$\lambda = \left(\frac{\nu^3}{\varepsilon} \right)^{\frac{1}{4}} \dots\dots\dots (2.23)$$

where λ is the Kolmogorov microscale, ν the kinematic viscosity and ε is the rate of energy dissipation.

The Navier-Stokes equations have intrinsically incorporated turbulence, but to properly simulate the small scale of turbulent motion (size about the Kolmogorov microscale), they would require an impractically fine mesh and unacceptable computational time. Therefore, for proper modeling of the hydrodynamics, the equations are averaged over a time scale which is long compared over the turbulent fluctuations (Abdel-Gawad, 1983; De Clercq, 2003). This idea was proposed by Reynolds and leads to the so-called Reynolds-averaged Navier-Stokes equations that include the Reynolds stresses (White, 1991; Hirsch, 1997). This modification introduces a “closure problem” (the number of unknowns exceeds the number of equations). To close the system a turbulence model

must be included which approximates the correlation of the turbulence structure and the average flow. A comprehensive review in this matter can be found in Abdel-Gawad (1983).

Turbulence models can be divided into two categories: 1) models based on the eddy viscosity concept, and 2) models that employ differential transport equation to evaluate the Reynolds stresses. The eddy viscosity is a common way of introducing turbulence effects on the momentum and transport equations, basically replacing the laminar viscosity ν by the turbulent eddy viscosity ν_t . The eddy viscosity is not a fluid property; its value is defined by the state of turbulence. The eddy viscosity concept has been widely used in the SST modelling; basically three different models have been applied:

- 1) Models that use a constant eddy viscosity, which is usually based on experimental values (e.g. Imam et al., 1983; Krebs, 1991; Krebs et al., 1992, 1995).
- 2) Models that use the Prandtl Mixing-Length theory to relate the eddy viscosity to the local mean velocity gradient and the mixing length l_m .

$$\nu_t = G l_m^2 \dots\dots\dots (2.24)$$

Example of application of the mixing-length model can be found in Larsen (1977), and Abdel-Gawad and McCorquodale (1984a, 1984b, 1985a).

- 3) Models based in the transport of turbulence kinetic energy (k) and the turbulence dissipation rate (ε). The k - ε model relates the eddy viscosity ν_t to k and ε by

$$\nu_t = C_\mu \frac{k^2}{\varepsilon} \dots\dots\dots (2.25)$$

where C_μ is a constant usually equal to 0.09. The k - ε model has been the most popular model for turbulence simulation in settling tanks (e.g. Schamber and Larock, 1981; Celik

et al., 1985; Celik and Rodi, 1988; Stamou et al., 1989; Adams and Rodi, 1990; Zhou and McCorquodale, 1992a, 1992b, 1992c; Zhou et al., 1992; Lyn et al., 1992; Dahl et al., 1994; Krebs et al., 1996; Vitasovic et al., 1997; Gerges and McCorquodale, 1997; Mazzolani et al., 1998; Lakehal et al., 1999; Stamou et al., 2000; Armbruster et al., 2001). The distributions of k and ε are obtained from semi-empirical differential transport equations (Rodi, 1980):

$$\frac{\partial k}{\partial t} + u \frac{\partial k}{\partial r} + v \frac{\partial k}{\partial y} = \frac{1}{r^m} \frac{\partial}{\partial r} \left(r^m \frac{\nu_t}{\sigma_k} \frac{\partial k}{\partial r} \right) + \frac{1}{r^m} \frac{\partial}{\partial y} \left(r^m \frac{\nu_t}{\sigma_k} \frac{\partial k}{\partial y} \right) + P\varepsilon + P_2 \dots \dots \dots (2.26)$$

and

$$\frac{\partial \varepsilon}{\partial t} + u \frac{\partial \varepsilon}{\partial r} + v \frac{\partial \varepsilon}{\partial y} = \frac{1}{r^m} \frac{\partial}{\partial r} \left(r^m \frac{\nu_t}{\sigma_\varepsilon} \frac{\partial \varepsilon}{\partial r} \right) + \frac{1}{r^m} \frac{\partial}{\partial y} \left(r^m \frac{\nu_t}{\sigma_\varepsilon} \frac{\partial \varepsilon}{\partial y} \right) + C_1 \frac{\varepsilon}{k} P C_2 \frac{\varepsilon^2}{k} \dots \dots \dots (2.27)$$

where C_1 and C_2 are constant, P is the production of turbulent energy by the mean velocity gradients, and P_2 is a buoyancy correction term. Equations 2.26 and 2.27 have to be solved along with the momentum and continuity equations.

$$P = \nu_t \left[2 \left(\frac{\partial u}{\partial r} \right)^2 + 2 \left(\frac{\partial v}{\partial y} \right)^2 + 2 \left(\frac{u}{r} \right)^2 m + \left(\frac{\partial u}{\partial y} + \frac{\partial v}{\partial r} \right)^2 \right] \dots \dots \dots (2.28)$$

$$P_2 = \frac{\nu_t}{\sigma} \frac{g}{\rho_r} \frac{\partial(\rho - \rho_r)}{\partial y} \dots \dots \dots (2.29)$$

Comment on Turbulence Models

Since the eddy viscosity depends on the state of turbulence in the settling tank, the selection of a constant value is just a gross estimate of the turbulence effects on the flow. Obviously it doesn't account for local effects, and the extrapolation from tank to tank is almost impossible. This critical problem is resolved in both the mixing-length and the k -

ε models that do include local effects. Based on this, these two models will be discussed more thoroughly below:

- A) The mixing-length model intrinsically assumes that the turbulence is dissipated where it is generated; there is not direct transport of turbulence. However, a good estimation of the l_m value overcomes this limitation. The $k-\varepsilon$ model does not present this inconvenience.
- B) Both models assume an isotropic eddy viscosity. This assumption is partially corrected with the Schmidt numbers applied in the x-r and y directions.
- C) Both have been partially questioned: Launder and Spalding (1972) and Rodi (1980) found the mixing-length model inadequate in recirculating flows. Zhou et al. (1994) expressed that the $k-\varepsilon$ partially miss the damping effect on the vertical direction due to buoyant effects. Adams and Rodi (1990) reported that “apparently too little mixing was generated by the $k-\varepsilon$ model.”
- D) Both models are strongly dependent on the boundary conditions.
- E) When applied to similar cases both models have predicted similar clarifier removal efficiency (e.g. Stamou et al., 1989; and Abdel-Gawad and McCorquodale, 1985a).
- F) The $k-\varepsilon$ model adds two additional transport equations, which make it computationally more demanding than the mixing-length model, both in time and capacity.

It seems indubitable that the $k-\varepsilon$ is a more general model with wider applicability than the mixing-length. However, for specific cases, like the flow in SST, the success of any model strongly depends on the knowledge of the flow to be modelled. The author believes that for the simulation of flow in SST both models can be successfully applied.

2.2.4 Sludge Rheology in Settling Tanks

The Rheology of a body defines its deformation (strain) under the influence of stresses (Dentel, 1997). In general the rheology describes the viscous characteristics of the fluid. In Newtonian fluids the shear stress is linearly related to the shear rate according to Equation 2.30.

$$\tau = \mu \frac{dv}{dy} \dots\dots\dots (2.30)$$

where τ is the shear stress, μ is the dynamic viscosity and dv/dy is the shear rate.

Wastewater sludges are non-Newtonian fluids, so the shear rate is not linearly proportional to the shear stress. Several rheological models have been proposed, such as the Ostwald equation (pseudoplastic model), Bingham equation (plastic model), and Herschel-Bulkley equations (yield pseudoplastic model) shown in Equation 2.31, 2.32 and 2.33, respectively (Dentel, 1997; Slatter, 1997).

$$\tau = \eta_p \left(\frac{dv}{dy} \right)^n \dots\dots\dots (2.31)$$

$$\tau = \tau_o + \eta_p \left(\frac{dv}{dy} \right) \dots\dots\dots (2.32)$$

$$\tau = \tau_o + \eta_p \left(\frac{dv}{dy} \right)^n \dots\dots\dots (2.33)$$

where τ_o is the yield stress, η_p is the plastic viscosity, and n is an empirical exponent less than one. τ_o and η_p are both functions of the SS concentrations. τ_o , the initial resistance of the sludge to deformation, must tend to zero as the concentration approaches zero as

shown by different researches (e.g. Dahl et al., 1994; Slatter, 1997). Slatter (1997) showed that n may also depend on the sludge concentration.

There is not a good agreement about which one is the best model to describe the rheology of activated sludges. In the Water Science and Technology edition about sludge rheology (1997) different authors expressed different conclusions. Battistoni (1997) concluded that both plastic and pseudoplastic models could be applied to all sludges. Lotito (1997) showed a better correlation for the pseudoplastic model when compared to the plastic. Lotito found excellent correlation when comparing data for individual types of sludge, but not so good when correlating data for different types. He suggested that concentration is the main parameter affecting the sludge rheological behavior, but it was not enough for a complete understanding of the property. Santos Monteiro (1997) suggested that the methods including the yield stress (Bingham and Herschel-Bulkley models) were better to represent the rheological behavior of raw and anaerobically digested sludges. Finally, Sozanski et al. (1997) concluded that the Bingham model was the best approach when modeling thickened sludge.

Bokil (1972) and Bokil and Bewtra (1972) suggested an experimental exponential function for the plastic viscosity. This relationship is presented in Figure 2.3 (adapted from Ekama et al. 1997) as effective kinematic viscosity versus sludge concentration.

Dahl et al. (1994) applied Equation 2.32 (Bingham plastic) for the simulation of the rheology characteristics of the sludge in their numerical modeling simulation of a rectangular clarifier. They proved that a good description of the rheology is indispensable in order to make the calculated profiles match the measured ones. Lakehal et al. (1999) and Armbruster et al. (2001) followed a similar approach to Dahl et al. (1994). Lakehal et al. (1999) also compared the Bingham model to the approach of Bokil and Bewtra (1972). They argued that the Bokil and Bewtra model over predicted the viscosity values causing an excessive elevation of the modeled sludge blanket.

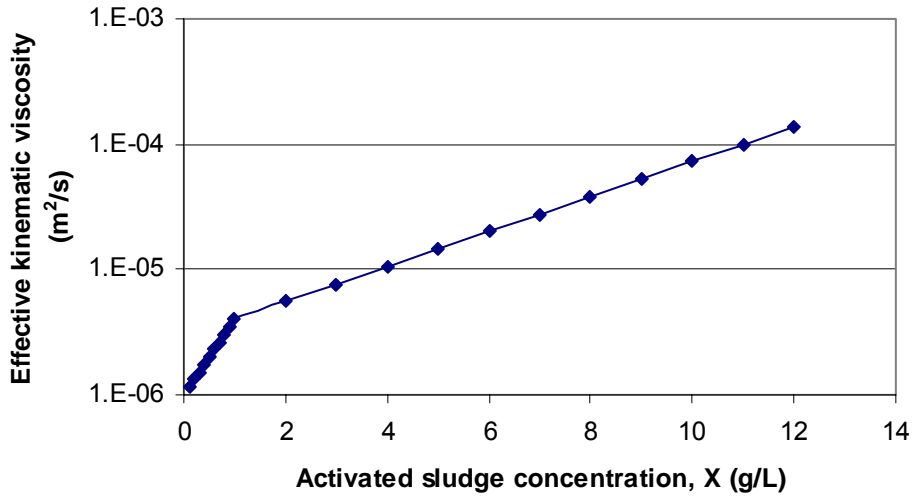


Figure 2.3 Effective kinematic viscosity of activated sludge (after Bokil, 1972)

De Clercq (2003) applied a modified Herschel-Bulkley model to simulate the rheology of activated sludges. Their model is written as:

$$\tau = \left[\frac{\tau_o}{\gamma^*} (1 - e^{-m\gamma^*}) + \eta_p \gamma^{*(n-1)} \right] \left(\frac{dv}{dy} \right) \dots\dots\dots (2.34)$$

where γ^* is the magnitude of the strain rate, m is the stress growth exponent, and n is the flow behavior index.

Maybe the most important aspect in De Clercq (2003) research in sludge rheology is that low-shear measurements showed that a true yield stress does not exist; consistently with this, they found that in CFD simulations the increased viscosity a very low shear rate may cause exaggerated elevation of the solids blanket. Their model does not apply a true yield stress, but it does incorporate high viscosities at low shears.

De Clercq (2003) compared his model to the Bingham model presented by Dahl et al. (1994) and Lakehal et al. (1999), and to the Bokil model (Figure 2.3) in order to evaluate their respective effects on the settling tank performance (using CFD simulations). He studied two cases: 1) zeolite-treated sludge, which improved the solids settling properties (the influence of zeolite in rheology was not considered), and 2) untreated sludge. In case 1, he found that the Dahl et al. (1994) model over predicted the sludge blanket height, while his proposed model and Bokil's seems to correctly predict the observed behavior. In the case of untreated sludge, he found that both Dahl's and his proposed model resulted in elevated sludge blankets, while the Bokil model showed shallow solids blankets. He suggested that the problem might arise from the yield stress included in Dahl's and his proposed model (as said before he did not apply a true yield stress, but did incorporate high viscosities at low shears).

2.2.5 Flocculation Process in Settling Tanks

Background

The effects of flocculation in clarifier performance and the causes that promote flocculation in settling tanks have been largely acknowledged. Camp (1945) recognized that flocculation in settling tanks is due to two causes:

1. Differences in the settling velocities of the particles whereby faster settling particles overtake those which settle more slowly and coalesce with them; and
2. Velocity gradients in the liquid, which cause particles in a region of higher velocity to overtake those in adjacent stream paths moving at slower velocity.

The flocculation due to difference in the settling velocities is known as differential settling, and the one due to velocity gradients is referred to as orthokinetic flocculation. These two types are known together as macroflocculation (Tchobanoglous et al. 2003) since it mostly affects the aggregation of particles greater than about 1 μm . The term microflocculation is used to refer to the aggregation of smaller particles (from about 0.001 to 1 μm) that are brought together through the random thermal “Brownian” motion of the particles; this is commonly referred to as perikinetic flocculation.

In ST the macroflocculation predominates as a mechanism to promote particle growth; this statement is based on the analysis of the size distribution and settling velocities of activated sludge particles. In this respect, Parker et al. (1970) found a bimodal distribution with a theoretical portion of “primary particles” in the size range of 0.5 to 5 μm and flocs between 10 μm and 5,000 μm . The experimental primary particles of Parker et al were based on the weight concentration of suspended solids after 30 minutes of settling. Li and Ganczarczyk (1986), in a detailed study about activated sludge flocs, found only flocs larger than about 2.5 μm . These studies support the idea that macroflocculation predominates over microflocculation, but more important is the fact that particles between 0.001 and 1 μm are basically part of the non-settleable portion

(based on the velocity distribution presented by Li and Ganczarczyk, 1987). Therefore, even if these smaller particles (0.001 to 1 μm) are brought together through perikinetic flocculation, the probability that they are removed in a settling tank is minimal.

In drinking water treatment plants, the flocculation process usually follows chemical coagulation, since coagulated water must be gently stirred to promote the growth of the flocs. In wastewater, the flocculation process usually follows biological coagulation; this is known as bioflocculation (biological flocculation). Bioflocculation is the ability of microorganisms to self-associate in a suspended growth environment; this can be a biological reactor or a SST. Under normal operating conditions activated sludge flocculates naturally. This process is thought to occur as a result of extracellular polymeric substance (EPS) secreted by microorganisms present in the mixed liquor (Das et al., 1993). The effect of EPS on bioflocculation has been largely studied and considerable efforts have been made to understand their role in biosolids-liquid separations in the activated sludge and solids contact processes (Liao et al., 2001). Recently, research into the nature of activated sludge floc has focused on the role of biopolymers in sludge thickening and dewatering. Because biopolymers play a central role in bacterial coagulation it seems reasonable that the amount of polymers affects the settling and dewatering characteristics of the sludge (Novak and Haugan, 1981). However, the precise role of EPS is not well understood, and contradictory studies have been presented in this matter, e.g., Chao and Keinath (1979) and Urbain et al. (1993) have shown that the settling properties of the sludge are enhanced when the EPS content in the sludge increases, while Goodwin and Forster (1985) have shown an opposite effect. Alternatively, Liao et al. (2001) found no correlation between the settling properties and the EPS concentration.

The major drawback in the study of the role of EPS on bioflocculation and sludge thickening and dewatering is that there is not a universal method for extraction of the polymers from the activated sludge and not even a good agreement in the way the extracted substance should be quantified. A few examples of extraction methods and

quantification techniques can be reviewed in Pavoni et al. (1972), Brown and Lester (1980), Novak and Haugan (1981), Frolund et al. (1996) and Azeredo et al. (1998).

Probably the most common way of describing the floc formation through polymer effects is polymer bridging (Tenney and Stumm, 1965; Busch and Stumm, 1968; Parker et al., 1970; Pavoni et al., 1972; Dickinson and Eriksson, 1991; Eriksson and Alm, 1991; Urbain et al., 1993). Hogg (1999) described the flocculation by means of polymer bridging as a dynamic process involving polymer adsorption, particle-to-particle collisions leading to floc formation and growth, and floc degradation in the presence of mechanical agitation.

Flocculation Zone in Clarifiers

Parker et al. (1970, 1971, 1972) demonstrated the utility of a flocculation zone previous to the final settling stage. They showed that often, the highly turbulent condition in the aeration chamber is so intense that it favors floc breakup over aggregation, resulting in a high level of dispersed solids (similar results were found by Starkey and Karr, 1984; Das et al., 1993; Wahlberg et al., 1994). They recommended additional flow conditioning, through the incorporation of a mildly stirred flocculation step between the aeration basin and the clarifier to promote the incorporation of dispersed particles into the floc. This practice became popular to improve the final effluent of attached growth systems e.g. trickling filter-solids contact processes (TF/SC). The idea has been supported by other researchers (Das et al., 1993; Wahlberg et al., 1994; La Motta et al., 2003; Jimenez et al. 2003). Wahlberg et al. presented an evaluation of 21 full-scale wastewater treatment plants (WWTP) that showed that the provision of additional flocculation would reduce the supernatant SS (SSS).

The inclusion of flocculation zones inside the SSTs is a relatively new practice. Knop (1966) reported, on the basis of pilot plant studies, that the placement of a flocculator in the inlet zone of a rectangular SST improved effluent transparency. Lately, a full-scale plant was constructed including two sets of paddle flocculators. The induced flocculation

in the clarifier improved the effluent SS by about 5 mg/L. Flocculation wells (FWs) were initially operated with mixers to impart G values of $20 - 70 \text{ s}^{-1}$, levels that had been found optimal in bench scale research (Parker et al., 1970, 1971). Parallel operation of SSTs showed that turning the mixer off had no effect on effluent quality, whereas testing showed that flocculation nevertheless proceeded efficiently (Ekama et al., 1997). This can be explained due to the G values presented in the flocculation well produced by energy loss and turbulence mixing.

Parker (1983), Parker and Stenquist (1986), and Parker et al. (1996) presented full-scale research in circular clarifiers that showed that clarifiers equipped with flocculator centerwell (FCW) can yield good ESS with high overflow rates. Parker and Stenquist concluded that “deep flocculator-clarifiers can achieve low suspended solids at overflow rates high enough to cause conventional shallow clarifiers to deteriorate.” Even though they are comparing deep with shallow clarifiers, and it has been recognized that the distance of the sludge blanket from the effluent weir has a direct relation to effluent quality (Parker, 1983), the beneficial effects of the FCW are well defined in the aforementioned researches.

The common way of sizing FW in clarifiers is based on detention time. A 20 minutes residence time (based in the work presented by Wahlberg et al., 1994) is used in conjunction with the average dry weather flow (ADWF) and a 50% RAS to determine the volume (Ekama et al., 1997).

FSS and DSS Tests

Wahlberg et al. (1994) found an average-equilibrium SSS of 6.8 mg/L after batch flocculation, with 25 of 30 evaluations well below 8.5 mg/L. This value represents the SS in an ideal clarifier; however, real clarifiers usually perform poorer than that. However, it is a clear indication that ESS may be lowered by improving flocculation and/or the internal hydrodynamic of the tank.

Wahlberg et al. (1995) identified that high ESS in SSTs occurs primarily by one or more of the following reasons: (1) hydraulic short-circuiting or resuspension of solids from the surface of sludge blankets; (2) thickening overloads resulting in high sludge blankets; (3) denitrification occurring in the SST causing solids to float to the surface; and (4) flocculation problems as a result of either floc breakup or poor floc formation before the secondary clarifier. Wahlberg et al. (1995) developed the dispersed suspended solids (DSS) and flocculated suspended solids (FSS) tests as a way to distinguish between the first and fourth of the reasons.

DSS are defined as the solids remaining in the supernatant after 30 minutes settling; the DSS level identifies the MLSS state of flocculation at the place and moment it is taken. FSS are defined as the solids remaining in the supernatant after 30 minutes of settling in a sludge that has been flocculated for 30 minutes (In Appendix B are presented the laboratory procedures for measuring DSS and FSS). The FSS attempts to quantify the optimum degree to which the sample can be flocculated (Wahlberg et al. 1995). With a data set of the DSS at inlet and outlet of the ST, FSS test and ESS concentration, a diagnostic-evaluation can be done on the performance of the clarifier. For example, Low DSSs-Low FSS-High ESS is a clear indication that the sludge is well flocculated with no indication of important breakup floc in the clarifier. The problem may be the result of poor sludge blanket management (e.g., thickening overloads) or poor hydrodynamics in the tank. A good description of different scenarios with the data set is presented in Wahlberg et al. (1995) and Ekama et al. (1997).

Flocculation Models

The net flocculation in a turbulent environment depends upon the balance of the opposing processes of aggregation and floc breakup (Parker et al., 1972; Oles, 1992; Spicer and Pratsinis, 1996; Serra and Casamitjana, 1998). At steady state a successful flocculation model should include the balance between particle growth and breakage. Spicer and Pratsinis (1996) described the dynamic of floc formation; they indicated that several phases of floc growth occur during flocculation: initially floc growth is dominant,

particles combine in the presence of polymers (coagulation), and their size increases rapidly. As the floc grows larger, porous and open structures are formed that are more susceptible to fragmentation by fluid shear. Parker et al. (1972), Galil et al. (1991) and Biggs and Lant (2000) found that the floc size on activated sludge decreased with increasing shear; similar results have been found in the flocculation of inorganic systems (Spicer and Pratsinis, 1996; Serra and Casamitjana, 1998).

Parker et al. (1971) identified two breaking mechanisms: 1) floc breakup as a result of erosion caused by surface shearing forces exceeding the shear strength of the bonds joining the primary particles to the floc, releasing primary particles in the suspension; and 2) floc breakup as a result of filament fracture that occurs when excessive tensile stresses are applied on the floc (which produces fragmentation of the floc instead of primary particles).

Based on a detailed theoretical analysis Parker et al. (1970, 1971) developed a differential equation describing the overall kinetic of flocculation in turbulent mixing:

$$\frac{dn}{dt} = K_B \cdot X \cdot G^m - K_A \cdot X \cdot n \cdot G \dots\dots\dots (2.35)$$

where X is the MLSS concentration (g/L), G the root-mean-square velocity gradient (s^{-1}), K_A a floc aggregation coefficient (L/g), K_B a floc breakup rate coefficient (number. S^{m-1}/g), m the floc breakup rate exponent (dimensionless), and n is the primary particle number concentration (numbers/L). Parker's experimental primary particle concentration was based on the weight concentration of SS in the supernatant after 30 minutes of settling. They performed a series of flocculation tests in a continuous-flow reactor (CFSTR) to support their development. A mass balance of primary particles for a CFSTR without recycle yields at steady state the following equation:

$$\frac{n_o}{n_t} = \frac{(1 + K_A \cdot X \cdot G \cdot \bar{t})}{(1 + K_B \cdot D \cdot G^m \cdot \bar{t})} \dots\dots\dots (2.36)$$

Other researchers have supported the development presented by Parker and his co-workers. Wahlberg et al. (1994) presented an integrated form of Equation 2.35 for the calculation of flocculation in a batch flocculator; Wahlberg et al. assumed K_A and K_B as true constants and used a value of m equal to 2 [$m = 2$ was selected based on analysis presented by Parker et al. (1971); this number indicates that floc breakup occurs by erosion of primary particles from floc surfaces due to eddies in the viscous dissipation range] :

$$n_t = \frac{K_B \cdot G}{K_A} + \left(n_o - \frac{K_B \cdot G}{K_A} \right) \cdot e^{-K_A \cdot X \cdot G \cdot t} \dots\dots\dots (2.37)$$

where n_o is the initial concentration of primary particles (numbers/L) and n_t is the primary particle number concentration in the reactor at time t .

Setting G as a constant and for a given MLSS concentration, Equation 2.37 can be expressed in the form:

$$n_t = \alpha + \beta e^{-\lambda t} \dots\dots\dots (2.38)$$

in Equation 2.38 $\alpha = K_B \cdot G / K_A$ is the equilibrium primary particle number concentration (number/L), $\beta = n_o - \alpha$, is the difference between the initial and equilibrium primary particle number concentration, and $\lambda = K_A \cdot X \cdot G$ is the overall primary particle removal rate (s^{-1}).

Wahlberg et al. (1994) tested Equation 2.37 and 2.38 with activated sludges obtained at 21 full-scale facilities with different aeration methods. They measured the primary particle concentration as the turbidity of the supernatant after 30 minutes of settling; turbidity was later correlated to SS mass concentration. They observed that the flocculation data was well described by the curves, concluding the applicability of the theoretical development of Parker et al. (1970, 1971) to the description of batch

flocculation data. Their study presents that 99% flocculation was achieved within 10 minutes under batch conditions for most sludge. They concluded that a similar performance improvement could be obtained in the field using a completely-mixed flocculation zone with a residence time of at least 20 minutes. The authors reported values of K_A , K_B , n_o , α , β and λ for 30 activated sludge samples.

Jimenez (2002) and La Motta et al. (2003) used equations similar to Equation 2.36 and 2.38 to evaluate the removal of SS and Particulate COD (PCOD) in continuous flow and batch flocculators. For a batch reactor, operated a constant G , they presented:

$$C = a + (C_o - a) \cdot e^{-k \cdot t \cdot X} \dots\dots\dots (2.39)$$

where C (mg/L) is the concentration of unflocculated particles remaining in the supernatant at reaction time t (min) after 30 minutes settling, a is the residual concentration of particles (mg/L), k is the reaction rate coefficient, C_o is the initial concentration of influent particles (mg/L), and X is the MLSS concentration (mg/L).

For a continuous flow mixed reactor, operated at constant G , Jimenez (2002) and La Motta et al. (2003) presented:

$$C = \frac{C_i \cdot (1 + \alpha) + a \cdot k \cdot \bar{t} \cdot X}{(1 + \alpha) + k \cdot \bar{t} \cdot X} \dots\dots\dots (2.40)$$

here α is the recycle ratio (recycle flow rate/plant flow rate) and C_i is the concentration of unflocculated particles concentration in the influent to the CFSTR.

$$C_i = \frac{C_o + \alpha \cdot C_R}{1 + \alpha} \dots\dots\dots (2.41)$$

where C_R is the concentration of particles of the recycle sludge after 30 minutes of

sedimentation. Since obtaining the supernatant of highly concentrated sludge is a hard task, Jimenez (2002) and La Motta et al. (2003) recommend finding C_i by mixing the influent to the aeration chamber and the recycle sludge in proportion to Q and αQ , respectively, and by measuring the suspended solids concentration of the supernatant of the mixture after 30 minutes of settling.

In a Pilot Plant study, using a CFSTR, Jimenez (2002) found that significant removal of suspended solids could be achieved at low detention times. He found that less than 30 mg/L could be obtained with only a hydraulic retention time (HRT) of 10 minutes, and 88% removal could be achieved during 30 minutes of flocculation. The values of the constants a and k were found to be 8.5 mg/L and 1.54×10^{-4} L/mg SS min, respectively ($kX = 0.477 \text{ min}^{-1}$). Figure 2.4 shows the results presented by Jimenez (2002), when evaluating the effect of HRT on SSS removal in the continuous flow flocculator.

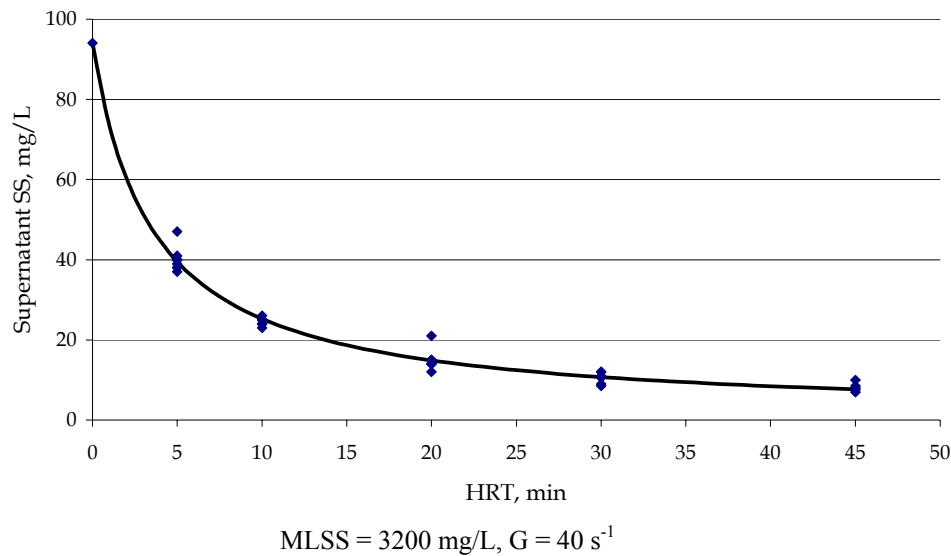


Figure 2.4 Effect of HRT on the SSS removal (After Jimenez 2002)

Modern flocculation models recognized the aggregates as fractal objects. One of the most important properties of fractal aggregates is that their porosity is a function of the aggregate size; porosity increases and density decreases with increasing size (Thomas et

al., 1999). The relationship between particle size and density is defined through the fractal dimension (D) that takes values between 0 and 3. In general, the lower the fractal dimension the more porous the aggregate. Li and Logan (1997a) proposed an expression to calculate the collision frequency between fractal aggregates and small particles in shear-induced flocculation:

$$\beta(a,p) = 0.01 \times 10^{-0.9D} d_a^{3.3-0.63D} G^{1-0.33D} \dots\dots\dots (2.42)$$

where $\beta(a,p)$ is the collision frequency function between the aggregate and small particles, D is the fractal dimension, d_a is the size of the aggregate, and G is the mean shear rate of the fluid.

Li and Logan (1997b) also presented an expression to calculate the collision frequency of fractal aggregates with small particles by differential sedimentation:

$$\beta_{frac-s} = \frac{9\pi d_a^2 U \left(1 - \frac{\tanh \xi}{\xi}\right) \left[1 - \exp\left(-\frac{3}{2s}(1-E)\alpha_{filt}\eta d_a^{1-b}\right)\right]}{4\alpha \left[2\xi^2 + 3\left(1 - \frac{\tanh \xi}{\xi}\right)\right]} \dots\dots\dots (2.43)$$

in Equation 2.43 β_{frac-s} is the collision frequency function between the aggregate and small particles by differential sedimentation, d_a is the size of the aggregate, U is the actual settling velocity of the aggregate, η is the single collector efficiency, E is the porosity of the fractal aggregate, α_{filt} is the particle sticking coefficient between the material comprising the aggregate and the particles in the fluid flowing through the aggregate, α is the collision efficiency, s and b are empirical coefficients relating the size of the clusters (d_c) and d_a through $d_c = s d_a^b$. Finally, $\xi = d_a/(2\kappa^{1/2})$ where κ is the permeability of the aggregate. The porosity of the fractal aggregate, E , is calculated with the expression (Li and Logan, 1997b):

$$E = 1 - 6c d_a^{D-3}/\pi \dots\dots\dots (2.44)$$

in Equation 2.44 c is a system-specific constant.

Equation 2.42 and 2.43 are used in conjunction with Equation 2.46 to find the rate of flocculation (R_f) in the sheared fluid:

$$R_f = \alpha(a,p) \beta^* N_p \dots \dots \dots (2.45)$$

where $\alpha(a,p)$ is the corresponding collision efficiency, β^* is $\beta(a,p)$ or $\beta_{\text{frac-s}}$, and N_p is the concentration of the small particles.

Other flocculation models have been presented by Camp and Stein (1943), Pearson et al. (1984, Cited by Valioulis and List, 1984a), Berlin et al. (1992), Han and Lawler (1992) and Hogg (1999).

Energy Dissipation and the Root-Mean-Square Velocity Gradient (G)

Since Camp and Stein (1943) introduced the root-mean-square velocity gradient (G) as an approximation to the fluid shear velocity (du/dy) and substituted it in the Smouchowski's equation for orthokinetic flocculation, the use of G to quantify the mixing intensity in flocculation systems has become widely accepted (Argman and Kaufman, 1970; Parker et al., 1970; Pearson et al., 1984; Wahlberg et al., 1994; Li and Logan, 1997a; Hogg, 1999; Jimenez, 2002; La Motta et al., 2003).

Camp and Stein (1943) linked G to the rate of energy dissipation ε and the kinematic viscosity of the water, ν :

$$G = (\varepsilon / \nu)^{1/2} \dots \dots \dots (2.46)$$

Camp and Stein (1943) proposed the following equations to estimate G values in aeration tanks:

$$G = (P/V \cdot \mu)^{1/2} \dots\dots\dots (2.47)$$

where P is the total energy loss or the power imparted to the water, V is the aerator volume and μ is the absolute viscosity of the fluid. Parker et al. (1970) suggested that for air induced turbulence P can be expressed as a function of the air-flow rate (Qa), the liquid specific weight (γ) and the diffuser depth (h):

$$P = Qa \cdot \gamma \cdot h \dots\dots\dots (2.48)$$

In the case of paddle-wheel mixers, the water power is given by (Qasim et al. 2000):

$$P = C_D \cdot A \cdot \rho \cdot v_r^3 / 2 \dots\dots\dots (2.49)$$

where C_D is the drag coefficient, A is the area of paddles, ρ is the water density and v_r is the velocity of the paddle relative to the water.

Larsen (1977) developed equations to estimate G values based on the energy dissipation at the inlet of the settling tank. For round jets Larsen presented:

$$G = (14.2 \, v^{-1} D^3 u_o^3 X^{-4})^{1/2} \dots\dots\dots (2.50)$$

in Equation 2.50 v is the water kinematic viscosity, D is the diameter of the inlet, u_o is the inlet velocity and X is the horizontal distance from the inlet.

For plane jets Larsen obtained based on inlet opening height (B):

$$G = 1.53 \, v^{-1/2} B^{3/4} u_o^{3/2} X^{-5/4} \dots\dots\dots (2.51)$$

Flocculation Models in Clarifier Modeling

The effect of flocculation in the clarifier performance has been largely acknowledged and a well demonstrated fact for many researches. However, the inclusion of flocculation models in general clarifier models has been scarce, and has been limited to the application in primary clarifiers.

Larsen (1977) recognized that settling of suspended matter depends strongly on properties of the particles, and in addition to the density of the particles, their ability to adhere to each other to form clusters is very important. He also recognized that the opportunity of contact between particles depends on fluid mechanics in terms of fall velocity and turbulence. As Larsen did, other researchers (Devantier and Larock, 1987; Lakehal et al., 1999; McCorquodale, 2004) have recognized the limitations in their models caused by the lack of a flocculation model.

A first attempt to model flocculation in a 2D clarifier model was done by Valioulis and List (1984a, 1984b). They introduced equations for Brownian motion, turbulent shear and differential sedimentation in a simple hydrodynamic model that assumed idealized spatially homogenous flow without buoyancy effects. The rate of turbulent energy dissipation (ε) was estimated using Equation 2.52:

$$\varepsilon = \kappa u^* z \left(1 - \frac{z}{H}\right) \left(\frac{du}{dz}\right)^2 \dots\dots\dots (2.52)$$

where κ is von Karman's constant, u^* is the shear velocity, z is the vertical coordinate, and H is the depth of the tank.

The collision function for Brownian motion (Equation 2.53) was calculated using an equation presented by Smoluchowski in 1916. For turbulent shear and differential sedimentation the collision functions (Equation 2.54 and 2.55 respectively) were calculated using equations presented by Pearson et al. (1984).

$$\beta_b = \frac{2kT}{3\mu} \frac{(r_i + r_j)^2}{r_i r_j} Eb \dots\dots\dots (2.53)$$

$$\beta_{sh} = \Theta (r_i + r_j)^3 (\varepsilon / \nu)^{1/2} Esh \dots\dots\dots (2.54)$$

$$\beta_{ds} = \frac{0.7g(\rho_p - \rho_f)}{\mu} (r_i + r_j)^2 |r_i^2 - r_j^2| Eds \dots\dots\dots (2.55)$$

β_b , β_{sh} , and β_{ds} are the collection functions for Brownian motion, turbulent shear and differential settling, respectively; k is Boltzmann's constant; T is the absolute temperature; r_i , r_j , are the particle radius; μ and ν are the dynamic and kinematic viscosity of the water; Θ is a proportionality constant assumed equal to 2.3; ρ_p and ρ_f are the particle and fluid density; and Eb , Esh and Eds are the collision efficiencies that express the influence of hydrodynamic and other interparticle forces on the collision process. Expression for evaluating Eb , Esh and Eds are presented in the paper by Valioulis and List (1984a).

In their application to the simulation of a primary rectangular tank Valioulis and List (1984b) found that the particle collision efficiencies affected dramatically both the characteristics of the effluent size distribution and the overall tank performance.

Lyn et al. (1992) presented a 2D steady state model to simulate the settling of discrete particles in rectangular tanks with a settling velocity distribution (SVD). In this relatively sophisticated flow model they included a simple flocculation model; floc breakup was not modelled. They assumed the shear-induced flocculation as the dominant mechanism (neglecting Brownian motion and differential settling), and particles were assumed to be of a size smaller than the Kolmogorov length scale. Furthermore, their model assumed that only particles of the same size coagulate, neglecting the addition between particles of

different sizes. Lyn et al. (1992) presented a modified solids transport equation to account for the flocculation of the i th-class,

$$\frac{\partial(uCi)}{\partial x} + \frac{\partial[(v - v_{si})Ci]}{\partial y} = \frac{\partial}{\partial x}(\nu_{sx} \frac{\partial Ci}{\partial x}) + \frac{\partial}{\partial y}(\nu_{sy} \frac{\partial Ci}{\partial y}) + F_{floc}^i \dots\dots\dots (2.56)$$

where the Ci , v_{si} are the concentration and the settling velocity of the i th-size particle respectively; ν_{sx} , ν_{sy} are the eddy diffusivity of suspended solids in the x -direction and in the y -direction; and F_{floc}^i is the flocculation model. For each size class F_{floc} was expressed in terms of Ci as

$$F_{floc}^i = \left(\frac{\varepsilon}{\nu}\right)^2 (\alpha_{i-1} C_{i-1}^2 - \alpha_i C_i^2) \dots\dots\dots (2.57)$$

The first term of Equation 2.57 represents a source of particles of the i th-size class due to flocculation of particles from the $(i-1)$ th-size class, and the second term is a sink term of the i th-size class that will appear in the term F_{floc}^{i+1} . The proportionality constant α_i is an empirical coefficient [normally varying from 0.4 to 2.3 (Pearson et al. 1984)], Lyn et al. (1992) evaluated the sensitivity of their model to two α_i values, 1 and 2, assuming the value equal for each class.

In contrast to Valioulis and List (1984b), Lyn et al. (1992) suggested that turbulent shear-induced flocculation plays only a minor role in a settling tank. Based on model observations, they concluded that for the studied conditions of relatively small concentrations, the effects of the shear-induced flocculation do not affect the flow field, and the effects on the concentration field and the removal efficiency may be of secondary importance.

De Cock et al. (1999) modeled the shear flocculation in the inlet zone of a sedimentation basin with a SVD. They used an equation similar to Equation 2.54, but the term $(\varepsilon/\nu)^{1/2}$ was substituted by a constant G value (47s^{-1}), and the proportionality constant, Θ , was assumed equal to $4/3$ (according to Spicer and Pratsinis, 1996) and $12\pi/\sqrt{15}$ (according to Tambo and Watanabe, 1979). For an influent suspended solids concentration of 164 mg/L and using $\Theta = 4/3$, De Cock et al. found a 1.6% improvement in the tank efficiency when compared to the case with no flocculation (80.5% efficiency). For the same influent concentration but for $\Theta = 12\pi/\sqrt{15}$, the improvement was 3.8% . They reported that with the addition of coagulant the settling efficiency could increase until 90% .

2.2.6 Temperature Effects on Settling Tanks

The effects of temperature on settling velocities and sedimentation in general have been largely recognized and debated. Hazen (1904) suggested that particles settle faster as the water becomes warmer. He stated that “a given sedimentation basin will do twice as much work in summer as in winter.” This is maybe a bold statement, but the influence of temperature differentials in the settling tank performance have been demonstrated by several researches. In this respect, Wells and LaLiberte (1998a, 1998b) suggested that in the presence of temperature gradients in the clarifier, such as during periods of winter cooling, the temperature effects are important and should be included in the modeling of the settling tank. The atmospheric cooling process was earlier studied by Larsen (1977); he suggested that the cooled-denser water sinks and is replaced by rising warmer water. He also suggested the removal efficiency of a tank may vary over the year with a minimum during the winter season when cooling rates are at a maximum. Similar effects were observed by Kinnear (2004) at the Littleton Englewood Wastewater Treatment Facility. Kinnear (2004) found that the excess effluent suspended solids increases as the air temperature decreases. Kinnear (2004) defined the excess effluent suspended solids (EESS) as the difference between the ESS and the FSS of the sample.

McCorquodale (1976, 1977) showed that a diurnal variation in the influent of the order of $\pm 0.2^{\circ}\text{C}$ may produce short circuiting in primary clarifiers. Larsen (1977) and McCorquodale (1987) showed that the direction of the density current in PST may be defined by the difference between the inflow and ambient fluid temperature. A cooler influent produces a bottom density current, while in the cases of a warmer influent the density current is along the surface. Studies done by Godo and McCorquodale (1991), Zhou et al. (1994), Moursi et al. (1995) and Wells and LaLiberte (1998b) support these findings. Wells and LaLiberte (1998b) found that temperature differences affect the hydrodynamic of SST.

Zhou et al. (1994) presented a numerical model that includes an equation of state for the local fluid density as a function of temperature and a convection-diffusion equation to determine the temperature field in the tank (Equation 2.58). They used this model to investigate the unsteady flow regime and the temperature mixing in temperature-stratified primary rectangular settling tanks. The following energy equation can be used to model the temperature field (Zhou et al., 1994; Ekama et al., 1997; McCorquodale, 2004):

$$\rho \left(\frac{\partial T}{\partial t} + u_j \frac{\partial T}{\partial x_j} \right) = \frac{\partial}{\partial x_i} \left[\lambda \frac{\partial T}{\partial x_i} - \rho \overline{u_i T'} \right] \dots\dots\dots (2.58)$$

where T and T' are respectively the mean and fluctuating component of the temperature, and λ is molecular diffusivity.

The temperature effects are commonly included in the reference density and kinetic viscosity of the water by means of equations of state. The following expressions represent examples of such equations:

$$\begin{aligned} \rho_{\text{ref}} = & [999.8396 + 18.224944 \times T - 0.00792221 \times T^2 - 55.4486 \times 10^{-6} \times T^3 + \\ & 14.97562 \times 10^{-8} \times T^4 - 39.32952 \times 10^{-11} \times T^5 + (0.802 - 0.002 \times T) \times \text{TDS}] / \\ & [1 + 0.018159725 \times T] \dots\dots\dots (2.59) \end{aligned}$$

$$\mu_{ref} = (2.414 \times 10^{-5}) \times 10^{\left[\frac{247.8}{T+133.15} \right]} \dots\dots\dots (2.60)$$

in Equations 2.59 and 2.60 T is the water temperature in °C, ρ_{ref} is the water reference density in g/L, TDS is the total dissolved solids in g/L, and μ_{ref} is the water dynamic viscosity in Kg /(m.s).

Another temperature-effect to take into consideration is probably the direct effect on the settling properties of the sludge. Surucu and Cetin (1990) suggested that the zone settling velocity decreases as the temperature of the reactor increases. The opposite effect is presented in Equations 2.11 and 2.22. Equation 2.11 (Stokes' law) shows that the settling velocity of discrete particles is affected by the viscosity of the water, which depends on temperature. Equation 2.22 (Kinnear, 2002) shows a similar effect for the hindered and compression settling regimes. In general these equations predict that the warmer the water the faster the particle will settle. The rest of the reviewed equations in Section 2.2.2 do not include temperature effects.

CHAPTER 3

3 RESEARCH ON SETTLING PROPERTIES. DEVELOPMENT OF A COMPOUND SETTLING MODEL

3.1 Research on Settling Properties

Section 2.2.2 presented a detailed review of published settling velocity models. Based on this review, and even though important advances have been made in this field, the author agrees with Larsen, who in 1977 expressed, “No single mathematical expression exists that describes the relationship between suspension settling rate and concentration in the full range of concentration encountered.” To the knowledge of the author, no such single equation has been published.

Lately, the Takacs model (Takacs et al., 1991) has been the most used model to simulate the settling properties in SST (e.g. Zhou and McCorquodale, 1992a, 1992b, 1992c; McCorquodale and Zhou, 1993, 1994b; Samstag et al., 1992; Krebs et al., 1996; Ji et al., 1996; Vitasovic et al., 1997; Zhou et al., 1998; Lakehal et al., 1999; Armbruster et al., 2001; Stamou et al., 2000; Kleine and Reddy, 2002; De Clercq, 2003); basically, it is used for its ability to simulate the settling of smaller slow-settling particles and the non-settleable portion of the sludge.

Even though the Takacs model has been used with relative success, several researches have presented its use as a shortcoming in clarifier modeling (e.g. Krebs, 1995; Mazzolani et al., 1998; Lakehal et al., 1999; Ekama, 2002). In this respect, Mazzolani et al. (1998) expressed “numerical models for the prediction of turbulent flow field and suspended solid distribution in sedimentation tanks are characterized by refined modeling of hydrodynamics, but apparently weak modeling of settling properties of suspensions.”

One of the major goals in this study is to develop an appropriate relationship for the simulation of the settling velocities on the entire curve of suspended solids usually encountered in SST. The next sections of this report discuss this development.

3.1.1 Study on Wall Effects and Effects of the Stirring Mechanism

In order to avoid wall effects, the batch settling tests for the determination of the settling properties of the sludge, were performed using a 2 liter stiro-settlometer. This laboratory equipment is manufactured by MCR Process and Technology; it is provided with a stirring mechanism consisting of two thin rods extended the length of the column and positioned within two rod diameters of the cylinder wall, the rods rotate at about 1 rpm. The stirring mechanism avoids any possible wall effect as recommended by Standard Method 2710 E and 2710 D for the evaluation of zone settling velocity and sludge volume index respectively.

Wall effects were studied using a relatively high concentrated suspension (About 3800 mg/L) and performing the settling test using three different equipments. The solids liquid interface depth versus time was recorded using: (a) the Stiro-settlometer with the stirring mechanism, (b) the stiro-settlometer without the stirring mechanism (2 liter cylinder), and (c) a 1 liter cylinder without stirring mechanism. The results of this experiment are presented in Figure 3.1. From the results of this simple test it is obvious that wall effects in small equipment may lead to erroneous values of the settling properties, yielding results that are not fully representative of what is really occurring in the SST. This problem may be overcome using equipment provided with a stirring mechanism such as the Stiro-settlometer.

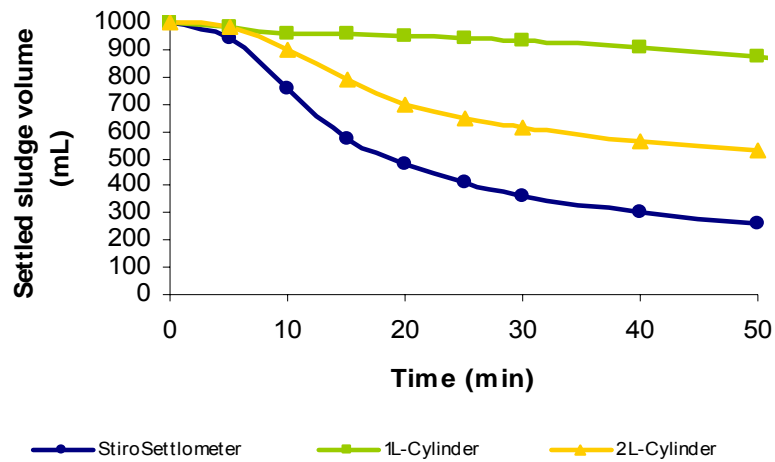


Figure 3.1 Solid Liquid Interface Depth vs. Time Using 3 Different Apparatus for a MLSS = 3800 mg/L

3.1.2 Study on Discrete Settling

Krebs (1995), Krebs et al. (1996), Mazzolani et al. (1998), Lakehal et al. (1999) and Ekama (2002) all expressed their concern about the way the settling properties are treated in current settling tank models. They were referring to the shortcomings in the use of the Takacs model. A generalized comment is that it was developed for 1D clarifier model and is used in 2D modelling. This is true, but the settling velocity is in nature a 1D process. Moreover, the calibration of the settling properties using a more sophisticated method than a 1D batch test equipped with a stirring mechanism, will limit the usage of any model. Hence, the settling velocity model to be incorporated in the 2D hydrodynamic equations should be based in a simple test procedure. On the other hand; the presumption that the Takacs equation does not predict correctly the settling behaviour of diluted concentration and of thickened sludge is a drawback in the simulation. In this respect, Krebs (1995) and Krebs et al. (1996) expressed that the Takacs model presents some

drawbacks when used in the regions of low concentration. Mazzolani et al. (1998) indicated that a concentration-dependent equation can not simulate accurately particle settling in the low concentration region. They proposed to use individual settling velocities in the low concentration region and a mass settling velocity in regions where settling is hindered by high concentration. The model proposed by Mazzolani et al. (1998) is expressed as follow:

$$V_s = fV_{si} + (1 - f)V_o e^{-kX} \dots\dots\dots (3.1)$$

where V_{si} represents the discrete settling velocity of the i class; V_o and k are the settling parameters of the Vesilind Equation; and f is a partition function, which is dependent on suspended solids concentration X . f is equal to one when $X \leq X_{min}$ and is equal to zero when $X \geq X_{max}$. Where X_{min} is the value of X below which discrete settling conditions are dominant and X_{max} is the value above which hindered settling conditions are dominant.

Mazzolani et al. (1998) did not indicate the way that the threshold X_{min} and X_{max} should be determined, and they proposed the estimation of V_{si} as a function of particle diameter. In this respect, they used the equations proposed by Li and Ganczarczyk (1987, Equations 2.12 and 2.13). However, their model does account for hindered and discrete particle settling, and eliminates the use of the k_2 parameter of the Takacs equations, which is still very difficult to estimate without calibration data.

The approach in this research is similar to Mazzolani et al. (1998) but is generalized to include all settling processes from non-settleable particles to the compression of the sludge blanket.

Several researches have measured the discrete settling velocity of individual flocs. Multi-exposure photographic methods (e.g. Li and Ganczarczyk, 1987) and digital video techniques (e.g. Kinnear, 2002) have been successfully used for the measurement of the settling velocity and size of activated sludge flocs. However, as proposed by Mazzolani et al. (1998) a dilute activated sludge suspension is composed by an infinite number of floc sizes each with a settling velocity. Hence assumptions have to be made, and the

suspension is usually divided into a few fractions each one with a representative settling velocity.

In this research a simple procedure was developed that allows the calculation of three different fractions with three settling velocities in addition to a non settleable class. In this respect, the suspension has been divided into the following fractions: (1) large flocs, (2) medium flocs, and (3) small flocs. This classification is based on a visual inspection, measurement of settling velocities, and solid fluxes. The term “small flocs” refers to flocs that have a settling velocity lower than about 1.50 m/hr, the term “medium flocs” refers to flocs with a settling velocity between 1.50 m/hr and about 6 m/hr, and the term “large flocs” refers to individual flocs with a settling velocity faster than about 6 m/hr. The measurement of the fractions and discrete settling velocities are explained in the next sections and in Appendix D.

3.1.2.1 Measurement of Discrete Settling Velocities

Large and Medium Flocs

The measurement of the discrete settling velocity of a MLSS sample starts with the identification of the “threshold for hindered settling”, the “threshold for discrete particle settling”, and the “lag time”.

The “threshold for hindered settling” refers to the total suspended solids concentration below which it is not possible to identify a clear interface in a batch column test. This threshold is obtained by performing successive dilutions to the MLSS sample. Experimental results obtained with samples taken at The Marrero Wastewater Treatment Plant (Marrero WWTP) and using a pilot plant (See Appendix A for a description of the Marrero WWTP, and Appendix C for a description of the pilot plant facility) indicate that this threshold is in the range of 1000 to 1400 mg/L.

The “threshold for discrete particle settling” refers to the total suspended solids concentration below which the particles settle in a complete discrete settling regime;

particles settle as individual units with no significant interaction with neighboring particles. Experimental results obtained at the Marrero WWTP and pilot plant facility indicate that this threshold is in the range of 500 to 650 mg/L. Once the “threshold for hindered settling” has been identified, it can be assumed that the “threshold for discrete settling” is half of this value. A transition zone occurs between the two thresholds.

The “lag time” is the time at the beginning of the column batch test during which a predominant vertical movement of the particles is not observed. Prior to the test, the sample is agitated in order to produce a homogenous distribution of solids in the column. After that the column is collocated in the upright position, an initial energy and momentum dissipation produce the lag time. The lag time lasts for about 1 to 1.5 minutes before the discrete settling starts.

Even though the settling velocity of individual flocs can be measured using a digital video technique or a more sophisticated photographic technique, the settling velocity of “large” and “medium” flocs can also be obtained by visual inspection and direct measurement: using a halogen light to backlight the settling column, the individual flocs can be identified and followed, and the settling velocity can be measured using a scale and stopwatch. The procedure has to be repeated several times in order to get an appropriated number of individual floc measurements. Kinnear (2002) used 50 individual measurements for obtaining an average floc settling velocity. In this research average “large flocs” and “medium flocs” settling velocities were obtained with at least 15 individual measurements for each class. Appendix D presents the results of the discrete floc velocity measurements, and additional details of these results are presented in Chapter 5.

Small Flocs

The settling velocity of “small flocs” is obtained using a procedure based on the concentration profiles at two different times: Time 1 (t_1) is the time required for a

“medium floc” to travel a distance $H/2$, where H is the total height of the column (See Figure 3.2). After this time no “medium floc” can be identified by visual inspection.

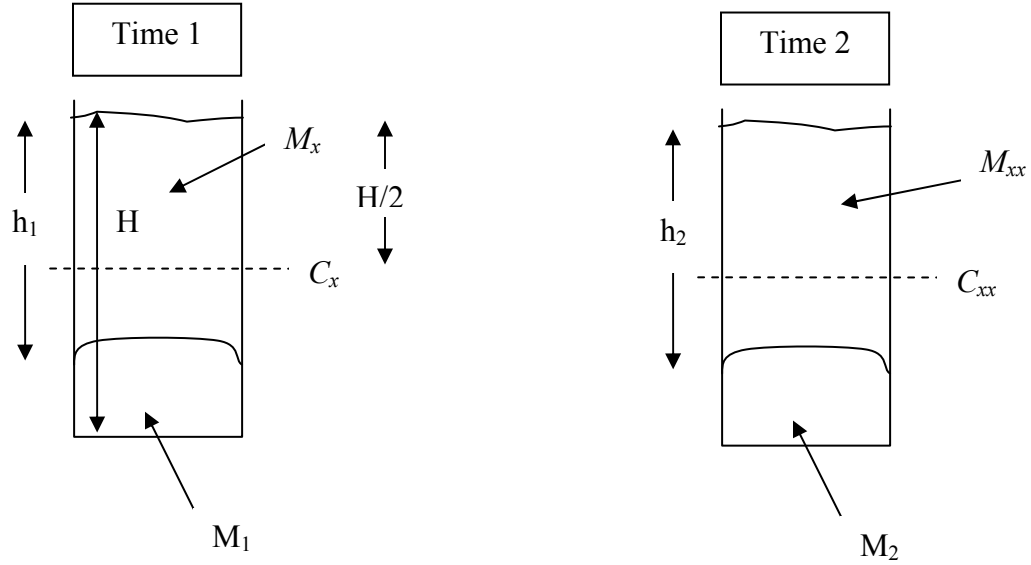


Figure 3.2 Sketch of Settling Column

The time 2 (t_2) is selected arbitrarily, but it should be at least double the value of t_1 . The mass of solids remaining in the upper-mid portion of the settling column is measured at t_1 and t_2 , and are referred to as M_x and M_{xx} respectively. The TSS concentrations at the middle of the column are also measured at t_1 and t_2 ; these values are referred to as C_x and C_{xx} respectively. The average flux of solids through a horizontal plane at the middle of the column between t_1 and t_2 can be calculated as:

$$\Delta t \left(\frac{V_x C_x + V_{xx} C_{xx}}{2} \right) \approx \frac{M_x - M_{xx}}{A_c} \dots \dots \dots (3.2)$$

where $\Delta t = t_2 - t_1$, V_x and V_{xx} are the average settling velocities of flocs at the hypothetical horizontal plane at the middle of the column at t_1 and t_2 respectively, and A_c is the area of the settling column defined by the intersection with a horizontal plane. Equation 3.2 can also be expressed as

$$\Delta t (\bar{V}_{x-xx} \bar{C}_{x-xx}) \approx \frac{M_x - M_{xx}}{A_c} \dots\dots\dots (3.3)$$

where $\bar{C}_{x-xx} = (C_x + C_{xx})/2$ and \bar{V}_{x-xx} is an average settling velocity between t_1 and t_2 . Assuming the average “small flocs” settling velocity (V_{sm}) as the average \bar{V}_{x-xx} , this velocity can be calculated from Equation 3.3:

$$V_{sm} \approx \frac{(M_x - M_{xx})}{A_c \Delta t \bar{C}_{x-xx}} \dots\dots\dots (3.4)$$

3.1.2.2 Calculation of the Discrete Settling Fractions

As explained in the previous section, the dilute suspension is divided into three settling fractions each with a representative settling velocity. However if three settling classes are considered, a fourth class should be added: the non-settleable portion. In this respect, a dilute concentration ($C_d \leq \text{Threshold for discrete particle settling}$) can be represented as the sum of four different concentrations, C_1 to C_4 each one corresponding to a different fraction:

$$C_1 + C_2 + C_3 + C_4 = C_d \dots\dots\dots (3.5)$$

where C_1 is the concentration of “large flocs”, C_2 is the concentration of “medium flocs”, C_3 is the concentration of “small flocs”, and C_4 is the concentration of the non-settleable particles. An ideal clarifier would have an ESS equal to the C_4 concentration. Since the FSS attempts to quantify the optimum degree to which the sample can be flocculated and settled, the value of the C_4 concentration can be approximated as the FSS of the sample. Based on this, Equation 3.5 can be rewritten as:

$$C_1 + C_2 + C_3 + FSS = C_d \dots\dots\dots (3.6)$$

The values of the different settling fractions can be calculated as:

$$f_i = \frac{C_i}{C_d - FSS}; \quad i = 1, 2, 3 \dots \dots \dots (3.7)$$

Obviously $\sum_{i=1}^n f_i = 1$.

In order to apply Equation 3.7 the C_i concentrations need to be calculated. Similar to the determination of the settling velocity of “small flocs”, these concentrations are obtained using a procedure based on the concentration profiles and mass of the sludge blanket at two different times. At t_1 the total mass in the sludge blanket (M_1 , See Figure 3.2) of the settling column can be calculated as:

$$A_c (V_{S1} \Delta t_{1-1} C_1 + V_{S2} \Delta t_{1-2} C_2 + V_{S3} \Delta t_{1-3} C_3) = M_1 \dots \dots \dots (3.8)$$

where V_{S1} , V_{S2} , and V_{S3} are the settling velocities of the “large”, “medium” and “small” flocs respectively. Δt_{j-i} refers to the settling time of the fraction i at time j (f_i at t_j), this settling time is calculated as:

$$\Delta t_{j-i} = \min \left(t_j - \text{Lag time}, \frac{h_j}{V_{si}} \right) \dots \dots \dots (3.9)$$

where h_j is the distance from the water surface to the top of the sludge blanket in the settling column at time j .

At t_2 the total mass in the sludge blanket (M_2 , See Figure 3.2) of the settling column can be calculated as:

$$A_c (V_{S1} \Delta t_{2-1} C_1 + V_{S2} \Delta t_{2-2} C_2 + V_{S3} \Delta t_{2-3} C_3) = M_2 \dots \dots \dots (3.10)$$

In Equation 3.8, the settling time Δt_{j-i} is calculated using Equation 3.9. The C_i concentrations are calculated using Equations 3.6, 3.8 and 3.10, and the f_i fractions are obtained with Equation 3.7.

Appendix D presents the results of the discrete floc fraction calculations, and additional details of this procedure are presented in Chapter 5.

3.1.3 Study on Compression Settling

Equation 3.1 treats the compression zone of the settling curve in the similar way that the Takacs equation does: as an extension of the Vesilind equation. In this respect, Lakehal et al. (1999) found that the Takacs or the Vesilind equation significantly underestimated the values of the settling velocities in the sludge blanket. To investigate this point, a simple experiment was designed (this procedure was performed using a pilot plant, which is described in Appendix C):

MLSS and RAS samples were taken from the contact chamber and from the recirculation line of the secondary clarifier respectively. Three dilutions were obtained from an initial MLSS concentration of about 4200 mg/L and from an initial RAS concentration of about 18000 mg/L respectively. The six dilutions were obtained by mixing the MLSS with effluent from the secondary clarifier. The zone settling velocity of the six samples were measured using the procedure and equipment described in Section 5.1.1.2. The zone settling velocity was plotted in semi-logarithmic paper versus concentration; this graph is presented in Figure 3.3. Obviously, if the Vesilind equation (exponential model) predicts the settling velocity for all the range of studied concentrations, all the points should align in a straight line. As observed in Figure 3.3, this was not the case. The data follow two straight lines, clearly indicating that the determination of the Vesilind settling parameters based on typical hindered concentrations in the MLSS underestimates the settling velocities of higher concentrations (similar to the typical values encountered in the sludge blanket)

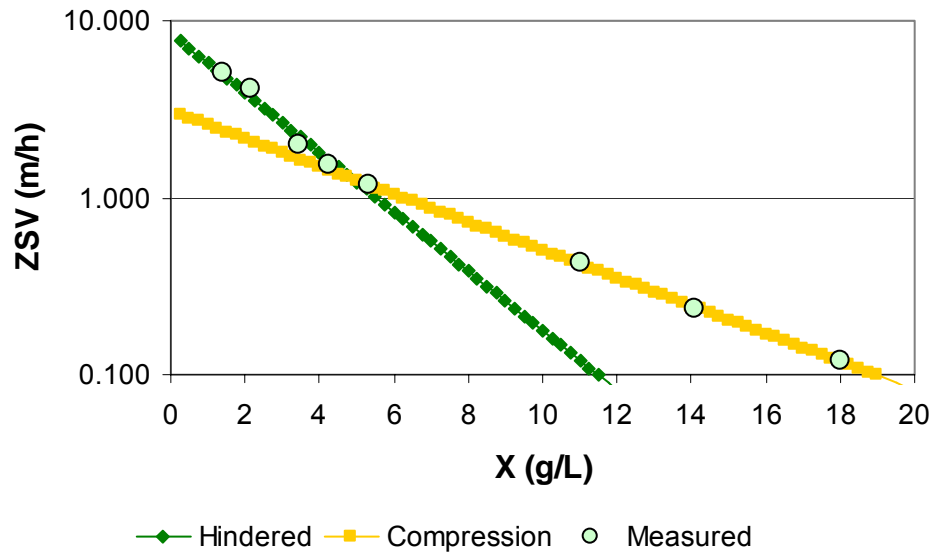


Figure 3.3 Settling Velocities for Hindered and Compression Zone

These results indicate that the straight application of the Takacs model or the Model proposed by Mazzolani et al. (1998) may lead to improper estimation of sludge blanket settling properties. An alternative approach is the application of a settling model based on the analogy between the filtration and the sedimentation processes; these models seem to adequately simulate the hindered and compression settling regimes. But, as previously discussed in Section 2.2.2, these models tend to overestimate the settling velocities of low concentration dilutions. More results on the study on compression settling are presented in Appendix E, and additional details of this procedure are presented in Chapter 5.

Previous discussion clearly demonstrates that the direct application of a single settling velocity model is not possible. The next section discusses the development of a compound model that accounts for the settling properties of activated sludge in five categories: (a) non-settleable particles, (b) discrete settling particles, (c) transition-flocculent settling, (d) hindered (zone) settling, and (e) compression settling.

3.2 Development of the Settling Model

In order to account for the settling velocity of the entire curve of suspended solids usually encountered in activated sludge and trickling filter-solids contact systems, the settling velocities have been divided in five settling regions. Table 3.1 indicates the regions and predominant settling regimes based on the total suspended solids concentration.

Table 3.1 Settling Regions Based on the TSS Concentration

Total Suspended Solids Concentration (X)	Settling Region	Settling Model
$X \leq FSS$	Non-settleable	$V_s = 0$
$FSS < X \leq \text{Discrete Threshold}$	Discrete settling	Individual floc settling velocity
$\text{Discrete Threshold} < X \leq \text{Hindered Threshold}$	Flocculent settling	Transition zone
$\text{Hindered Threshold} < X \leq \text{Compression Threshold}$	Hindered settling	Exponential model
$X > \text{Compression Threshold}$	Compression settling	Exponential model

For every settling region there is a different settling velocity sub-model. The compound settling velocity model is represented by Equation 3.11

$$V_s = 0 \quad X \leq FSS$$

$$V_s = V_{si} \text{ for } i = 1, 2, \dots, n$$

$$X = \sum_{i=1}^n X_i + FSS \quad FSS < X \leq \text{Discrete Threshold } (Xd)$$

$$X_i = f_i(X - FSS)$$

$$\begin{aligned}
V_s &= \zeta V_o e^{-k_l X} + (1 - \zeta) V_{sd}^* \\
\zeta &= \frac{(X - Xd)}{(Xh - Xd)} \quad Xd < X \leq \text{Hindered Threshold } (Xh) \\
V_{sd}^* &= \sum_{i=1}^3 f_i V_{si} \\
V_s &= V_o e^{-k_l X} \quad \text{Hindered Threshold } (Xh) < X \leq \text{Compression Threshold} \\
V_s &= V_c e^{-k_c X} \quad X > \text{Compression Threshold} \\
&\dots\dots\dots (3.11)
\end{aligned}$$

where X is the suspended solids concentration, V_s is the settling velocity, V_{si} is the discrete settling velocity of the i floc class, f_i is the i settling fraction for discrete settling, V_o and k_l are settling parameters for the hindered settling model, and V_c and k_c are settling parameters for the compression settling model.

3.3 Effects of Temperature on Settling Velocities

The traditional discrete settling model proposed by the Stoke's law (Equation 2.11) suggests that the settling velocity of discrete particles depends indirectly on the temperature of the fluid since the settling velocity is inversely proportional to the kinematic viscosity of the liquid. A similar relationship is presented in the compression rate model proposed by Kinnear (2002) in which the settling velocity is inversely proportional to the dynamic viscosity of the fluid (Equation 2.22). The models proposed by Stoke's law and Kinnear (2002) indicate that the settling velocity of discrete particles and the compression rate of the sludge are influenced by the temperature of the mixture.

In order to define a correction factor for the settling velocities based on temperature difference, the temperature effect on the zone settling velocity has to be determined. In

this respect a modified column batch test was conducted: in addition to the normal batch test for determining the zone settling velocity a second batch test was carried out. The additional batch test was conducted modifying the temperature of the sample using a submerge bath. The sludge samples were submitted to a 30 minute cooling process, after which the settling velocities were measured. During the measuring process the column was kept in a cold bath in order to avoid a major heating of the sample. Even though a major alteration of the sample was not expected during the 30 minutes cooling process; the TSS and VSS of the samples were measured before and after the cooling process and after the completion of the settling test. These measurements were performed to verify if the composition of the samples change during the test. In none of the cases was found an important alteration in the TSS and VSS values. The sludge samples were taken from the contact chamber of the experimental pilot plant at Marrero.

Table 3.2 presents the settling velocities measured for different samples at two different conditions: (a) zone settling velocity measured at normal (field conditions) temperature, and (b) zone settling velocity measured at a cooled temperature. This table also shows the temperature of the sample at the beginning and at the end of the test, and the respective dynamic viscosity of the mixture calculated using Equation 2.60. Additional results are presented in Appendix F.

Assuming the viscosity as the only variable in the models proposed by Stoke's law and Kinnear (2002), the settling velocity of discrete particles and the compression rate of activated sludges can be expressed as:

$$V_s = \frac{K}{\mu} \dots\dots\dots (3.12)$$

where K is a constant independent of temperature but dependent on all other parameters affecting settling.

Table 3.2 Settling Velocities and Dynamic Viscosities for Samples at Normal and Cooled Temperature

Sample at Normal Temperature (T_n)				
Sample TSS (mg/L)	Settling Velocity (V_{sT_n}, m/h)	Initial Temperature (T_o, °C)	Final Temperature (T_f, °C)	Dynamic Viscosity (μ_{T_n}, Kg/ m.s)
5713	1.5	27.5	27.5	8.42E-04
4500	1.7	27.5	27.5	8.42E-04
3205	2.73	26	26	8.70E-04
2152	4.52	25.3	25.3	8.84E-04
Sample at Cooled Temperature (T_c)				
Sample TSS (mg/L)	Settling Velocity (V_{sT_c}, m/h)	Initial Temperature (T_o, °C)	Final Temperature (T_f, °C)	Dynamic Viscosity (μ_{T_c}, Kg/ m.s)
5713	0.96	10	10	1.30E-03
4500	1.02	8.6	8.8	1.35E-03
3205	1.8	9.8	10.8	1.29E-03
2152	3.12	9	10.9	1.30E-03

For a fixed value of K in Equation 3.12, and two different temperatures T_1 and T_2 , Equation 3.12 can be rearranged as:

$$V_{sT_1} \mu_{T_1} = V_{sT_2} \mu_{T_2} = K \dots\dots\dots (3.13)$$

where V_{sT_1} and V_{sT_2} are the settling velocities at temperatures T_1 and T_2 respectively, and μ_{T_1} and μ_{T_2} are the dynamic viscosities of the mixtures at temperatures T_1 and T_2 respectively. Table 3.3 shows the value of the relationship V_{sT_1}/V_{sT_2} and μ_{T_2}/μ_{T_1} for the data presented in Table 3.2 at temperatures T_n (normal temperature) and T_c (cooled temperature), and Figure 3.4 displays graphically this information

Table 3.3 Ratios of $V_{s_{T_1}}/V_{s_{T_2}}$ and μ_{T_2}/μ_{T_1} for Different Samples

Sample TSS (mg/L)	$V_{s_{T_n}}/V_{s_{T_c}}$	μ_{T_c}/μ_{T_n}
5713	1.56	1.54
4500	1.67	1.60
3205	1.52	1.48
2152	1.45	1.47

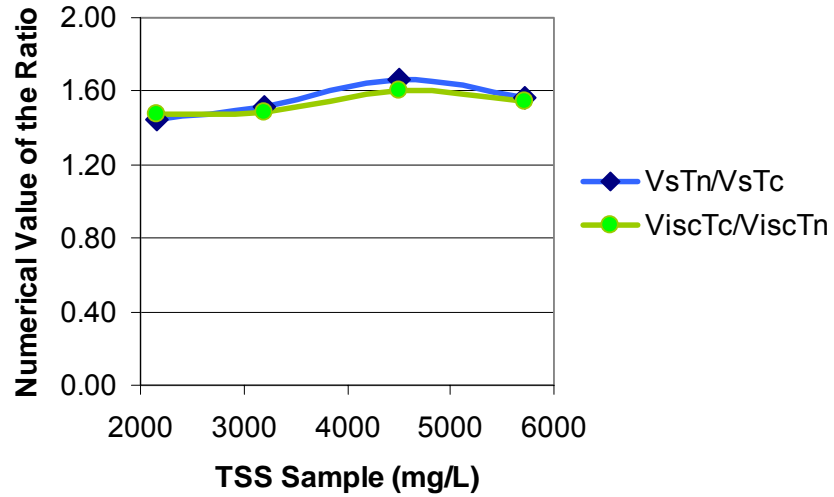


Figure 3.4 Ratios of $V_{s_{T_1}}/V_{s_{T_2}}$ and μ_{T_2}/μ_{T_1} for Different TSS Concentrations

From Figure 3.4 and Table 3.3 can be observed that the numerical values of the ratios $V_{s_{T_1}}/V_{s_{T_2}}$ and μ_{T_2}/μ_{T_1} are very close, suggesting that an easy correction in the zone settling velocity for different temperatures can be made with a correction factor based on the dynamic viscosity of the water at the two temperatures. Figure 3.5 shows an extended data set indicating the relationships between the ratios $V_{s_{T_1}}/V_{s_{T_2}}$ and μ_{T_2}/μ_{T_1} .

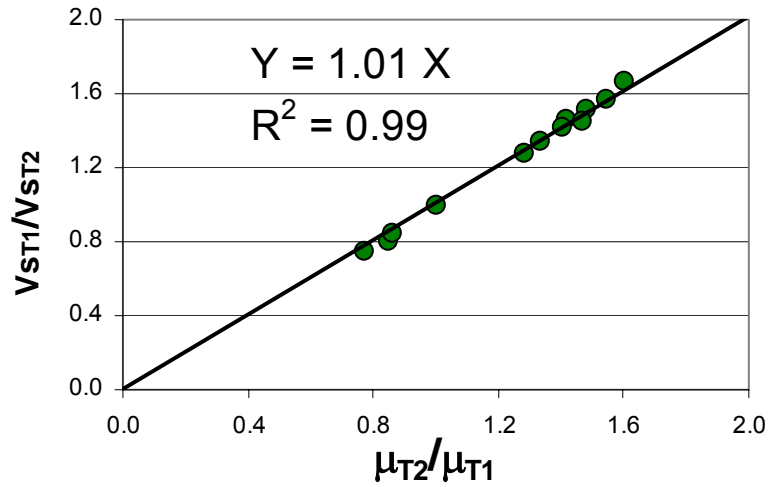


Figure 3.5 Effect of Temperature on Zone Settling Velocity

Fitting a straight line to the data points presented in Figure 3.5 and using Equation 2.60 we can find a correction factor for the settling velocities based on temperature

$$V_{sT2} = V_{sT1} \left(\frac{10^{\left[\frac{247.8}{T1+133.15} \right]}}{10^{\left[\frac{247.8}{T2+133.15} \right]}} \right) \dots\dots\dots (3.14)$$

Equation 3.14 can be applied to correct the settling velocities for difference in temperatures in whichever of the four types of sedimentation described by Equation 3.11, i.e., unflocculated discrete settling, flocculated discrete settling, hindered (zone) settling and compression. In this equation $T1$ could be the temperature at which the settling properties were measured, e.g. laboratory temperatures, and $T2$ would be the temperature of the fluid in the field. Even though Equation 3.14 can be used for a sensitivity analysis on the performance of the model for different seasons, e.g. summer and winter, there is no evidence that the settling properties can be accurately extrapolated from one season to another. Equation 3.14 was developed using the same sludge, changing only the temperatures of the samples, while the effect of seasonal variations in the sludge properties were not studied.

CHAPTER 4

4 SETTling TANK MODEL DEVELOPMENT

4.1 Development of Quasi 3D (Q3D) Settling Tank Model

The development of a numerical model for settling tanks involves five steps (McCorquodale et al., 1991):

- 1) A mathematical formulation to describe the hydrodynamics and other important processes in the tank.
- 2) The application of numerical methods to discretise the governing partial differential equations and to solve the set of resulting algebraic equations.
- 3) A computer code to run the model.
- 4) Calibration of the model, which involves adapting the model to predict the observed results in a specific facility (field or scale model data).
- 5) Validation of the model, which involves comparing the model response to actual measured field data that was not used in the calibration. Scale model and published data can also be used in the validation.

This chapter is organized following the five aforementioned steps.

4.1.1 Governing Equations

The major assumption in the development of the model is that the flow is axisymmetric and incompressible; therefore, a 2-dimensional geometry can be used to properly simulate the general features of the hydrodynamic processes in the clarifier. However, in order to include important three dimensional effects, like swirl momentum and turbulence produced by inlet vanes and rotating scraper mechanisms, a third velocity component in the θ direction is included. In this way, the model development starts with the momentum equations in three directions.

The governing equations of motion for three dimensional, incompressible, unsteady, stratified, incompressible, and turbulent- average flow in cylindrical coordinates (r, θ , y) are as follows (Jensen et al., 1979):

continuity equation

$$\frac{\partial ru}{\partial r} + \frac{\partial rv}{\partial y} + \frac{\partial rv_{\theta}}{r \partial \theta} = 0 \dots\dots\dots (4.1)$$

r-momentum component

$$\begin{aligned} \frac{\partial \rho u}{\partial t} + u \frac{\partial \rho u}{\partial r} + \frac{v_{\theta}}{r} \frac{\partial \rho u}{\partial \theta} - \frac{\rho v_{\theta}^2}{r} + v \frac{\partial \rho u}{\partial y} = - \frac{\partial p}{\partial r} + \\ \frac{1}{r} \frac{\partial}{\partial r} \left(r \mu_{eff} \frac{\partial u}{\partial r} \right) + \frac{1}{r^2} \frac{\partial}{\partial \theta} \left(\mu_{eff} \frac{\partial u}{\partial \theta} \right) - \frac{2}{r^2} \mu_{eff} \frac{\partial v_{\theta}}{\partial \theta} + \frac{\partial}{\partial y} \left(\mu_{eff} \frac{\partial u}{\partial y} \right) + \rho g_r \end{aligned} \quad (4.2)$$

θ - momentum component

$$\begin{aligned} \frac{\partial \rho v_{\theta}}{\partial t} + u \frac{\partial \rho v_{\theta}}{\partial r} + \frac{v_{\theta}}{r} \frac{\partial \rho v_{\theta}}{\partial \theta} + \frac{\rho v_{\theta} u}{r} + v \frac{\partial \rho v_{\theta}}{\partial y} = - \frac{1}{r} \frac{\partial p}{\partial \theta} + \\ \frac{1}{r} \frac{\partial}{\partial r} \left(r \mu_{eff} \frac{\partial v_{\theta}}{\partial r} \right) + \frac{1}{r^2} \frac{\partial}{\partial \theta} \left(\mu_{eff} \frac{\partial v_{\theta}}{\partial \theta} \right) + \frac{2}{r^2} \mu_{eff} \frac{\partial u}{\partial \theta} + \frac{\partial}{\partial y} \left(\mu_{eff} \frac{\partial v_{\theta}}{\partial y} \right) + \rho g_{\theta} \end{aligned} \quad (4.3)$$

y- momentum component

$$\begin{aligned} \frac{\partial \rho v}{\partial t} + u \frac{\partial \rho v}{\partial r} + \frac{v_{\theta}}{r} \frac{\partial \rho v}{\partial \theta} + v \frac{\partial \rho v}{\partial y} = - \frac{\partial p}{\partial y} + \\ \frac{1}{r} \frac{\partial}{\partial r} \left(r \mu_{eff} \frac{\partial v}{\partial r} \right) + \frac{1}{r^2} \frac{\partial}{\partial \theta} \left(\mu_{eff} \frac{\partial v}{\partial \theta} \right) + \frac{\partial}{\partial y} \left(\mu_{eff} \frac{\partial v}{\partial y} \right) + \rho \frac{\rho - \rho_r}{\rho_r} g_y \end{aligned} \quad (4.4)$$

in which u , v , and v_θ are temporal mean velocity components in the r -, y - and θ - directions respectively; μ_{eff} is the effective viscosity; p is the general pressure less the hydrostatic pressure at reference density ρ_r ; ρ is the fluid-solid mixture density; g is the component of gravitational acceleration and $(\frac{\rho - \rho_r}{\rho_r} g_y)$ is a density gradient term for the simulation of buoyant effects.

As previously performed by Larsen (1977), Imam et al. (1983), McCorquodale et al. (1991), Samstag et al.(1992), Ji et al. (1996), and Gerges and McCorquodale (1997) the pressure terms from Equations 4.2 to 4.4 are going to be eliminated by using the vorticity - stream function formulation. The vorticity ω is defined as:

$$\omega = \frac{\partial v}{\partial r} - \frac{\partial u}{\partial y} \dots\dots\dots (4.5)$$

The stream function formulation defines the two-dimensional flow field and guarantees liquid continuity. The net flow per unit width passing through two points in the grid is given by the difference of stream function at the two given points. The mean velocity component in the r - and y - directions can be obtained from the stream function ψ using the following equations (Ji et al. 1996):

$$u = \frac{1}{r} \frac{\partial \psi}{\partial y} \quad ; \quad v = -\frac{1}{r} \frac{\partial \psi}{\partial r} \dots\dots\dots (4.6)$$

Combining Equations 4.5 and 4.6 we get working Equation 4.7 that is used to get the field values of ψ .

$$\frac{\partial^2 \psi}{\partial r^2} - \frac{1}{r} \frac{\partial \psi}{\partial r} + \frac{\partial^2 \psi}{\partial y^2} = -\omega r \dots\dots\dots (4.7)$$

Using the vorticity definition and the axisymmetric assumption $\left[\frac{\partial(\dots)}{\partial \theta} \cong 0 \right]$ the momentum equations in the r- and y- components are reduced to the following vorticity transport equation:

$$\frac{\partial \rho \omega}{\partial t} + \frac{\partial \rho u \omega}{\partial r} + \frac{\partial \rho v \omega}{\partial y} + \frac{\partial}{\partial y} \left(\rho \frac{v_{\theta}^2}{r} \right) = \frac{1}{r} \frac{\partial}{\partial r} \left(\rho r v_{eff} \frac{\partial \omega}{\partial r} \right) + \frac{\partial}{\partial y} \left(\rho v_{eff} \frac{\partial \omega}{\partial y} \right) + \rho \frac{\partial g'}{\partial r} + \hat{S}_{\omega} \dots \quad (4.8)$$

where $g' = \frac{\rho - \rho_r}{\rho_r} g$ and \hat{S}_{ω} is a vorticity source term. The mixture density ρ is related to the water reference density and suspended solids concentration through the following equation of state (Larsen, 1977)

$$\rho = \rho_{ref} + \left(1 - \frac{1}{S_s} \right) X \dots \quad (4.9)$$

where X is the SS concentration, S_s is the specific gravity of the dry solids, and ρ_{ref} is the water reference density. As expressed in Chapter 2 the ρ_{ref} is a function of water temperature (T) and water dissolved solids content (TDS). This equation is recapitulated below.

$$\rho_{ref} = [999.8396 + 18.224944 \times T - 0.00792221 \times T^2 - 55.4486 \times 10^{-6} \times T^3 + 14.97562 \times 10^{-8} \times T^4 - 39.32952 \times 10^{-11} \times T^5 + (0.802 - 0.002 \times T) \times \text{TDS}] / [1 + 0.018159725 \times T] \dots \quad (2.59)$$

Typical reported S_s values for activated sludges range from 1.2 to 1.70 (e.g. Larsen, 1977; Smith and Coackley, 1984; Li and Ganczarczyk, 1992; Namer and Ganczarczyk,

1993; Hilligardt and Hoffman, 1997; Kinnear, 2002). In this study an average $S_s = 1.45$ is used as default value.

Equation 4.8 differs from the previously presented vorticity transport equation due to the presence of the correction term $\frac{\partial}{\partial y} \left(\frac{v_{\theta}^2}{r} \right)$. The v_{θ} velocities are obtained from a simplified Equation 4.3. Making all gradients with respect to θ equal zero, Equation 4.3 is reduced to:

$$\frac{\partial \rho v_{\theta}}{\partial t} + u \frac{\partial \rho v_{\theta}}{\partial r} - \frac{\rho v_{\theta} u}{r} + v \frac{\partial \rho v_{\theta}}{\partial y} = \frac{1}{r} \frac{\partial}{\partial r} \left(\rho r v_{eff} \frac{\partial v_{\theta}}{\partial r} \right) + \frac{\partial}{\partial y} \left(\rho v_{eff} \frac{\partial v_{\theta}}{\partial y} \right) + \hat{S}_{\theta} \quad (4.10)$$

in which \hat{S}_{θ} is a circumferential momentum source term. Notice that the continuity equation (Equation 4.1) is also reduced to only two terms.

Szalai et al. (1994) presented a similar equation to Equation 4.10 but for steady state. They used the circumferential momentum to simulate swirl effects in a neutrally buoyant flow environment. They observed that swirl effects strongly influence the radial flow, and the inclusion of such effect results in a better prediction of the FTC curves. As they expressed, their results (which did not include density effects or particle settling) are of relative importance for primary clarifiers only. In this research, the swirl effects are included in the simulation of secondary clarifiers where the flow is dominated by density effects. As mentioned before, the effects of density gradients due to solids and temperature are incorporated in the model. The effects of solids transport and particle settling, which modeling is discussed next, are included as well.

Equation 4.8 is controlled by density effects, and density depends on suspended solids concentration and temperature as shown by Equations 4.9 and 2.59. Moreover the function of the settling tank is to remove SS from water; hence, the overall efficiency of a SST model relies on the accurate prediction of the solids transport and settling

phenomena. The advection-diffusion equation for solids transport was presented in Section 2 and is recapitulated below.

$$\frac{\partial \rho X}{\partial t} + \frac{\partial \rho u X}{\partial r} + \frac{\partial \rho v X}{\partial y} = \frac{1}{r} \frac{\partial \rho r \nu_{sr}}{\partial r} \frac{\partial X}{\partial r} + \frac{1}{r} \frac{\partial \rho r \nu_{sy}}{\partial y} \frac{\partial X}{\partial y} + \frac{1}{r} \frac{\partial \rho r V_s X}{\partial y} \dots\dots\dots (4.11)$$

Equation 4.11 differs from Equation 2.6 since it includes the density of the mixture as a variable. As in Equation 2.6 X is concentration of SS; ν_{sr} is the eddy diffusivity of suspended solids in the r - direction; ν_{sy} is eddy diffusivity of suspended solids in the y -direction; and V_s is particle settling velocity. These two last variables will be further discussed in the next two sections.

4.1.2 Turbulence Model and Rheology of the Sludge

The importance and different approaches for modelling turbulence and rheology were discussed in sections 2.2.2 and 2.2.3 respectively. In this section the two concepts, even though different in nature, are used together to define the diffusion effects in Equation 4.8, 4.10 and 4.11.

The effective viscosity ν_{eff} presented in this chapter includes both the molecular viscosity ν and the turbulent eddy viscosity ν_t , i.e.

$$\nu_{eff} = \nu + \nu_t \dots\dots\dots (4.12)$$

Generally the eddy diffusivity term has been presented as the ratio of the eddy viscosity ν_t and the turbulent Schmidt number σ_s (Equations 2.7 and 2.8). Usually the eddy diffusivity has been assumed as an isotropic property (e.g. Lakehal et al., 1999; Stamou et al., 2000; Armbruster et al., 2001; De Clercq, 2003) with similar Schmidt numbers in the r - (x) and y - directions; however, as expressed by Larsen (1977), in the case of density stratified flow with buoyant effects (when buoyancy dominates over kinetic energy),

turbulence is subdued (this occurs basically in the vertical direction) and the diffusion coefficient of momentum and solids transport are reduced. Therefore, different Schmidt numbers should be used in the two directions (e.g. Samstag et al., 1992; Zhou et al., 1994). Samstag et al. (1992) found the best fit to experimental data when using a 10 times higher eddy diffusivity in the radial direction with respect to the vertical one.

In this study the eddy diffusivity is defined as:

$$\nu_{sr} = \nu + \Gamma_r \nu_t \dots \dots \dots (4.13)$$

$$\nu_{sy} = \nu + \Gamma_y \nu_t \dots \dots \dots (4.14)$$

where Γ_r and Γ_y are the effective diffusion coefficient in the r- and y- directions respectively. The effective diffusion coefficients may be regarded as the inverse of the turbulent Schmidt numbers.

The molecular viscosity ν is a property of the fluid-solids mixture, defined by the rheology of the sludge. The eddy viscosity ν_t is not a fluid property but depends on the structure of the turbulence.

As presented in Section 2.2.4, several models have been proposed to simulate the rheology of non-Newtonian sludges, such as the Ostwald equation (pseudoplastic model), Bingham equation (plastic model), and Herschel-Bulkley equations (yield pseudoplastic model). The plastic and yield pseudoplastic models include a yield stress as the initial resistance of the sludge to deformation. Other approaches are presented by Bokil (1972) and De Clercq (2003).

As mentioned earlier, different authors have expressed different conclusions about the best model to describe the rheology of activated sludges. In SST modeling the simulation of rheology effects has been too limited to be conclusive. Despite the fact that most

models (Dahl et al. 1994, Lakehal et al. 1999, Armbruster et al. 2001) have applied a Bingham-type model simulation, this study uses the model proposed by Bokil (1972) as an initial approach. Three reasons can be argued for this selection:

- 1) De Clercq (2003) showed that a true yield stress does not exist (the Bingham model supposes a yield stress while the Bokil model doesn't). When comparing their model (a Herschel-Bulkley-type model) to the Bingham model and to the Bokil model, they found that the Bokil model resulted in the best prediction of the sludge blanket height.
- 2) Three-parameter models do not seem to have any advantage over two-parameter models. Hence for simplicity it is better to select a two-parameter model. In fact, the lack of agreement in this respect makes almost any initial selection equally good.
- 3) The Bokil model is straightforward and easy to implement. It suggests an exponential function for the molecular kinematic viscosity based on sludge concentration.

The relationship proposed by Bokil (1972) is presented in Figure 2.3 (adapted from Ekama et al. 1997) as the effective molecular kinematic viscosity versus sludge concentration. From this graph we can extrapolate the following relationship:

$$\begin{aligned} \nu &= 1 \times 10^{-6} e^{1.386X} & X \leq 1 \text{ g/L} \\ \nu &= 2.9 \times 10^{-6} e^{0.322X} & X > 1 \text{ g/L} \end{aligned} \tag{4.15}$$

in which X is SS in g/L and ν is the mixture kinematic viscosity in m^2/s .

As discussed in Section 2.2.3 the eddy viscosity concept for introducing turbulence effects on the momentum and transport equations has been by far the most popular among researches in settling tank modeling. Basically, three different approaches have been used: 1) a constant eddy viscosity, 2) relation of the eddy viscosity to the local mean

velocity gradient G and the mixing length l_m , and 3) relation of the eddy viscosity to the turbulence kinetic energy (k) and the turbulence dissipation rate (ε).

As earlier commented, a constant eddy viscosity does not account for the heterogeneous nature of the turbulence in settling tanks, while models based on mixing length and k - ε theory do. Both models (mixing length and k - ε) have been used with success in settling tank modelling, predicting similar removal efficiencies and agreeing with experimental data. However, Rodi (1980, cited by Imam et al., 1983) reported that mixing length models are not satisfactory for recirculating flows, due to the difficulty in describing l_m . In this respect, Imam et al. (1983) argued that it could be true if no experimental calibration is used. Larsen (1977) and Abdel-Gawad and McCorquodale (1984a, 1984b, 1985a, 1985b) showed that the solids removal is not very sensitive to the actual distribution of the diffusion coefficient, and the main hydraulic features of flow in clarifiers could be reproduced with a simple-modified mixing length model. On the other hand, as presented in a previous section, the efficiency of the k - ε model has also been questioned. What cannot be questioned is that the k - ε model is considerably more demanding than the mixing-length model with respect to computational time and storage. The k - ε model adds two additional transport equations that have to be solved at every time step.

In addition to the above statements, it is important to recognize that as for any model, the efficiency of a turbulent model strongly depends on the applied boundary conditions and the knowledge of the flow to be modelled. As Abdel-Gawad (1983) pointed out: “the more knowledge of the flow the modeller has, the greater the chance he has to describe a simple turbulence model.” Based on this discussion, the initial approach in this study will be to use a modified-calibrated mixing length model. This approach is presented next.

As presented in Section 2.2.3, the hypothesis on the mixing length model relates the eddy viscosity ν_t to the mixing length l_m and the local mean velocity gradient G .

$$v_t = Gl_m^2 \dots\dots\dots (2.24)$$

In Equation 2.24 G is defined as the mean gradient of the radial and vertical velocities with respect to y and r respectively.

$$G = \sqrt{\left(\frac{\partial u}{\partial y}\right)^2 + \left(\frac{\partial v}{\partial r}\right)^2} \dots\dots\dots (4.16)$$

The l_m field is obtained by means of a calibrated Poisson Equation. In cylindrical coordinates this equation is expressed as:

$$\frac{\partial^2 l_m}{\partial r^2} - \frac{1}{r} \frac{\partial l_m}{\partial r} + \frac{\partial^2 l_m}{\partial y^2} = K_{l_m} \dots\dots\dots (4.17)$$

where K_{l_m} is a calibration constant.

4.1.3 Settling Model

The development of the settling model was presented in Chapter 3. As discussed in that chapter, a compound settling velocity model was developed which is represented by Equation 3.11. This model accounts for the settling velocity of the entire curve of suspended solids usually encountered in activated sludge and trickling filter-solids contact systems. Five different settling regimes are included in the model (see Chapter 3): (a) non-settleable particles, (b) discrete settling particles, (c) transition-flocculent settling, (d) hindered (zone) settling, and (e) compression settling.

4.1.4 Flocculation Sub-Model

Section 2.3.4 presented a detailed explanation of the flocculation process, including its modelling and effects on clarifier performance. It was discussed that early researches in PST (e.g. Larsen, 1977; Valioulis and List, 1984a; Devantier and Larock, 1987; Lyn et al., 1992) recognized the importance of the flocculation process in this type of clarifier, but only Valioulis and List (1984a, 1984b) and Lyn et al. (1992) included a flocculation sub-model in the general PST model. Valioulis and List (1984a, 1984b) introduced equations for Brownian motion, turbulent shear and differential sedimentation in a very simple hydrodynamic model. Lyn et al. (1992) used a relative sophisticated hydrodynamic model, but a simple flocculation approach. They simulated only shear-induced flocculation without floc breakup. The outcomes in these two researches were very different; while Valioulis and List (1984b) found that the flocculation process affects dramatically the suspended solids removal efficiency, Lyn et al. (1992) found that the shear-induced flocculation scarcely affects it. A third study was presented recently by De Cock et al. (1999); they studied the feasibility of flocculation in a storage sedimentation basin using a previous flocculation zone. Similar to Lyn et al. (1992), De Cock et al. (1999) simulated only the shear-induced flocculation, but they found the flocculation step does improve the basin efficiency.

It has been shown (Parker et al. 1970, 1971, 1972; Das et al., 1993; La Motta et al., 2003) that a flocculation zone previous to the final settling stage can improve the general suspended solids removal efficiency. It has been also stated that a flocculation zone inside the tank improves the performance of the SST. Parker et al. (1996) found that SSTs equipped with a flocculation center-well perform better than tanks without it. They expressed that “the main purpose of the flocculation center-well (FCW) is to encourage the aggregation of dispersed settleable solids.” Interestingly, Merrill et al. (1992) found that the optimum placement of a FCW coincided with the optimum diameter recommended for flocculation. The interesting point is that Merrill et al. (1992) did not modelled flocculation, but the hydrodynamic flow pattern in a SST using a 2D model. These results open the discussion about the real effect of the FCW in the clarifier

performance: is it promoting flocculation or is it improving the hydrodynamics of the tank? A study aimed at answering this question is presented in Chapter 6.

In order to define the role of flocculation and FCW in SSTs, a flocculation sub-model that accounts for the effects of shear-induced and differential settling flocculation was included in the general Q3D settling tank model. The equations that compose this sub-model are presented and discussed in the next two sections.

4.1.4.1 Shear Induced Flocculation

The differential equation presented by Parker et al. (1970, 1971) is used to model the floc aggregation and break up in a turbulent environment. This equation was presented in Section 2.3.4 and is recapitulated below.

$$\frac{dn}{dt} = K_B \cdot X \cdot G^m - K_A \cdot X \cdot n \cdot G \dots\dots\dots (2.35)$$

The studies of Wahlberg et al. (1994), Jimenez (2002), and La Motta et al. (2003) support the use of this model. Beyond the fact that this model has been used widely; it was selected in the basis of its simplicity and kinetic constant documentation.

Equations 2.47 and 2.51 are used to simulate the G values in the inlet zone, and Equation 4.16 is used to simulate G values in the rest of the tank. These equations were described in Chapter 2 and Section 4.1.2 of this chapter respectively.

$$G = \sqrt{\frac{P}{V\mu}} = \frac{u_o}{\sqrt{t}v} \dots\dots\dots (2.47)$$

$$G = 1.53 v^{-1/2} B^{3/4} u_o^{3/2} X^{-5/4} \dots\dots\dots (2.51)$$

$$G = \sqrt{\left(\frac{\partial u}{\partial y}\right)^2 + \left(\frac{\partial v}{\partial r}\right)^2} \dots\dots\dots (4.16)$$

The calibration of the shear induced flocculation model is presented in Chapter 5.

4.1.4.1 Differential Settling Flocculation

The differential settling flocculation is due to the differences in the settling velocities of the particles whereby large particles overtake smaller particles during the settling process. The particles coalesce increasing the mass and settling at a faster rate. McCorquodale et al. (2004) developed a differential equation predicting the rate of change of primary particles into flocs due to differential settling (Equation 4.18). The development of this equation is presented in Appendix H.

$$\frac{dC_1}{dt} = -\frac{9}{4}k_{ds} \frac{C_1C_2}{\rho_1\rho_2} \left(1 + 2\frac{d_1}{d_2}\right)^2 \frac{C_1}{d_1}(V_{S2} - V_{S1}) \dots\dots\dots (4.18)$$

In Equation 4.18 C_1 and C_2 are the concentrations of unflocculated–primary and flocculated–flocs particles respectively, d_1 and d_2 are the cross sectional diameters of unflocculated and flocculated particles respectively, ρ_1 and ρ_2 are the densities of the primary and flocculated particles respectively, t is time, k_{ds} is a kinetic constant between 1 and 2 accounting for the increase in the rate of collision due to the turbulence in the flow, and V_{S1} and V_{S2} are the settling velocities of the primary particles and flocs respectively.

The cross sectional diameter is a physical characteristic of the floc that requires a sophisticated technique for its determination; technique that is not available in most wastewater treatment installations. In order to avoid this limitation, the determination of the cross sectional diameter is based on the equation proposed by Li and Ganczarczyk

(1987) that relates the settling velocity of the individual activated sludge floc to the cross sectional diameter. This equation was presented in Section 2.2.2 and is recapitulated below:

$$V_{si(mm/s)} = 0.35 + 1.77 d_{pi(mm)} \dots\dots\dots (2.12)$$

where V_{si} is the settling velocity of the i floc class, and d_{pi} is the cross sectional diameter of the i floc class. Table 4.1 presents an estimation of the cross sectional diameter for different types of flocs based on their settling velocities.

Table 4.1 Settling Velocities and Cross Sectional Diameters for Different Particles

Type of Particle		Settling Velocity (m/h)	Cross Sectional Diameter (microns)*
Settling Model	Flocculation Model		
Small Floc	Primary Particles	< 1.50	< 37
Medium Floc	Flocculated Particles	$1.5 \leq V_s < 6$	$37 \leq d < 740$
Large Floc	Flocculated Particles	≥ 6	≥ 740

* Cross sectional diameter estimation based on Equation 2.12

4.1.4.2 Transfer of Primary Particles to Flocs in the Flocculation Sub-Model

Section 4.1.3 divided the suspended solids in the mixture in three classes: (1) large flocs, (2) medium flocs, and (3) small flocs. Each class has a representative settling velocity range. The flocculation sub-model presented in the previous section proposed the aggregation of primary-unflocculated particles into flocs. In the general model, what are called “small flocs” for settling velocity purposes become the primary particles that are going to be flocculated into larger units using Equations 2.35 and 4.18. In this respect, the flocculation sub-model propose the conversion of “small flocs” into “medium” and

“large” flocs in a way proportional to the initial fractions in the incoming MLSS. At the same time, the model proposes the conversion of “medium flocs” into “large flocs”. If break up occurs, the flocculation model will promote the conversion of “large flocs” into “medium” and “small” flocs using a similar approach.

4.1.5 Temperature Sub-Model

Larsen (1977), Wells and LaLiberte (1998a, 1998b) and Kinnear (2004) found that the removal efficiency of settling tanks may vary over the year with a minimum during the winter season. McCorquodale (1976, 1977) showed that temperature differences in the influent of PST in the order of $\pm 0.2^{\circ}\text{C}$ induce strong density currents and may produce short circuiting. Zhou et al. (1994) presented a numerical model for PST that includes the simulation of the temperature stratification effects on the flow pattern. This model described the major features of a flow pattern affected by a warm influent, and that was described using a physical model by Godo (1990) and Godo and McCorquodale (1991).

These thermal density currents may be more important in PSTs than in SSTs (McCorquodale 1976, 1977, 1987). However as expressed by Ekama et al. (1997), for a realistic simulation in SST, it is necessary to consider the combination of thermal and suspended solids-induced density effects as well as heat exchange through the boundaries. So far, most SST models do not include temperature as a variable (McCorquodale, 2004); in fact no reference was found describing the modeling of temperature effects on SST.

This model intends to estimate the surface heat exchange by simulating the solar shortwave radiation, the atmospheric longwave radiation, and the water dependent terms (water longwave radiation, conduction and convection, and evaporation and condensation). The model incorporates a temperature transport equation, and in addition to the solids-induced density effects, the thermal density currents (due to influent temperature differences and surface heat exchange) are modelled in the tank.

In summary the temperature sub-model is formed by five components: (1) simulation of the influent wastewater temperature, (2) an advection-diffusion equation for the transport of temperature in the tank, (3) surface heat exchange, (4) effects of temperature on density and molecular viscosity, and (5) effects of temperature on the settling properties of the sludge. The treatment of these components is discussed in the following sections.

4.1.5.1 Influent Wastewater Temperature and Transport

The temperature of the incoming wastewater is treated in the model as an advective (open) boundary condition. The values of the influent temperature are incorporated in the tank, and are then transported using an advection-diffusion partial differential equation. In the model the heat exchange through solid boundaries is neglected, but the surface heat exchange is incorporated. The differential equation for modeling the transport of temperature is expressed as:

$$\frac{\partial \rho T}{\partial t} + \frac{\partial \rho u T}{\partial r} + \frac{\partial \rho v T}{\partial y} = \frac{1}{r} \frac{\partial \rho r \nu_{sr}}{\partial r} \frac{\partial T}{\partial r} + \frac{1}{r} \frac{\partial \rho r \nu_{sy}}{\partial y} \frac{\partial T}{\partial y} + SHE \dots\dots\dots (4.19)$$

where T is the temperature, ρ is the density of the mixture, ν_{sr} is the eddy diffusivity of suspended solids in the r - direction; ν_{sy} is eddy diffusivity of suspended solids in the y -direction; and SHE is the source term for the surface heat exchange. The SHE term is only applied to the surface cells.

The temperature is an intensive property (it is not dependent on size), while heat is an extensity quantity (it depends on the mass of the substance). For a volume of water V , the heat (H) is related to the temperature by

$$H = T \rho C_p V \dots\dots\dots (4.20)$$

The total surface heat flux (J_{she}) can be represented as

$$J_{she} = J_{sn} + J_{an} - (J_{br} + J_{cc} + J_{ec}) \dots \dots \dots (4.22)$$

where J_{sn} is the net solar shortwave radiation, J_{an} is the net atmospheric longwave radiation, J_{br} is the water longwave radiation, J_{cc} is the heat transfer due to conduction and convection, and J_{ec} is the heat transfer due to evaporation and condensation. The surface heat fluxes have units of $\text{Jm}^{-2}\text{d}^{-1}$.

Solar Shortwave Radiation (J_{sn})

The insolation I_o at outer limit of earth's atmosphere is given by (Eagleson, 1970)

$$I_o = W_{BO} \sin \alpha \dots \dots \dots (4.23)$$

where W_{BO} is a solar constant equal to $2.00 \text{ cal cm}^{-2} \text{ min}^{-1}$, and α is the angle of the radiation with the horizontal (this values is usually refereed as the solar altitude); which is given, from spherical trigonometry, by

$$\sin \alpha = \text{Max}[(\sin \delta \sin \Phi + \cos \delta \cos \Phi \cos \tau); 0] \dots \dots \dots (4.24)$$

where δ is the declination angle in degrees, Φ is the local latitude in degrees, and τ is the sun's hour angle in degrees. The maximum function is used in Equation 4.24 because negative values of α indicate that the sun is below the observer's true horizon.

The solar declination in degrees is defined by the following equation (Lee, 1978):

$$\delta = 23.45 \sin \left[\frac{2\pi(284 + JD)}{365} \right] \dots \dots \dots (4.25)$$

where JD is the Julian date. Figure 4.2 shows the variation of the declination angle and its cosine and sine with respect to the Julian date.

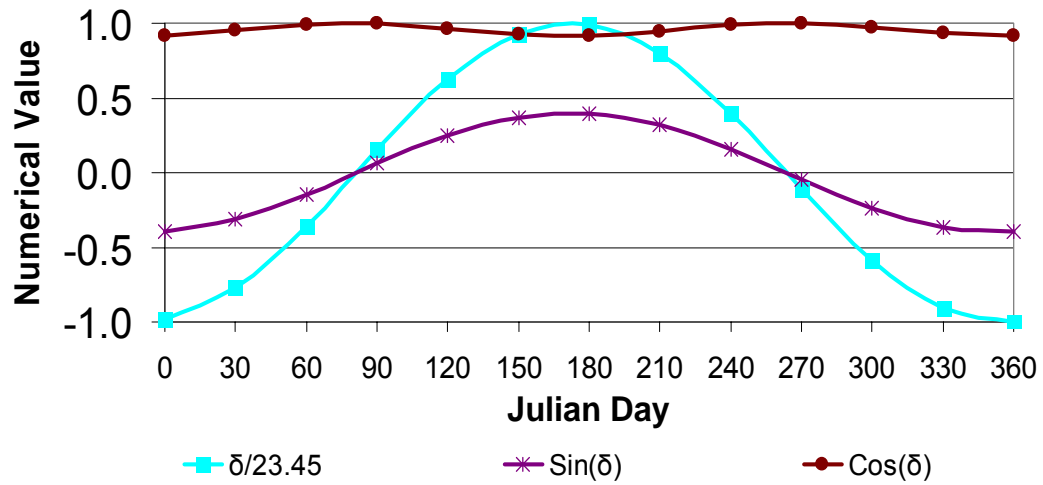


Figure 4.2 Declination Angle, Sine and Cosine of the Declination Angle

Figure 4.3 shows the variation of the cosine and sine functions for the local latitude.

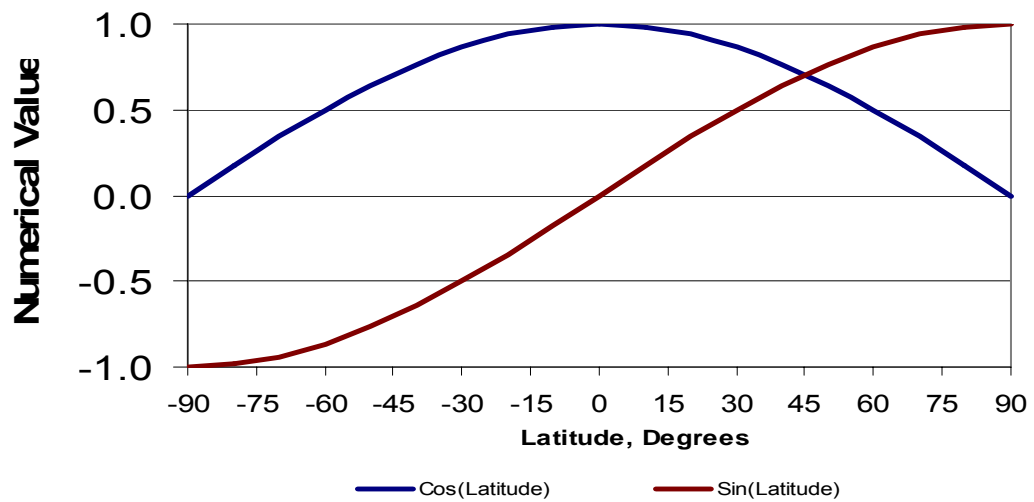


Figure 4.3 Local Latitude

The sun's hour angle changes with time during the day, according to the relationship:

$$\tau = \frac{180(t-12)}{12} \dots\dots\dots (4.26)$$

where τ is the sun's hour angle in degrees, and t is the hour of day in a 24 hour clock (e.g. $t = 10$ for 10:00 am, $t = 22$ for 10:00 pm). Figure 4.4 shows the variation of the cosine of the sun's hour angle with respect to the day's hour.

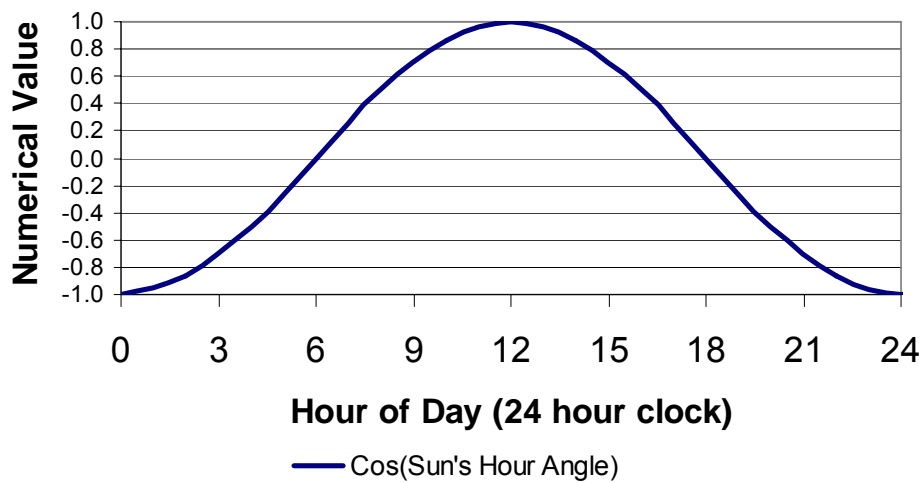


Figure 4.4 Cosine of the Sun's Hour Angle

Including the loss of the shortwave radiation due to molecular and particulate scattering and due to absorption (See Eagleson, 1970) the direct, cloudless sky insolation at earth's surface (I_c) can be found using the following expression:

$$I_c = I_o e^{(-n a_1 m)} \dots\dots\dots (4.27)$$

where n is the turbidity factor of the air, which varies from about 2.0 for clear mountain air to as high as 5 for smoggy urban areas; m is the relative thickness of air mass and is equal to the cosecant of solar altitude α ; and a_1 is a molecular scattering coefficient = $0.128 - 0.054 \log m$. In a cloudy sky the surface insolation will be further reduced due to

diffusion. Under these conditions the direct and diffuse insolation at earth's surface (I_s) may be estimated from:

$$I_s = I_c \left[1 - \left(0.82 - 2.4 \times 10^{-5} z \right) N \right] \dots\dots\dots (4.28)$$

where z is the cloud-base altitude in feet, and N is the fraction of the sky obscured by clouds (i.e., $N=1$ for an overcast sky).

The effective incoming shortwave radiation (I_e) is equal to the direct incident shortwave radiation (I_s) minus the reflected radiation by the surface. Based on the albedo of the surface this effective radiation can be estimated as

$$I_e = I_s (1 - A) \dots\dots\dots (4.29)$$

where A is the albedo or reflection coefficient. The albedo depends on the type of surface and the angle of the radiation with the horizontal (the solar altitude). Figure 4.5 presents the values the water's albedo based on the solar altitude.

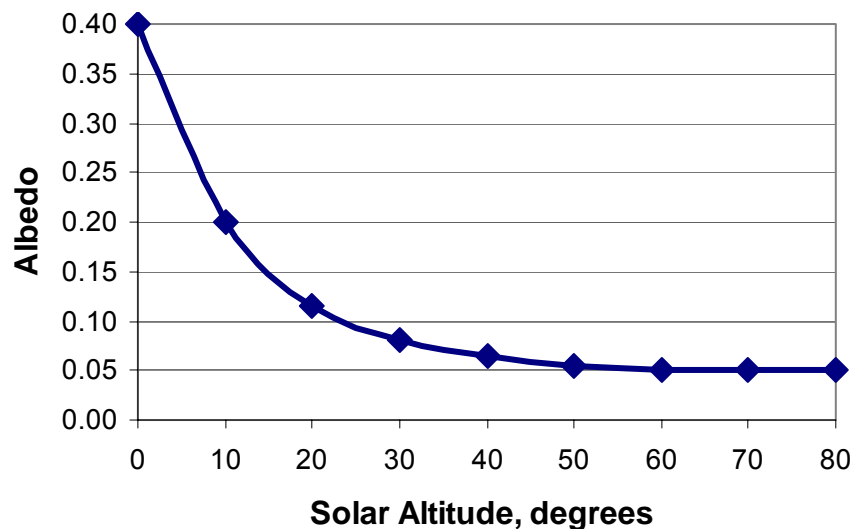


Figure 4.5 Albedo of the Water (Adapted from Eagleson 1970)

Atmospheric Longwave Radiation (J_{an})

The atmosphere by itself emits longwave radiation. This radiation may be represented as a modification of the Stefan-Boltzmann law (Chapra, 1997),

$$J_{an} = \sigma (T_{air} + 273)^4 \times Ea \times 0.97 \dots\dots\dots (4.30)$$

where σ = the Stefan-Boltzmann constant = $4.9 \times 10^{-3} \text{ J(m}^2 \text{ d } ^\circ\text{K}^4)^{-1}$

T_{air} = air temperature ($^\circ\text{C}$)

Ea = atmospheric emissivity = $[0.740 + 0.00653 e_{air}] [1 + (0.1662 - 0.0039 e_{air})N]$

e_{air} = air vapor pressure (mmHg) = $4.596e^{\frac{17.27Td}{237.3+Td}}$

Td = dew point temperature, $^\circ\text{C}$

Water Longwave Radiation (J_{br})

The water longwave effective back radiation can also be represented by the Stefan-Boltzmann law (Chapra, 1997),

$$J_{br} = \varepsilon \sigma (T_{sw} + 273)^4 \dots\dots\dots (4.31)$$

where T_{sw} = water surface temperature ($^\circ\text{C}$)

ε = emissivity of water = 0.97

Conduction and Convection (J_{cc})

Conduction is heat transfer from molecule to molecule (due to temperature gradients) and convection is the heat transfer due to the mass movements of the fluid. Conduction and convection occur at the water surface (air-water interface) and can be estimated from:

$$J_{cc} = c_1 f(U_w)(T_{sw} - T_{air}) \dots \dots \dots (4.32)$$

where c_1 = Bowen's coefficient ≈ 0.47 mmHg/°C

$$f(U_w) = 19.0 + 0.95U_w^2$$

U_w = wind speed measured in m/s at a height of 7 m above the water surface.

Evaporation and Condensation (J_{ec})

The heat loss due to evaporation or the heat gain due to condensation can be represented by Dalton's law (Chapra, 1997),

$$J_{ec} = f(U_w)(e_s - e_{air}) \dots \dots \dots (4.33)$$

where e_s = saturation vapor pressure (mmHg) = $4.596e^{\frac{17.27T_{sw}}{237.3+T_{sw}}}$

If $e_s > e_{air}$ heat will be lost from the clarifier by evaporation.

4.1.6 Scraper Sub-Model

Despite the fact that solids removal mechanisms are a major consideration in the design of SST, the function of the scraper in sludge removal is still under debate. Traditionally, it has been accredited with the function of transporting the settled sludge towards the hopper (e.g. Gunthert, 1984; Billmeier, 1988; Albertson and Okey, 1992); but, lately such function has been questioned. Some researches (e.g. Kinnear and Deines, 2001; De Clercq, 2003) have found out that typical scraper velocities are not conveying the solids, but are merely resuspending it. In this matter, McCorquodale (2004) believes more research is required in order to determine the effectiveness of scrapers. An own conclusion about this topic is expected to be obtained with this research.

Even though, the flow has been basically simulated in 2D, Equations 4.8 and 4.10 account for swirl effects. In this way, scrapper effects are included as an additional momentum source in the radial and the theta directions respectively.

r- direction

The scraper effect is introduced in the vorticity equation following the approach described below.

$$\frac{\tau_{rr}}{\rho} = \nu_{eff} \frac{\partial u}{\partial y} \Phi_t \approx -\nu_{eff} \frac{\partial \omega_{br}}{\partial t} \dots\dots\dots (4.34)$$

$$\frac{\tau_{rr}}{\rho} = \frac{\partial \frac{F_{scr}}{\rho}}{\partial A_p} \Phi_t \approx \frac{\frac{1}{2} C_d V_r |V_r| \partial A_{br}}{\partial A_p} \Phi_t \dots\dots\dots (4.35)$$

in which τ_{rr} is the shear stress exerted by the scraper in the radial direction, ρ is the viscosity of the mixture, ν_{eff} is the effective viscosity, Φ_t is a on-off function depending on time, ω_{br} is the additional vorticity generated by the scraper in the radial boundary,

F_{scr} is the force parallel to area A_p (one radian) induced by the scraper, C_d is the drag coefficient, V_r is the relative velocity of the blade (velocity of the blade minus the velocity of the mixture) and A_{br} is the area of the blade in the radial direction. Figures 4.6 and 4.7 show schematic representations of the areas and velocities.

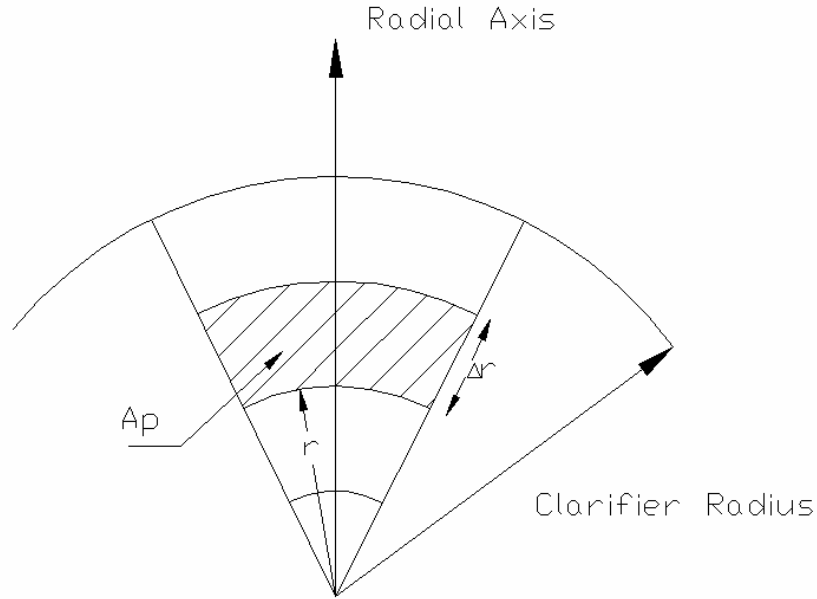


Figure 4.6 Scheme of Circular Settling Tank for Scraper Definition

∂A_p and ∂A_{br} are defined as (See Figures 4.6 and 4.7):

$$\partial A_p = \left(r + \frac{\Delta r}{2} \right) \Delta r \dots\dots\dots (4.36)$$

$$\partial A_{br} = Hb \Delta r \tan \theta \dots\dots\dots (4.37)$$

where r is the radius of the differential area, Δr is the dimension of the differential area in the r - direction, Hb is the height of the blade, and θ is the inclination angle of the blade.

In Equation 4.35 the term $V_r |V_r|$ accounts for the direction of the stress. As described before the relative velocity of the blade V_r is defined as the velocity of the blade in the

radial direction V_{br} minus the velocity of liquid-solids mixture u . V_{br} is a function of the tangential velocity V_t and the inclination angle of the blade.

$$V_{br} = V_t \cos \theta \sin \theta \dots\dots\dots (4.38)$$

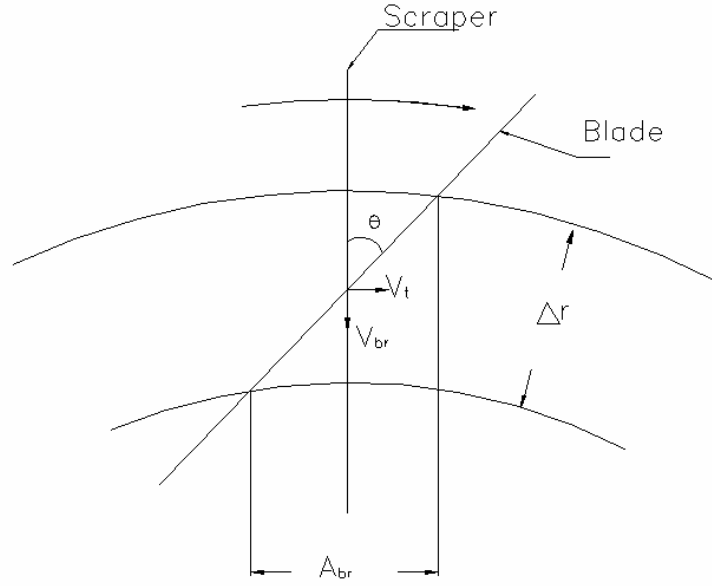


Figure 4.7 Scheme of Scraper, Tangential and Radial Velocity

The Φ_t function is set equal to 1 when the scraper is passing through the simulated sector (1 radian) and equal to 0 when is not.

$$\Phi_t = 0 \quad t_i \leq \left(\frac{2\pi}{N\Omega} i - \frac{1}{\Omega} \right), \quad i = 1, 2, \dots, n \quad (4.39)$$

$$\Phi_t = 1 \quad \left(\frac{2\pi}{N\Omega} i - \frac{1}{\Omega} \right) \leq t_i \leq \frac{2\pi}{N\Omega} i, \quad i = 1, 2, \dots, n$$

where t_i is the continuous time of the simulation, N is the number of arm, Ω is the scraper angular velocity (radians/time), and i is the cycle number; i can be obtained by adding 1 to the integer part of the ratio $t_i / \left(\frac{2\pi}{N\Omega} \right)$.

θ- direction

In the θ- direction the scraper is introduced as a circumferential source term in the momentum equation of v_θ .

$$\hat{S}_\theta = \frac{\partial \tau_{r\theta}}{\partial r} \dots\dots\dots (4.40)$$

where \hat{S}_θ is a circumferential momentum source term and $\tau_{r\theta}$ is the shear stress applied by the scraper in the θ- direction. The force applied by the scraper is averaged over the complete differential area (See Figure 4.8). The shear stress $\tau_{r\theta}$ is defined as:

$$\tau_{r\theta} = \frac{\partial F_\theta}{\partial A_{r\theta}} \approx \frac{\frac{1}{2} \rho N C_d V_{r\theta}^2 \partial A_{b\theta}}{\partial A_{r\theta}} \dots\dots\dots (4.41)$$

in which F_θ is the force applied by the scraper over the differential area $A_{r\theta}$, $V_{r\theta}$ is the relative velocity of the scraper in the θ- direction, $A_{b\theta}$ is the area of the blade in the θ- direction, and N is the number of arms. The differential areas are defined as:

$$\partial A_{b\theta} = Hb \Delta r \dots\dots\dots (4.42)$$

$$\partial A_{r\theta} = 2\pi r \Delta r \dots\dots\dots (4.43)$$

and, the relative velocity is

$$V_{r\theta} = (r\Omega - v_\theta) \dots\dots\dots (4.44)$$

where Hb is the height of the blade, r is the radius of the differential section, and Ω is the angular velocity of the blade.

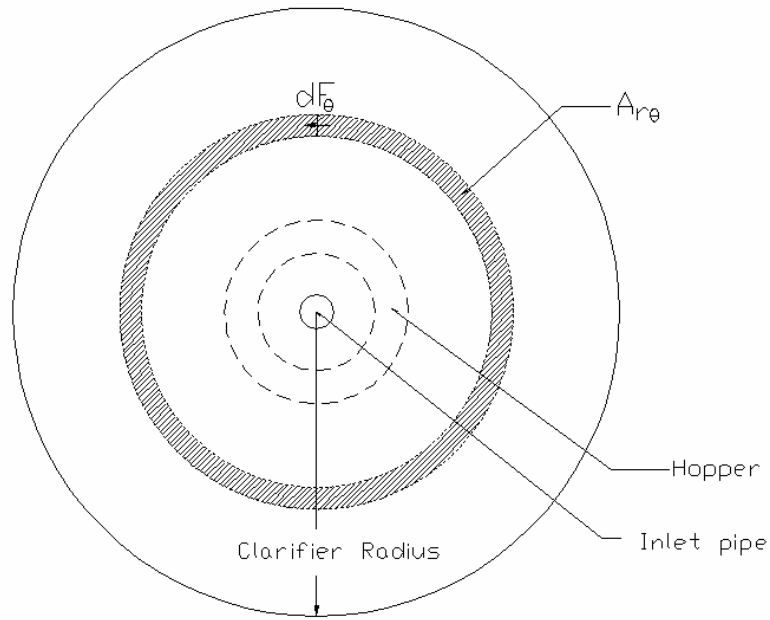


Figure 4.8 Scheme of Scraper Effect in the θ - direction

4.2 Numerical Methods

This research aims at developing its own code to solve the set of partial differential equations (PDEs) described in previous sections. This task requires the selection of the appropriated numerical techniques for solving such equations; this research does not pretend to be a comprehensive study in the subject but shows the application and limitations of the methods that have been selected. Hence, the numerical techniques are briefly discussed, and the reader is encouraged to look for details of these methods elsewhere (e.g. Patankar, 1980; Versteeg and Malalasekera, 1995; Gerges and McCorquodale, 1997; Burden and Faires, 2001; De Clercq, 2003; McCorquodale, 2004).

The numerical solution of PDEs is obtained in two major steps: 1) discretisation, which breaks the PDEs into a system of algebraic equations, and 2) solution of the system of discretised equations. There are three commonly applied discretisation techniques: the finite difference method (FDM), the finite element (FEM) and the finite volume method (FVM). The FDM replaces each of the derivatives in the differential equation with an

appropriate difference-quotient approximation, usually using a truncated Taylor series expansion (Burden and Faires, 2001). The FDM needs a structured grid. The FEM uses simple piecewise functions valid on elements to describe the local variations of unknown variables (Versteeg and Malalasekera, 1995). In general, the FEM is very flexible, unstructured grids can have high conformity with local refinement.

The FVM applies a formal integration of the governing equations over all the control volumes of the solution domain (finite number of cells). Even though variable cell shapes are possible, the FVM is usually limited to structured grids; making difficult to represent irregular boundaries. According to Versteeg and Malalasekera (1995) the control volume integration expresses the conservation of properties in each cell. In general, the FVM is locally and globally conservative, showing better conservation of mass in transport equations than the other two methods. Based on this property, the FVM is selected for solving the transport equations in this research.

In settling tank modeling the three aforementioned techniques have been used with success. For example, the FDM has been used in clarifiers models by Imam et al. (1983), Zhou and McCorquodale (1992a), and Zhou et al. (1992, 1994). Examples of FEM applications are found in Schamber and Larock (1981), DeVantier and Larock (1987), Lindeborg et al. (1996), Ji et al. (1996), and Kleine and Reddy 2002. While, Celik et al. (1985), Adams and Rodi (1990), Lyn and Zhang (1989), Lyn et al. (1992), Szalai et al. (1994), Gerges and McCorquodale (1997), Lakehal et al. (1999), and Armbruster et al. (2001) used different approaches of FVM to simulate the hydrodynamic of settling tanks. The FVM is also the based method in the commercial CFD codes PHOENICS and FLUENT.

In this study the vorticity and solids transport equations (Equations 4.8 and 4.11) are solved using the FVM, while the circumferential momentum equation (Equation 4.10) and the Poisson-type equations (Equations 4.7 and 4.17) are discretised using FDM techniques. Equations 4.7 and 4.17 are solved using a Hybrid Scheme, while the time-dependent equations are discretised using the hybrid differencing scheme in the spatial

variation and the Crank-Nicolson approach for the time variation. The selection of these schemes is briefly discussed next. For details of these numerical schemes the reader is referred to Versteeg and Malalasekera (1995), and Burden and Faires (2001).

Spatial Schemes

Although the FDM and FVM are different in approach, they use similar spatial and time discretisation schemes. The most used spatial differencing schemes are briefly discussed here. Based on Figure 4.9, assume a convection-diffusion process with horizontal flow in the positive direction, $u_w > 0$ and $u_e > 0$.

- The central differencing scheme: for a uniform grid, the central differencing scheme calculates the cell face value ϕ_e of property ϕ as the average of the adjacent nodal values of the property (ϕ_E and ϕ_P):

$$\phi_e = (\phi_E + \phi_P)/2 \text{ and } \phi_w = (\phi_W + \phi_P)/2 \quad (4.45)$$

- The upwind difference scheme: the upwind differencing scheme takes into account the direction of the flow when determining the value of the cell face:

$$\phi_e = \phi_P \text{ and } \phi_w = \phi_W \quad (4.46)$$

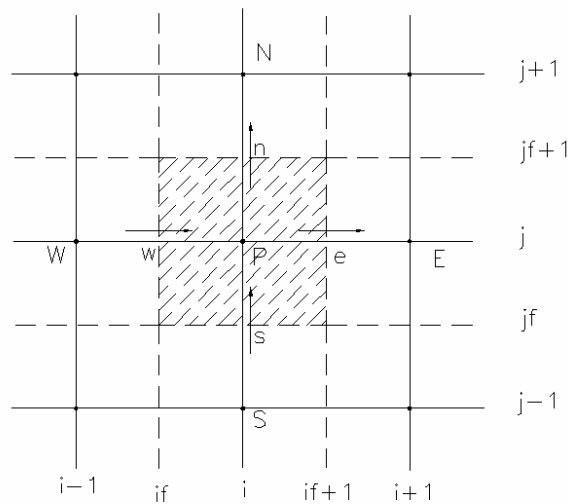


Figure 4.9 Scalar Control Volume Used for Discretisation Schemes

The central differencing scheme is second order accurate according to the Taylor series truncation error; it is conservative and generally stable for small Peclet Numbers (Pe). The central differencing scheme does not identify the direction of the flow, it does not account for transportiveness of the property at high Pe. Meanwhile, the upwind differencing scheme does take into account the flow direction, but the accuracy is only first order (it is based on the backward differencing formula). The scheme is conservative and stable, but as expressed by Versteeg and Malalasekera (1995) a major drawback of the scheme is that it introduces numerical errors when the flow is not aligned with the grid lines. This error is commonly referred as numerical or false diffusion.

- The hybrid differencing scheme: the hybrid differencing scheme combines the favourable properties of the central and upwind differencing schemes. It evaluates the Peclet number at the face of the control volume. For example, at the west face

$$Pe = \frac{F_w}{D_w} = \frac{(\rho u)_w}{\nu_{sr-w} \rho / \Delta r} \dots\dots\dots (4.47)$$

where F_w and D_w are the convective mass flux per unit area and diffusion conductance at the west face, ν_{sr-w} is the eddy diffusivity in the r- direction evaluated at the west face and Δr is the width of the cell. Based on this evaluation, the hybrid scheme employs the central differencing scheme for small Peclet numbers ($Pe < 2$), and the upwind scheme at high Peclet number ($Pe \geq 2$), accounting for transportiveness under this condition. The scheme is totally conservative and highly stable, and also, since the coefficients involved in the scheme are always positive, it is unconditionally bounded which assures convergence.

Logically, a natural concern when using a hybrid differencing scheme is the appearance on the solution of numerical diffusion. Some researches have expressed their concern about using this scheme in settling tank modelling and have compared its performance to

higher order methods. Adams and Rodi (1990) presented a comparison on FTC predicted respectively by the hybrid and the QUICK schemes with experimental data; they found that the hybrid scheme underpredicted the experimental peak of the FTC by about 5%, while the QUICK scheme overpredicted the peak by about 15%. McCorquodale and Zhou (1993) aware that the hybrid schemes tends to be numerically diffusive, tested the grid dependence using three different grids (12 x 24, 18 x 34 and 24 x 42) and did not found significant difference in the flow pattern for all three grids. Zhou et al. (1994) reported that in a previous study, when comparing the hybrid scheme with a high-order accuracy numerical method, i.e. semi-implicit skew upwind method (SISUM); they did not found a significant difference for the case of density stratified flow. Gerges and McCorquodale (1997) compared the hybrid scheme with the skew third-order upwinding scheme (STOUS) and concluded that hybrid suffers from numerical diffusion. In this study, where no density effects were included, the STOUS scheme overpredicted the peak of the FTC by 20%.

In resume, in the case of density-driven flow like in SST, where the flow is mainly orthogonal to the grid; the use of hybrid scheme does not seem to be limited by false diffusion errors. However, since the appearance of this error can be reduced by using a finer grid, a grid dependence test should be carried out to determine such effects.

Time-Variation Schemes

In the case of the time-dependent equations, the finite volume integration over a control volume must be augmented with a further integration over a finite time step. Backward, central or forward differencing schemes in time may be used. When the old time levels of the variables are used to find the new time levels (backward differencing), the resulting scheme is called explicit. When only unknown variables at the new time levels are used on both sides of the equation, the scheme is called fully implicit. Both, explicit and fully implicit are only first order accurate. When central differencing is applied, the new time level variable at the node is found using a weighting average (weighting coefficient = $\frac{1}{2}$) of old time and new time level surrounding variables, it is called the

Crank-Nicolson scheme. Since it is based on central differencing, the Crank-Nicolson scheme is second order accurate in time.

Iterative Techniques for Solving the Systems of Discretised Equations

The schemes presented in the previous section result in a system of linear algebraic equations which needs to be solved. There are two major groups of solution techniques for solving linear algebraic systems, i.e. direct methods and indirect or iterative methods. Direct methods are based on a finite number of arithmetic operations leading to the exact solution of a system of n equations with n unknowns. Iterative methods start with an initial approximation and repeat a relative simple algorithm leading to converge after a finite number of repetitions. In the cases of CFD applications the number of arithmetic operations is very large, and usually iterative methods are more efficient in terms of both computer storage and computation (Burden and Faires, 1991; Versteeg and Malalasekera, 1995). The traditional Gauss-Seidel iterative technique and the accelerate-convergence over-relaxation method are applied in this study.

4.3 Boundary Conditions

4.3.1 Stream Function Boundary Conditions

Figure 4.10 shows the type of stream function boundary conditions that can be prescribed for the settling tank. These boundary conditions can be steady or unsteady state conditions. The boundary conditions of the stream function define the flow entering and leaving the settling tank, i.e. influent flow rate (Q_{in}), effluent flow rate (Q_{out}), and recirculation flow rate (Q_{ras}). The convention for prescribing the stream function is positive increasing in the counter-clockwise direction and outward normal flow is positive. The “Mask” presented in Figure 4.10 defines the solid boundary conditions in the internal part of the tank. A value of the Mask equal to 0 is assigned to the cells defining the solid boundaries. The value of wz that is presented in Figure 4.10 is set equal to 2π in the case of radial coordinates and is equal to the width of the tank in Cartesian coordinates.

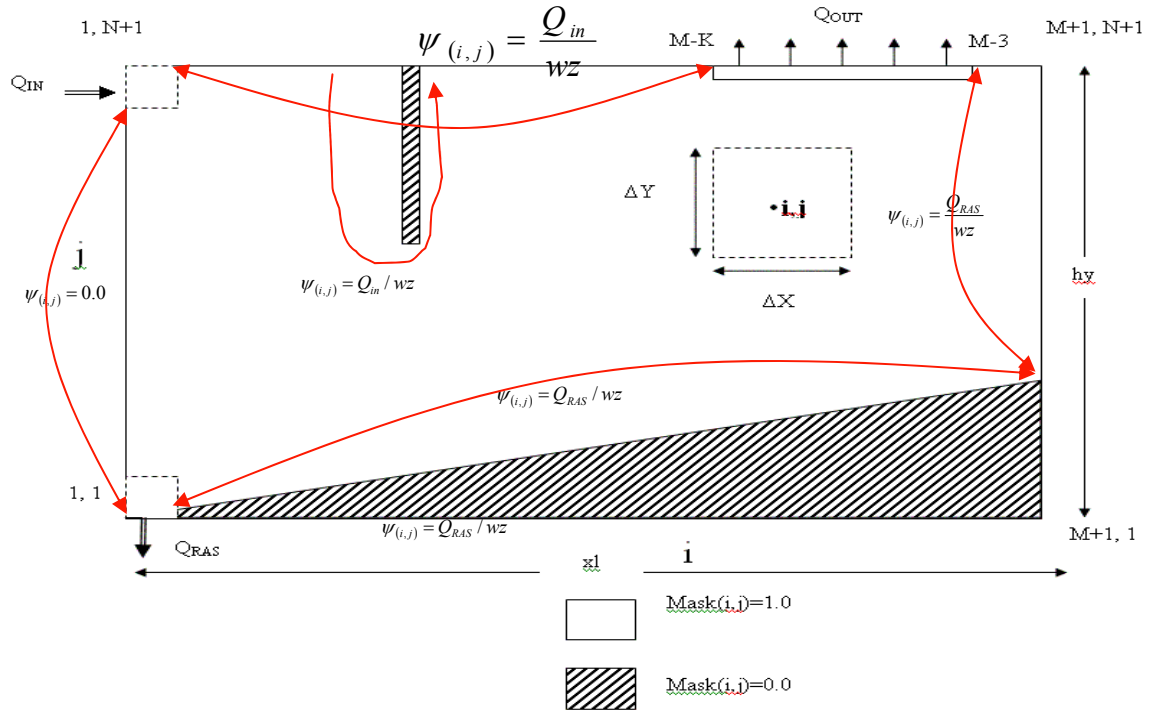


Figure 4.10 Stream Function Boundary Conditions

The vorticity boundary conditions are shown in Figure 4.11. These boundary conditions can be steady or unsteady state conditions and typically respond to the interior solution. The convention for prescribing the vorticity is positive increasing in the counter-clockwise direction. The boundary condition at the bottom is modified by the shear applied by the scraper. At the surface is assigned a vorticity equal to 0. As in the case of solids the vorticity is removed through the open boundaries like launder and hopper.

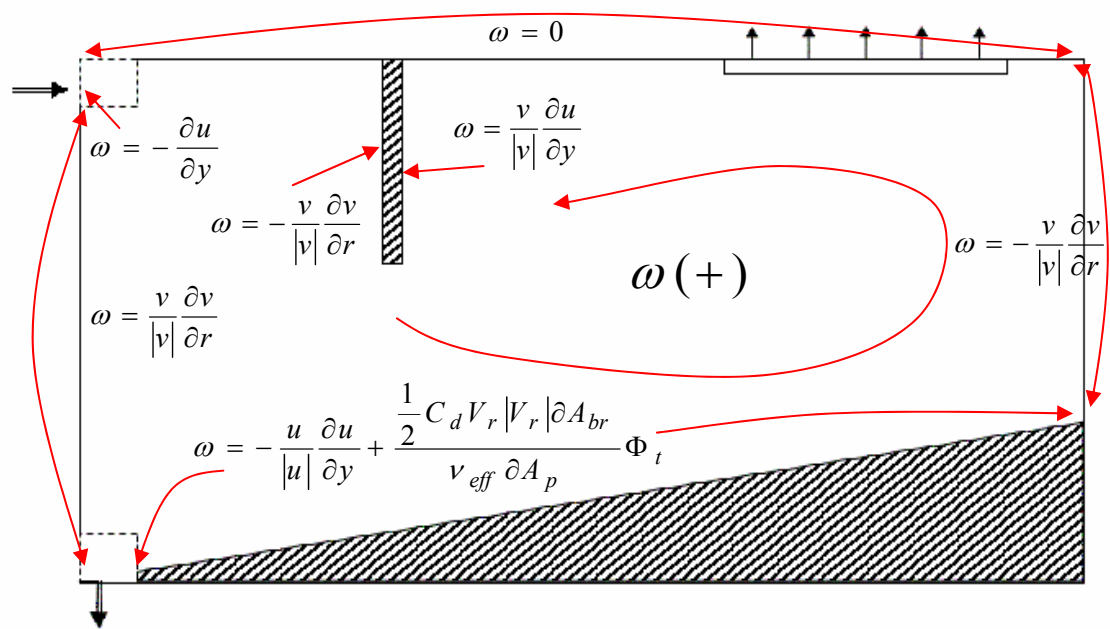


Figure 4.11 Vorticity Boundary Conditions

4.3.3 Solids Boundary Conditions

The solids boundary conditions are shown in Figure 4.12. These boundary conditions can be steady or unsteady state conditions. The convention for prescribing the solids flux is positive in the outward normal direction. The advective flux is defined by $F_r = u\rho_r r\Delta y$ and $F_y = v\rho_y r\Delta r$. The diffusive flux is defined by $D_y = \frac{A_y \rho_y v_{sy}}{2\pi\Delta y}$ and $D_r = \frac{A_r \rho_r v_{sr}}{2\pi\Delta r}$.

The advective and diffusive fluxes are defined equal to 0 at the solid boundaries and also at the surface, except for the case when an inboard launder is simulated.

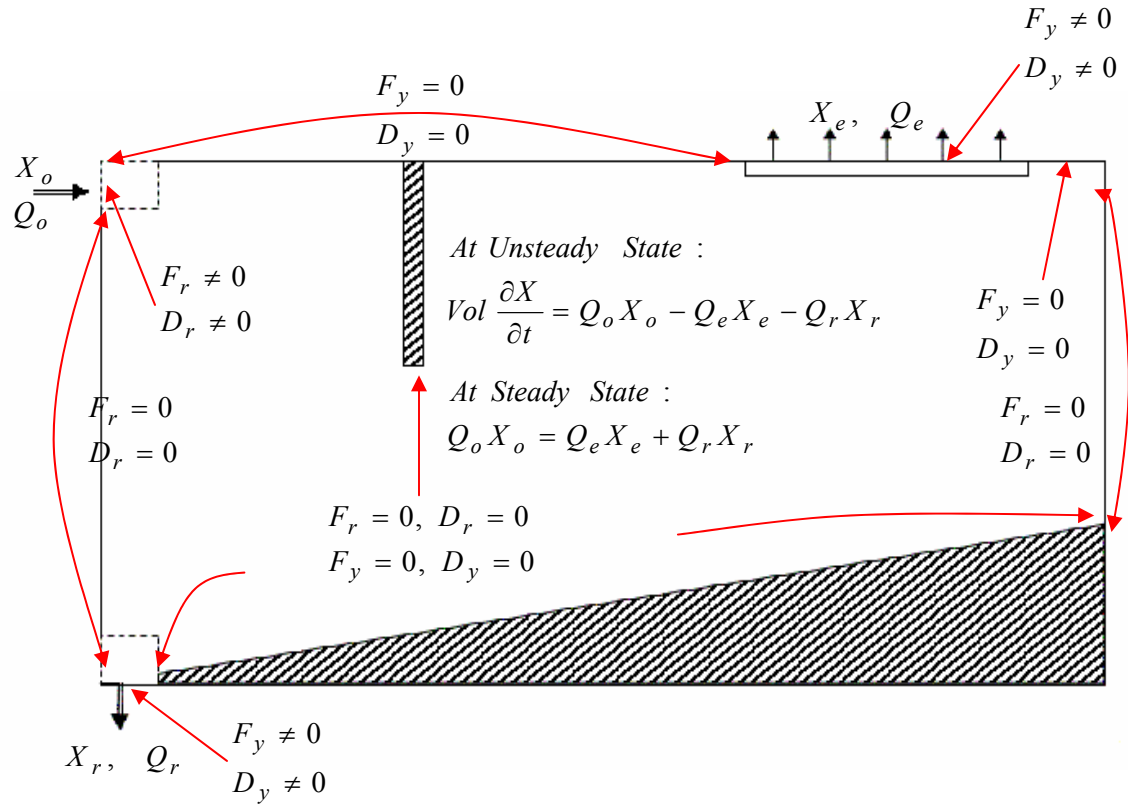


Figure 4.12 Solids Boundary Conditions

4.3.4 Thermal Boundary Conditions

Figure 4.13 summarizes the boundary conditions that were applied to the water temperature variable. The atmospheric exchange was treated as diurnal and seasonal with user specified latitude, air minimum and maximum temperatures, dew point temperature and cloud cover. The parameters for the surface heat exchange were defined in Section 4.1.5.

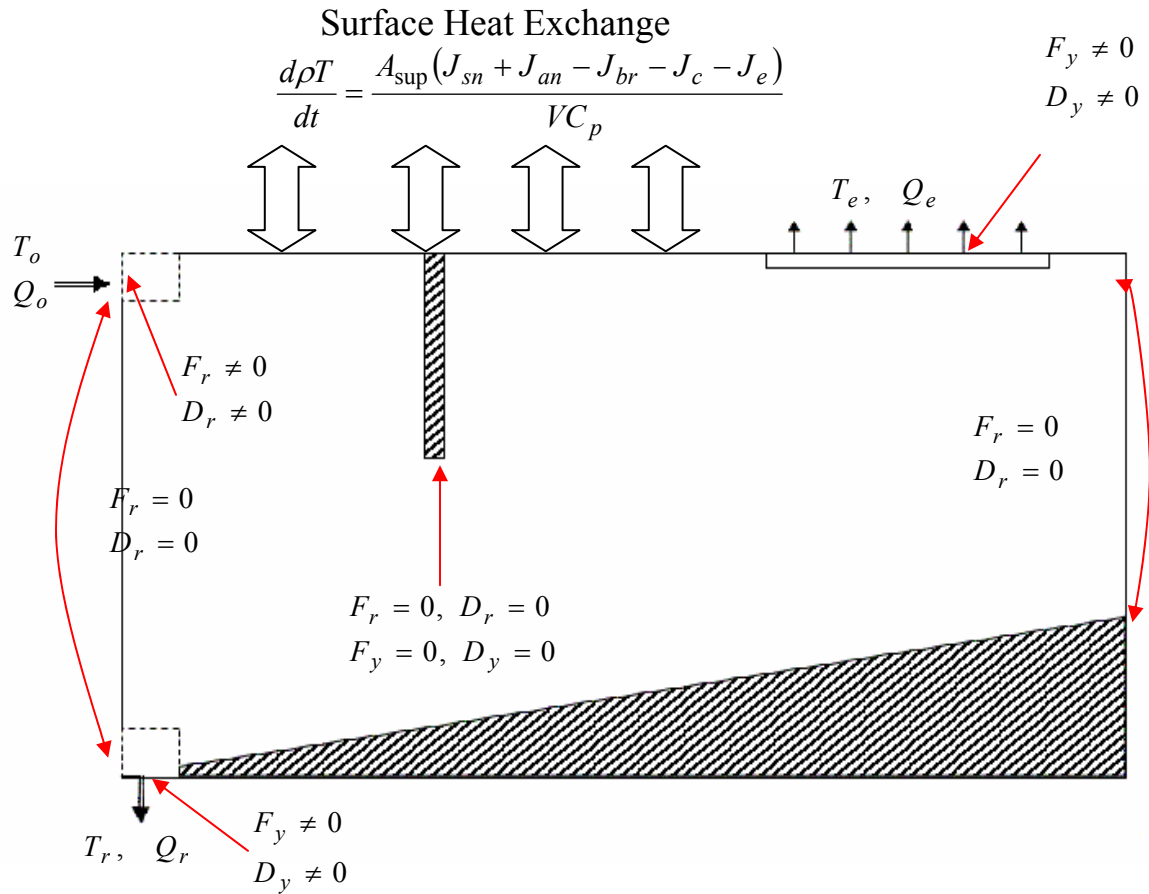


Figure 4.13 Heat Exchange Boundary Conditions

Specific Heat Coefficient: C_p Solar Shortwave Radiation: $J_{\text{sn}} = f(\text{Solar altitude, scattering and absorption, reflection, shading})$; Atmospheric Longwave Radiation: J_{an} ; Water Longwave Radiation: J_{br} ; Conduction and Convection: J_{c} ; Evaporation and Condensation: J_{e} .

4.3.5 Swirl Boundary Conditions

Figure 4.14 gives the boundary conditions that were applied to the θ -velocity. No shear was assumed at the free surface and no slip was applied at the end wall and the center well or other internal solid baffles. The inlet has an option of including a deflector. Figure 4.14 shows the equations used in the calculation of the θ - and radial components of the velocity, i.e. v_θ and u respectively. In these equations Q_o is the inlet volumetric flow rate and A_{inlet} is the area of the inlet. The rake or suction arm introduces a local velocity. The development of this relationship was presented in Section 4.1.6.

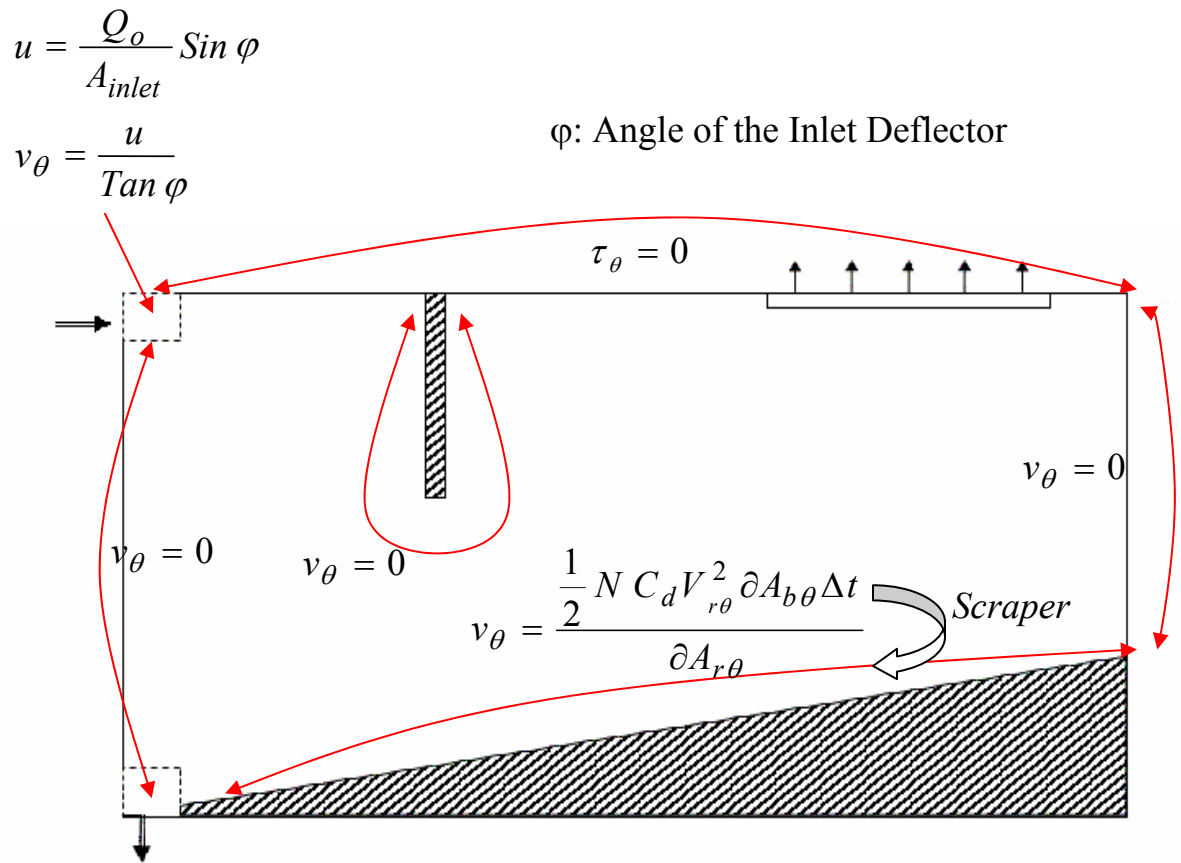


Figure 4.14 Swirl Boundary Conditions

4.3.6 Turbulence Model Boundary Conditions

A simplified mixing length based turbulence model is used in the study. The boundary conditions for the mixing length are shown in Figure 4.15. Three constants are used in the definition of the turbulence model and its boundary conditions, i.e. K_1 , K_2 and K_{lm} . K_1 is defined equal to the roughness of the solid surface in units of length, K_2 is a constant approximately equal to 1% of K_1 which is used at the water surface boundary, and K_{lm} is a calibration constant which was presented in Section 4.1.2.

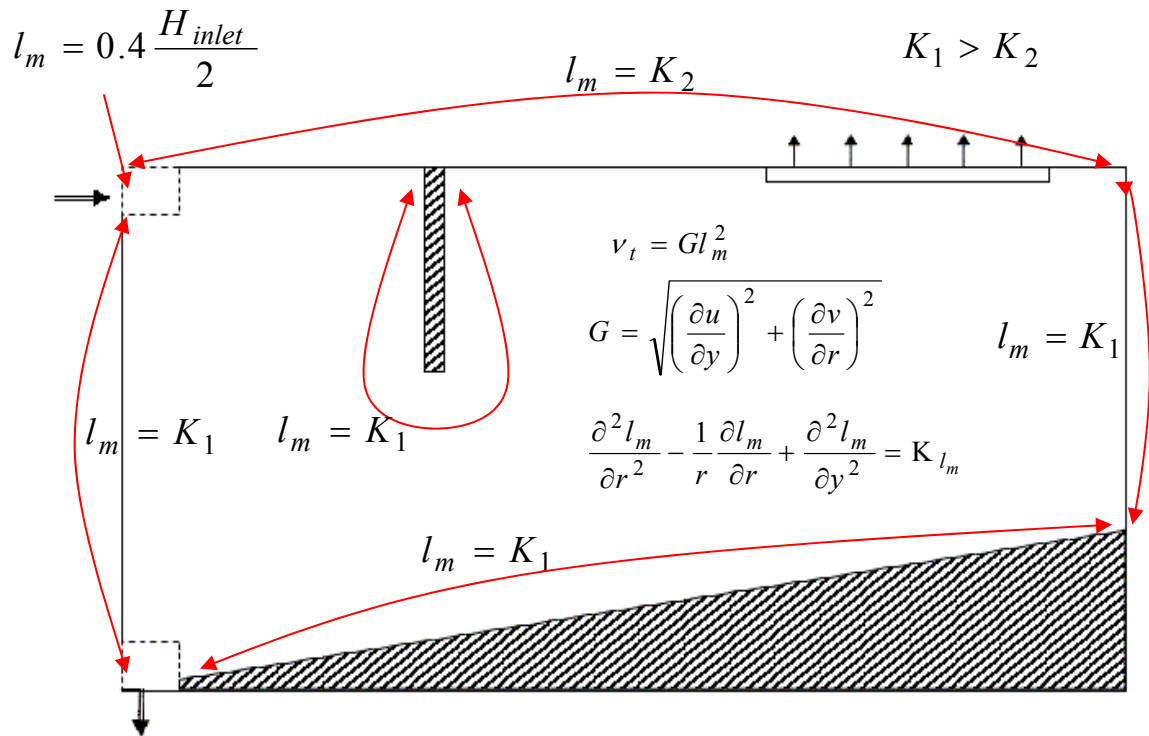


Figure 4.15 Boundary Conditions for the Simplified Turbulence Model

CHAPTER 5

5. MODEL CALIBRATION, TESTING AND VALIDATION

The Quasi 3D mathematical model developed in the previous two sections, was coded in FORTRAN and calibrated using field data from a full-scale plant. As discussed next, the model is mass conservative and realistically reproduces the effluent and recirculation concentrations, and the main circulation patterns in clarifiers. Appendix J presents the FORTRAN source code that has been written during the development of this dissertation, and Appendix K shows the input files used for running the source code. At this point, the capabilities of the model include:

- Modeling of circular clarifiers. Inlet, settling and outlet zones.
- Steady and unsteady conditions for mass and hydraulic loadings.
- Simulation of Center Well, Canopy, Mid-Tank (Crosby) Baffle and Peripheral (Stamford) Baffle; positive or negative slope; inboard or outboard launder and simple inlet arrangements. See Figure 5.1.
- Simulation of the sludge removal systems: hopper or suction, constant or proportional recirculation flow rate and scraper simulation.
- Simulation of the total dissolved solids (TDS) density currents.
- Simulation of the dynamic inventory of the sludge blanket.

For post-processing the data, the computer code uses the commercial plotting software called TECPLOT. This software helps to explore the output data of the *Q3D-Clarifier Software* and to produce two dimensional graphical representations of the information. With TECPLOT it is possible to produce animations and movies of the clarifier data. The visualization tools include:

- Grid display
- General geometry of the tank including baffles
- Suspended solids concentrations
- Velocity vectors
- Dye concentrations

- Stream function values
- Other parameters like vorticity, gradients and viscosity

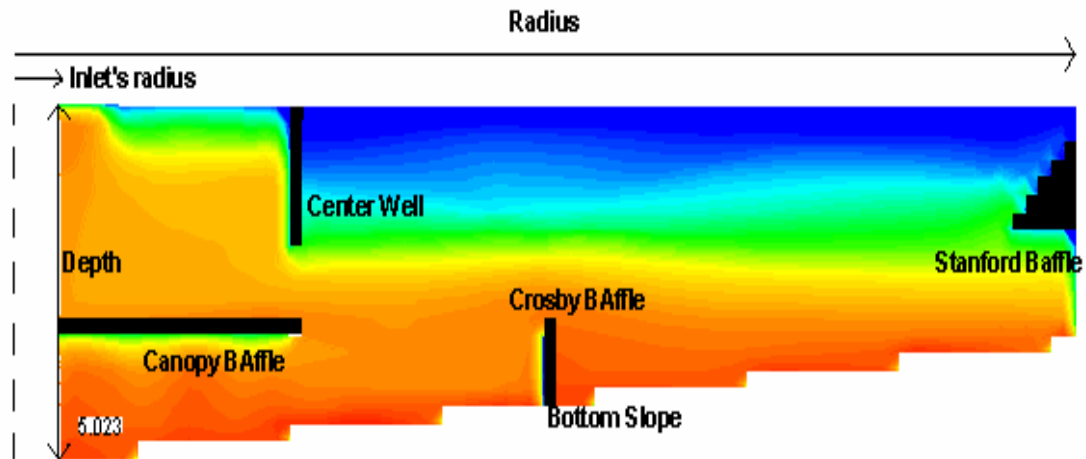


Figure 5.1 Geometry Capabilities of the Model

5.1 Calibration of the model. Case Study: Marrero WWTP.

The calibration process involved adapting the model to predict the results of a specific facility. During the calibration process actual field data was taken at a specific full-scale facility and the model prediction was adjusted by changing the diffusion and advection coefficients that are used in the transport equations.

The calibration process was carried out at The Marrero Wastewater Treatment Plant (Marrero WWTP) located at 6250 Lapalco Boulevard, Marrero, LA. The Marrero Plant is a municipal trickling filter/solids contact WWTP with an average flow of about 9.2 MGD (Appendix A presents a general description of the plant); it has two secondary settling tanks, which dimensions and main operating characteristics are shown in Table 5.1

Table 5.1 Dimensions and Operating Characteristics of the SST at the Marrero WWTP
(After Retana, 1999)

ITEM	VALUE
Number of Units	2
Flow rate through each unit	4.6 MGD
Diameter	115 ft
Depth	14 ft
Center Well Diameter	29.5 ft
Center Well Depth	8.4 ft
Bottom Slope	8.33%
Weir Length	361.28 ft
Total surface area	10386.9 ft ²
Net surface area	9675 ft ²
Surface overflow rate	475.45 gpd/ft ²
Hydraulic retention time	5.68 h
Weir overflow rate	12732.4 gpd/ft
Return sludge flow rate	1944000 gal/day
Sludge wastage	16617.6 gal/day
Sludge TSS	2800 mg/L
Solids loading rate	0.05 lb TSS/ft ² .h
Sludge blanket depth	10 in

For the calibration process a 24 hours period with more or less constant flow rate was selected. During the selected period the following parameters were recorded:

- Settling properties of the sludge
- Flocculation parameters

- MLSS in the contact chamber, measured as total suspended solids concentration (TSS)
- Effluent suspended solids concentration (ESS) in the clarifier, measured as TSS
- Recirculation suspended solids concentration (RAS SS)
- Plant flow rate (Q_p) and recirculation ratio (RAS)
- Sludge blanket height

5.1.1 Calibration of the Settling Sub-Model

The settling parameters of the settling sub-model were determined using sludge samples taken from the contact chamber of the Marrero WWTP (this sample is the MLSS) and from the hopper of the secondary clarifier (this sample is the RAS). The hindered (X_h) and discrete (X_d) threshold were identified by performing successive dilution to the MLSS sample. Table 5.2 indicates the values of the TSS concentration for the MLSS, RAS, X_h and X_d .

Table 5.2 MLSS, RAS and Threshold Concentration

MLSS Concentration (mg/L)	RAS Concentration (mg/L)	Hindered Threshold (mg/L)	Discrete Threshold (mg/L)
2800	8500	1200	600

The calibration of the settling sub-model involves determining the individual floc discrete settling velocities and fractions, the concentration of the non-settleable component, and the settling constants used in the exponential models for hindered settling and compression rate. These determinations are presented in the next sections.

5.1.1.1 Discrete Settling

As discussed in Chapter 3 the discrete settling characteristics of the sludge are determined using a sludge sample with a concentration equal (or lesser than) to the discrete threshold concentration. The sample is divided into three settling fractions and a non-settleable portion. The three settling fractions are referred as: (1) large flocs, (2) medium flocs, and (3) small flocs. This division is based on size and individual floc settling velocities. Table 3.2 presents the range of settling velocities and cross sectional diameter for the division.

The settling velocities of large and medium flocs are found by direct measurement in a column batch test using a light source, a scale and a stopwatch (See Section 3.1.2.1). The results of the individual measurements of these two types of flocs are reported in Tables 5.3 and 5.4

Table 5.3 Discrete Settling Velocities of Large Flocs

Large Flocs							
Floc No.	H (cm)	Time(s)	V(m/h)	Floc No.	H (cm)	Time(s)	V(m/h)
1	3	10.5	10.3	11	3	14.0	7.7
2	3	14.2	7.6	12	3	12.3	8.8
3	3	9.3	11.6	13	3	14.3	7.6
4	3	14.3	7.6	14	3	9.5	11.4
5	3	11.3	9.6	15	3	9.9	10.9
6	3	15.5	7.0	16	3	10.4	10.3
7	3	15.0	7.2	17	3	6.5	16.6
8	3	6.8	15.9	18	3	8.1	13.4
9	3	7.7	14.0	19	3	6.5	16.6
10	3	11.6	9.3	20	3	9.1	11.9
Average Large Flocs Settling Velocity:				10.8 m/h			
Standard Deviation:				3.16			
Maximum:				16.6 m/h			
Minimum:				7.0 m/h			

Table 5.4 Discrete Settling Velocities of Medium Flocs

Medium Flocs							
Floc No.	H (cm)	Time(s)	V(m/h)	Floc No.	H (cm)	Time(s)	V(m/h)
1	3	26.5	4.1	11	3	25	4.3
2	3	47.3	2.3	12	3	30.2	3.6
3	3	46	2.3	13	3	29	3.7
4	3	45	2.4	14	3	26	4.2
5	3	30	3.6	15	3	30	3.6
6	3	47.9	2.3	16	3	29	3.7
7	3	46.5	2.3	17	3	45	2.4
8	3	49	2.2	18	3	38	2.8
9	3	28	3.9	19	3	58	1.9
10	3	40.7	2.7	20	3	40	2.7
Average Large Flocs Settling Velocity:				3.0 m/h			
Standard Deviation:				0.79			
Maximum:				4.3 m/h			
Minimum:				1.9 m/h			

As described in Chapter 3 the settling velocity of small flocs is obtained using a procedure based on the concentration profile of settling batch columns at two different times and using Equation 3.4. Figure 3.2 presents a sketch of the settling column at the two different times.

$$V_{sm} \approx \frac{(M_x - M_{xx})}{A_c \Delta t \bar{C}_{x-xx}} C_f \dots\dots\dots (3.4)$$

where C_f is a conversion factor. The results of the test for the determination of the small floc settling velocities, conducted during the calibration day, are presented in Table 5.5

Table 5.5 Data for the Calculation of the Discrete Settling Velocity of Small Flocs

Area of the Settling Column (Ac)	71.4 cm ²
Time 1 (t ₁)	4 min
Time 2 (t ₂)	13 min
Mass of Solids in the upper-mid portion of the settling column at t ₁ (M _x)	131.45 mg
Mass of Solids in the upper-mid portion of the settling column at t ₂ (M _{xx})	57.48 mg
TSS Concentration at the middle of the column at t ₁ (C _x)	141 mg/L
TSS Concentration at the middle of the column at t ₂ (C _{xx})	61 mg/L
Conversion factor for the units presented in this table (C _f)	600
Small Floc Settling Velocity (Equation 3.4)	0.68 m/h

Determination of the Discrete Settling Fractions

The procedure for determining the settling fractions was presented in Chapter 3. According to this procedure the dilute concentration ($C_d \leq \text{Threshold for discrete particle settling}$) is divided in four components: three settling fractions and a non-settleable portion. The non-settleable concentration is estimated as the FSS of the sample (Appendix B presents the required procedure for the determination of the FSS); this value was found to be 5.0 mg/L.

The three settling fractions are calculated using the procedure described in Section 3.1.2.2 and using Equation 3.5 to 3.10 These equations are recapitulated below.

$$C_1 + C_2 + C_3 + FSS = C_d \dots\dots\dots (3.5)$$

$$f_i = \frac{C_i}{C_d - FSS}; \quad i = 1, 2, 3 \dots\dots\dots (3.7)$$

$$A_c (V_{S1} \Delta t_{1-1} C_1 + V_{S2} \Delta t_{1-2} C_2 + V_{S3} \Delta t_{1-3} C_3) = M_1 \dots\dots\dots (3.8)$$

$$\Delta t_{j-i} = \min \left(t_j - \text{Lag time}, \frac{h_j}{V_{si}} \right) \dots\dots\dots (3.9)$$

$$A_c (V_{S1} \Delta t_{2-1} C_1 + V_{S2} \Delta t_{2-2} C_2 + V_{S3} \Delta t_{2-3} C_3) = M_2 \dots\dots\dots (3.10)$$

The information required for the determination of the fractions (including the results of the batch column tests) is presented in Table 5.6

Table 5.6 Data for the Calculation of the Discrete Settling Fractions

Area of the settling column (Ac)			71.4 cm ²
Dilute Concentration (Cd)			600 mg/L
FSS of the sample			5 mg/L
Lag Time			1.5 min
Time 1 (t ₁)			4 min
Time 2 (t ₂)			13 min
Distance from the water surface to the top of the sludge blanket at t ₁ (h ₁)			25.5 cm
Distance from the water surface to the top of the sludge blanket at t ₂ (h ₂)			25.4 cm
Mass of Solids in the sludge blanket of the settling column at t ₁ (M ₁)			939.70 mg
Mass of Solids in the sludge blanket of the settling column at t ₂ (M ₂)			1077.64 mg
Fraction i	V _{si} (m/h)	Δtime _{1-i} (min)	Δtime _{2-i} (min)
1	10.8	1.42	1.41
2	3	2.50	5.08
3	0.68	2.50	11.50

Table 5.7 summarizes the discrete settling velocities and fractions obtained during the calibration period.

Table 5.7 Discrete Settling Velocities and Fractions

Type of Particle		Settling Velocity V_{si} (m/h)*	Concentration C_i (mg/L)	Fraction f_i
Description	Class (i)			
Big Floc	1	10.80	441.5	0.742
Medium Floc	2	3.00	151.9	0.255
Small Floc	3	0.68	1.6	0.003
Non-Settleable	4	0.00	5.0	----
		Total =	600.0	1.000

*The settling velocities presented in this table were measured at 26.5 °C

5.1.1.2 Zone and Compression Settling

The zone settling velocity and the compression rate are both simulated in the model using exponential equations similar to the Vesilind's equation. Each individual model has two settling parameter: V_o and k_l for zone settling and V_c and k_c for the compression rate.

$$V_s = V_o e^{-k_l X} \quad \text{Hindered Threshold } (Xh) < X \leq \text{Compression Threshold}$$

$$V_s = V_c e^{-k_c X} \quad X > \text{Compression Threshold}$$

The two parameters of the exponential equations are determined in a batch settling test. The settling velocity is measured as the maximum slope of the curve solids-liquid interface depth versus time obtained during the test. An example of such curve is presented in Figure 5.2.

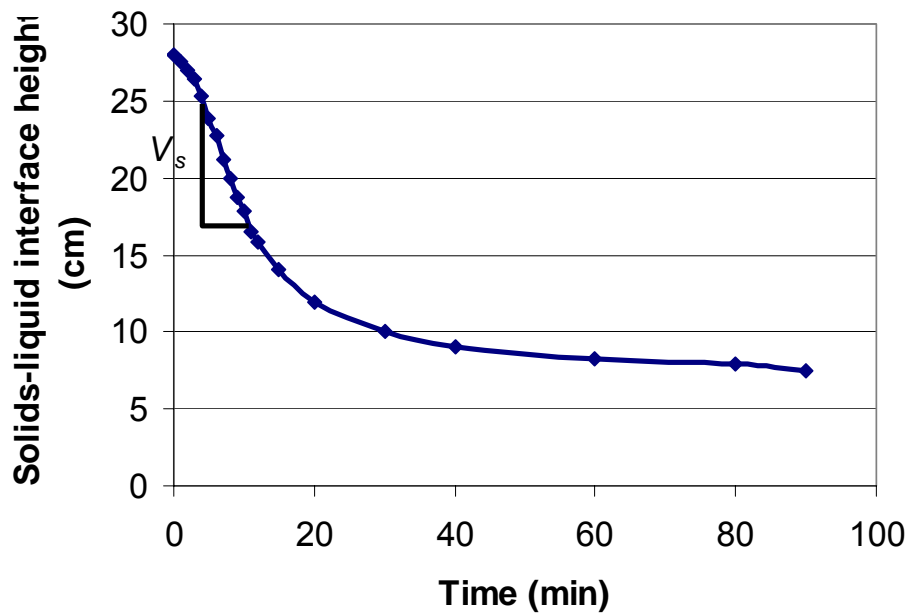


Figure 5.2 Solids-Liquid Interface vs. Time in a Batch Settling Test

The batch settling test was performed using a 2 liter Stiro-settlometer. This laboratory equipment is manufactured by MCR Process and Technology; it is equipped with a stirring mechanism consisting of two thin rods extended the length of the column and positioned within two rod diameters of the cylinder wall, the rods rotate at about 1 rpm. The stirring mechanism avoids any possible wall effect as recommended by Standard Method 2710 E and 2710 D for the evaluation of zone settling velocity and sludge volume index respectively.

Zone Settling

In order to obtain the settling velocity as a function of solids concentration, the batch settling test was conducted using five different concentrations. From an initial MLSS concentration of 2800 mg/L, taken from the contact chamber, two dilutions and two composite samples were obtained. The dilutions were obtained by mixing the MLSS with effluent from the secondary clarifier, and the thickened samples were obtained by decanting the supernatant from a previous batch test. The resulting settling velocities

were subsequently utilized to estimate the settling parameter V_o and k_l from the exponential equation. Table 5.8 shows the zone settling velocity measured for the five samples (these samples are identified as A, B, C, D and E) and Figure 5.3 shows the exponential fitting for the data set. The fitted values of V_o and k_l are 10.54 m/h and 0.40 L/g respectively. These values indicate good settling properties for the analyzed sludge.

Table 5.8 Field Data for the Determination of the Settling Parameter of the Zone Settling and Compression Rate Exponential Equations

SAMPLE	Concentration (g/L)	Settling Velocity (m/h)	Sample Obtained from
A	1.5	6.00	Dilution of MLSS
B	2.2	4.08	Dilution of MLSS
C	2.8	3.50	MLSS
D	4.8	1.56	Thickened of MLSS
E	5.4	1.20	Thickened of MLSS, Dilution of RAS
F	8.4	0.64	RAS
G	11.0	0.43	Thickened of RAS
H	14.06	0.23	Thickened of RAS

*The settling velocities presented in this table were measured at 26.5 °C

Compression Rate

The settling parameters of the exponential equation for the simulation of the compression rates are obtained following the same procedure used for the determination of the zone settling parameters but using a RAS or a waste sample. From an initial RAS concentration of 8400 mg/L, taken from the hopper of the secondary clarifier, one dilution and two composite samples were obtained. As in the previous case the dilution was obtained by mixing the RAS with effluent from the secondary clarifier, and the thickened samples were obtained by decanting supernatant from a previous batch test. The resulting settling velocities were subsequently utilized to estimate the settling parameter V_c and k_c from the exponential equation. Table 5.8 shows the compression

settling velocity measured for the four samples (these samples are identified as E, F, G and H) and Figure 5.3 shows the exponential fitting for the data set. The fitted values of V_c and k_c are 3.20 m/h and 0.184 L/g respectively.

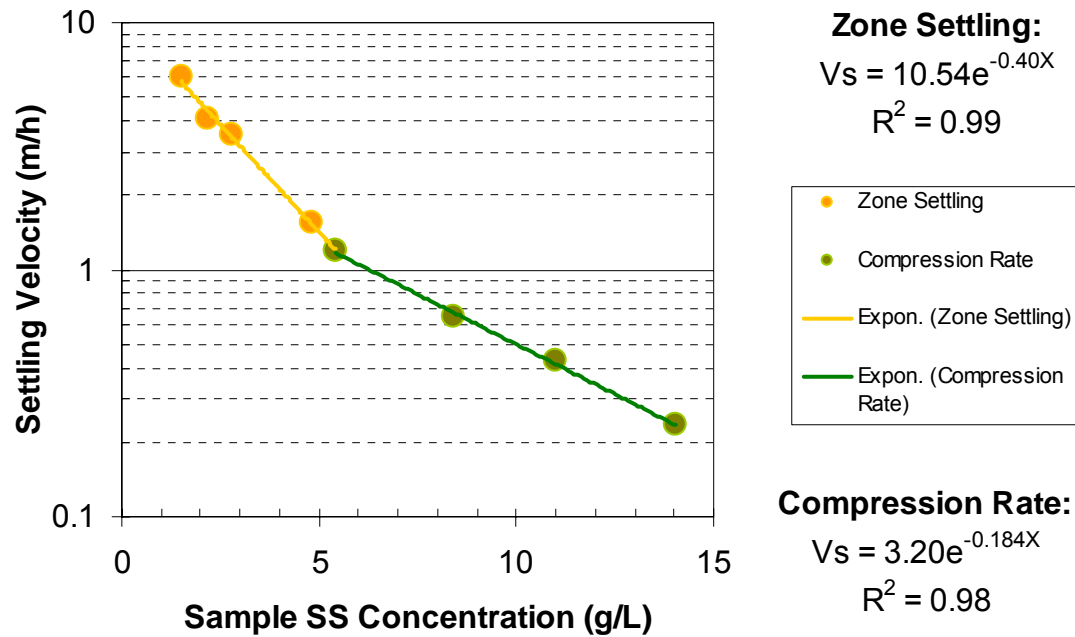


Figure 5.3 Field data and Fitted Exponential Equations for Zone Settling and Compression Rate

The calibrated parameters of the exponential equations are summarized in Table 5.9

Table 5.9 Calibrated Settling Parameter of the Hindered and Compression Settling Equations

Parameter	Value*
V_o (m/h)	10.54
k_1 (L/g)	0.40
V_o (m/h)	3.20
K_c (L/g)	0.184

*The settling properties presented in this table were measured at 26.5 °C

5.1.2 Calibration of the Flocculation Sub-Model

A simple batch flocculation test was conducted in order to determine the flocculation constants used in the shear induced flocculation model. The flocculation test was performed on-site at the Marrero WWTP, and is similar to the test carried out by Jimenez (2002) for the determination of the flocculation kinetic constant. A six-paddle stirrer (Phipps and Bird Stirrer) was used to flocculate the activated sludge samples. Flocculation was induced mechanically by stirring at a rotational velocity the samples inducing a G value of about 40 s^{-1} . The stirrers were equipped with rectangular flat-blades of $2.54 \times 7.62 \text{ cm}$ ($1.0 \times 3.0 \text{ in}$) that rotate in a horizontal plane about the centerline of their long axis. The bottoms of the paddles were situated approximately 5 cm (1.97 in) above the bottom of the jar during the tests. Square, $15 \times 15 \text{ cm}$ ($5.91 \times 5.91 \text{ in}$), glass jars were used for the flocculation tests, in order to prevent vortexing.

The activated sludge samples were taken from the contact chamber of the Marrero WWTP (MLSS sample). The average concentration of the MLSS samples was 2800 mg/L . Two liters of MLSS were poured in each jar, and a flocculation time was assigned to each jar. The selected flocculation times were 0, 2.5, 5, 10 and 20 minutes. After the prescribed flocculation time had elapsed, the jar was removed carefully from the stirrer. After 30 minutes of settling, approximately 250 mL of supernatant were withdrawn very carefully by a siphon mechanism avoiding suction of floating solids. Each supernatant sample was analyzed for TSS. The C_O concentration was measured from a sample taken from the inlet zone of the Marrero contact chamber (SS concentration at time equal zero, see Equation 2.39), this value can also be determined experimentally by mixing the influent to the solids contact chamber and recycle sludge in proportion to the influent flow rate (Q) and the recycle flow rate (αQ), respectively, and by measuring the SS concentration of the supernatant of the mixture after 30 minutes of settling, this procedure according to the recommendation presented by La Motta et al. (2003).

As discussed in the Section 4.1.4 the differential equation (Equation 2.35) presented by Parker et al. (1970) is used to model the shear induced flocculation.

$$\frac{dn}{dt} = K_B \cdot X \cdot G^m - K_A \cdot X \cdot n \cdot G \dots\dots\dots (2.35)$$

Wahlberg et al. (1994) presented an integrated form of Equation 2.35 for the calculation of flocculation in a batch flocculator. Wahlberg et al. assumed K_A and K_B as true constant and used a value of m equal to 2 [$m = 2$ was selected based on analysis presented by Parker et al. (1971); this number indicates that floc breakup occurs by erosion of primary particles from floc surfaces due to eddies in the viscous dissipation range] This equation was presented in Section 2.3.4 and is recapitulated below:

$$n_t = \frac{K_B \cdot G}{K_A} + \left(n_o - \frac{K_B \cdot G}{K_A} \right) \cdot e^{-K_A \cdot X \cdot G \cdot t} \dots\dots\dots (2.37)$$

Jimenez (2002) and La Motta et al. (2003) used an equation similar to Equation 2.37 to evaluate the removal of SS in batch flocculators. For a batch reactor, operated at constant G , they presented:

$$C = a + (C_O - a) \cdot e^{-k_f \cdot t \cdot X} \dots\dots\dots (2.39)$$

The flocculation characteristics were defined by the parameters a and k_f . Estimates of the parameters were made by fitting Equation 2.39 to the experimental data. The experimental constants a and k_f were determined by a non-linear regression analysis.

Figure 5.4 shows the removal of the supernatant suspended solids with the flocculation time. This figure shows a good correlation between the model proposed by Equation 2.39 and the measured field data. The flocculation constant a and $k_F \cdot X$ were obtained by a non-linear regression analysis. The values obtained were $a = 4.3$ mg/L, and $k_F \cdot X = 0.497 \text{ min}^{-1}$. A value of $k_F = 0.1776 \text{ L/g SS min}$ is obtained by dividing $k_F \cdot X$ by the MLSS concentration. The values of the flocculation kinetic constants obtained with the batch test are similar to values reported in the literature by Parker et al. (1970), Wahlberg

et al. (1994), Jimenez (2002) and La Motta et al. (2003).

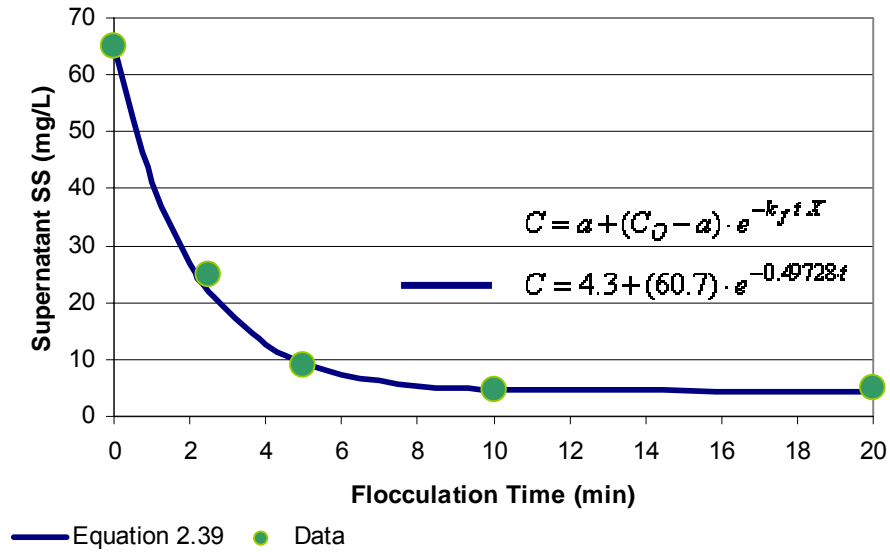


Figure 5.4 Supernatant SS versus Flocculation Time in a Batch Test

With the values of a , k_F , C_O , G and X the values of the kinetic constant were calculated by comparing Equations 2.37 and 2.39. Table 5.10 summarizes the values of the flocculation kinetic constant found during the calibration period.

Table 5.10 Kinetic Constant for the Flocculation Sub-Model

Batch Test Information	Value
C_o	65 mg/L
MLSS (X)	2800 mg/L
Velocity Gradient (G)	40 s^{-1}
Flocculation Kinetic Constant for Equation 2.39	Value
a	4.3 mg/L
K_f	$0.1776 \text{ L/g SS min}$
Flocculation Kinetic Constant for Equations 2.35 and 2.37	Value
K_A	$7.4 \times 10^{-5} \text{ L/g SS}$
K_B	$8.00 \times 10^{-9} \text{ s}$

5.1.3 MLSS, ESS, Flow Rates and RAS

MLSS, ESS and TSS were measured twice during the 24 hours period, and the Q_p and RAS were obtained from the plant operator recorded data. The sludge blanket depth was also obtained from the plant operator. Appendix B presents a description of the laboratory techniques utilized for measuring these concentrations. Table 5.11 presents the average values of the suspended solids concentrations and the standard deviation of the estimates. These values are used in the model test case that is presented below.

Table 5.11 Suspended Solids Concentrations Measured During the Calibration Period

	X (mg/L)	sd(X) (mg/L)
MLSS	2800	106
ESS	10.20	1.4
RASS	8500	790

The average clarifier effluent flow rate (Q_{eff}), recirculation flow rate (Q_{ras}), surface over flow rate (SOR), RAS and sludge blanket depths in the inlet and outer zone are presented in Table 5.12.

Table 5.12 Flow Rates, SOR and RAS During the Calibration Period

Variable	Value
Q_{eff}	972 m ³ /h
Q_{ras}	488 m ³ /h
SOR	1.00
RAS	0.50
Sludge Blanket Height at the inlet zone	40 inches
Sludge Blanket Height at the outer zone	10 inches

5.1.4 Model Simulation

The calibrated and measured data presented in the previous section was given as input to the computer code. For this initial calculation a medium grid of 60 cells in the radial direction and 20 cells in the vertical direction was used, this grid is referred as 60x20. This grid was selected after a grid dependency test that is discussed in the next section. For the time-dependent equations a time step of two seconds was selected. Table 5.13 shows a summary of the input data to the model. Table 5.13 indicates that the compression threshold is equal to 5400 mg/L; the computer model selects this value by applying the following equations:

$$V_s = MAX[V_o e^{-k_1 X}; V_c e^{-k_c X}] \text{ for } X > \text{Hindered Threshold } (Xh) \dots \quad (5.1)$$

The duration of the run for the 540 minutes simulation time and 2 seconds time step was about 195 minutes; this is called the run time. This time is encouraging when compared with simulations done by Ekama and Marais (2002) and Armbruster et al. (2001) with similar models that lasted about 100 hours. Steady conditions were reached at about 270 minutes of simulation time. A mass balance was calculated at every time step and displayed every ten minutes (simulation time); during the complete simulation the mass balance error was less than 0.2%. Figure 5.5 presents the evolution of RAS and ESS concentrations versus the simulation time (from this point the simulation time will be referred as time). While the RAS SS concentration steadily increases until it reaches the equilibrium value, the ESS effluent presents a peak value at about 20 minutes. The simulation starts with a clean-water full tank, the incoming solids are immediately affected by the density current which produces a strong bottom current that travels near the floor of the tank until it reaches the end wall. When the density current reaches the end wall it produces a rebound that is characterized by the high ESS concentration. Part of the flow exits the tank through the weirs and part of it creates a reverse flow. After the initial momentum is dissipated, the ESS concentration starts to decrease until it reaches an equilibrium value.

Table 5.13 Input Data for the Clarifier Model Simulation

Run Control	Value
Number of cells in r- direction	60
Number of cells in y- direction	20
Time step	2 s
Simulation time	540 min
Geometry	Value
Radius of the clarifier	17.6 m
Radius of the inlet pipe	0.5 m
Depth of outer wall	4.3 m
Bottom Slope	8.33%
Center well radius	4.5 m
Center well depth	2.5 m
Outboard launder	----
Radial length of hopper	2.0 m
Loading	Value
SOR	1.0 m/h
RAS Ratio	0.5
Qeffluent	972 m ³ /h
Qras	486 m ³ /h
MLSS	2800 mg/L
Discrete Settling Properties	Value
Discrete Settling Threshold	1200 mg/L
V_{s1}	10.8 m/h
<i>Fraction 1 (Dimensionless)</i>	0.742
V_{s2}	3.0 m/h
<i>Fraction 2 (Dimensionless)</i>	0.255
V_{s3}	0.68 m/h
<i>Fraction 3 (Dimensionless)</i>	0.003
Zone Settling Properties	Value
Zone Settling Threshold	600 mg/L
V_o	10.54 m/h
k_1	0.4 L/g
Compression Rate Properties	Value
Compression Settling Threshold	5400 mg/L
V_o	3.20 m/h
K_c	0.184 L/g

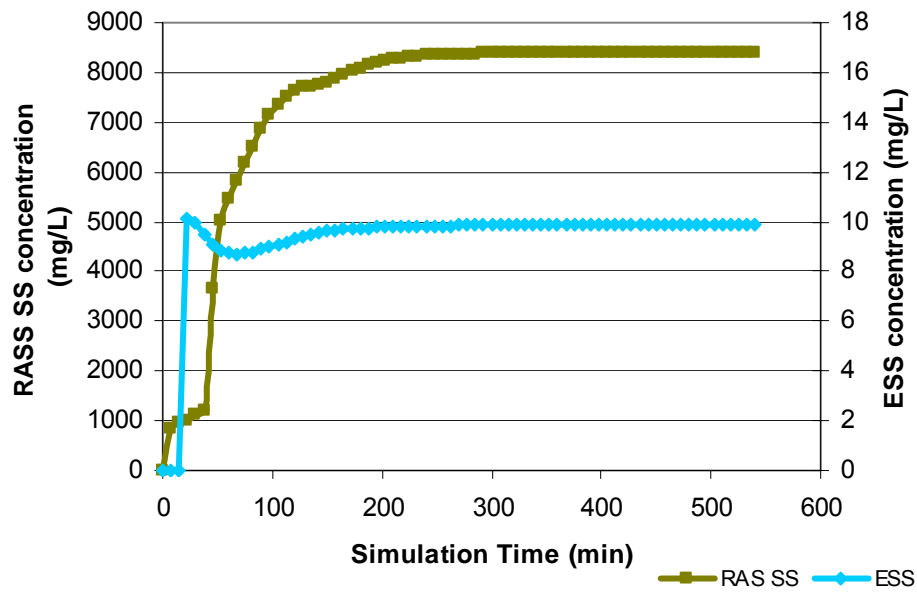


Figure 5.5 RAS SS and ESS Concentration Predicted by the Model

As presented in Figure 5.5 the steady RAS and ESS concentrations were about 8390 mg/L and 10.0 mg/L respectively. A comparison with the measured values is presented in Table 5.14. In general, measured and predicted values are in good agreement. In order to get this agreement different combinations of effective diffusion coefficient in the r- and y- direction were tested. Values of $\Gamma_r = 5.0$ and $\Gamma_y = 0.1$ gave the best prediction of the measured data.

Table 5.14 Comparison between Measured and Predicted Values for Calibrated Model

	Measured Concentration (mg/L)	Predicted Concentration (mg/L)	Difference %
MLSS	2800	2800	0
ESS	10.20	10	2.0
RAS SS	8500	8390	1.3

Figures 5.6a and 5.6b show the concentration contours and the flow stream lines and velocity vectors resulting from the computation of the Marrero test case. Figure 5.6c shows the velocity vectors and different trajectory paths.

Figure 5.6a shows a stable stratified field with approximately horizontal layers in the settling zone. The inlet zone shows evidence of entrainment and dilution with clarified liquid. The sludge blanket presented concentration between 6000 mg/L and 9000 mg/L, with a depth in the inlet zone of about 110 cm (43 inches) and 28 cm (11 inches) in the outer zone. These depths agree with the reported values for the day (Table 5.12).

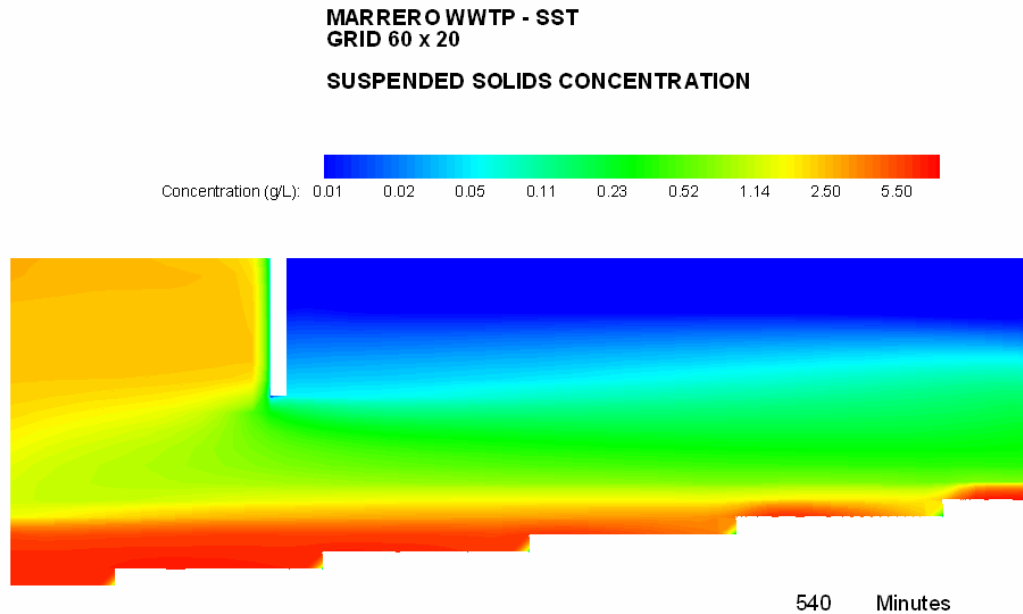


Figure 5.6a Concentration Contours at 540 minutes of simulation time for the Marrero WWTP Test Case using a 60x20 grid

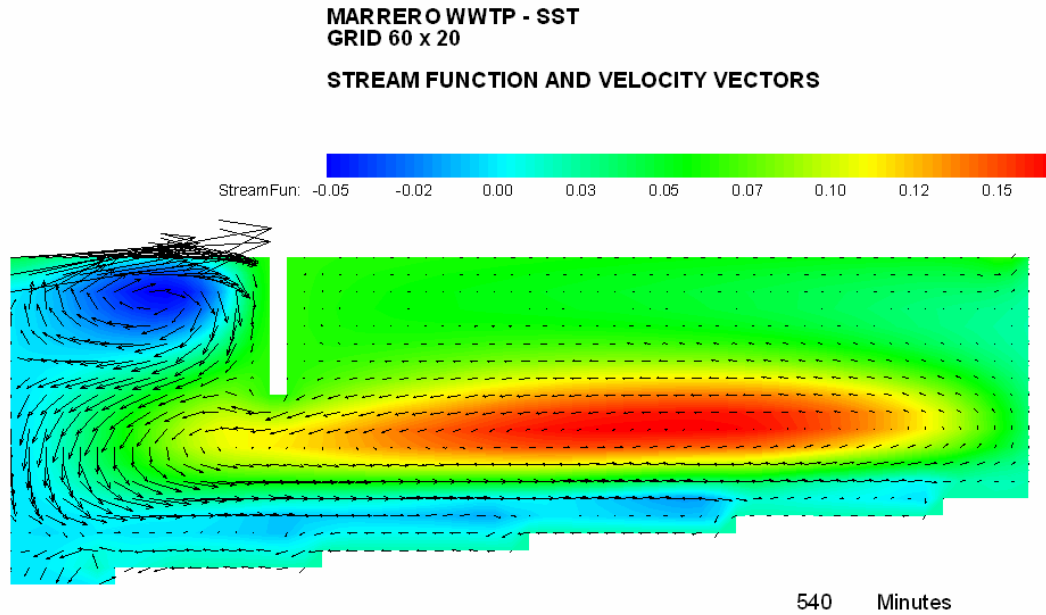


Figure 5.6b Stream Function and Velocity Vectors at 540 minutes of simulation time for the Marrero WWTP Test Case using a 60x20 grid

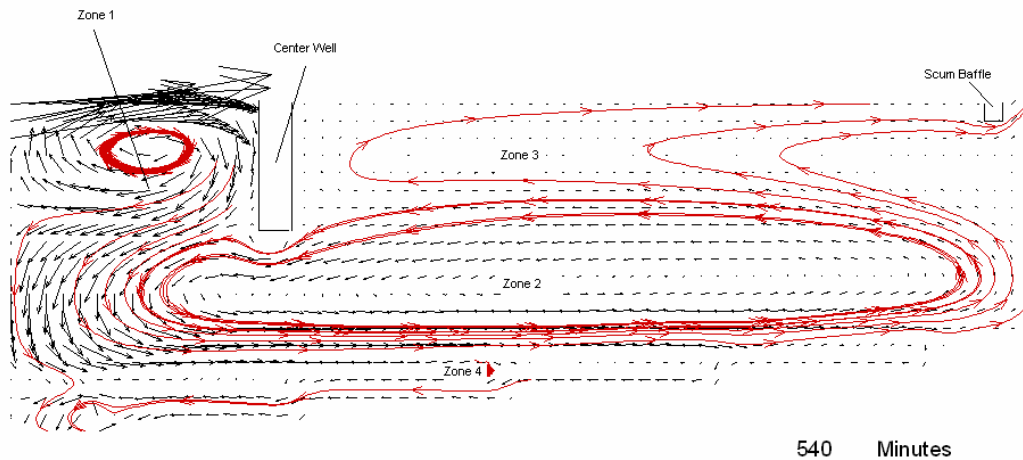


Figure 5.6c Trajectory Paths and Zones for the 60x20 grid. Marrero WWTP.

Figures 5.6b and 5.6c show a complex flow pattern where can be recognized the major characteristics describing the flow in settling tanks. As previously presented in Section

2.2.1 these characteristics have been identified and reported by many researches. A short description of the predicted flow field by the model is presented next.

As shown in Figure 5.6c the settling tank was divided into 4 zones: Zone 1 is the inlet region, Zone 2 is located in the settling region and is the zone dominated by the density currents, Zone 3 is located at the top of the settling region, and Zone 4 is defined by the sludge blanket. The inlet zone (Zone 1) shows strong turbulence and mixing and the development of a density waterfall, this is due to density difference between the influent and the ambient liquid. The entrainment of clarified liquid from the clarification zone (Zones 2 and 3) and the increasing in the total flow can also be observed. As indicated by Larsen (1977) the potential energy of SS is partly dissipated and partly converted into kinetic energy through the density current. In this case there is no evidence of short circuiting from the inlet zone to the RAS zone, since the density current is developed over the sludge blanket. The density current totally dominates the flow pattern in Zone 3. The bottom density current travels over the sludge blanket towards the periphery, hits and rebounds at the end wall and produces a reverse current; this reverse current entrains in the inlet zone. Near the outer wall, part of the flow coming with the bottom density current exits the clarifier through the peripheral launder.

Similar to the flow pattern described by van Marle and Kranenburg (1994) and Krebs et al. (1998) from experimental observations; the predicted flow field presents a three layer structure. Over the two density current layers, flowing in opposite directions, a third layer (Zone 3) is developed. This layer, which is considerably weaker than the other two, presents a flow that is directed towards the effluent weir. Close to the center well the layer is almost stagnant; the mixture moves very slow at about 0.1 cm/s in the horizontal direction. The mixture accelerates as it approaches the weir and reaches a velocity of about 1.3 cm/s close to the end wall.

A fourth layer (Zone 4) can be observed in Figures 5.6a, b and c. This zone is defined by the sludge blanket movement towards the central sludge withdrawal. This zone is clearly developed under the bottom density current, and is characterized by high SS

concentrations and slow movement of the mixture probably affected by rheology effects. Commonly, this fourth layer has not been reported in laboratory experiments (e.g. van Marle and Kranenburg, 1994; Krebs et al., 1998) basically due to limitations in the physical model. But, it has been detected in full scale measurements (e.g. Kinnear and Deines, 2001) and numerical models (e.g. Lakehal et al., 1999; Armbruster et al., 2001).

5.2 Testing: Grid Dependency Test

In order to analyze the grid dependency of the solution, three mesh sizes were evaluated. These meshes are referred to as coarse, medium and fine. Table 5.15 summarizes the studied meshes.

Table 5.15 Grid Sizes Evaluated in the Dependency Test

GRID	Number of cells		Time Step	Simulation Time	Run Time
	r- direction	y- direction			
Coarse	40	15	3 s	540 min	60 min
Medium	60	20	2 s	540 min	195 min
Fine	90	30	0.75 s	540 min	900 min

The time step presented in Table 5.15 was the minimum required after a time-dependency test was done. This time guarantees that the solution is not affected by the step size; however, it was found that the different solutions are only slightly affected by bigger time steps until the solution becomes unstable. In general, the finer the grid the smaller the time step that is required.

Figure 5.7 shows the evolution of the RAS and ESS concentrations with respect to the simulation time for the 3 grids. From a qualitative point of view, only the ESS of the coarsest grid deviates from the equilibrium value with respect to the other two. The grids 90x30 and 60x20 reach a value of about 10.0 mg/L, while the coarsest grid predicts a

value around 14.0 mg/L. The exact values are presented in Table 5.16. It can be noticed that the three grids present a different peak ESS, which does not seem to be dependent on the grid size. It is suspected that these differences may be caused by the difference in initial momentum caused by different effective inlet openings, which depends on the cell- y dimension. With respect to the RAS concentration, it can be observed that at equilibrium conditions similar values are reached with the 3 grids; however, slightly difference may be found during the simulation time. The most important different occurs at the beginning of the simulation time, when the sludge blanket starts developing. It can be observed that the finer the grid the sooner the RAS concentration develops. This might be due to the effective size of the withdrawal opening. However, this early variations are not affecting the predicted values at equilibrium conditions.

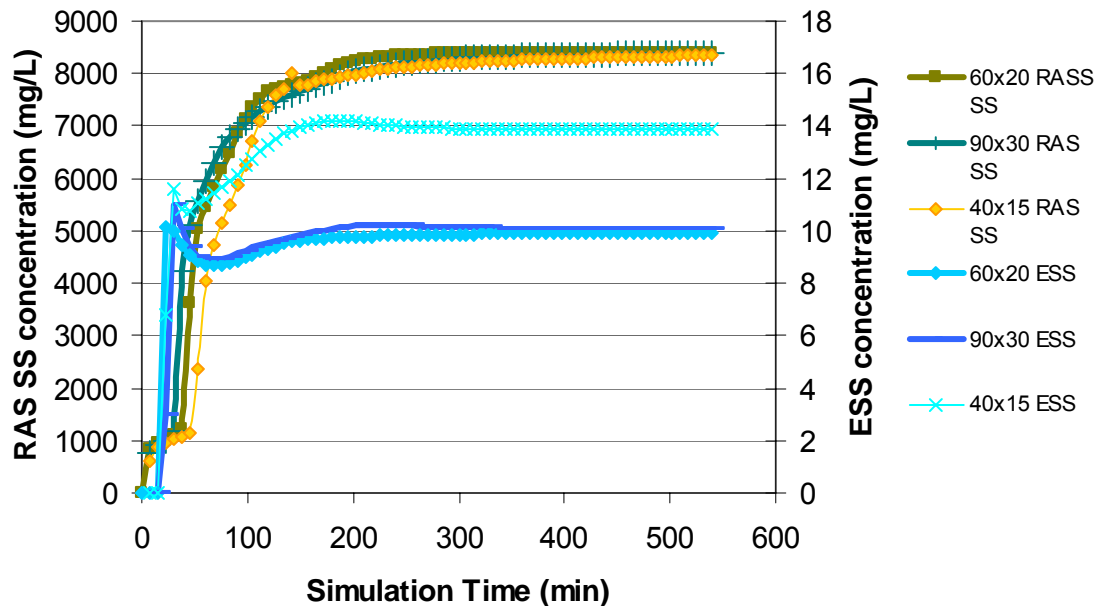


Figure 5.7 RAS and ESS Concentrations for Different Grid Sizes

Table 5.16 summarizes the concentrations at equilibrium conditions showed by the 3 grids.

Figure 5.8 shows the concentration fields for the three different grids, and Figure 5.9 shows the velocity vectors and stream function values for the same cases.

Table 5.16 ESS and RAS SS Concentrations at Equilibrium Conditions for 3 Grid Sizes

GRID	ESS Concentration (mg/L)	RAS SS Concentration (mg/L)
90x30	10.1	8385
60x20	10.0	8390
40x15	13.9	8341

In Figure 5.8, only minor differences can be found with respect to concentration contours. The 40x15 contours field shows a thicker sludge blanket close to the end wall and slightly higher concentrations close to the outlet. The 60x20 and 90x30 contour concentrations are virtually identical. Due to limitations with the cell size the 60x20 and 40x15 grids do not show the scum baffle, which can be observed in the 90x30 grid.

The flow patterns described by the stream functions in Figure 5.9 are very similar. The major difference in the three grids is that the 40x15 grid presents a thicker eddy in the settling zone apparently producing higher concentration in this region. In the three grids can be identified the flow of water under the scum baffle towards the peripheral launder.

From this simple test, it can be concluded that numerical diffusion and grid dependency may affect the result when coarse grids are used; however, such grids may be useful for initial-quick estimations, since the general flow pattern and concentration contours do not change too much with respect to finer grids. These differences in the flow and concentration patterns diminish as the grid refinement increase, which proves that the model converges to a unique solution.

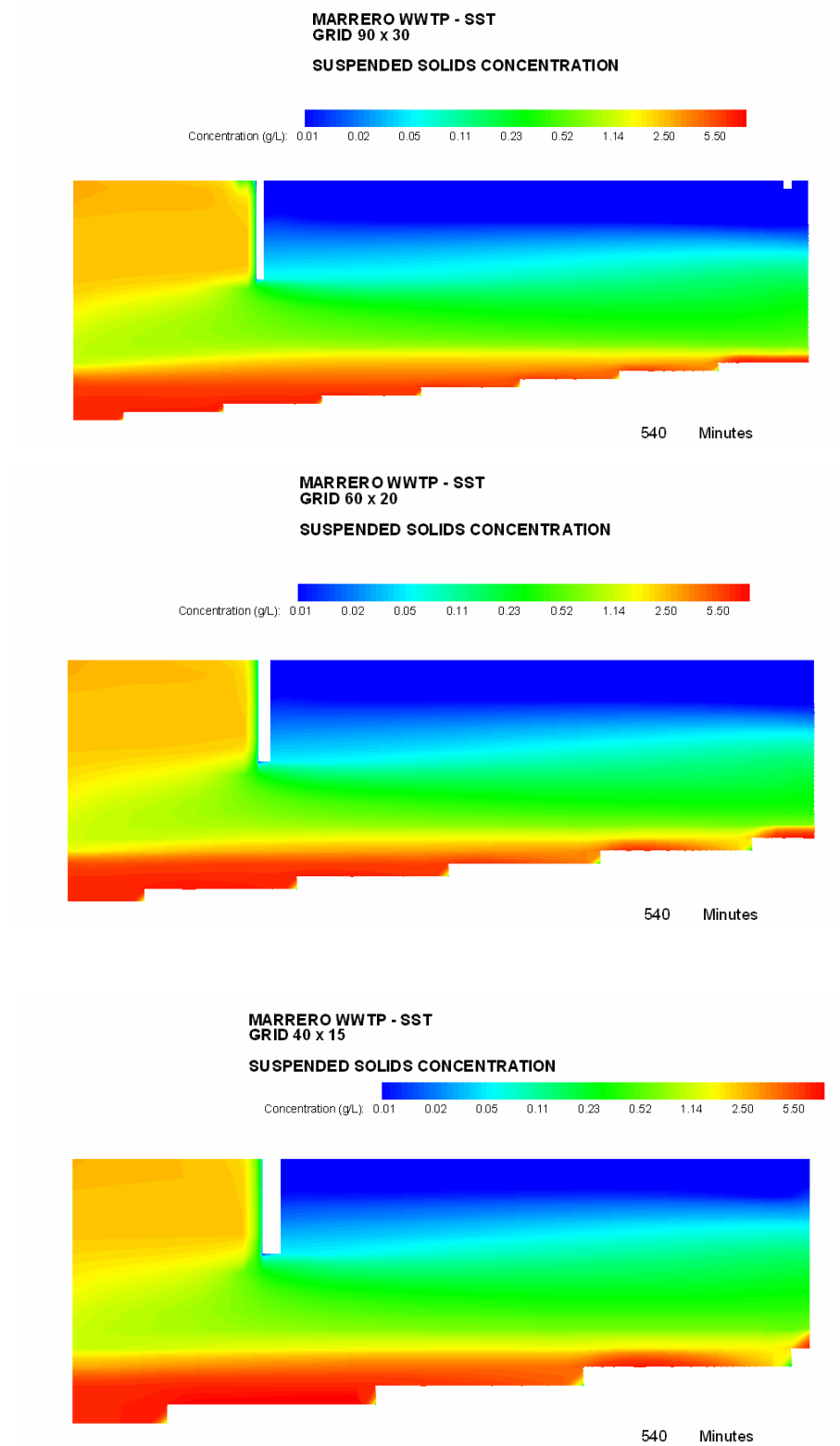


Figure 5.8 Concentration Contours for 3 Different Grids Used in the Marrero Test Case

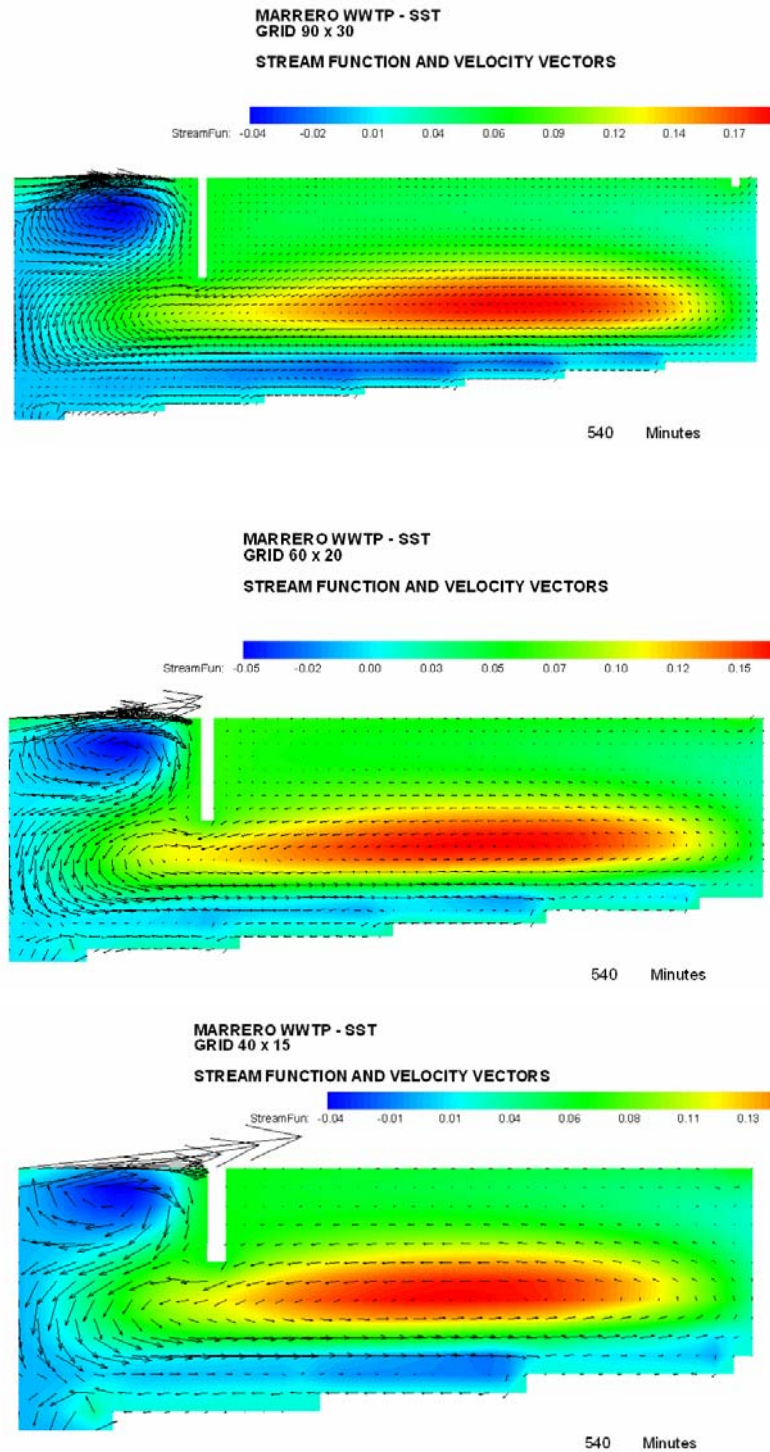


Figure 5.9 Stream Function Contours and Velocity Vectors for 3 Different Grids Used in the Marrero Test Case

5.3 Validation of the Model

After the calibration of the model a validation process was carried out. The validation process involves comparing the model response to actual measured data that was not used during the calibration. The model was validated using additional data from the Marrero WWTP and using independent-published data. During the validation process the settling parameters and flocculation constants were updated whenever was possible, but the diffusion coefficients remained the same.

5.3.1 Marrero WWTP

After the calibration process was carried out, additional data was gathered at the Marrero WWTP SST in order to validate the model. MLSS, ESS and TSS were measured twice during a 6 hours period, and the effluent flow rate and RAS ratio were obtained from the plant operator recorded data. The sludge blanket depth was also obtained from the plant operator. Table 5.17 presents the average values of the suspended solids concentrations and the standard deviation of the estimates. These values were used during the validation of the model

Table 5.17 Suspended Solids Concentrations Measured at the Marrero WWTP During the Validation Period

	X (mg/L)	sd(X) (mg/L)
MLSS	3100	56
ESS	15.00	1.2
RASS	9200	520

Table 5.18 presents the general information gathered during the validation process at the Marrero WWTP, including the settling properties of the sludge. The procedures for

gathering and processing this information were the same procedures described in Section 5.1. Appendix G presents the data obtained during the validation.

Table 5.18 General Data for the Validation of the Q3D Model – Marrero WWTP

Loading	Value
SOR	0.90 m/h
RAS Ratio	0.5
Qeffluent	875 m ³ /h
Qras	438 m ³ /h
MLSS	3100 mg/L
Sludge Blanket Height at the inlet zone	40 inches
Sludge Blanket Height at the outer zone	10 inches
Discrete Settling Properties	Value
Discrete Settling Threshold	1200 mg/L
V_{s1}	9.96 m/h
<i>Fraction 1 (Dimensionless)</i>	0.7
V_{s2}	3.0 m/h
<i>Fraction 2 (Dimensionless)</i>	0.256
V_{s3}	0.62 m/h
<i>Fraction 3 (Dimensionless)</i>	0.044
Zone Settling Properties	Value
Zone Settling Threshold	600 mg/L
V_o	8.46 m/h
k_1	0.386 L/g
Compression Rate Properties	Value
Compression Settling Threshold	5400 mg/L
V_o	3.08 m/h
K_c	0.181 L/g
Flocculation Kinetic Constant for Equation 2.39*	Value
a	4.3 mg/L
K_f	0.1776 L/g SS min
Flocculation Kinetic Constant for Equations 2.35 and 2.37*	Value
K_A	7.4×10^{-5} L/g SS
K_B	8.00×10^{-9} s

*The same flocculation kinetics constant obtained during the calibration were used for the validation of the model

The field measured data presented Table 5.18 were given as input to the Q3D model. The model was run using a 60x20 grid and a 2 seconds time step. Figure 5.10 presents the evolution of RAS and ESS concentrations versus the simulation time.

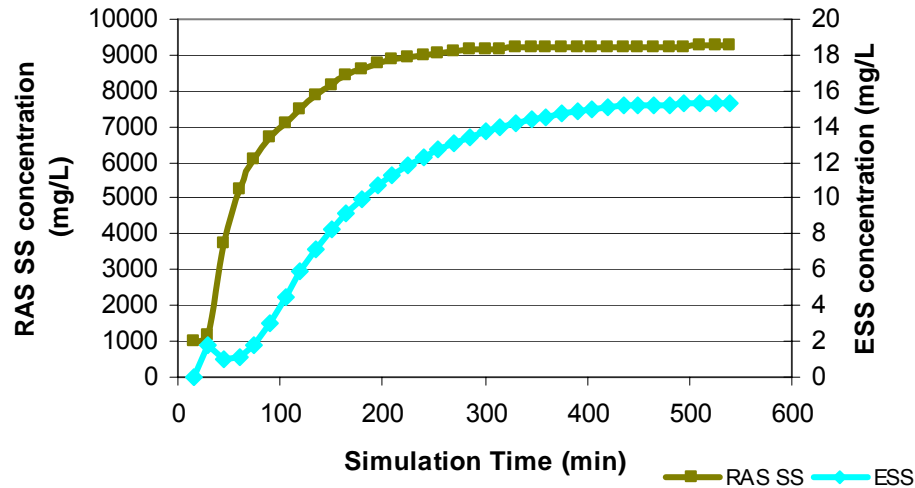


Figure 5.10 RAS SS and ESS Concentration Predicted by the Model During the Validation

As indicated in Figure 5.10 the steady RAS and ESS concentrations were about 9250 mg/L and 15.5 mg/L respectively. A comparison with the measured values is presented in Table 5.19. Without further calibration an excellent agreement was found between measured and predicted values.

Table 5.19 Comparison between Measured and Predicted Values During the Validation of the Q3D Model

	Measured Concentration (mg/L)	Predicted Concentration (mg/L)	Difference %
MLSS	3100	3100	0
ESS	15.0	15.5	3.3
RAS SS	9200	9250	0.5

Figure 5.11 shows the concentration contours resulting from the computation of the Validation - Marrero case. The sludge blanket presented concentration between 6000 mg/L and 9000 mg/L, with a depth in the inlet zone of about 110 cm (43 inches) and 28 cm (11 inches) in the outer zone. These depths agree with the reported values for the day (Table 5.18).

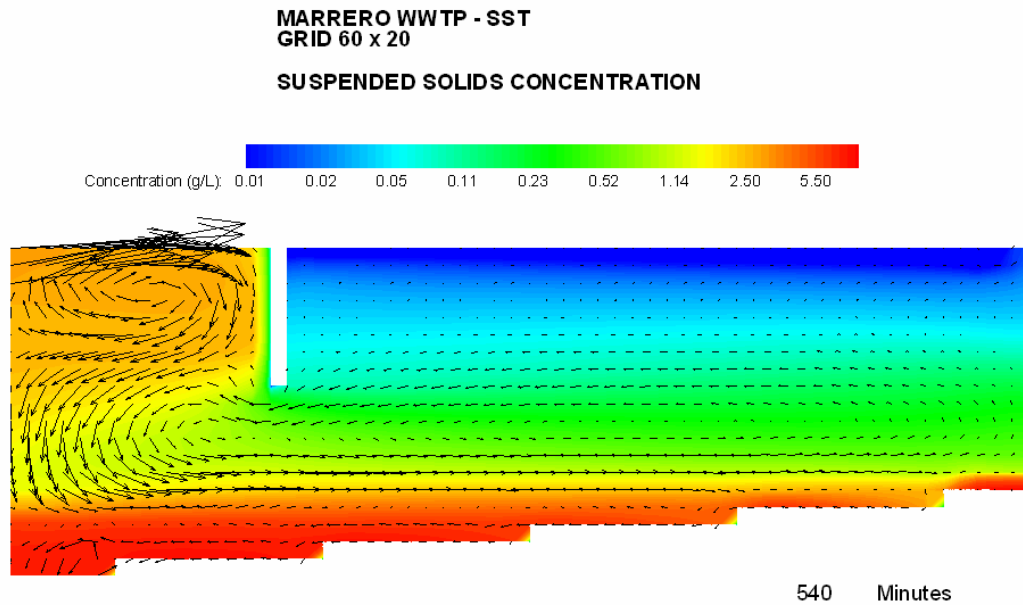


Figure 5.11 Concentration Contours at 540 minutes of simulation time for the Validation - Marrero WWTP Test Case using a 60x20 grid

The concentration contours predicted with the Q3D model at steady state conditions were compared with pseudo-steady-state solids concentration profile measured at the mid-radius of the clarifier at 8.8 m radial distance. The field concentration profile was obtained by sampling the middle column of the Marrero WWTP using a two-and-a-half-liter Kemmerer sampler supplied by Wildlife Supply Company. The sampler was lowered into the SST at different depths, and closed by a messenger once it was positioned at the required depth. Ten different depths above floor were sampled, i.e. 0, 1, 1.5, 2, 2.5, 3, 3.5, 4, 4.5 and 5 meters above the floor in the mid-radius position. The samples were later taken to the laboratory for the TSS test. Figure 5.12 shows the comparison between the

measured solids profile and the profile predicted by the model for the same position. For this validation case, an excellent agreement was found between the two solids profiles.

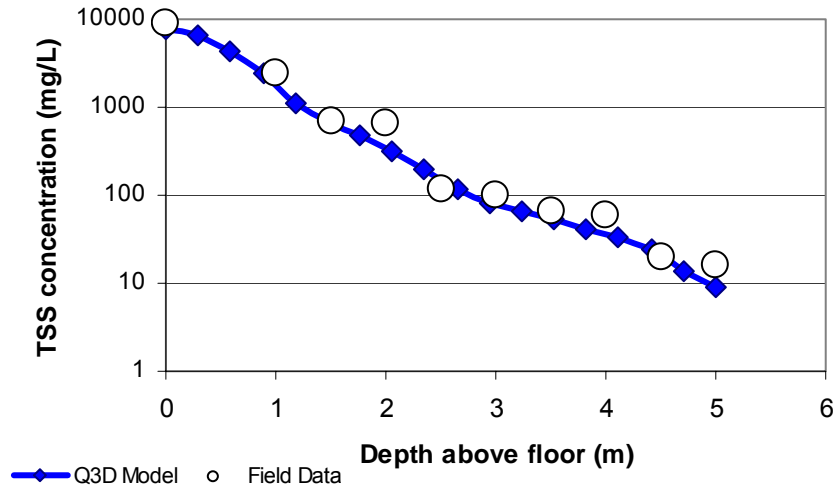


Figure 5.12 Measured and Predicted Concentration Profiles at 8.8 m Radial Distance for the Marrero SST

5.3.1.1 Marrero WWTP – Early Validation

After the development of the hydrodynamic model, turbulence and rheology model, but prior to the development of the compound settling model, the clarifier model was tested using the Takacs' equation as the settling model. During this period a validation of the hydrodynamic and ESS prediction was carried out adjusting the K_2 parameter of the Takacs' equation. The ESS predicted by the model was tested during seven days (from a 10 day period) showing a very good agreement with the field data. Figure 5.13 shows the comparison of the model prediction and the field data during the aforementioned seven days trial.

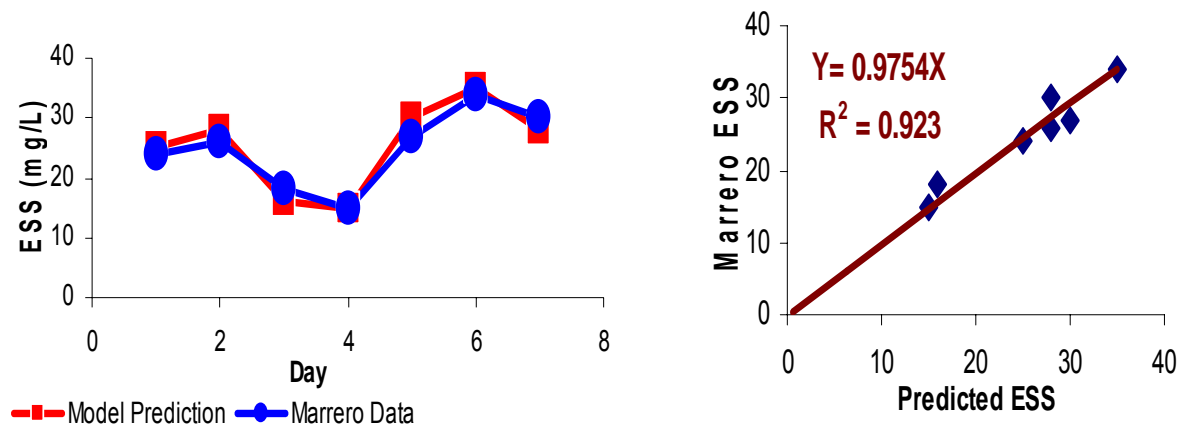


Figure 5.13 Early Validation of the ESS Simulated by the Model

As observed in Figure 5.13 in this early stage the clarifier model presented a very good agreement between the predicted and measured ESS. As mentioned previously the data shown in Figure 5.13 corresponds to simulation executed with the Takacs' model. Despite the good correlation between field data and predictions, it is noted that the K_2 parameter of the Takacs equation (Equation 2.18) was used as a calibration parameter instead of a measured settling property.

5.3.2 Oxley Creek WWTP

The Oxley Creek WWTP is located in Brisbane Australia. It is a conventional activated sludge treatment plant built to remove only carbon and equipped with circular sloped floor secondary clarifiers. A special feature of the system at the time of the study was the continuous dosing of zeolite ZELfloc to improve the settling properties and the nitrification capacity (De Clercq, 2003). This WWTP was selected for a case study by De Clercq (2003) and the information presented in this section was taken from his report. De Clercq (2003) used this treatment plant for the calibration and validation of a CFD clarifier model, this model simulated the settling properties using the Takacs' equation (Equation 2.18) and did not included the simulation of the flocculation process. Therefore the data presented next does not include the flocculation parameters and the settling properties are restricted to those in the Takacs' model. Table 5.20 summarizes the settling properties of the zeolite-composite sludge obtained by De Clercq and used for the calibration of his model

Table 5.20 Settling Properties (Takacs' Model) for the Oxley Creek WWTP
(After De Clercq, 2003)

Parameter	Value
V_o (m/h)	19.88
k_1 (L/g)	0.26
k_2 (L/g)	4.00
X_{min} (g/L)	0.003

Table 5.21 presents the general geometry of the Oxley Creek SST and the average loading information obtained during the study period presented by De Clercq. This table also includes the settling properties measured by De Clercq and an estimation of the compression settling parameter. Since no information was available in the compression rate properties, the values of V_c and K_c were estimated as the 40% of the value of V_o and K_l respectively.

Table 5.21 Summary of Oxley Creek WWTP SST Characteristics
(After De Clercq, 2003)

Geometry	Value
Radius of the clarifier	9.9 m
Radius of the inlet pipe	0.3 m
Depth of outer wall	2.5 m
Bottom Slope	29.30%
EDI radius	0.75 m
EDI Depth	1.31 m
Center Well radius	2.50 m
Center Well Depth	2.41 m
Stamford Baffle Depth	0.6 m
Stamford Baffle Length	0.75 m
Outboard launder	----
Radial length of hopper	4.0 m
Loading	Value
Average SOR	0.88 m/h
Average Qeffluent	272 m ³ /h
Average Qras	200 m ³ /h
Average MLSS	2090 mg/L
Settling Properties*	Value
V_o	19.88 m/h
k_1	0.26 L/g
k_2	4.00 L/g
X_{min}	0.003 g/L
Compression Rate Properties**	Value
V_c	7.95 m/h
K_c	0.104 L/g

* These are the settling parameters included in the Takacs' model (Equation 2.18)

**The compression rate properties V_c and K_c were estimated as the 40% of the value of V_o and K_l respectively. The 40% was selected based on studies done in the Marrero WWTP and might be different for the Oxley case, but no other information was available.

Figure 5.14 shows the dynamic inlet solids concentration profile and flow rates that were obtained by the De Clercq during the study period. The SOR of the SST is also included in this figure.

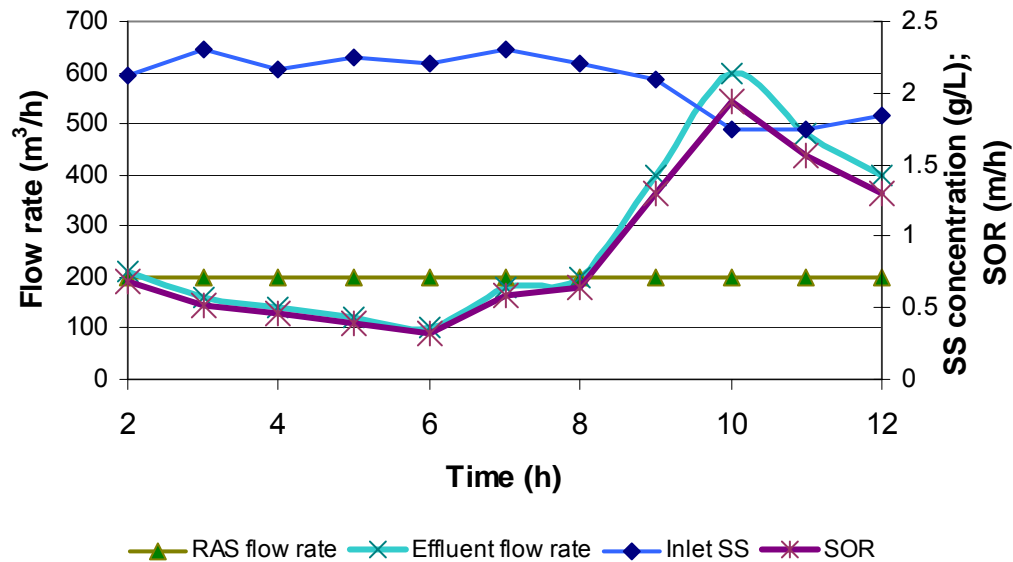


Figure 5.14 Flow Rates and Inlet Solids Concentration During at The Oxley Creek WWTP SST (After De Clercq, 2003)

Using the information presented in Table 5.21 and in Figure 5.14 the Q3D model was run for two different scenarios: (a) steady-state simulation, using the average loading values presented in Table 5.21; and (b) unsteady-state simulation, using the dynamic loading values presented in Figure 5.14. The simulations were carried out using a coarse 40x20 grid (the 40x20 grid was selected instead of a 60x20 in order to have approximately square cells). Since no information about flocculation or discrete settling (including fractions) was available, the Q3D model was run without the flocculation sub-model and using the Takacs equation with the K_2 parameter instead of the discrete settling model ($K_2 = 4 \text{ L/g}$, estimated by De Clercq). The results for the steady-state simulation and the comparison with the average field values (measured by De Clercq, 2003) are presented in Table 5.22.

Table 5.22 Predicted and Measured ESS and RAS SS Concentration Under Steady State Conditions for the Oxley Creek WWTP SST Simulation

	Average Measured Concentration (mg/L)	Q3D Model Predicted Concentration (mg/L)	Difference %
MLSS	2090	2090	0
ESS	6.14	6.7	-9.1
RAS S	4759	4483	5.8

The results presented in Table 5.22 indicate that the Q3D model accurately predicts the ESS and the RAS SS for the SST of the Oxley Creek WWTP. These results were obtained after steady-state conditions were reached at 420 minutes of simulation time for the 40x20 grid. Figure 5.15 shows the suspended solids concentration contours after the steady-state conditions.

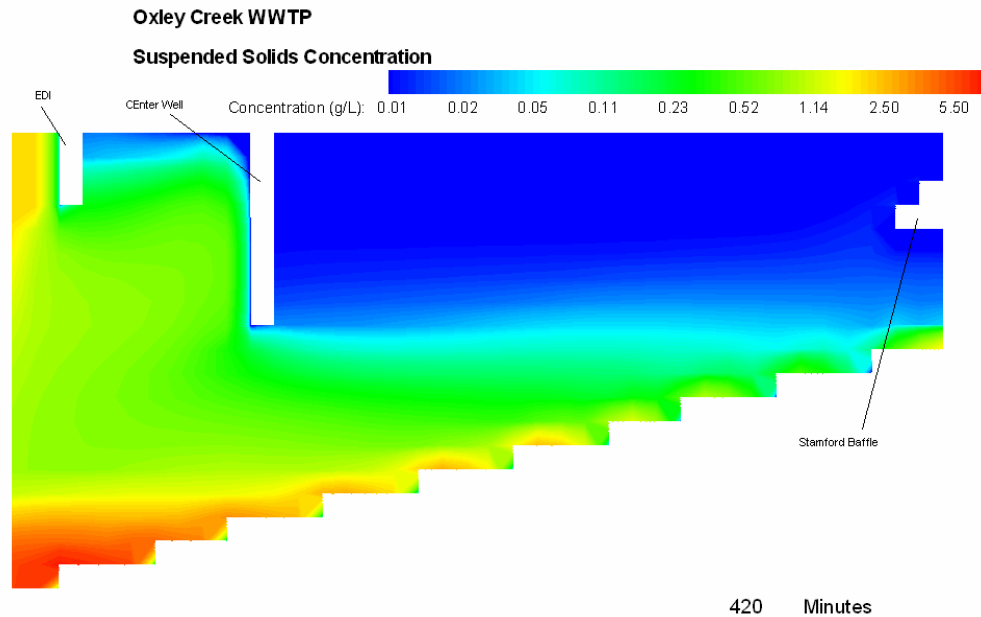


Figure 5.15 Concentration Contours at 420 minutes of simulation time for the Oxley WWTP Validation Case using a 40x20 grid

The concentration contours predicted by the Q3D model at steady state conditions were compared with pseudo-steady-state solids concentration profiles measured at 3 different radial distances, i.e. 2.6, 4.7 and 8.2 m, all situated outside of the center well [the reader is referred to De Clercq (2003) for details in the measurement procedure]. The results are shown in Figure 5.16. For this validation case, an excellent agreement was found between simulations and measurements.

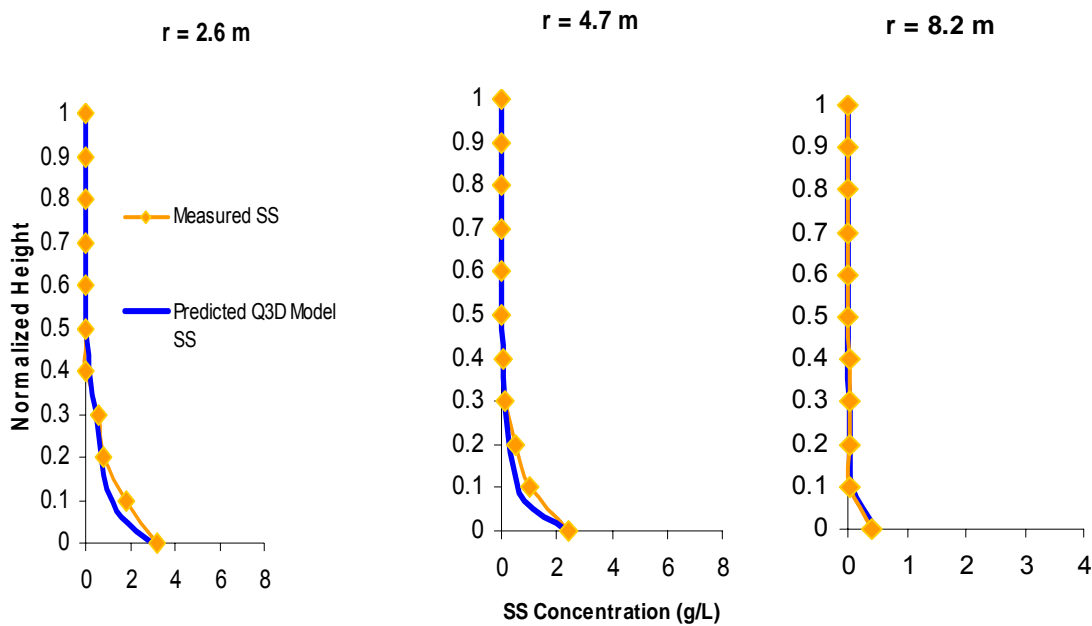


Figure 5.16 Measured and Predicted Concentration Profiles at Different Radial Distances for the SST of the Oxley Creek WWTP

The second validation condition for the Oxley Creek study case focused on the solids flow dynamics by considering ESS and RAS SS time distributions. The simulation basically consists in a “step” change in SOR and influent suspended solids keeping constant the recirculation flow rate. The information of the dynamic loading is presented in Figure 5.14, and the geometry and settling properties information is presented in Table 5.21. Figure 5.17 shows the results of the unsteady simulation. The evolution of the predicted RAS SS concentration shows an excellent agreement with the measured field data, the predicted underflow concentrations closely follow the field values. This tendency suggests that the compression submodel is working adequately and also

suggests that the 40% reduction in the V_c and K_c parameters with respect to the values of V_o and K_l is an appropriate estimation for this case. The good agreement observed in the SS profiles shown in Figure 5.16 also indicates that the compression submodel is performing well.

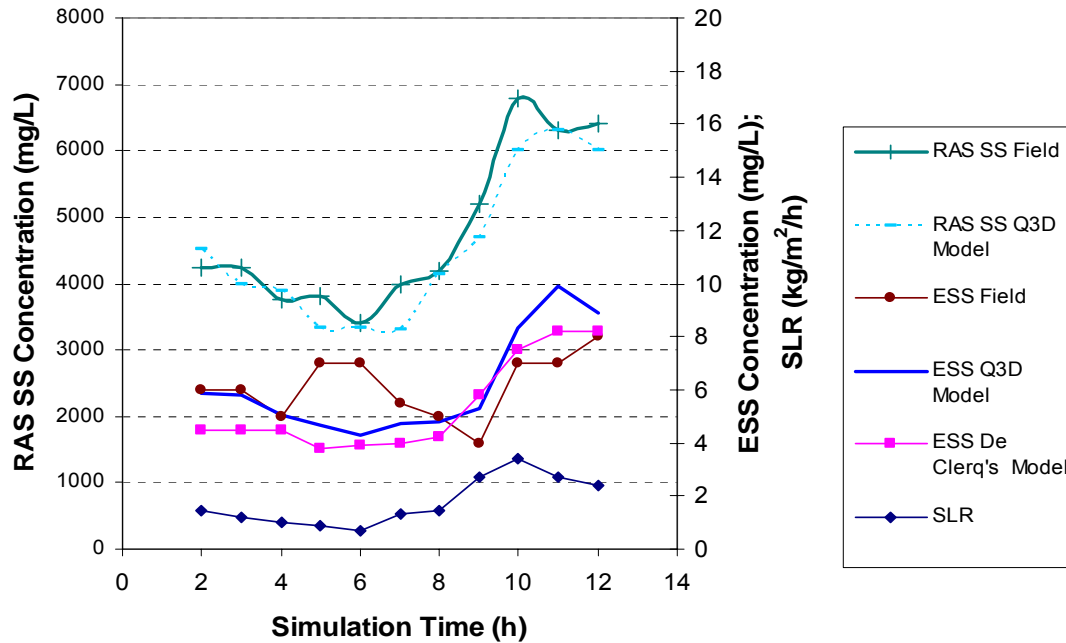


Figure 5.17 ESS, RAS SS and SLR for the Unsteady Simulation of the Oxley Creek WWTP SST

The simulation of the effluent suspended solids concentration also shows a good agreement with the measured values. However slight discrepancies are observed at two points during the simulation: (1) at hours 5 and 6 of the simulation time the model predicts the lower ESS values (about 4 mg/L) and the field data indicate higher values around 7 mg/L; nevertheless, the prediction of the model is reasonable since this time corresponds to the lowest SLRs and SORs. The high measured ESS could be due to an external not-modeled cause, e.g. wind. (2) The model predicts a peak ESS at 11 hours of simulation time, and field data shows the peak at 12. The values of the peak are also different (10 mg/L for the model and 8 mg/L for the field value); in general the predicted and the measured values are close. Also the prediction of the Q3D is similar in trend and

magnitude to the results that De Clercq obtained using a commercial CFD model (FLUENT).

5.3.3 Darvill WWTP New SSTs

Ekama and Marais (2002) presented the application of the 2D hydrodynamic model Settler CAD (Zhou et al., 1998; Vitasovic et al, 1997) to the simulation of full scale circular SSTs with the principle aim to: “establish whether or not it automatically reproduces a flux rating < 1.0 with respect to the steady state 1D idealized flux theory (1DFT), where the flux rating is the capacity of the SST as a % of the 1DFT calculated maximum surface overflow rate (SOR) and solids loading rate (SLR), and determine what factors influence this flux rating.” To do this Ekama and Marais (2002) simulated stress tests reported in the literature. The first tests that they reported were:

- Four tests done by de Haas et al. (1998, Reported by Ekama and Marais, 2002) on four 35 m diameter SSTs with Stamford baffle of the Darvill WWTP, Pietermaritzburg, South Africa.

The stress tests completed by de Haas et al. (1998) and the simulations conducted by Ekama and Marais (2002) in the Darvill WWTP SSTs are going to be used in this report for the validation of the Q3D model. The model used by Ekama and Marais (2002) did not include a flocculation sub-model, and the settling properties of the sludge were simulated using the Takacs' equation. Therefore the simulations presented herein with the Q3D were done without the flocculation sub-model and using the Takacs equation with the K_2 parameter instead of the discrete settling model. Nevertheless, Ekama and Marais (2002) did not report the value of K_2 , and therefore a K_2 equal to 10 L/g was assumed in this report.

According to Ekama and Marais (2002) de Haas et al. performed stress test in two types of clarifiers at the Darvill WWTP; these types were referred to as old and new clarifiers. The old are flat bottom suction type clarifiers and the new ones are sloped bottom

scraped to central hopper circular clarifiers. This part of their report deals with the new clarifiers. The general geometry of new SSTs at the Darvill WWTP is presented in Table 5.23. The information from the stress tests performed by de Haas et al. and reported by Ekama and Marais is presented in Table 5.24.

Table 5.23 Geometry of Darvill WWTP New SSTs.

Geometry	Value
Radius of the clarifier	17.5 m
Area	962 m ²
Radius of the inlet pipe	0.5 m
Depth of outer wall	4.1 m
Bottom Slope	10.00%
Center Well radius	3.0 m
Center Well Depth	2.7 m
Stamford Baffle Depth	0.6 m
Stamford Baffle Length	1.7 m
Outboard launder	Peripheral Launder
Radial length of hopper	4.0 m
Sludge Collection	Scraper

Table 5.24 Summary of the Four SLR Stress Test Done on the Darvill WWTP New SSTs
(After Ekama and Marais, 2002)

Loading	Test 1	Test 2	Test 3	Test 4
Average SOR (m/h)	0.866	0.715	0.985	2.49
Average Qeffluent (m ³ /h)	833	688	948	2395
Recycle Ratio	0.80	0.97	0.79	0.30
Average Qras (m ³ /h)	667	667	750	709
Underflow rate (m/h)	0.693	0.694	0.779	0.737
Average MLSS (mg/L)	4600	4300	3600	3450
Applied Flux (SLR KgSS/m ² /h)	7.17	6.06	6.35	11.13

Table 5.25 shows the 1DFT predicted maximum SOR and SLR calculated with the values of V_o and K_l presented in Table 5.27. The values presented in Table 5.25 were presented by Ekama and Marais (2002). Table 5.26 shows the results of the stress test done on the Darvill SSTs.

Table 5.25 1 DFT Predicted Maximum SOR
(After Ekama and Marais, 2002)

1DFT Predicted Limits	Test 1	Test 2	Test 3	Test 4
Maximum SLR (KgSS/m ² /h)	8.26	6.31	8.22	12.19
Overflow Rate (SOR, m/h)	1.104	0.775	1.503	2.796
Qeffluent (m ³ /h)	1062	746	1446	2690

Table 5.26 Darvill WWTP New SST Stress Test Results
(After Ekama and Marais, 2002)

Test No.	Test 1	Test 2	Test 3	Test 4
Applied Flux (SLR KgSS/m ² /h)	7.17	6.06	6.35	11.13
Feed Conc. (MLSS, mg/L)	4600	4300	3600	3450
Recycle Conc. (RAS SS, mg/L)	10000	9000	9000	15000
Sludge Blanket Depth ¹	2.20	2.60	2.70	----
Effluent Conc. (ESS, mg/L)	17	5	10	----
Test Duration (hours)	10.5	12.0	10.0	5.0
Test Outcome Safe/Fail ²	Safe	Safe	Safe	Fail

¹ Sludge blanket depth is the depth of the top of the sludge blanket from the water surface.

² SST failure interpreted as raised sludge blanket to the water surface and gross solids loss.

The values of the settling properties reported by Ekama and Marais (2002) for the four stress tests are presented in Table 5.27. Since no information was available in the compression rate properties, the values of V_c and K_c were estimated as 40% of the value of V_o and K_l respectively.

Table 5.27 Sludge Settleability Parameters for the Darvill WWTP
(After Ekama and Marais, 2002)

Settling Properties*	Test 1	Test 2	Test 3	Test 4
V_o (m/h)	7.71	7.83	8.00	9.08
k_1 (L/g)	0.390	0.513	0.430	0.290
k_2 (L/g)	10	10	10	10
X_{min} (mg/L)	0.005	0.005	0.005	0.005
Compression Rate Properties**	Test 1	Test 2	Test 3	Test 4
V_c (m/h)	3.08	3.13	3.20	3.63
K_c (L/g)	0.156	0.205	0.172	0.116

* These are the settling parameters included in the Takacs' model (Equation 2.18).

**The compression rate properties V_c and K_c were estimated as the 40% of the value of V_o and K_1 respectively. The 40% was selected based on studies done in the Marrero WWTP and might be different for the Darvill case, but no other information was available.

With the information presented in Tables 5.23, 5.24 and 5.27 the Q3D clarifier model was run for the four tests. The simulations were executed using 60x20 grid and the runs were sufficiently long to establish a final steady state condition or to predict the failure of the SST (Failure was identified as a raise of the sludge blanket to the water surface or as a ESS value higher than 50 mg/L; the 50 mg/L threshold was selected as a limit by Ekama and Marais). Steady state conditions were assumed to be reached when the RAS SS concentration was within $\pm 2\%$ or less of the equilibrium value obtained with a mass balance of suspended solids around the secondary clarifier, provided that the ESS of the simulation did not change more of a 5% in the last 30 minutes of simulation. For the four cases the simulations were as long as the time of the stress test reported in Table 5.26 or longer. Figure 5.18 shows the ESS and RAS SS concentrations predicted by the Q3D model versus the simulation time. As observed in this figure, Test 1, 2 and 3 were run for 720 minutes (12 hours) and all of them ended in steady state conditions. The Q3D model predicts that the three SLRs evaluated in these tests are safe; i.e. the new SSTs of the Darvill WWTP do not fail under such loadings. This prediction agrees with the stress tests performed by de Haas et al. (1998) and reported by Ekama and Marais (2002). The run of Test 4 was stopped after 345 minutes of simulation time because the tank showed a

gross solids loss. The Q3D prediction for Test 4 is that the new SST fails under the loading conditions due to an excessive rise of the sludge blanket and very high ESS. This prediction also agrees with the outcome of the stress test conducted by de Haas et al. (1998)

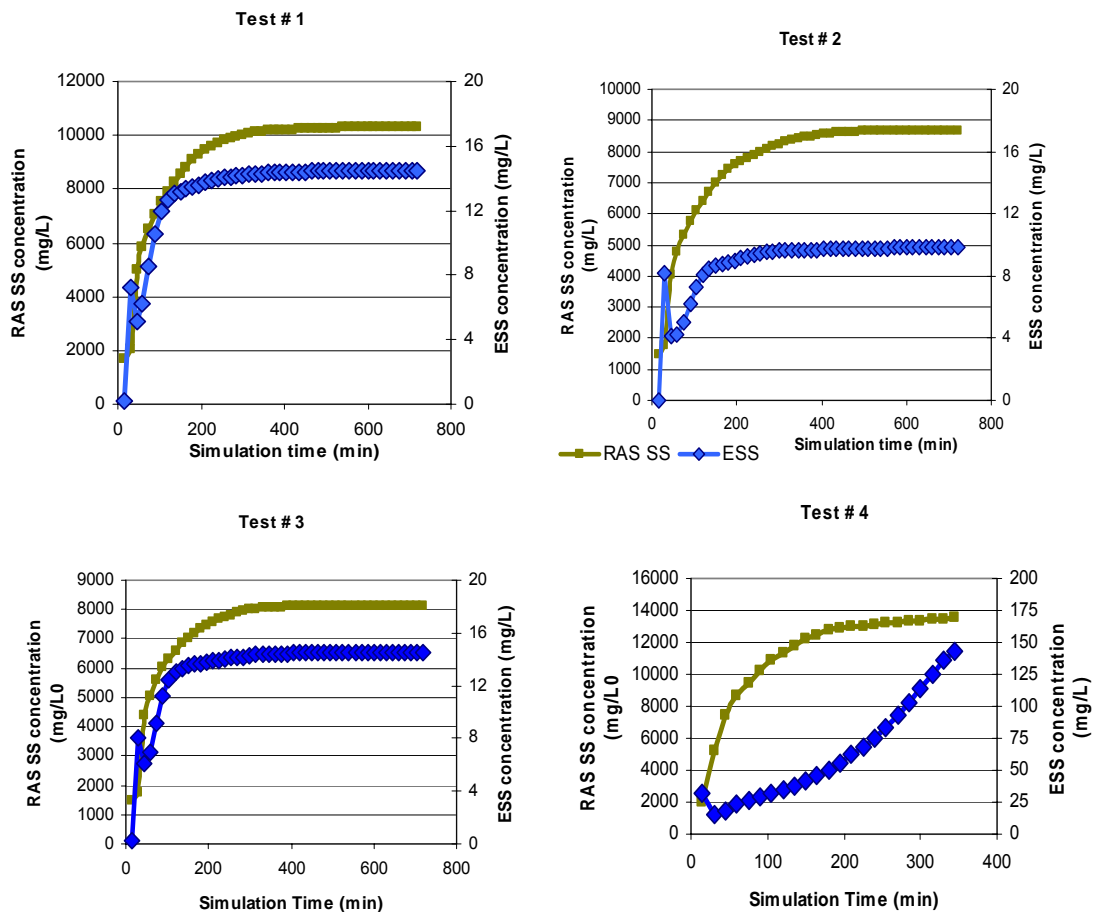
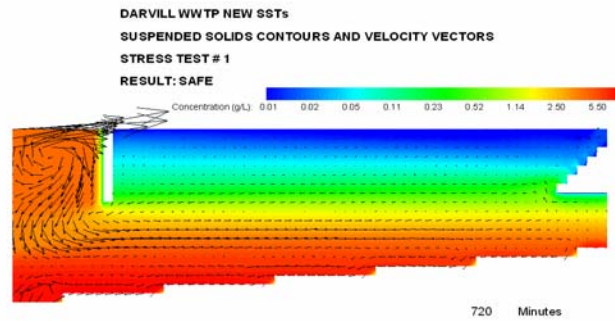
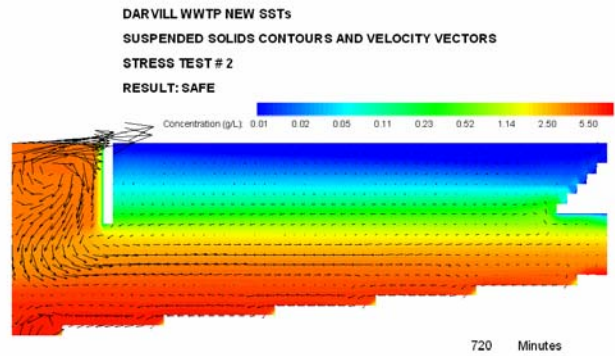


Figure 5.18 ESS and RAS SS Predicted by the Q3D Model for the Stress Test on the Darvill WWTP New SSTs

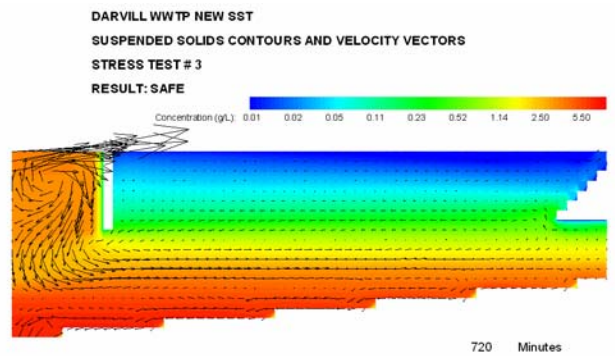
Figure 5.19 shows the suspended solids contours and velocity vectors for the four study cases. This figure indicates that the position of the sludge blanket for the safe cases and the raised sludge blanket for the fail case (Test 4). For the safe cases the top of the sludge blankets were between 2.30 and 2.70 m below the water surface. The actual predicted values are reported in Table 5.28.



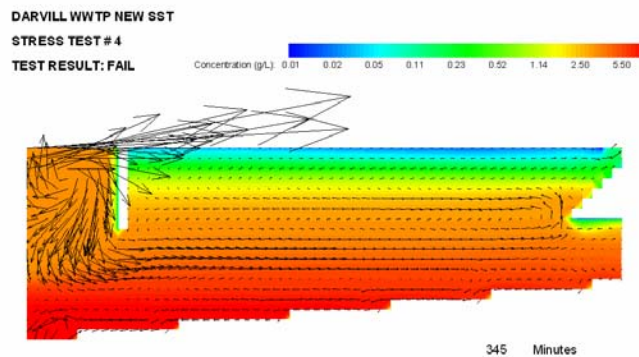
Stress Test # 1: Safe



Stress Test # 2: Safe



Stress Test # 3: Safe



Stress Test # 4: Fail

Figure 5.19 Suspended Solids Contours and Velocity Vector for the Four Stress Test on the Darvill WWTP New SSTs

Table 5.28 presents a summary of the predicted values by the Q3D model for the four cases. The values of the stress tests and the prediction results reported by Ekama and

Marais (2002) using the SettlerCAD 2D hydrodynamic model are also reported in this Table. The Q3D model agrees with the “safe” prediction of SettlerCAD 2D model for Test 3 and “Failure” for Test 4 but does not agree with the SettlerCAD 2D for the other two tests.

Table 5.28 Summary of the Q3D Model Simulation Results for the Stress Test 1 to 4 on the Darvill WWTP New SSTs. Comparison with the Actual Stress Tests and with SettlerCAD Simulations.

Actual Stress Tests*	Test 1	Test 2	Test 3	Test 4
Sludge Blanket Depth ¹	2.20	2.60	2.70	----
Effluent Conc. (ESS, mg/L)	17	5	10	---
Recycle Conc. (RAS SS, mg/L)	10000	9000	9000	15000
Test Duration (hours)	10.5	12.0	10.0	5.0
Test Outcome Safe/Fail ²	Safe	Safe	Safe	Fail
SettlerCAD Results*	Test 1	Test 2	Test 3	Test 4
Applied Flux (SLR KgSS/m ² /h)	7.17	6.06	6.35	11.13
Feed Conc. (MLSS, mg/L)	4600	4300	3600	3450
Recycle Conc. (RAS SS, mg/L)	9558	7517	8148	12863
Effluent Conc. (ESS, mg/L)	495	933	2.1	647
Test Outcome Safe/Fail ²	Fail	Fail	Safe	Fail
Q3D Model Results	Test 1	Test 2	Test 3	Test 4
Applied Flux (SLR KgSS/m ² /h)	7.17	6.06	6.35	11.13
Feed Conc. (MLSS, mg/L)	4600	4300	3600	3450
Recycle Conc. (RAS SS, mg/L)	10310	8690	8130	13530
Sludge Blanket Depth ¹	2.30	2.30	2.70	----
Effluent Conc. (ESS, mg/L)	14.8	9.8	14.5	143.0
Test Duration (hours)	12.0	12.0	12.0	5.8
Test Outcome Safe/Fail ²	Safe	Safe	Safe	Fail
Equilibrium Values	Test 1	Test 2	Test 3	Test 4
Recycle Conc. (RAS SS, mg/L) ³	10300	8700	8150	15100

*Values reported by Ekama and Marais (2002).

¹ Sludge blanket depth is the depth of the top of the sludge blanket from the water surface.

² SST failure interpreted as raised sludge blanket to the water surface and gross solids loss.

³ The equilibrium recycle suspended solids concentration is obtained by performing a mass balance at steady state conditions around the SST.

As noticed in Table 5.28, the Q3D model correctly predicted the outcome of the four stress tests on the new SSTs of the Darvill WWTP. This is a positive result; the Q3D model was more accurate than the SettlerCAD model that only predicted correctly two of the four tests. These results indicate that the assumptions made with respect to the compression rate properties are accurate, and might also be an indication that a compression sub-model is indispensable for the correct representation of the SLR on secondary clarifiers. For the runs that ended on steady state condition, i.e. Test 1, 2 and 3, the Q3D Model predicted ESS and RAS SS values that are very close to the values reported in the stress tests. All predicted ESS values are within a ± 5 mg/L difference or less with respect to the reported values; this is a very good agreement taking into account that the K_2 parameter of the Takacs' equation was assumed constant for the four cases. The predicted and measured RAS SS are also in good agreement, except for Test 4 that did not reach steady state conditions. Test 3 presents a 10% difference between the reported and predicted recycle concentrations, but the predicted value is much closer to the equilibrium value than the measured value. In the three safe cases the predicted RAS SS concentration values were approximately equal to the theoretical equilibrium values. A possible reason why the Q3D does a better prediction than SettlerCAD is that Q3D includes the compression phase.

CHAPTER 6

6 MODEL APPLICATIONS AND RESULTS

6.1 Influence of the Flocculation State on the Secondary Settling Tank Performance

The influence of the flocculation state of the incoming MLSS in the secondary clarifier performance was evaluated by simulating the Marrero SST under three different cases. Each case simulates a different flocculation state for the MLSS represented by different discrete settling fractions. Case 1 is the case presented during the calibration of the model in Section 5.1; Case 2 is the case presented during the calibration but with the settling fractions measured during the validation, and presented in Section 5.3; and Case 3 is a hypothetical case. The input data for the clarifier model simulation is the same data presented in Tables 5.10 and 5.13, with the exception of the discrete settling fractions which are different for cases 2 and 3 (for better comparison, the loadings, the settling and flocculation properties were assumed to be the same for the three cases). Table 6.1 presents the discrete settling fractions for the three cases.

Table 6.1 Discrete Settling Fractions for Three Study Cases

Fractions	Typical Vs m/h	Case 1	Case 2	Case 3
Large Flocs (f_1)	10.8	0.742	0.700	0.700
Medium Flocs (f_2)	3.0	0.255	0.256	0.200
Small Flocs (f_3)	0.68	0.003	0.044	0.100

The information presented in Table 6.1 indicates that the MLSS for Case 1 is better flocculated than the other two cases, and the MLSS for Case 3 is the poorest flocculated.

Table 6.2 presents the values of the ESS and RAS SS for the three cases after 360 minutes of simulation time, and Figure 6.1 shows the evolution of the ESS during the 360 minutes.

Table 6.2 ESS and RAS SS for Three Study Cases with Different Discrete Settling Fractions.

Fractions	Case 1	Case 2	Case 3
Large Floccs (f_1)	0.742	0.700	0.700
Medium Floccs (f_2)	0.255	0.256	0.200
Small Floccs (f_3)	0.003	0.044	0.100
ESS (mg/L)	9.9	15.3	25.8
RAS SS (mg/L)	8390	8364	8335

Simulation time = 360 min

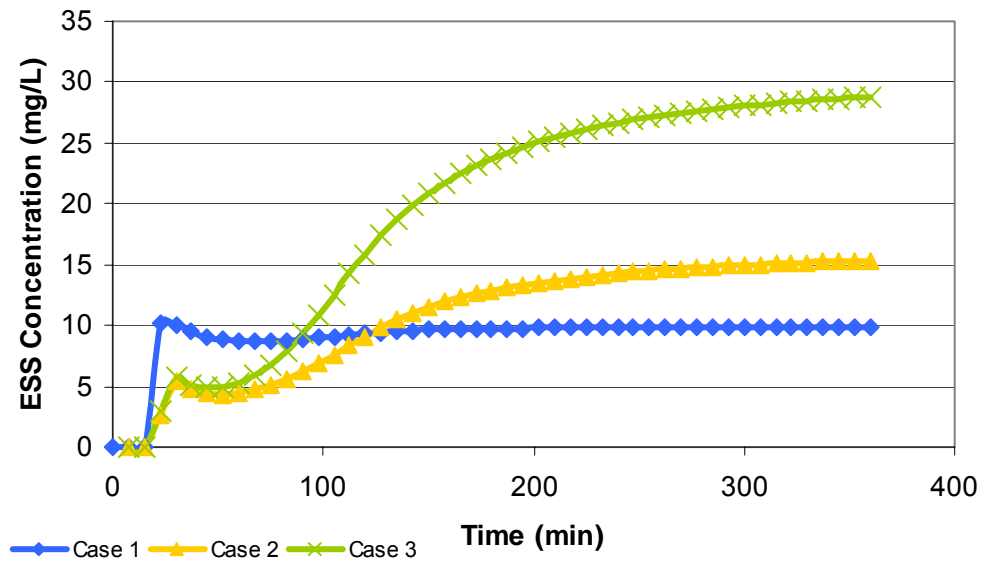


Figure 6.1 ESS for Three Study Cases with Different Initial Discrete Settling Fractions

Figure 6.1 and Table 6.2 show that the ESS is strongly related to the degree of flocculation of the MLSS prior to the settling tank. The better the flocculation state of the sample the lower the ESS. Several researches have demonstrated this conclusion by showing that a flocculation zone prior to the final settling stage can improve the general suspended solids removal efficiency (e.g. Parker et al., 1970, 1971, 1972; Das et al., 1993; La Motta et al., 2003). Furthermore, these results indicate that even when flocculation occurs in the clarifier, the effect might not be enough for getting a low effluent suspended solids when the influent to the clarifier is poorly flocculated.

6.2 Flocculation in Secondary Settling Tanks

In order to evaluate the effect of the flocculation process on the clarifier performance the simulation conditions for Case 2 presented in the previous section were repeated but deactivating the flocculation sub-model, i.e. shear and differential settling flocculation was not allowed inside the SST. Table 6.3 shows the values of the ESS and RAS SS concentration for Case 2 with and without flocculation effects after 360 minutes of simulation time. The ESS for the case with the activated flocculation submodel was 15.3 mg/L and for the case without flocculation was 24.6 mg/L. From this simple study case, it can be concluded that flocculation plays a major role in the performance of the secondary clarifier. For the Marrero Case and the study conditions used in Case 2 the flocculation process in the SST reduced the ESS by about 38%. Apparently the value of the RAS SS is not affected by the flocculation model; the slight difference presented in Table 6.3 appears to be due to different equilibrium RAS SS values caused by different ESS concentrations.

Table 6.3 ESS and RAS SS for a Study Case with and without Simulation of the Flocculation Process in the SST

Suspended Solids Concentration (mg/L)	Case 2: Flocculation Sub-Model On	Case 2: Flocculation Sub-Model Off
ESS	15.3	24.6
RAS	8364	8335

6.3 Effects of Center Well on Flocculation and Hydrodynamics

As observed in the previous sections, the flocculation in the SST plays an important role on the clarifier performance. In this respect, Parker et al. (1996) expressed that in order to encourage the aggregation of dispersed settleable solids in SSTs, these units should be equipped with a center well. They stated that the main function of the center well is to promote flocculation. Meanwhile, Merrill et al. (1992), using a 2D hydrodynamic model without modelling flocculation, found that the Center Well significantly improves the performance of SST. Interestingly both studies agreed on the optimum placement of the center well.

To clarify the effect of the center well on hydrodynamics and on flocculation a sensitivity study was conducted. Starting with the conditions presented for the “Case 2” discussed in the previous two sections, four conditions were studied: (1) Case 2 with center well and flocculation submodel on, (2) Case 2 with center well and flocculation submodel off, (3) Case 2 without center well and flocculation submodel on, and (4) Case 2 without center well and flocculation submodel off. Table 6.4 presents the values of the ESS and RAS SS concentration after 360 minutes of simulation time for the four conditions, and Figure 6.2 shows the evolution of the ESS with the simulation time.

Table 6.4 ESS and RAS SS for Three Study Cases in Center Well’s Effects

Suspended Solids Concentration (mg/L)	Case 2: Center Well Flocculation On	Center Well Flocculation Off	No Center Well Flocculation On	No Center Well Flocculation Off
ESS	15.3	24.6	108.6	126.2
RAS	8364	8335	8086	8044

From the results presented in Figure 6.2 and Table 6.4 it can be concluded that the center well promotes flocculation, but its most important contribution is the improvement of the tank hydrodynamics. The center well promotes flocculation by allowing enough contact time for the mixture in a zone of high velocity gradient (as can be observed in Figure 6.4), but the dominant role of the center well is the control of the re-entrainment of clarified fluid with the influent flow thus inducing a stronger upflow at the launder.

Figure 6.3 shows that the density current and the upflow velocities at the outlet zone are stronger for the tank without the center well. The center well decreases the strength of the density current by controlling the entrainment in the inlet zone; however, entrainment still occurs under the center well, suggesting that the dimensions of the center well could be improved.

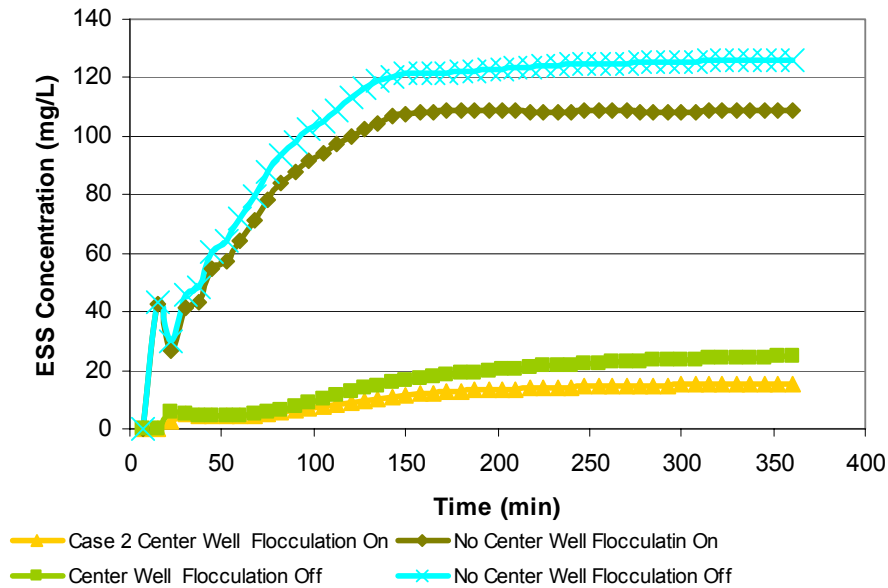


Figure 6.2 ESS for 4 Study Cases in Center Well Effects.

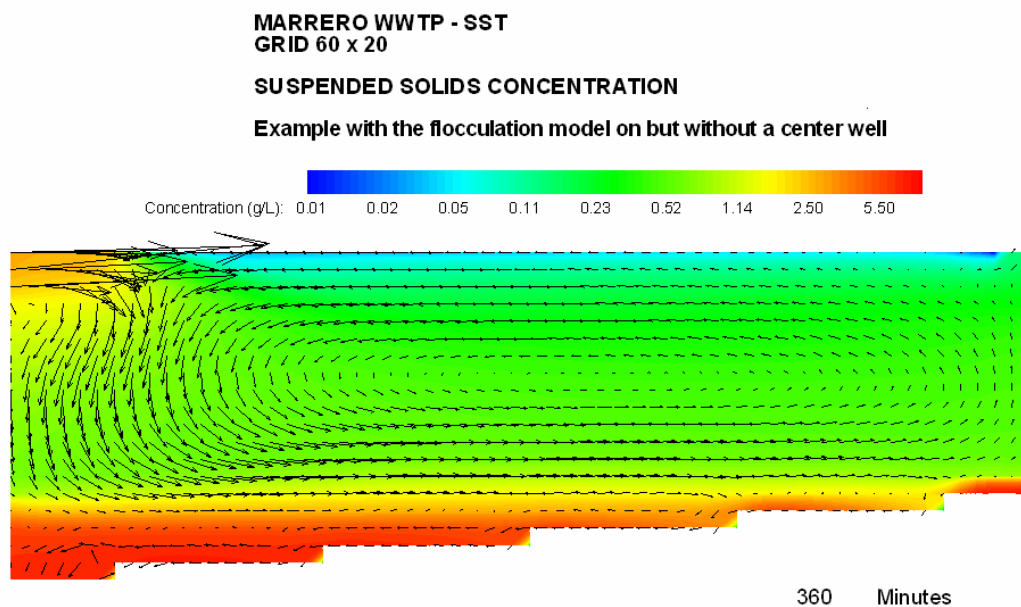
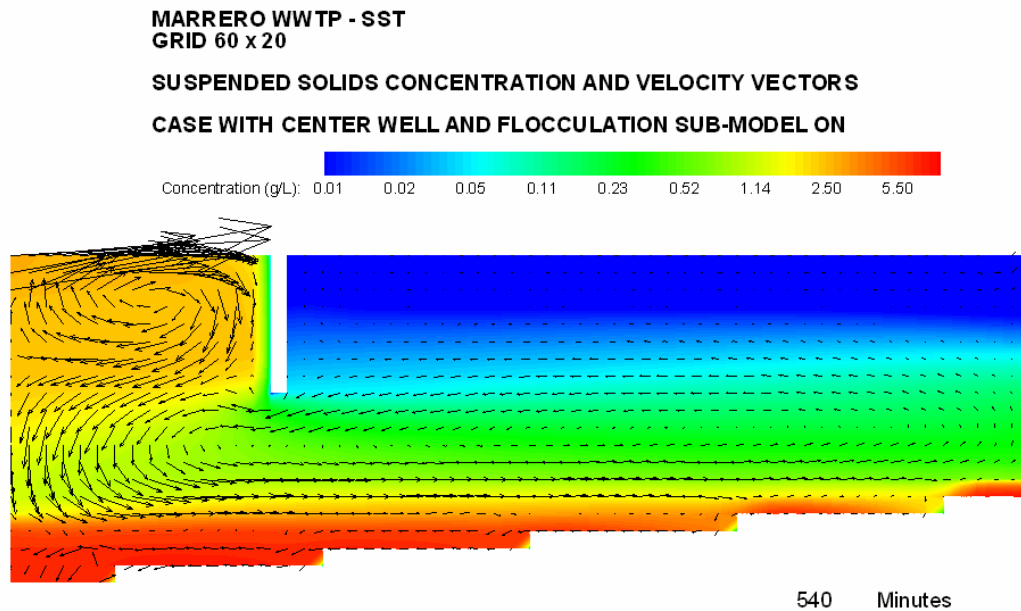


Figure 6.3 Concentration Contours and Velocity Vectors for the Marrero SST with and without Center Well.

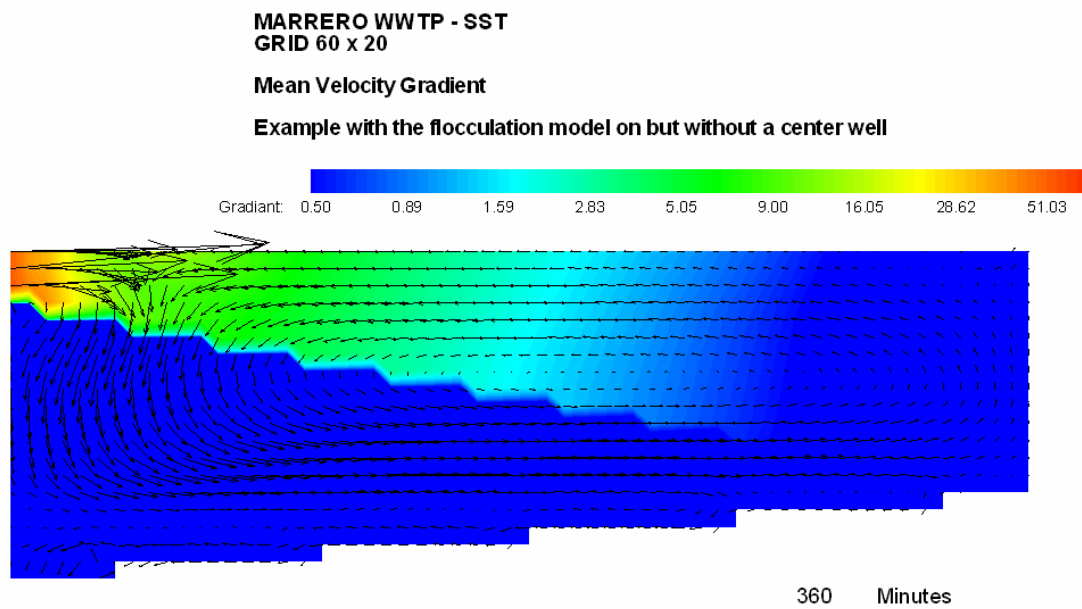
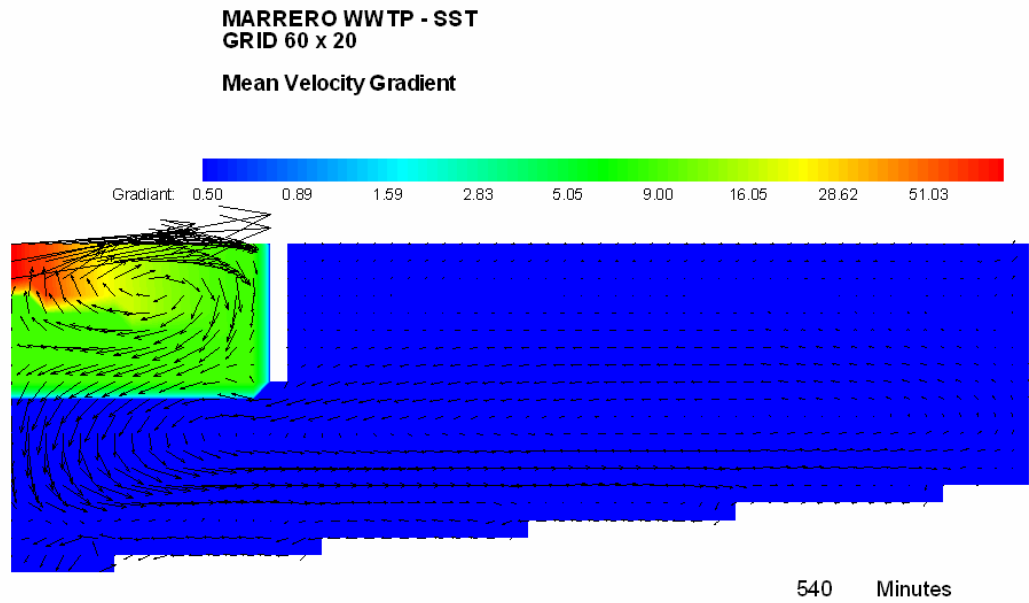


Figure 6.4 Mean Square Velocity Gradient for Marrero SST with and without Center Well.

6.4 Optimum Dimensions for the Center Well

The effect of the position of the center well on the clarifier performance was evaluated by simulating “Case 2” presented in Table 6.1 with different center well radius. The input data to the Q3D model is the same data presented in Tables 5.10 and 5.13 for the Marrero SST but with the settling fractions presented in Table 6.1 for “Case 2.” Figure 6.5 presents the values of the ESS and RAS SS for different radius of the center well.

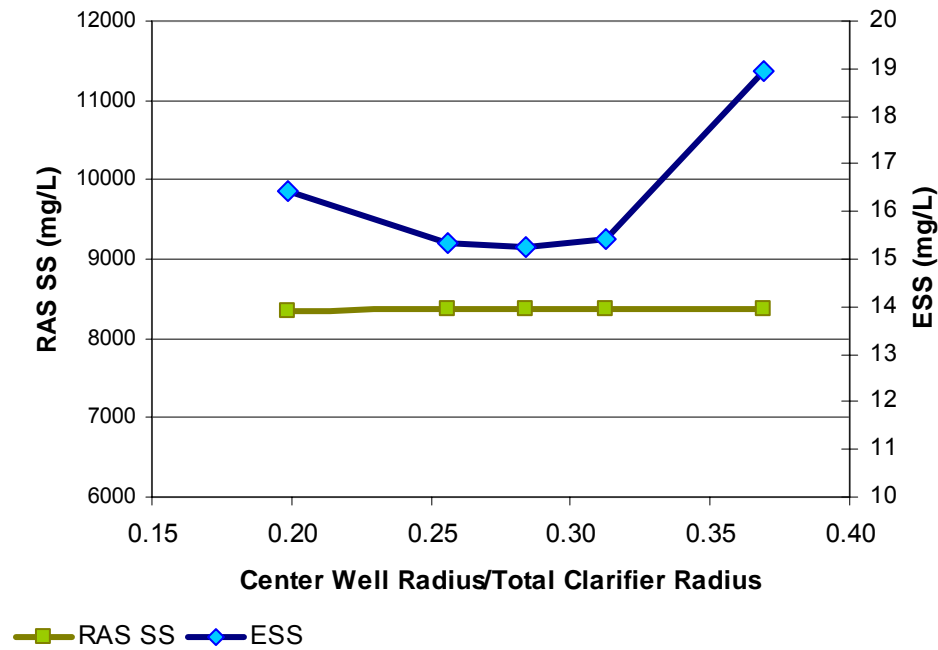


Figure 6.5 Effect of Center Well Radius on Clarifier Performance
(Baffle Depth = 2.6m, SOR = 1 m/h, SLR= 4.20 kg/m³, RAS = 50%)

According to Figure 6.5 the optimum radius for the center well under the study loading conditions (SOR= 1 m/h, MLSS = 2.8 Kg/m³, Recirculation Ratio = 0.5, SLR = 4.20 Kg/m²/h) is about 28% of the total clarifier radius for the 2.6 m baffle depth. The 28% of the total clarifier radius yields a 5 m baffle radius and allows a HRT for flocculation of about 8 minutes in the center well, based on the influent flow rate and only the volume of the flocculation well itself. If the volume below the center well is included in the calculation, the HRT is about 18 minutes. These values agree with the design recommendations presented by Ekama et al. (1997) who recommended a 20 minute detention time (based on the work of Wahlberg et al., 1994) and a center well diameter

extending from 20% to 35% of the tank diameter. Under slightly different loading conditions Merrill et al. (1992) concluded that the optimum center well diameter is in the range of 32 to 35 percent of the clarifier diameter. Similarly, Vitasovic et al. (1997) showed that drastic improvement could be found in a circular clarifier by decreasing the diameter of the center well from 45% to 28% of the clarifier diameter. Figure 6.6 shows the flow pattern and suspended solids contours for the optimum position (5 m radius), and for a smaller (3.5 m radius) and larger center well (6.5 m).

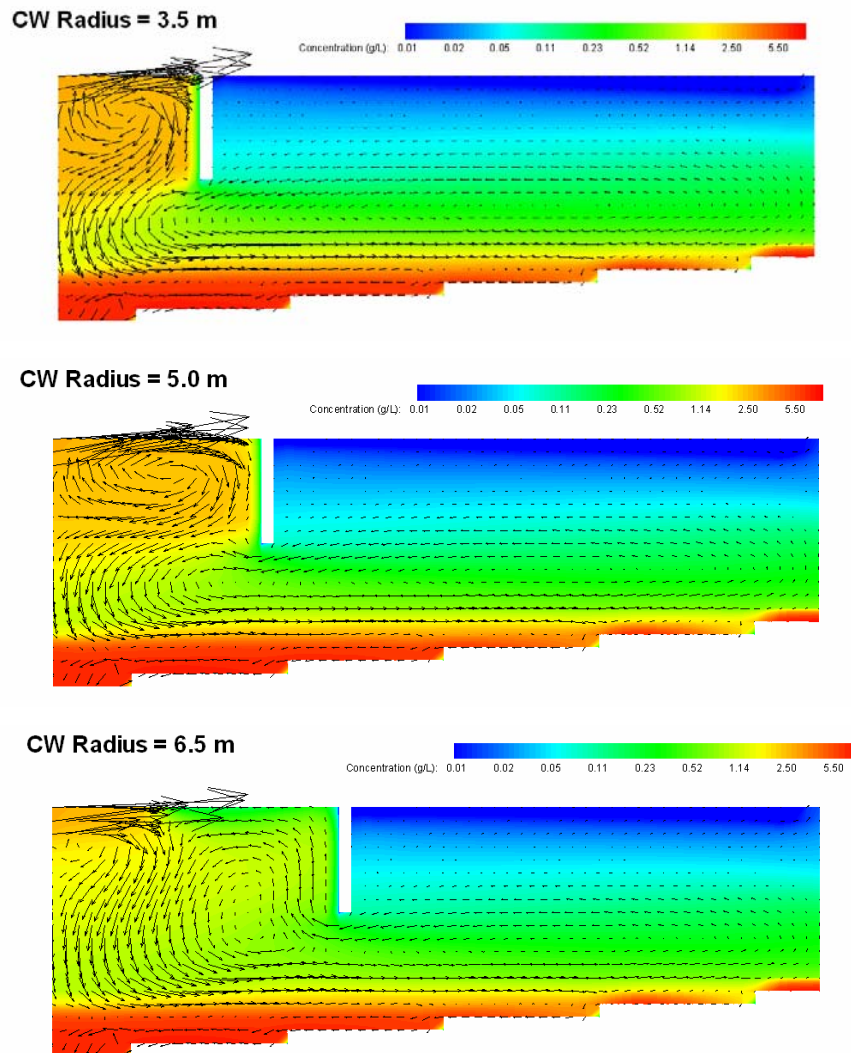


Figure 6.6 Effect of Center Well Radius on the Clarifier's Flow Pattern (Baffle Depth = 2.6m, SOR = 1 m/h, SLR= 4.20 kg/m³, RAS = 50%)

It seems that small center wells do not provide enough contact time for flocculation and slightly decrease the strength of the density current. On the other hand, large center wells do not provide good control of the re-entrainment of the fluid from the sedimentation zone, resulting in a strengthened density current. As discussed before, the optimum dimension for the study conditions was a 5 m baffle radius; however, even though this case produces the lowest ESS, it can be observed that re-entrainment is still occurring under the center well. This suggests that a deeper baffle could improve the hydrodynamics by further controlling the re-entrainment. Figure 6.7 shows the effect of the baffle depth on the ESS of the SST under the loading conditions presented in Table 5.10.

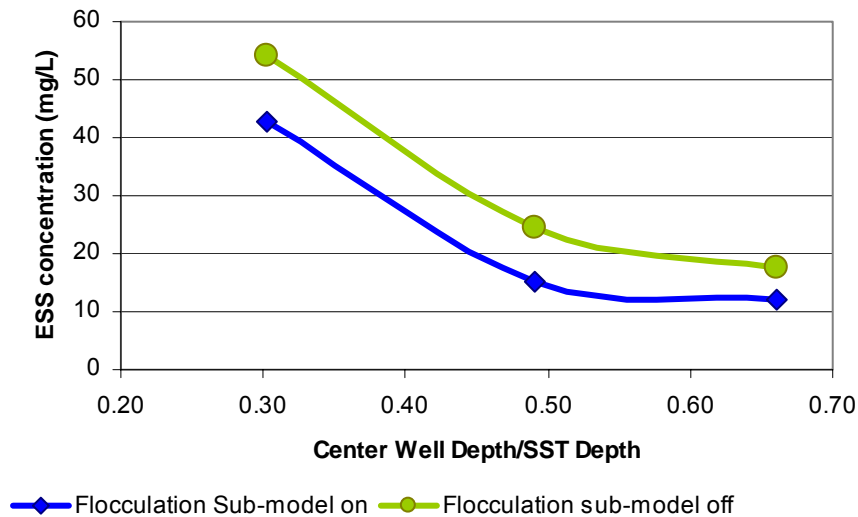


Figure 6.7 Effect of Center Well Depth on the ESS
(Baffle Radius = 5.0 m, SOR = 1 m/h, SLR= 4.20 kg/m³, RAS = 50%)

As suspected the deeper center well further controls the re-entrainment and decreases the strength of the density current, thus producing a lower ESS. This effect may be observed in Figure 6.8. Similarly a shallow baffle does not provide good control of the re-entrainment. Figure 6.7 suggests that the decreasing of the ESS with the baffle depth reaches an asymptote at about 70%, even though it was safe for the study conditions, it has been recognized that very deep center wells may be counter-productive to the performance of the SST when the sludge blanket approaches the bottom of the baffle. To evaluate the possible negative impact of a deep center well in the performance of the SST, the case studied in this section was re-run but under extreme loading conditions.

Using a high SOR (SOR=2.5 m/h) and keeping the MLSS constant (MLSS= 2.8 Kg/m³) the performance of the settling tanks with the baffles at 2.6m and 3.5 m depths were evaluated until the solution reached steady state conditions. Figure 6.9 shows the progression of the ESS values with the simulation time for the two baffle-depths. The tank with the deeper baffles (3.5 m depth) fails under the loading conditions at about 600 minutes while its RAS SS never reached the equilibrium value (Equilibrium RAS SS = 8400 mg/L), meanwhile the tank with the “normal” baffle (2.6 m depth) reached steady state at about 600 minutes for both ESS and RAS SS. Figure 6.10 shows the flow pattern and suspended solids contours for the 3.5 m and 2.6 m baffle depths at 780 and 1200 minutes of simulation time respectively. The solution was allowed to run until 1200 minutes to examine any evidence of failure. As seen in Figures 6.9 and 6.10 the tank with the normal depth (e.g. 2.6 m) is capable of producing a decent ESS under the extreme loading conditions.

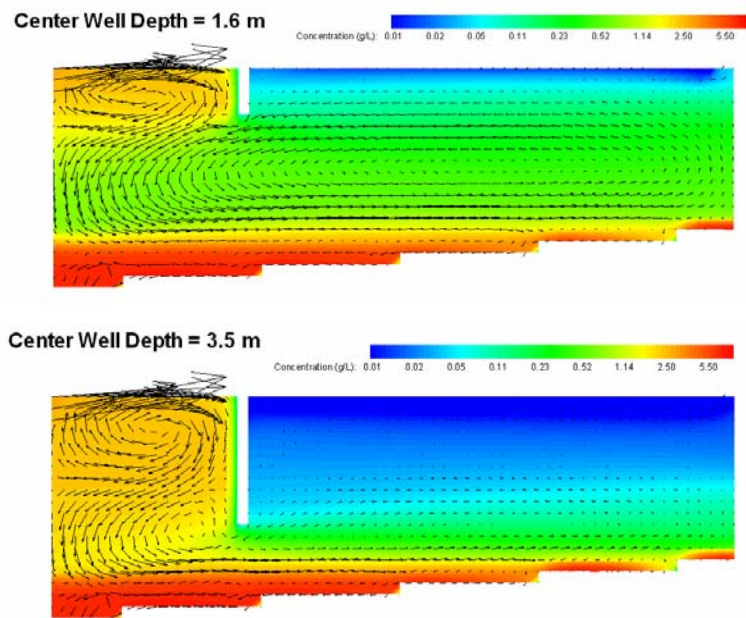


Figure 6.8 Effect of Center Well Depth on the Clarifier’s Flow Pattern (Baffle Radius = 5.0 m, SOR = 1 m/h, SLR= 4.20 kg/m³, RAS = 50%)

To further evaluate the effect of the center well on hydrodynamics and on flocculation, the cases presented in Figure 6.7 (for different baffles depth) were also simulated but turning off the flocculation sub-model. In all the cases the predicted ESS was lower when

the flocculation sub-model was on, reinforcing the point that the flocculation process in the center well improves the performance of the settling tank. For the case with the baffle depth at 50% of the total depth, the flocculation sub-model improved the ESS by about 38%; and for the case with the deeper baffle (66% of the total depth) the flocculation sub-model improved the ESS by 31%, even though the flocculation zone was bigger. These results indicate that the major effect of the deeper baffle is the control of the re-entrainment instead of providing a larger detention time for the flocculation process.

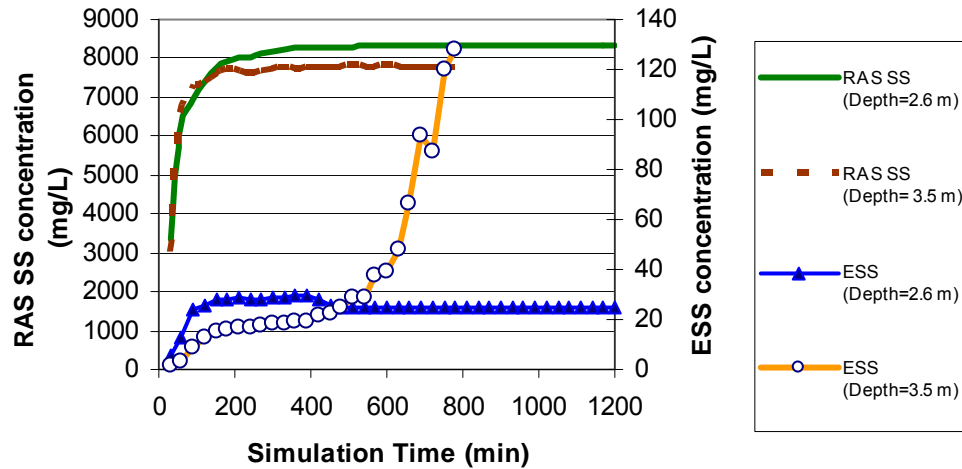


Figure 6.9 Comparison of Two Different Center Well Depths under Extreme Loading Conditions (Baffle Radius = 4.5 m, SOR = 2.5 m/h, MLSS = 2. kg/m³, RAS = 50%)

It may be argued that it is not necessary to have a deeper baffle to provide a larger flocculation time, since the region below the center well is well mixed and therefore its volume can be used for the calculation of the detention time; however, the values of the velocity gradient found with the Q3D model in the region below the baffles are not high enough to really promote shear flocculation (see Figure 6.4).

The model shows (see Figure 6.4 and 6.8) that the major energy dissipation and hence major G values occur in the zone defined by the actual center well.

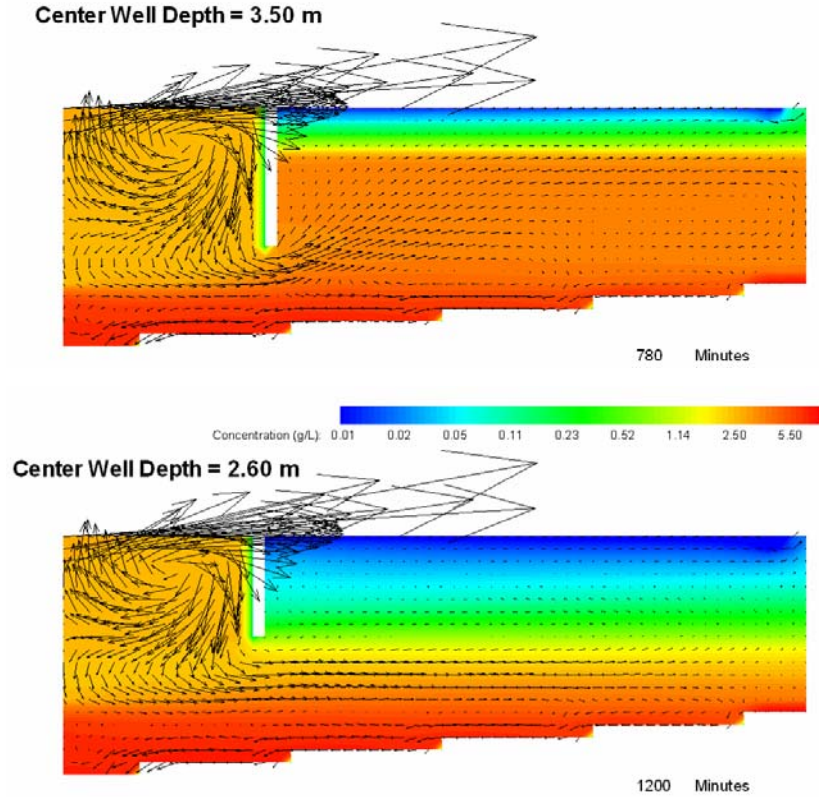


Figure 6.10 Flow Pattern and SS Contours for Two Different Center Well Depths under Extreme Loading Conditions
(Baffle Radius = 4.5 m, SOR = 2.5 m/h, MLSS = 2.8 kg/m³, RAS = 50%)

Due to this double functionality, i.e. promoting flocculation and improving hydrodynamics, the optimum dimension of the center well could be affected by distinct factors such as hydraulic and solids loading. The study of the effects of these factors on the optimum dimensions of the center well is presented in the next sections.

6.5 Effects of SLR (Constant SOR) on the Optimum Dimensions of the Center Well

The effect of the center well radius on the ESS concentration was evaluated for different SLR by keeping constant the SOR (1 m/h) and the recirculation ratio (0.5) and changing the MLSS (e.g., 1.8, 2.8, and 4.2 Kg/m³). The results are presented in Figure 6.11.

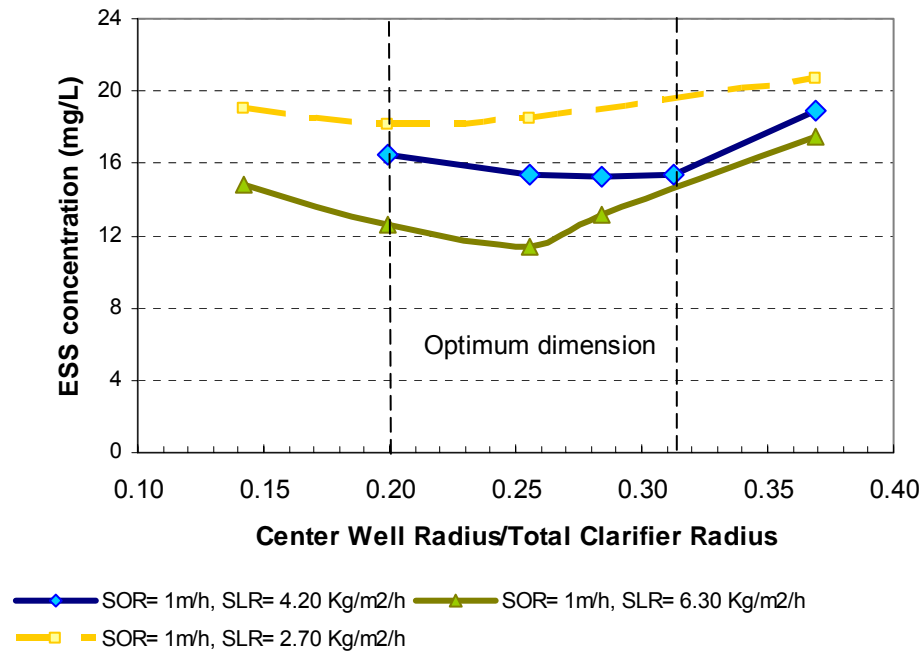


Figure 6.11 Effect of SLR on Optimum Position of the Center Well
(Baffle Depth = 2.6m, SOR = 1 m/h, SLR= Variable; RAS = 50%)
Note : SLR is defined as suggested by Ekama and Marais (2002) by $MLSS \cdot (SOR + UFR)$, where $UFR = SOR \cdot RAS$

Even though there is a defined optimum radius of the center well and the SLR (for low SLR and a constant SOR), the curves in Figure 6.11 indicate that an optimum placement of the center well becomes more distinct as the SLR increases. In general the optimum radius of the center well is between the 20 and 32 percent of the clarifier radius. This range is almost in the same design range proposed by Ekama et al. (1997) who recommend a center well diameter extending from 20% to 35% of the tank diameter.

An interesting and somewhat surprising finding in Figure 6.11 is that the ESS concentration decreases as the SLR (with a constant SOR) increases. This phenomenon is studied further in Section 6.7.

6.6 Effects of SOR (Constant MLSS, Variable SLR) on the Optimum Dimensions of the Center Well

To define the effect of the SOR on the optimum dimension of the center well, different baffle positions were evaluated under different SORs. The recirculation ratio (0.5) and the MLSS (2.8 kg/m^3) were kept constant during the simulations, thus changing the SLR with the change on the SOR. The SORs evaluated were 0.75, 1.0, 1.5 and 2.0 m/h and the baffle positions were defined during the runs to find the optimum radius for each SOR. The ESS was affected by the baffle position, while it did not seem to have any effect on the RAS SS. The results for the ESS concentrations are shown in Figure 6.12.

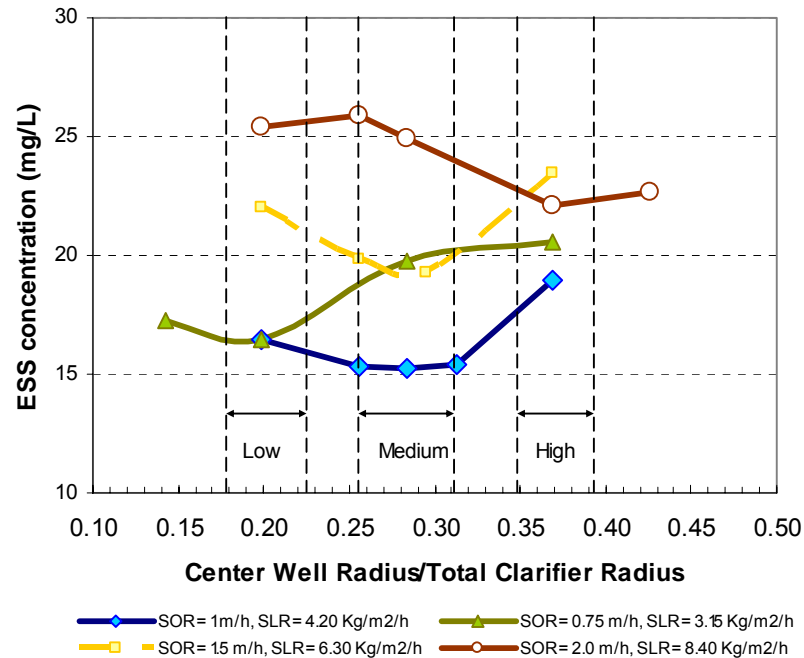


Figure 6.12 Effect of SOR on Optimum Position of the Center Well
(Baffle Depth = 2.6m, MLSS = 2.8 Kg/m^3 , SLR= Variable, RAS = 50%)

Figure 6.12 shows that the optimum size of the center well decreases as the SOR decreases: (1) for the low SOR the optimum radius is about a 20% of the total clarifier radius, (2) for the medium SORs the optimum radius were about a 28% of the total radius, and (3) for the high SOR the optimum radius increased to a 37%. This tendency can be observed in Figure 6.13. For SORs between 0.75 and 2.0 m/h the optimum

dimension of the center well radius changes in a range from 20 to 37%. This range is similar to the one presented in Figure 6.11 and agrees with the same design range proposed by Ekama et al. (1997).

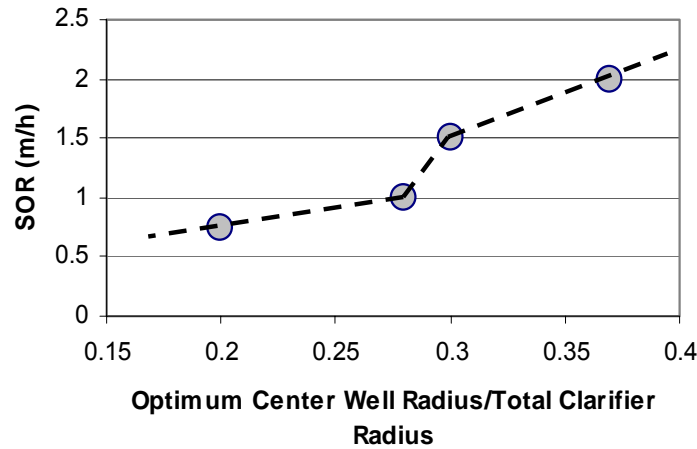


Figure 6.13 Optimum Center Well Radius versus SOR
(Baffle Depth = 2.6m, MLSS = 2.8 Kg/m³, SLR= Variable, RAS = 50%)

The reason for the behavior exhibited in Figure 6.13 is in the control of the re-entrainment and the promotion of the flocculation in the center well. As discussed before, large center wells do not provide a good control of the re-entrainment; but this statement is true for low and medium SORs. In the presence of high SORs the turbulence and eddy motion dominates the flow in the center well restringing the re-entrainment of the fluid from the sedimentation zone. Obviously, the same effect will occur with smaller baffles and high SOR, but in the case of the larger baffle there is more contact time for the flocculation process at adequate G values produced by the conversion of the high inlet kinetic energy. Figure 6.14 shows how the re-entrainment of the clarified fluid in the center well significantly decreases as the SOR increases for the large baffle.

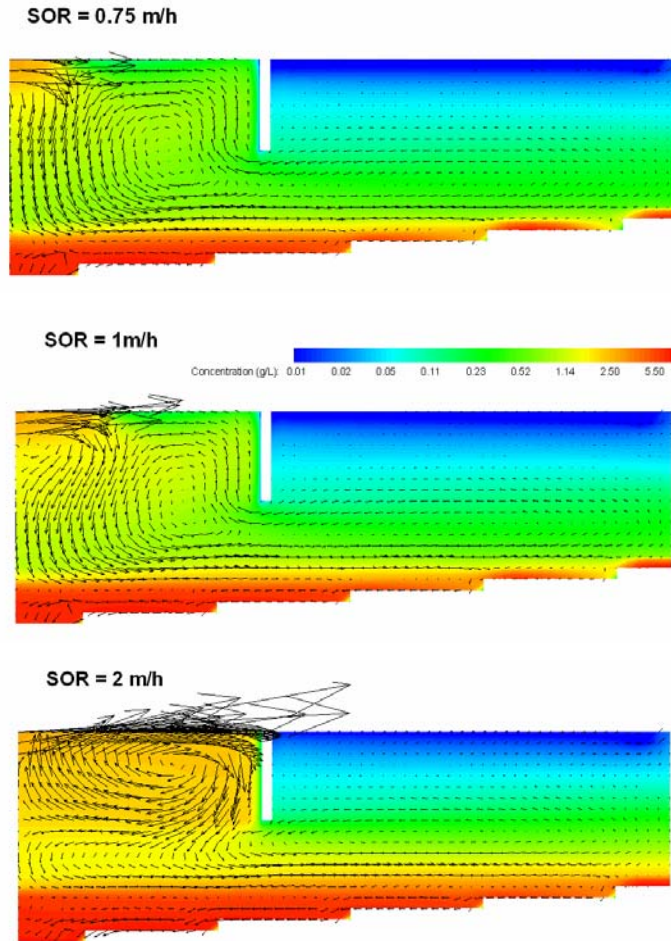


Figure 6.14 Flow Pattern and SS Contours for a Large Center Well under Different SOR Loadings
(CW Radius = 6.5 m, CW Depth = 2.6 m, MLSS = 2.8 kg/m³, RAS = 50%)

6.7 Solids Flux Limiting Analysis for the Marrero WWTP - Maximum SLR

6.7.1 1D Solids Flux Analysis

Using the 1D solids flux analysis presented by Tchobanoglous et al. (2003), the limiting solids flux for the Marrero WWTP was found using two different analyses. In the first analysis the measured settling properties for zone settling, i.e., $V_o = 10.54$ m/h and $K_I = 0.40$ L/g, were applied to the complete range of suspended solids concentration used in

the solids flux analysis. The SOR was set equal to 1.0 m/h, and the recirculation ratio equal to 0.5. Figure 6.15A shows the fluxes used in the analysis; from the solids-flux curves presented in Figure 6.15A, the limiting solids flux for this analysis was found to be equal to 6.93 Kg/m².h

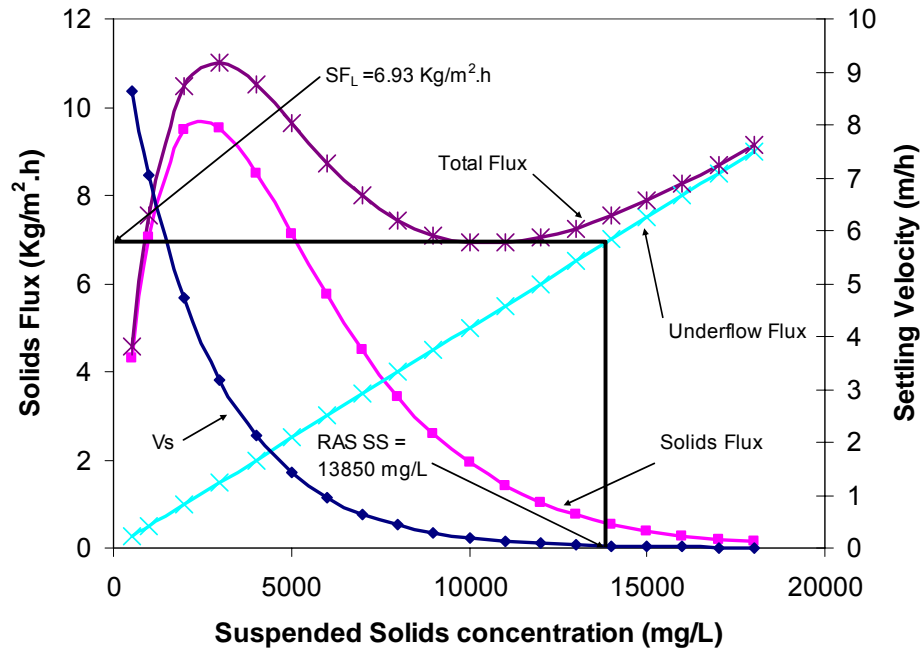


Figure 6.15A 1D Solids Flux Analysis for the Marrero WWTP using the Zone Settling Properties
($V_o = 10.54$ m/h and $K_I = 0.40$ L/g)

The second analysis was conducted using the settling properties for zone settling but also the settling properties for compression rate, according to Equation 5.10. These settling properties were presented in Table 5.9 and are recapitulated in Table 6.5 indicating the zone and compression settling thresholds.

Table 6.5 Settling Properties used in the Solids Flux Analysis

Zone Settling Properties	Value
Zone Settling Threshold	600 mg/L
V_o	10.54 m/h
k_1	0.4 L/g
Compression Rate Properties	Value
Compression Settling Threshold	5400 mg/L
V_o	3.20 m/h
K_c	0.184 L/g

Figure 6.15B shows the fluxes used in the second analysis. From the solids-flux curves presented in Figure 6.15B, the limiting solids flux under for this analysis was found to be equal to 9.15 Kg/m².h

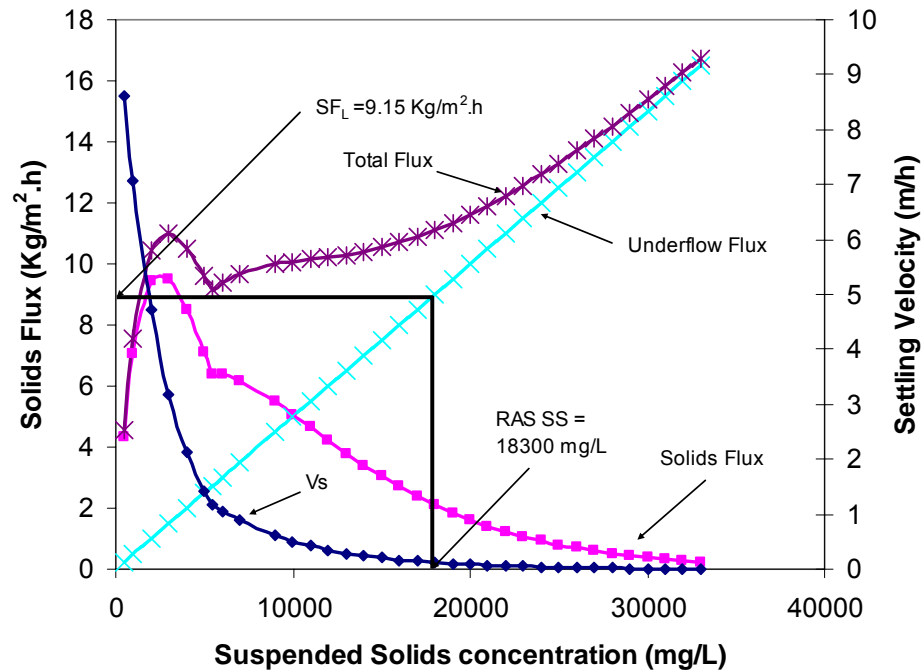


Figure 6.15B 1D Solids Flux Analysis for the Marrero WWTP using the Zone Settling and Compression Rate Properties
(V_o = 10.54 m/h, K_1 = 0.40 L/g, V_c = 3.20 m/h, K_c = 0.184 L/g)

The results found with the two different 1D solids flux analysis indicate the sensitivity of this procedure to the settling properties. The predicted limiting solids flux using only the zone settling properties was 76% of the predicted flux using both the zone settling and the compression rate properties. The second analysis should be more accurate since it has a better representation of the settling properties of the sludge. However, some researchers have indicated that the 1D solids flux analysis consistently over predicts the limiting solids flux, and reduction factors have been recommended. For example, Ekama et al. (1997) recommended an 80% reduction in the SLR found with the 1DFT, but there is no evidence that this factor should be applied for all SSTs. Based on this consideration there are some uncertainties about which limiting solids flux is more realistic, i.e., 6.93 or 9.15 Kg/m².h. In order to better define the limiting solids flux for the Marrero WWTP, and to compare it with the 1D analyses, several runs were conducted using the Q3D Model (until steady state conditions were reached). In this runs the SOR and the RAS ratio were kept constant and the MLSS was changed in order to simulate different SLR. These tests are discussed in the next section.

6.7.2 Q3D Solids Flux Analysis

Setting the SOR and the underflow rate (UFR) constant at 1.0 m/h and 0.5 m/h respectively, the Marrero WWTP SST was simulated under different MLSS loadings, i.e., 1.8, 2.8, 4.2, 4.5, 4.7, 4.8, 5.0 and 5.1 Kg/m³. The different MLSS reproduce different SLRs (see Table 6.6). The SLR was slightly increased with every simulation to define the maximum allowable SLR for the Marrero clarifier. The simulations were run until steady conditions were reached, or until failure of the clarifier (Failure was identified as a rise of the sludge blanket to the water surface or as an ESS value higher than 30 mg/L). Steady state conditions were assumed to be reached when the RAS SS concentration was $\pm 2\%$ or less of the equilibrium value obtained with a mass balance of suspended solids around the secondary clarifier, provided that the ESS of the simulation did not change more of than 5% in the last 30 minutes of simulation. The simulated SOR, MLSS, SLR, the expected RAS SS, and the predicted ESS and RAS SS concentrations are presented in Table 6.6. Figure 6.16 shows the ESS concentration for each SLRs.

Table 6.6 Simulated Data and Predicted ESS and RAS SS in the Solids Flux Analysis of the Marrero WWTP SST (RAS = 50%)

MLSS (mg/L)	SOR (m/h)	UFR (m/h)	SLR (kg/m ² .h)	ESS (mg/L)	RAS SS (mg/L)	Expected RAS SS* (mg/L)	Test Result**
1800	1.0	0.5	2.70	18.5	5360	5400	Safe
2800	1.0	0.5	4.20	15.3	8370	8400	Safe
4200	1.0	0.5	6.30	11.4	12550	12600	Safe
4500	1.0	0.5	6.75	10.5	13463	13500	Safe
4700	1.0	0.5	7.05	11.9	14060	14100	Safe
4800	1.0	0.5	7.20	12.2	14312	14400	Safe
5000	1.0	0.5	7.50	12.2	14940	15000	Safe
5100	1.0	0.5	7.65	123	14565	15300	Fails

*The expected RAS SS values are found applying a mass balance around the SST, in this case the ESS concentration was neglected in the balance.

** SST failure interpreted as raised sludge blanket to the water surface or an ESS 30 mg/L.

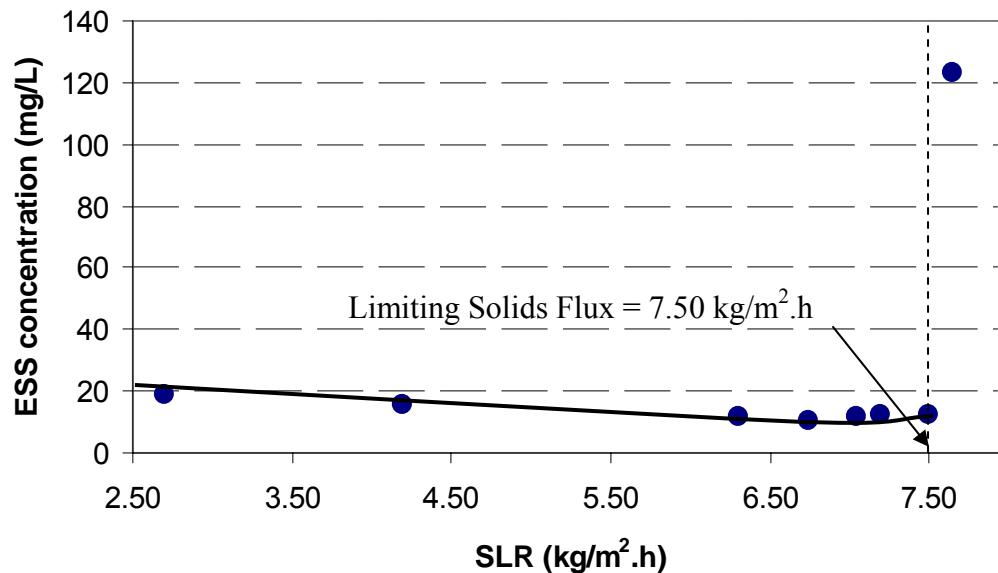


Figure 6.16 ESS vs SLR. Limiting Solids Flux Analysis.
(SOR= 1 m/h, UFR= 0.5 m/h, MLSS= Variable, RAS =50%)

The Q3D model predicted a limiting SLR equal to 7.50 Kg/m².h. This value is slightly higher than the 1D prediction using the zone settling properties (6.93 Kg/m².h), but is 82% of the limiting solids flux predicted with the 1D model when the compression rate properties were taken into consideration (9.15 Kg/m².h). Assuming that the Q3D model is the real limiting SLR, the prediction of the first 1D analysis would be closer to this target (8% under-prediction); but, as mentioned before the second 1D analysis should be the more accurate (because it used a more realistic settling model). However the second analysis over predicted the SLR by a higher 22%. Assuming that the second 1D analysis is the correct one, the 80% reduction in the 1D predicted limiting flux is an accurate correction factor, and it can be concluded that the Q3D model “automatically” reproduces a flux rating < 1.0 with respect to the 1DFT, where the flux rating is the capacity of the SST as a % of the 1DFT. If it were assumed that the first 1D analysis is the correct one and the 80% correction factor were applied, the suggested limiting SLR by the 1D model would be 5.54 Kg/m².h (a value 26% lower than the real one). This would be an important under-prediction of the real clarifier capacity. If a 1D model is used, the recommendation would be to perform the 1D procedure with settling values for the entire curve of suspended solids concentrations used in the analysis, and applied an adequate correction factor. Due to the uncertainty of the correction factor’s value, it seems that the better approach is to use an accurate 2D model for the final estimates.

The failure of the Marrero WWTP for a SLR higher than 7.50 Kg/m².h (for SOR = 1 m/h and UFR= 0.5 m/h) and a MLSS higher than 5.0 Kg/m³ occurs due to an excessive rise of the sludge blanket produced by the accumulation of sludge due to the incapacity of the tank to reach the equilibrium “expected” RAS SS concentration. In fact in all the safe cases the predicted RAS SS was very close to the expected equilibrium value (less than 1% difference) presented in Table 6.6. In the predicted limiting SLR the depth to the sludge blanket (measured from the water surface to the top of the sludge blanket) reached a higher equilibrium-safe value of 2.60 m even after 72 hours of simulation time. In the next simulation (SLR = 7.65 Kg/m².h, and MLSS = 5.1 Kg/m³) the sludge blanket almost reached the water surface and the clarifiers failed with very high ESS (before the 72 hours of simulation time). These conditions are represented in Figure 6.17.

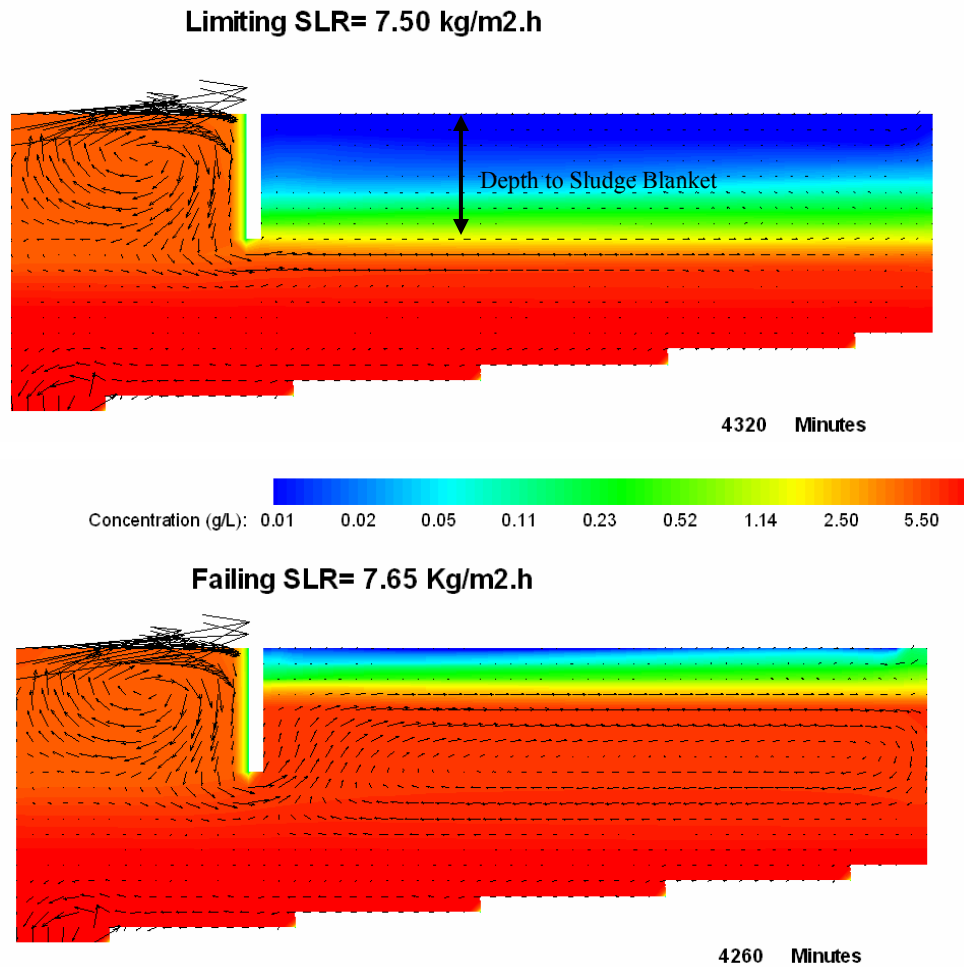


Figure 6.17 Sludge Blanket Position for Limiting and Failing SLRs
(SOR= 1 m/h, UFR= 0.5 m/h, MLSS= Variable, RAS = 50%)

Figures 6.9 and 6.16 show a similar tendency; the ESS concentration decreases as the SLR increases. In Figure 6.16 the ESS decreases as the SLR increases until the ESS reaches a minimum value and then it starts increasing again until it suddenly fails. In these graphs the SLR increases due to a rise in the incoming MLSS because the SOR and the UFR were kept constant at 1 m/h and 0.5 m/h respectively. Since the SOR was kept constant, the reason for the improvement may not be an improved hydrodynamics, since the density current is strengthened as the MLSS increases due to a higher density differential with the ambient fluid. The reason for this behavior is an improvement of the

flocculation process with increasing MLSS, basically for two reasons: (1) when the MLSS concentration increases, the concentration in the center well obviously increases and with it the shear flocculation rate, due to a higher opportunity of contact between the particles. Equations 2.35, 2.37 and 2.39 support this concept. (2) The increase of the MLSS also increases the sweep flocculation in the center well. The sweep flocculation occurs due to the trapping of small particles in the matrix formed during the zone settling process.

Based on the preceding discussion, the improvement in the ESS concentration with the increasing SLR is not necessary true for the case of an increasing SOR. The study of the influence of the SOR on the clarifier performance is presented in the next section.

6.8 Effect of the SOR on the Performance of the SST – Marrero Case

The effect of the SOR on the clarifier performance was evaluated by simulating different SORs using the geometry and settling properties of the Marrero SST. During the simulations the MLSS and the recirculation ratio were kept constant at 2.8 Kg/m^3 and 0.5 respectively. The UFR and the SLR increased as the simulated SOR increased. Table 6.7 presented a summary of the simulated SOR, UFR and SLR and the ESS and RAS SS concentrations predicted by the model. The simulations were run until steady conditions were reached or until failure of the clarifier, following the same criteria used in Section 6.7.2. A mass balance around the SST (for a constant recirculation ratio) yielded an equilibrium RAS SS concentration close to 8400 mg/L ; all the tests that reached steady state conditions, i.e. the outcome was safe, presented a RAS SS very close to this value. The SOR and the SLR did not seem to have any influence in the RAS SS concentration for the test that ended as “safe” (see Table 6.7). The test that showed the failure of the clarifier did not reach the equilibrium RAS SS concentration.

Figure 6.18 shows the ESS concentration as a function of the SOR and the SLR. This figure shows that the ESS slightly increases as the SOR increases; however, the ESS is almost independent of the SOR until the tank suddenly fails.

Table 6.7 Simulated Data and Predicted ESS and RAS SS in the Study of the Effect of the SOR on the Performance of the Marrero SST

SOR (m/h)	UFR (m/h)	MLSS (mg/L)	SLR (kg/m ² .h)	ESS (mg/L)	RAS SS* (mg/L)	Test Result**
0.65	0.325	2800	2.73	15.72	8367	Safe
0.75	0.375	2800	3.15	16.00	8364	Safe
1.00	0.5	2800	4.20	15.75	8370	Safe
1.50	0.75	2800	6.30	19.84	8359	Safe
1.70	0.85	2800	7.14	23.12	8352	Safe
1.80	0.9	2800	7.56	20.10	8358	Safe
1.90	0.95	2800	7.98	22.31	8354	Safe
2.00	1.0	2800	8.40	25.90	8347	Safe
2.20	1.1	2800	9.24	25.78	8347	Safe
2.50	1.25	2800	10.50	24.97	8349	Safe
3.00	1.5	2800	12.60	183.00	7937	Fails

*The expected RAS SS values is 8400 mg/L.

** SST failure interpreted as raised sludge blanket to the water surface or an ESS 30 mg/L

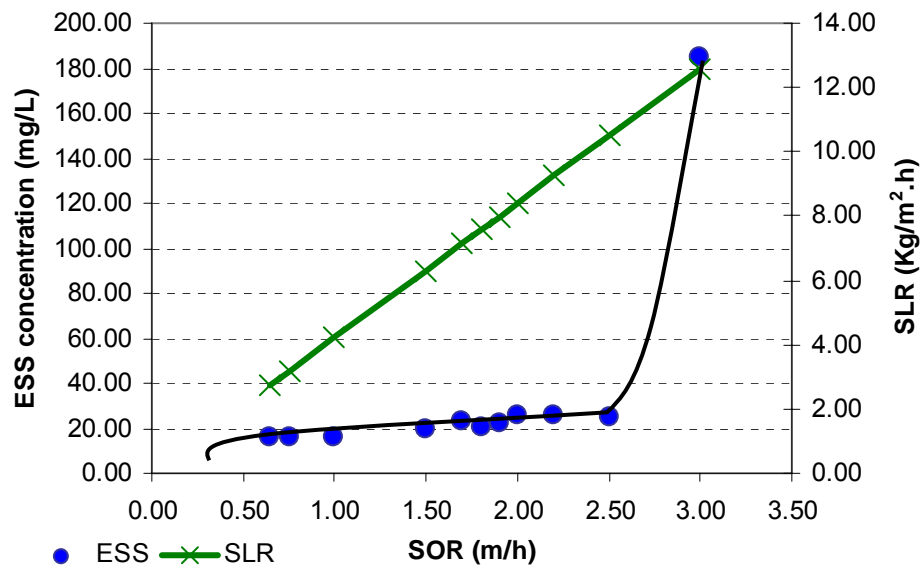


Figure 6.18 ESS vs SOR. Limiting Solids Flux Analysis.
(SOR= Variable, UFR= 0.5xSOR, MLSS= 2.8 Kg/m³)

As can be noticed in Figure 6.19 the failure of the tank occurs because of solids overload, causing the exaggerated rise of the sludge blanket with the consequent gross loss of solids. On the other hand, even though the relationship presented in Figure 6.18 between the SOR and the ESS is relatively flat, indicating that the ESS is almost independent of the SOR, the tendency shows that the ESS slightly increases as the SOR increases. This increase appears to be due to a rise of the sludge blanket as the SLR increases with the SOR instead of a direct effect of the high volumetric flow. Figure 6.19 shows the position of the sludge blanket for some of the tests.

Section 6.7.2 indicated that the limiting solids flux for the Marrero SST (for $SOR = 1$ m/h, and $UFR = 0.5$ m/h) was $7.50 \text{ Kg/m}^2\cdot\text{h}$, and also that this value was the 82% of the limiting solids flux predicted with the 1D model when the compression rate properties were taken into consideration. Figure 6.18 shows that increasing the SOR can increase the limiting solids flux of the Marrero clarifier. The reason for this is the increase in the underflow flux, caused by the higher UFR. Figure 6.19 indicates that the maximum SLR found by increasing the SOR, and keeping the MLSS and the recirculation ratio constant, is about $10.50 \text{ Kg/m}^2\cdot\text{h}$.

The value of limiting solids flux predicted by the Q3D model was compared to the limiting solids flux predicted by a 1D model using the same procedure presented in Section 6.7.1. Again the 1D limiting solids flux was found using two sets of settling properties: (1) using only the zone settling properties, and (2) using the zone settling and the compression rate properties. The limiting solids fluxes were found to be 13.23 and $13.27 \text{ Kg/m}^2\cdot\text{h}$ for the first and second case respectively. This time, both predictions were higher than the Q3D model prediction; however, if an 80% reduction is applied to the second case the two predicted limiting SLRs are very close (10.6 and $10.5 \text{ Kg/m}^2\cdot\text{h}$). The 1D limiting solids flux analyses are presented in Appendix I.

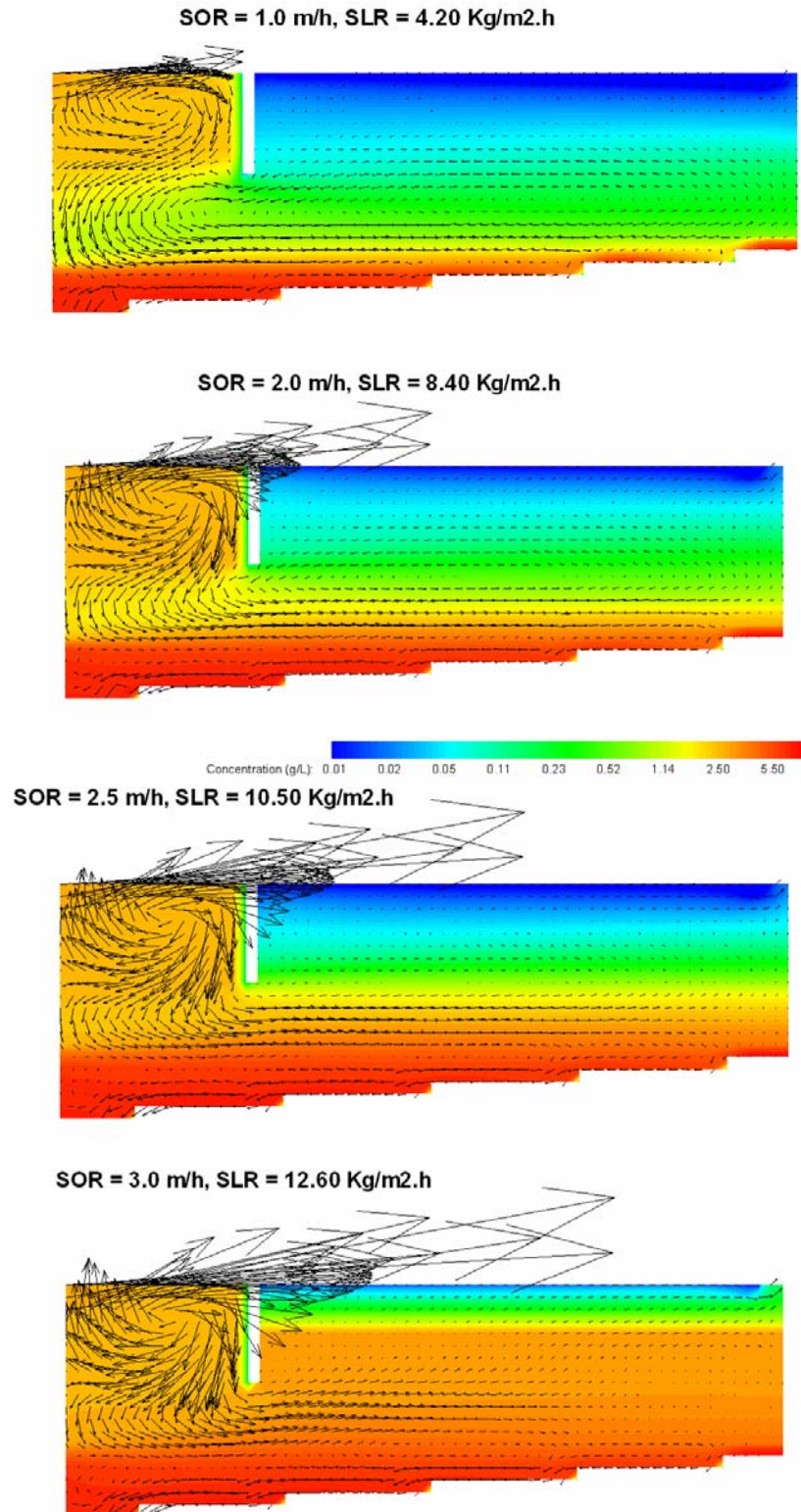


Figure 6.19 Influence of SOR in the Flow Pattern and the Position of the Sludge Blanket (SOR= Variable, UFR= 0.5xSOR, MLSS= 2.8 Kg/m³)

6.9 Effect of the SOR and the MLSS on the Performance of the SST for a Constant SLR – Marrero Case

Section 6.7 described the evaluation of the performance of the Marrero SST with a constant SOR and changing the MLSS and the SLR; it was found that the performance was improved with an increase of the SLR until a certain point, where it slowly started to perform poorly until it suddenly failed by a solids overload. Section 6.8 evaluated the performance of the Marrero SST with a constant MLSS and by changing the SOR and the SLR; it was found that the ESS of the SST is almost independent of the SOR until it suddenly failed, again due to a solids overload. In this section the effect of the SOR and MLSS was evaluated by setting constant the SLR at a value equal to $4.20 \text{ Kg/m}^2\cdot\text{h}$ (normal operating conditions of the Marrero WWTP with $\text{SOR} = 1\text{m/h}$, $\text{UFR} = 0.5 \text{ m/h}$ and $\text{MLSS} = 2.8 \text{ Kg/m}^3$). Five different conditions were simulated by changing the SOR, the UFR and the MLSS and keeping constant the SLR and the recirculation ratio (0.5). Table 6.8 presents a summary of the loading conditions and the predicted ESS and RAS SS using the Q3D model. Similar to the previous cases, the simulations were run until they reached steady conditions or showed evidence of failure (as in the other sections the failure was identified as a exaggerated rise of the sludge blanket or as an ESS higher than 30 mg/L , and the steady conditions were assumed to be reached with a RAS SS within $\pm 2\%$ or less of the expected equilibrium value).

Table 6.8 Simulated Data and Predicted ESS and RAS SS in the Study of the Effect of the SOR and MLSS with Constant SLR on the Performance of the SST

MLSS (mg/L)	SOR (m/h)	UFR (m/h)	SLR (kg/m ² .h)	ESS (mg/L)	RAS SS (mg/L)	Expected RAS SS (mg/L)	Test Result
5600	0.50	0.25	4.20	9.15	16122	16800	Fail
5000	0.56	0.28	4.20	10.00	14860	14964	Safe
2800	1.00	0.50	4.20	15.75	8370	8369	Safe
1800	1.56	0.78	4.21	29.27	5345	5362	Safe
1400	2.00	1.00	4.20	36.66	4131	4163	Fail

From the five simulations presented in Table 6.8, three were identified as “safe” and two as “fail” cases. The first fail case correspond to $SOR = 0.5$ m/h and $MLSS = 5600$ mg/L; even though the reported ESS for this case is only 9.15 mg/L, the case is reported as a “fail” because the RAS SS concentration did not reach equilibrium after 96 hours of simulation time and the sludge blanket was still rising (see Figure 6.21). This failure is due to a solids overload. The second fail case correspond to $SOR = 2.0$ m/h and $MLSS = 1400$ mg/L. In this case, the run reached steady state conditions, and the RAS SS concentration was very close to the expected equilibrium value (less than 1% difference). The sludge blanket for this case was very thin (see Figure 6.21). As can be observed in Figure 6.21, the failure was due to the excessive carry over of suspended solids by the upward current towards the effluent weir.

Figure 6.20 shows the ESS concentrations predicted by the model as a function of the SOR and the MLSS for a constant SLR ($4.20 \text{ Kg/m}^2 \cdot \text{h}$).

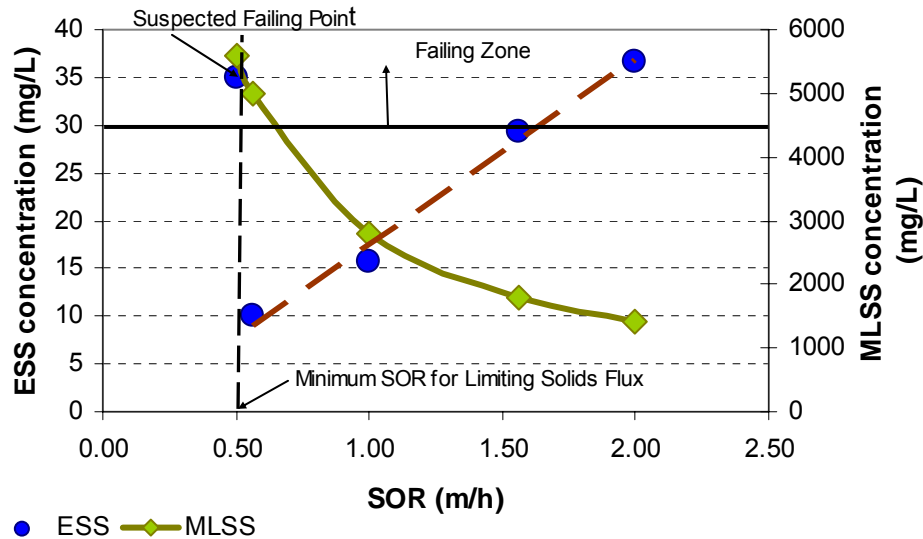
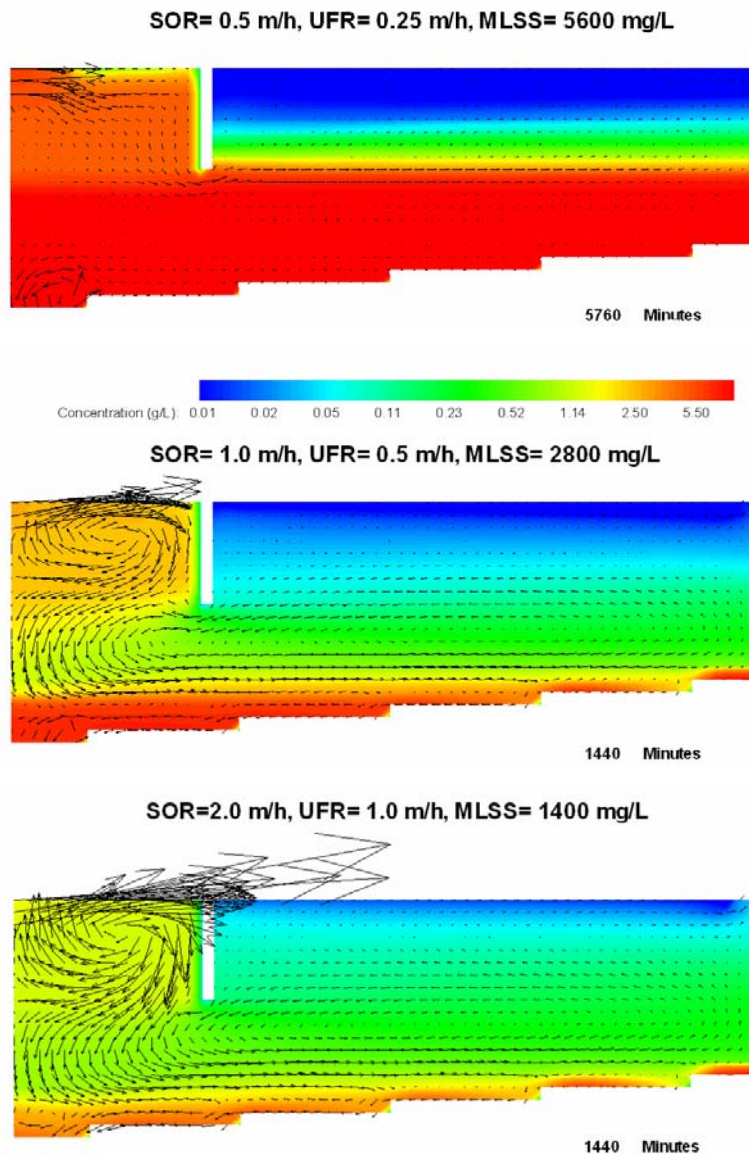


Figure 6.20 Performance of the SST for a Constant SLR and Variables SOR and MLSS (SOR= Variable, UFR= $0.5 \times SOR$, MLSS= Variable, SLR= $4.20 \text{ Kg/m}^2 \cdot \text{h}$)

Figure 6.20 shows a direct relationship between the SOR and the ESS for the constant SLR and constant recirculation ratio. The ESS linearly increases as the SOR increases and the MLSS decreases. The curve has already passed the failing limit (30 mg/L) for a

SOR equal to 2.0 m/h and a MLSS equal to 1400 mg/L. As mentioned before, the failure exhibited at this point is produced by the high outflow velocity and the carry of suspended solids by the upward current towards the outboard launder. This is a failure associated with a high SOR. However, Figure 6.18 shows that the Marrero SST exhibits an ESS lower than 30 mg/L with a 2.0 m/h SOR and even at higher SORs, but the MLSS and the SLR presented in Figure 6.18 are higher.



**Figure 6.21 Effects of the MLSS and SOR with a Constant SLR on the SST
Suspended Solids Contours**
(SOR= Variable, UFR= 0.5xSOR, MLSS= Variable, SLR= 4.20 Kg/m².h)

The fact that the SST performs better (at the SOR equal to 2.0 m/h) with the higher MLSS, supports the trend presented in Figure 6.16, and the conclusion that the flocculation process in the SST may improve with higher MLSS due to the higher opportunity of contact between the particles, as well as the trapping of small particles in the matrix formed during the hindered sedimentation. The increased contact between particles improves the shear flocculation process, and the trapping of particles in the solids matrix is a type of sweep flocculation process. In order to define the relative significance of these two flocculation processes on the improvement of the settling tank performance, the simulations for the Marrero SST with SOR equal to 2.0 m/h and MLSS equal to 1400 and 2800 mg/L were repeated but turning off the flocculation model. These simulations are presented in the next section.

As mentioned before the SST showed evidence of failure at the SLR equal to 4.20 Kg/m².h when the SOR is 0.5 m/h, the UFR = 0.25 m/h and the MLSS is equal to 5600 mg/L; this SLR would be the limiting solids flux under such loading conditions. The limiting solids flux predicted by the Q3D model was again compared with the limiting solids flux predicted by a 1D model. Once again the 1D limiting solids flux was found using two set of settling properties: (1) using only the zone settling properties, and (2) using the zone settling and the compression rate properties. This time the limiting solids fluxes were found to be equal to 4.00 and 6.50 Kg/m².h (see Appendix I) for the first and second case respectively. The 1D limiting solids flux prediction using only the zone settling properties is slightly lower than the Q3D prediction; if an 80% reduction were applied to this value then the SST would be over-designed. On the other hand the prediction of the limiting solids flux with the complete settling model (including the compression rate properties) predicted a limiting value almost 50% higher than the Q3D value; if an 80% reduction were applied to the 1D predicted limiting flux the clarifier would be under- designed. These results confirm the findings that the Q3D model “intrinsically” reproduces a flux rating less than 1 with respect to the 1D flux theory when the 1D is performed with a complete settling model, and are also an indication that a 0.80 correction factor in the 1D predicted limiting solids flux should not be applied to every case.

6.10 Evaluation of the Different Component of the Flocculation Sub-Model.

As discussed in Section 4.1.4 the flocculation sub-model is composed by two parts: (1) the shear induced flocculation equation, and (2) the differential settling flocculation equation. The sweep flocculation is intrinsically simulated in the model by the trapping of particles in the zone settling region where the same settling velocity is applied to all the fractions, assigning to the small particles the sedimentation rate of the matrix. To evaluate the weight of the different types of flocculation on the performance of the tank, the Marrero SST was simulated with a SOR= 2.0 m/h and two different MLSS (1400 and 2800 mg/L). Three different simulations were performed for each MLSS for a total of six simulations. The simulations were: (1) with the flocculation sub-model on, (2) with the flocculation sub-model off, and (3) only simulating the differential settling flocculation. The results of these simulations are presented in Table 6.9 and in Figure 6.22

The results presented in Table 6.9 clearly indicate that the shear induced flocculation is the most important flocculation process in the clarifier. The performance of the tank drastically improved when the complete flocculation sub-model is on, while the improvement was small when only the differential settling flocculation was simulated.

TABLE 6.9 Evaluations of the Flocculation Processes on SST at High SOR

SOR (m/h)	MLSS (mg/L)	ESS (mg/L)	RAS SS (mg/L)	Observation
2.00	2800	25.90	8347	Flocculation Sub-Model ON
2.00	1400	36.66	4131	Flocculation Sub-Model ON
2.00	2800	46.10	8301	Flocculation Sub-Model OFF
2.00	1400	48.73	4101	Flocculation Sub-Model OFF
2.00	2800	44.90	4101	Only Differential Settling Flocculation
2.00	1400	47.54	4101	Only Differential Settling Flocculation

When the flocculation sub-model was on, the difference in the ESS for the two modeled MLSSs was about 10.8 mg/L (about a 30% difference); meanwhile, when the flocculation

sub-model was off, the difference in the two ESS was much smaller, only 2.6 mg/L (about a 5% difference). These results are shown in Figure 6.22.

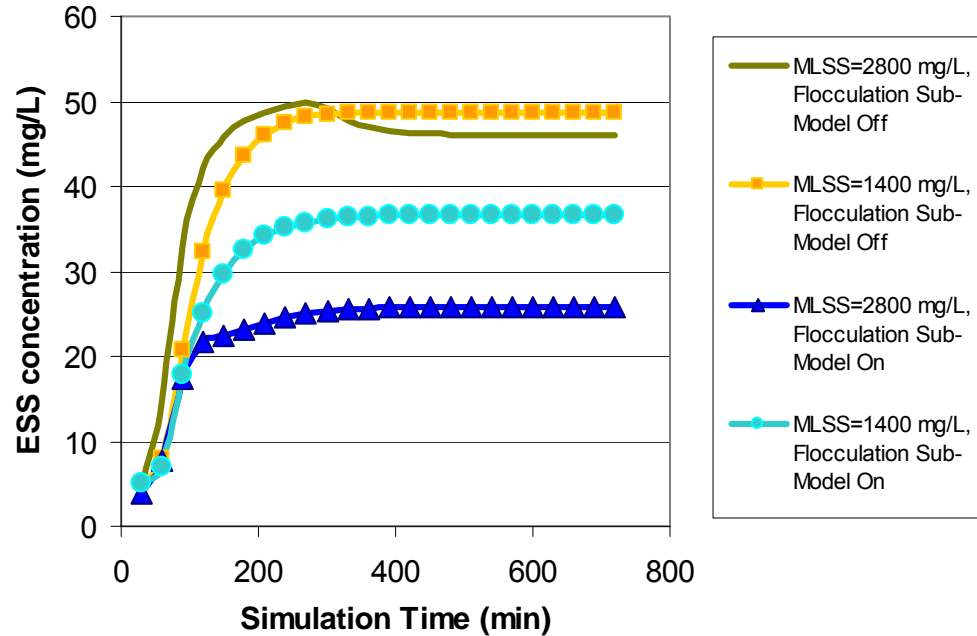


Figure 6.22 Evaluations of the Flocculation Processes at Different MLSS (SOR= 2.0 m/h)

The fact that the difference in the ESS increases when the flocculation sub-model is on, is an indication that the increased MLSS improves the flocculation process in the tank, and that the shear induced flocculation is more important than the sweep flocculation. The fact that the ESS for the 2800 mg/L MLSS is lower than the ESS for the 1400 mg/L MLSS when the flocculation sub-model is off, is an indication that the aforementioned sweep flocculation is occurring in the tank (as mentioned before, this type of flocculation is automatically modeled in the tank, and is not deactivated when the flocculation sub-model is turned off). However, as concluded before the results indicate that the shear flocculation is the most important type of flocculation in SSTs.

If the flocculation process is responsible for lowering the ESS from 48.73 mg/L to 25.90 mg/L, it can be concluded that 2.63 mg/L are due to the sweep flocculation (about

11.5%), 1.20 mg/L are due to the differential settling flocculation (about 5.3%) and about 19.00 mg/L are due to the shear induced flocculation (about 83.2%).

6.11 Effect of Sludge Withdrawal Systems on the Settler Performance

The Q3D model is capable of performing simulations with different withdrawal systems including hopper and suction, and the simulation of rake and spiral type scrapers. In order to evaluate the effect of the sludge withdrawal systems on the performance of the SST, different simulations were performed combining the possibilities available. The simulations were conducted with two different set of the settling properties, one set representing good settling and other representing poor settling. Table 6.10 presents the value of the two sets of settling properties and Table 6.11 presents a summary of these simulations. The discrete and zone settling thresholds were set at 600 and 1200 mg/L respectively.

Table 6.10 Settling Properties Used in the Evaluation of the Sludge Withdrawal Systems

GOOD SETTLING	
Zone Settling Properties	Value
V_o (m/h)	10.54
k_f (L/g)	0.40
Compression Rate Properties	Value
V_c (m/h)	3.20
K_c (L/g)	0.184
POOR SETTLING	
Zone Settling Properties	Value
V_o (m/h)	7.00
k_f (L/g)	0.50
Compression Rate Properties	Value
V_c (m/h)	2.00
K_c (L/g)	0.250

Table 6.11 Effect of the Sludge Withdrawal Systems on the SST Performance

Type of Withdrawal System	Type of Scraper ¹	Slope of the Bed	ESS (mg/L)	RAS SS (mg/L)	Thickness of the Sludge Blanket ² (m)
Good Settling					
Hopper	None	8.33%	15.75	8367	0.52
Hopper	Rake	8.33%	15.70	8391	0.48
Hopper	Spiral	8.33%	15.73	8368	0.50
Suction	None	Flat Bed ³	22.56	8345	0.40
Suction	None	8.33% ⁴	15.08	8369	0.42
Poor Settling					
Hopper	None	8.33%	17.02	8364	1.42
Hopper	Rake	8.33%	16.98	8297	1.30
Hopper	Spiral	8.33%	17.01	8363	1.40
Suction	None	Flat Bed ³	21.66	8338	0.75
Suction	None	8.33% ⁴	16.47	8362	1.20

¹The velocity of the scraper was set equal to 0.033 rpm.

²The thickness of the sludge blanket is measured at the mid-radius position, and is measured as the distance from the bottom of the clarifier to the top of the sludge blanket.

³The depth of the tank for the suction system with flat bed was selected equal to 5.0 m that is the average depth of the Marrero SST.

⁴For comparison purpose the SST was modeled with suction and sloping bed.

The results presented in Table 6.11 indicate that the benefit effects of the scraper on the ESS are minimal, and may be associated with thinner sludge blankets. However, the effects of the scraper in the sludge blanket are also small. In general, the simulations with a suction system reported a thinner sludge blanket, and the case with suction and sloping bed reported the lowest ESS. The flat bed clarifier shows the highest ESS in both cases (good and poor settling). These high ESS values are associated with poor hydrodynamics compared to the sloping bed; these cases are presented in Figure 6.23A. An interesting result that can be observed in Table 6.11 and in Figure 6.23A is that the flat bottom tank presents a higher ESS for the good settling when compared to the poor settling case. Figure 6.23A shows that the density current is stronger in the good settling case, apparently strengthened by the fast settling rate of the particles which traduces in a higher ESS. The case shown in Figure 6.23A for the good settling properties shows

strong evidence of short-circuiting, a condition that is obviously in detriment of the clarifier performance. Figure 6.23B shows how the short-circuiting may be avoided by decreasing the recirculation ratio from 0.5 to 0.3. With this recirculation ratio the flat-bottom clarifier predicts an ESS equal to 16.75 mg/L and a RAS SS concentration equal to 12050 mg/L (the expected equilibrium value is about 12130 mg/L).

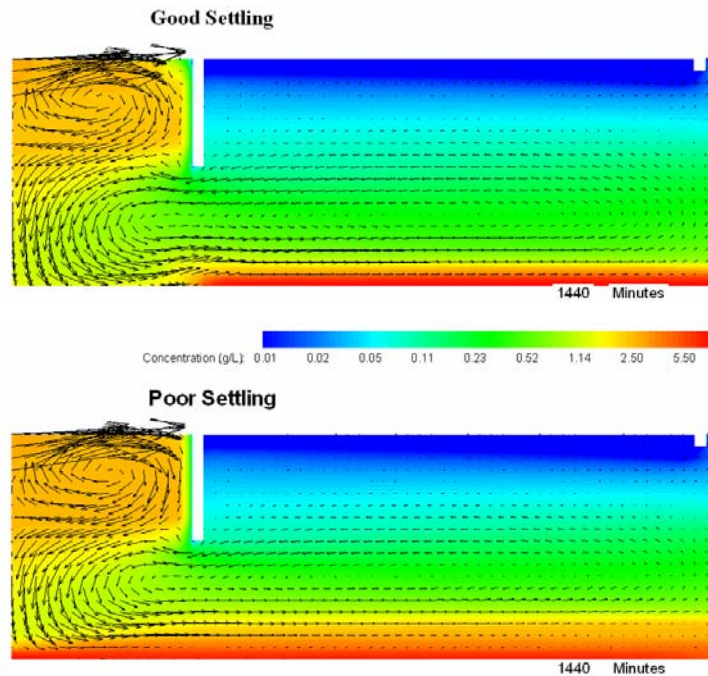


Figure 6.23A Flat Bed Clarifier with Suction Withdrawal System (Depth = 5.0m, SOR= 1.0 m/h, UFR= 0.5 m/h, MLSS= 2800mg/L)

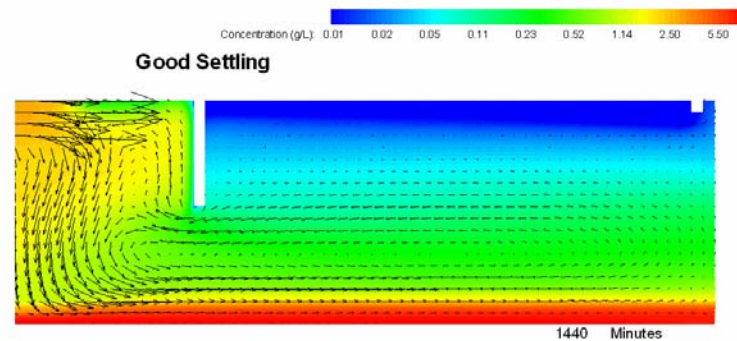


Figure 6.23B Flat Bed Clarifier with Suction Withdrawal System – Lower RAS Ratio (Depth = 5.0m, SOR= 1.0 m/h, UFR= 0.3 m/h, MLSS= 2800mg/L)

Even though the case presented in Figure 6.23B presents a lower ESS with respect to the cases presented in Figure 6.23A, this value is still not as good as the ESS predicted with the sloping bottom tank. This may be attributed to the fact that this clarifier presents a higher re-entrainment in the inlet zone, apparently associated with the decrease in the initial momentum of the inlet flow. The total incoming flow is decreased due to the lower recirculation ratio.

An important effect observed with the scraper simulations, was that this equipment introduced waves and a “pulse” type movement of the sludge towards the hopper. This effect introduces oscillations in the RAS SS concentrations, and in general makes the Q3D more sensitive and unstable. Figure 6.24 shows the oscillations in the RAS SS concentration due to the scraper simulation.

The oscillations induced by the Rake type scraper are almost eliminated in the simulation of the spiral type scraper. Although both types of scrapers are simulated in the Q3D model by the application of a shear force at the bottom of the tank, in the case of the spiral type scraper the force is average over a larger surface area which makes the effect smoother.

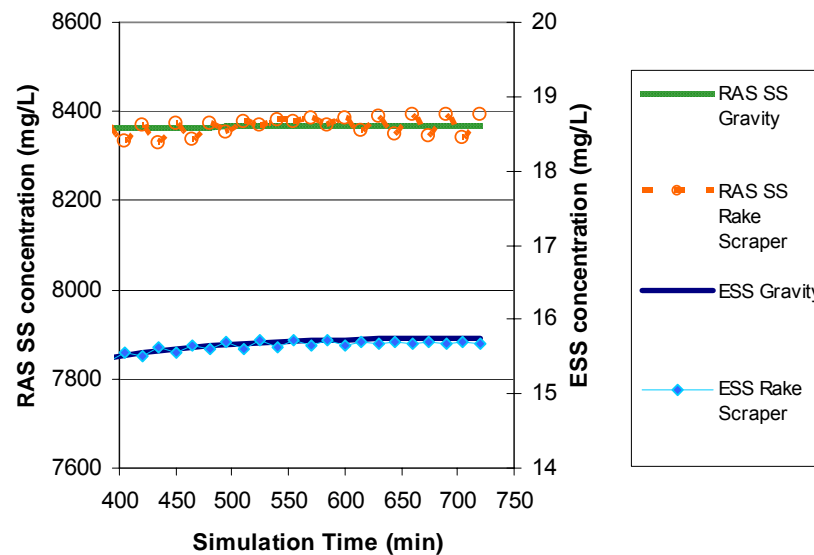


Figure 6.24 Oscillation Presented in the RAS SS and ESS Concentration with the Simulation of the Rake Type Scraper

6.12 Comparison between Gravity and Rake Induced Flows. Effectiveness of the Scraper

The comparison presented in Figure 6.24 between the gravity and the rake induced flows, for the sloping bed clarifier (at 8.33% bottom slope), shows negligible difference in the average ESS and RAS SS concentrations. The scraper simulation induces oscillations in the ESS and RAS SS values, probably associated with each pass of the scraper for the modeled radian sector every 30 minutes. Since the gravity flow steadily reached the average expected value, it seems that the scraper is retarding the movement of the sludge towards the hopper, at least in the region close to the outlet. In order to prove this statement the velocities of the gravity flow and of the scraper were analyzed. Figure 6.25 shows the horizontal velocities at steady conditions for the case of the gravity flow with the 8.33% slope. Table 6.12 presents a summary of the predicted gravity flow velocities and the calculated scraper velocities for a typical angular velocity equal to 0.033 rpm and a blade angle equal to 45°.

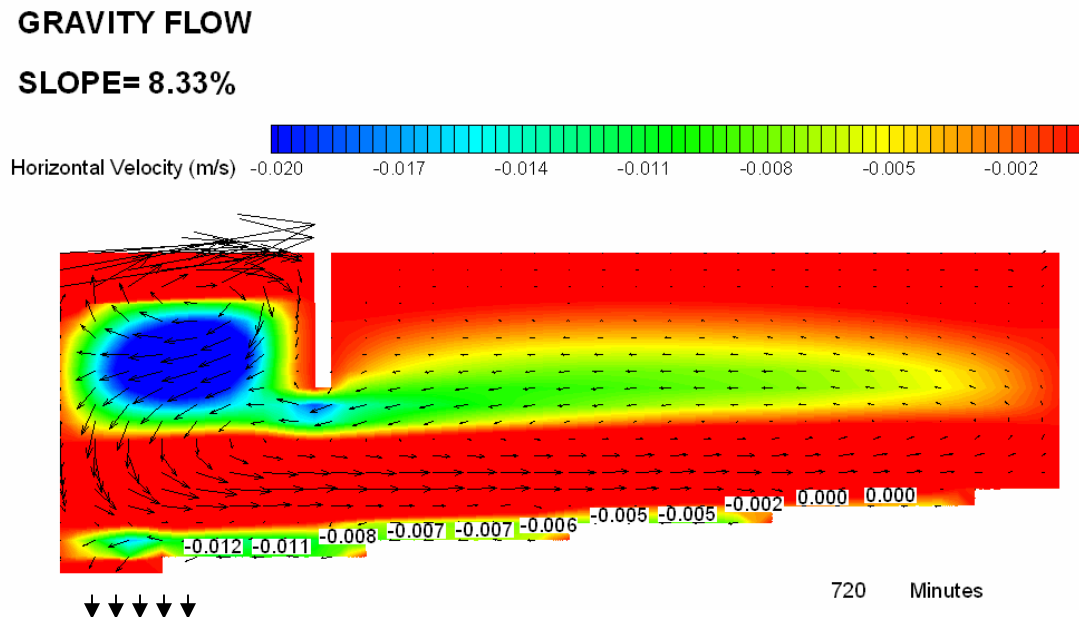


Figure 6.25 Horizontal Velocities in a Gravity Flow for a Sloping Bed Circular Clarifier (Bottom Slope= 8.33%)

Table 6.12 Scraper and Gravity Flow Velocities

Angular Velocity (rpm)	Radius (m)	Sludge Blanket Velocity (m/s)	Scraper Tangential Velocity (cm/s)	Scraper Radial Velocity* (cm/s)
0.033	2.9	1.20	0.98	0.49
0.033	4.0	1.10	1.37	0.68
0.033	5.1	0.85	1.76	0.88
0.033	6.8	0.70	2.32	1.16
0.033	7.9	0.70	2.71	1.35
0.033	9.1	0.60	3.10	1.55
0.033	10.2	0.50	3.49	1.74
0.033	11.3	0.50	3.88	1.94
0.033	12.5	0.20	4.27	2.14
0.033	13.6	0.00	4.66	2.33
0.033	17.6	1.00	6.03	3.01

*The scraper radial velocities are calculated using Equation 3.52.

The information presented in Table 6.12 is presented graphically in Figure 6.26. This figure clearly indicates that the gravity induced radial velocities in the sludge blanket are higher than the radial velocities of the scraper in the region close to the hopper, and therefore the blades are not effective in conveying the sludge towards the outlet in this region.

According to Figure 6.26 the blades would be effective at a radial distance larger than 5.0 m, which is typically outside of the center well zone. Hence, a scraper mechanism should avoid the use of blades in this region, possibly using radial rods for mixing the sludge blanket, to avoid long retention times of portions of the sludge blanket which could promote the denitrification process.

The conclusions presented in the two previous paragraphs could not be validated with field data, and therefore field data should be gathered and more research should be conducted on the effect of blades' position in order to come up with a better design of the scraper mechanism.

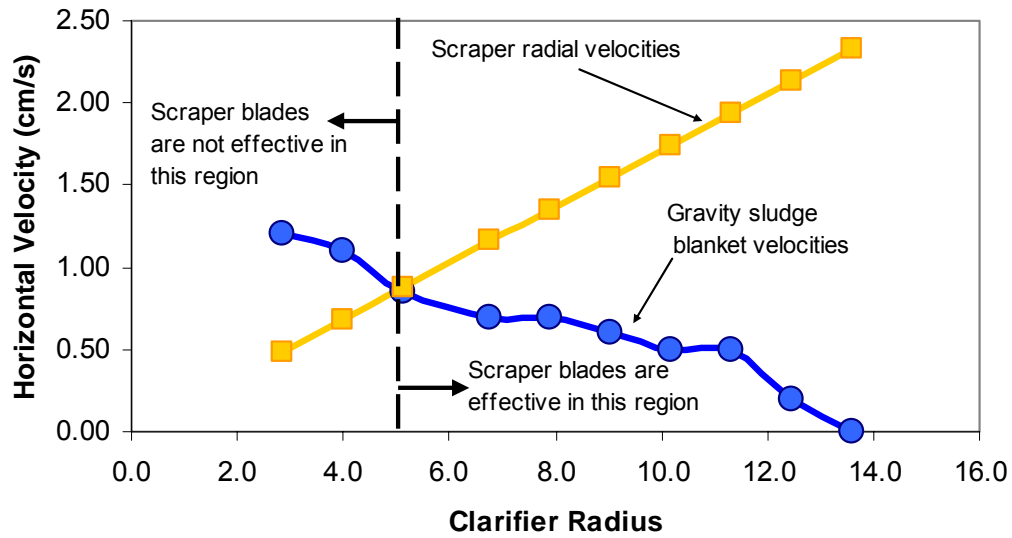


Figure 6.26 Horizontal Velocities in a Gravity Flow for a Sloping Bed Circular Clarifier and Comparison with the Radial Velocities of the Scraper (Bottom Slope= 8.33%, Scraper Velocity = 0.033 rpm, Blade Angle= 45°)

6.13 Effect of Swirl Components on the Settler Performance

The effects of the swirl components on the SST performance were evaluated by simulating the Marrero SST with and without an inlet deflector. The swirl effects of the inlet deflector were evaluated with two different SOR, i.e. 1.0 and 1.5 m/h, and two different sets of settling properties representing good and poor settling. The simulated settling properties are the same used in Section 6.11 and presented in Table 6.10. Table 6.13 presents a summary of these simulations after steady conditions were reached.

A consistent result, independent of the SOR or the type of settling, is that the Q3D model predicts higher ESSs when the inlet deflector is simulated. These results do not seem to be consistent with the information provided in the literature, e.g. Ekama et al. (1997) reported that simple inlet ports can introduce high-velocity jets into the SST, creating unwanted turbulence that can upset the SST.

Table 6.13 Predicted ESS and RAS SS Concentration with and without an Inlet Deflector for Good and Poor Settling

SOR (m/h)	Inlet Deflector	ESS (mg/L)	RAS SS (mg/L)
Good Settling			
1.0	None	15.75	8367
1.0	45°	18.18	8361
1.5	None	19.84	8359
1.5	45°	23.68	8350
Poor Settling			
1.0	None	17.02	8364
1.0	45°	19.76	8357

Ekama et al. (1997) also stated that the introduction of tangential flow is one way of managing inlet headloss in a positive way. Similarly, Krebs et al. (1995) stated that increasing the energy dissipation may produce a less-pronounced bottom current, improving the tank hydrodynamics. Even though, other authors agrees in the benefit of the inlet deflector as energy dissipater, a conclusive and well supported study in this matter was not found. If in fact, the inlet deflector improves the performance of the SST, then this simulation seems to be a limitation of the Q3D model. Independently of the realism of the simulations, the reason why the Q3D model predicts better ESS without the inlet deflectors seems to be in the flocculation sub-model. Figure 6.27 shows the values of the velocity gradients for the cases with and without the inlet deflector, it can be noticed that the G values are significantly higher for the case without the inlet deflector. The G values are calculated based on the horizontal velocity of the inlet jet as proposed by Equations 2.47 and 2.51. The higher G values will induce a better flocculation and indeed a better ESS. The Q3D simulation indicates that the center well is effective in dissipating the initial kinetic energy and the density current is formed by the conversion of the potential energy into additional kinetic energy.

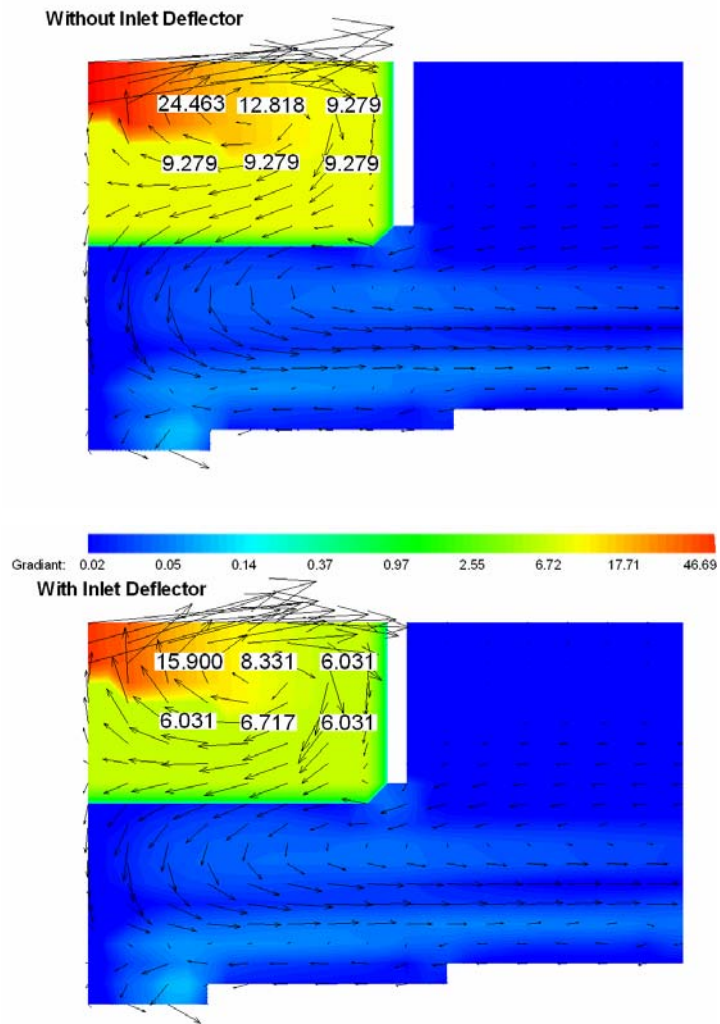


Figure 6.27 Simulated Velocity Gradients with and without Inlet Deflector (SOR= 1.0 m/h)

Figure 6.27 shows that the inlet deflector in fact reduces the initial kinetic energy, but this reduction does not seem to have any effect on the development of the density current.

In order to define if the reason for a lower ESS in the case without the inlet deflector is a higher prediction of the flocculation process for this case, the two simulations presented in Figure 6.27 were repeated turning off the flocculation sub model. Under these conditions, the case with the inlet deflector predicted a final ESS concentration equal to 22.77 mg/L, while the case without the inlet deflector predicted a final ESS concentration

equal to 22.98 mg/L (both solution after steady state conditions were reached). These results clearly indicate that the prediction of a lower ESS for the case without an inlet deflector is due to the prediction of higher G values that results in a better flocculation of the incoming MLSS. The realism of this prediction needs to be further investigated.

6.14 Effect of Temperature and Seasonal Variation on Clarifier Performance

6.14.1 Effect of temperature on settling velocity due to change of viscosity

In Section 3.3, a correction factor for the settling velocities due to the effect of the temperature on the viscosity of the water was developed. It was also discussed that this correction factor, which is recapitulated below, should be applied for the correction of the settling velocities in all of the four types of sedimentation described in Section 3.2, i.e., unflocculated discrete settling, flocculated discrete settling, hindered (zone) settling and compression.

$$V_{sT2} = V_{sT1} \left(\frac{10^{\left[\frac{247.8}{T1+133.15} \right]}}{10^{\left[\frac{247.8}{T2+133.15} \right]}} \right) \dots\dots\dots (3.47)$$

Table 5.13 presented the set of settling properties measured during the main calibration of the Q3D model. As mentioned in Chapter 5 these settling properties were measured at about 26.5 °C. Table 6.14 presents a comparison between the values of the aforementioned settling properties and the respective settling properties at a water temperature of 15 °C, modified applying Equation 3.47. As indicated in this table, the values of the settling velocities at 15 °C are about the 75.6% of the values at 26.5 °C; obviously the decrease in the settling velocities will be reflected in a poorer performance of the settling tank under the same loading conditions.

Table 6.14 Comparison between Settling Properties at 26.5 and 15.0 °C. Correction
Based on the Change of Viscosity

Discrete Settling Properties	Value at 26.5 °C	Value at 15.0 °C
Discrete Settling Threshold (mg/L)	1200	1200
V_{s1} (m/h)	10.8	8.18
<i>Fraction 1 (Dimensionless)</i>	0.742	0.742
V_{s2} (m/h)	3.0	2.27
<i>Fraction 2 (Dimensionless)</i>	0.255	0.255
V_{s3} (m/h)	0.68	0.52
<i>Fraction 3 (Dimensionless)</i>	0.003	0.003
Zone Settling Properties	Value at 26.5 °C	Value at 15.0 °C
Zone Settling Threshold (mg/L)	600	600
V_o (m/h)	10.535	7.98
k_1 (L/g)	0.40	0.40
Compression Rate Properties	Value at 26.5 °C	Value at 15.0 °C
Compression Settling Threshold	5400	5400
V_c (m/h)	3.2	2.42
K_c (L/g)	0.184	0.184

The effects of the change on the settling properties due to the different viscosity at 15.0 and 26.5 °C on the performance of the settling tank were evaluated by simulating the Marrero SST with the two set of sedimentation properties. Figure 6.28 shows the predicted ESS and RAS SS concentrations for the two cases. As expected the cases with the cooler temperature presents a higher ESS, naturally originated by the lower sedimentation rates. This kind of pattern could be one of the reasons why several plants perform poorer during the winter. The change on the settling properties did not have any important effect on the RAS SS concentration; but, as can be expected, the decreases in the values of the zone settling and compression rate properties will decreases the limiting solids of the clarifier.

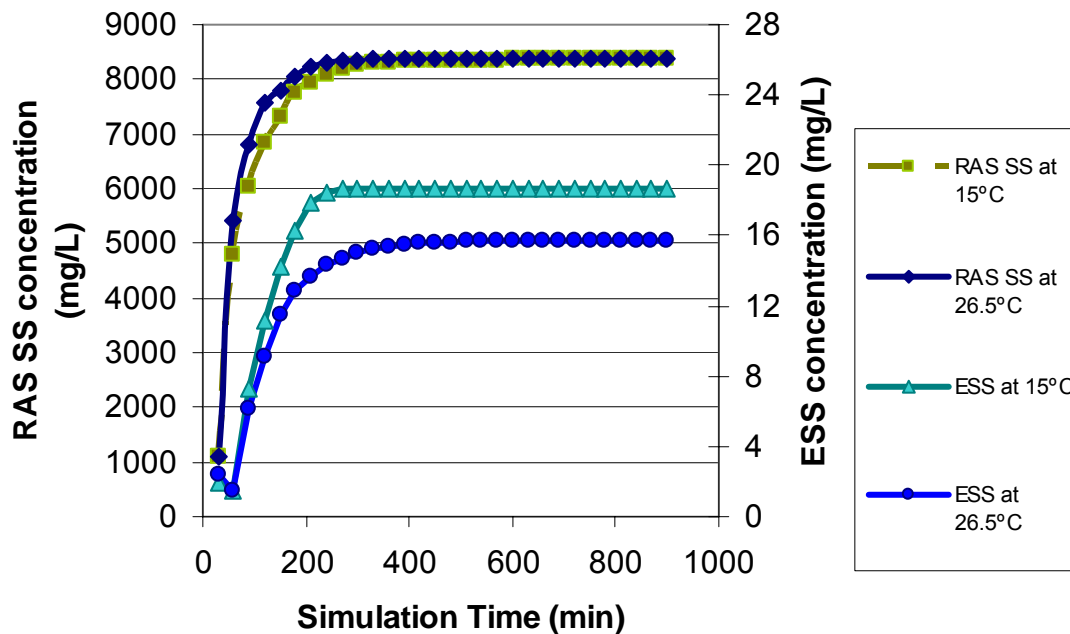


Figure 6.28 Predicted ESS and RAS SS Concentrations with Settling Properties Corrected for Different Temperatures due to Change of Viscosity

6.14.2 Effect of Influent Temperature Variation and Heat Exchange on the Hydrodynamics and Performance of Clarifiers

The effects of the influent temperature variations on the hydrodynamics and the performance of the settling tank were evaluated by simulating the Marrero SST with an influent temperature difference of $\pm 1^{\circ}\text{C}$, and two different MLSS, i.e. 300 and 2800 mg/L. The low MLSS was selected in order to simulate loading conditions similar to those found in PSTs. The heat exchange for these simulations was set up for summer and winter conditions. Tables 6.15 and 6.16 show the general data used in the simulations. Table 6.15 also shows the peak ESS found during the simulations. Table 6.16 presents the values used for the simulation of the surface heat exchange. The values presented in Table 6.16 represent two specific sets of data for the City of Marrero, Louisiana. These values were obtained from the website www.wunderground.com, the winter data corresponds to 01/11/2004, and the summer data corresponds to 07/11/2004.

Table 6.15 Predicted ESS values for Different Temperature Variations

MLSS (mg/L)	SOR (m/h)	Influent Temperature Variation	Heat Exchange ¹	Peak ESS (mg/L)
2800	1.0	+1°C	Summer	46.24
2800	1.0	-1°C	Summer	16.25
2800	1.0	0°C	Summer	16.05
2800	1.0	0°C	Winter	43.65
2800	1.0	0°C	Off	15.75
300	1.0	+1°C	Summer	83.90
300	1.0	-1°C	Summer	81.19
300	1.0	0°C	Summer	81.00
300	1.0	0°C	Winter	110.19
300	1.0	0°C	Off	80.60

Table 6.16 Heat Exchange Parameters Summer and Winter Conditions

Heat Exchange Parameters	Summer	Winter
Starting Time of the Run	10:00 AM	10:00 PM
Julian Day	192	11
Local Latitude (Degrees)	30	30
Atmospheric Turbidity Factor	3	3
Fraction of Sky Covered by Clouds	0.1	0.1
Dew Point Temperature (°C)	23.9	5.0
Maximum Air Temperature (°C)	32.8	16.0
Minimum Air Temperature (°C)	25.0	5.0
Wind Speed (m/s)	2.22	2.22

The values of the peak ESS presented in Table 6.15 indicate that the influent temperature variations and the heat exchange have an important effect on the performance of the SST.

For both MLSS the critical cases are the incoming warmer water and the surface cooling process. Figure 6.29 shows the variation of ESS with the change in the influent temperature for the MLSS equal to 2800 mg/L.

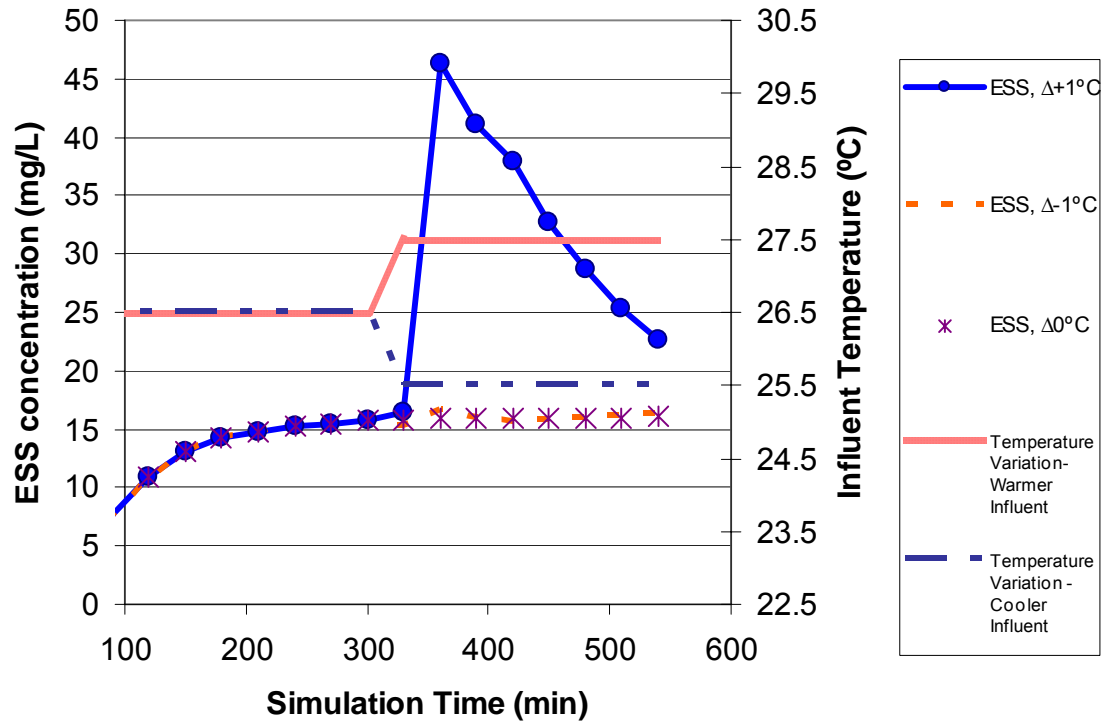


Figure 6.29 Effect of Influent Temperature Variation on the ESS Concentration (SOR= 1.0 m/h, MLSS= 2800 mg/L)

It can be observed how the ESS suddenly rises when the warmer water comes inside the settling zone of the tank. Figure 6.30 shows that the warmer influent did not produce a change in the direction of the density current, but it temporally strengthened it and produced a rise of the ESS. When the influent temperature rises the suspended solids keep the warmer, but still denser inflow, close to the bottom. When the current reaches the end of the clarifier and most of the solids have settled out, the plume rises reinforced by the vertical acceleration of the buoyant effect of the warmer water. This process results in a transient strengthening of the density current, and a higher ESS. As the warmer water keeps coming in, the temperature differential decreases and the density

current goes back to the original position with the corresponding decrease of the ESS. These effects are demonstrated in Figures 6.29, 6.30 and 6.31

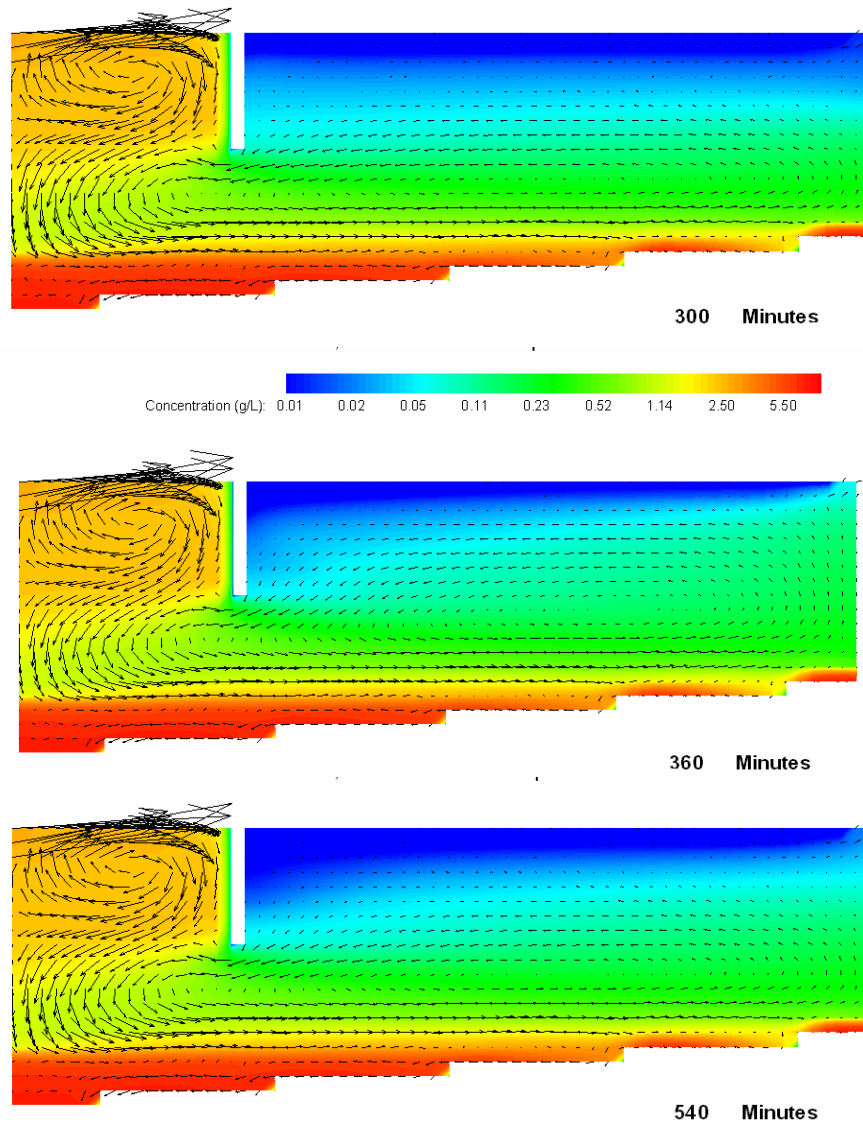


Figure 6.30 Effect of Influent Temperature Variation on the Suspended Solids Contours ($\Delta T = +1^\circ\text{C}$, $\text{SOR} = 1.0 \text{ m/h}$, $\text{MLSS} = 2800 \text{ mg/L}$)

Figure 6.31 shows the temperature changes in the SST with the warmer influent and the heat exchange for the summer conditions. This figure shows that the surface heat exchange warms up the surface water. Since this is a stable stratification gradient there is

little mixing between the surface and the inner layers. This figure also shows the incoming water plume traveling near the bottom until it rises close to the end wall. A study presented by Wells and LaLiberte (1998a) on prototype circular secondary clarifiers showed similar results to those presented herein.

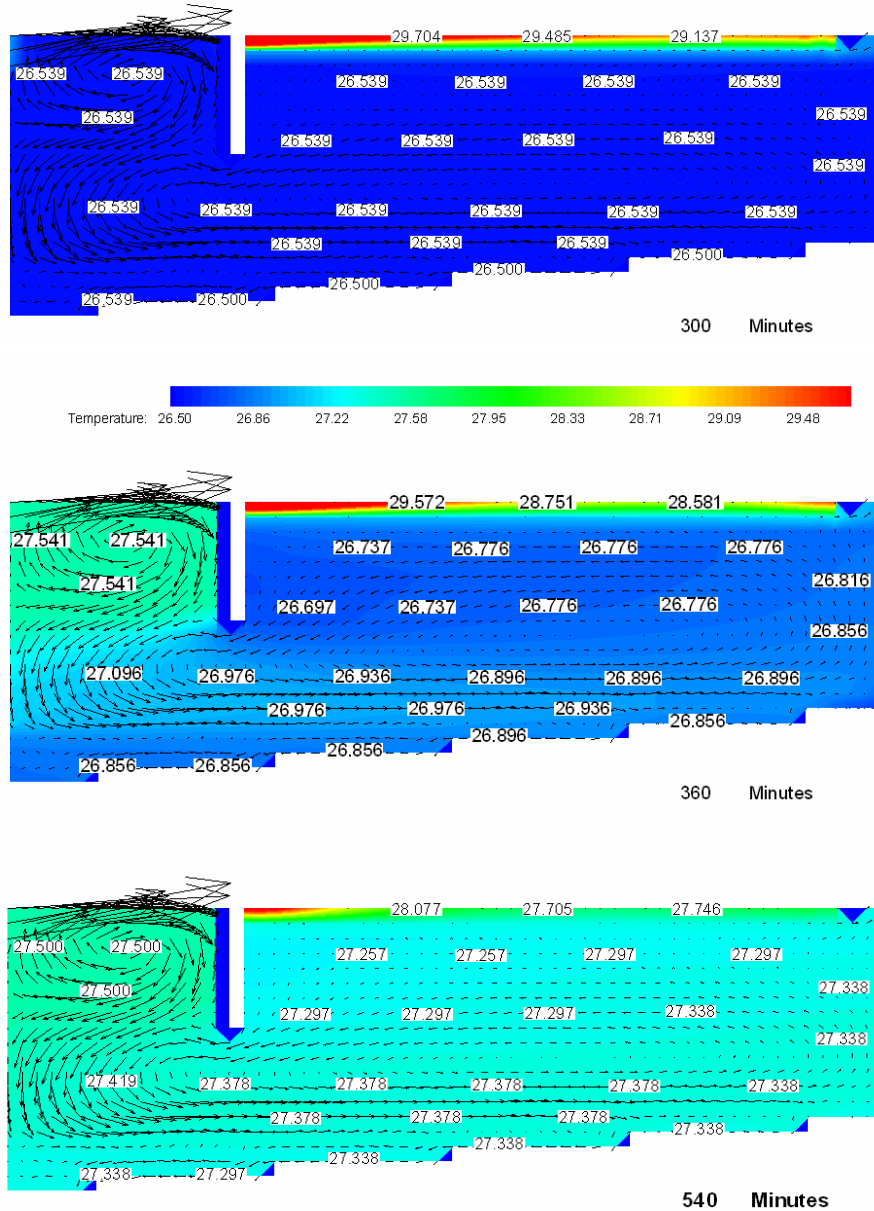


Figure 6.31 Effect of Influent Temperature Variation on the Internal Temperature Distribution
($\Delta T = +1^\circ\text{C}$, $\text{SOR} = 1.0 \text{ m/h}$, $\text{MLSS} = 2800 \text{ mg/L}$)

The case with the cooler influent and the MLSS equal to 2800 mg/L shows a rise of the ESS when the cooler water enters the settling zone, but the rise is much smaller than the case with the warmer influent. In this case the cooler influent makes the inflow even denser which strengthen the density current. This effect is dissipated as the cooler water keeps entering and the difference in temperatures decreases. The generation of a stable stratification of the vertical density gradients seems to suppress the turbulence in the vertical direction and to damp the diffusion of the suspended solids.

The simulations with the lower MLSS (300 mg/L) and the warmer influent ($\Delta T = +1^\circ\text{C}$) shows a different flow pattern. In this case the clarifier shows a rising buoyant plume that changes the direction of the density current, i.e. previous to the change in temperature the density current rotates counterclockwise and then it changes to a clockwise rotation. The warmer influent impacts the center well and is deflected downward. Immediately after passing below the center well the flow shows a strong rising plume which reaches the surface and develops a surface density current. The surface density current travels at the surface, impacts the end wall and is deflected downward, and then is recirculated as an underflow current. The flow in the surface density current is higher than the effluent flow due to the entrainment of the underflow current. As the temperature in the tank becomes more uniform, the counter flow becomes weaker, eventually returning to the counterclockwise density current dominated by the suspended solids. This flow pattern can be observed in Figure 6.32. Similar results to those presented herein have been presented by McCorquodale (1976, 1977, 1987), Godo (1990), and McCorquodale and Godo (1991) in studies conducted with physical models and full scale facilities and also by Zhou et al. (1994) in numerical simulations of PSTs.

In Figure 6.32, at 420 minutes of simulation time, there is a stable density interface between the cooler fluid at the bottom and the warmer fluid at the top. Little mixing is observed between these two layer, and the cooler water is withdrawn from the tank through the hopper. A similar stable-sharp interface is observed at the top of the tank between the surface water (heated by the solar radiation) and the cooler water below it.

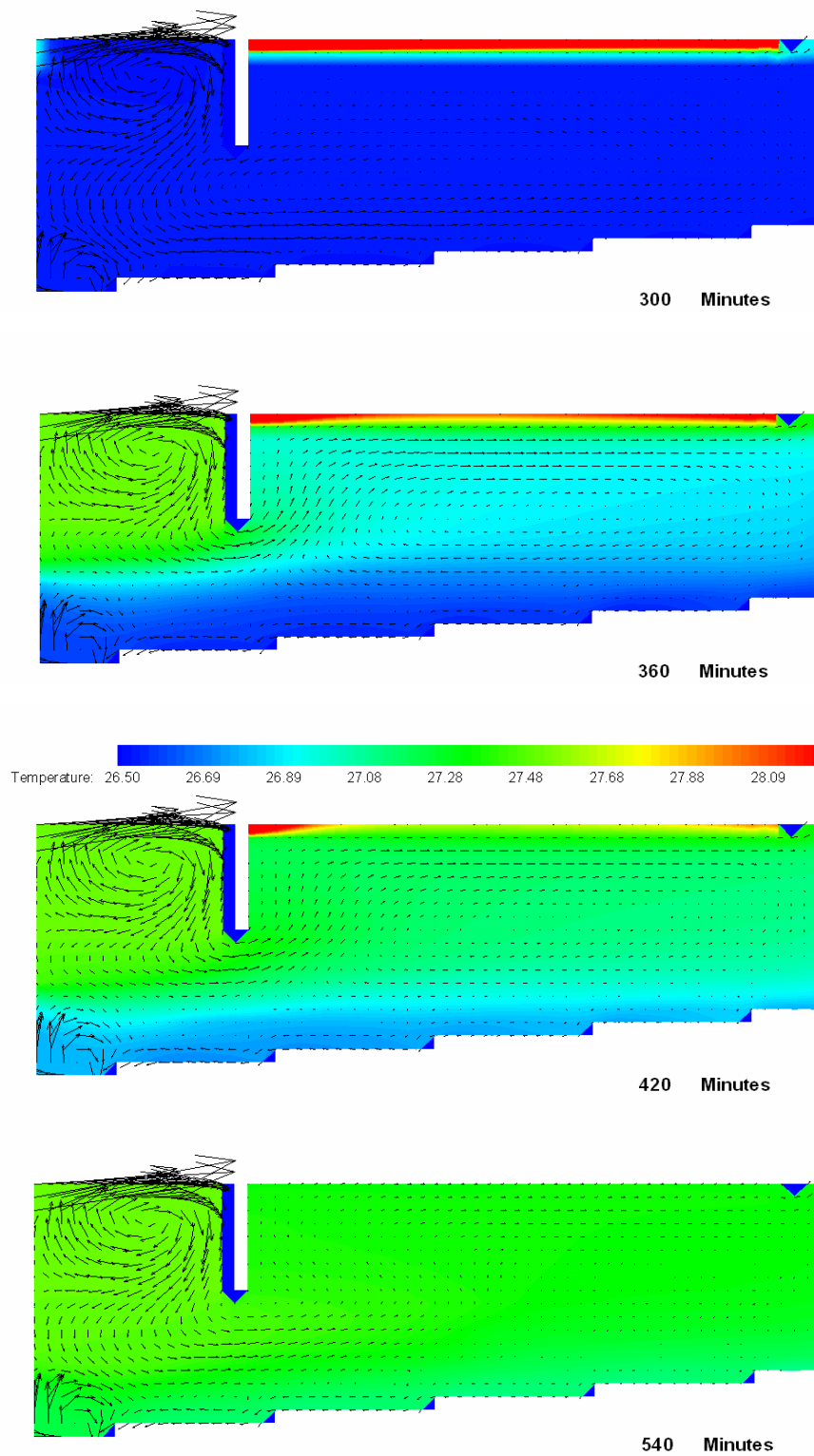


Figure 6.32 Effect of Influent Temperature Variation on the Internal Temperature Distribution for a Low incoming MLSS ($\Delta T = +1^{\circ}\text{C}$, $\text{SOR} = 1.0 \text{ m/h}$, $\text{MLSS} = 300 \text{ mg/L}$)

The results presented in Table 6.16 indicate that the performance of the clarifier strongly decreases under the influence of the surface cooling process presented during winter conditions. These results agree with the findings of Larsen (1977), Wells and LaLiberte (1998a, 1998b) and Kinnear (2004) who found that the removal efficiency of settling tanks may vary over the year with a minimum during the winter season. The differences in the ESS for the heat exchange simulation for winter (on a clear cool night case) and summer (on a sunny day), a with no surface heat exchange are presented in Figure 6.33.

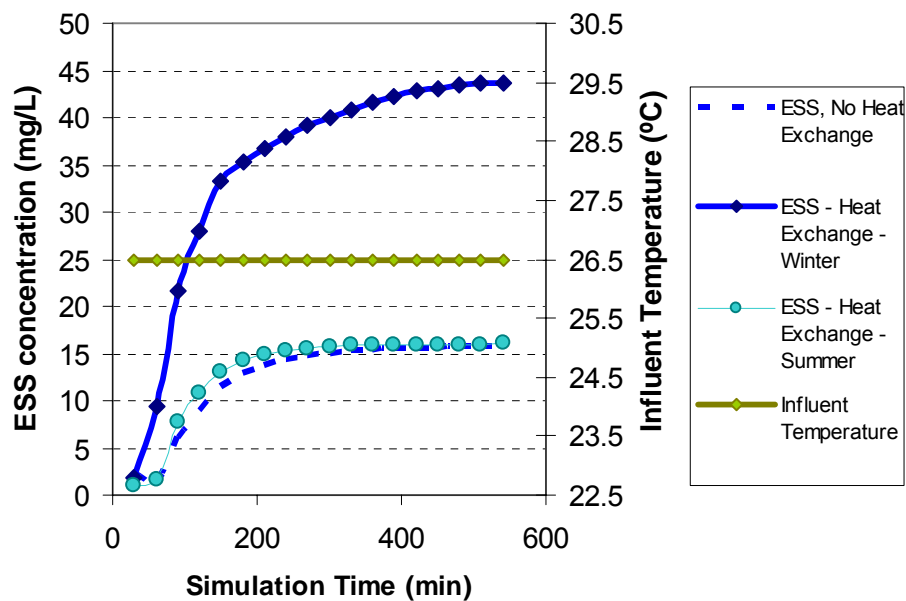


Figure 6.33 Effect of Seasonal Variation on the Performance of the SST (SOR= 1.0 m/h, MLSS= 2800 mg/L)

The warming up process of the surface originated by the heat exchange during the summer conditions practically does not affect the performance of the settling tank. As presented in Figures 6.31 and 6.32 these conditions create a stable density stratification which has negligible effects on the overall hydrodynamics and performance of the tank.

As mentioned before the surface cooling process has a negative impact in the hydraulics and solids distribution of the SST. Figure 6.34 shows the suspended solids contours of the

clarifier under the effect of the surface cooling process. Apparently the surface cooling process is strengthening the density current, creating higher upflow velocities close to the end wall, and increasing the vertical mixing.

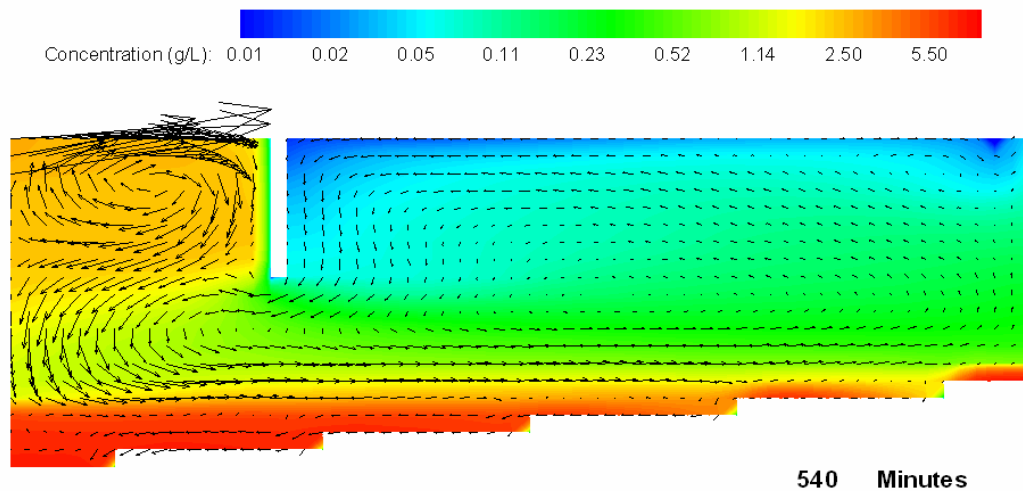


Figure 6.34 Effect of Surface Cooling on the Suspended Solids Contours

When the surface water becomes cooler it develops an unstable stratification density gradient promoting the mixing with the lower layers. As the cooler-denser water coming from the surface penetrates the tank, the counterclockwise density current carries the denser water towards the inlet region, where it impacts the center well and is deflected downward. This denser plume mixes with the warmer influent, warming up and traveling with the bottom density current. This cycle creates a radial density gradient that promotes positive vorticity in the settling zone reinforcing the strength of the density current and increasing the suspended solids carrying capacity of the upward current. Close to the clarifier outlet, the current towards the effluent weirs obligates the surface denser water to pass below the scum baffle creating a density gradient in the opposite direction to the main gradient developed in the settling zone, this condition creates a small eddy that rotates in the opposite direction to the main density current. This eddy is apparently counteracting the upward flow of suspended solids, but its effect is too local

and small to avoid the high ESS at the outlet. Figure 6.35 shows the unstable temperature stratification that develops under the surface cooling process. The effect presented herein might have been exaggerated for the relative warm influent for “winter” conditions, i.e., 26.5°C. To evaluate the conditions for a cooler influent, the test was repeated using a constant influent temperature equal to 16.0°C. Figure 6.36 shows the temperature field pattern for this influent temperature; this figure shows the same pattern observed in Figure 6.35. In this case the peak ESS was 27.15 mg/L, 10 mg/L higher than the “summer” conditions, which supports the statements about the effects of the surface cooling process presented in the previous paragraphs.

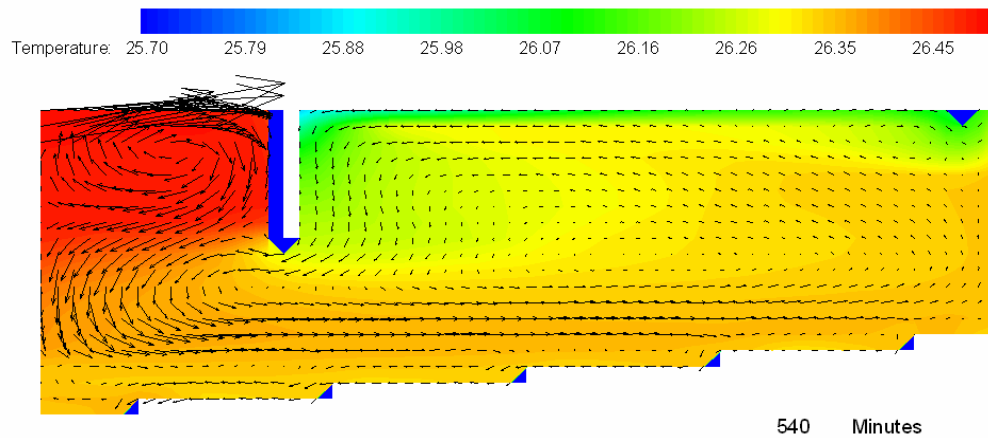


Figure 6.35 Temperature Stratification under the Effect of a Surface Cooling Process for an Influent Temperature Equal to 26.5°C

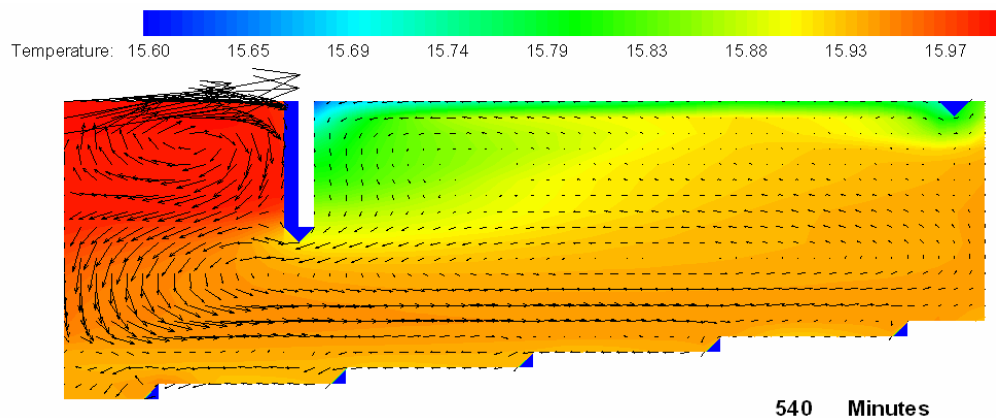


Figure 6.36 Temperature Stratification under the Effect of a Surface Cooling Process for an Influent Temperature Equal to 16.0°C

6.15 Stability Criteria Analysis

As mentioned in Section 4.2 of Chapter 4 two different discretisation techniques were used in this study for solving the partial differential equations: the vorticity and solids transport equations (Equations 4.8 and 4.11) were solved using the FVM, while the circumferential momentum equation (Equation 4.10) and the Poisson-type equations (Equations 4.7 and 4.17) were discretised using FDM techniques. Equations 4.7 and 4.17 were solved using a Hybrid Scheme, while the time-dependent equations were discretised using the hybrid differencing scheme in the spatial variation and the Crank-Nicolson approach for the time variation (the selection of these schemes was discussed in Section 4.2). Similarly, in Section 5.2 the dependency of the solution with the grid size was evaluated. It was proved that the grid-related errors are reduced with the use of finer grids and also that the model converges to a unique solution. In general the spatial and time variations schemes used in the development of the model are very robust and stable. However, an extensive investigation was conducted to define the criteria that guarantee the stability of the numerical diffusion. In general the procedure performed was the following: given a grid size and a stable solution from a numerical point of view, the SOR and the time step were successively increased until the solution became unstable; calculating for every case the Courant number (the Courant number is usually associated with computation stability conditions). Similarly, the effect of the scraper applied shear stress on the stability of the solution was evaluated for different scraper velocities and blades heights. As conclusion of these tests, the recommendations for the constraint of the time step and the grid size based on the Courant number are defined in Equations 6.1 to 6.3.

$$Courant\ No. = \frac{u_r \times \Delta t}{\Delta r} \leq 2.50 \dots\dots\dots (6.1)$$

$$Courant\ No. = \frac{V_\theta \times \Delta t}{r_{in}} \leq 2.50 \dots\dots\dots (6.2)$$

$$Courant \ No = \frac{\omega \times r \times \cos(\theta) \times \sin(\theta) \times \Delta t \times H_{bl}}{0.30 \times \Delta r} \leq 0.30 \dots\dots\dots (6.3)$$

where u_r is the inlet horizontal velocity (m/s), Δt is the computational time step (seconds), Δr is the radial dimensions of the computational cells (m), V_θ is the inlet velocity in the theta direction (m/s), r_{in} is the radius of the clarifier's inlet (m), ω is the angular velocity of the scraper (radians/s), r is the radius of the clarifier (m), θ is the angle of the blades, and H_{bl} is the height of the blades.

CHAPTER 7

7 CONCLUSIONS AND RECOMMENDATIONS

The main purpose of this investigation was to develop a CFD clarifier model capable of simulating the major processes that control the performance of secondary settling tanks, this goal was achieved. The accomplished objectives of this research include: the development of a compound settling model that includes the representation of the settling velocities for the entire curve of suspended solids usually encountered in this type of tank; the inclusion of swirl effects, a flocculation sub-model, and a temperature sub-model. These types of sub-models have not been previously incorporated in CFD SST models. The model was rigorously tested and validated. The validation process confirms the utility and accuracy of the model. An important benefit of this research is that it has contributed to a better understanding of the processes in SSTs. The results presented in this research clarify important points that have been debated by previous researchers. This research may also open the discussion for future research and different ways for improving the performance of existing and new clarifiers. In summary, this research has led to a more complete understanding of the processes affecting the performance of secondary settling tanks, and provides a useful tool for the optimization of these cornerstone units in water treatment. The major conclusions, general and specifics, obtained from this research are:

7.1 General Conclusions

- The performance of settling tanks depends on several interrelated processes and factors that include: hydrodynamics, settling, turbulence, sludge rheology, flocculation, temperature changes and heat exchange, geometry, loading, the nature of the floc, the atmospheric conditions and the total dissolved solids concentration.
- A Quasi-3D (Q3D) clarifier model has been developed to include the following factors: axisymmetric hydrodynamics (including the swirl component), four types

of settling, turbulence, sludge rheology, flocculation with four classes of particles, temperature changes and surface heat exchange with the atmosphere, various external and internal geometries, unsteady solids and hydraulic loading, the nature of the floc settling/interaction. The model includes: shear flocculation, differential settling flocculation and sweep flocculation due to the trapping of particles in the matrix formed during the zone settling process.

- A compound settling model has been developed. This mathematical model accounts for the settling velocities of the suspended solids under five different settling regimes, i.e. non-settleable particles, discrete settling, flocculent settling, zone or hindered settling and blanket compression. Compared with the Takacs' model, the developed model has a better representation of the discrete settling and the compression rate. In the discrete settling region the new model avoids the use of the k_2 parameter, and substitutes it by a finite number of fractions with individual settling velocities. While the Takacs' model uses the same representation for zone settling and blanket compression, the new model incorporates two new settling parameters that allow a better representation of the consolidation of the sludge blanket. The major drawback of the new settling model is a longer and slightly complicated calibration procedure when compared with previous model, e.g. Vesilind and Takacs Models.
- A field testing procedure is presented that addresses all of the settling regimes that are encountered in a Secondary Settling Tank, i.e. non-settling particles, unflocculated primary particles, partially flocculated particles, highly flocculated particles with discrete settling, hindered settling and compression. This procedure is used for the calibration of the settling model.
- The Q3D model reproduces the major features of the hydrodynamic processes and solids distribution on secondary clarifiers. When the model is executed with the field derived settling characteristics as recommended in this dissertation, it can accurately predict the effluent and recirculation suspended solids concentration.

- The Q3D model accurately predicts the limiting solids flux of the SST. When compared with a 1D solids flux analysis performed including the zone settling and the compression rate properties, the Q3D model consistently predicts a flux rating less than one, where the flux rating is the capacity of the SST as a fraction of the 1DFT predicted maximum solids loading rate. In this case the flux rating varied between 0.82 and 0.65 (for simulations of the Marrero WWTP). When compared with a 1D solids flux analysis performed using only the zone settling properties, both predictions, i.e. the Q3D and the 1D limiting solids flux, are closer. Apparently, ignoring the 2D effects on the hydrodynamics, which tends to predict higher limiting solids fluxes, and ignoring the compression rate properties, which tends to predict lower limiting solids fluxes, are somehow compensating in the 1D analysis allowing an apparently “accurate” representation of the limiting solids flux value of the clarifier. However, caution should be used in interpreting 1D analysis, and the results of 1D analysis should be verified using 2D simulations.
- The model has been formulated and confirmed to conserve fluid, tracer and solids mass.
- The accuracy in predicting ESS and RAS SS concentrations, limiting solids flux, flow pattern, suspended solids stratification, and the ability to simulate different geometry configurations makes the Q3D a useful tool for designing, evaluating and modifying clarifiers. This model can be a good complement for 1D flux limiting models.

7.2 Specific Conclusions

- The flocculation process plays a major role in the ESS on secondary clarifiers. The potential improvement due to flocculation is very sensitive to the difference between the DSS and the minimum FSS, i.e. the fraction of unflocculated flocculatable particles.

- The extent of actual flocculation depends on several factors that include: the design of the center well, the MLSS concentration, and the G values in the inlet zone. Even though the clarifier can be designed to optimize its flocculation function, the effects might not be enough to get a good effluent when the influent MLSS to the clarifier is poorly flocculated.
- Preliminary results obtained from the simulation of the Marrero WWTP indicate that the shear induced flocculation is the most important flocculation process in SST, followed by the sweep flocculation.
- Increasing the MLSS increases the flocculation rate in the clarifier. If the SOR is kept constant, the increase in the MLSS may yield a lower ESS until an optimum MLSS value is reached. For the case of the Marrero WWTP the optimum MLSS is about 4500 mg/L. If the MLSS is increased beyond the optimum value, the ESS starts to slowly increase until it suddenly fails due to a solids overload.
- The center well promotes flocculation, but its most important benefit is the improvement on the tank hydrodynamics. Model sensitivity studies indicate that the dominant role of the center well is the control of the re-entrainment of clarified fluid with the influent flow thus inducing a stronger upflow at the launder.
- The optimum dimension of the center well diameter is between 20% to 35% of the total clarifier diameter. The incoming MLSS does not seem to have any effect on the optimum dimension, while it appears that the optimum dimension tends to increase as the SOR increases. The increase in the UFR might also affect the optimum dimension of the center well in the same way the SOR does.
- The performance of SST depends on several interrelated processes and therefore its behavior can not be explained with a single variable. Clarifiers should not be

designed in the basis of a single parameter, e.g. the SOR alone can not accurately provide the dimensions of secondary clarifiers.

- When the MLSS and the recirculation ratio are kept constant and the SOR is increased, the Marrero SST shows almost no correlation between the SOR and the ESS (until it suddenly fails due to a solids overload, i.e. rising of the sludge blanket). When the SLR and the recirculation ratio are kept constant, the SOR and the ESS show a linear correlation, i.e. the ESS increases as the SOR increases. In this case the failure of the clarifier is gradual and is due to an excessive carry over of suspended solids by the upward current towards the effluent weir.
- The water temperature affects the settling velocities via the fluid viscosity. The Stokes' Law relationship was shown to adequately describe the effect of temperature on a selected floc. This relationship can be applied to correct the settling velocities for difference in temperatures in whichever of the four types of sedimentation settling processes, i.e., unflocculated discrete settling, flocculated discrete settling, hindered (zone) settling and compression.
- The changes in temperature on secondary clarifiers play an important role in the performance of secondary settling tanks. A warmer inflow produces a transient strengthening of the density current which results in a higher ESS; the creation of an unstable stratification density gradient in the vertical direction magnifies this effect. A cooler inflow also results in a strengthening of the density current, but in this case the stable vertical density gradient seems to suppress the turbulence in the vertical direction and to damp the diffusion of the suspended solids.
- In SST the direction of the density current will be probably dominated by the gradient due to the suspended solids. A warmer inflow would travel near the bottom until it rises after the suspended solids have settled out. In the case of low SS at the influent, e.g. typical concentrations in primary settling tanks, water temperature difference might define the nature of the density current, i.e. buoyant or sinking. A

warmer influent might result in a rising plume downstream of the center well and in a surface density current in the settling zone.

- The surface cooling process, typical of winter or night conditions, has a negative impact in the hydrodynamics and solids distribution of the SST. The creation of an unstable density gradient in the vertical direction, and the entrainment of the surface-denser water in the density current results in a density gradient in the radial direction that reinforces the counterclockwise rotation of the density current, thus increasing the suspended solids carrying capacity of the upward current. This effect in conjunction with the decrease in the values of the settling properties explains some of the differences that have been observed in “summer” and “winter”, and “day” and “night” ESS concentrations.
- The warming up process of the water surface originated by the heat exchange during the summer conditions has a relatively small effect on the performance of the settling tank. These conditions create a stable density stratification which has negligible effects on the overall hydrodynamics and performance of the tank.
- In circular tanks with scrapers, the blades are not highly effective in conveying the solids in the region near the hopper. The gravity induced radial velocities in the sludge blanket are higher than the radial velocities of the scraper in this region. In fact the scraper might retard the sludge blanket movement towards the hopper, forcing it to move as a “pulse” and promoting the creation of internal waves.
- The use of inlet swirl vanes does not appear to have an important benefit on the tank hydrodynamics.

7.3 Recommendations

Even though this research makes some important advances in the modeling of secondary settling tanks, the model makes use of simplifying assumptions that limit its applicability. The following are suggestions for additional developments to address these limitations:

- The Q3D model does not include the effects of wind shear. The actual model should be expanded to 3-dimensions in order to accurately predict the effects of wind.
- The Q3D model assumes the solids-liquid mixture as a homogenous suspension for the solution of the transport, momentum and stream function equations. The solids-liquid mixture is really a two-phase flow. The simulation of a two-phase flow might lead to a more realistic representation of the compression of the sludge blanket.
- Even though the Q3D model includes the simulation of total dissolved solids variations, the effect of the TDS in the hydrodynamics needs to be validated.
- The Q3D model neglects the effects of the Brownian motion flocculation in the general flocculation process, partly because it leads to the aggregation of particles that fall into the non-settleable portion. However, the effects of the Brownian motion flocculation inside the SST needs to be further investigated.
- The FSS test as proposed by Wahlberg et al. (1995) is based on the flocculation of the sludge sample at a specific G value. Since the G values might be different in the clarifier and the objective of the test is to quantify the flocculation potential of a specific sample, the FSS test should be conducted with different G values to get the optimum value for flocculation. This procedure will provide a better representation of the flocculation potential of the sample.

- The flocculation sub-model should be used with field derived data including aggregation and breakup constants, and FSS. The FSS should be obtained with the optimum G value.
- The effect of poorly flocculated sludge on the performance of SST should be further evaluated. Even though it is suspected that a good representation of the discrete settling fractions, a FSS based on an optimum G value, and representative kinetic flocculation constants should yield an accurate simulation of this type of incoming sludge, this assumption needs to be validated.
- The effects of bulking sludges on the zone settling parameters and compression rate properties need to be investigated. Similarly, the Q3D model needs to be validated under these conditions.
- The methods proposed in this research for the determination of the discrete settling fractions and the discrete settling velocities should be further evaluated. The methods presented herein require a considerable effort in both time and precision. Since it has been demonstrated that the final effluent strongly depends on the values of the initial fractions, the accurate representation of the discrete settling fractions is vital for a good simulation. Research on improved column tests to derive the data should be investigated.
- In Chapter 3, Equation 3.14 proposes a relationship for the correction of the settling properties for difference in temperatures. Even though this relationship can be used to conduct a sensitivity analysis in the performance of the model for different seasons, e.g. summer and winter, there is no evidence that the settling properties can be accurately extrapolated from one season to another. More research is needed to define the effect of seasonal variations on the settling characteristics and other sludge's properties like rheology and the flocculation kinetic constants.

- Few attempts have been made trying to relate the settling properties to the biological unit processes. More research is needed to link the settling properties to the conditions in the aerator, including the effects of bio-polymers, dissolved oxygen (DO), HRT, sludge retention time (SRT), pH, food/microorganism ratio, and temperature.
- Studies are needed to link the conditions in the biological unit to the kinetic constants involved in the flocculation sub-model. An implicit assumption is that particles can be flocculated because there is an adequate amount of polymers in the incoming MLSS; however, if the conditions in the aerator are not adequate (e.g., SRT, HRT, pH, DO) the amount of polymer might be significantly affected. Studies are required to determine whether the discrete fraction, the flocculation kinetic constants and the FSS of the sample are sufficient for a good representation of the flocculation potential of the mixed liquor, or are other parameters needed. In any case, an extensive research is needed including a wide range of conditions from very poor to well flocculated sludges.
- There are some uncertainties in the G values predicted by the model when inlet deflectors are used. Apparently these G values need to be corrected, accounting for the fact that the real inlet velocity is higher than the horizontal component of the velocity. Similarly, the model could be modified to include the simulation of other types of inlet configurations when such information becomes available by future research.
- The Q3D model neglects the biological processes in the clarifier. For example, if denitrification occurs in the clarifier, the rising bubbles might cause alterations on the hydrodynamics and on the suspended solids contours. Similarly, the conversion of COD is not included in the model. However, since the clarifier can promote the aggregation of dispersed particles, it could also promote the reduction of the particulate and colloidal CODs. On the other hand, the oxygen level in some portions of the clarifier might be enough to produce additional removal of dissolved

substrate. In treatment systems with short retention time in the biological reactor, e.g. bioflocculation systems, there might be a remaining dissolved substrate on the effluent; with adequate dissolved oxygen levels the consumption of dissolved substrate could continue in the SST. This is a research topic that needs to be addressed.

- Even though important advances have been made in the representation of the rheology of the sludge, it is not clear which model would better represent the rheology of activated sludges. As indicated by McCorquodale (2004) “more research is needed to relate rheological properties to the biological unit processes.”
- This research concluded that, “In circular tanks with scrapers, the blades are not highly effective in conveying the solids in the region near the hopper.” However, field data should be gathered and more research should be conducted on the effect of blades’ position in order to come up with a better design of the scraper mechanism.
- Researches presented by McCorquodale (1976, 1977, 1987), Godo (1990), Wells and LaLiberte (1998a, 1998b) and Zhou et al. (1994) show similar results to those presented herein in the evaluation of the temperature effects on secondary and primary clarifiers. However, it is necessary to collect more field data to calibrate and validate this sub-model.
- The Q3D model does not include the representation of the floatable fraction. New versions of the model should incorporate this simulation.
- Future efforts should be made to couple the Q3D model to the biological unit in the treatment plant. This would allow a better representation of the solids inventory of the systems and more dynamics simulations. With slight modifications the Q3D model can be used for the simulation of primary settling tanks which makes the implementation of the coupled system shown in Figure 7.1 easier.

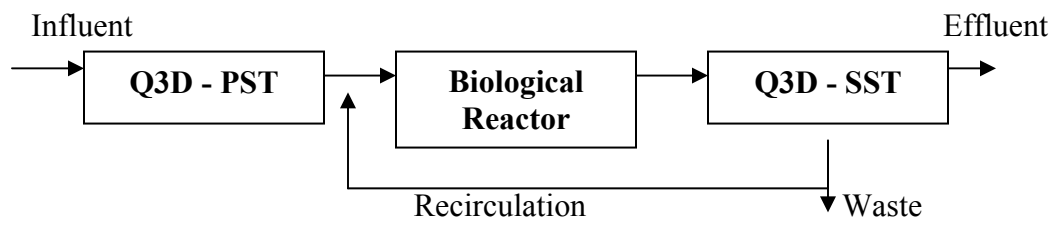


Figure 7.1 Recommended Coupled System

REFERENCES

- Abdel-Gawad, S.M. (1983). *Simulation of settling tanks by the strip integral method*. Ph.D. thesis, University of Windsor, Windsor, Ontario.
- Abdel-Gawad, S.M., and McCorquodale, J.A. (1984a). Strip integral method applied to settling tanks. *Journal of Hydraulic Engineering*, 110(1), pp. 1-17.
- Abdel-Gawad, S.M., and McCorquodale, J.A. (1984b). Hydrodynamics of circular primary clarifiers. *Canadian Journal of Civil Engineering*, 11(2), pp. 299-307.
- Abdel-Gawad, S.M., and McCorquodale, J.A. (1985a). Numerical simulation of rectangular settling tanks. *Journal of Hydraulic Research*, 23(2), pp. 85-96.
- Abdel-Gawad, S.M., and McCorquodale, J.A. (1985b). Simulation of particle concentration distribution in primary clarifiers. *Canadian Journal of Civil Engineering*, 12(3), pp. 454-463.
- Adams, E.W., and Rodi, W. (1990). Modelling flow and mixing in sedimentation tanks. *Journal of Hydraulic Engineering*, 116(7), pp. 895-913.
- Albertson, O., and Okey, R., (1992). Evaluating scraper designs. *Water Environment and Technology*, 4(1), pp. 52-58.
- Anderson, N.E. (1945). Design of settling tanks for activated sludge. *Sewage Works Journal*, 17(1), pp. 50-63.
- APHA (1999). *Standard methods for the examination of water and wastewater*. 20th Edition, American Public Health Association, Washington D.C. (1999)

Argaman, Y., and Kaufman, W.J. (1970). Turbulence and flocculation. *Journal of the Sanitary Engineering Division, ASCE* , 96(2), pp. 223-241.

Armbruster, M., Krebs, P., and Rodi, W. (2001). Numerical modelling of dynamic sludge blanket behaviour in secondary clarifiers. *Water Science and Technology*, 43 (11), pp. 173-180.

Azeredo, J., Oliveira, R., and Lazarova, V. (1998). A new method for extraction of exopolymers from activated sludges. *Water Science and Technology*, 37(4-5), pp. 367-370.

Battistoni, P. (1997). Pre-treatment, measurement execution procedure and waste characteristics in the rheology of sewage sludges and the digested organic fraction of municipal solid wastes. *Water Science and Technology*, 36(11), pp. 33-41.

Baumer, P., Volkart, P., and Krebs, P. (1996). Dynamic loading test for final settling tanks. *Water Science and Technology*, 34(3-4), pp. 267-274.

Berlin, A.A., Kislenko, V.N., and Moldovanov, M.A. (1992). Mathematical model of suspension flocculation kinetics. *Colloid and Polymer Science*, 270, pp. 1042-1045.

Bhargava, D.S., and Rajagopal, K. (1993). Differentiation between transition zone and compression in zone settling. *Water Research*, 27(3), pp. 457-463.

Biggs, C.A., and Lant, P.A. (2000). Activated sludge flocculation: on-line determination of floc size and the effect of shear. *Water Research*, 34(9), pp. 2542-2550.

Billmeier, E. (1988). The influence of blade height on the removal of sludge from activated sludge settling tanks. *Water Science and Technology*, 20(4-5), pp. 165-175.

Bokil, S.D. (1972). *Effect of mechanical blending on the aerobic digestion of waste activated sludge*. PhD dissertation, Department of Civil and Engineering, University of Windsor, Ontario, Canada.

Bokil, S.D., and Bewtra, J.K. (1972). Influence of mechanical blending on aerobic digestion of waste activated sludge. *Proceedings 6th IAWPRC Conference on Water Pollution Research*, pp.. 421-438, Jerusalem, Israel.

Brouckaert, C.J., and Buckley, C.A. (1999). The use of computational fluid dynamics for improving the design and operation of water and wastewater treatment plants. *Water Science and Technology*, 40(4-5), pp. 81-89.

Brown, M. J. and Lester, J. N. (1980). Comparison of bacterial extracellular polymer extraction methods. *Applied and Environmental Microbiology*, 40(2), pp.179-185.

Burden, R.L., and Faires, J.D. (2001). *Numerical Analysis*. 7th Edition, Wadsworth Group. Brooks/Cole. Pacific Grove, CA.

Busch, P. L., and Stumm, W. (1968). Chemical interactions in the aggregation of bacteria- bioflocculation in waste treatment. *Environmental Science and Technology*, 2, pp. 49.

Camp, T., and Stein, P.C. (1943). Velocity gradients and internal work in fluid motion. *Journal Boston Society of Civil Engineers*, 30, pp. 219-237

Camp, T.R. (1945). Sedimentation and the design of settling tanks. *Transactions of the American Society of Civil Engineers*, Paper No. 2285, pp. 895-958.

Camp, T.R. (1952). Studies of sedimentation basin design. *Sewage Works*, 25(1), pp.1-14.

Catunda, P., and van Haandel, A.C. (1992). Activated sludge settling part I: experimental determination of activated sludge settleability. *Water SA*, 18(3), pp. 165-172

Celik, I., and Rodi, W. (1988). Modeling suspended sediment transport in nonequilibrium situations. *Journal of Hydraulic Engineering*, 114(10), pp. 1157-1191.

Celik, I., and Rodi, W., and Stamou, A. (1985). Prediction of hydrodynamic characteristics of rectangular settling tanks. *Proceedings of the International Symposium on Refined Flow Modelling and Turbulence Measurements*, Iowa City, Iowa, 641-651.

Chao, A. C., and Keinath, T. M. (1979). Influence of process loading intensity on sludge clarification and thickening characteristics. *Water Research*, 13, pp. 1213-1223.

Chapra, S. C. (1997). *Surface Water-Quality Modeling*. WCB/McGraw-Hill, New York, N.Y., 844 pp.

Chebbo, G., Forgues, N., Lucas-Aiguier, E., and Berthebaud, S. (1998). A stochastic approach to modeling solid transport in settling tanks. *Water Science and Technology*, 37(1), pp. 277-284.

Cho, S.H., Colin, F., Sardin, M., and Prost, C. (1993). Settling velocity model of activated sludge. *Water Research*, 27(7), pp. 1237-1242.

Coulson, J.M., and Richardson, G. (1955). *Chemical Engineering*, Vol. 2. McGraw-Hill, New York.

Dahl, C., Larsen, T., and Petersen, O. (1994). Numerical modelling and measurement in a test secondary settling tank. *Water Science and Technology*, 30(2), pp. 219-228.

Das, D., Keinath, T. M., Parker, D. S, and Wahlberg, E. J. (1993). Floc breakup in activated sludge plants. *Water Environment Research*, 65(2), pp. 138-145.

De Cock, W., Blom, P., and Berlamont, J. (1999). The feasibility of flocculation in a storage sedimentation basin. *Water Science and Technology*, 39(2), pp. 75-83.

DeClercq, B. (2003). *Computational Fluid Dynamics of Settling Tanks: Development of Experiments and Rheological, Settling and Scraper Submodels*. Ph.D. Thesis. University of Ghent, Belgium.

Deininger, A., Gunthert, F., and Wilderer, P. (1996). The influence of currents on circular secondary clarifier performance and design. *Water Science and Technology*, 34(3-4), pp. 405-412.

Dentel, S. (1997). Evaluation and role of rheological properties in sludge management. *Water Science and Technology*, 36(11), pp. 1-8.

DeVantier, B.A., and Larock, B. E. (1987). Modelling sediment-induced density currents in sedimentation basins. *Journal of Hydraulic Engineering*, 113(1), pp. 80-94.

DeVantier, B.A., and Larock, B.E. (1986). Modeling a recirculation density-driven turbulent flow. *International Journal for Numerical Methods in Fluids*, 6 (4), pp. 241-253.

Dick, R.I. (1972). Role of activated sludge final settling tanks. *Journal of the Sanitary Engineering Division, ASCE* , 96, pp. 423.

Dickinson, E., and Eriksson, L. (1991). Particle flocculation by adsorbing polymers. *Advances in Colloid and Interface Science*, 34, pp. 1-29.

Dobbins, W.E. (1944). Effect of turbulence on sedimentation. *Transactions of the American Society of Civil Engineers*, 109, pp. 629-656.

Dupont, R., and Dahl, C. (1995). A one-dimensional model for a secondary settling tank including density current and short-circuiting. *Water Science and Technology*, 31(2), pp. 215-224.

Dupont, R., and Henze, M. (1992). Modelling of the secondary clarifier combined with the activated sludge model No. 1. *Water Science and Technology*, 25(6), pp. 285-300.

Eagleson, P.S. (1970). *Dynamic Hydrology*. McGraw-Hill, New York, N.Y.

Ekama, G.A., and Marais, P. (2002). *Hydrodynamic Modelling of Secondary Settling Tanks*. WRC Report No. 835/1/02 Part 1. Water Resources Group, Department of Civil Engineering, University of Cape Town, South Africa.

Ekama, G.A., Barnard, J., Gunthert, F., Krebs, P., McCorquodale, J.A., Parker, D.S., and Wahlberg, E.J. (1997). *Secondary Settling Tanks: Theory, Modelling, Design and Operation*. Published by the International Association on Water Quality, STR No. 6, 1997, Richmond, UK.

Eriksson, L., and Alm, B. (1991). Study of flocculation mechanisms by observing effects of a complexing agents on activated sludge properties. *Water Science and Technology*, 24, pp. 21-28.

Frolund, B., Palmgren, R., Keiding, K., and Nielsen, P. H. (1996). Extraction of extracellular polymers from activated sludge using a cation exchange resin. *Water Research*, 30(8), pp.1749-1758.

Galil, N., Stahl, N., Novak, J.T., and Rebhum, M. (1991). The influence of mixing on the physical characteristics of biological flocs. *Journal Water Pollution Control Federation*, 63(5), pp. 768-772.

Gerges, H., and McCorquodale, J.A. (1997). Modelling of flow in rectangular sedimentation tanks by an explicit third-order upwinding technique. *International Journal for Numerical Methods in Fluids*, 24, pp. 537-561.

Godo, A., and McCorquodale, J.A. (1991). Effect of diurnal temperature variation on the hydraulics of clarifiers. *Canadian Journal of Civil Engineering*, 18(6), pp. 1084-1087.

Godo, A.M. (1990). Density currents in rectangular settling tanks. M.S. thesis, University of Windsor, Windsor, Ontario.

Goodwin, J. A., and Forster, C. F. (1985). A further examination into the composition of the activated sludge surfaces in relation to their settlement characteristics. *Water Research*, 19, 527.

Gorczyca, B., and Ganczarczyk, J. (2002). Flow rates through alum coagulation and activated sludge flocs. *Water Quality Research Journal of Canada*, 37(2), pp. 389-398.

Grijpspeerd, K., Vanrolleghem, P., and Verstraete, W. (1995). Selection of one-dimensional sedimentation: models for on-line use. *Water Science and Technology*, 31(2), pp. 193-204.

Gunthert, F.W. (1984). Thickening zone and sludge removal in circular final settling tanks. *Water Science and Technology*, 16, pp. 303-316.

Hamilton, J., Jain, R., Antoniou, P., Svoronos, S.A., Koopman, B., and Lyberatos, G. (1992). Modeling and pilot-scale experimental verification for predenitrification process. *Journal of Environmental Engineering*, 118, pp. 38-55.

Han, M., and Lawler, D.F. (1992). The relative insignificance of G in flocculation. *Research and Technology*, AWWA, 8, pp. 79-91.

Hazen, A. (1904). On Sedimentation. Transactions of the American Society of Civil Engineers, Paper No. 980, pp. 45 -88.

Hilligard, D., and Hoffmann, E. (1997). Particle size analysis and sedimentation properties of activated sludge flocs. *Water Science and Technology*, 36(4), pp. 167-175.

Hirschc, C. (1997). *Numerical computation of internal and external flows. Vol. 1, Fundamentals of numerical discretisation.* John Wiley & Sons, West Sussex, U.K., 515 pp.

Hogg, R. (1999). The role of polymer adsorption kinetics in flocculation. *Colloids and Surface A: Physicochemical and Engineering Aspects*, 146, pp. 253-263.

Imam, E., McCorquodale, J.A., and Bewtra, J.K. (1983). Numerical modelling of sedimentation tanks. *Journal of Hydraulic Engineering*, 109(12), pp. 1740-1754.

Islam, M.A., and Karamisheva, R.D. (1998). Initial settling rate/concentration relationship in zone settling. *Journal of Environmental Engineering*, 124(1), pp. 39-42.

Jayanti, S., and Narayanan, S. (2004). Computational study of particle-eddy interaction in sedimentation tanks. *Journal of Environmental Engineering*, 130(1), pp. 37-49.

Jensen, D.E., Spalding, D.G., Tatchell, D.G., and Wilson, A.S. (1979). *Computation of structure of flames with recirculating flow and radial pressure gradients.* Numerical prediction of flow, heat transfer, turbulence and combustion. Edited by D.B. Spalding. 1983. Pergamon Press, Elmsford, N.Y.

Ji, Z., McCorquodale, J.A., Zhou, S.P., and Vitasovic, Z. (1996). A dynamic solids inventory model for activated sludge systems. *Water Environment Research*, 68(3), pp 329-337.

Jimenez, J.A. (2002). *Kinetics of cod removal in the activated sludge process*. Ph.D. Thesis, University of New Orleans, New Orleans, Louisiana.

Jimenez, J.A., La Motta, E.J., and Parker, D.S., (2003). Kinetic of removal of particulate COD in the activated sludge process. *Proceedings Water Environment Federation 76th Annual Conference and Exhibition*, Los Angeles, California, October 11-15.

Karl, J., and Wells, S.A. (1999). Numerical model of sedimentation/thickening with inertial effects. *Journal of Environmental Engineering*, 125(9), pp. 792-806.

Kinnear, D. J. (2002). *Biological Solids Sedimentation: A Model Incorporating Fundamental Settling Parameters*. Ph.D. Thesis, University of Utah.

Kinnear, D.J., (2004). *Littleton Englewood Wastewater Treatment Facility, Personal Communication*.

Kinnear, D.J., and Deines, K. (2001). Acoustic Doppler current profiler: clarifier velocity measurement. *Proceedings Water Environment Federation 74th Annual Conference and Exposition, Atlanta, Georgia, October 13-17*.

Kleine, D., and Reddy, B.D. (2002). *Hydrodynamic Modelling of Secondary Settling Tanks*. WRC Report No. 835/1/02 Part 2. Water Resources Group, Department of Civil Engineering, University of Cape Town, South Africa.

Knop, E. (1966). Design studies for the Emscher Mouth treatment plant. *Journal Water Pollution Control Federation*, 38(7), pp. 1194-1207.

Krebs, P., Armbruster, M., and Rodi, W. (1998). Laboratory experiments of buoyancy-influenced flow in clarifiers. *Journal of Hydraulic Research*, 36(5), pp. 831-851.

Krebs, P., Stamou, A.I., Garcia-Heras, J.L., and Rodi, W. (1996). Influence of inlet and outlet configuration on the flow in secondary clarifiers. *Water Science and Technology*, 34(5-6), pp. 1-9.

Krebs, P., Vischer, D., and Gujer, W. (1992). Improvement of secondary clarifier efficiency by porous walls. *Water Science and Technology*, 25(5-6), pp. 1147-1156.

Krebs, P., Vischer, D., and Gujer, W. (1995). Inlet structure design for final clarifiers. *Journal of Environmental Engineering*, 121(8), pp. 558-564.

Krebs, P. (1991). The hydraulics of final settling tanks. *Water Science and Technology*, 23(4-6), pp. 1037-1046.

Krebs, P. (1995). Success and shortcomings of clarifier modelling. *Water Science and Technology*, 31(2), pp. 181-191.

La Motta, E.J., and Josse, J.C. (1996). *Prefeasibility study of the Jefferson Parish Wastewater Treatment Plant Privatization Project*. Final Report submitted by Cochran, Sternhell and Associates, Inc. to Jefferson Parish, Louisiana

La Motta, E.J., Jimenez, J.A., Josse, J.A., and Manrique, A. (2004a). The Role of Bioflocculation on COD Removal In the Solids Contact Chamber of the TF/SC Process. Accepted for publication in *Journal of Environmental Engineering*, ASCE.

La Motta, E.J., Jimenez, J.A., Parker, D., and McManis, K.L. (2003). Removal of Particulate COD by Bioflocculation in the Activated Sludge Process. *Water Pollution VII, Modelling, Measuring and Prediction*, edited by C.A. Brebbia, D. Almorza, and D. Sales, WIT Press, Southampton, Boston, pp. 349-358.

La Motta, E.J., McCorquodale, J.A., Griborio, A.G., and Rojas, J. (2004b). *Personal communication*.

- Laikari, H. (1989). Simulation of the sludge blanket of a vertical clarifier in activated sludge process. *Water Science and Technology*, 21(6-7), pp. 621-629.
- Laine, S., Phan, L., Pellarin, P., and Robert, P. (1999). Operating diagnostics on a flocculator-settling tank using FLUENT CFD software. *Water Science and Technology*, 39(4), pp. 155-162.
- Lakehal, D., Krebs, P., Krijgsman, J. and Rodi, W. (1999). Computing shear flow and sludge blanket in secondary clarifiers. *Journal of Hydraulic Engineering*, 125 (3), pp 253-262.
- Larsen, P. (1977). *On the hydraulics of rectangular settling basins, experimental and theoretical studies*. Report no. 1001, Dept. of Water Resour. Engrg., Lund Inst. of Tech., Lund Univ., Lund, Sweden.
- Launder, B.E., and Spalding, D.B. (1972). *Lectures in mathematical models of turbulence*. Academic Press, London, UK.
- Lee, R. (1978). *Forest Microclimatology*. Columbia University Press, New York, N.Y.
- Levine A. D., Tchobanoglous G., and Asano T. (1991). Size distribution of particulate contaminants in wastewater and their impact on treatability. *Water Research*, 25(8), pp. 911-922.
- Li, D.H., and Ganczarczyk, J.J. (1986). Application of image analysis system for study of activated sludge. *Water Pollution Research Journal of Canada*, 21, pp. 130-140.
- Li, D.H., and Ganczarczyk, J.J. (1987). Stroboscopic determination of settling velocity, size and porosity of activated sludge flocs. *Water Research*, 31(3), pp. 257-262.

- Li, D.H., and Ganczarczyk, J.J. (1992). Advective transport in activated sludge flocs. *Water Environment Research*, 64, pp. 236-240.
- Li, X., and Logan, B.E. (1997a). Collision frequencies between fractal aggregates and small particles in a turbulently sheared fluid. *Environmental Science and Technology*, 31(4), pp. 1237-1242.
- Li, X., and Logan, B.E. (1997b). Collision frequencies of fractal aggregates with small particles by differential sedimentation. *Environmental Science and Technology*, 31(4), pp. 1229-1236.
- Liao, B.Q., Allen, D.G., Droppo, I.G., Leppard, G.G., and Liss, S.N. (2001). Surface properties of sludge and their role in bioflocculation and settleability. *Water Research*, 35(2), pp. 339-350.
- Lindeborg, C., Wiberg, N., and Seyf, A. (1996). Studies of the dynamic behaviour of a primary sedimentation tank. *Water Science and Technology*, 34(3-4), pp. 213-222.
- Lotito, V., Spinosa, L., Mininni, G., and Antonacci, R. (1997). The Rheology of Sewage Sludge at Different Steps of Treatment. *Water Science and Technology*, 36(11), pp. 79-85.
- Lumley, D.J., Balmer, P., and Adamsson, J. (1988). Investigations of secondary settling at a large treatment plant. *Water Science and Technology*, 20(4-5), pp. 133-142.
- Lyn, D.A., and Zhang, Z. (1989). Boundary-fitted numerical modelling of sedimentation tanks. *Proceedings 23rd International Association for Hydraulic Research (IAHR), Ottawa, Canada, A-331-A-338*.

Lyn, D.A., Stamou, A.I., and Rodi, W. (1992). Density currents and shear-induced flocculation in sedimentation tanks. *Journal of Hydraulic Engineering*, 118(6), pp. 849-867.

Malcherek, A. (1994). Numerical modeling of cohesive settling velocities. *International Journal of Sediment Research*. Pp. 97-106.

Mazzolani, G., Pirozzi, F., and D'Antonio, G. (1998). A generalized settling approach in the numerical modeling of sedimentation tanks. *Water Science and Technology*, 38(3), pp. 95-102.

McCorquodale, J.A., Griborio, A.G., and Georgiou, I. (2004). *Personal communication*.

McCorquodale, J.A., and Zhou, S.P. (1994a). Application of numerical models in the design of clarifiers. *Proceedings 1994 National Conference on Environmental Engineering, ASCE*, Boulder, Colorado, July 11-13, pp. 186-193.

McCorquodale, J.A., and Zhou, S.P. (1994b). Use of numerical models in clarifier design: optimization of inlet structures. *Proceedings Water Environment Federation 67th Annual Conference & Exposition*, Chicago, Illinois, October 15-19, pp. 349-360.

McCorquodale, J.A. (1976). Hydraulic study of the circular settling tanks at the West Windsor Pollution Control Plant. Report submitted to Lafontaine, Cowie, Buratto and Associated, Limited, Consulting Engineers, Windsor, Ontario, Canada.

McCorquodale, J.A. (1977). Temperature profiles in primary settling tanks. IRI Report, University of Windsor.

McCorquodale, J.A. (1987). Density currents in clarifiers. *Proceedings of Hydraulic Division, ASCE Conference*, Williamsburg, VA, pp. 56-61.

McCorquodale, J.A. (2004). Manual of practice for clarifiers. Chapter 6: Mathematical modelling of settling tank (Draft). Water Environmental Federation.

McCorquodale, J.A., and Zhou, S.P. (1993). Effect of hydraulic and solids loading on clarifier performance. *Journal of Hydraulic Research*, IAHR, 31(4), pp. 461-470.

McCorquodale, J.A., Yuen, E.M., Vitasovic, Z., and Samstag, R.W. (1991). Numerical simulation of unsteady conditions in clarifiers. *Water Pollution Research Journal of Canada*, 26(2), pp. 201-222.

Merrill, M.S., Tetreault, M., Parker, D.S., Vitasovic, Z., McCorquodale, J.A., and Ji, Z. (1992). Mathematical simulation of secondary clarifiers coupled with activated sludge reactors. *Proceedings Water Environment Federation 65th Annual Conference & Exposition*, New Orleans, Louisiana, September 20 – 24, pp. 229-240.

Moursi, A., McCorquodale, J.A., and El-Sebakhy, I. (1995). Experimental studies on heavy radial density currents. *Journal of Environmental Engineering*, 121(12), pp. 920-929.

Namer, J., and Ganczarczyk, J.J. (1993). Settling properties of digested sludge particle aggregates. *Water Research*, 27(8), pp. 1285-1294.

Novak, J.T., and Haugan, B.E. (1981). Polymer extraction from activated sludge. *Journal Water Pollution Control Federation*, 53(9), pp. 1420-1424.

Oles, V. (1992). Shear-induced aggregation and break up of polystyrene latex particles. *Journal of Colloid and Interface Science*, 154, pp. 351-358.

Otterpohl, R., and Freund, M. (1992). Dynamic models for clarifiers of activated sludge plants with dry and wet weather flows. *Water Science and Technology*, 26(5-6), pp. 1391-1400.

Parker, D.S. (1983). Assessment of secondary clarification design concepts. *Journal of Water Pollution Control Federation*, 55(4), pp. 349.

Parker, D. S., Kaufman, W. J., and Jenkins, D. (1970). Characteristics of biological flocs in turbulent regime. SERL Report No. 70-5, University of California, Berkeley, California.

Parker, D. S., Kaufman, W. J., and Jenkins, D. (1971). Physical conditioning of activated sludge flocs. *Journal Water Pollution Control Federation*, 43(9), pp. 1817-1834.

Parker, D., and Stenquist, R. (1986). Flocculator-clarifier performance. *Journal of Water Pollution Control Federation*, 58(3), pp. 214-219.

Parker, D., Buttler, R., Finger, R., Fisher, R., Fox, W., Kido, W., Merrill, S., Newman, G., Pope, R., Slapper, J., and Wahlberg, E. (1996). Design and operations experience with flocculator-clarifiers in large plants. *Water Science and Technology*, 33(12), pp. 163-170.

Parker, D.S., Kaufman, and W.J., Jenkins, D. (1972). Floc breakup in turbulent processes. *Journal of the Sanitary Engineering Division, ASCE*, SA1, pp. 79-99.

Parker, D.S., Kaufman, W.J., and Jenkins, D. (1970) Characteristics of Biological Floc in Turbulent Regimes, SERL Report 70-5. University of California, Berkeley.

Patankar, S.V. (1980). *Numerical Heat Transfer and Fluid Flow*. Hemisphere Publishing Corporation. McGraw-Hill, New York, N.Y.

Patankar, S.V., and Spalding, D.B. (1972). A calculation procedure for heat, mass and momentum transfer in three-dimensional parabolic flows. *International Journal of Heat and Mass Transfer*, 15, pp. 1787-1806.

Pavoni, J., Tenney, M., and Echelberger, W. (1972). Bacterial exocellular polymers and biological flocculation. *Journal of Water Pollution Control Federation*, 44(3), pp. 414-431.

Pearson, H.J., Valioulis, I.A., and List, E.J. (1984). Monte Carlo simulation of coagulation in discrete particle size distributions. Part 1: Brownian motion and fluid shearing. *Journal of Fluid Mechanics*, 143, June, pp. 367-385.

Qasim, S.R., Motley, E.M., and Zhu, G. (2000). *Water Works Engineering Planning Design and Operations*. 1st Edition, Prentice Hall PTR, 844 pp.

Rasmussen, M.R., and Larsen, T. (1996). A method for measuring sludge settling characteristics in turbulent flows. *Water Research*, 30(1), pp. 2363-2370

Retana, A.G. (1999). *Full-scale comprehensive evaluation of the dual trickling filter/solids contact process*. M.S. thesis, University of New Orleans, New Orleans, Louisiana.

Rodi, W. (1980). *Turbulence models and their application in hydraulics*. A state-of-the-art review. IAHR, Delft, The Netherlands.

Samstag, R.W., Dittmar, D.F., Vitasovic, Z., and McCorquodale, J.A. (1992). Underflow geometry in secondary sedimentation. *Water Environment Research*, 64(3), pp. 204-212.

Santos Monteiro, P. (1997). The influence of the anaerobic digestion process on the sewage sludges rheological behaviour. *Water Science and Technology*, 36(11), pp. 61-67.

Schamber, D.R., and Larock, B.E. (1981). Numerical analysis of flow in sedimentation basins. *Journal Hydraulic Division*, ASCE 107 (HY5), pp. 595-591.

Scott, K.J. (1966). Mathematical models of mechanism of thickening. *Journal of Industrial and Engineering Chemistry*, 5, pp. 109-113.

Serra T., and Casamitjana, X. (1998). Modelling the aggregation and break-up of fractal aggregates in a shear flow. *Applied Scientific Research Journal*, 59, pp. 225-268.

Slatter, P. (1997). The rheological characterisation of sludges. *Water Science and Technology*, 36(11), pp. 9-18.

Smith, P.G., and Coackley, P. (1984). A method for determining specific surface area of activated sludge by dye absorption. *Water Research*, 17, pp. 595-598.

Smollen, M., and Ekama, G. (1984). Comparison of empirical settling velocity equations in flux theory for secondary settling tanks. *Water SA*, 10 (4), pp. 175-184.

Sozanski, M., Kempa, E., Grocholski, K., and Bien, J. (1997). The rheology experiment in sludge properties research. *Water Science and Technology*, 36(11), pp. 69-78.

Spicer, P., and Pratsinis, S. (1996). Shears-induced flocculation: the evolution of floc structure and the shape of the size distribution at steady state. *Water Research*, 30(5), pp. 1049-1056.

Stamou, A.I., Adams, E.W., and Rodi, W. (1989). Numerical modeling of flow and settling in primary rectangular clarifiers. *Journal of Hydraulic Research*, 27(5), pp. 665-682

Stamou, A.I., Latsa, M., and Assimacopoulos, D. (2000). Design of two-storey final settling tanks using mathematical models. *Journal of Hydroinformatics*, 2(4), pp. 235-245.

Starkey, J., and Karr, J. (1984). Effect of low dissolve oxygen concentration on effluent turbidity. *Journal Water Pollution Control Federation*, 56(7), pp. 837-843.

Steinour, H.H. (1944). Rated of sedimentation, nonflocculated suspensions of uniform spheres. *Journal of Industrial and Engineering Chemistry*, 36(7), pp.618-624.

Surucu, G., and Cetin F.D. (1990). Effects of temperature, pH, and D.O. concentration on settleability of activated sludge. *Environmental Technology*, 11, pp. 205-212.

Szalai, L., Krebs, P., and Rodi, W. (1994). Simulation of flow in circular clarifier with and without swirl. *Journal of Hydraulic Engineering*, 120(1), pp. 4-21.

Tambo, N., and Watanabe, Y. (1979). Physical aspect of the flocculation process-I. Fundamental treatise. *Water Research*, 13, pp. 429-439

Takacs, I., Patry, G.G., and Nolasco, D. (1991). A dynamic model of the clarification-thickening process. *Water Research*, 25(10), pp. 1263-1271.

Tchobanoglous, G., Burton, F., and Stensel, D. (2003). *Wastewater Engineering: Treatment and Reuse*. Metcalf & Eddy, Inc. 4th Edition. McGraw-Hill, New York, N.Y., 1819 pp.

Tenney, M.W., and Stumm, W. (1965). Chemical flocculation of microorganisms in biological waste treatment. *Journal of Water Pollution Control Federation*, 37, pp.1370.

Thomas, D.N., Judd, S.J., and Fawcett, N. (1999). Flocculation modelling: a review. *Water Research*, 33(7), pp. 1579-1592.

Urbain, V., Block, J., and Manem, J. (1993). Bioflocculation in activated sludge: an analytic approach. *Water Research*, 27(5), pp. 829-838.

Valioulis, I., and List, J. (1984a). Numerical simulation of a sedimentation basin. 1. Model development. *Environmental Science and Technology*, 18, pp. 242-247.

Valioulis, I., and List, J. (1984b). Numerical simulation of a sedimentation basin. 2. Design application. *Environmental Science and Technology*, 18, pp. 248-253.

van Haandel, A.C. (1992). Activated sludge settling part II: settling theory and application to design and optimization. *Water SA*, 18(3), pp. 173-180.

van Marle, C., and Kranenburg, C. (1994). Effects of gravity currents in circular secondary clarifiers. *Journal of Environmental Engineering*, 120(4), pp. 943-960.

Vanderhasselt, A., Aspegren, H., Vanrolleghem, P., and Verstraete, W. (1999). Settling characterisation using on-line sensors at a full-scale wastewater treatment plant. *Water SA*, 25(4), pp. 1-6.

Vanrolleghem, P., Vand der Schueren D., Krikilion, G., Grijspeerdt, K., Willems, P., and Verstraete, W. (1996). On-line quantification of settling properties with in-sensor-experiments in an automated settlometer. *Water Science and Technology*, 33(1), pp. 37-51.

Versteeg, H.K., and Malalasekera, W. (1995). *An Introduction to Computational Fluid Dynamics: The Finite Volume Method*. Prentice Hall, Harlow, England.

Vesilind, P.A., (1968). Design of prototype thickeners from batch settling tests. *Water and Sewage Works*, 115 (July), 115-307.

Vitasovic, Z., Zhou, S.P., McCorquodale, J.A., and Lingren, K. (1997). Secondary clarifier analysis using data from the Clarifier Research Technical Committee Protocol. *Water Environmental Research*, 69(5), pp. 999-1007.

Wahlberg, E.J., Keinath, T.M., and Parker, D.S. (1994). Influence of activated sludge flocculation time on secondary clarification. *Water Environment Research*, 66 (6), pp. 779-786.

Wahlberg, E.J., Merrill, D.T., and Parker, D.S. (1995). Troubleshooting activated sludge secondary clarifier performance using simple diagnostic test. *Proceedings Water Environment Federation 68th Annual Conference & Exposition*, Miami, Florida, Vol. 1, pp. 435-444.

Wahlberg, E.J., Peterson, M.A., Flancher, D.W., Johnson, D., and Lynch, C.S. (1993). Field application of the CRTC's protocol for evaluating secondary clarifier performance: a comparison of sludge removal mechanisms in circular clarifiers. *Rocky Mountain Water Pollution Control Association Annual Meeting*, Albuquerque, New Mexico, September 20.

Weber, W. J. (1972). *Physical Chemical Processes for Water Quality Control*. Wiley, New York.

Wells, S., and LaLiberte, D., (1998a). Modeling density currents in circular clarifiers. *Fluid Particle Separation Journal*, 11(1), pp. 48-54.

Wells, S., and LaLiberte, D., (1998b). Winter Temperature Gradients in Circular Clarifiers. *Water Environment Research*, 70(7), pp. 1274-1279.

White, F.M. (1991). *Viscous fluid flow*. McGraw-Hill, Singapore, 614 pp.

Zheng, Y., and Bagley, D.M. (1999). Numerical simulation of batch settling process. *Journal of Environmental Engineering*, 125(11), pp. 1007-1013.

Zhou, S., and McCorquodale, J.A. (1992a). Influence of skirt radius on performance of circular clarifier with density stratification. *International Journal for Numerical Methods in Fluids*, 14, pp. 919-934.

Zhou, S., and McCorquodale, J.A. (1992b). Modelling of rectangular settling tanks. *Journal of Hydraulic Engineering*, 118(10), pp. 1391-1405.

Zhou, S., and McCorquodale, J.A. (1992c). Mathematical modelling of a circular clarifier. *Canadian Journal of Civil Engineering*, 19, pp. 365-374.

Zhou, S., McCorquodale, J.A., and Godo, A.M. (1994). Short circuiting and density interface in primary clarifiers. *Journal of Environmental Engineering*, 120(9), pp. 1060-1080.

Zhou, S., McCorquodale, J.A., and Vitasovic, Z. (1992). Influences of density on circular clarifiers with baffles. *Journal of Environmental Engineering*, 118 (6), pp. 829-847.

Zhou, S., Pfeil, R., Strand, E., Ji, Z., and Vitasovic, C. (1998). SettlerCAD (formerly Clarity or MZSettler) Release 1.1. A 2D hydrodynamic model for secondary clarifiers. Reid Crowther Consulting, Seattle, WA.

APPENDIX A

MARRERO WASTEWATER TREATMENT PLANT

The Marrero WWTP is located at 6250 Lapalco Boulevard, Marrero, Louisiana, and serves Marrero and the central part of the West Bank. The plant, which is a Dual trickling filter-solids contact (TF/SC) process that treats mainly domestic sewage, has a design average flow rate capacity of 6.4 MGD; however, actually the average flow is about 9.0 MGD. The Marrero plant has the following units: prechlorination, 2 mechanical bar screens and 1 manual bar screen, 2 covered aerated grit chambers, 2 covered primary settling tanks, 2 covered 4"-rock trickling filters, 2 aeration basins, 2 secondary clarifiers, 2 chlorine contact chambers, 3 aerobic sludge digesters, and 2 new belt presses for sludge dewatering. According to Retana (1997) and La Motta and Josse (1996) the average influent BOD₅ is about 146mg/L, and the average TSS is 147 mg/L. The values reported by Jimenez (2002) for the wastewater characterization at the Marrero WWTP are presented in Table A.1

Table A.1. Wastewater Composition for the Marrero WWTP (after Jimenez, 2002)

Parameter	Value (mg/L)
Raw Wastewater	
TSS	190
TCOD	350
PCOD	302
CCOD	50
DCOD	48
Primary Clarifier Effluent	
TSS	115
TCOD	220
PCOD	176
CCOD	49
DCOD	44

The dimensions and operating characteristics of the SST at the Marrero WWTP were presented in Tables 5.1 and 5.2

APPENDIX B

LABORATORY PROCEDURES

Total Suspended Solids (TSS)

The TSS test was used to quantify the amount of suspended solids in a specific sample. TSS tests were performed using Method 2540B of Standard Methods (APHA, 1999). After filtration, the solids remaining in the 0.45-mm pore size filter paper were dried at $103^{\circ}\text{C} \pm 1^{\circ}\text{C}$. The difference in weights, after and before drying, divided by the volume of the sample gives the TSS.

Dispersed Suspended Solids (DSS)

The DSS test quantifies the state of flocculation at the moment and location that the sample is taken. Ekama et al. (1997) defined the DSS as the TSS remaining in the supernatant of a sample after 30 minutes of settling. The samples are collected with a Kemmerer sampler; the sampler is a clear tube, 105 mm in diameter and 600 mm tall with upper and lower closures. The closures are locked in the open position before the sampler is lowered into the mixed liquor to be sampled. Once submerged, the sampler is closed by dropping a weighted messenger.

Flocculated Suspended Solids (FSS)

The FSS test quantifies the flocculation potential of a specific sample. Wahlberg et al. (1995) defined the FSS of a sample as the SS remaining in the supernatant after 30 minutes of settling preceded by 30 minutes of flocculation. The FSS test procedures uses a six-paddle stirrer. The sample is flocculated in a square jar for 30 minutes at a rotational velocity of 30 rpm (the measured G value is about 15 s^{-1}). After flocculation the sample is allowed to settle for 30 minutes. After settling, the TSS concentration of the supernatant is measured.

APPENDIX C

EXPERIMENTAL PILOT PLANT

The experimental plant is located at the Marrero Wastewater Treatment Plant, Marrero, Louisiana. The pilot plant is composed by the following parts: a rotating screen, an inlet mechanism, an aeration tank, a mechanical flocculator and a secondary clarifier. The unit was designed for an average flow rate of $7.5\text{m}^3/\text{d}$ (2000 gal/d) and a hydraulic retention time in the contact chamber of about 30 minutes. The rotating screen receives the wastewater from the primary clarifier of the Marrero full-scale treatment plant. The effluent from the rotary screen is pumped out to a mixed-storage tank, from where is pumped to the aeration basin.

The pilot plant aeration basin consists of a 152-L polyethylene tank, equipped with 8 heat-bonded silica fine-pore diffusers. The volume of the aeration tank can be modified to account for different hydraulic retention times; also, this can be done varying the plant flow rate. After residing in the aeration tank, the MLSS moves by gravity to the next unit, which can be either the mechanical flocculator or the secondary settling tank depending on the experimental requirements.

The secondary clarifier consists of a 280-L (70-gal) polyethylene conical tank with a side water depth of 1.07 m (3.5 ft). The inlet structure is formed by a 38-mm (1-½ inch) PVC pipe that transports the water from the aeration chamber. The secondary clarifier is equipped with a 20-cm (8-inch) diameter center well. A scraper arm is placed at the bottom of the unit to avoid the formation of solids clumps and to prevent sludge bridging at the sludge withdrawal point (Jimenez, 2002).

The sludge returns and sludge wastage systems are placed at the bottom of the clarifier. The pumps are controlled by two repeat-cycle timers. Flow rate control is achieved by adjusting valves located at the discharge of each pump. This configuration allows for different RAS and different sludge retention times (SRT).

In figure C.1 is presented a sketch of the experimental pilot plant.

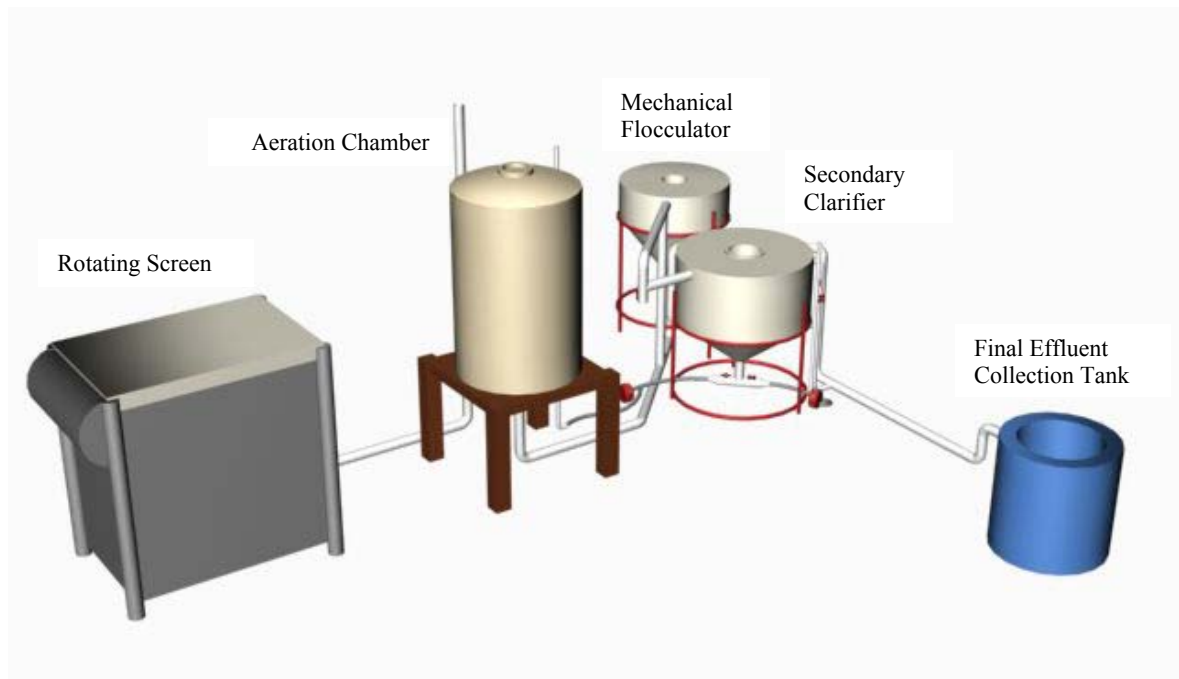


Figure C.1 Experimental Pilot Plant (after Jimenez, 2002)

APPENDIX D

DISCRETE FRACTIONS AND DISCRETE SETTLING VELOCITIES

The data presented in this Appendix was collected both at Marrero WWTP SST and at the Experimental Pilot Plant located in the same treatment plant (see Appendices A and C).

D.1

Date: November 16, 2004

Site: Experimental Pilot Plant

Table D.1 shows the discrete settling velocities measured for large flocs, and Table D.2 shows the discrete settling velocities measured for medium flocs.

Table D.1 Discrete Settling Velocities for Large Flocs Measured at the Experimental Pilot Plant (11/16/2004)

Dilution=		200	Sludge
Dilute Concentration=		630	mg/L
Big Flocs			
Floc	H (cm)	Time(s)	Vs(m/h)
1	3	9.9	10.91
2	3	13.5	8.00
3	3	10	10.80
4	3	10.33	10.45
5	3	7.45	14.50
6	3	8.7	12.41
7	3	11.3	9.56
8	3	7	15.43
9	3	9.7	11.13
10	3	11.0	9.79
11	3	8.7	12.41
12	3	10.5	10.29
13	3	9.7	11.13
14	3	14.5	7.45
15	3	12.0	9.00
Vs(m/h)=			10.88
Std.Dev.			2.26

Table D.2 Discrete Settling Velocities for Medium Flocs Measured at the Experimental Pilot Plant (11/16/2004)

Dilution=		200	Sludge
Dilute Concentration=		634	mg/L
Medium Flocs			
Floc	H (cm)	Time(s)	Vs(m/h)
1	3	32	3.38
2	3	20	5.40
3	3	46	2.35
4	3	32.3	3.34
5	3	40	2.70
6	3	54	2.00
7	3	42	2.57
8	3	35	3.09
9	3	40	2.70
10	3	38.2	2.83
11	3	36.4	2.97
12	3	46	2.35
13	3	32.3	3.34
14	3	40	2.70
15	3	26.5	4.08
Vs(m/h)=			3.05
Std.Dev.			0.93

Table D.3 shows the results of the test for the determination of the small floc settling velocities using Equation 3.4

Determination of the Discrete Settling Fractions

The procedure for determining the settling fractions was presented in Chapter 3. The three settling fractions are calculated using the procedure described in Section 3.1.2.2 and using Equation 3.5 to 3.10. These equations are recapitulated below.

$$C_1 + C_2 + C_3 + FSS = C_d \dots\dots\dots (3.5)$$

$$f_i = \frac{C_i}{C_d - FSS}; \quad i = 1, 2, 3 \dots\dots\dots (3.7)$$

$$A_c(V_{S1}\Delta t_{1-1}C_1 + V_{S2}\Delta t_{1-2}C_2 + V_{S3}\Delta t_{1-3}C_3) = M_1 \dots\dots\dots (3.8)$$

$$\Delta t_{j-i} = \min\left(t_j - Lag\ time, \frac{h_j}{V_{si}}\right) \dots\dots\dots (3.9)$$

$$A_c(V_{S1}\Delta t_{2-1}C_1 + V_{S2}\Delta t_{2-2}C_2 + V_{S3}\Delta t_{2-3}C_3) = M_2 \dots\dots\dots (3.10)$$

Table D.3 Data for the Calculation of the Discrete Settling Velocity of Small Flocs
Obtained at the Experimental Pilot Plant (11/16/2004)

Area of the Settling Column (Ac)	71.4 cm ²
Time 1 (t ₁)	4 min
Time 2 (t ₂)	14 min
Mass of Solids in the upper-mid portion of the settling column at t ₁ (M _x)	146.19 mg
Mass of Solids in the upper-mid portion of the settling column at t ₂ (M _{xx})	59.47 mg
TSS Concentration at the middle of the column at t ₁ (C _x)	152 mg/L
TSS Concentration at the middle of the column at t ₂ (C _{xx})	63 mg/L
Conversion factor for the units presented in this table (C _f)	600
Small Floc Settling Velocity (Equation 3.4)	0.68 m/h

The discrete settling fractions were obtained using equations 3.5 to 3.10. The following section provides the information of the data collected on November 18, 2004, the calculation of the delta time values with Equation 3.9, and the setting and resolution of the matrix resulting from Equations 3.5, 3.8 and 3.10.

Fraction Calculation

Date:	16-Nov					
Diluted Concentration=	630	mg/L	Fractions	Vs(m/h)	Δ time1	Δ time2
DSS=	23	mg/L	1	10.8	1.417	1.411
FSS=	10	mg/L	2	3.05	2.2	4.997
Lag time=	1.8	min	3	0.68	2.2	12.200
Time1=	4	min				
Time2=	14	min				
Column Length=	28	cm				
Blanket Height at time1=	2.5	cm				
Blanket Height at time2=	2.6	cm				
Blanket Mass at time1=	13409	mg*cm/L				
Blanket Mass at time2=	15603	mg*cm/L				

Input

Coefficient Matrix	1	1	1
	25.50	11.18	2.49
	25.40	25.40	13.78

Inverse Matrix	0.547	0.070	-0.052
	-		
	1.734	-0.070	0.138
	2.186	0.000	-0.086

Result Matrix:

620
13408.5
15602.5

Results:

457.13	f1	0.743
156.28	f2	0.254
1.59	f3	0.003
615	Σ=	1.000

D.2

Date: November 17, 2004

Site: Experimental Pilot Plant

Table D.4 shows the discrete settling velocities measured for large flocs, and Table D.5 shows the discrete settling velocities measured for medium flocs. Table D.6 shows the results of the test for the determination of the small floc settling velocities using Equation 3.4

Table D.4 Discrete Settling Velocities for Large Flocs Measured at the Experimental Pilot Plant (11/17/2004)

Dilution= Dilute Concentration=		200 514	Sludge mg/L
		Big Flocs	
Floc	H (cm)	Time(s)	Vs(m/h)
1	3	7	15.43
2	3	7.5	14.40
3	3	14	7.71
4	3	9.7	11.13
5	3	9.8	11.02
6	3	16.6	6.51
7	3	9.3	11.61
8	3	7	15.43
9	3	12.3	8.78
10	3	11.7	9.23
11	3	12.1	8.93
12	3	8.0	13.50
13	3	9.9	10.91
14	3	10.0	10.80
15	3	9.5	11.37
16	3	9.5	11.37
17	3	5.8	18.62
18	3	7	15.43
19	3	11.5	9.39
20	3	12.9	8.37
21	3	9.6	11.25
22	3	10.7	10.09
23	3	11.5	9.39
24	3	8.3	13.01
25	3	15.0	7.20
26	3	10.5	10.29
27	3	10.3	10.49
28	3	7.4	14.59
29	3	7.2	15.00
30	3	9.3	11.61
		Vs(m/h)=	11.40
		Std.Dev.	2.95

Table D.5 Discrete Settling Velocities for Medium Floccs Measured at the Experimental Pilot Plant (11/17/2004)

Medium Floccs			
Floc	H (cm)	Time(s)	Vs(m/h)
1	3	24	4.50
2	3	27.5	3.93
3	3	44	2.45
4	3	29.7	3.64
5	3	46.2	2.34
6	3	36.6	2.95
7	3	29.3	3.69
8	3	47	2.30
9	3	57.2	1.89
10	3	27.5	3.93
11	3	54	2.00
12	3	48.2	2.24
13	3	36.5	2.96
14	3	36.6	2.95
15	3	29.3	3.69
Vs(m/h)=			3.00
Std.Dev.			0.89

Table D.6 Data for the Calculation of the Discrete Settling Velocity of Small Floccs Obtained at the Experimental Pilot Plant (11/17/2004)

Area of the Settling Column (A_c)	71.4 cm ²
Time 1 (t_1)	4 min
Time 2 (t_2)	14 min
Mass of Solids in the upper-mid portion of the settling column at t_1 (M_x)	182.9 mg
Mass of Solids in the upper-mid portion of the settling column at t_2 (M_{xx})	86.96 mg
TSS Concentration at the middle of the column at t_1 (C_x)	209 mg/L
TSS Concentration at the middle of the column at t_2 (C_{xx})	97 mg/L
Small Floc Settling Velocity (Equation 3.4)	0.53 m/h

The discrete settling fractions were obtained using equations 3.5 to 3.10. The following section provides the information of the data collected on November 17, 2004, the calculation of the delta time values with Equation 3.9, and the setting and resolution of the matrix resulting from Equations 3.5, 3.8 and 3.10.

Fraction Calculation

Date=	17-Nov					
Diluted Concentration=	514	mg/L	Fractions	Vs(m/h)	Δ time1	Δ time2
DSS=	23	mg/L	1	11.4	1.358	1.353
FSS=	3	mg/L	2	3	2.5	5.140
Lag time=	1.5	min	3	0.53	2.5	12.500
Time1=	4	min				
Time2=	14	min				
Column Length=	28	cm				
Blanket Height at time1=	2.2	cm				
Blanket Height at time2=	2.3	cm				
Blanket Mass at time1=	9033	mg*cm/L				
Blanket Mass at time2=	11814	mg*cm/L				

Input

Coefficient Matrix	1	1	1
	25.80	12.50	2.20
	25.70	25.70	10.98
Inverse Matrix	0.41281	0.075188	0.05263
	-1.1588	-0.07519	0.12057
	1.74597	1.21E-17	0.06794

Result Matrix:

511
9032.6
11814.35

Results:

268.27	f1	0.525
153.17	f2	0.300
89.56	f3	0.175
511		1.000

D.3

Date: November 18, 2004

Site: Marrero WWTP SST

Table D.7 shows the discrete settling velocities measured for large flocs, and Table D.8 shows the discrete settling velocities measured for medium flocs.

Table D.7 Discrete Settling Velocities for Large Flocs Measured at the Marrero WWTP
(11/18/2004)

Large Flocs							
Floc No.	H (cm)	Time(s)	V(m/h)	Floc No.	H (cm)	Time(s)	V(m/h)
1	3	10.5	10.3	11	3	14.0	7.7
2	3	14.2	7.6	12	3	12.3	8.8
3	3	9.3	11.6	13	3	14.3	7.6
4	3	14.3	7.6	14	3	9.5	11.4
5	3	11.3	9.6	15	3	9.9	10.9
6	3	15.5	7.0	16	3	10.4	10.3
7	3	15.0	7.2	17	3	6.5	16.6
8	3	6.8	15.9	18	3	8.1	13.4
9	3	7.7	14.0	19	3	6.5	16.6
10	3	11.6	9.3	20	3	9.1	11.9
Average Large Flocs Settling Velocity:				10.8 m/h			
Standard Deviation:				3.16			
Maximum:				16.6 m/h			
Minimum:				7.0 m/h			

Table D.8 Discrete Settling Velocities for Medium Flocs Measured at the Marrero
WWTP (11/18/2004)

Medium Flocs							
Floc No.	H (cm)	Time(s)	V(m/h)	Floc No.	H (cm)	Time(s)	V(m/h)
1	3	26.5	4.1	11	3	25	4.3
2	3	47.3	2.3	12	3	30.2	3.6
3	3	46	2.3	13	3	29	3.7
4	3	45	2.4	14	3	26	4.2
5	3	30	3.6	15	3	30	3.6
6	3	47.9	2.3	16	3	29	3.7
7	3	46.5	2.3	17	3	45	2.4
8	3	49	2.2	18	3	38	2.8
9	3	28	3.9	19	3	58	1.9
10	3	40.7	2.7	20	3	40	2.7
Average Large Flocs Settling Velocity:				3.0 m/h			
Standard Deviation:				0.79			
Maximum:				4.3 m/h			
Minimum:				1.9 m/h			

Table D.9 shows the results of the test for the determination of the small floc settling velocities using Equation 3.4

Table D.9 Data for the Calculation of the Discrete Settling Velocity of Small Flocs
Obtained at the Marrero WWTP (11/18/2004)

Area of the Settling Column (A_c)	71.4 cm ²
Time 1 (t_1)	4 min
Time 2 (t_2)	13 min
Mass of Solids in the upper-mid portion of the settling column at t_1 (M_x)	131.45 mg
Mass of Solids in the upper-mid portion of the settling column at t_2 (M_{xx})	57.48 mg
TSS Concentration at the middle of the column at t_1 (C_x)	141 mg/L
TSS Concentration at the middle of the column at t_2 (C_{xx})	61 mg/L
Conversion factor for the units presented in this table (C_f)	600
Small Floc Settling Velocity (Equation 3.4)	0.68 m/h

The discrete settling fractions were obtained using equations 3.5 to 3.10. The following section provides the information of the data collected on November 18, 2004 at the Marrero WWTP, the calculation of the delta time values with Equation 3.9, and the setting and resolution of the matrix resulting from Equations 3.5, 3.8 and 3.10.

Fraction Calculation

Date:	18-Nov					
Diluted Concentration=	600	mg/L	Fractions	Vs(m/h)	Δ time1	Δ time2
DSS=	23	mg/L	1	10.8	1.417	1.411
FSS=	5	mg/L	2	3	2.5	5.080
Lag time=	1.5	min	3	0.68	2.5	11.500
Time1=	4	min				
Time2=	13	min				
Column Length=	28	cm				
Blanket Height at time1=	2.5	cm				
Blanket Height at time2=	2.6	cm				
Blanket Mass at time1=	13161	mg*cm/L	Unit Area			
Blanket Mass at time2=	15093	mg*cm/L	Unit Area			

Input

Result Matrix:

595
13161
15093

Results:

441.48	f1	0.742
151.90	f2	0.255
1.63	f3	0.003
595		1.000

Coefficient Matrix	1	1	1
	25.50	12.50	2.85
	25.40	25.40	13.11
Inverse Matrix	0.572	0.077	-0.060
	-1.638	-0.077	0.142
	2.066	0.000	-0.081

Table D.10 summarizes the discrete settling velocities and fractions obtained the day 11/18/2004.

Table D.10 Discrete Settling Velocities and Fractions Obtained at the Marrero WWTP (11/18/2004)

Type of Particle		Settling Velocity V_{si} (m/h)*	Concentration C_i (mg/L)	Fraction f_i
Description	Class (i)			
Big Floc	1	10.80	441.48	0.742
Medium Floc	2	3.00	151.90	0.255
Small Floc	3	0.68	1.63	0.003
Non-Settleable	4	0.00	5.0	----
		Total =	600.0	1.000

*The settling velocities presented in this table were measured at 26.5 °C

APPENDIX E

RESEARCH ON ZONE SETTLING AND COMPRESSION RATE PROPERTIES

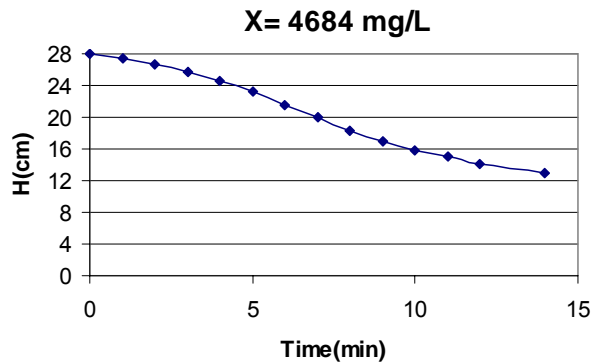
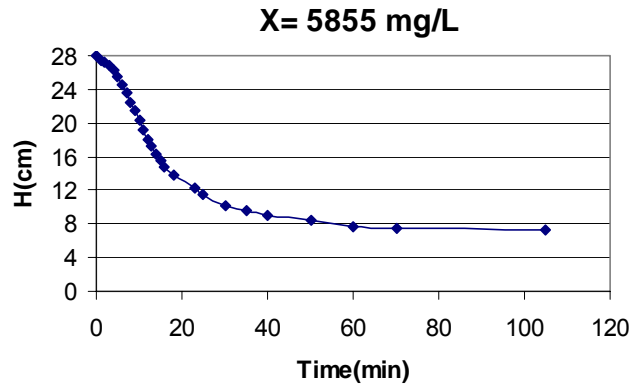
The data presented in this Appendix was collected both at Marrero WWTP SST and at the Experimental Pilot Plant located in the same treatment plant (see Appendices A and C).

E.1

Date: October 24, 2004

Site: Experimental Pilot Plant

Figure E.1 shows different batch settling tests performed with different suspended solids concentrations during the evaluation of the zone settling properties. The different SS concentrations were obtained from a MLSS equal to 4684 mg/L through dilutions and thickening.



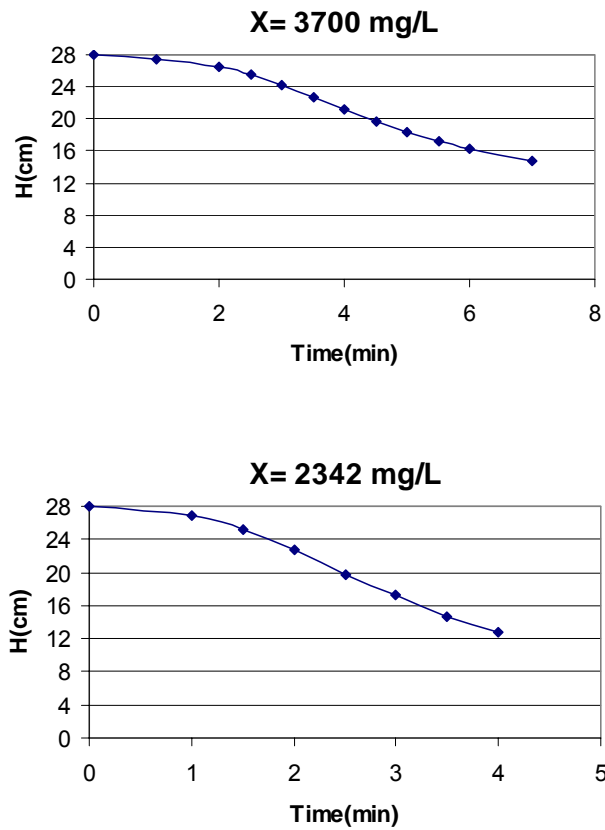


Figure E.1 Batch Settling Tests for the Determination of the Zone Settling Properties
(10/24/2004)

Table E.1 shows the zone settling velocities obtained from the batch curves presented in Figure E.1.

Table E.1 Zone Settling Velocities (10/24/2004)

Settling Velocities Calculations			
X(mg/L)	Vs(m/h)	Log(Vo)	X(kg/m3)
5855	0.7	-0.1549	5.855
4684	0.990	-0.00436	4.684
3700	1.76	0.24551	3.700
2342	3.473	0.54075	2.342

Figure E.2 shows the exponential fitting for the data set presented in Table E.1.

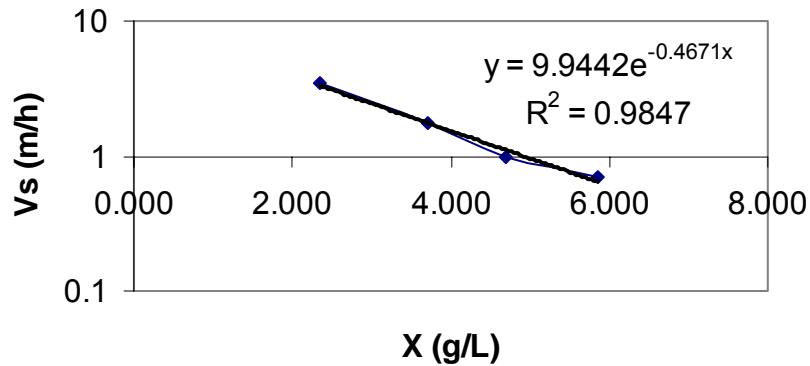
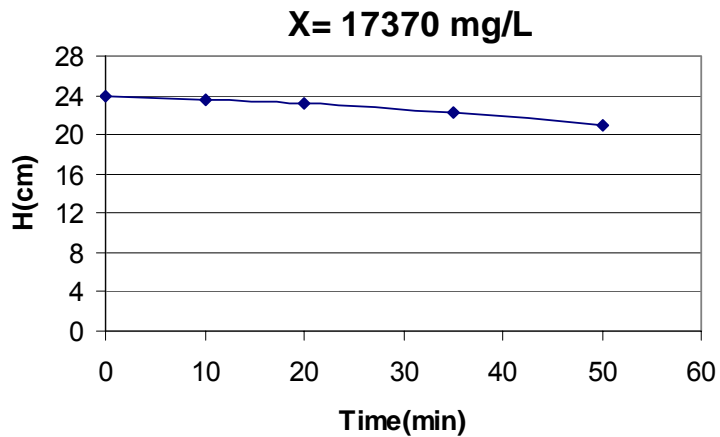


Figure E.2 Field Data and Fitted Exponential Equation for Zone Settling
(10/24/2004)

Figure E.3 shows different batch settling tests used for the determination of the compression settling properties. The different SS concentrations were obtained from the RAS sludge through dilutions and thickening.



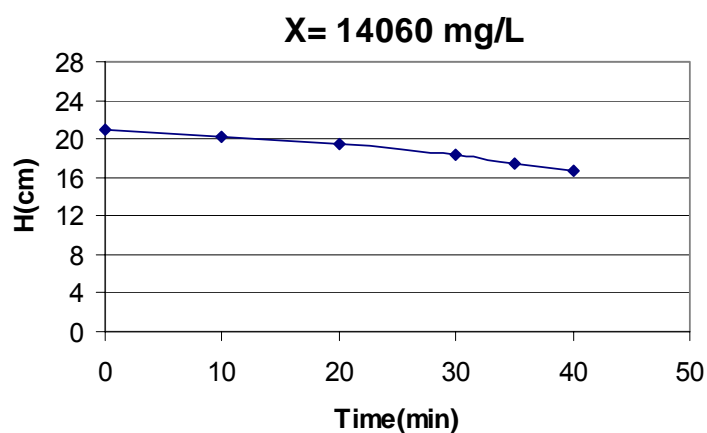


Figure E.3 Batch Settling Tests for the Determination of the Compression Rate Properties (10/24/2004)

Table E.2 shows the compression velocities obtained from the batch curves presented in Figure E.3.

Table E.2 Compression Velocities (10/24/2004)

Settling Velocities-Compression Calculations			
X(mg/L)	Vs(m/h)	Log(Vo)	X(kg/m ³)
5855	0.7	-0.1549	5.855
11450	0.129	-0.88941	11.450
14060	0.102	-0.9914	14.060
17370	0.046	-1.33724	17.370

Figure E.4 shows the exponential fitting for the data set presented in Table E.2, and Figure E.5 shows the comparison between the zone settling and the compression rate properties.

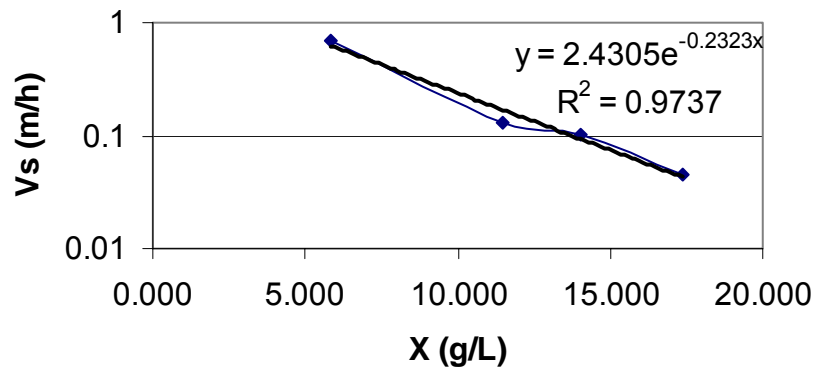


Figure E.4 Field Data and Fitted Exponential Equation for Compression Settling
(10/24/2004)

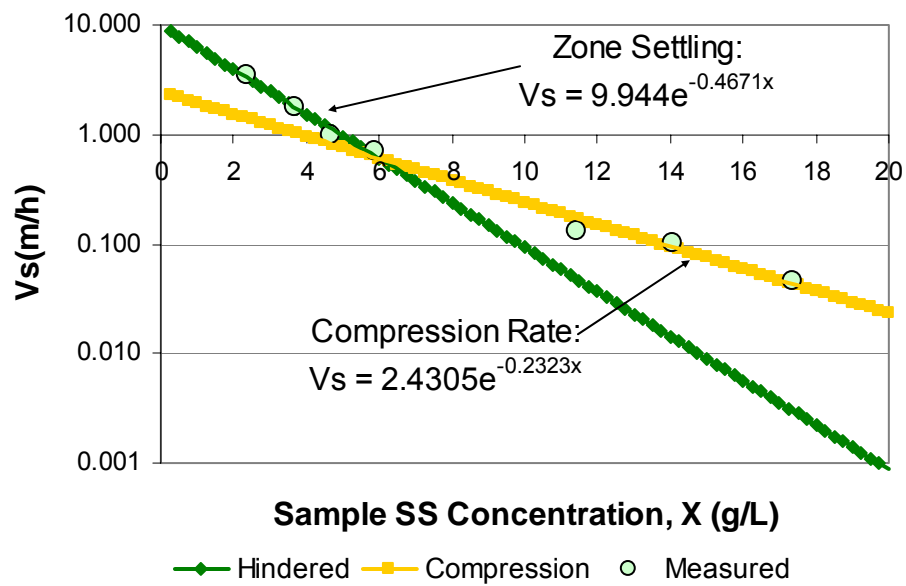


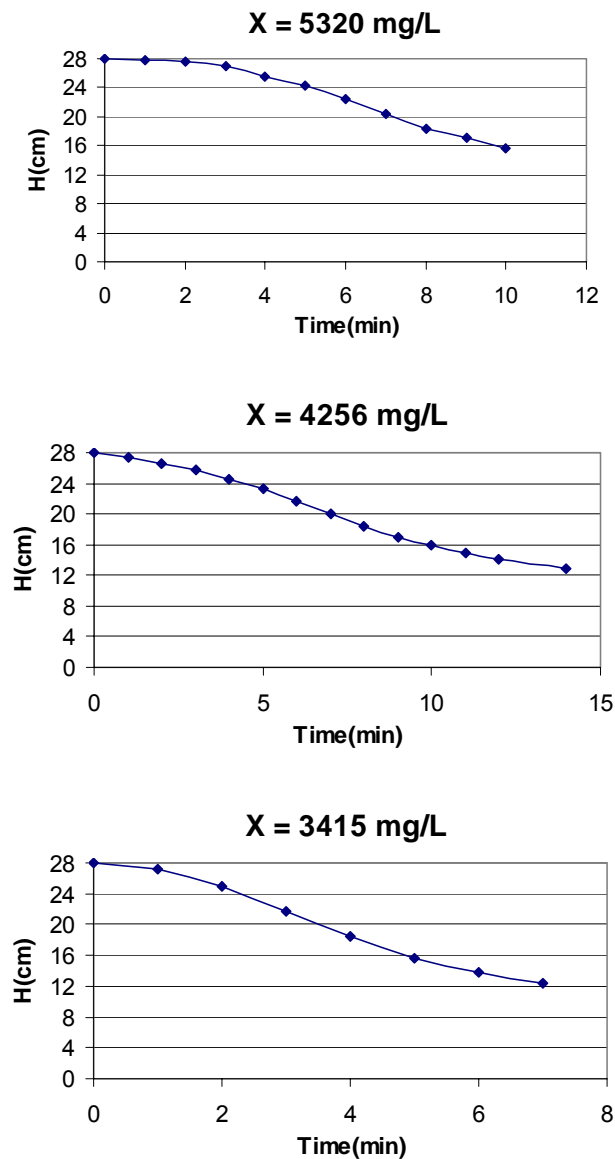
Figure E.5 Field Data and Fitted Exponential Equation for Zone Settling and
Compression Rate (10/24/2004)

E.2

Date: November 24, 2004

Site: Marrero WWTP SST

Figure E.6 shows different batch settling tests performed with different suspended solids concentrations during the evaluation of the zone settling properties. The different SS concentrations were obtained from a MLSS equal to 3415 mg/L through dilutions and thickening.



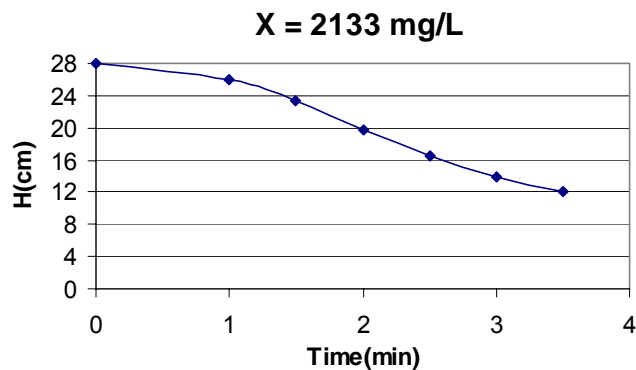


Figure E.6 Batch Settling Tests for the Determination of the Zone Settling Properties
(11/24/2004)

Table E.3 shows the zone settling velocities obtained from the batch curves presented in Figure E.6.

Table E.3 Zone Settling Velocities (11/24/2004)

Settling Velocities Calculations			
X(mg/L)	Vs(m/h)	LogVo	X(kg/m ³)
5320	1.18	0.07188	5.320
4256	1.550	0.19033	4.256
3415	1.98	0.29667	3.415
2133	4.080	0.61066	2.133

Figure E.7 shows the exponential fitting for the data set presented in Table E.3.

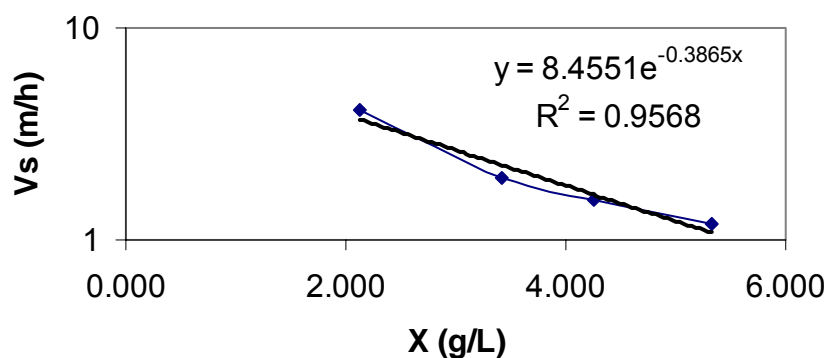


Figure E.7 Field Data and Fitted Exponential Equation for Zone Settling
(11/24/2004)

Figure E.8 shows different batch settling tests used for the determination of the compression settling properties. The different SS concentrations were obtained from the RAS sludge through dilutions.

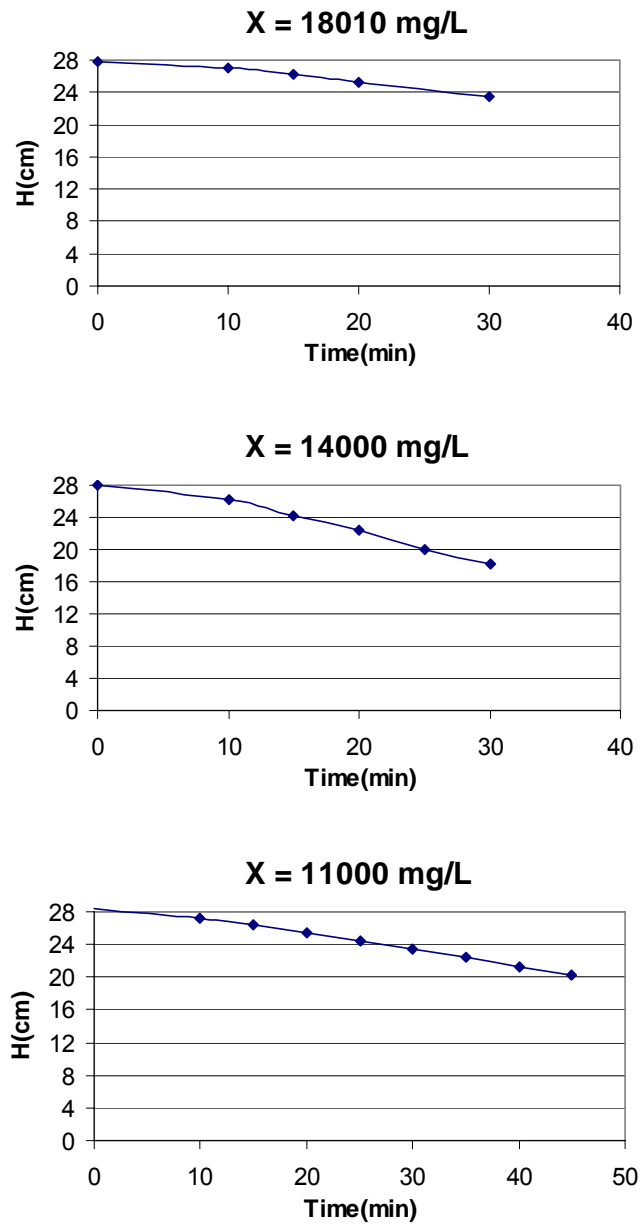


Figure E.8 Batch Settling Tests for the Determination of the Compression Rate Properties (11/24/2004)

Table E.4 shows the compression velocities obtained from the batch curves presented in Figure E.8.

Table E.4 Compression Velocities (11/24/2004)

Settling Velocities-Compression Calculations			
X(mg/L)	Vs(m/h)	LogVo	X(kg/m3)
5320	1.180	0.07188	5.320
11000	0.425	-0.92082	11.000
14060	0.234	-0.63078	14.060
18010	0.120	-0.92082	18.010

Figure E.9 shows the exponential fitting for the data set presented in Table E.4, and Figure E.10 shows the comparison between the zone settling and the compression rate properties.

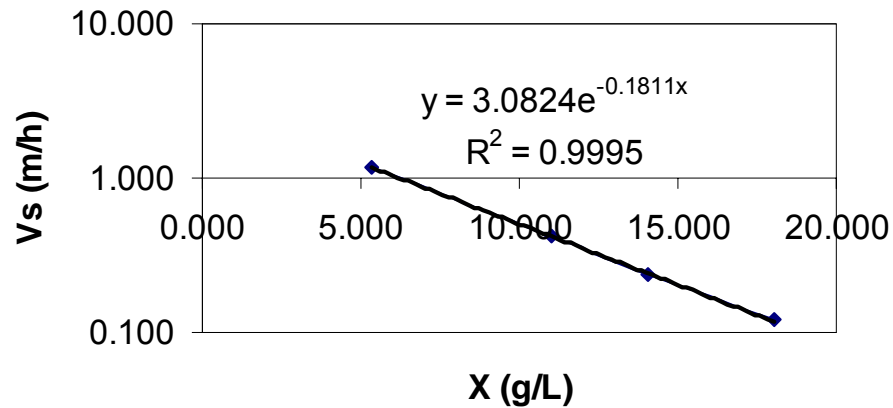


Figure E.9Field Data and Fitted Exponential Equation for Compression Settling (11/24/2004)

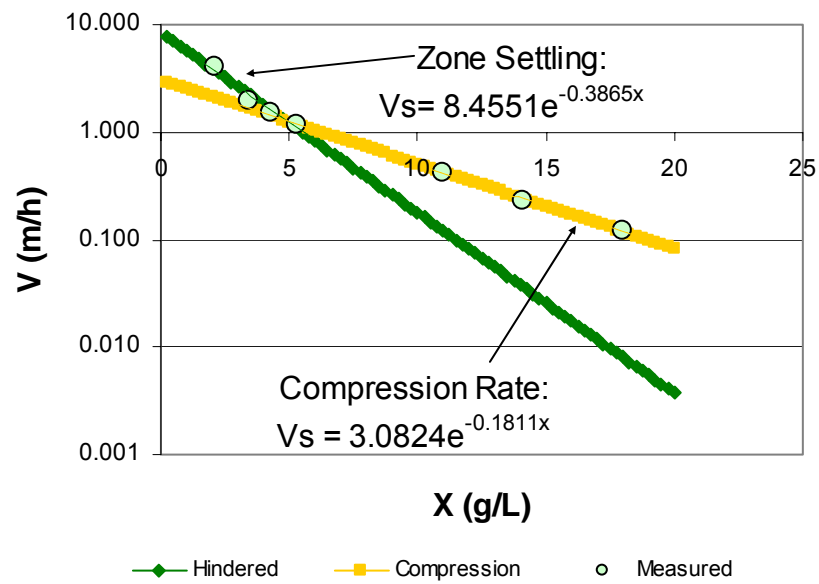


Figure E.10 Field Data and Fitted Exponential Equation for Zone Settling and Compression Rate (11/24/2004)

E.3

Date: November 04, 2004

Site: Experimental Pilot Plant

Figure E.11 shows different batch settling tests performed with different suspended solids concentrations during the evaluation of the zone settling properties. The different SS concentrations were obtained from a MLSS equal to 4530 mg/L through dilutions and thickening.

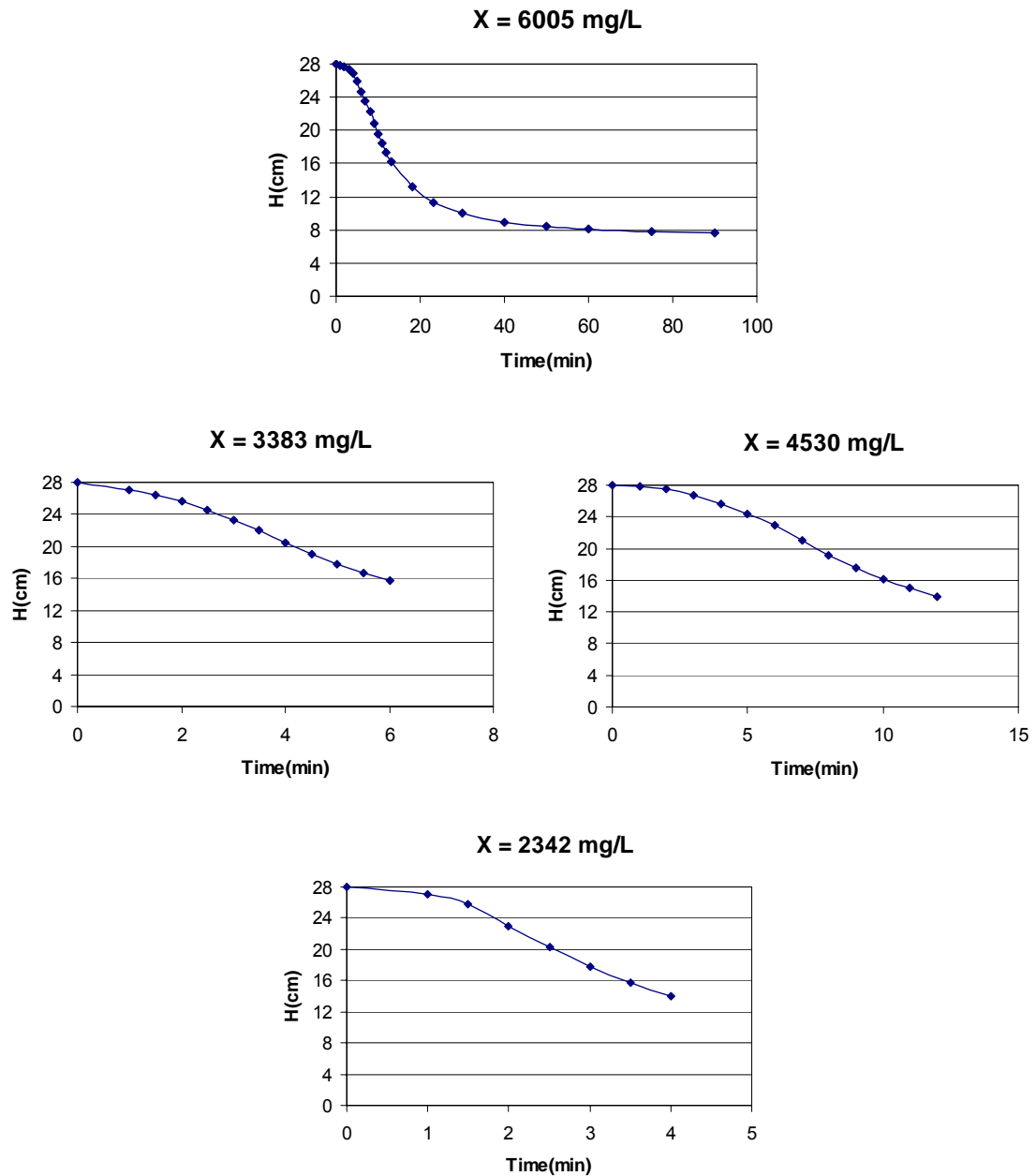


Figure E.11 Batch Settling Tests for the Determination of the Zone Settling Properties
(11/04/2004)

Table E.5 shows the zone settling velocities obtained from the batch curves presented in Figure E.11.

Table E.5 Zone Settling Velocities (11/04/2004)

Settling Velocities Calculations			
X(mg/L)	Vs(m/h)	LogVo	X(kg/m3)
6005	0.84	-0.07572	6.005
4530	1.140	0.0569	4.530
3383	1.8	0.25527	3.383
2342	3.280	0.51587	2.342

Figure E.12 shows the exponential fitting for the data set presented in Table E.5.

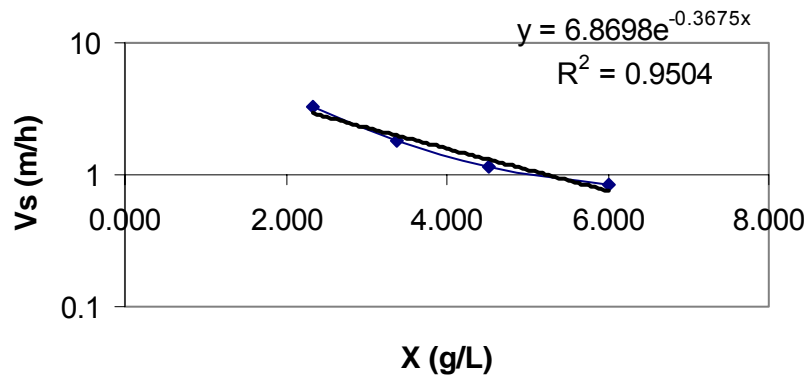
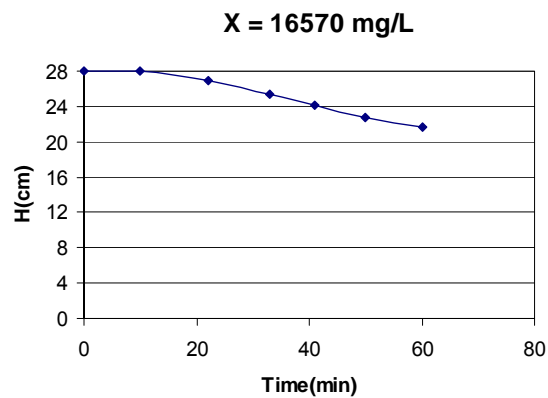


Figure E.12 Field Data and Fitted Exponential Equation for Zone Settling
(11/04/2004)

Figure E.13 shows different batch settling tests used for the determination of the compression settling properties. The different SS concentrations were obtained from the RAS sludge through dilutions and thickening.



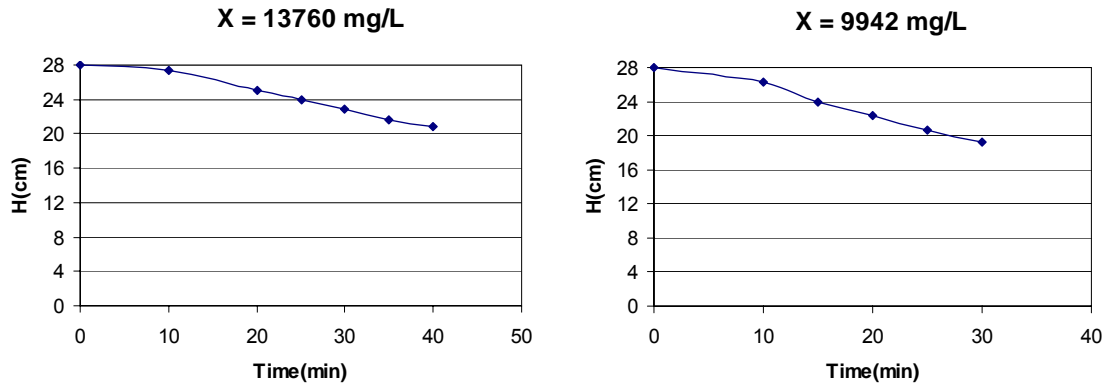


Figure E.13 Batch Settling Tests for the Determination of the Compression Rate Properties (11/04/2004)

Table E.6 shows the compression velocities obtained from the batch curves presented in Figure E.13.

Table E.6 Compression Velocities (11/04/2004)

Settling Velocities-Compression Calculations			
$X(\text{mg/L})$	$V_s(\text{m/h})$	$\text{Log}V_o$	$X(\text{kg/m}^3)$
6005	0.840	-0.07572	6.005
9942	0.228	-0.92082	9.942
13760	0.138	-0.86012	13.760
16570	0.092	-1.03582	16.570

Figure E.14 shows the exponential fitting for the data set presented in Table E.6, and Figure E.15 shows the comparison between the zone settling and the compression rate properties.

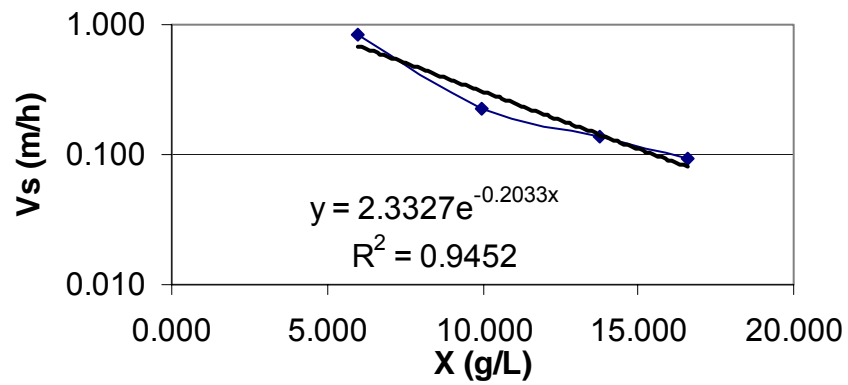


Figure E.14 Field Data and Fitted Exponential Equation for Compression Settling
(11/04/2004)

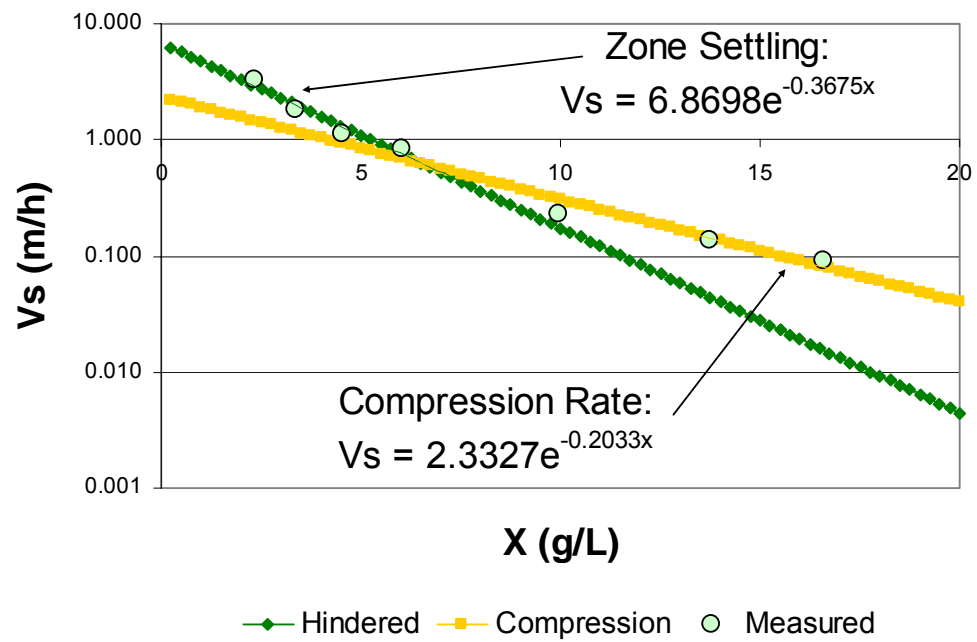


Figure E.15 Field Data and Fitted Exponential Equation for Zone Settling and
Compression Rate (11/04/2004)

E.4

Date: November 06, 2004

Site: Experimental Pilot Plant

Tables E.7 and E.8 show the settling velocity data obtained at the experimental pilot plant the date 11/06/2004.

Table E.7 Zone Settling Velocities (11/06/2004)

Settling Velocities Calculations			
X(mg/L)	Vs(m/h)	LogVo	X(kg/m3)
4910	1.02	0.0086	4.910
4355	1.550	0.19033	4.355
3133	2.16	0.33445	3.133
2193	3.460	0.53908	2.193

Figure E.16 shows the exponential fitting for the data set presented in Table E.7.

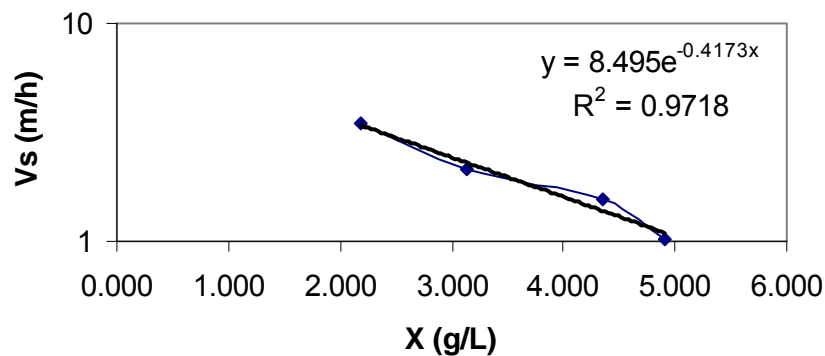


Figure E.16 Field Data and Fitted Exponential Equation for Zone Settling
(11/06/2004)

The SS concentrations presented in Table E.7 were obtained from the MLSS of the contact chamber and successive dilutions, and the SS concentrations presented in Table E.8 were obtained from the RAS line, diluting and compositing the RAS sample.

Table E.8 Compression Velocities (11/06/2004)

Settling Velocities-Compression Calculations			
X(mg/L)	Vs(m/h)	LogVo	X(kg/m3)
4910	1.020	0.0086	4.910
11032	0.220	-0.92082	11.032
14710	0.132	-0.87943	14.710
18387	0.096	-1.01773	18.387

Figure E.17 shows the exponential fitting for the data set presented in Table E.8, and Figure E.18 shows the comparison between the zone settling and the compression rate properties.

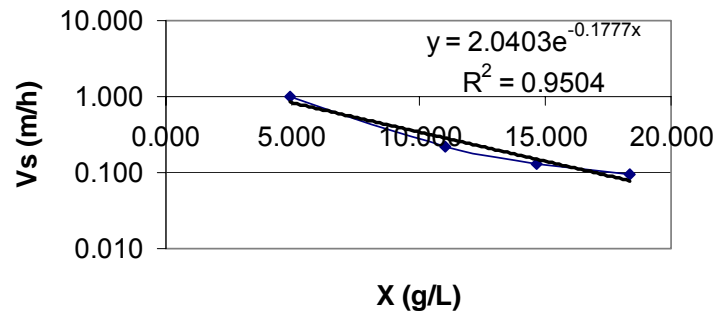


Figure E.17 Field Data and Fitted Exponential Equation for Compression Settling (11/06/2004)

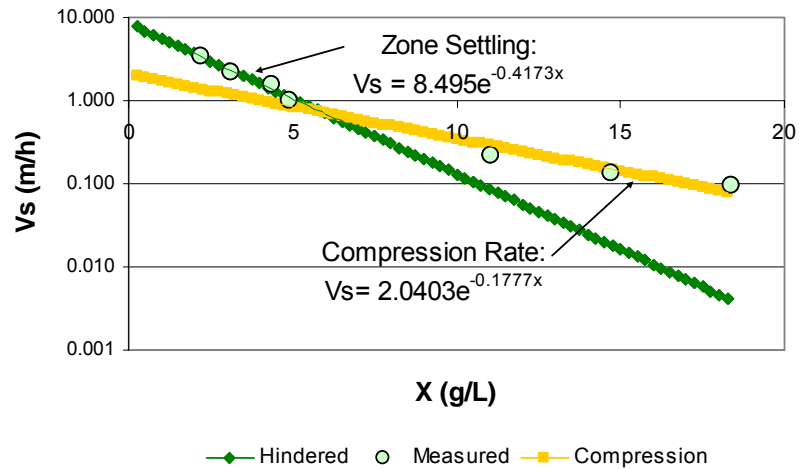


Figure E.18 Field Data and Fitted Exponential Equation for Zone Settling and Compression Rate (11/06/2004)

APPENDIX F

RESEARCH ON TEMPERATURE EFFECTS ON ZONE SETTLING

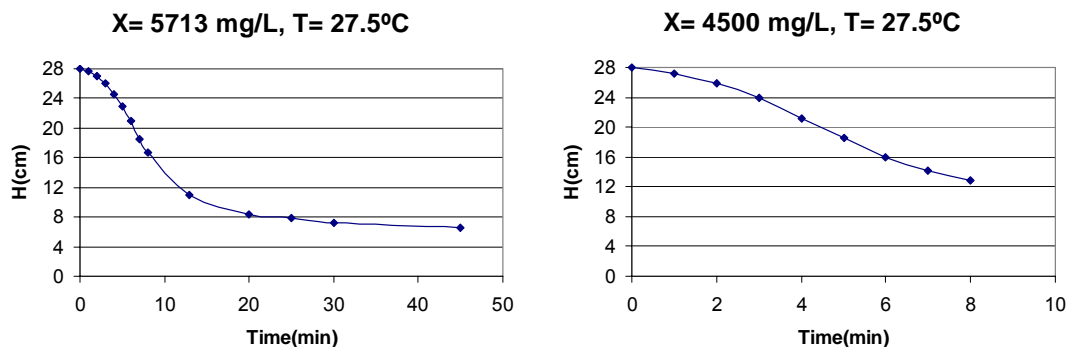
The data presented in this appendix was collected at the Experimental Pilot Plant located at the Marrero WWTP. This appendix shows the results of the procedure presented in Section 3.3 aimed at determining a correction factor for the zone settling velocities based on temperature difference. As presented herein, in every case two batch tests were conducted: (1) a normal batch column test, and (2) an additional batch column test that was conducted modifying the temperature of the sample using a submerge bath. The sludge samples were submitted to a 30 minutes cooling process, after which the temperature and the settling velocities were measured.

F.1

Date: October 07, 2004

Site: Experimental Pilot Plant

Figure F.1 shows different batch settling tests performed with different suspended solids concentrations during the evaluation of the zone settling properties at normal temperature. The different SS concentrations were obtained from a MLSS equal to 4500 mg/L through dilutions and thickening. Table F.1 shows the zone settling velocities obtained from the batch curves presented in Figure F.1.



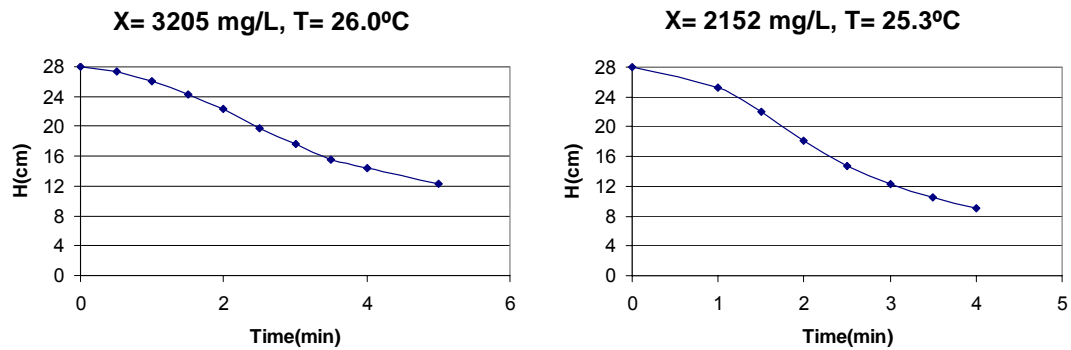


Figure F.1 Batch Settling Tests for the Determination of the Zone Settling at Normal Temperature (10/07/2004)

Table F.1 Zone Settling Velocities at Normal Temperature (10/07/2004)

Settling Velocities at Normal Temperature			
X(mg/L)	Vo(m/h)	LogVo	X(kg/m ³)
5713	1.5	0.17609	5.713
4500	1.695	0.22917	4.500
3205	2.73	0.43616	3.205
2152	4.52	0.65514	2.152

Figure F.2 shows different batch settling tests performed with different suspended solids concentrations during the evaluation of the zone settling properties at a cooled temperature. The different SS concentrations were obtained from a MLSS equal to 4500 mg/L through dilutions and thickening. Table F.2 shows the zone settling velocities obtained from the batch curves presented in Figure F.2.

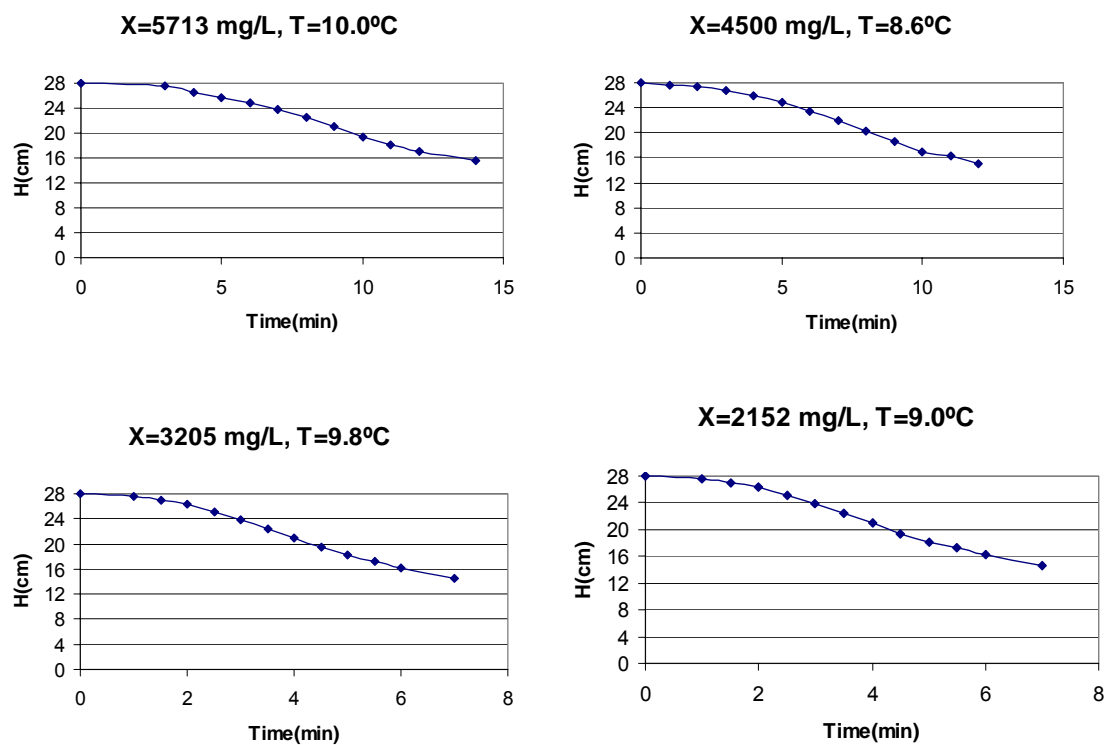


Figure F.2 Batch Settling Tests for the Determination of the Zone Settling at a Cooled Temperature (10/07/2004)

Table F.2 Zone Settling Velocities at Cooled Temperature (10/07/2004)

Settling Velocities at Cooled Temperature			
X(mg/L)	Vo(m/h)	LogVo	X(kg/m3)
5713	0.96	-0.01773	5.713
4500	1.020	0.0086	4.500
3205	1.8	0.25527	3.205
2152	3.12	0.49415	2.152

Table F.3 summarizes the settling velocities measured at different temperatures, and shows the value of the relationship $V_{s_{T_n}}/V_{s_{T_c}}$ and μ_{T_2}/μ_{T_1} for the values of settling velocities and dynamic viscosities at temperatures T_n (normal temperature) and T_c (cooled temperature). Figure F.3 displays graphically this information.

Table F.3 Settling Velocities and Dynamic Viscosities for Samples at Normal and Cooled Temperature (10/07/2004)

TSS (mg/L)	Sample at Normal Temperature (Tn)				Sample at Cooler Temperature (Tc)				Ratios	
	Vsn (m/h)	To (°C)	Tf (°C)	μ_n (Kg/m.s)	Vsc (m/h)	To (°C)	Tf (°C)	μ_c (Kg/m.s)	Vsn/Vsc	μ_c/μ_n
5713	1.50	27.5	27.5	0.000842	0.96	10	10	0.0013	1.56	1.54
4500	1.70	27.5	27.5	0.000842	1.02	8.6	8.8	0.00135	1.67	1.60
3205	2.73	26	26	0.00087	1.80	9.8	10.8	0.00129	1.52	1.48
2152	4.52	25.3	25.3	0.000884	3.12	9	10.9	0.00130	1.45	1.47

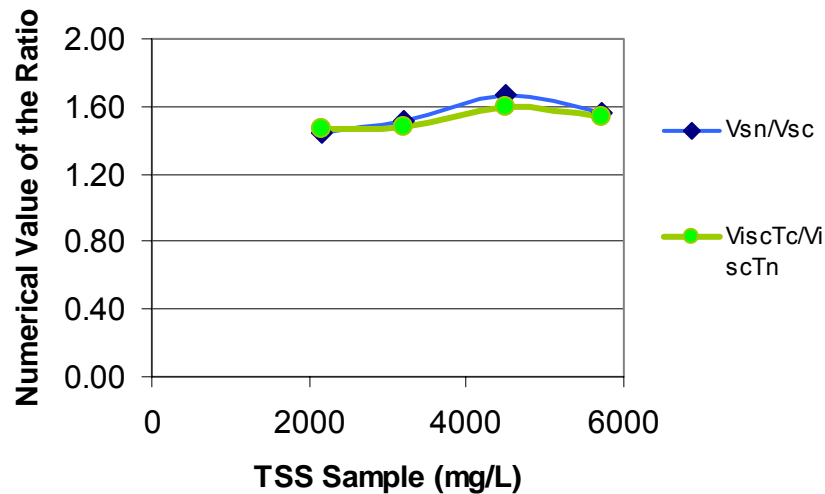


Figure F.3 Ratios $V_{s_{T_1}}/V_{s_{T_2}}$ and μ_{T_2}/μ_{T_1} for Different TSS Concentrations (10/07/2004)

F.2

Date: October 16, 2004

Site: Experimental Pilot Plant

Figure F.4 shows different batch settling tests performed with different suspended solids concentrations during the evaluation of the zone settling properties at normal temperature. The different SS concentrations were obtained from a MLSS equal to 4800 mg/L through dilutions and thickening. Table F.4 shows the zone settling velocities obtained from the batch curves presented in Figure F.4.

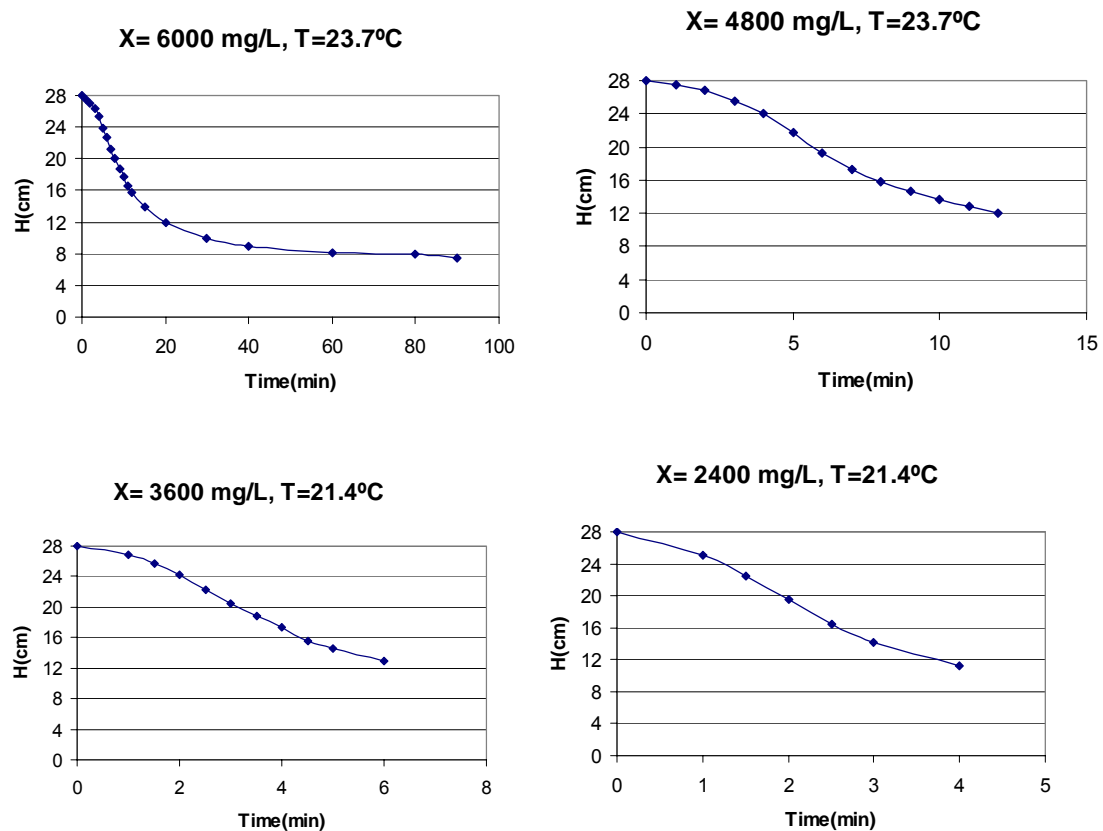


Figure F.4 Batch Settling Tests for the Determination of the Zone Settling at Normal Temperature (10/16/2004)

Table F.4 Zone Settling Velocities at Normal Temperature (10/16/2004)

Settling Velocities at Normal Temperature			
X(mg/L)	Vo(m/h)	LogVo	X(kg/m ³)
6000	0.82	-0.08619	6.000
4800	1.440	0.15836	4.800
3600	2.28	0.35793	3.600
2400	3.60	0.5563	2.400

Figure F.5 shows different batch settling tests performed with different suspended solids concentrations during the evaluation of the zone settling properties at a cooled temperature. Table F.5 shows the zone settling velocities obtained from the batch curves presented in Figure F.5.

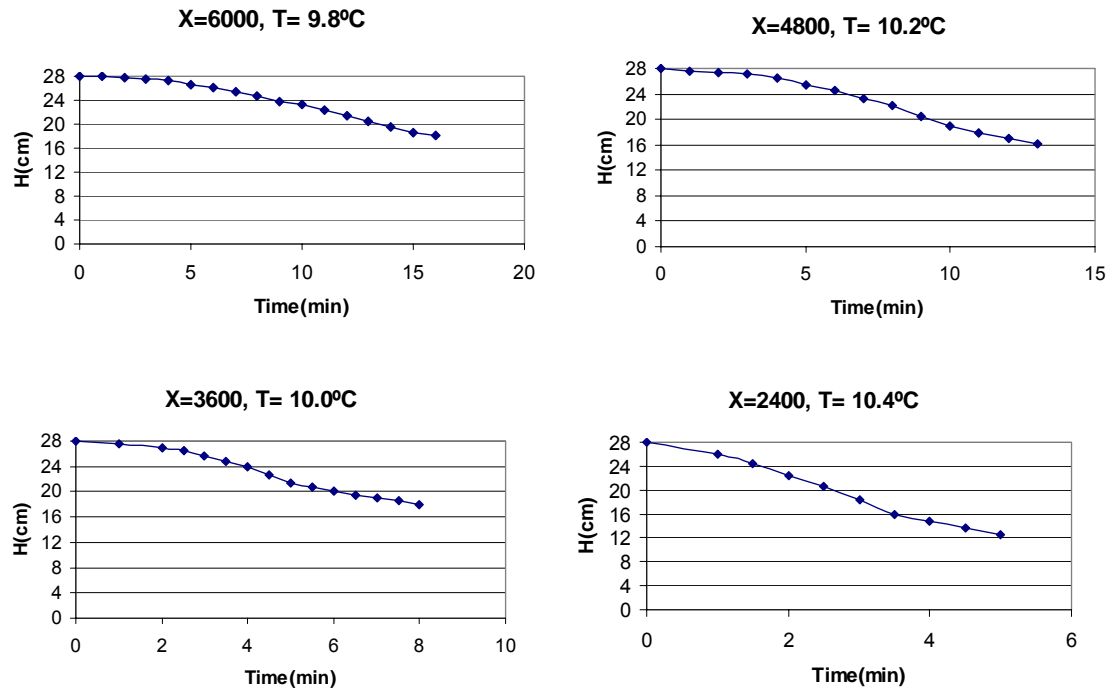


Figure F.5 Batch Settling Tests for the Determination of the Zone Settling at a Cooled Temperature (10/16/2004)

Table F.5 Zone Settling Velocities at Cooled Temperature (10/16/2004)

Settling Velocities at Cooled Temperature			
X(mg/L)	Vo(m/h)	LogVo	X(kg/m3)
6000	0.56	-0.25181	6.000
4800	1.020	0.0086	4.800
3600	1.62	0.20952	3.600
2400	2.76	0.44091	2.400

Table F.6 summarizes the settling velocities measured at different temperatures, and shows the value of the relationship V_{sT_n}/V_{sT_c} and μ_{T_2}/μ_{T_1} for the values of settling velocities and dynamic viscosities at temperatures T_n (normal temperature) and T_c (cooled temperature). Figure F.6 displays graphically this information.

Table F.6 Settling Velocities and Dynamic Viscosities for Samples at Normal and Cooled Temperature (10/16/2004)

TSS (mg/L)	Sample at Normal Temperature (Tn)				Sample at Cooler Temperature (Tc)				Ratios	
	Vsn (m/h)	To (°C)	Tf (°C)	μ_n (Kg/m.s)	Vsc (m/h)	To (°C)	Tf (°C)	μ_c (Kg/m.s)	Vsn/Vsc	μ_c/μ_n
6000	0.82	23.7	23.7	0.000917	0.56	9.8	10	0.0013	1.46	1.42
4800	1.44	23.7	23.7	0.000917	1.02	10.2	10.4	0.00129	1.41	1.40
3600	2.28	21.4	21.4	0.000969	1.62	10	10.8	0.00129	1.41	1.33
2400	3.6	21.4	21.4	0.000969	2.76	10.4	11.6	0.00126	1.30	1.31

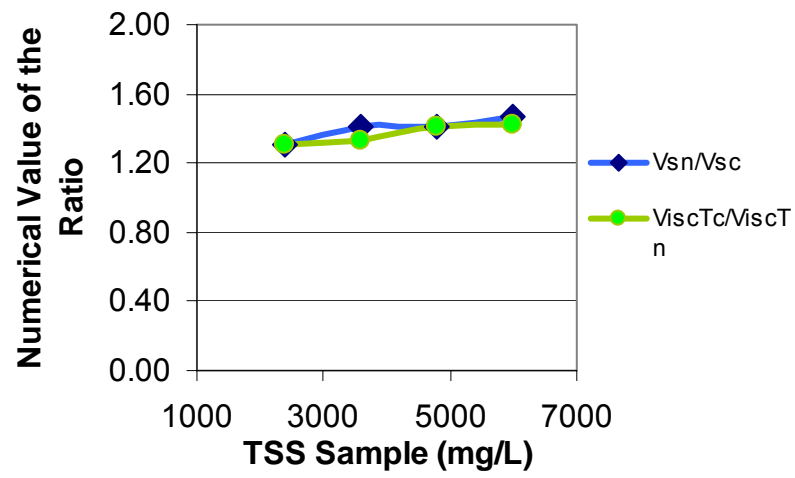


Figure F.6 Ratios $V_{s_{T_1}}/V_{s_{T_2}}$ and μ_{T_2}/μ_{T_1} for Different TSS Concentrations (10/16/2004)

APPENDIX G

DATA COLLECTED DURING THE VALIDATION OF THE MODEL

Date: November 24, 2004

Site: Marrero WWTP SST

Table G.1 shows the suspended solids concentration measured at the SST of Marrero during the calibration period.

Table G.1 Suspended Solids Concentrations Measured at the Marrero WWTP During the Validation Period

	X (mg/L)	sd(X) (mg/L)
MLSS	3100	56
ESS	15.00	1.2
RASS	9200	520

Tables G.2 and G.3 show the discrete settling velocities for big and medium flocs measured during the calibration of the model. As described in Chapter 3 the settling velocity of small flocs is obtained using a procedure based on the concentration profile of settling batch columns at two different times and using Equation 3.4.

$$V_{sm} \approx \frac{(M_x - M_{xx})}{A_c \Delta t \bar{C}_{x-xx}} C_f \dots\dots\dots (3.4)$$

where C_f is a conversion factor. The results of the test for the determination of the small floc settling velocities, conducted during the validation day, are presented in Table G.4

Table G.2 Discrete Settling Velocities for Large Flocs Measured During the Validation

Large Flocs							
Floc No.	H (cm)	Time(s)	V(m/h)	Floc No.	H (cm)	Time(s)	V(m/h)
1	3	11.4	9.5	11	3	13.3	8.1
2	3	16.5	6.5	12	3	9.5	11.4
3	3	9.5	11.4	13	3	9.5	11.4
4	3	8.3	13.0	14	3	17.3	6.2
5	3	8.4	12.9	15	3	10.5	10.3
6	3	9.5	11.4	16	3	10.8	10.0
7	3	16.2	6.7	17	3	11.5	9.4
8	3	10.3	10.5	18	3	12.4	8.7
9	3	9.6	11.3	19	3	9.4	11.5
10	3	9.4	11.5	20	3	14.1	7.7
Average Large Flocs Settling Velocity (m/h):				9.96			
Standard Deviation:				2.0			
Maximum (m/h):				13.0			
Minimum (m/h):				6.2			

Table G.3 Discrete Settling Velocities for Medium Flocs Measured During the Validation

Medium Flocs							
Floc No.	H (cm)	Time(s)	V(m/h)	Floc No.	H (cm)	Time(s)	V(m/h)
1	3	33.3	3.2	11	3	51.2	2.1
2	3	29.2	3.7	12	3	29.5	3.7
3	3	35.2	3.1	13	3	36.2	3.0
4	3	30.5	3.5	14	3	41.2	2.6
5	3	48.3	2.2	15	3	44.6	2.4
6	3	26.8	4.0	16	3	36.4	3.0
7	3	44.5	2.4	17	3	47.5	2.3
8	3	49.1	2.2	18	3	51.2	2.1
9	3	47.9	2.3	19	3	26.3	4.1
10	3	30.5	3.5	20	3	25.1	4.3
Average Large Flocs Settling Velocity (m/h):				3.00			
Standard Deviation:				0.73			
Maximum (m/h):				4.30			
Minimum (m/h):				2.11			

Table G.4 Data for the Calculation of the Discrete Settling Velocity of Small Floccs
Obtained During the Validation of the Model

Area of the Settling Column (Ac)	71.4 cm ²
Time 1 (t ₁)	4 min
Time 2 (t ₂)	14 min
Mass of Solids in the upper-mid portion of the settling column at t ₁ (M _x)	156.18 mg
Mass of Solids in the upper-mid portion of the settling column at t ₂ (M _{xx})	69.47 mg
TSS Concentration at the middle of the column at t ₁ (C _x)	162 mg/L
TSS Concentration at the middle of the column at t ₂ (C _{xx})	73 mg/L
Conversion factor for the units presented in this table (C _f)	600
Small Floc Settling Velocity (Equation 3.4)	0.62 m/h

Determination of the Discrete Settling Fractions

The procedure for determining the settling fractions was presented in Chapter 3. The three settling fractions are calculated using the procedure described in Section 3.1.2.2 and using Equation 3.5 to 3.10. These equations are recapitulated below.

$$C_1 + C_2 + C_3 + FSS = C_d \dots\dots\dots (3.5)$$

$$f_i = \frac{C_i}{C_d - FSS}; \quad i = 1, 2, 3 \dots\dots\dots (3.7)$$

$$A_c (V_{S1} \Delta t_{1-1} C_1 + V_{S2} \Delta t_{1-2} C_2 + V_{S3} \Delta t_{1-3} C_3) = M_1 \dots\dots\dots (3.8)$$

$$\Delta t_{j-i} = \min \left(t_j - \text{Lag time}, \frac{h_j}{V_{si}} \right) \dots\dots\dots (3.9)$$

$$A_c (V_{S1} \Delta t_{2-1} C_1 + V_{S2} \Delta t_{2-2} C_2 + V_{S3} \Delta t_{2-3} C_3) = M_2 \dots\dots\dots (3.10)$$

The information required for the determination of the fractions (including the results of the batch column tests) obtained during the validation is presented in Table G.5

Table G.5 Data for the Calculation of the Discrete Settling Fractions Obtained During the Validation of the Model

Area of the settling column (A_c)		71.4 cm ²	
Dilute Concentration (C_d)		600 mg/L	
FSS of the sample		5 mg/L	
Lag Time		1.5 min	
Time 1 (t_1)		4 min	
Time 2 (t_2)		13 min	
Distance from the water surface to the top of the sludge blanket at t_1 (h_1)		25.5 cm	
Distance from the water surface to the top of the sludge blanket at t_2 (h_2)		25.4 cm	
Mass of Solids in the sludge blanket of the settling column at t_1 (M_1)		899.2 mg	
Mass of Solids in the sludge blanket of the settling column at t_2 (M_2)		1055.9 mg	
Fraction i	V_{si} (m/h)	Δtime_{1-i} (min)	Δtime_{2-i} (min)
1	9.96	1.536	1.530
2	3.00	2.5	5.080
3	0.62	2.5	12.500

Table G.6 summarizes the discrete settling velocities and fractions obtained during the validation period. Table G.7 shows the zone settling properties and compression rate parameters obtained during the validation, these values were obtained following the procedure explained in Section 5.11.2. The data and figures used for the calculation of the settling properties presented in Table G.7 were presented in Appendix E.

Table G.6 Discrete Settling Velocities and Fractions Obtained During the Validation

Type of Particle		Settling Velocity V_{si} (m/h)*	Concentration C_i (mg/L)	Fraction f_i
Description	Class (i)			
Big Floc	1	9.96	416.45	0.700
Medium Floc	2	3.00	152.55	0.256
Small Floc	3	0.62	26.00	0.044
Non-Settleable	4	0.00	5.00	----
		Total =	600.0	1.000

*The settling velocities presented in this table were measured at 26.0 °C

Table G.7 Measured Settling Parameter of the Hindered and Compression Settling Equations

Parameter	Value*
V_o (m/h)	8.46
k_1 (L/g)	0.386
V_o (m/h)	3.08
K_c (L/g)	0.181

*The settling properties presented in this table were measured at 26.0 °C

APPENDIX H **DEVELOPMENT OF THE DIFFERENTIAL SETTLING FLOCCULATION** **EQUATION**

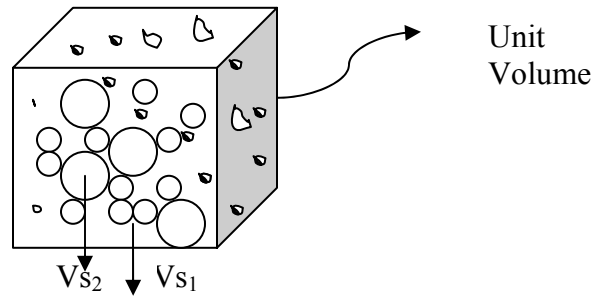


Figure H.1 Unit Volume

Assuming C_1 as the concentration of primary-unfloculated particles and C_2 as the concentration of flocculated particles. The number of particles 1 per unit volume is defined as:

$$\frac{\text{No. Particles}}{\text{Unit Volume}} = \frac{\left(\frac{C_1}{\rho_1} \right)}{\left[\pi \frac{4}{3} \left(\frac{d_1}{2} \right)^3 \right]} = \frac{6C_1}{\pi \rho_1 d_1^3} \dots\dots\dots \text{H.1}$$

where ρ_1 is the density of the C_1 particles and d_1 is the diameter

The number of particles in the control volume presented in Figure H.2 is:

$$\frac{\text{No. Particles}}{\text{Control Volume}} = \frac{6C_1}{\pi \rho_1 d_1^3} \delta_y \dots\dots\dots \text{H.2}$$

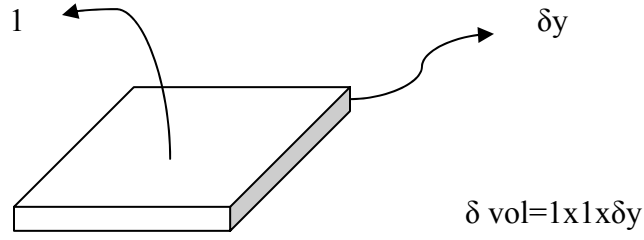


Figure H.2 Control Volume

The probability ($p1$) that there will be an area of small particles projected into a plane orthogonal to the direction of the settling velocity is given by:

$$p1 = \frac{\Sigma A_1}{1} \approx \frac{6C_1}{\pi \rho_1 d_1^3} \delta_y \frac{\pi d_1^2}{4 \times 1} = \frac{3}{2} \frac{C_1 \delta_y}{\rho_1 d_1} \dots\dots\dots H.3$$

The probability that particles 1 fall in the near free path of particles 2 is approximately:

$$p_{cell} = p1 p2 = \left(\frac{3}{2} \frac{C_1 \delta_y}{\rho_1 d_1} \right) \frac{\frac{\pi}{4} (d_2 + 2d_1)^2}{\frac{\pi}{6} d_2^3} \delta_y \left(\frac{C_2}{\rho_2} \right) \dots\dots\dots H.4$$

$$\text{where } p2 = \frac{\frac{\pi}{4} (d_2 + 2d_1)^2}{\frac{\pi}{6} d_2^3} \delta_y \left(\frac{C_2}{\rho_2} \right) \dots\dots\dots H.5$$

Equation H.4 can be simplified to

$$p_{cell} = p1 p2 = \left(\frac{9}{4} \delta_y^2 \right) \left\{ \frac{C_1 C_2}{\rho_1 \rho_2} \frac{(d_2 + 2d_1)^2}{d_1 d_2^3} \right\} \dots\dots\dots H.6$$

Assuming $\delta v = \delta y / \delta t$, and $\delta y = d_2$, we can define:

$$p_{ct} = \frac{p_{cell}}{\delta t} = \frac{p_{cell}}{\delta y} \delta v = \frac{p_{cell}}{d_2} \delta v \dots\dots\dots \text{H.7}$$

From Equations H.6 and H.7 we can get Equation H.8

$$p_{ct} = \left(\frac{9}{4} \right) \left\{ \frac{C_1 C_2}{\rho_1 \rho_2} \frac{\left(1 + 2 \frac{d_1}{d_2} \right)^2}{d_1} \right\} \delta v \dots\dots\dots \text{H.8}$$

where p_{ct} is the rate of collision. For each collision a C_1 particle joins a C_2 and C_2 increases and C_1 decreases. The rate of change of particles C_1 is define as:

$$\frac{dC_1}{dt} = -p_{ct} C_1 \dots\dots\dots \text{H.9}$$

Substituting Equation H.8 into Equation H.9,

$$\frac{dC_1}{dt} = - \left(\frac{9}{4} \right) \left\{ \frac{C_1 C_2}{\rho_1 \rho_2} \frac{\left(1 + 2 \frac{d_1}{d_2} \right)^2}{d_1} \right\} \delta v C_1 \dots\dots\dots \text{H.10}$$

Since $\delta v = V_{S2} - V_{S1}$ (difference in settling velocities), and introducing a kinetic constant accounting for the increase in the rate of collision due to the turbulence in the flow, we obtain:

$$\frac{dC_1}{dt} = -\frac{9}{4}k_{ds} \frac{C_1 C_2}{\rho_1 \rho_2} \left(1 + 2\frac{d_1}{d_2}\right)^2 \frac{C_1}{d_1} (V_{S2} - V_{S1}) \dots\dots\dots \text{H.11}$$

where C_1 and C_2 are the concentrations of unflocculated–primary and flocculated–flocs particles respectively, d_1 and d_2 are the cross sectional diameters of unflocculated and flocculated particles respectively, ρ_1 and ρ_2 are the densities of the primary and flocculated particles respectively, t is time, k_{ds} is a kinetic constant between 1 and 2, and V_{S1} and V_{S2} are the settling velocities of the primary particles and flocs respectively.

APPENDIX I

1D ANALYSES

I.1 1D Limiting Solids Flux Analysis for SOR= 1.0 m/h, UFR= 0.5 m/h, V_o = 10.54 m/h, K_I = 0.40 L/g.

Table I.1 presents the data used for the 1D limiting solids flux analysis, using only the zone settling properties, i.e, V_o = 10.54 m/h, K_I = 0.40 L/g, with SOR= 1.0 m/h, UFR= 0.5 m/h. Figure I.1 shows the solids-flux curves used in the analysis.

Table I.1 Data for 1D Limiting Solids Flux Analysis Using Only the Zone Settling Properties for a UFR= 0.5 m/h.

MLSS (mg/L)	V_s (m/h)	Solids Flux (Kg/m ² /h)	Underflow Rate (m/h)	Underflow flux (Kg/m ² /h)	Solids + Underflow flux (Kg/m ² /h)
500	8.63	4.31	0.5	0.25	4.56
1000	7.06	7.06	0.5	0.5	7.56
2000	4.73	9.47	0.5	1	10.47
3000	3.17	9.52	0.5	1.5	11.02
4000	2.13	8.51	0.5	2	10.51
5000	1.43	7.13	0.5	2.5	9.63
6000	0.96	5.73	0.5	3	8.73
7000	0.64	4.48	0.5	3.5	7.98
8000	0.43	3.44	0.5	4	7.44
9000	0.29	2.59	0.5	4.5	7.09
10000	0.19	1.93	0.5	5	6.93
11000	0.13	1.42	0.5	5.5	6.92
12000	0.09	1.04	0.5	6	7.04
13000	0.06	0.76	0.5	6.5	7.26
14000	0.04	0.55	0.5	7	7.55
15000	0.03	0.39	0.5	7.5	7.89
16000	0.02	0.28	0.5	8	8.28
17000	0.01	0.20	0.5	8.5	8.70
18000	0.01	0.14	0.5	9	9.14

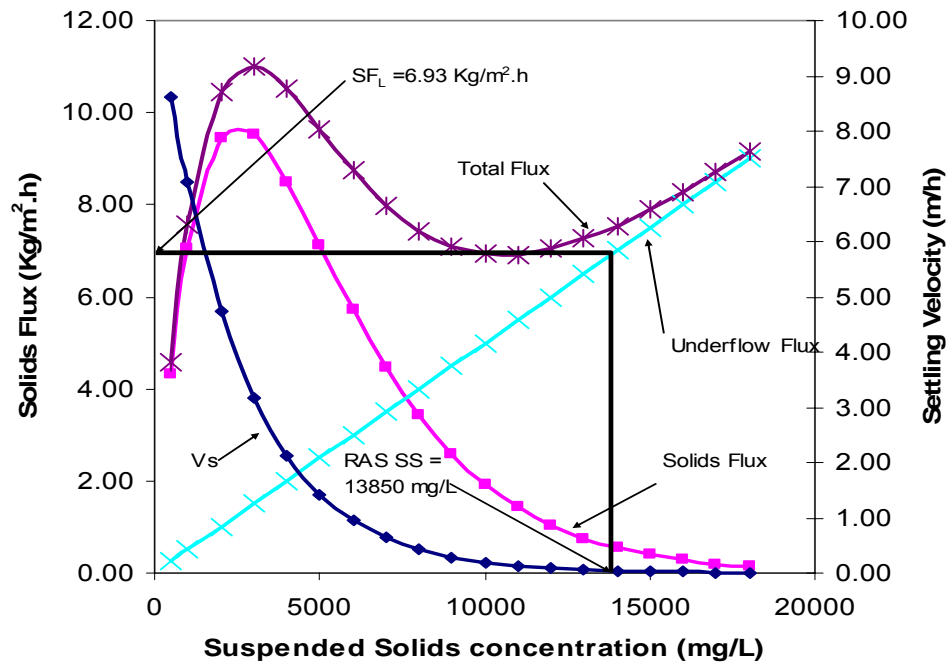


Figure I.1 1D Solids Flux Analysis for the Marrero WWTP using the Zone Settling Properties for a UFR= 0.5 m/h
($V_o = 10.54$ m/h and $K_I = 0.40$ L/g)

I.2 1D Limiting Solids Flux Analysis for SOR= 1.0 m/h, UFR= 0.5 m/h, $V_o = 10.54$ m/h, $K_I = 0.40$ L/g, $V_c = 3.20$ m/h, $K_c = 0.184$ L/g.

Table I.2 presents the data used for the 1D limiting solids flux analysis using the zone settling and the compression rate properties, i.e, $V_o = 10.54$ m/h, $K_I = 0.40$ L/g, $V_c = 3.20$ m/h, $K_c = 0.184$ L/g, with SOR= 1.0 m/h, UFR= 0.5 m/h. Figure I.2 shows the solids-flux curves used in the analysis. In this analysis the compression settling threshold was 5400 mg/L.

The evaluation of solids-flux curves presented in Figure I.1 yields a limiting solids flux equal to $6.93 \text{ kg/m}^2\text{.h}$, and the evaluation of Figure I.2 yields a limiting value equal to $9.15 \text{ kg/m}^2\text{.h}$.

Table I.2 Data for 1D Limiting Solids Flux Analysis using the Zone Settling and the Compression Rate Properties for a UFR= 0.5 m/h.

MLSS (mg/L)	Vs (m/h)	Solids Flux (Kg/m²/h)	Underflow Rate (m/h)	Underflow flux (Kg/m²/h)	Solids + Underflow flux (Kg/m²/h)
500	8.63	4.31	0.5	0.25	4.56
1000	7.06	7.06	0.5	0.50	7.56
2000	4.73	9.47	0.5	1.00	10.47
3000	3.17	9.52	0.5	1.50	11.02
4000	2.13	8.51	0.5	2.00	10.51
5000	1.43	7.13	0.5	2.50	9.63
5500	1.16	6.40	0.5	2.75	9.15
6000	1.06	6.37	0.5	3.00	9.37
7000	0.88	6.18	0.5	3.50	9.68
9000	0.61	5.50	0.5	4.50	10.00
10000	0.51	5.08	0.5	5.00	10.08
11000	0.42	4.65	0.5	5.50	10.15
12000	0.35	4.22	0.5	6.00	10.22
13000	0.29	3.80	0.5	6.50	10.30
14000	0.24	3.41	0.5	7.00	10.41
15000	0.20	3.04	0.5	7.50	10.54
16000	0.17	2.70	0.5	8.00	10.70
17000	0.14	2.38	0.5	8.50	10.88
18000	0.12	2.10	0.5	9.00	11.10
19000	0.10	1.84	0.5	9.50	11.34
20000	0.08	1.61	0.5	10.00	11.61
21000	0.07	1.41	0.5	10.50	11.91
22000	0.06	1.23	0.5	11.00	12.23
23000	0.05	1.07	0.5	11.50	12.57
24000	0.04	0.93	0.5	12.00	12.93
25000	0.03	0.80	0.5	12.50	13.30
26000	0.03	0.70	0.5	13.00	13.70
27000	0.02	0.60	0.5	13.50	14.10
28000	0.02	0.52	0.5	14.00	14.52
29000	0.02	0.45	0.5	14.50	14.95
30000	0.01	0.38	0.5	15.00	15.38
31000	0.01	0.33	0.5	15.50	15.83
32000	0.01	0.28	0.5	16.00	16.28
33000	0.01	0.24	0.5	16.50	16.74

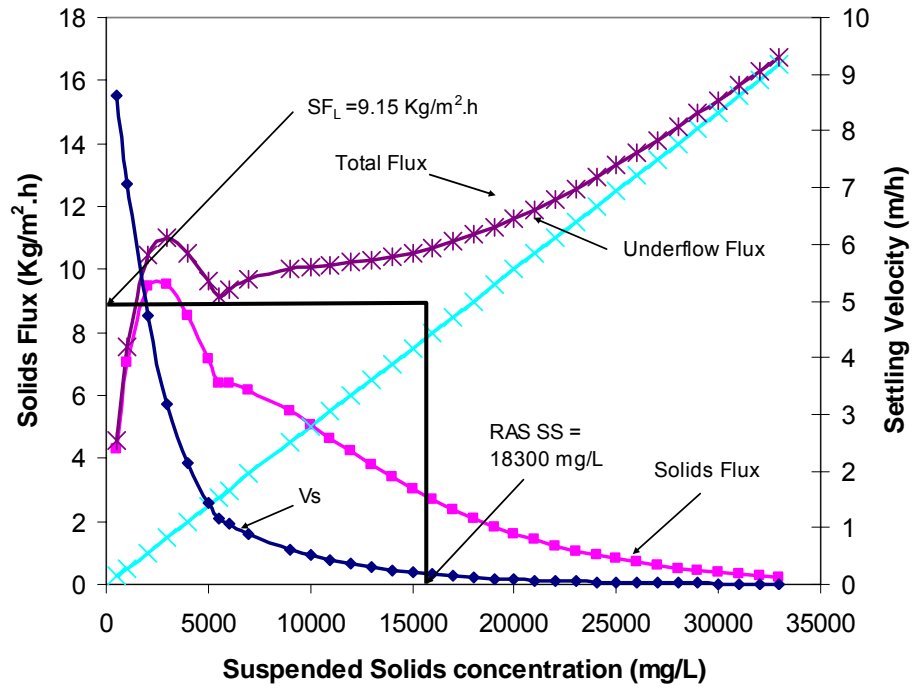


Figure I.2 1D Solids Flux Analysis for the Marrero WWTP using the Zone Settling and Compression Rate Properties for a UFR= 0.5 m/h.
($V_o = 10.54$ m/h and $K_I = 0.40$ L/g, $V_c = 3.20$ m/h, $K_c = 0.184$ L/g)

I.3 1D Limiting Solids Flux Analysis for SOR= 2.5 m/h, UFR= 1.25 m/h, $V_o = 10.54$ m/h, $K_I = 0.40$ L/g.

Table I.3 presents the data used for the 1D limiting solids flux analysis, using only the zone settling properties, i.e, $V_o = 10.54$ m/h, $K_I = 0.40$ L/g, for a SOR= 2.50 m/h, and UFR= 1.25 m/h. Figure I.3 shows the solids-flux curves used in the analysis.

The evaluation of the fluxes presented in Figure I.3 yields a limiting solids flux equal to $13.23 \text{ kg/m}^2\cdot\text{h}$.

Table I.3 Data for 1D Limiting Solids Flux Analysis Using Only the Zone Settling
Properties for a UFR= 1.25 m/h.

MLSS (mg/L)	Vs (m/h)	Solids Flux (Kg/m ² /h)	Underflow Rate (m/h)	Underflow flux (Kg/m ² /h)	Solids + Underflow flux (Kg/m ² /h)
500	8.63	4.31	1.25	0.63	4.94
1000	7.06	7.06	1.25	1.25	8.31
2000	4.73	9.47	1.25	2.50	11.97
3000	3.17	9.52	1.25	3.75	13.27
4000	2.13	8.51	1.25	5.00	13.51
5000	1.43	7.13	1.25	6.25	13.38
6000	0.96	5.73	1.25	7.50	13.23
7000	0.64	4.48	1.25	8.75	13.23
8000	0.43	3.44	1.25	10.00	13.44
9000	0.29	2.59	1.25	11.25	13.84
10000	0.19	1.93	1.25	12.50	14.43
12000	0.09	1.04	1.25	15.00	16.04
14000	0.04	0.55	1.25	17.50	18.05
16000	0.02	0.28	1.25	20.00	20.28
18000	0.01	0.14	1.25	22.50	22.64

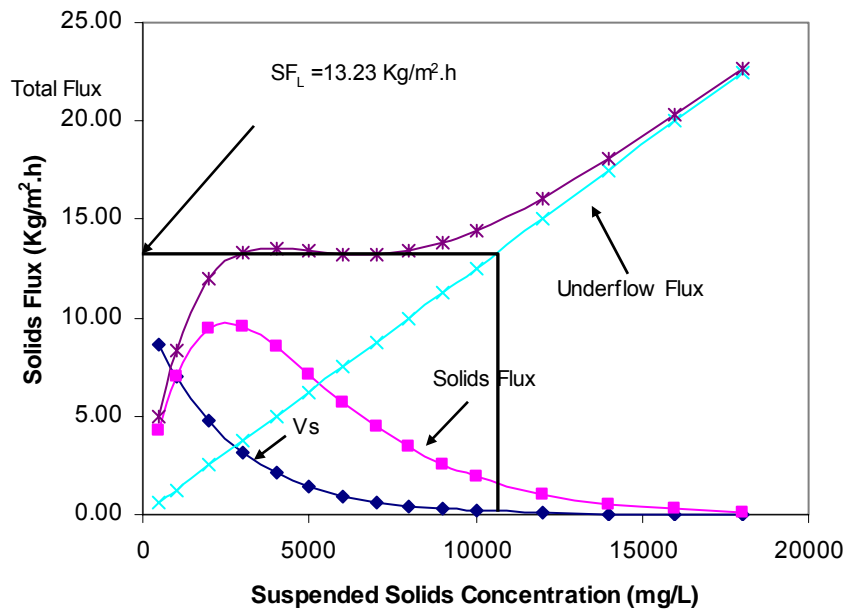


Figure I.3 1D Solids Flux Analysis for the Marrero WWTP using the Zone Settling
Properties for a UFR= 1.25 m/h
(V_o = 10.54 m/h and K_I = 0.40 L/g)

I.4 1D Limiting Solids Flux Analysis for SOR= 2.5 m/h, UFR= 1.25 m/h, V_0 = 10.54 m/h, K_1 = 0.40 L/g, V_c = 3.20 m/h, K_c = 0.184 L/g.

Table I.4 presents the data used for the 1D limiting solids flux analysis using the zone settling and the compression rate properties, i.e, V_0 = 10.54 m/h, K_1 = 0.40 L/g, V_c = 3.20 m/h, K_c = 0.184 L/g, for a SOR= 2.50 m/h, and UFR= 1.25 m/h. Figure I.4 shows the solids-flux curves used in the analysis. In this analysis the compression settling threshold was 5400 mg/L.

Table I.4 Data for 1D Limiting Solids Flux Analysis using the Zone Settling and the Compression Rate Properties for a UFR= 1.25 m/h.

MLSS (mg/L)	V_s (m/h)	Solids Flux (Kg/m ² /h)	Underflow Rate (m/h)	Underflow flux (Kg/m ² /h)	Solids + Underflow flux (Kg/m ² /h)
500	8.63	4.31	1.25	0.63	4.94
1000	7.06	7.06	1.25	1.25	8.31
2000	4.73	9.47	1.25	2.50	11.97
3000	3.17	9.52	1.25	3.75	13.27
4000	2.13	8.51	1.25	5.00	13.51
5000	1.43	7.13	1.25	6.25	13.38
5500	1.16	6.40	1.25	6.88	13.27
6000	1.06	6.37	1.25	7.50	13.87
7000	0.88	6.18	1.25	8.75	14.93
9000	0.61	5.50	1.25	11.25	16.75
10000	0.51	5.08	1.25	12.50	17.58
11000	0.42	4.65	1.25	13.75	18.40
12000	0.35	4.22	1.25	15.00	19.22
13000	0.29	3.80	1.25	16.25	20.05
14000	0.24	3.41	1.25	17.50	20.91
15000	0.20	3.04	1.25	18.75	21.79
16000	0.17	2.70	1.25	20.00	22.70
17000	0.14	2.38	1.25	21.25	23.63
18000	0.12	2.10	1.25	22.50	24.60
19000	0.10	1.84	1.25	23.75	25.59
20000	0.08	1.61	1.25	25.00	26.61
25000	0.03	0.80	1.25	31.25	32.05

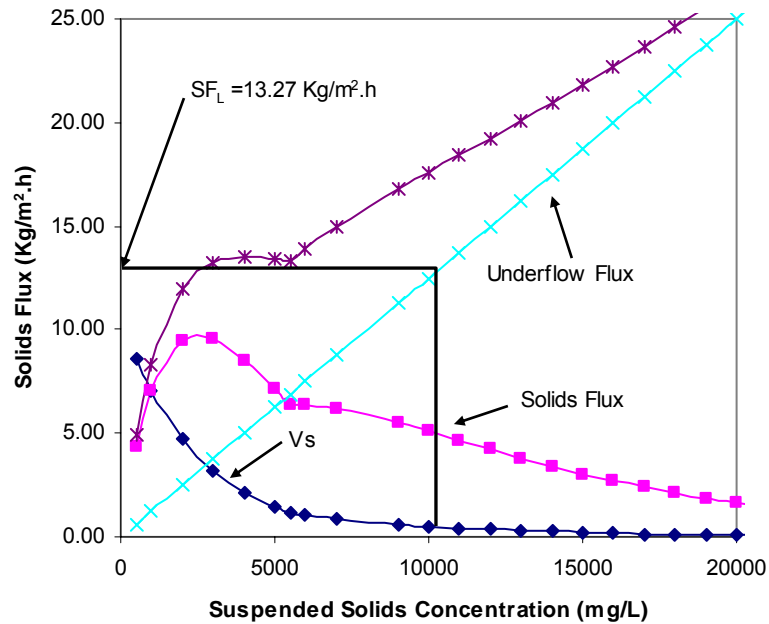


Figure I.4 1D Solids Flux Analysis for the Marrero WWTP using the Zone Settling and Compression Rate Properties for a UFR= 1.25 m/h.
($V_o = 10.54$ m/h and $K_I = 0.40$ L/g, $V_c = 3.20$ m/h, $K_c = 0.184$ L/g)

The evaluation of solids-flux curves presented in Figure I.4 yields a limiting solids flux equal to $13.27 \text{ kg/m}^2 \cdot \text{h}$.

I.5 1D Limiting Solids Flux Analysis for SOR= 0.50 m/h, UFR= 0.25 m/h, $V_o = 10.54$ m/h, $K_I = 0.40$ L/g.

Table I.5 presents the data used for the 1D limiting solids flux analysis, using only the zone settling properties, i.e, $V_o = 10.54$ m/h, $K_I = 0.40$ L/g, for a SOR= 0.50 m/h, and UFR= 0.25 m/h. Figure I.5 shows the solids-flux curves used in the analysis.

The evaluation of the fluxes presented in Figure I.5 yields a limiting solids flux equal to $4.00 \text{ kg/m}^2 \cdot \text{h}$.

Table I.5 Data for 1D Limiting Solids Flux Analysis Using Only the Zone Settling
Properties for a UFR= 0.25 m/h.

MLSS (mg/L)	Vs (m/h)	Solids Flux (Kg/m ² /h)	Underflow Rate (m/h)	Underflow flux (Kg/m ² /h)	Solids + Underflow flux (Kg/m ² /h)
500	8.63	4.31	0.25	0.13	4.44
1000	7.06	7.06	0.25	0.25	7.31
2000	4.73	9.47	0.25	0.50	9.97
3000	3.17	9.52	0.25	0.75	10.27
4000	2.13	8.51	0.25	1.00	9.51
5000	1.43	7.13	0.25	1.25	8.38
6000	0.96	5.73	0.25	1.50	7.23
7000	0.64	4.48	0.25	1.75	6.23
8000	0.43	3.44	0.25	2.00	5.44
9000	0.29	2.59	0.25	2.25	4.84
10000	0.19	1.93	0.25	2.50	4.43
12000	0.09	1.04	0.25	3.00	4.04
14000	0.04	0.55	0.25	3.50	4.05
16000	0.02	0.28	0.25	4.00	4.28
18000	0.01	0.14	0.25	4.50	4.64

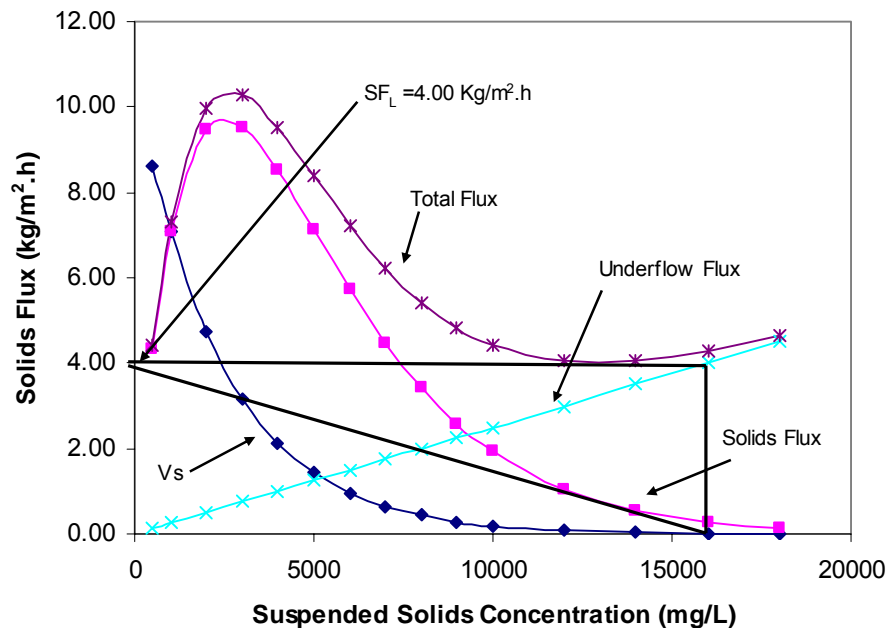


Figure I.5 1D Solids Flux Analysis for the Marrero WWTP using the Zone Settling
Properties for a UFR= 0.25 m/h
($V_o = 10.54$ m/h and $K_I = 0.40$ L/g)

I.6 1D Limiting Solids Flux Analysis for SOR= 0.5 m/h, UFR= 0.25 m/h, $V_0= 10.54$ m/h, $K_1= 0.40$ L/g, $V_c= 3.20$ m/h, $K_c= 0.184$ L/g.

Table I.6 presents the data used for the 1D limiting solids flux analysis using the zone settling and the compression rate properties, i.e, $V_0= 10.54$ m/h, $K_1= 0.40$ L/g, $V_c= 3.20$ m/h, $K_c= 0.184$ L/g, for a SOR= 0.50 m/h, and UFR= 0.25 m/h. Figure I.6 shows the solids-flux curves used in the analysis. In this analysis the compression settling threshold was 5400 mg/L.

Table I.6 Data for 1D Limiting Solids Flux Analysis using the Zone Settling and the Compression Rate Properties for a UFR= 0.25 m/h.

MLSS (mg/L)	V_s (m/h)	Solids Flux (Kg/m ² /h)	Underflow Rate (m/h)	Underflow flux (Kg/m ² /h)	Solids + Underflow flux (Kg/m ² /h)
500	8.63	4.31	0.25	0.13	4.44
1000	7.06	7.06	0.25	0.25	7.31
2000	4.73	9.47	0.25	0.50	9.97
3000	3.17	9.52	0.25	0.75	10.27
4000	2.13	8.51	0.25	1.00	9.51
5000	1.43	7.13	0.25	1.25	8.38
5500	1.16	6.40	0.25	1.38	7.77
6000	1.06	6.37	0.25	1.50	7.87
7000	0.88	6.18	0.25	1.75	7.93
9000	0.61	5.50	0.25	2.25	7.75
10000	0.51	5.08	0.25	2.50	7.58
15000	0.20	3.04	0.25	3.75	6.79
20000	0.08	1.61	0.25	5.00	6.61
25000	0.03	0.80	0.25	6.25	7.05
30000	0.01	0.38	0.25	7.50	7.88
35000	0.01	0.18	0.25	8.75	8.93

The evaluation of solids-flux curves presented in Figure I.6 yields a limiting solids flux equal to 6.50 kg/m².h.

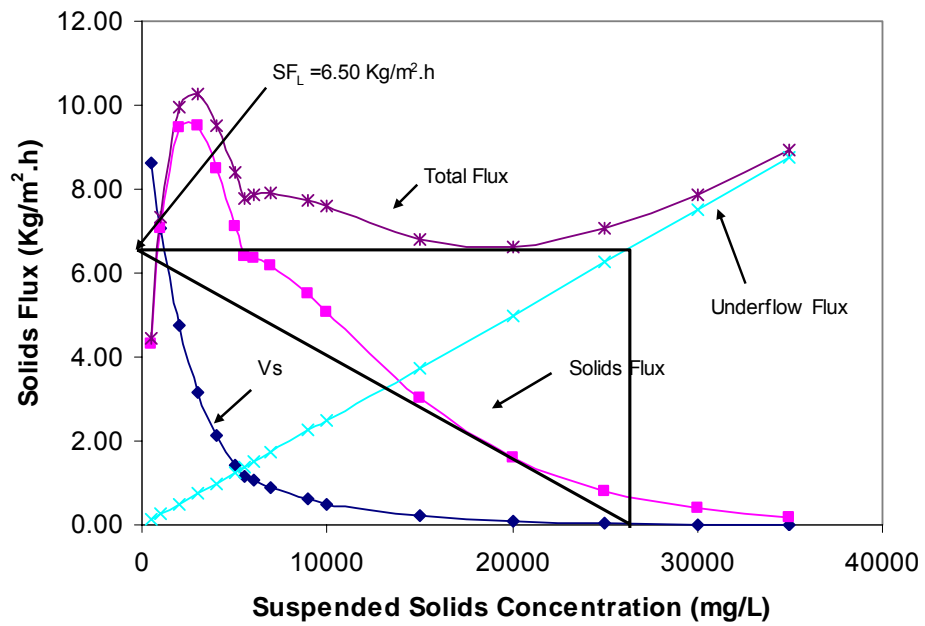


Figure I.6 1D Solids Flux Analysis for the Marrero WWTP using the Zone Settling and Compression Rate Properties for a UFR= 0.25 m/h.
 (V_o = 10.54 m/h and K_I = 0.40 L/g, V_c = 3.20 m/h, K_c = 0.184 L/g)

APPENDIX J

FORTTRAN SOURCE CODE FOR THE Q3D CLARIFIER MODEL

```
c          UNIVERSITY OF NEW ORLEANS
c          Q3D COMPUTER CODE
c          PARED FOR THE DISSERTATION
c          SECONDARY CLARIFIER MODELING: A MULTI-
c          PROCESS APPROACH
c          BY
c          ALONSO G GRIBORIO
c          ADVISER: DR. J. A. McCORQUODALE

c  Main EXPLICIT MODIFIED IMPLICIT COEFFICIENT-Weighted
c  Coefficient
c          CALCULATION IN TWO DIRECTION
c          Change in Boundary Conditions
c          Bottom Slope - Baffles
c          Settler-Mask
c          2-D Settler FVM
c          include 'comdeck3'

c  CIRCULAR-CLARIFIER
c  Include Horizontal Baffle at the inlet wall
c  Include Stamford and Crosby Baffle
c  Include Hopper and Suction
c  Include Inboard or Outboard Launder
c  Included Canopy Baffle and EDI
c  Digital Version
c  Version with Scraper included
c  Transport equation for vorticity
c  Modifications in boundary conditions for vorticity.
c  Include subroutine for change in Temperature
c  Version Temp 2-1, Includes Initial To Average or User Input
c  Include variable Cd base on Reynolds

c          Include 'comdeck3.h'
c          REAL nuo, nut,LL,mask,maskk,NBl,Inlet,maski,maske
c          INTEGER IPRINT
c          psi= streamfunction, vort = vorticity
c          u= x velocity, v= y velocity, p = pressure
c          phi=scalar variable, C = Concentration, rho= density
c          Temp(200,100), nut(200,100), Con(200,100)
c          Fnb = face value of advection flux, Dnb=face value of diffusion flux, XX=?
c          nuo = kinematic viscosity
c          anb = neighbouring coefs, aP = diagonal coef, b = source/sink, DF=adv coef
```

```

        open (unit=29, file= 'Runcontrol3.dat', status = 'unknown')
        open (unit=30, file= 'control.dat', status = 'unknown')
        open (unit=31, file= 'settler.dat', status = 'unknown')
        open (unit=32, file= 'Loading.dat', status = 'unknown')
        open (unit=33, file= 'geometry3.dat', status = 'unknown')
        open (unit=37, file= 'Launder.dat', status = 'unknown')
        open (unit=38, file= 'HopperSuction.dat', status = 'unknown')
        open (unit=39, file= 'Scraper3.dat', status = 'unknown')
        open (unit=40, file= 'TimeSerie3.dat', status = 'unknown')
        open (unit=41, file= 'Output.out', form= 'formatted',
& status = 'unknown')
        open (unit=42, file= 'HeatExc.dat', status = 'unknown')
        Read(30,*) DCy  !Diffusion Coefficient in the Y direction
        Read(30,*) DCr  !Diffusion Coefficient in the R direction
        Read(30,*) Alpha !Coefficient for the Source Term in Vorticity Transport Eq.
        Read(30,*) Spegra !Specific Gravity of the Solid Particles
        Read(30,*) Densre !Reference density
        Read(30,*) Vlsl  ! 1 mm, roughness coefficient for Turbulence Model
        Read(30,*) gravi ! gravity m/s2
        Read(30,*) Cd    ! Drag coefficient
        Read(30,*) RheEx ! nonNewtonian exponent
        Read(30,*) Wt    ! Implicit weighting factor!Weighted Coefficient (Wt= 1
Fully Implicit, Wt= 0 Explicit Solution) =
        Read(30,*) STDS  !Salinity Concentration in Kg/m3 , STDS
        Read(30,*) Wbo   !Isolation at the outer limit of earth's atmosphere, cal/(cm2*d)
        Read(30,*) Cloub  !Cloud-Base altitude
        Read(30,*) Cp     !Specific heat
        Read(30,*) Bowen  !Bowen's Coefficient
        Read(30,*) SteBol !Stefan-Boltzmann Constan

SGC=(1.-1./Spegra)

Write(*,*) 'GRID AND RUN INFORMATION'

        Read(29,*) M  !Number of cells in X direction
        Read(29,*) N  !Number of cells in Y direction (default=25)
        Read(29,*) Dt !Time Step
        Read(29,*) Iswitch !Run dye (Yes=0, No=1)

c      Read(29,*) Wt !Weighted Coefficient (Wt= 1 Fully Implicit, Wt= 0 Ex
c      &      !plicit Solution) =
        Read(29,*) Iserie !Time Series,Iserie (Function=0, Time Serie =1)
        Read(29,*) Itemp !Modeling Temperature (No=0, Yes=1)

```

```

Read(29,*) Intem !Initial Tank Temperature(User defined=1, Average of
Influent Temp.=2)

```

```

If(Intem.eq.1) then

```

```

    Read(29,*) TemI

```

```

Else

```

```

    Read(29,*) Dummy

```

```

endif

```

```

read(29,*) NTs !Number of time step (integer)

```

```

read(29,*) aaa2 !Every how many time steps would you like to PRINT?

```

```

read(29,*) Tserie !Time Step for Time Serie, Constant (minutes)

```

```

pi=4.0*atan(1.0)

```

```

OveR=4./(2.+sqrt(4.-(cos(pi/M)+cos(pi/N))*2))

```

```

Write(*,292) 'Number of cells in X direction ',M

```

```

Write(*,292) 'Number of cells in Y direction ',N

```

```

Write(*,291) 'Time Step (seconds) ',Dt

```

```

Write(*,292) 'Run dye (Yes=0, No=1)',Iswitch

```

```

Write(*,291) 'Weighted Coefficient', Wt

```

```

Write(*,291) 'Over Relaxation Coefficient', OveR

```

```

Write(*,*)'_____ '

```

```

c*****Initial Water Temperature Calculation*****

```

```

Icount=Int(Nts*dt/(60.*Tserie)+0.00001)

```

```

Write(*,*) 'Icount',Icount

```

```

291 Format (1X,A,2X,1F5.2)

```

```

292 Format (1X,A,2X,1I4)

```

```

293 Format (1X,A,2X,1F10.0)

```

```

294 Format (1X,A,2X,1F6.4)

```

```

295 Format (1X,A,2X,1F8.1,2X,A)

```

```

296 Format (A,A,A,A)

```

```

297 Format (1X,A,2X,1F6.2)

```

```

299 Format (1X,A,2X,1F10.1,2X,1F6.3,2X,1F6.3)

```

```

300 Format (1X,A,2X,1F6.1,2X,1F6.1,2X,1F6.1)

```

```

301 Format (1X,A,2X,1F8.2)

```

```

302 Format (1X,1F9.2,6X,1F8.2,15X,1F8.2)

```

```

303 Format (1X,A,2X,1F8.2,2X,A)

```

```

304 Format (1X,A,1X,1I3,1X,A,1X,1F5.1,1X,A)

```

```

Write(*,*) 'LOADING INFORMATION'

If(Iserie.eq.0) then
  read(32,*) SORA
  SORA=SORA/3600.
  Write(*,291) 'Average SOR (m/h)' ,SORA*3600
  read(32,*) Pfact
  Write(*,291) 'Ratio of Diurnal Peak SOR to Ave SOR',Pfact
  read(32,*) Tdi
  Write(*,291) 'Period in Hours of "diurnal flow"' ,Tdi
  read(32,*) Dyeo
  Write(*,291) 'MLSS Concentration Kg/m3',Dyeo
  read(32,*) Cfact
  Write(*,291) 'Ratio of MLSS Peak to Ave' ,Cfact
  read(32,*) Tcdi
  Write(*,291) 'Period of "diurnal Concentration"' ,Tcdi
  read(32,*) Iras
  Write(*,292) 'Proportional(1) or Constant(2) Recirculation Flow
&Rate"',Iras

  Tdi=Tdi*3600.
  Tcdi=Tcdi*3600.

  If (Iras.eq.1) then
    read(32,*) Ras
    Write(*,291) 'Recirculation Ratio' ,Ras
  Else
    read(32,*) Dummy
    read(32,*) Qras
    Write(*,294) 'Recirculation Flow Rate' ,Qras
  endif

Else If(Iserie.eq.1) then

read(40,296) dummy1, dummy1, dummy1, dummy1

  Do ii= 1, Icount+1

    read(40,*) TScountt(ii), SORAa(ii), Dyeoo(ii), Tempoo(ii)
  enddo

  If (Intem.eq.2) then
    TemI=0.0
    Do iii=1,Icount
      TemI= TemI+Tempoo(iii)

```

```

enddo
Temi=Temi/Icount
endif

```

```

SORA=SORAa(1)
Tscout= Tscoutt(1)
Dyeo=Dyeoo(1)
Tempo=Tempoo(1)
SORA=SORA/3600.

```

```

Write(*,291) 'Initial SOR (m/h)' ,SORA*3600
Write(*,297) 'Initial Tscout(min)' ,Tscout

```

```

read(32,*) Dummy          !SOR
read(32,*) Dummy          !Pfact
read(32,*) Dummy          !Tdi
read(32,*) Dummy          !Dyeo
Write(*,291) 'MLSS Initial Concentration Kg/m3',Dyeo
Write(*,291) 'Initial Water Temperature in °C' ,TemI
read(32,*) Dummy          !Cfact
read(32,*) Dummy          !Tcdi
read(32,*) Iras

```

```

Write(*,292) 'Proportional(1) or Constant(2) Recirculation Flow
&Rate"',Iras

```

```

If (Iras.eq.1) then
read(32,*) Ras
Write(*,291) 'Recirculation Ratio' ,Ras
Else
read(32,*) Dummy
read(32,*) Qras
Write(*,294) 'Recirculation Flow Rate' ,Qras
endif
endif
endif

```

c ***** Initial Density Calculations

```

Do i=1,M+1
do j=1,N+1

```

```

Densr(i,j)=(999.8396+18.224944*TemI-0.00792221*TemI**2
&-(55.4486E-6)*TemI**3+(149.7562E-9)*TemI**4-
&(393.2952E-12)*TemI**5+(0.802-0.002*TemI)*STDS)/
&(1+0.018159725*TemI)

```

```

        enddo
    enddo

    Write(*,301)'Initial Water Density', Densr(1,1)

    call infile

c*****Radius Calculations*****

    do j=1,N+1
        do i=1,M+1

            r(i,j)=rin+(i-1)*Dr

        enddo
    enddo

c*****Boundary Conditions for Turbulence*****
c    Vls1=0.001
        j=1
        Do 120 i=1,M+1
120    Turb(i,j)=Vls1

        j=N+1
        Do 121 i=1,M+1
            Turb(i,j)=Vls1/100.0
121    Turb(i,N)=Turb(i,N+1)

        i=1
        Do 221 iii=1,Ninl+1
            j=N+1-(iii-1)
221    Turb(i,j)=0.4*Inlet/2.0

        i=1
        Do 122 j=1,N-Ninl
122    Turb(i,j)=Vls1

        i=M+1
        Do 123 j=1,N+1
123    Turb(i,j)=Vls1

c***** Mixing Length Turbulence Model *****
    do 124 L=1,5000

        do 124 j=2,N

```

```

do 124 i=2,M

  if(mask(i,j-1).eq.0) then

    Turb(i,j)=Vlsl

    else if(maskk(i,j).eq.0) then
    Turb(i,j)=Vlsl

    else if(maski(i,j).eq.0) then
    Turb(i,j)=Vlsl

    else if(maske(i,j).eq.0) then
    Turb(i,j)=Vlsl

    else

      PPhi(i,j)=0.38          !0.45

      turb(i,j)=(1.-OveR)*turb(i,j)+OveR*
&(turb(i-1,j)+turb(i+1,j) +(turb(i,j-1)+
&turb(i,j+1))*rf*rf+(turb(i+1,j)-turb(i-1,j))*(0.5*Dr/(r(i,j)))
&+PPhi(i,j)*Dr*Dr)
&/(2*(1.+rf*rf))

c      turb(i,j)=(turb(i-1,j)+turb(i+1,j) +(turb(i,j-1)+
c      &turb(i,j+1))*rf**2+(turb(i+1,j)-turb(i-1,j))*(0.5*Dr/(r(i,j)))
c      &+PPhi(i,j)*Dr**2)
c      &/(2*(1.+rf**2))

    endif

124  continue

c*****Boundary Conditions for 3D Theta Velocity- Thevel
*****
c      Vlsl=0.001
      j=1
      Do 420 i=1,M
        Vth(i,j,3)=0.0
420  Vth(i,j,2)=0.0

      j=N
      Do 421 i=1,M
        Vth(i,j,3)=0.0
421  Vth(i,j,2)=0.0

```



```

i=1
  Do 422 j=1,N
    Vth(i,j,3)=0.0
422 Vth(i,j,2)=0.0

```

```

i=M
  Do 423 j=1,N
    Vth(i,j,3)=0.0
423 Vth(i,j,2)=0.0

```

```

do i=2,M-1
do j=2,N-1
Vth(i,j,2)=0.00
Vth(i,j,3)=0.00
enddo
enddo

```

c*****Initial Solution*****

```

      do 5 i=2,M
      do 5 j=2,N
c      vort(i,j)=0.0/100000
      C(i,j)=2.
c      rho(i,j)=Densr(i,j)
c      Temp(i,j,2)=Tempo
5      psi(i,j)=psio

      open (unit=10, file= 'settler.out', status = 'unknown')

      do i = 1, M+1

        do j= 1, N+1
          rho(i,j)=Densr(i,j)
          Temp(i,j,2)=TemI
          Temp(i,j,3)=TemI
          write(10,*)'psi(i,j) = ',i,j,psi(i,j)
        enddo
      enddo

```

c*****

c Iterative Solution

c Simple dye transport - Hybrid FVM

c***MAIN PROGRAM*******

```
Write(*,304) 'Simulation Time: ',INT(NTs*Dt/3600.),  
&'hours', 60*(NTs*Dt/3600.-INT(NTs*Dt/3600.)), 'minutes'
```

```
WRITE(*,292) 'Every how many time steps would you like to PRINT?',  
&jfix(aaa2)
```

```
If (Iserie.eq.1) Then
```

```
Write(*,295) 'Time Serie for Flow Rate, SOR every:', Tserie,'minutes'  
endif
```

```
Write(*,303) 'Time for Tecplot:', aaa2*dt/60,'minutes'
```

```
close(29)
```

```
close(30)
```

```
close(31)
```

```
close(32)
```

```
close(33)
```

```
close(37)
```

```
close(38)
```

```
close(39)
```

```
close(40)
```

```
call radius
```

```
mm=1
```

```
do nn=1,50
```

```
call hydrod(mm)
```

```
enddo
```

c***TECPLOT OUTPUT (Initial conditions) *******

```
IPRINT=AAA2
```

```
aaa=0.
```

C 2D SOLUTION

```
open (unit=16, file= '2DOutput.plt', form= 'formatted',  
& status = 'unknown')
```

C TIME SERIES Con. INLET-OUTLET

```

write(16,*)'variables="i","j","Velo(U)","Velo(V)","StreamFun",'
write(16,*)'"Conce","MAsk","Baffle","Canopi","Stamford",'
write(16,*)'"Viscosity","Vorticity","Turbulence",'
write(16,*)'"Froud","Gradiant","Dye","Temperature","Density"'
write(16,*)'"ThetaVel"'

write(16,*)'zone i='m,j'='n,f=point'
do j= 1, N
do i = 1, M
write(16,*) i,j,U(i,j),V(i,j),psi(i,j),con(i,j,1),Mask(i,j),
&Maskk(i,j),Maski(i,j),Maske(i,j),nut(i,j,2),Vort(i,j,2),Turb(i,j),
&Froud(i,j),Gf(i,j),Dye(i,j,2),Temp(i,j,2),Rho(i,j),Vth(i,j,2)
enddo
enddo

Write(41,*)' Time(min), Effluent (mg/L), Recirculation Conc.(mg/L)'
c***** Time stepping *****
do 8 mm= 2, NTs
if(ILOAD.eq.0) call load(mm)

call hydrod(mm)

call rhofac(mm)

call Turmod(mm)

call advdif(mm)

call coefs(mm)

call TheVel(mm)

if (Itemp.eq.1) call Temsub(mm)

do ifrac=3,Nfraction*2+1,2

call Concen(mm)

enddo

do i=1,M+1
do j=1,N+1

Con(i,j,1)=Con(i,j,3)+Con(i,j,5)+Con(i,j,7)

```

```

Con(i,j,2)=Con(i,j,4)+Con(i,j,6)+Con(i,j,8)

enddo
enddo
do i=1,M+1
do j=1,N+1

Fracc(i,j,1)=Con(i,j,4)/Max(Con(i,j,2),0.0001)

Fracc(i,j,2)=Con(i,j,6)/Max(Con(i,j,2),0.0001)

Fracc(i,j,3)=Con(i,j,8)/Max(Con(i,j,2),0.0001)

enddo
enddo

if (Ifloc.eq.1) call Floccu(mm)

if (Iswitch.eq.0) call dyetra(mm)

call vortic(mm)

If(Mrecir.EQ.2.AND.NSlope.eq.0.And.NCrosby.eq.0) then
j=1
Sum=0.0
Sum2=0.0
do i=1,M
Sum=Sum+con(i,j,2)
Sum2=Sum2+Dye(i,j,3)
Davg=Sum2/M
Avg=Sum/M
enddo
Else If(Mrecir.EQ.2.AND.NSlope.eq.0.And.NCrosby.eq.1) then
j=1
Sum=0.0
Sum2=0.0
do i=1,M
Sum=Sum+con(i,j,2)
Avg=(Sum+Con(icrosby+1,j,3))/M
Sum2=Sum2+Dye(i,j,3)
DAvg=(Sum2+Dye(icrosby+1,j,3))/M

enddo

```

```

Else if(Mrecir.EQ.2.AND.NSlope.gt.0) then
Sum=0.0
Sum2=0.0
j=1

      do i=1,M
Sum=Sum+con(i,j,2)*mask(i,j)
Sum2=Sum2+Dye(i,j,3)*mask(i,j)
      enddo

      do j=2,N
      do i=1,M
Sum=Sum+con(i,j,2)*mask(i,j)*(1-mask(i,j-1))
Sum2=Sum2+Dye(i,j,3)*mask(i,j)*(1-mask(i,j-1))
Davg=Sum2/M
Avg=Sum/M
      enddo
      enddo

endif

if(Mrecir.EQ.1) then
Sum2=0.0
Sum=0.0
j=1
do i=ihopst,ihopper-1
Sum=Sum+con(i,j,2)*mask(i,j)
Sum2=Sum2+Dye(i,j,3)*mask(i,j)

      enddo

      do j=2,N/2
      do i=ihopst,ihopper-1
Sum=Sum+con(i,j,2)*mask(i,j)*(1-mask(i,j-1))
Sum2=Sum2+Dye(i,j,3)*mask(i,j)*(1-mask(i,j-1))
Avg=Sum/(ihopper-ihopst)
DAvg=Sum2/(ihopper-ihopst)
      enddo
      enddo
endif

If(NLaundry.eq.2) then

      Avg2=Con(M,N,2)

```

```

Davg2=Dye(M,N,2)

Else if (Nlaunder.eq.1) Then
Sum2=0.0
Sum3=0.0
Count=0
j=N
do i=1,M
  If (Vn(i,j).gt.0) then
    Count=Count+1
    Sum2=Sum2+con(i,j,2)
    Sum3=Sum3+Dye(i,j,3)
  endif
enddo
Avg2=Sum2/Count
DAvg2=Sum3/Count

endif

```

c ***MASS BALANCE*******

```

BCon=0.0
Bcon2=0.0
Bdye=0.0
Bdye2=0.0
do i=1,M
do j=1,N
BCon=Bcon+con(i,j,2)*Vol(i,j)
Bcon2=Bcon2+con(i,j,1)*Vol(i,j)
Bdye=Bdye+Dye(i,j,3)*Vol(i,j)
Bdye2=Bdye2+Dye(i,j,2)*Vol(i,j)
enddo
enddo

```

c ***TEC PLOT TIME VARYING SOLUTION*******

```

IF(MM.GE.IPRINT) THEN
aaa=(float(mm)/float(nts))*100.
print*,aaa, ' % completed'
Write(*,299)'Seconds,SOR',mm*Dt,SOR*3600
Write(*,301)'MLSS Loading (mg/L)', Dyeo*1000.
Write(*,300)'Qin,Qout,Qras (L/s)', Q1*1000.,Q*1000.,Qras*1000.
Write(*,301) 'Effluent Concentration (mg/L)',Avg2*1000.

```

```

Write(*,301) 'Recirculation Concentration (mg/L)',Avg*1000.
Write(41,302) mm*Dt/60., Avg2*1000.,Avg*1000.
BMASS=Q1*DYEO*dt-dt*Q*Avg2-dt*Qras*Avg-(Bcon-Bcon2)*2*pi
BMASS2=Q1*DYEO*dt-dt*Q*DAvg2-dt*Qras*DAvg-(Bdye-Bdye2)*2*pi

Write(*,291)'Mass Balance of Concentration.%',BMASS*100/
&(Q1*DYEO*dt)

```

```

write(16,*)'zone i=',m,'j=',n,'f=point'
do j= 1, N
do i = 1, M
U(i,j)=(Uw(i,j)+Ue(i,j))*0.5
V(i,j)=(Vn(i,j)+Vs(i,j))*0.5
write(16,*) i,j,U(i,j),V(i,j),psi(i,j),con(i,j,1),Mask(i,j),
&Maskk(i,j),Maski(i,j),Maske(i,j),nut(i,j,2),Vort(i,j,2),Turb(i,j),
&Froud(i,j),Gf(i,j),Dye(i,j,2),Temp(i,j,2),rho(i,j),Vth(i,j,2)
enddo
enddo

```

```

IPRINT=IPRINT+AAA2
END IF

```

```

8    continue

```

```

c *****

```

```

open (unit=51, file= 'Veloc2.out',form= 'formatted',
& status = 'unknown')

```

```

Write(51,52) (i,i=1,M+1)
52  Format(15X, 200I10)

```

```

do j = N, 1, -1
Write(51,53) j,(Uw(i,j),Ue(i,j),i=1,M)
enddo

```

```

Write(51,54) (i,i=1,M+1)
53  Format (1X,'j=',I3,3X,'Uw and Ue',220F5.3)
54  Format(15X, 200I10)

```

```

do j = N, 1, -1
Write(51,55) j,(Vn(i,j),i=1,M)
Write(51,56) j,(Vs(i,j),i=1,M)

```

```

55  Format (1X,'j=',I3,3X,'Vn',7X,120E10.3)
56  Format (1X,'j=',I3,3X,'Vs',7X,120E10.3)
    enddo

    open (unit=155, file= 'Vorticity2.out', form= 'formatted',
    & status = 'unknown')

        Write(155,157) (i,i=1,M)

157  Format(15X, 200I10)

    do j = N, 1,-1
        Write(155,156) j,(Vort(i,j,2),i=1,M)
156  Format (1X,'j=',I3,3X, 'Vorticity=',200E10.3)
    enddo

    open (unit=165, file= 'Concentration2.out', form= 'formatted',
    & status = 'unknown')

        Write(165,167) (i,i=1,M)

167  Format(15X, 200I10)

    do j = N, 1,-1

        Write(165,166) j,(con(i,j,1),i=1,M)

166  Format (1X,'j=',I3,3X, 'Concent.=',200E10.3)
    enddo
    open (unit=191, file= 'Fracc.out',form= 'formatted',
    & status = 'unknown')

        Write(191,192) (i,i=1,M+1)
192  Format(21X, 200I15)

    do j = N, 1, -1
        Write(191,193) j,(Fracc(i,j,1),Fracc(i,j,2),Fracc(i,j,3),
    &i=1,M)
    enddo

193  Format (1X,'j=',I3,3X,'Frac(1), Frac(2), Frac(3)=' ,100F5.3,2X,

```



```

&100F5.3,2X,100F5.3)
c 54  Format(15X, 200I10)

```

```

open (unit=168, file= 'densi2.out', form= 'formatted',
& status = 'unknown')

```

```

Write(168,169) (i,i=1,M)

```

```

169  Format(15X, 200I10)

```

```

do j = N, 1,-1

```

```

Write(168,170) j,(rhonb(i,j,1),i=1,M)

```

```

Write(168,170) j,(rhonb(i,j,2),i=1,M)

```

```

enddo

```

```

do j = N, 1,-1

```

```

Write(168,170) j,(rho(i,j),i=1,M)

```

```

enddo

```

```

170  Format (1X,'j=',I3,3X, 'Densities=. ',200f10.1)

```

```

c*****Eddy Viscosity*****

```

```

open (unit=172, file= 'viscosity.out', form= 'formatted',
& status = 'unknown')

```

```

Write(172,173) (i,i=1,M)

```

```

173  Format(15X, 200I10)

```

```

do j = N, 1,-1

```

```

Write(172,174) j,(nut(i,j,2),i=1,M)

```

```

174  Format (1X,'j=',I3,3X, 'Visc=',200E10.3)

```

```

enddo

```

```

c*****Turbulence Function*****

```

```

open (unit=175, file= 'TurbFunc.out', form= 'formatted',
& status = 'unknown')

```

```

        Write(175,176) (i,i=1,M+1)

176  Format(15X, 200I10)

        do j = N+1, 1,-1
            Write(175,177) j,(Turb(i,j),i=1,M+1)
177  Format (1X,'j=',I3,3X, 'Turb(l)=' ,200E10.3)
        enddo
c*****Radius *****
        open (unit=178, file= 'radius.out', form= 'formatted',
            & status = 'unknown')

        Write(178,179) (i,i=1,M)

179  Format(15X, 200I10)

        do j = N, 1,-1
            Write(178,180) j,(r(i,j),i=1,M)
180  Format (1X,'j=',I3,3X, 'radius=' ,200f10.3)
        enddo
c*****Stream Function*****

        open (unit=181, file= 'StreamFunc.out', form= 'formatted',
            & status = 'unknown')

        Write(181,182) (i,i=1,M+1)

182  Format(15X, 200I10)

        do j = N+1, 1,-1

            Write(181,183) j,(psi(i,j),i=1,M+1)

183  Format (1X,'j=',I3,3X, 'Psi(i,j)=' ,200E10.3)
        enddo

c*****Theta Velocity*****

        open (unit=192, file= 'TheTaVeloc.out', form= 'formatted',
            & status = 'unknown')

        Write(192,182) (i,i=1,M+1)

```

```
c 182  Format(15X, 200I10)
```

```
do j = N+1, 1,-1
```

```
Write(192,184) j,(Vth(i,j,2),i=1,M+1)
```

```
184  Format (1X,'j=',I3,3X, 'Vth(i,j)=' ,200E10.3)
      enddo
```

```
open (unit=193, file= 'DragCoeff.out', form= 'formatted',
& status = 'unknown')
```

```
Write(193,179) (i,i=1,M)
```

```
do j = N, 1,-1
```

```
Write(193,185) j,(CDv(i,j),i=1,M)
```

```
enddo
```

```
185  Format (1X,'j=',I3,3X, 'DragCo=' ,200f10.3)
```

```
If(Mrecir.EQ.2.AND.NSlope.eq.0.And.NCrosby.eq.0) then
```

```
j=1
```

```
Sum=0.0
```

```
do i=1,M
```

```
Sum=Sum+con(i,j,1)
```

```
Avg=Sum/M
```

```
enddo
```

```
Write(*,*)'Avg Recirculation Con', Avg
```

```
Else If(Mrecir.EQ.2.AND.NSlope.eq.0.And.NCrosby.eq.1) then
```

```
j=1
```

```
Sum=0.0
```

```
do i=1,M
```

```
Sum=Sum+con(i,j,1)
```

```
Avg=(Sum+Con(icrosby+1,j,2))/M
```

```
enddo
```

```
Write(*,*)'Avg Recirculation Con', Avg
```

```

Else if(Mrecir.EQ.2.AND.NSlope.gt.0) then
  Sum=0.0
  j=1
  do i=1,M
    Sum=Sum+con(i,j,1)*mask(i,j)

  enddo

  do j=2,N
    do i=1,M
      Sum=Sum+con(i,j,1)*mask(i,j)*(1-mask(i,j-1))
    enddo
  enddo
  Avg=Sum/M
  Write(*,*)'Avg Recirculation Con', Avg

endif

if(Mrecir.EQ.1) then
  Sum=0.0
  j=1
  do i=ihopst,ihopper-1
    Sum=Sum+con(i,j,1)*mask(i,j)
  enddo

  do j=2,N/2
    do i=ihopst,ihopper-1
      Sum=Sum+con(i,j,1)*mask(i,j)*(1-mask(i,j-1))
    enddo
  enddo
  Avg=Sum/(ihopper-ihopst)
  Write(*,*)'Avg Recirculation Con', Avg
endif

If(NLaunder.eq.2) then

  Write(*,*)'Outlet Concentration', Con(M,N,2)

  Else if (Nlaunder.eq.1) Then
    Sum2=0.0
    Count=0
    j=N
    do i=1,M

```

```

        If (Vn(i,j).gt.0) then
        Count=Count+1
        Sum2=Sum2+con(i,j,1)
        endif
    enddo
    Avg2=Sum2/Count
    Write(*,*)'Outlet Concentration', Avg2

    endif
    write(*,*)'no. ',mm
stop
end

```

```

c*****MODEL SUBROUTINES*****
c*****

```

```

c*****
c*****SUBROUTINE: INFILE*****

```

```

    subroutine infile
    Include 'comdeck3.h'
    REAL nuo, nut,LL,mask,maskk,NBl,Inlet,maski,maske
    INTEGER IPRINT

```

```

        SOR = SORA
        Write(*,*)'_____ '

```

```

c*****SETTLING PROPERTIES*****

```

```

        read(31,*) Vmax
        Write(*,500) 'Maximum Settling Velocity (m/h) = ',Vmax
        Vmax = Vmax/3600.0

        read(31,*) Fsp

        Write(*,500) 'Floc Settling Parameter (m^3/Kg) = ',Fsp

        read(31,*) Csp

        Write(*,500) 'Colloids Settling Parameter (m^3/Kg) = ',Csp

        read(31,*) Cmin

        Write(*,501) 'Concentration of nonsettling floc (Kg/m3) =',Cmin

```

```

c      read(31,*) Dummy                                !nonNewtonian exponent

      read(31,*) Vcom

      Write(*,500) 'Compression Settling velocity (m/h) =' ,Vcom
      Vcom = Vcom/3600.0

      read(31,*) Fcom

      Write(*,500) 'Compression Settling Parameter (m^3/Kg) =' ,Fcom

      read(31,*) IFloc

c*****FLOCCULATION KINETIC CONSTANTS*****

      Write(*,*) 'Modeling Flocculation (Yes=1, No= 2)' ,IFloc

      If (Ifloc.eq.1) then

        read(31,*) FKds

        Write(*,500) 'Flocculation Constant for Diff. Settling (Turb.)=',
        &FKds

        read(31,*) FKa

        Write(*,505) 'Flocculation Constant for Aggregation,Ka (L/g)=' ,FKa

        read(31,*) FKb

        Write(*,505) 'Flocculation Constant for Breakup, Kb (sec)= ' ,FKb

        read(31,*) Fm

        Write(*,500) 'Floc Breakup rate coefficient= ' ,Fm

        read(31,*) Thind

        Write(*,506) 'Threshold for hindered Settling (mg/L) = ' ,Thind

        Thind=Thind/1000.0

        read(31,*) Tdis

        Write(*,506) 'Threshold for discrete Settling (mg/L) = ' ,Tdis

```

```

Tdis=Tdis/1000.0

read(31,*) Nfraction

Write(*,507) 'Number of Fractions for Discretes Particles =',
&Nfraction

Do i=1,Nfraction

read(31,*) frac(i)

Write(*,508) 'Fraction', i , 'in influent = ', frac(i)

read(31,*) Vfrac(i)

Write(*,509) 'Settling velocity for fraction ',i',(m/h) =',
& Vfrac(i)

enddo

Else if(Ifloc.eq.2) then

FKds = 0.0

FKa = 0.0

FKb = 0.0

Fm=0.0

Read(31,*) Dummy

Read(31,*) Dummy

Read(31,*) Dummy

Read(31,*) Dummy

read(31,*) Thind

Write(*,506) 'Threshold for hindered Settling (mg/L) = ',Thind

Thind=Thind/1000.0

```

```

read(31,*) Tdis

Write(*,506) 'Threshold for discrete Settling (mg/L) = ',Tdis

Tdis=Tdis/1000.0

read(31,*) Nfraction

Write(*,507) 'Number of Fractions for Discretes Particles =',
&Nfraction

Do i=1,Nfraction

read(31,*) frac(i)

Write(*,508) 'Fraction', i , 'in influent = ', frac(i)

read(31,*) Vfrac(i)

Write(*,509) 'Settling velocity for fraction ',i, '(m/h) =',
& Vfrac(i)

Enddo

Else

Write(*,*) 'Warning! Do you want to run the flocculation submodel?'

Endif
c*****GEOMETRY DATA*****
Read(33,*)rmaxin
Read(33,*)rin
Read(33,*)hy
Read(33,*)slope
Read(33,*) Inlet
Read(33,*) WidthIn
Read(33,*) Nport
Read(33,*) InDef !Modeling Inlet Deflector (yes=1, no=0)
Read(33,*) DefAng
IDefAng=Int(DefAng+.001)
DefAng=Defang*pi/180.0

Write(*,*)'_____'
```



```

rinreal=rin

hyyy=hy+slope*(rmaxin-rin)/100.0
Dyyy=hyyy/float(N)

Ninlyy=int((Inlet+.0001)/Dyyy)

Heinlet=Ninlyy*Dyyy

Aopen=Nport*Inlet*WidthIn

Atotal=2*Pi*rinreal*Inlet

rin=Aopen/(2*pi*Heinlet)

VortBoun=1.15*Min(0.5*Rinreal,0.25*Inlet)

Write(*,*)'Atotal,Aopen,Fopen, VortBoun',Atotal,rin,VortBoun

c*****Correction in Inlet Velocity - Momentum by deflector effects

If (InDef.eq.1.And.Sin(DefAng).NE.0) rin=rin/sin(DefAng)

c*****

Write(*,*) 'Cells dimensions (m)'
Write(*,501) 'Dy (m)=' ,Dyyy

Write(*,500) 'Radius of the Clarifier (including inlet,m)' ,rmaxin

Write(*,500) 'Radius of the inlet (m)',rinreal

Write(*,500) 'Effective Radius of the Inlet(m)',Rin

Write(*,500)'Inlet opening Height, m' ,Inlet

Write(*,500)'Effective Inlet opening Height, m' ,Heinlet

Write(*,500)'Inlet opening Width, m' ,WidthIn

Write(*,*)'Number of Ports',Nport

Write(*,*)'Modeling Inlet Deflector (yes=1, no=0)',InDef

If(InDef.eq.1) then

```

```

Write(*,500) 'Deflector Angle (degrees) =',DefAng*180./pi

Write(*,501) 'Deflector Angle (radians) =',DefAng

endif

Write(*,500) 'End Wall Depth of circular tank (m)',hy

Write(*,500) 'Bottom slope (%)',slope

hy=hy+slope*(rmaxin-rinreal)/100.0

Write(*,500) 'Inlet Wall Depth of circular tank (m)',hy

NSlope=Int(Slope+0.9)
If(slope.lt.0.0) then
NSlope=Int(slope-0.9)
endif

c*****Radius calculations*****
rmax=rmaxin-rin
c*****Grid Calculations*****

Dr=rmax/float(M)

Dy=hy/float(N)

rf= Dr/Dy

c*****Ninl Calculation
Ninl=int((Inlet+.0001)/Dy)
c*****
Write(*,*)'Inlet cells', Ninl

Write(*,*)'_____ '
Write(*,*) 'Cells dimensions (m)'
Write(*,501) 'Dr (m)=' ,Dr
Write(*,501) 'Dy (m)=' ,Dy

c*****Mask****Bottom Slope*****
c Bed Slope

```

```

IB=1
  LS=1
  L=1
  xs(L,IB,1)=0.0
  ys(L,IB,1)=0.0
  xs(L,IB,2)=rmax      !
  ys(L,IB,2)=Slope*(rmaxin-rinreal)/100.0    ! Usually +ve
  if(slope.lt.0.0) then
    ys(L,IB,1)= -ys(L,IB,2)
    ys(L,IB,2)=0.0
  Write(*,*)'Slope if',Slope,NSlope
  endif
  So(L)=(ys(L,IB,2)-ys(L,IB,1))/(xs(L,IB,2)-xs(L,IB,1))
  Write(*,*)'Slope ',So(L),NSlope

c*****
*****
      g=9.81
      pi=4.0*atan(1.0)
      nuo=0.000001
      wz=2*pi
c    wz = perimeter of a circumference
      xl=rmax
c    xl = equivalent length
c    hy = depth of circular tank
c    ras = recycle ratio

      Q=SOR*pi*(rmaxin*rmaxin - rinreal*rinreal)
      If (Iras.eq.1) then

        Qras=ras*Q

      Endif
      Q1=Q+Qras
      psio=Q1/wz
      xxm=xl/Dr +.1
  Write(*,*)'_____ '

  Write(*,502) 'Average Influent Flow Rate (m3/s)',Q1
  Write(*,502) 'Average Effluent Flow Rate (m3/s)',Q
  Write(*,502) 'Average Recirculation Flow Rate (m3/s)',Qras

c*****Vorticity and Dye Concentration at T=0*****

  do 1 i=1,M+1

```

```

        do 1 j=1,N+1
        rho(i,j)=Densr(i,j)
        Con(i,j,1)=0.0
        vort(i,j,1)=0.0
        Maske(i,j)=1.0

        nut(i,j,1)=nuo
        nut(i,j,2)=nuo
1      psi(i,j)=0.0

c*****Mask for Boundary Condition-Psi Function*****

        L=1
        IB=1
        do 101 i=1,M
        do 101 j=1,N
        Mask(i,j)=1.0
        Maskk(i,j)=1.0
        Maski(i,j)=1.0
c      Maske(i,j)=1.0

        xss=(float(i)-0.5)*Dr
        yss=(float(j)-0.5)*Dy
        ybc=So(L)*xss+ys(L,IB,1)

        if (yss.le.ybc.AND.Slope.gt.0.0) then
        Mask(i,j)=0.0
        psi(i,j)=(Q1-Q)/wz
        psi(i,j+1)=(Q1-Q)/wz

        Else if (yss.le.ybc.AND.Slope.lt.0.0) then
        Mask(i,j)=0.0
        psi(i,j)=(0.0)/wz
        psi(i,j+1)=(0.0)/wz

        endif
101  continue
C*****BAFFLES*****
*****
c*****Baffle at Center Well (Maskk) *****
        Write(*,*)'_____ '
        read(33,*) NCenter
        Write(*,*) 'Modeling Center Well(yes=1, no=0)' ,Ncenter

        If(NCenter.eq.1) then

```

```

    read(33,*) RCenter
    Write(*,500) 'Center Well Radius (m)' ,Rcenter

    RCenter=RCenter-rin

    read(33,*) HCenter
    Write(*,500) 'Center Well Depth (m)' ,Hcenter

    icenter=int((RCenter+0.0001)/Dr+0.5)+1    !Modified 01/09/2004
    Write(*,*)'Icenter',icenter
    jcenter=int((HCenter+0.0001)/Dy)
    jcenter=N+1-jcenter
    Write(*,*)'jcenter',jcenter

    i=icenter
    do 111 j=jcenter,N
    Maskk(i,j)=0.0

111  continue

    Else
        read(33,*) Dummy
        read(33,*) Dummy
    endif

c*****EDI*****

    read(33,*) NCenter2
    Write(*,*) 'Modeling Vertical- E.D.I. (yes=1, no=0)' ,Ncenter2

    If(NCenter2.eq.1) then
        read(33,*) RCenter2
        Write(*,500) 'EDI Radius (m)' ,Rcenter2

        RCenter2=RCenter2-rin

        read(33,*) HCenter2
        Write(*,500) 'EDI Depth (m)' ,Hcenter2

        icenter2=int((RCenter2+0.0001)/Dr+0.5)+1
        Write(*,*)'Icenter2',icenter2
        jcenter2=int((HCenter2+0.0001)/Dy)
        jcenter2=N+1-jcenter2

```

```

Write(*,*)'jcenter2',jcenter2

i=icenter2

do 112 j=jcenter2,N

Maskk(i,j)=0.0

112 continue

Else
read(33,*) Dummy
read(33,*) Dummy
endif

c*****SCUM BAFFLE*****

read(33,*) NCenter3
Write(*,*) 'Modeling Scum Baffle (yes=1, no=0)' ,Ncenter3

If(NCenter3.eq.1) then
read(33,*) RCenter3
Write(*,500) 'Scum Baffle Radius (m)' ,Rcenter3

RCenter3=RCenter3-rin

read(33,*) HCenter3
Write(*,500) 'Scum Baffle Depth (m)' ,Hcenter3

icenter3=int((RCenter3+0.0001)/Dr+0.5)
Write(*,*)'Icenter3',icenter3
jcenter3=int((HCenter3+0.0001)/Dy)
jcenter3=N+1-jcenter3
Write(*,*)'jcenter3',jcenter3

i=icenter3

do 113 j=jcenter3,N

Maskk(i,j)=0.0

113 continue

```

```

Else
    read(33,*) Dummy
    read(33,*) Dummy
endif

Write(*,*)'_____ '

c***** Baffles at Inlet Wall (Maski) *****
    read(33,*) NBainl
    Write(*,*) 'Canopy Baffle at the Inlet Wall(yes=1, no=0)' ,NBainl

    If(NBainl .eq.1) then

        read(33,*) RBainl
        Write(*,500) 'Canopy Baffle Radius (m)',RBainl

        RBainl=RBainl-rin

        read(33,*) HBainl
        Write(*,500) 'Canopy Baffle Depth (m)' ,HBainl

        iBainl=int((RBainl+0.0001)/Dr+0.5)
        Write(*,*)'iBainl',iBainl

        jBainl=int((HBainl+0.0001)/Dy)
        jBainl=N-jBainl
        Write(*,*)'jBainl',jBainl

        j=jBainl
        do i=1,iBainl
            Maski(i,j)=0.0
        enddo
        Else
            read(33,*) Dummy
            read(33,*) Dummy
        endif
    c 112 continue
c***** Baffles at Outer Wall (Maske) *****
read(33,*) NBAoule
    Write(*,*) 'Modeling Peripheral Baffle (yes=1, no=0)',
    & NBAoule

```

```

    If(NBaoule.eq.1) then

        read(33,*) HBaoule
        Write(*,500) 'Peripheral Baffle Depth (m)',HBaoule

        read(33,*) RBaoule
        Write(*,500) 'Peripheral Baffle Length(m)',RBaoule

        jBaoule=Int(Hbaoule/Dy+0.5)

        iBaoule=Int(RBaoule/Dr+0.5)

        j=N-jBaoule-iBaoule+1
        do i=M+1,M+1-iBaoule,-1
Maske(i,j)=0.0
        enddo

        Do j=N-jBaoule-iBaoule+2,N-jBaoule

            do i=M+1,M+1-iBaoule,-1

                if (Maske(i-1,j-1).eq.0) then
                    Maske(i,j)=0.0
                endif
            enddo

        enddo
    Else
        read(33,*) Dummy
        read(33,*) Dummy
    endif
c***** Crosby Vertical Baffles or Mid-Radius Baffle*****
        read(33,*) NCrosby
        Write(*,*) 'Modeling Mid-radius Baffle (yes=1, no=0)',NCrosby

        If(NCrosby.eq.1) then
            read(33,*) RCrosby
            Write(*,500) 'Mid-radius Baffle Radius (m)', RCrosby
c 366 Format (1X,A,2X,1F5.2)
            RCrosby=RCrosby-rin

            read(33,*) HCrosby
            Write(*,500) 'Mid-radius Baffle Height (m)', HCrosby

```



```

        icrosby=int((RCrosby+0.0001)/Dr+0.5)
        Write(*,*)'Icrosby',icrosby
        jcrosby=int((HCrosby+0.0001)/Dy)
        Write(*,*)'jcrosby',jcrosby

        i=icrosby

        Hinitial=Slope*(i*Dr)/100.0
        jini=Max(Int(Hinitial/Dy),1)

        Do j=jini,jini+jcrosby-1,1
            Mask(i,j)=0.0
c        Write(*,*)'i,j,Mask(i,j)',i,j,Mask(i,j)
        enddo
        Else
            read(33,*) Dummy
            read(33,*) Dummy
        endif

c*****Boundary Condition for Psi Function*****

        i=1
        do ii=1,Ninl
            j=N-(ii-1)
            psi(i,j)=(Ninl-ii)*Q1/((Ninl)*Wz)
        enddo

        Write(*,*)'_____ '
        read(37,*) NLaundry
        Write(*,*) 'Type of Outlet: Inboard=1, Outboard=2 ',NLaundry

        If(NLaundry.eq.1) then

            read(37,*) LL
            Write(*,500) 'Width of Laundry(m) = ',LL

            mt=int(LL/Dr+0.0001)

            read(37,*) EW
            Write(*,500) 'End Wall Clearance (m) = ',EW

```

```

        Iew = jfix(ew/Dr+0.00001)

        i=M+1
        do 2 j=1,N+1
2      psi(i,j)=(Q1-Q)/wz

        j=N+1
        do 3 i=1,M+1-(mt+Iew)
3      psi(i,j)=Q1/wz

        j=N+1
        do 35 mtt=1,mt-1

        i=M+1-(mt+Iew-mtt)
        psi(i,j)=(Q1-Q*mtt/mt)/wz

35    HL=mt*Dr
        Write(*,*)'Length of Launder = ',HL
        write(*,*)'End Wall Clearance = ',EW

        j=N+1
        do 30 i=M+1-Iew,M+1
30    psi(i,j)=(Q1-Q)/wz

        Else If(NLaunder.eq.2) then

        j=N+1
        do 33 i=1,M+1
33    psi(i,j)=Q1/wz

        i=M+1
        do 22 j=1,N-1
22    psi(i,j)=(Q1-Q)/wz

        i=M+1
        j=N
        psi(i,j)=(Q1-Q)/(wz)

        endif

        Write(*,*)'
        Read(38,*) Mrecir

```

```

        Write(*,*)'Type of Outlet Recirculation:Hopper=1, Suction =2',
        & Mrecir
c jam needs modification for -ve slopes
        If(Mrecir.eq.1) then
            Read(38,*) Ahopper
            Write(*,500)'Length of Hopper = ',Ahopper

Read(38,*) Rhopper
        Write(*,500)'Starting radius of hopper = ',Rhopper

        ihopst=jfix((rhopper-rin)/Dr + 1.)
        ihopper=Int(Ahopper/Dr+0.00001)+ihopst
        write(*,*)'ihopst',ihopst,ihopper

        do i=1,ihopst
            do j=1,N
                if (Mask(i,j).eq.0.or.j.eq.1)then
                    psi(i,j)=0.0
                endif
            enddo
        enddo

        do i=ihopst+1,ihopper
            do j=1,N
                if (Mask(i,j).eq.0.or.j.eq.1)then
                    psi(i,j)=(Q1-Q)*(i-ihopst)/(wz*(ihopper-ihopst))
                endif
            enddo
        enddo

        j=1
        do i=ihopper,M+1
            do j=1,N
                if (Mask(i,j).eq.0.or.j.eq.1)then
                    psi(i,j)=(Q1-Q)/wz
                endif
            enddo
        enddo

        else if(Mrecir.eq.2.AND.NCrosby.eq.0) then
            j=1
            do i=2,M
                do j=1,N
                    if (Mask(i,j).eq.0.or.j.eq.1)then

```

```

    psi(i,j)=(Q1-Q)*(i-1)/(wz*M)
    endif
enddo
enddo

    do 44 j=1,N+1
do 44 i=2,M+1

    if (yss.le.ybc) then

        psi(i,j)=(Q1-Q)*(i-1)/(wz*M)
        psi(i,j+1)=(Q1-Q)*(i-1)/(wz*M)

    endif
44 continue

    else if(Mrecir.eq.2.AND.NCrosby.eq.1) then

        j=1
        do i=2,M
psi(i,j)=(Q1-Q)*(i-1)/(wz*M)
enddo

        do 45 j=1,N+1
do 45 i=2,Icrosby

    if (yss.le.ybc) then

        psi(i,j)=(Q1-Q)*(i-1)/(wz*M)
        psi(i,j+1)=(Q1-Q)*(i-1)/(wz*M)

    endif
45 continue

        do 46 j=1,N+1
do 46 i=Icrosby+2,M+1

    if (yss.le.ybc) then

        psi(i,j)=(Q1-Q)*(i-1)/(wz*M)
        psi(i,j+1)=(Q1-Q)*(i-1)/(wz*M)

    endif
46 continue

        do 47 j=jini,jini+jcrosby,1
do 47 i=icrosby,icrosby+1

```

```

        psi(i,j)=(Q1-Q)*(icrossby-1)/(wz*M)
47 continue
    endif
c***** Boundary for Negative Slope *****

    if (Slope.lt.0.0) then

        j=1

        do i=1,M+1

            psi(i,j)=0.0

        enddo

    endif

c*****Scrapper Input Data*****
    Write(*,*)'_____ '
    read(39,*) NScraper
    Write(*,*) 'Simulating Scrapper. yes=1 no=2 ',NScraper

    read(39,*) NSctype

    If(NSctype.eq.1.AND.NScrapper.eq.1) then

        Write(*,*)'Simulating Rake Type Scrapper'

        Fscr=1.0

    Else If(NSctype.eq.2.AND.NScrapper.eq.1) then

        Write(*,*)'Simulating Spiral Type Scrapper'

        Fscr=pi

    Else If(NScraper.eq.1) then

        Write(*,*)'Warning: Type of Scrapper?'

    endif

    Write(*,500)'Scrapper Factor',Fscr

```

```

Write(*,*)'Drag Coefficient: Variable'

if(NScraper.EQ.2) then
  HBL=0.0
  NBL=0.0
  WBL=0.00167/60.0
  Fscr=1.0

  else
    read(39,*) HBl
    Write(*,500) 'Height of Blade (m) = ',HBl

    read(39,*) WBl
    Write(*,502) 'Angular Velocity of the blades (rpm) =',
    &WBl

    WBL=WBL*2.0*Pi/60.0
    read(39,*)   BlaAng
    Write(*,500) 'Angle of the Blade (degrees) =',BlaAng

    BlaAng=BlaAng*pi/180.0

    read(39,*) Narm
    Write(*,*) 'Number of Arms =',Narm

c*****Scrapper Cycle*****

    NScycle=Int((2*pi)/(Narm*Wbl))

    If(NSctype.eq.1) then      !Rake

    NScontrol=Int(1/Wbl)

    Else

    NScontrol=Int(pi/Wbl)      !Spiral

    Endif

    Write(*,500)'Scrapper Starts at (minutes)',(NScycle-NScontrol)/60.

!Quasi - 3D approach

```

C*****SURFACE HEAT EXCHANGE DATA*****

Write(*,*)'_____'

read(42,*) Nheat

Write(*,*) 'Modeling Heat Exchange. yes=1 no=2 ',Nheat

If (Nheat.eq.1) then

read(42,*) Stim

Write(*,500) 'Starting Time of Run (hours) =',Stim

read(42,*) Hday

Write(*,503) 'Julian day =',Hday

read(42,*) HLati

Write(*,504) 'Local Latitude =',HLati

Decl=23.45*Sin((2*pi*(284+Hday)/365))

Write(*,504) 'Declination Angle, degrees =',Decl

Sins=Sin(Decl*pi/180)*Sin(HLati*pi/180)

Coss=Cos(Decl*pi/180)*Cos(HLati*pi/180)

read(42,*) Nturb

Write(*,*) 'Turbidity Factor =',Nturb

read(42,*) ClouN !Fraction of Sky obscured by clouds

Clouf=(1.-(1.-(0.18+0.024*ClouN/1000.))*ClouN)

Write(*,500) 'Cloud Cover Factor =',Clouf

read(42,*) Tdew

```

Write(*,500) 'Dew Point Temperature, C degrees=',Tdew

      eair=4.596*exp(17.27*Tdew/(237.3+Tdew))

Write(*,500) 'Air vapor pressure, mm Hg=',eair

      Ea=(0.740+0.00653*eair)*(1+(0.1662-0.0039*eair)*ClouN)

Write(*,500) 'Ea =',Ea

      read(42,*) Tama

Write(*,500) 'Maximum Air Temperature, C degrees=',Tama

      read(42,*) Timi

Write(*,500) 'Minimum Air Temperature, C degrees=',Timi

      read(42,*) Uwind

Write(*,500) 'Wind Speed (at 7 m), m/s =',Uwind

      FUw=19.0+0.95*(Uwind*Uwind)    !cal/(cm2 d mmHg)

Write(*,500) 'FUw=',FUw

      endif


500 Format (1X,A,2X,1F5.2)

501 Format (1X,A,2X,1F6.3)

502 Format (1X,A,2X,1F7.5)

503 Format (1X,A,2X,1F4.0)

504 Format (1X,A,2X,1F5.1)

505 Format (1X,A,2X,1E10.3)

506 Format (1X,A,2X,1F8.2)

507 Format (1X,A,1X,1I3)

```


508 Format (1X,A,I2,2X,A,1F6.3)

509 Format (1X,A,I2,1X,A,1F6.2)

return
end

C*****
*****LOADING SUBROUTINE*****

```
subroutine load(mm)
  Include 'comdeck3.h'
  REAL nuo, nut,LL,mask,maskk,NBl,Inlet,maski,maske
  INTEGER IPRINT

  g=9.81
  pi=4.0*atan(1.0)
  nuo=0.000001

  If(Iserie.eq.0) then
    t=dt*float(mm)
  if(t.le.Tdi) then
    SOR=SORA*(1. - (pfact - 1.)*cos(2.*pi*t/Tdi))
  else
    SOR=SORA*(1. - (pfact - 1.))*(1./(1. + t/Tdi))
  endif

  Else if(Iserie.eq.1) then
    t=dt*float(mm)

    If(t.lt.(TScount*60.+Tserie*60.)) then  !Minutes to seconds
      SOR=SORA

    Else

      ITcount=Int(t/(60.*Tserie)+1.00001)

      SORA=SORAa(ITcount)

      Tscount= Tscountt(ITcount)

      Dyeo=Dyeoo(ITcount)

      Tempo=Tempoo(ITcount)
```

SORA=SORA/3600.

```
        Write(*,*) 'ITcount',ITcount
        Write(*,303) 'Change on SOR, minutes', mm*dt/60.
Write(*,291) 'SOR (m/h)',SORA*3600
Write(*,303) 'Tscout(min)',Tscout
Write(*,291) 'Influent Temperature in degrees Celsius',Tempo
        SOR=SORA
        endif
    endif
291 Format (1X,A,2X,1F5.2)
294 Format (1X,A,2X,1F6.4)
296 Format (A,A,A)
297 Format (1X,A,2X,1F6.2)
303 Format (1X,A,2X,1F8.1)
```

```
Q=SOR*pi*(rmaxin*rmaxin - rin*rin)
If (Iras.eq.1) then
```

```
Qras=ras*Q
```

```
Endif
Q1=Q+Qras
```

```
psio=Q1/wz
```

c***Boundary Condition for Psi Function*******

```
        i=1
        do ii=1,Ninl

            j=N-(ii-1)
            psi(i,j)=(Ninl-ii)*Q1/((Ninl)*Wz)

        enddo
```

```
        If(NLaundry.eq.1) then
```

```
        Iew = jfix(ew/Dr+0.00001)
```

```
        i=M+1
        do 2 j=1,N+1
```

```

2   psi(i,j)=(Q1-Q)/wz

      j=N+1
      do 3 i=1,M+1-(mt+Iew)
3   psi(i,j)=Q1/wz
      j=N+1
      do 35 mtt=1,mt-1

        i=M+1-(mt+Iew-mtt)
        psi(i,j)=(Q1-Q*mtt/mt)/wz

35  HL=mt*Dr

      j=N+1
      do 30 i=M+1-Iew,M+1
30  psi(i,j)=(Q1-Q)/wz

      Else If(NLaunder.eq.2) then

        j=N+1
        do 33 i=1,M+1
33  psi(i,j)=Q1/wz

        i=M+1
        do 22 j=1,N-1
22  psi(i,j)=(Q1-Q)/wz

        i=M+1
        j=N
        psi(i,j)=(Q1-Q)/(wz)

      endif

      If(Mrecir.eq.1) then

        ihopst=jfix((rhopper-rin)/Dr + 1.)
        ihopper=Int(Ahopper/Dr+0.00001)+ihopst

        do i=1,ihopst
          do j=1,N
            if (Mask(i,j).eq.0.or.j.eq.1)then
              psi(i,j)=0.0
            endif
          enddo
        enddo
      enddo

```

```

do i=ihopst+1,ihopper
do j=1,N
if (Mask(i,j).eq.0.or.j.eq.1)then
psi(i,j)=(Q1-Q)*(i-ihopst)/(wz*(ihopper-ihopst))
endif
enddo
enddo

j=1
do i=ihopper,M+1
do j=1,N
if (Mask(i,j).eq.0.or.j.eq.1)then
psi(i,j)=(Q1-Q)/wz
endif
enddo
enddo

else if(Mrecir.eq.2.AND.NCrosby.eq.0) then
j=1
do i=2,M
do j=1,N
if (Mask(i,j).eq.0.or.j.eq.1)then
psi(i,j)=(Q1-Q)*(i-1)/(wz*M)
endif
enddo
enddo

do 44 j=1,N+1
do 44 i=2,M+1

if (yss.le.ybc) then

psi(i,j)=(Q1-Q)*(i-1)/(wz*M)
psi(i,j+1)=(Q1-Q)*(i-1)/(wz*M)

endif
44 continue

else if(Mrecir.eq.2.AND.NCrosby.eq.1) then

j=1
do i=2,M
psi(i,j)=(Q1-Q)*(i-1)/(wz*M)
enddo

```

```

        do 45 j=1,N+1
        do 45 i=2,Icrosby

            if (yss.le.ybc) then

                psi(i,j)=(Q1-Q)*(i-1)/(wz*M)
                psi(i,j+1)=(Q1-Q)*(i-1)/(wz*M)

            endif
45 continue
        do 46 j=1,N+1
        do 46 i=Icrosby+2,M+1

            if (yss.le.ybc) then

                psi(i,j)=(Q1-Q)*(i-1)/(wz*M)
                psi(i,j+1)=(Q1-Q)*(i-1)/(wz*M)

            endif
46 continue
        do 47 j=jini,jini+jcrosby,1
        do 47 i=icrosby,icrosby+1
            psi(i,j)=(Q1-Q)*(icrosby-1)/(wz*M)
47 continue
        endif
c***** Boundary for Negative Slope *****

        if (Slope.lt.0.0) then
            j=1
            do i=1,M+1
                psi(i,j)=0.0
            enddo
        endif
        return
    end

c*****
c*****SUBROUTINE: RADIUS*****

    subroutine radius
        Include 'comdeck3.h'
        REAL nuo, nut,LL,mask,maskk,NBl,Inlet,maski,maske
        INTEGER IPRINT

        do j=1,N
            do i=1,M

```

```

r(i,j)=rin+float(i-1)*Dr
bf(i,j)=Dr/(2.*r(i,j))
af(i,j)=(rf*rf)*(1. - bf(i,j)*bf(i,j))

c*****Vtc - Calculation
Vtc(i,j)=(r(i,j)*dr+dr*dr/2.0)/(r(i,j)+dr/2.0)
c*****

Vol(i,j)=dy*(r(i,j)*dr+dr*dr/2.0)

If (NSlope.ne.0) then
Vbl(i,j)=-Slope*Wbl*(r(i,j)+dr/2.0)*sin(BlaAng)*Cos(BlaAng)
&/Abs(slope)

else
Vbl(i,j)=-Wbl*(r(i,j)+dr/2.0)*sin(BlaAng)*Cos(BlaAng)
endif

enddo
enddo
return
end
c*****
c*****SUBROUTINE: HYDROD*****

subroutine hydrod(mm)
c face densities from node densities
c include 'comdeck'
Include 'comdeck3.h'
REAL nu0, nut,LL,mask,maskk,NBl,Inlet,maski,maske
INTEGER IPRINT

c Iterative Solution

c Hydrodynamic - Check Output
c*****Hydrodynamic Modified by Mask*****
do 7 L=1,2*(M+N) !500

do 7 j=2,N
do 7 i=2,M
xss=(float(i)-0.5)*Dr

```

```

yss=(float(j)-0.5)*Dy
ybc=Slope*xss/100.

if(Slope.ge.0.0.AND.mask(i,j-1)*mask(i,j).eq.0.AND.Mrecir.eq.1.
&AND.i.le.(ihopst)) then

    psi(i,j)=0.0
    psi(i,j+1)=0.0

    else if(Slope.ge.0.0.AND.mask(i,j-1)*mask(i,j).eq.0.AND.Mrecir.
&eq.1.AND.i.ge.(ihopst+1).AND.i.le.(ihopper-1)) then

        psi(i,j)=(Q1-Q)*(i-ihopst)/(wz*(ihopper-ihopst))
        psi(i,j+1)=(Q1-Q)*(i-ihopst)/(wz*(ihopper-ihopst))

        else if(Slope.ge.0.0.AND.mask(i,j-1)*mask(i,j).eq.0.
&AND.Mrecir.eq.1) then

            psi(i,j)=(Q1-Q)/wz
            psi(i,j+1)=(Q1-Q)/wz

            else if(Slope.ge.0.0.AND.mask(i-1,j)*mask(i-1,j-1).eq.0.
&AND.Mrecir.eq.1) then
                psi(i,j)=(Q1-Q)/wz

c*****Psi for Negative Slope*****
    else if(Slope.lt.0.0.AND.mask(i,j-1)*mask(i,j)*mask(i-1,j-1).eq.0)
&then
        psi(i,j)=(0.0)/wz
c*****
    else if(maskk(i,j).eq.0) then

        psi(i,j)=(Q1)/wz
        psi(i,j+1)=(Q1)/wz

        else if(maskk(i-1,j).eq.0) then
            psi(i,j)=(Q1)/wz
            psi(i,j+1)=(Q1)/wz

        else if(maski(i,j).eq.0) then

            psi(i,j)=(0.0)/wz
            psi(i,j+1)=(0.0)/wz

            else if(maski(i-1,j).eq.0) then

```

```

psi(i,j)=(0.0)/wz
    psi(i,j+1)=(0.0)/wz

    else if(maski(i-1,j-1).eq.0) then
psi(i,j)=(0.0)/wz
    else if(maski(i,j-1).eq.0) then
psi(i,j)=(0.0)/wz

    else if(maske(i,j).eq.0) then

psi(i,j)=(Q1-Q)/wz
    psi(i,j+1)=(Q1-Q)/wz

    else if(maske(i,j).eq.1. AND. maske(i+1,j).EQ.0. AND.
& maske(i,j-1).EQ.1) then
psi(i+1,j)=(Q1-Q)/wz
    psi(i+1,j+1)=(Q1-Q)/wz

    psi(i,j)=(1.-OveR)*psi(i,j)+OveR*
&(psi(i-1,j)+psi(i+1,j) +(psi(i,j-1)+psi(i,j+1))*af(i,j)
&-(psi(i+1,j)-psi(i-1,j))*bf(i,j)+
&((vort(i,j,2)+vort(i-1,j,2)+vort(i-1,j-1,2)+vort(i,j-1,2))*r(i,j)
&/4.0)*af(i,j)*Dy*Dy)/(2.*(1.+af(i,j)))

c    psi(i,j)=(psi(i-1,j)+psi(i+1,j) +(psi(i,j-1)+psi(i,j+1))*af(i,j)
c    &-(psi(i+1,j)-psi(i-1,j))*bf(i,j)+
c    &((vort(i,j,2)+vort(i-1,j,2)+vort(i-1,j-1,2)+vort(i,j-1,2))*r(i,j)
c    &/4.0)*af(i,j)*Dy**2)/(2.*(1.+af(i,j)))

    else if(maske(i,j-1).eq.0) then
psi(i,j)=(Q1-Q)/wz

c*****
    else if(Mrecir.eq.2.AND.NCrosby.eq.0.AND.mask(i,j-1).eq.0) then

psi(i,j)=(Q1-Q)*(i-1)/(wz*M)
psi(i,j+1)=(Q1-Q)*(i-1)/(wz*M)

    else if(Mrecir.eq.2.AND.NCrosby.eq.1.AND.i.le.icrosby.
&AND.mask(i,j-1).eq.0) then

psi(i,j)=(Q1-Q)*(i-1)/(wz*M)
psi(i,j+1)=(Q1-Q)*(i-1)/(wz*M)

```



```

        else if(Mrecir.eq.2.AND.NCrosby.eq.1.AND.i.ge.(icrossby+2).
&AND.mask(i,j-1).eq.0) then

            psi(i,j)=(Q1-Q)*(i-1)/(wz*M)
            psi(i,j+1)=(Q1-Q)*(i-1)/(wz*M)

        else if(Mrecir.eq.2.AND.NCrosby.eq.1.AND.i.eq.(icrossby).
&AND.(j.ge.jini.AND.j.le.(jini+jcrossby))) then
            psi(i,j)=(Q1-Q)*(icrossby-1)/(wz*M)

        else if(Mrecir.eq.2.AND.NCrosby.eq.1.AND.i.eq.(icrossby+1).
&AND.(j.ge.1.AND.j.le.(jini+jcrossby))) then      !Change jini by 1

            psi(i,j)=(Q1-Q)*(icrossby-1)/(wz*M)

c *****
        else if(mm.eq.1) then

            psi(i,j)=(1.-OveR)*psi(i,j)+OveR*
            &(psi(i-1,j)+psi(i+1,j) +(psi(i,j-1)+psi(i,j+1))*af(i,j)
            &-(psi(i+1,j)-psi(i-1,j))*bf(i,j)+
            &((vort(i,j,1)+vort(i-1,j,1)+vort(i-1,j-1,1)+vort(i,j-1,1))*r(i,j)
            &/4.0)*af(i,j)*Dy*Dy)/(2.*(1.+af(i,j)))

        else
c      Successive Over-Relaxation Iterative Technique

            psi(i,j)=(1.-OveR)*psi(i,j)+OveR*
            &(psi(i-1,j)+psi(i+1,j) +(psi(i,j-1)+psi(i,j+1))*af(i,j)
            &-(psi(i+1,j)-psi(i-1,j))*bf(i,j)+
            &((vort(i,j,2)+vort(i-1,j,2)+vort(i-1,j-1,2)+vort(i,j-1,2))*r(i,j)
            &/4.0)*af(i,j)*Dy**2)/(2.*(1.+af(i,j)))

        endif

7    continue

        return
        end

c *****End Subroutine hydrodynamic*****
c *****

```

```

c*****
c*****SUBROUTINE: RHOFAC*****

```

```

subroutine rhofac(mm)
c   face densities from node densities
c   include 'comdeck'
   Include 'comdeck3.h'
   REAL nuo, nut,LL,mask,maskk,NBl,Inlet,maski,maske
   INTEGER IPRINT

c   psi= streamfunction, vort = vorticity
c   u= x velocity, v= y velocity, p = pressure
c   phi=scalar variable, C = Concentration, rho= density
c   Temp(200,100), nut(200,100), Con(200,100)
c   Fnb = face value of advection flux, Dnb=face value of diffusion flux, XX=??
c   rhonb(200,100,nf)= face density of fluid, nf = 1 vert face, nf = 2 horiz face
c   nuoinematic viscosity

   Do i=1,M
      do j=1,N

         Densr(i,j)=(999.8396+18.224944*Temp(i,j,2)
&-0.00792221*Temp(i,j,2)**2
&-(55.4486E-6)*Temp(i,j,2)**3+(149.7562E-9)*Temp(i,j,2)**4-
&(393.2952E-12)*Temp(i,j,2)**5+(0.802-0.002*Temp(i,j,2))*STDS)/
&(1+0.018159725*Temp(i,j,2))

         enddo
      enddo

      do 10 j=1,N
         rho(1,j)=Densr(i,j)+Con(1,j,2)*(1.-1./Spegra)

         rhonb(1,j,1)=rho(1,j)

         rho(M,j)=Densr(i,j)+Con(M,j,2)*(1.-1./Spegra)

         rhonb(M+1,j,1)=rho(M,j)

         rho(M,N)=Densr(i,j)+Con(M,N,2)*(1.-1./Spegra)

         rhonb(M+1,N+1,1)=rho(M,N)

         rhonb(1,N+1,1)=rho(1,N)

```

```

do 10 i=2,M
rho(i,j)=Densr(i,j)+con(i,j,2)*(1.-1./Spegra)

10  rhonb(i,j,1)=(rho(i,j)+rho(i-1,j))/2.
do 11 i=1,M
rho(i,1)=Densr(i,j)+Con(i,1,2)*(1-1./Spegra)

rhonb(i,1,2)=rho(i,1)

rhonb(M+1,1,2)=rho(M,1)
rhonb(M+1,N+1,2)=rho(M,N)
rhonb(i,N+1,2)=rho(i,N)

do 11 j=2,N
c  rhonb(1,j,2)=rho(1,j)
rhonb(M+1,j,2)=rho(M,j)

rho(i,j)=Densr(i,j)+con(i,j,2)*(1-1./Spegra)
11  rhonb(i,j,2)=(rho(i,j)+rho(i,j-1))/2.

c  write(*,*)'rhonb ',rhonb(25,10,1),rhonb(10,20,2)
return
end

c*****
c*****SUBROUTINE: TURMOD*****
c*****Subroutine for the Turbulence Model*****
subroutine Turmod(mm)
c  face densities from node densities
c  include 'comdeck'

Include 'comdeck3.h'
REAL nuo, nut,LL,mask,maskk,NBl,Inlet,maski,maske
INTEGER IPRINT

c  psi= streamfunction, vort = vorticity
c  u= x velocity, v= y velocity, p = pressure
c  phi=scalar variable, C = Concentration, rho= density
c  Temp(200,100), nut(200,100), Con(200,100)
c  Fnb = face value of advection flux, Dnb=face value of diffusion flux, XX=?
c  rhonb(200,100,nf)= face density of fluid, nf = 1 vert face, nf = 2 horiz face
c  nuo = kinematic viscosity
do 110 j=1,N+1

```

```

Gradnb(1,j,1)=0.0

Gradnb(M+1,j,1)=0.0

do 110 i=2,M+1

Gradnb(i,j,1)=(Vs(i,j)-Vs(i-1,j))/Dr

Gradnb(i,j+1,1)=(Vn(i,j)-Vn(i-1,j))/Dr

Gradnb(i+1,j,1)=(Vs(i+1,j)-Vs(i,j))/Dr

110 Gradnb(i+1,j+1,1)=(Vn(i+1,j)-Vn(i,j))/Dr
cccjam write(*,*)'j='j
      j=N+1
do 111 i=1,M+1
cccjam   write(*,*)'i,j='i,j

Gradnb(1,j,2)=0.0

Gradnb(M+1,j,2)=0.0

do 111 j=2,N+1

Gradnb(i,j,2)=(Uw(i,j)-Uw(i,j-1))/Dy

Gradnb(i,j+1,2)=(Uw(i,j+1)-Uw(i,j))/Dy

Gradnb(i+1,j,2)=(Ue(i,j)-Ue(i,j-1))/Dy

111 Gradnb(i+1,j+1,2)=(Ue(i,j+1)-Ue(i,j))/Dy
cccjam   write(*,*)'i,j='i,j


Do i=1,M
Do j=1,N

Grad(i,j)=(sqrt(Gradnb(i,j,1)**2+ Gradnb(i,j,2)**2)+
&sqrt(Gradnb(i,j+1,1)**2+ Gradnb(i,j+1,2)**2)+
&sqrt(Gradnb(i+1,j,1)**2+ Gradnb(i+1,j,2)**2)+
&sqrt(Gradnb(i+1,j+1,1)**2+ Gradnb(i+1,j+1,2)**2))/4.0

enddo
enddo
Do 118 i=1,M
Do 118 j=1,N

```

```

Drho = -rho(i,j+1)+rho(i,j)

Rich(i,j)=Gravi*Drho*Dy/(
&Max((((Uw(i,j)+Ue(i,j))/2)**2),0.0005)*Densr(i,j))

if(Rich(i,j).lt.-10.) then
Rich(i,j)=-10.
ENDIF
if(Rich(i,j).gt.10.) then
Rich(i,j)=10.
ENDIF

If (Rich(i,j).lt.0) then

Damp=Min(10.,Exp(-1.5*Rich(i,j)))

Else

Damp=Max(0.02, Exp(-0.5*Rich(i,j))) !-1.0

endif

If ((con(i,j,1).LE.1).And.(i.le.icenter)) Then

nut(i,j,1)=(0.000001*Exp(1.386294361*con(i,j,1)) +
&1.0*Dcr*Grad(i,j)*(((Turb(i,j)+Turb(i,j+1)+Turb(i+1,j)+
&Turb(i+1,j+1))/4.0)**2)*1.0)

nut(i,j,2)=(0.000001*Exp(1.386294361*con(i,j,1)) +
&Dcy*Grad(i,j)*(((Turb(i,j)+Turb(i,j+1)+Turb(i+1,j)+
&Turb(i+1,j+1))/4.0)**2)*Damp)

Else If (con(i,j,1).LE.1) Then

nut(i,j,1)=(0.000001*Exp(1.386294361*con(i,j,1)) +
&Dcr*Grad(i,j)*(((Turb(i,j)+Turb(i,j+1)+Turb(i+1,j)+
&Turb(i+1,j+1))/4.0)**2)*1.0)

nut(i,j,2)=(0.000001*Exp(1.386294361*con(i,j,1)) +
&Dcy*Grad(i,j)*(((Turb(i,j)+Turb(i,j+1)+Turb(i+1,j)+
&Turb(i+1,j+1))/4.0)**2)*Damp)

Else if (i.le.icenter) then

```

```

      nut(i,j,1)=(0.0000029*Exp(0.3218875825*con(i,j,1))+
&1.0*Dcr*Grad(i,j)*(((Turb(i,j)+Turb(i,j+1)+Turb(i+1,j)+
&Turb(i+1,j+1))/4.0)**2)*1.0)

```

```

      nut(i,j,2)=(0.0000029*Exp(0.3218875825*con(i,j,1))+
&Dcy*Grad(i,j)*(((Turb(i,j)+Turb(i,j+1)+Turb(i+1,j)+
&Turb(i+1,j+1))/4.0)**2)*Damp)

```

```

      Else

```

```

      nut(i,j,1)=(0.0000029*Exp(0.3218875825*con(i,j,1))+
&Dcr*Grad(i,j)*(((Turb(i,j)+Turb(i,j+1)+Turb(i+1,j)+
&Turb(i+1,j+1))/4.0)**2)*1.0)

```

```

      nut(i,j,2)=(0.0000029*Exp(0.3218875825*con(i,j,1))+
&Dcy*Grad(i,j)*(((Turb(i,j)+Turb(i,j+1)+Turb(i+1,j)+
&Turb(i+1,j+1))/4.0)**2)*Damp)

```

```

    endif

```

```

118 continue

```

```

      return

```

```

    end

```

```

c*****
c*****SUBROUTINE: ADVDIF*****
c*****Subroutine for the calculation of the advection and diffusion coefficients*****

```

```

      subroutine advdif(mm)

```

```

c      face advection flux and face diffusion flux

```

```

c      include 'comdeck'

```

```

      Include 'comdeck3.h'

```

```

      REAL nuo, nut,LL,mask,maskk,NBl,Inlet,maski,maske

```

```

      INTEGER IPRINT

```

```

c      psi= streamfunction, vort = vorticity

```

```

c      u= x velocity, v= y velocity, p = pressure

```

```

c      phi=scalar variable, C = Concentration, rho= density

```

```

c      Temp(200,100), nut(200,100), Con(200,100)

```

```

c      Fnb = face value of advection flux, Dnb=face value of diffusion flux, XX=??

```

```

c      rhonb(200,100,nf)= face density of fluid, nf = 1 vert face, nf = 2 horiz face
c      nuo = kinematic viscosity
      dyr=Dy/Dr
      dry=Dr/Dy
      do 10 j=1,N
        Dnb(1,j,1)= 0.0
        Dnb(M+1,j,1)= 0.0
        Fnb(1,j,1)= rhonb(1,j,1)*(psi(1,j+1)-psi(1,j))
        Fnb(M+1,j,1)=rhonb(M+1,j,1)*(psi(M+1,j+1)-psi(M+1,j))
      do 10 i=2,M
        Dnb(i,j,1)= r(i,j)*dyr*rhonb(i,j,1)*(nut(i-1,j,1)+nut(i,j,1))/2.
10      Fnb(i,j,1)=rhonb(i,j,1)*(psi(i,j+1)-psi(i,j))
c      Horizontal Velocities
      do i = 1, M
        do j= 1, N
          Uw(i,j)= Fnb(i,j,1)/(Dy*rhonb(i,j,1)*r(i,j))
          Ue(i,j)= Fnb(i+1,j,1)/(Dy*rhonb(i+1,j,1)*r(i+1,j))
        enddo
      enddo

      do 11 i=1,M
        Dnb(i,1,2)= 0.0
        Dnb(i,N+1,2)= 0.0
        Fnb(i,1,2)= rhonb(i,1,2)*(psi(i,1)-psi(i+1,1))
        Fnb(i,N+1,2)=rhonb(i,N+1,2)*(psi(i,N+1)-psi(i+1,N+1))
        Snb(i,1,2)= rhonb(i,1,2)*(r(i,1)*Dr+Dr*Dr/2.)
        Snb(i,N+1,2)=rhonb(i,N+1,2)*(r(i,N+1)*Dr+Dr*Dr/2.)
        do 11 j=2,N
          Dnb(i,j,2)=((r(i,j)*Dr+Dr*Dr/2.)/Dy)*rhonb(i,j,2)*      !Dy correction
&(nut(i,j,2)+nut(i,j-1,2))/2.
          Fnb(i,j,2)=rhonb(i,j,2)*(psi(i,j)-psi(i+1,j))
11      Snb(i,j,2)=rhonb(i,j,2)*(r(i,j)*Dr+Dr*Dr/2.)
c      Vertical Velocities
      do i = 1, M
        do j= 1, N
          Vs(i,j)=Fnb(i,j,2)/(Dr*rhonb(i,j,2)*(r(i,j)+r(i+1,j))/2.)
          Vn(i,j)=Fnb(i,j+1,2)/(Dr*rhonb(i,j+1,2)*(r(i,j)+r(i+1,j))/2.)
        enddo
      enddo
      ss=      Fnb(8,8,1)-Fnb(9,8,1)+
&      Fnb(8,8,2)-Fnb(8,9,2)
      return
      end

```

```

c*****
c*****SUBROUTINE: THEVEL*****

```

c*****Subroutine for the calculation of velocities in the theta direction*****

subroutine TheVel(mm)

Include 'comdeck3.h'

REAL nuo, nut,LL,mask,maskk,NBl,Inlet,maski,maske
INTEGER IPRINT

do i=2,M-1
do j=2,N
Vth(i,j,2)=Vth(i,j,3)
enddo
enddo

Do i=2,M
Do j=2,N

$C1(i,j) = DCr * (nut(i,j,1) * (r(i,j) + dr/2.)) / ((dr**2) * (2. * r(i,j) + 1.5 * dr))$

$C2(i,j) = DCr * (nut(i,j,1) * (r(i,j) + dr/2.)) / ((dr**2) * (2. * r(i,j) + 0.5 * dr))$

$C3(i,j) = DCr * (nut(i,j,1) * (r(i+1,j) + dr/2.)) /$
& $((dr**2) * (2. * r(i,j) + 1.5 * dr))$

$C4(i,j) = DCr * (nut(i,j,1) * (r(i-1,j) + dr/2.)) /$
& $((dr**2) * (2. * r(i,j) + 0.5 * dr))$

$C5(i,j) = (Ue(i,j) + Uw(i,j)) / (4.0 * (r(i,j) + dr/2.))$

$C6(i,j) = (2 * DCy) * Nut(i,j,2) / (Dy**2.0)$

$C7(i,j) = (Vs(i,j)) / (4.0 * Dy)$

$C8(i,j) = (Uw(i,j)) / (4.0 * Dr)$

enddo
enddo

i=1
do j=1,N-Ninl

Vth(i,j,3)=0.0
Vth(i,j,2)=0.0
enddo


```

i=1
do j=N-Ninl+1,N
  if(Indef.eq.1.AND.IdefAng.eq.90) then
    Vth(i,j,3)=0.0
    Vth(i,j,2)=0.0
  else if(Indef.eq.1.AND.IdefAng.eq.0) then
    Vth(i,j,3)=0.25*Uw(i,j)      !Vth(i,j,3)=Uw(i,j)
    Vth(i,j,2)=Vth(i,j,3)      !Vth(i,j,2)=Vth(i,j,3)
  else if(Indef.eq.1) then
    Vth(i,j,3)=Uw(i,j) / Tan(DefAng)
    Vth(i,j,2)=Vth(i,j,3)
  else
    Vth(i,j,3)=0.0
    Vth(i,j,2)=0.0
  endif
enddo

Do 80 LLLL=1, 500

j=1
do i=2,M-1

  Vth(i,j,3)=((-C8(i+1,j)+C3(i,j))*(Vth(i+1,j,3)+Vth(i+1,j,2))
&+(1/Dt-C1(i,j)-C2(i,j)-C5(i,j)-C6(i,j))*Vth(i,j,2)+
&(C8(i,j)+C4(i,j))*(Vth(i-1,j,3)+Vth(i-1,j,2))+
&(-C7(i,j+1)+C6(i,j)/2.)*(Vth(i,j+1,3)+Vth(i,j+1,2))
&+(C7(i,j)+C6(i,j)/2.)*(Vth(i,j,3)+Vth(i,j,2))
& + 0.5*(Narm*0.5*(Hbl*dr)*CDv(i,j)*
&(Wbl*(r(i,j)+dr/2.)-Vth(i,j,2))**2)/(2*pi*(r(i,j)+dr/2.)*dr*dr)
&+ 0.5*(Narm*0.5*(Hbl*dr)*CDv(i,j)*

&(Wbl*(r(i,j)+dr/2.)-Vth(i,j,3))**2)/(2*pi*(r(i,j)+dr/2.)*dr*dr)
&*mask(i,j) / (1/Dt+C1(i,j)+C2(i,j)+C5(i,j)+C6(i,j))

enddo

j=N
do i=2,M-1

  Vth(i,j,3)=((-C8(i+1,j)+C3(i,j))*(Vth(i+1,j,3)+Vth(i+1,j,2))
&+(1/Dt-C1(i,j)-C2(i,j)-C5(i,j)-C6(i,j))*Vth(i,j,2)+
&(C8(i,j)+C4(i,j))*(Vth(i-1,j,3)+Vth(i-1,j,2))+
&(-C7(i,j+1)+C6(i,j)/2.)*(Vth(i,j,3)+Vth(i,j,2))
&+(C7(i,j)+C6(i,j)/2.)*(Vth(i,j-1,3)+Vth(i,j-1,2)))*maskk(i,j)/

```

```

&(1/Dt+C1(i,j)+C2(i,j)+C5(i,j)+C6(i,j))

    enddo

do 80 j=2,N-1
do 80 i=2,M-1

    if(mask(i,j-1).eq.0) then

        Vth(i,j,3)=((-C8(i+1,j)+C3(i,j))*(Vth(i+1,j,3)+Vth(i+1,j,2))
&+(1/Dt-C1(i,j)-C2(i,j)-C5(i,j)-C6(i,j))*Vth(i,j,2)+
&(C8(i,j)+C4(i,j))*(Vth(i-1,j,3)+Vth(i-1,j,2))+
&(-C7(i,j+1)+C6(i,j)/2.)*(Vth(i,j+1,3)+Vth(i,j+1,2))
&+(C7(i,j)+C6(i,j)/2.)*(Vth(i,j,3)+Vth(i,j,2))
& + 0.5*(Narm*0.5*(Hbl*dr)*CDv(i,j)*                                !0.5
&(Wbl*(r(i,j)+dr/2.)-Vth(i,j,2))**2)/(2*pi*(r(i,j)+dr/2.)*dr*dr)
&+ 0.5*(Narm*0.5*(Hbl*dr)*CDv(i,j)*
                                !0.5
&(Wbl*(r(i,j)+dr/2.)-Vth(i,j,3))**2)/(2*pi*(r(i,j)+dr/2.)*dr*dr))
&*mask(i,j) / (1/Dt+C1(i,j)+C2(i,j)+C5(i,j)+C6(i,j))

    else if(maskk(i,j).eq.0) then
        Vth(i,j,3)=0.0

    else if(maski(i,j).eq.0) then
        Vth(i,j,3)=0.0

    else if(maske(i,j).eq.0) then
        Vth(i,j,3)=0.0

    else

        Vth(i,j,3)=((-C8(i+1,j)+C3(i,j))*(Vth(i+1,j,3)+Vth(i+1,j,2))
&+(1/Dt-C1(i,j)-C2(i,j)-C5(i,j)-C6(i,j))*Vth(i,j,2)+
&(C8(i,j)+C4(i,j))*(Vth(i-1,j,3)+Vth(i-1,j,2))+
&(-C7(i,j+1)+C6(i,j)/2.)*(Vth(i,j+1,3)+Vth(i,j+1,2))
&+(C7(i,j)+C6(i,j)/2.)*(Vth(i,j-1,3)+Vth(i,j-1,2)))
& / (1/Dt+C1(i,j)+C2(i,j)+C5(i,j)+C6(i,j))

    endif

80    continue
return
end

```

```

c*****
c*****SUBROUTINE: VORTIC*****
c*****Subroutine for the calculation of the vorticity*****

```

```

      subroutine vortic(mm)
c This subroutine computes the Vorticity Transport Equation
c      Called from Main
c      Calls: none
c      include 'comdeck'

```

```

      Include 'comdeck3.h'
      REAL nuo, nut,LL,mask,maskk,NBl,Inlet,maski,maske
      INTEGER IPRINT

```

```

c      psi= streamfunction, vort = vorticity
c      u= x velocity, v= y velocity, p = pressure
c      phi=scalar variable, C = Concentration, rho= density
c      Temp(200,100), nut(200,100), Con(200,100)
c      Fnb = face value of advection flux, Dnb=face value of diffusion flux, XX=?
c      rhonb(200,100,nf)= face density of fluid, nf = 1 vert face, nf = 2 horiz face
c      nuo = kinematic viscosity
c      dyr=Dy/Dr
c      dry=Dr/Dy
c Boundary Conditions

```

```

      If((NScycle-NScontrol).le.Int(mm*dt)) then
      NScf=1
      Else
      NScf=0
      endif

```

```

      If(NScycle.le.Int(mm*dt)) then
      NScycle=NScycle+Int((2*pi)/(Narm*Wbl))
      endif

```

```

      do i=1,M
      do j=1,N
      vort(i,j,2)=vort(i,j,3)
      enddo
      enddo

```

```

do 110 mmm=1,100

i=1
j=N

vort(1,N,3)=0.0
i=1
j=1

vort(i,j,3)=maski(i,j)*maske(i,j)*
& maskk(i,j)*mask(i,j)*((aW(i,j)*vort(i,j,3)+
& aS(i,j)*vort(i,j,3)+
& aE(i,j)*vort(i+1,j,3)+
& aN(i,j)*vort(i,j+1,3))*Wt+
& (aW(i,j)*vort(i,j,2)+
& aS(i,j)*vort(i,j,2)+
& aE(i,j)*vort(i+1,j,2)+
& aN(i,j)*vort(i,j+1,2))*(1.-Wt)+
& aPo(i,j)*vort(i,j,2)-Wt*Alpha*(1-1/Spegra)*rho(i,j)*
& ((r(i,j)+Dr)*(con(i,j,2)+con(i+1,j,2))-
& 1.00*Dr*(2.0*con(i,j,2))-
& r(i,j)*(con(i,j,2)+con(i,j,2)))
& *Dy*Gravi/(2.*Densr(i,j))-(1.-Wt)*Alpha*(1-1/Spegra)
& *rho(i,j)*((r(i,j)+Dr)*(con(i,j,1)+con(i+1,j,1))-
& 1.00*Dr*(2.0*con(i,j,1))-
& r(i,j)*(con(i,j,1)+con(i,j,1)))
& *Dy*Gravi/(2.*Densr(i,j))+
& (2.0*rho(i,j)*(Dr/(r(i,j)+Dr/2.))*(
& nut(i,j+1,2)*Uw(i,j+1)-
& nut(i,j,2)*Uw(i,j))) + rho(i,j)*Wt*((Vth(i,j,3)+Vth(i,j,3))**2-
& (Vth(i,j+1,3)+Vth(i,j,3))**2)*Vtc(i,j)/4.0+rho(i,j)*(1-Wt)*
& ((Vth(i,j,2)+Vth(i,j,2))**2-(Vth(i,j+1,2)+Vth(i,j,2))**2)
& *Vtc(i,j)/4.0)/aP(i,j)

Vort(1,1,3)=max(Vort(1,1,3),0.0)
i=1
do j=2,N-2
vort(i,j,3)=(7.*(2./7.)*(Vn(i,j)+Vs(i,j))/(Dr*2))

enddo

i=1
do ii=1,Ninl
j=N-(ii-1)

```

```

vort(i,j,3)=1.0*((psi(i,j)-psi(i,j-1))-(psi(i,j+1)-psi(i,j)))
& /((r(i,j)+dr/2.)*Dy*VortBoun)+(0.5)*(Vn(i,j)+Vs(i,j))/(Dr*2) !Dy
enddo

```

```

j=N
do i=1,M-(mt+3)
  Vort(i,j,3)=0.0
enddo
j=N
do mtt=1,mt-1
  i=M-(mt+3-mtt)
  Vort(i,j,3)=-((psi(i,j+1)+psi(i+1,j+1))+(psi(i,j-1)+
& psi(i+1,j-1))-2*(psi(i,j)+psi(i+1,j)))/(r(i,j)*2*Dy**2)
enddo

```

```

j=N
do i=M-3,M-1
  Vort(i,j,3)=0.0
enddo

```

```

do 10 i=2,M-1
do 10 j=2,N-1
  if(Mask(i,j-1).EQ.0 .AND. Mask(i+1,j).EQ.0) then
    vort(i,j,3)=maskk(i,j)*mask(i,j)*((-Vn(i,j)/(Dr)-Uw(i,j)/(Dy))
& +(Tan(BlaAng)*0.5*CDv(i,j)*Hbl*NScf*
& (VBl(i,j)-(Ue(i,j)+Uw(i,j))/2.0)*
& Abs((VBl(i,j)-(Ue(i,j)+Uw(i,j))/2.0)))/((r(i,j)+Dr/2.0)*Fscr*
& MAX(nut(i,j,1),0.000001)))
    else if(Mask(i,j-1).eq.0) then
      vort(i,j,3)=((-7.0/7.0)*((psi(i,j+1)-psi(i,j))/r(i,j)+
& (psi(i+1,j+1)-psi(i+1,j))/r(i+1,j))/(2*Dy**2)
& +(Tan(BlaAng)*0.5*CDv(i,j)*Hbl*NScf*
& (VBl(i,j)-(Ue(i,j)+Uw(i,j))/2.0)*
& Abs((VBl(i,j)-(Ue(i,j)+Uw(i,j))/2.0)))/((r(i,j)+Dr/2.0)*Fscr*
& MAX(nut(i,j,1),0.000001)))

```

```

    else if(Mask(i,j-1).eq.0) then
      vort(i,j,3)=(-2.0/7.0)*((psi(i,j+1)-psi(i,j))/r(i,j)+
& (psi(i+1,j+1)-psi(i+1,j))/r(i+1,j))/(2*Dy**2)

```

```

    else if(Mask(i,j+1).eq.0) then

```

```

      vort(i,j,3)=+(2.0/7.0)*((psi(i,j+1)-psi(i,j))/r(i,j)+
& (psi(i+1,j+1)-psi(i+1,j))/r(i+1,j))/(2*Dy**2)

```

```

else if(Maske(i,j-1).eq.0) then

    vort(i,j,3)=(-2.0/7.0)*((psi(i,j+1)-psi(i,j))/r(i,j)+
& (psi(i+1,j+1)-psi(i+1,j))/r(i+1,j))/(2*Dy**2)
    else if(Maske(i,j+1).eq.0) then

    vort(i,j,3)=+(2.0/7.0)*((psi(i,j+1)-psi(i,j))/r(i,j)+
& (psi(i+1,j+1)-psi(i+1,j))/r(i+1,j))/(2*Dy**2)

else if(maskk(i+1,j).eq.0) then

vort(i,j,3)=-(Vn(i,j)+Vs(i,j))/(Dr)

else if(maskk(i-1,j).eq.0) then

vort(i,j,3)=(Vn(i,j)+Vs(i,j))/(Dr)

else if(maskk(i+1,j+1).eq.0) then

    vort(i,j,3)=2.0*vort(i,j+1,3)

else

    vort(i,j,3)=maski(i,j)*maske(i,j)*
& maskk(i,j)*mask(i,j)*((aW(i,j)*vort(i-1,j,3)+
& aS(i,j)*vort(i,j-1,3)+
& aE(i,j)*vort(i+1,j,3)+
& aN(i,j)*vort(i,j+1,3))*Wt+
& (aW(i,j)*vort(i-1,j,2)+
& aS(i,j)*vort(i,j-1,2)+
& aE(i,j)*vort(i+1,j,2)+
& aN(i,j)*vort(i,j+1,2))*(1.-Wt)+
& aPo(i,j)*vort(i,j,2)-Wt*Alpha*rho(i,j)*((r(i,j)+Dr)*
& (SGC*(con(i,j,2)+con(i+1,j,2))+Densr(i,j)+Densr(i+1,j))-
& Dr*(SGC*2.0*con(i,j,2)+2.0*Densr(i,j))-r(i,j)*
& (SGC*(con(i,j,2)+con(i-1,j,2))+Densr(i,j)+Densr(i-1,j))))
& *Dy*Gravi/(2.*Densr(i,j))-
& (1.-Wt)*Alpha*rho(i,j)*((r(i,j)+Dr)*
& (SGC*(con(i,j,1)+con(i+1,j,1))+Densr(i,j)+Densr(i+1,j))-
& Dr*(SGC*2.0*con(i,j,1)+2.0*Densr(i,j))-r(i,j)*
& (SGC*(con(i,j,1)+con(i-1,j,1))+Densr(i,j)+Densr(i-1,j))))
& *Dy*Gravi/(2.*Densr(i,j))+
& 1.0*(2.*rho(i,j)*(Dr/(r(i,j)+Dr/2.))*(
& nut(i,j+1,2)*Uw(i,j+1)-
& nut(i,j,2)*Uw(i,j)))+

```

```

& rho(i,j)*Wt*((Vth(i,j,3)+Vth(i,j-1,3))**2-
& (Vth(i,j+1,3)+Vth(i,j,3))**2)*Vtc(i,j)/4.0+rho(i,j)*(1-Wt)*
& ((Vth(i,j,2)+Vth(i,j-1,2))**2-(Vth(i,j+1,2)+Vth(i,j,2))**2)
& *Vtc(i,j)/4.0)/aP(i,j)

endif

vort(i,N+1,3)=vort(i,N,3)
vort(M+1,j,3)=vort(M,j,3)
10 continue

i =M
do j = 2,N-1

vort(i,j,3)=mask(i,j)*(2./7.)*(-(Vn(i,j)+Vs(i,j))/(2*Dr))

enddo

j=1
If (Mrecir.eq.1) then
do i=2,ihopper-1
vort(i,j,3)=maski(i,j)*maske(i,j)*
& maskk(i,j)*mask(i,j)*((aW(i,j)*vort(i-1,j,3)+
& aS(i,j)*vort(i,j,3)+
& aE(i,j)*vort(i+1,j,3)+
& aN(i,j)*vort(i,j+1,3))*Wt+
& (aW(i,j)*vort(i-1,j,2)+
& aS(i,j)*vort(i,j,2)+
& aE(i,j)*vort(i+1,j,2)+
& aN(i,j)*vort(i,j+1,2))*(1.-Wt)+
& aPo(i,j)*vort(i,j,2)-Wt*Alpha*rho(i,j)*((r(i,j)+Dr)*
& (SGC*(con(i,j,2)+con(i+1,j,2))+Densr(i,j)+Densr(i+1,j))-
& Dr*(SGC*2.0*con(i,j,2)+2.0*Densr(i,j))-r(i,j)*
& (SGC*(con(i,j,2)+con(i-1,j,2))+Densr(i,j)+Densr(i-1,j))))
& *Dy*Gravi/(2.*Densr(i,j))-
& (1.-Wt)*Alpha*rho(i,j)*((r(i,j)+Dr)*
& (SGC*(con(i,j,1)+con(i+1,j,1))+Densr(i,j)+Densr(i+1,j))-
& Dr*(SGC*2.0*con(i,j,1)+2.0*Densr(i,j))-r(i,j)*
& (SGC*(con(i,j,1)+con(i-1,j,1))+Densr(i,j)+Densr(i-1,j))))
& *Dy*Gravi/(2.*Densr(i,j))+
& (2.*rho(i,j)*(Dr/(r(i,j)+Dr/2.))*
& nut(i,j+1,2)*Uw(i,j+1)-
& nut(i,j,2)*Uw(i,j))+rho(i,j)*Wt*((Vth(i,j,3)+Vth(i,j,3))**2-
& (Vth(i,j+1,3)+Vth(i,j,3))**2)*Vtc(i,j)/4.0+rho(i,j)*(1-Wt)*
& ((Vth(i,j,2)+Vth(i,j,2))**2-(Vth(i,j+1,2)+Vth(i,j,2))**2)

```

```

&    *Vtc(i,j)/4.0)/aP(i,j)

    enddo

    do i=ihopper,M-1
        vort(i,j,3)=((-7.0/7.0)*((psi(i,j+1)-psi(i,j))/r(i,j)+
& (psi(i+1,j+1)-psi(i+1,j))/r(i+1,j))/(2*Dy**2)
& +(Tan(BlaAng)*0.5*CDv(i,j)*Hbl*NScf*
& (VBl(i,j)-(Ue(i,j)+Uw(i,j))/2.0)*
& Abs((VBl(i,j)-(Ue(i,j)+Uw(i,j))/2.0)))/((r(i,j)+Dr/2.0)*Fscr*
& MAX(nut(i,j,1),0.000001)))*Mask(i,j)

    enddo

    Else

    do i=2,M-1

        vort(i,j,3)=((-2.0/7.0)*((psi(i,j+1)-psi(i,j))/r(i,j)+
& (psi(i+1,j+1)-psi(i+1,j))/r(i+1,j))/(2*Dy**2)
& +(Tan(BlaAng)*0.5*CDv(i,j)*Hbl*NScf*
& (VBl(i,j)-(Ue(i,j)+Uw(i,j))/2.0)*
& Abs((VBl(i,j)-(Ue(i,j)+Uw(i,j))/2.0)))/((r(i,j)+Dr/2.0)*Fscr*
& MAX(nut(i,j,1),0.000001)))*Mask(i,j)

    enddo
    endif

    i=M
    j=N

    vort(M,N,3)=mask(i,j)*(-(Vs(i,j))/(Dr))

    i=M
    j=1

    vort(i,j,3)=mask(i,j)*(-Vn(i,j)/(Dr)-Uw(i,j)/(Dy))

```

110 continue

c Calculation in the other direction

```

c*****Calculations in the other direction*****
do 120 mmm=1,100

```



```

i=1
j=N
vort(1,N,3)=0.0
i=1
j=1
vort(i,j,3)=maski(i,j)*maske(i,j)*
& maskk(i,j)*mask(i,j)*(
& (aW(i,j)*vort(i,j,3)+
& aS(i,j)*vort(i,j,3)+
& aE(i,j)*vort(i+1,j,3)+
& aN(i,j)*vort(i,j+1,3))*Wt+
& (aW(i,j)*vort(i,j,2)+
& aS(i,j)*vort(i,j,2)+
& aE(i,j)*vort(i+1,j,2)+
& aN(i,j)*vort(i,j+1,2))*(1.-Wt)+
& aPo(i,j)*vort(i,j,2)
& -Wt*Alpha*(1-1/Speggra)*rho(i,j)*((r(i,j)+Dr)*
& (con(i,j,2)+con(i+1,j,2))-
& 1.00*Dr*(2.0*con(i,j,2))-
& r(i,j)*(con(i,j,2)+con(i,j,2)))
& *Dy*Gravi/(2.*Densr(i,j))
& -(1.-wt)*Alpha*(1-1/Speggra)*rho(i,j)*((r(i,j)+Dr)*
& (con(i,j,1)+con(i+1,j,1))-
& 1.00*Dr*(2.0*con(i,j,1))-
& r(i,j)*(con(i,j,1)+con(i,j,1)))
& *Dy*Gravi/(2.*Densr(i,j))+
& (2.0*rho(i,j)*(Dr/(r(i,j)+Dr/2.)))*(
& nut(i,j+1,2)*Uw(i,j+1)-
& nut(i,j,2)*Uw(i,j))) + rho(i,j)*Wt*((Vth(i,j,3)+Vth(i,j,3))*2-
& (Vth(i,j+1,3)+Vth(i,j,3))*2)*Vtc(i,j)/4.0+rho(i,j)*(1-Wt)*
& ((Vth(i,j,2)+Vth(i,j,2))*2-(Vth(i,j,2)+Vth(i,j+1,2))*2)
& *Vtc(i,j)/4.0)/aP(i,j)

i=1
do j=2,N-2
vort(i,j,3)=2*(2./7.)*(Vn(i,j)+Vs(i,j))/(Dr*2)
enddo

i=1
do ii=1,Ninl
j=N-(ii-1)

vort(i,j,3)=1.0*((psi(i,j)-psi(i,j-1))-(psi(i,j+1)-psi(i,j)))
& /((r(i,j)+dr/2.)*Dy*VortBoun)+(0.5)*(Vn(i,j)+Vs(i,j))/(Dr*2)
enddo

```

```

j=N
do i=1,M-(mt+3)

Vort(i,j,3)=0.0

enddo

j=N
do mtt=1,mt-1

i=M-(mt+3-mtt)

Vort(i,j,3)=-((psi(i,j+1)+psi(i+1,j+1))+(psi(i,j-1)+
&psi(i+1,j-1))-2*(psi(i,j)+psi(i+1,j)))/(r(i,j)*2*Dy**2)

enddo

j=N

do i=M-3,M-1

Vort(i,j,3)=0.0
enddo


do 20 j=2,N-1
do 20 i=2,M-1

if(Mask(i,j-1).EQ.0.AND.Mask(i+1,j).EQ.0) then

vort(i,j,3)=maskk(i,j)*mask(i,j)*((-Vn(i,j)/(Dr)-Uw(i,j)/(Dy))
& +(Tan(BlaAng)*0.5*CDv(i,j)*Hbl*NScf*
& (VBl(i,j)-(Ue(i,j)+Uw(i,j))/2.0)*
& Abs((VBl(i,j)-(Ue(i,j)+Uw(i,j))/2.0)))/((r(i,j)+Dr/2.0)*Fscr*
& MAX(nut(i,j,1),0.000001)))

else if(Mask(i,j-1).eq.0) then

vort(i,j,3)=((-7.0/7.0)*((psi(i,j+1)-psi(i,j))/r(i,j)+
& (psi(i+1,j+1)-psi(i+1,j))/r(i+1,j))/(2*Dy**2)
& +(Tan(BlaAng)*0.5*CDv(i,j)*Hbl*NScf*
& (VBl(i,j)-(Ue(i,j)+Uw(i,j))/2.0)*
& Abs((VBl(i,j)-(Ue(i,j)+Uw(i,j))/2.0)))/((r(i,j)+Dr/2.0)*Fscr*
& MAX(nut(i,j,1),0.000001)))

```

```

        else if(Maski(i,j-1).eq.0) then

            vort(i,j,3)=(-2.0/7.0)*((psi(i,j+1)-psi(i,j))/r(i,j)+
& (psi(i+1,j+1)-psi(i+1,j))/r(i+1,j))/(2*Dy**2)

            else if(Maski(i,j+1).eq.0) then

                vort(i,j,3)=(2.0/7.0)*((psi(i,j+1)-psi(i,j))/r(i,j)+
& (psi(i+1,j+1)-psi(i+1,j))/r(i+1,j))/(2*Dy**2)

            else if(Maske(i,j-1).eq.0) then

                vort(i,j,3)=(-2.0/7.0)*((psi(i,j+1)-psi(i,j))/r(i,j)+
& (psi(i+1,j+1)-psi(i+1,j))/r(i+1,j))/(2*Dy**2)

            else if(Maske(i,j+1).eq.0) then

                vort(i,j,3)=(2.0/7.0)*((psi(i,j+1)-psi(i,j))/r(i,j)+
& (psi(i+1,j+1)-psi(i+1,j))/r(i+1,j))/(2*Dy**2)

            else if(maskk(i+1,j).eq.0) then

c          vort(i,j,mm+1)=ABS(-((psi(i+1,j)+psi(i+1,j+1))+(psi(i-1,j)+
c          & psi(i-1,j+1))-2*(psi(i,j)+psi(i,j+1)))/(2*Dr**2))

            vort(i,j,3)=-(Vn(i,j)+Vs(i,j))/(Dr)

            else if(maskk(i-1,j).eq.0) then

c          vort(i,j,3)= -((psi(i,j)+psi(i,j+1))+(psi(i+2,j)+
c          & psi(i+2,j+1))-2*(psi(i+1,j)+psi(i+1,j+1)))/(r(i,j)*2*Dr**2)

            vort(i,j,3)=(Vn(i,j)+Vs(i,j))/(Dr)

c          else if(maskk(i,j+1).eq.0) then

c          vort(i,j,mm+1)=maskk(i,j)*mask(i,j)*(-(Uw(i,j)+Ue(i,j))/Dy)

c*****
c          else if((maskk(i+1,j+1).eq.0).and.(Vn(i,j).gt.0)) then !try

c          vort(i,j,3)=vort(i+1,j,3)*0.0
c*****
            else if(maskk(i+1,j+1).eq.0) then

```

```

vort(i,j,3)=2.0*(vort(i,j+1,3))

else

vort(i,j,3)=maski(i,j)*maske(i,j)*
& maskk(i,j)*mask(i,j)*((aW(i,j)*vort(i-1,j,3)+
& aS(i,j)*vort(i,j-1,3)+
& aE(i,j)*vort(i+1,j,3)+
& aN(i,j)*vort(i,j+1,3))*Wt+
& (aW(i,j)*vort(i-1,j,2)+
& aS(i,j)*vort(i,j-1,2)+
& aE(i,j)*vort(i+1,j,2)+
& aN(i,j)*vort(i,j+1,2))*(1.-Wt)+
& aPo(i,j)*vort(i,j,2)-Wt*Alpha*rho(i,j)*((r(i,j)+Dr)*
& (SGC*(con(i,j,2)+con(i+1,j,2))+Densr(i,j)+Densr(i+1,j))-
& Dr*(SGC*2.0*con(i,j,2)+2.0*Densr(i,j))-r(i,j)*
& (SGC*(con(i,j,2)+con(i-1,j,2))+Densr(i,j)+Densr(i-1,j))))
& *Dy*Gravi/(2.*Densr(i,j))-
& (1.-Wt)*Alpha*rho(i,j)*((r(i,j)+Dr)*
& (SGC*(con(i,j,1)+con(i+1,j,1))+Densr(i,j)+Densr(i+1,j))-
& Dr*(SGC*2.0*con(i,j,1)+2.0*Densr(i,j))-r(i,j)*
& (SGC*(con(i,j,1)+con(i-1,j,1))+Densr(i,j)+Densr(i-1,j))))
& *Dy*Gravi/(2.*Densr(i,j))+
& 1.0*(2.*rho(i,j)*(Dr/(r(i,j)+Dr/2.)))*(
& nut(i,j+1,2)*Uw(i,j+1)-
& nut(i,j,2)*Uw(i,j)))+
& rho(i,j)*Wt*((Vth(i,j,3)+Vth(i,j-1,3))**2-
& (Vth(i,j+1,3)+Vth(i,j,3))**2)*Vtc(i,j)/4.0+rho(i,j)*(1-Wt)*
& ((Vth(i,j,2)+Vth(i,j-1,2))**2-(Vth(i,j+1,2)+Vth(i,j,2))**2)
& *Vtc(i,j)/4.0)/aP(i,j)

endif

vort(i,N+1,3)=vort(i,N,3)
vort(M+1,j,3)=vort(M,j,3)

20 continue
j=1
If (Mrecir.eq.1) then
do i=2,ihopper-1

vort(i,j,3)=maski(i,j)*maske(i,j)*
& maskk(i,j)*mask(i,j)*((aW(i,j)*vort(i-1,j,3)+
& aS(i,j)*vort(i,j,3)+
& aE(i,j)*vort(i+1,j,3)+
& aN(i,j)*vort(i,j+1,3))*Wt+

```

```

&      (aW(i,j)*vort(i-1,j,2)+
&      aS(i,j)*vort(i,j,2)+
&      aE(i,j)*vort(i+1,j,2)+
&      aN(i,j)*vort(i,j+1,2))*(1.-Wt)+
&      aPo(i,j)*vort(i,j,2)-Wt*Alpha*rho(i,j)*((r(i,j)+Dr)*
&      (SGC*(con(i,j,2)+con(i+1,j,2))+Densr(i,j)+Densr(i+1,j))-
&      Dr*(SGC*2.0*con(i,j,2)+2.0*Densr(i,j))-r(i,j)*
&      (SGC*(con(i,j,2)+con(i-1,j,2))+Densr(i,j)+Densr(i-1,j))))
&      *Dy*Gravi/(2.*Densr(i,j))-
&      (1.-Wt)*Alpha*rho(i,j)*((r(i,j)+Dr)*
&      (SGC*(con(i,j,1)+con(i+1,j,1))+Densr(i,j)+Densr(i+1,j))-
&      Dr*(SGC*2.0*con(i,j,1)+2.0*Densr(i,j))-r(i,j)*
&      (SGC*(con(i,j,1)+con(i-1,j,1))+Densr(i,j)+Densr(i-1,j))))
&      *Dy*Gravi/(2.*Densr(i,j))+
&      (2.*rho(i,j)*(Dr/(r(i,j)+Dr/2.))*(
&      nut(i,j+1,2)*Uw(i,j+1)-
&      nut(i,j,2)*Uw(i,j)))+rho(i,j)*Wt*((Vth(i,j,3)+Vth(i,j,3))*2-
&      (Vth(i,j+1,3)+Vth(i,j,3))*2)*Vtc(i,j)/4.0+rho(i,j)*(1-Wt)*
&      ((Vth(i,j,2)+Vth(i,j,2))*2-(Vth(i,j+1,2)+Vth(i,j,2))*2)
&      *Vtc(i,j)/4.0)/aP(i,j)

```

enddo

do i=ihopper,M-1

```

      vort(i,j,3)=((-7.0/7.0)*((psi(i,j+1)-psi(i,j))/r(i,j)+
&      (psi(i+1,j+1)-psi(i+1,j))/r(i+1,j))/(2*Dy**2)
&      +(Tan(BlaAng)*0.5*CDv(i,j)*Hbl*NScf*
&      (VBl(i,j)-(Ue(i,j)+Uw(i,j))/2.0)*
&      Abs((VBl(i,j)-(Ue(i,j)+Uw(i,j))/2.0)))/((r(i,j)+Dr/2.0)*Fscr*
&      MAX(nut(i,j,1),0.000001))))*Mask(i,j)

```

enddo

Else

do i=2,M-1

```

      vort(i,j,3)=((-2.0/7.0)*((psi(i,j+1)-psi(i,j))/r(i,j)+
&      (psi(i+1,j+1)-psi(i+1,j))/r(i+1,j))/(2*Dy**2)
&      +(Tan(BlaAng)*0.5*CDv(i,j)*Hbl*NScf*
&      (VBl(i,j)-(Ue(i,j)+Uw(i,j))/2.0)*
&      Abs((VBl(i,j)-(Ue(i,j)+Uw(i,j))/2.0)))/((r(i,j)+Dr/2.0)*Fscr*
&      MAX(nut(i,j,1),0.000001))))*Mask(i,j)

```

```

        enddo
    endif

    i = M
    do j = 2, N-1
        vort(i,j,3) = mask(i,j) * (2./7.) * (-(Vn(i,j) + Vs(i,j)) / (2 * Dr))
    enddo

    i = M
    j = N
    vort(M, N, 3) = mask(i, j) * (-(Vs(i, j)) / (Dr))

    i = M
    j = 1
    vort(i, j, 3) = mask(i, j) * (-Vn(i, j) / Dr - Uw(i, j) / Dy)

120    continue

    return
end

c*****
c*****SUBROUTINE: CONCEN*****
c*****Subroutine for the transport of the suspended solids*****
c*****Subroutine to Calculate Concentration *****
c*****
    subroutine Concen(mm)
c This subroutine computes the transport of a conservative scalar quality in 2-D and
Concentration.
c    Called from Main
c    Calls: none
c    include 'comdeck'

    Include 'comdeck3.h'
        REAL nuo, nut, LL, mask, maskk, NBI, Inlet, maski, maske
        INTEGER IPRINT

c    psi= streamfunction, vort = vorticity
c    u= x velocity, v= y velocity, p = pressure
c    phi=scalar variable, C = Concentration, rho= density
c    Temp(200,100), nut(200,100), Con(200,100)
c    Fnb = face value of advection flux, Dnb=face value of diffusion flux, XX=??
c    rhonb(200,100,nf)= face density of fluid, nf = 1 vert face, nf = 2 horiz face
c    nuo = kinematic viscosity
c    dyr=Dy/Dr

```

```

c      dry=Dr/Dy
      do i=1,M
      do j=1,N
      Con(i,j,ifrac)=Con(i,j,ifrac+1)
      enddo
      enddo

      do 110 mmm=1,100

      i=1
      j=N

      If (Con(i,j,2).eq.0.000) then

      Vsn(i,j,2)=0.00

      Vsn(i,j,3)=0.00

      Else If(Con(i,j,2).ge.Thind) then

      Vsn(i,j,2)=Max(Vmax*(exp(-Fsp*(Con(i,j,1)-Cmin))
      &-exp(-Csp*(Con(i,j,1)-Cmin))),Vcom*(exp(-Fcom*
      &(Con(i,j,1)-Cmin))
      &-exp(-Csp*(Con(i,j,1)-Cmin))))
      Vsn(i,j,3)=Max(Vmax*(exp(-Fsp*(Con(i,j,2)-Cmin))
      &-exp(-Csp*(Con(i,j,2)-Cmin))),Vcom*(exp(-Fcom*
      &(Con(i,j,2)-Cmin))
      &-exp(-Csp*(Con(i,j,2)-Cmin))))

      Else if (Con(i,j,2).le.Tdis) then

      Vsn(i,j,2)=Vfrac((ifrac-1)/2)/3600.0

      Vsn(i,j,3)=Vfrac((ifrac-1)/2)/3600.0

      Else

      Vsn(i,j,2)=(0.667*Vfrac((ifrac-1)/2)/3600.0+ 0.333*Vmax*
      &(exp(-Fsp*(Con(i,j,1)-Cmin))-exp(-Csp*(Con(i,j,1)-Cmin))))

      Vsn(i,j,3)=(0.667*Vfrac((ifrac-1)/2)/3600.0+ 0.333*Vmax*
      &(exp(-Fsp*(Con(i,j,2)-Cmin))-exp(-Csp*(Con(i,j,2)-Cmin))))

      endif

```

```

Con(i,j,ifrac+1)=maski(i,j)*maskk(i,j)*mask(i,j)*((aW(1,N)*
&   Dyeo*frac((ifrac-1)/2)+
&       aS(i,j)*Con(i,j-1,ifrac+1)+
&       aE(i,j)*Con(i+1,N,ifrac+1)+
&       aN(i,j)*Con(1,N,ifrac+1))*Wt+
&   (aW(1,N)*Dyeo*frac((ifrac-1)/2) +
&       aS(i,j)*Con(i,j-1,ifrac)+
&       aE(i,j)*Con(i+1,N,ifrac)+
&       aN(i,j)*Con(1,N,ifrac))*(1.-wt)+
&   aPo(i,j)*Con(1,N,ifrac)-wt*Vsn(1,N,3)*Snb(i,j,2)*
&   Con(1,N,ifrac+1)-(1.-wt)*Vsn(1,N,2)*Snb(i,j,2)*
&   Con(1,N,ifrac)
&   +(Sfloc(i,j,ifrac+1)+Sflds(i,j,ifrac+1))*Vol(i,j)*Rho(i,j)
&)/aP(i,j)

```

```

i=1
do ii=2,Ninl
j=N-(ii-1)

```

```

If (Con(i,j,2).eq.0.000) then

```

```

Vsn(i,j,2)=0.00

```

```

Vsn(i,j,3)=0.00

```

```

Else If(Con(i,j,2).ge.Thind) then

```

```

Vsn(i,j,2)=Max(Vmax*(exp(-Fsp*(Con(i,j,1)-Cmin))
&-exp(-Csp*(Con(i,j,1)-Cmin))),Vcom*(exp(-Fcom*
&(Con(i,j,1)-Cmin))
&-exp(-Csp*(Con(i,j,1)-Cmin))))
Vsn(i,j,3)=Max(Vmax*(exp(-Fsp*(Con(i,j,2)-Cmin))
&-exp(-Csp*(Con(i,j,2)-Cmin))),Vcom*(exp(-Fcom*
&(Con(i,j,2)-Cmin))
&-exp(-Csp*(Con(i,j,2)-Cmin))))

```

```

Else if (Con(i,j,2).le.Tdis) then

```

```

Vsn(i,j,2)=Vfrac((ifrac-1)/2)/3600.0

```

```

Vsn(i,j,3)=Vfrac((ifrac-1)/2)/3600.0

```

```

Else

```

```

Vsn(i,j,2)=(0.667*Vfrac((ifrac-1)/2)/3600.0+ 0.333*Vmax*
&(exp(-Fsp*(Con(i,j,1)-Cmin))-exp(-Csp*(Con(i,j,1)-Cmin))))

```



```

Vsn(i,j,3)=(0.667*Vfrac((ifrac-1)/2)/3600.0+ 0.333*Vmax*
&(exp(-Fsp*(Con(i,j,2)-Cmin))-exp(-Csp*(Con(i,j,2)-Cmin))))

```

```

endif

```

```

Con(i,j,ifrac+1)=maski(i,j)*maskk(i,j)*mask(i,j)*((aW(i,j)*
& Dyeo*frac((ifrac-1)/2) +
& aS(i,j)*Con(i,j-1,ifrac+1)+
& aE(i,j)*Con(i+1,j,ifrac+1)+
& aN(i,j)*Con(i,j+1,ifrac+1))*Wt+
& (aW(i,j)*Dyeo*frac((ifrac-1)/2) +
& aS(i,j)*Con(i,j-1,ifrac)+
& aE(i,j)*Con(i+1,j,ifrac)+
& aN(i,j)*Con(i,j+1,ifrac))*(1.-wt)+aPo(i,j)*
&Con(i,j,ifrac)
& -Wt*Vsn(i,j,3)*Snb(i,j,2)*maski(i,j-1)*maske(i,j-1)*
&Con(i,j,ifrac+1)
&*mask(i,j-1)-(1.-Wt)*Vsn(i,j,2)*Snb(i,j,2)*maski(i,j-1)*
&maske(i,j-1)*Con(i,j,ifrac)*mask(i,j-1)
&+Wt*Vsn(i,j+1,3)*Snb(i,j+1,2)*Con(i,j+1,ifrac+1)+(1.-Wt)*
&Vsn(i,j+1,2)*Snb(i,j+1,2)*Con(i,j+1,ifrac)
& +(Sfloc(i,j,ifrac+1)+Sflds(i,j,ifrac+1))*Vol(i,j)*Rho(i,j)
&)/aP(i,j)
enddo

```

```

i=1

```

```

j=1

```

```

If (Con(i,j,2).eq.0.000) then

```

```

Vsn(i,j,2)=0.00

```

```

Vsn(i,j,3)=0.00

```

```

Else If(Con(i,j,2).ge.Thind) then

```

```

Vsn(i,j,2)=Max(Vmax*(exp(-Fsp*(Con(i,j,1)-Cmin))
&-exp(-Csp*(Con(i,j,1)-Cmin))),Vcom*(exp(-Fcom*
&(Con(i,j,1)-Cmin))
&-exp(-Csp*(Con(i,j,1)-Cmin))))
Vsn(i,j,3)=Max(Vmax*(exp(-Fsp*(Con(i,j,2)-Cmin))
&-exp(-Csp*(Con(i,j,2)-Cmin))),Vcom*(exp(-Fcom*
&(Con(i,j,2)-Cmin))
&-exp(-Csp*(Con(i,j,2)-Cmin))))

```

```

Else if (Con(i,j,2).le.Tdis) then

Vsn(i,j,2)=Vfrac((ifrac-1)/2)/3600.0

Vsn(i,j,3)=Vfrac((ifrac-1)/2)/3600.0

Else

Vsn(i,j,2)=(0.667*Vfrac((ifrac-1)/2)/3600.0+ 0.333*Vmax*
&(exp(-Fsp*(Con(i,j,1)-Cmin))-exp(-Csp*(Con(i,j,1)-Cmin))))

Vsn(i,j,3)=(0.667*Vfrac((ifrac-1)/2)/3600.0+ 0.333*Vmax*
&(exp(-Fsp*(Con(i,j,2)-Cmin))-exp(-Csp*(Con(i,j,2)-Cmin))))

endif

Con(i,j,ifrac+1)=maski(i,j)*maskk(i,j)*mask(i,j)*((aW(i,j)*
&Con(1,1,ifrac+1)+
&          aS(i,j)*Con(i,j,ifrac+1)+
&          aE(i,j)*Con(i+1,j,ifrac+1)+
&          aN(i,j)*Con(i,j+1,ifrac+1))*Wt+
&          (aW(i,j)*Con(1,1,ifrac)+
&          aS(i,j)*Con(i,j,ifrac)+
&          aE(i,j)*Con(i+1,j,ifrac)+
&          aN(i,j)*Con(i,j+1,ifrac))*(1.-wt)+
&          aPo(i,j)*Con(i,j,ifrac)+Wt*Vsn(i,j+1,3)*Snb(i,j+1,2)*
&Con(i,j+1,ifrac+1)+(1.-Wt)*Vsn(i,j+1,2)*Snb(i,j+1,2)*
&Con(i,j+1,ifrac)
& +(Sfloc(i,j,ifrac+1)+Sflds(i,j,ifrac+1))*Vol(i,j)*Rho(i,j)
&)/aP(i,j)

i=1
do j=2,N-Ninl

If (Con(i,j,2).eq.0.000) then

Vsn(i,j,2)=0.00

Vsn(i,j,3)=0.00

Else If(Con(i,j,2).ge.Thind) then

Vsn(i,j,2)=Max(Vmax*(exp(-Fsp*(Con(i,j,1)-Cmin))
&-exp(-Csp*(Con(i,j,1)-Cmin))),Vcom*(exp(-Fcom*
&(Con(i,j,1)-Cmin))
&-exp(-Csp*(Con(i,j,1)-Cmin))))

```

```

Vsn(i,j,3)=Max(Vmax*(exp(-Fsp*(Con(i,j,2)-Cmin))
&-exp(-Csp*(Con(i,j,2)-Cmin))),Vcom*(exp(-Fcom*
&(Con(i,j,2)-Cmin))
&-exp(-Csp*(Con(i,j,2)-Cmin))))

Else if (Con(i,j,2).le.Tdis) then

Vsn(i,j,2)=Vfrac((ifrac-1)/2)/3600.0

Vsn(i,j,3)=Vfrac((ifrac-1)/2)/3600.0

Else

Vsn(i,j,2)=(0.667*Vfrac((ifrac-1)/2)/3600.0+ 0.333*Vmax*
&(exp(-Fsp*(Con(i,j,1)-Cmin))-exp(-Csp*(Con(i,j,1)-Cmin))))

Vsn(i,j,3)=(0.667*Vfrac((ifrac-1)/2)/3600.0+ 0.333*Vmax*
&(exp(-Fsp*(Con(i,j,2)-Cmin))-exp(-Csp*(Con(i,j,2)-Cmin))))

endif

Con(i,j,ifrac+1)=maski(i,j)*maskk(i,j)*mask(i,j)*((aW(i,j)*
&Con(i,j,ifrac+1)+
&          aS(i,j)*Con(i,j-1,ifrac+1)+
&          aE(i,j)*Con(i+1,j,ifrac+1)+
&          aN(i,j)*Con(i,j+1,ifrac+1))*Wt+
&      (aW(i,j)*Con(i,j,ifrac)+
&          aS(i,j)*Con(i,j-1,ifrac)+
&          aE(i,j)*Con(i+1,j,ifrac)+
&          aN(i,j)*Con(i,j+1,ifrac))*(1.-wt)+
&aPo(i,j)*Con(i,j,ifrac)-Wt*Vsn(i,j,3)*Snb(i,j,2)*maski(i,j-1)
&*maske(i,j-1)*Con(i,j,ifrac+1)*mask(i,j-1)-(1.-Wt)*Vsn(i,j,2)
&*Snb(i,j,2)
&*maski(i,j-1)*maske(i,j-1)*Con(i,j,ifrac)*mask(i,j-1)
&+Wt*Vsn(i,j+1,3)*Snb(i,j+1,2)*Con(i,j+1,ifrac+1)
&+(1.-Wt)*Vsn(i,j+1,2)*Snb(i,j+1,2)*Con(i,j+1,ifrac)
&  +(Sfloc(i,j,ifrac+1)+Sflds(i,j,ifrac+1))*Vol(i,j)*Rho(i,j)
&)/aP(i,j)
enddo

j=N
do i=2,M-1

If (Con(i,j,2).eq.0.000) then

Vsn(i,j,2)=0.00

```

```

Vsn(i,j,3)=0.00

Else If(Con(i,j,2).ge.Thind) then

Vsn(i,j,2)=Max(Vmax*(exp(-Fsp*(Con(i,j,1)-Cmin))
&-exp(-Csp*(Con(i,j,1)-Cmin))),Vcom*(exp(-Fcom*
&(Con(i,j,1)-Cmin))
&-exp(-Csp*(Con(i,j,1)-Cmin))))
Vsn(i,j,3)=Max(Vmax*(exp(-Fsp*(Con(i,j,2)-Cmin))
&-exp(-Csp*(Con(i,j,2)-Cmin))),Vcom*(exp(-Fcom*
&(Con(i,j,2)-Cmin))
&-exp(-Csp*(Con(i,j,2)-Cmin))))

Else if (Con(i,j,2).le.Tdis) then

Vsn(i,j,2)=Vfrac((ifrac-1)/2)/3600.0

Vsn(i,j,3)=Vfrac((ifrac-1)/2)/3600.0

Else

Vsn(i,j,2)=(0.667*Vfrac((ifrac-1)/2)/3600.0+ 0.333*Vmax*
&(exp(-Fsp*(Con(i,j,1)-Cmin))-exp(-Csp*(Con(i,j,1)-Cmin))))

Vsn(i,j,3)=(0.667*Vfrac((ifrac-1)/2)/3600.0+ 0.333*Vmax*
&(exp(-Fsp*(Con(i,j,2)-Cmin))-exp(-Csp*(Con(i,j,2)-Cmin))))

endif

Con(i,j,ifrac+1)=maski(i,j)*maskk(i,j)*mask(i,j)*((aW(i,j)*
&Con(i-1,j,ifrac+1)+
&          aS(i,j)*Con(i,j-1,ifrac+1)+
&          aE(i,j)*Con(i+1,j,ifrac+1)+
&          aN(i,j)*Con(i,j,ifrac+1))*Wt+
&      (aW(i,j)*Con(i-1,j,ifrac)+
&          aS(i,j)*Con(i,j-1,ifrac)+
&          aE(i,j)*Con(i+1,j,ifrac)+
&          aN(i,j)*Con(i,j,ifrac))*(1.-wt)+
&          aPo(i,j)*Con(i,j,ifrac)-Wt*Vsn(i,j,3)*Snb(i,j,2)*
&Con(i,j,ifrac+1)-(1.-Wt)*Vsn(i,j,2)*Snb(i,j,2)
&*Con(i,j,ifrac)
&  +(Sfloc(i,j,ifrac+1)+Sflds(i,j,ifrac+1))*Vol(i,j)*Rho(i,j)
&)/aP(i,j)
enddo

```

```

do 10 i=2,M-1
do 10 j=2,N-1

If (Con(i,j,2).eq.0.000) then

Vsn(i,j,2)=0.00

Vsn(i,j,3)=0.00

Else If(Con(i,j,2).ge.Thind) then

Vsn(i,j,2)=Max(Vmax*(exp(-Fsp*(Con(i,j,1)-Cmin))
&-exp(-Csp*(Con(i,j,1)-Cmin))),Vcom*(exp(-Fcom*
&(Con(i,j,1)-Cmin))
&-exp(-Csp*(Con(i,j,1)-Cmin))))
Vsn(i,j,3)=Max(Vmax*(exp(-Fsp*(Con(i,j,2)-Cmin))
&-exp(-Csp*(Con(i,j,2)-Cmin))),Vcom*(exp(-Fcom*
&(Con(i,j,2)-Cmin))
&-exp(-Csp*(Con(i,j,2)-Cmin))))

Else if (Con(i,j,2).le.Tdis) then

Vsn(i,j,2)=Vfrac((ifrac-1)/2)/3600.0

Vsn(i,j,3)=Vfrac((ifrac-1)/2)/3600.0

Else

Vsn(i,j,2)=(0.667*Vfrac((ifrac-1)/2)/3600.0+ 0.333*Vmax*
&(exp(-Fsp*(Con(i,j,1)-Cmin))-exp(-Csp*(Con(i,j,1)-Cmin))))

Vsn(i,j,3)=(0.667*Vfrac((ifrac-1)/2)/3600.0+ 0.333*Vmax*
&(exp(-Fsp*(Con(i,j,2)-Cmin))-exp(-Csp*(Con(i,j,2)-Cmin))))

endif

if(Mask(i,j-1).EQ.0 .AND. Mask(i+1,j).EQ.0) then
Con(i,j,ifrac+1)=maski(i,j)*maskk(i,j)*mask(i,j)*((aW(i,j)*
&Con(i-1,j,ifrac+1)+
& aS(i,j)*Con(i,j,ifrac+1))+
& (1.0*aE(i,j)*Con(i,j,ifrac+1))+
& aN(i,j)*Con(i,j+1,ifrac+1))*Wt+
& (aW(i,j)*Con(i-1,j,ifrac)+
& aS(i,j)*Con(i,j,ifrac)+
& (1.0*aE(i,j)*Con(i,j,ifrac))+
& aN(i,j)*Con(i,j+1,ifrac))*(1.-wt)+

```

```

& aPo(i,j)*Con(i,j,ifrac)-Wt*Vsn(i,j,3)*Snb(i,j,2)*
&Con(i,j,ifrac+1)*mask(i,j-1)-(1.-Wt)*Vsn(i,j,2)*Snb(i,j,2)*
&Con(i,j,ifrac)*mask(i,j-1)+Wt*Vsn(i,j+1,3)*Snb(i,j+1,2)*
&Con(i,j+1,ifrac+1)
&+(1.-Wt)*Vsn(i,j+1,2)*Snb(i,j+1,2)*Con(i,j+1,ifrac)
& +(Sfloc(i,j,ifrac+1)+Sflds(i,j,ifrac+1))*Vol(i,j)*Rho(i,j)
&)/aP(i,j)

```

```

else if(Mask(i,j-1).EQ.0 .AND. Mask(i-1,j-1).EQ.1) then

```

```

Con(i,j,ifrac+1)=maski(i,j)*maskk(i,j)*mask(i,j)*((
&(1.0*aW(i,j)*Con(i-1,j,ifrac+1)+0.0*aW(i,j)*Con(i-1,j-1,ifrac+1))+
& aS(i,j)*Con(i,j,ifrac+1)+
& aE(i,j)*Con(i+1,j,ifrac+1)+
& aN(i,j)*Con(i,j+1,ifrac+1))*Wt+
&((1.0*aW(i,j)*Con(i-1,j,ifrac)+0.0*aW(i,j)*Con(i-1,j-1,ifrac))+
& aS(i,j)*Con(i,j,ifrac)+
& aE(i,j)*Con(i+1,j,ifrac)+
& aN(i,j)*Con(i,j+1,ifrac))*(1.-Wt)+
& aPo(i,j)*Con(i,j,ifrac)-Wt*Vsn(i,j,3)*Snb(i,j,2)*
&Con(i,j,ifrac+1)*mask(i,j-1)-(1.-Wt)*Vsn(i,j,2)*Snb(i,j,2)*
&Con(i,j,ifrac)*mask(i,j-1)+Wt*Vsn(i,j+1,3)*Snb(i,j+1,2)*
&Con(i,j+1,ifrac+1)
&+(1.-Wt)*Vsn(i,j+1,2)*Snb(i,j+1,2)*Con(i,j+1,ifrac)
& +(Sfloc(i,j,ifrac+1)+Sflds(i,j,ifrac+1))*Vol(i,j)*Rho(i,j)
&)/aP(i,j)

```

```

else if(Mask(i,j-1).eq.0) then

```

```

Con(i,j,ifrac+1)=maski(i,j)*maskk(i,j)*mask(i,j)*((aW(i,j)*
&Con(i-1,j,ifrac+1)+
& aS(i,j)*Con(i,j,ifrac+1)+
& aE(i,j)*Con(i+1,j,ifrac+1)+
& aN(i,j)*Con(i,j+1,ifrac+1))*Wt+
& (aW(i,j)*Con(i-1,j,ifrac)+
& aS(i,j)*Con(i,j,ifrac)+
& aE(i,j)*Con(i+1,j,ifrac)+
& aN(i,j)*Con(i,j+1,ifrac))*(1.-Wt)+
& aPo(i,j)*Con(i,j,ifrac)-Wt*Vsn(i,j,3)*Snb(i,j,2)*
&Con(i,j,ifrac+1)*mask(i,j-1)-(1.-Wt)*Vsn(i,j,2)*Snb(i,j,2)*
&Con(i,j,ifrac)*mask(i,j-1)+Wt*Vsn(i,j+1,3)*Snb(i,j+1,2)*
&Con(i,j+1,ifrac+1)
&+(1.-Wt)*Vsn(i,j+1,2)*Snb(i,j+1,2)*Con(i,j+1,ifrac)
& +(Sfloc(i,j,ifrac+1)+Sflds(i,j,ifrac+1))*Vol(i,j)*Rho(i,j)
&)/aP(i,j)

```

```

    else if (Mask(i,j).EQ. 0 .OR. Maskk(i,j).EQ. 0. OR.
& Maski(i,j).EQ. 0. OR. Maske(i,j).EQ. 0) then

        Con(i,j,ifrac+1)=0.0

    else

        Con(i,j,ifrac+1)=maski(i,j)*maskk(i,j)*mask(i,j)*((aW(i,j)*
& Con(i-1,j,ifrac+1)+
&          aS(i,j)*Con(i,j-1,ifrac+1)+
&          aE(i,j)*Con(i+1,j,ifrac+1)+
&          aN(i,j)*Con(i,j+1,ifrac+1))*Wt+
&          (aW(i,j)*Con(i-1,j,ifrac)+
&          aS(i,j)*Con(i,j-1,ifrac)+
&          aE(i,j)*Con(i+1,j,ifrac)+
&          aN(i,j)*Con(i,j+1,ifrac))*(1.-Wt)+
&          aPo(i,j)*Con(i,j,ifrac)-Wt*Vsn(i,j,3)*Snb(i,j,2)*
& maski(i,j-1)*maske(i,j-1)*Con(i,j,ifrac+1)*mask(i,j-1)
& -(1.-Wt)*Vsn(i,j,2)*Snb(i,j,2)*
& maski(i,j-1)*maske(i,j-1)*Con(i,j,ifrac)*mask(i,j-1)
& +Wt*Vsn(i,j+1,3)*Snb(i,j+1,2)*Con(i,j+1,ifrac+1)
& +(1.-Wt)*Vsn(i,j+1,2)*Snb(i,j+1,2)*Con(i,j+1,ifrac)
& +(Sfloc(i,j,ifrac+1)+Sflds(i,j,ifrac+1))*Vol(i,j)*Rho(i,j)
& )/aP(i,j)
        endif
        Con(i,N+1,ifrac+1)=Con(i,N,ifrac+1)
        Con(M+1,j,ifrac+1)=Con(M,j,ifrac+1)

```

10 continue

```

    i =M
    do j = 2,N-1

        If (Con(i,j,2).eq.0.000) then

            Vsn(i,j,2)=0.00

            Vsn(i,j,3)=0.00

            Else If (Con(i,j,2).ge.Thind) then

                Vsn(i,j,2)=Max(Vmax*(exp(-Fsp*(Con(i,j,1)-Cmin))
& -exp(-Csp*(Con(i,j,1)-Cmin))),Vcom*(exp(-Fcom*
& (Con(i,j,1)-Cmin))
& -exp(-Csp*(Con(i,j,1)-Cmin))))
                Vsn(i,j,3)=Max(Vmax*(exp(-Fsp*(Con(i,j,2)-Cmin))

```

```

&-exp(-Csp*(Con(i,j,2)-Cmin))),Vcom*(exp(-Fcom*
&(Con(i,j,2)-Cmin))
&-exp(-Csp*(Con(i,j,2)-Cmin))))

Else if (Con(i,j,2).le.Tdis) then

Vsn(i,j,2)=Vfrac((ifrac-1)/2)/3600.0

Vsn(i,j,3)=Vfrac((ifrac-1)/2)/3600.0

Else

Vsn(i,j,2)=(0.667*Vfrac((ifrac-1)/2)/3600.0+ 0.333*Vmax*
&(exp(-Fsp*(Con(i,j,1)-Cmin))-exp(-Csp*(Con(i,j,1)-Cmin))))

Vsn(i,j,3)=(0.667*Vfrac((ifrac-1)/2)/3600.0+ 0.333*Vmax*
&(exp(-Fsp*(Con(i,j,2)-Cmin))-exp(-Csp*(Con(i,j,2)-Cmin))))

endif

Con(i,j,ifrac+1)=maski(i,j)*maskk(i,j)*mask(i,j)*maske(i,j)*
& ((aW(i,j)*Con(i-1,j,ifrac+1)+
& aS(i,j)*Con(i,j-1,ifrac+1)+
& aE(i,j)*Con(i,j,ifrac+1)+
& aN(i,j)*Con(i,j+1,ifrac+1))*Wt+
& (aW(i,j)*Con(i-1,j,ifrac)+
& aS(i,j)*Con(i,j-1,ifrac)+
& aE(i,j)*Con(i,j,ifrac)+
& aN(i,j)*Con(i,j+1,ifrac))*(1.-Wt)+
& aPo(i,j)*Con(i,j,ifrac)-Wt*Vsn(i,j,3)*Snb(i,j,2)*
& maske(i,j-1)*Con(i,j,ifrac+1)*mask(i,j-1)-
&(1.-Wt)*Vsn(i,j,2)*Snb(i,j,2)*
& maske(i,j-1)*Con(i,j,ifrac)*mask(i,j-1)
&+Wt*Vsn(i,j+1,3)*Snb(i,j+1,2)*Con(i,j+1,ifrac+1)
&+(1.-Wt)*Vsn(i,j+1,2)*Snb(i,j+1,2)*Con(i,j+1,ifrac)
& +(Sfloc(i,j,ifrac+1)+Sflds(i,j,ifrac+1))*Vol(i,j)*Rho(i,j)
&)/aP(i,j)
enddo

j=1
do i=2,M-1

If (Con(i,j,2).eq.0.000) then

Vsn(i,j,2)=0.00

```



```

Vsn(i,j,3)=0.00

Else If(Con(i,j,2).ge.Thind) then

Vsn(i,j,2)=Max(Vmax*(exp(-Fsp*(Con(i,j,1)-Cmin))
&-exp(-Csp*(Con(i,j,1)-Cmin))),Vcom*(exp(-Fcom*
&(Con(i,j,1)-Cmin))
&-exp(-Csp*(Con(i,j,1)-Cmin))))
Vsn(i,j,3)=Max(Vmax*(exp(-Fsp*(Con(i,j,2)-Cmin))
&-exp(-Csp*(Con(i,j,2)-Cmin))),Vcom*(exp(-Fcom*
&(Con(i,j,2)-Cmin))
&-exp(-Csp*(Con(i,j,2)-Cmin))))

Else if (Con(i,j,2).le.Tdis) then

Vsn(i,j,2)=Vfrac((ifrac-1)/2)/3600.0

Vsn(i,j,3)=Vfrac((ifrac-1)/2)/3600.0

Else

Vsn(i,j,2)=(0.667*Vfrac((ifrac-1)/2)/3600.0+ 0.333*Vmax*
&(exp(-Fsp*(Con(i,j,1)-Cmin))-exp(-Csp*(Con(i,j,1)-Cmin))))

Vsn(i,j,3)=(0.667*Vfrac((ifrac-1)/2)/3600.0+ 0.333*Vmax*
&(exp(-Fsp*(Con(i,j,2)-Cmin))-exp(-Csp*(Con(i,j,2)-Cmin))))

endif

Con(i,j,ifrac+1)=maski(i,j)*maskk(i,j)*mask(i,j)*((aW(i,j)*
&Con(i-1,j,ifrac+1))+
& aS(i,j)*Con(i,j,ifrac+1)+
& aE(i,j)*Con(i+1,j,ifrac+1)+
& aN(i,j)*Con(i,j+1,ifrac+1))*Wt+
& (aW(i,j)*Con(i-1,j,ifrac)+
& aS(i,j)*Con(i,j,ifrac)+
& aE(i,j)*Con(i+1,j,ifrac)+
& aN(i,j)*Con(i,j+1,ifrac))*(1.-Wt)+
& aPo(i,j)*Con(i,j,ifrac)+Wt*Vsn(i,j+1,3)*Snb(i,j+1,2)*
& Con(i,j+1,ifrac+1)
& +(1.-Wt)*Vsn(i,j+1,2)*Snb(i,j+1,2)*Con(i,j+1,ifrac)
& +(Sfloc(i,j,ifrac+1)+Sflds(i,j,ifrac+1))*Vol(i,j)*Rho(i,j)
&)/aP(i,j)
enddo

i=M

```

```

j=N

If (Con(i,j,2).eq.0.000) then

Vsn(i,j,2)=0.00

Vsn(i,j,3)=0.00

Else If(Con(i,j,2).ge.Thind) then

Vsn(i,j,2)=Max(Vmax*(exp(-Fsp*(Con(i,j,1)-Cmin))
&-exp(-Csp*(Con(i,j,1)-Cmin))),Vcom*(exp(-Fcom*
&(Con(i,j,1)-Cmin))
&-exp(-Csp*(Con(i,j,1)-Cmin))))
Vsn(i,j,3)=Max(Vmax*(exp(-Fsp*(Con(i,j,2)-Cmin))
&-exp(-Csp*(Con(i,j,2)-Cmin))),Vcom*(exp(-Fcom*
&(Con(i,j,2)-Cmin))
&-exp(-Csp*(Con(i,j,2)-Cmin))))

Else if (Con(i,j,2).le.Tdis) then

Vsn(i,j,2)=Vfrac((ifrac-1)/2)/3600.0

Vsn(i,j,3)=Vfrac((ifrac-1)/2)/3600.0

Else

Vsn(i,j,2)=(0.667*Vfrac((ifrac-1)/2)/3600.0+ 0.333*Vmax*
&(exp(-Fsp*(Con(i,j,1)-Cmin))-exp(-Csp*(Con(i,j,1)-Cmin))))

Vsn(i,j,3)=(0.667*Vfrac((ifrac-1)/2)/3600.0+ 0.333*Vmax*
&(exp(-Fsp*(Con(i,j,2)-Cmin))-exp(-Csp*(Con(i,j,2)-Cmin))))

endif

Con(M,N,ifrac+1)=maski(i,j)*maskk(i,j)*mask(i,j)*((aW(M,N)*
&Con(i-1,j,ifrac+1)+
&          aS(i,N)*Con(i,j-1,ifrac+1)+
&          aE(i,j)*Con(i,N,ifrac+1)+
&          aN(i,j)*Con(i,N,ifrac+1))*Wt+
&      (aW(M,N)*Con(i-1,j,ifrac) +
&          aS(i,N)*Con(i,j-1,ifrac)+
&          aE(i,j)*Con(i,N,ifrac)+
&          aN(i,j)*Con(i,N,ifrac))*(1.-Wt)+
&          aPo(i,j)*Con(i,N,ifrac)-Wt*Vsn(i,j,3)*Snb(i,j,2)*
&      Con(i,j,ifrac+1)

```

```

&-(1.-Wt)*Vsn(i,j,2)*Snb(i,j,2)*Con(i,j,ifrac)
& +(Sfloc(i,j,ifrac+1)+Sflds(i,j,ifrac+1))*Vol(i,j)*Rho(i,j)
&)/aP(i,j)

i=M
j=1

If (Con(i,j,2).eq.0.000) then

Vsn(i,j,2)=0.00

Vsn(i,j,3)=0.00

Else If(Con(i,j,2).ge.Thind) then

Vsn(i,j,2)=Max(Vmax*(exp(-Fsp*(Con(i,j,1)-Cmin))
&-exp(-Csp*(Con(i,j,1)-Cmin))),Vcom*(exp(-Fcom*
&(Con(i,j,1)-Cmin))
&-exp(-Csp*(Con(i,j,1)-Cmin))))
Vsn(i,j,3)=Max(Vmax*(exp(-Fsp*(Con(i,j,2)-Cmin))
&-exp(-Csp*(Con(i,j,2)-Cmin))),Vcom*(exp(-Fcom*
&(Con(i,j,2)-Cmin))
&-exp(-Csp*(Con(i,j,2)-Cmin))))

Else if (Con(i,j,2).le.Tdis) then

Vsn(i,j,2)=Vfrac((ifrac-1)/2)/3600.0

Vsn(i,j,3)=Vfrac((ifrac-1)/2)/3600.0

Else

Vsn(i,j,2)=(0.667*Vfrac((ifrac-1)/2)/3600.0+ 0.333*Vmax*
&(exp(-Fsp*(Con(i,j,1)-Cmin))-exp(-Csp*(Con(i,j,1)-Cmin))))

Vsn(i,j,3)=(0.667*Vfrac((ifrac-1)/2)/3600.0+ 0.333*Vmax*
&(exp(-Fsp*(Con(i,j,2)-Cmin))-exp(-Csp*(Con(i,j,2)-Cmin))))

endif

Con(i,j,ifrac+1)=maski(i,j)*maskk(i,j)*mask(i,j)*((aW(i,j)*
&Con(i-1,j,ifrac+1)+
& aS(i,j)*Con(i,j,ifrac+1)+
& aE(i,j)*Con(i,j,ifrac+1)+
& aN(i,j)*Con(i,j+1,ifrac+1))*Wt+
& (aW(i,j)*Con(i-1,j,ifrac)+

```

```

&          aS(i,j)*Con(i,j,ifrac)+
&          aE(i,j)*Con(i,j,ifrac)+
&          aN(i,j)*Con(i,j+1,ifrac))*(1.-Wt)+
&          aPo(i,j)*Con(i,j,ifrac)+Wt*Vsn(i,j+1,3)*Snb(i,j+1,2)*
&          Con(i,j+1,ifrac+1)
&+(1.-Wt)*Vsn(i,j+1,2)*Snb(i,j+1,2)*Con(i,j+1,ifrac)
& +(Sfloc(i,j,ifrac+1)+Sflds(i,j,ifrac+1))*Vol(i,j)*Rho(i,j)
&)/aP(i,j)
110 continue

```

c *****Calculations in the other direction *****

```

do 120 mmm=1,100

i=1
j=N

If (Con(i,j,2).eq.0.000) then

Vsn(i,j,2)=0.00

Vsn(i,j,3)=0.00

Else If(Con(i,j,2).ge.Thind) then

Vsn(i,j,2)=Max(Vmax*(exp(-Fsp*(Con(i,j,1)-Cmin))
&-exp(-Csp*(Con(i,j,1)-Cmin))),Vcom*(exp(-Fcom*
&(Con(i,j,1)-Cmin))
&-exp(-Csp*(Con(i,j,1)-Cmin))))
Vsn(i,j,3)=Max(Vmax*(exp(-Fsp*(Con(i,j,2)-Cmin))
&-exp(-Csp*(Con(i,j,2)-Cmin))),Vcom*(exp(-Fcom*
&(Con(i,j,2)-Cmin))
&-exp(-Csp*(Con(i,j,2)-Cmin))))

Else if (Con(i,j,2).le.Tdis) then

Vsn(i,j,2)=Vfrac((ifrac-1)/2)/3600.0

Vsn(i,j,3)=Vfrac((ifrac-1)/2)/3600.0

Else

Vsn(i,j,2)=(0.667*Vfrac((ifrac-1)/2)/3600.0+ 0.333*Vmax*
&(exp(-Fsp*(Con(i,j,1)-Cmin))-exp(-Csp*(Con(i,j,1)-Cmin))))

Vsn(i,j,3)=(0.667*Vfrac((ifrac-1)/2)/3600.0+ 0.333*Vmax*

```

```

&(exp(-Fsp*(Con(i,j,2)-Cmin))-exp(-Csp*(Con(i,j,2)-Cmin))))

endif

Con(i,j,ifrac+1)=maski(i,j)*maskk(i,j)*mask(i,j)*((aW(1,N)*
& Dyeo*frac((ifrac-1)/2)+
& aS(i,j)*Con(i,j-1,ifrac+1)+
& aE(i,j)*Con(i+1,N,ifrac+1)+
& aN(i,j)*Con(1,N,ifrac+1))*Wt+
& (aW(1,N)*Dyeo*frac((ifrac-1)/2) +
& aS(i,j)*Con(i,j-1,ifrac)+
& aE(i,j)*Con(i+1,N,ifrac)+
& aN(i,j)*Con(1,N,ifrac))*(1.-wt)+
& aPo(i,j)*Con(1,N,ifrac)-wt*Vsn(1,N,3)*Snb(i,j,2)*
& Con(1,N,ifrac+1)-(1.-wt)*Vsn(1,N,2)*Snb(i,j,2)*
& Con(1,N,ifrac)
& +(Sfloc(i,j,ifrac+1)+Sflds(i,j,ifrac+1))*Vol(i,j)*Rho(i,j)
&)/aP(i,j)

i=1
do ii=2,Ninl
j=N-(ii-1)

If (Con(i,j,2).eq.0.000) then

Vsn(i,j,2)=0.00

Vsn(i,j,3)=0.00

Else If(Con(i,j,2).ge.Thind) then

Vsn(i,j,2)=Max(Vmax*(exp(-Fsp*(Con(i,j,1)-Cmin))
&-exp(-Csp*(Con(i,j,1)-Cmin))),Vcom*(exp(-Fcom*
&(Con(i,j,1)-Cmin))
&-exp(-Csp*(Con(i,j,1)-Cmin))))
Vsn(i,j,3)=Max(Vmax*(exp(-Fsp*(Con(i,j,2)-Cmin))
&-exp(-Csp*(Con(i,j,2)-Cmin))),Vcom*(exp(-Fcom*
&(Con(i,j,2)-Cmin))
&-exp(-Csp*(Con(i,j,2)-Cmin))))

Else if (Con(i,j,2).le.Tdis) then

Vsn(i,j,2)=Vfrac((ifrac-1)/2)/3600.0

Vsn(i,j,3)=Vfrac((ifrac-1)/2)/3600.0

```

```

Else

Vsn(i,j,2)=(0.667*Vfrac((ifrac-1)/2)/3600.0+ 0.333*Vmax*
&(exp(-Fsp*(Con(i,j,1)-Cmin))-exp(-Csp*(Con(i,j,1)-Cmin))))

Vsn(i,j,3)=(0.667*Vfrac((ifrac-1)/2)/3600.0+ 0.333*Vmax*
&(exp(-Fsp*(Con(i,j,2)-Cmin))-exp(-Csp*(Con(i,j,2)-Cmin))))

endif

Con(i,j,ifrac+1)=maski(i,j)*maskk(i,j)*mask(i,j)*((aW(i,j)*
& Dyeo*frac((ifrac-1)/2) +
& aS(i,j)*Con(i,j-1,ifrac+1)+
& aE(i,j)*Con(i+1,j,ifrac+1)+
& aN(i,j)*Con(i,j+1,ifrac+1))*Wt+
& (aW(i,j)*Dyeo*frac((ifrac-1)/2) +
& aS(i,j)*Con(i,j-1,ifrac)+
& aE(i,j)*Con(i+1,j,ifrac)+
& aN(i,j)*Con(i,j+1,ifrac))*(1.-wt)+aPo(i,j)*
&Con(i,j,ifrac)
& -Wt*Vsn(i,j,3)*Snb(i,j,2)*maski(i,j-1)*maske(i,j-1)*
&Con(i,j,ifrac+1)
&*mask(i,j-1)-(1.-Wt)*Vsn(i,j,2)*Snb(i,j,2)*maski(i,j-1)*
&maske(i,j-1)*Con(i,j,ifrac)*mask(i,j-1)
&+Wt*Vsn(i,j+1,3)*Snb(i,j+1,2)*Con(i,j+1,ifrac+1)+(1.-Wt)*
&Vsn(i,j+1,2)*Snb(i,j+1,2)*Con(i,j+1,ifrac)
& +(Sfloc(i,j,ifrac+1)+Sflds(i,j,ifrac+1))*Vol(i,j)*Rho(i,j)
&)/aP(i,j)
enddo

i=1
j=1

If (Con(i,j,2).eq.0.000) then

Vsn(i,j,2)=0.00

Vsn(i,j,3)=0.00

Else If(Con(i,j,2).ge.Thind) then

Vsn(i,j,2)=Max(Vmax*(exp(-Fsp*(Con(i,j,1)-Cmin))
&-exp(-Csp*(Con(i,j,1)-Cmin))),Vcom*(exp(-Fcom*
&(Con(i,j,1)-Cmin))
&-exp(-Csp*(Con(i,j,1)-Cmin))))
Vsn(i,j,3)=Max(Vmax*(exp(-Fsp*(Con(i,j,2)-Cmin))

```

```

&-exp(-Csp*(Con(i,j,2)-Cmin)),Vcom*(exp(-Fcom*
&(Con(i,j,2)-Cmin))
&-exp(-Csp*(Con(i,j,2)-Cmin))))

Else if (Con(i,j,2).le.Tdis) then

Vsn(i,j,2)=Vfrac((ifrac-1)/2)/3600.0

Vsn(i,j,3)=Vfrac((ifrac-1)/2)/3600.0

Else

Vsn(i,j,2)=(0.667*Vfrac((ifrac-1)/2)/3600.0+ 0.333*Vmax*
&(exp(-Fsp*(Con(i,j,1)-Cmin))-exp(-Csp*(Con(i,j,1)-Cmin))))

Vsn(i,j,3)=(0.667*Vfrac((ifrac-1)/2)/3600.0+ 0.333*Vmax*
&(exp(-Fsp*(Con(i,j,2)-Cmin))-exp(-Csp*(Con(i,j,2)-Cmin))))

endif

Con(i,j,ifrac+1)=maski(i,j)*maskk(i,j)*mask(i,j)*((aW(i,j)*
&Con(1,1,ifrac+1)+
& aS(i,j)*Con(i,j,ifrac+1)+
& aE(i,j)*Con(i+1,j,ifrac+1)+
& aN(i,j)*Con(i,j+1,ifrac+1))*Wt+
& (aW(i,j)*Con(1,1,ifrac)+
& aS(i,j)*Con(i,j,ifrac)+
& aE(i,j)*Con(i+1,j,ifrac)+
& aN(i,j)*Con(i,j+1,ifrac))*(1.-wt)+
& aPo(i,j)*Con(i,j,ifrac)+Wt*Vsn(i,j+1,3)*Snb(i,j+1,2)*
&Con(i,j+1,ifrac+1)+(1.-Wt)*Vsn(i,j+1,2)*Snb(i,j+1,2)*
&Con(i,j+1,ifrac)
& +(Sfloc(i,j,ifrac+1)+Sflds(i,j,ifrac+1))*Vol(i,j)*Rho(i,j)
&)/aP(i,j)

i=1
do j=2,N-Ninl

If (Con(i,j,2).eq.0.000) then

Vsn(i,j,2)=0.00

Vsn(i,j,3)=0.00

Else If(Con(i,j,2).ge.Thind) then

```

```

Vsn(i,j,2)=Max(Vmax*(exp(-Fsp*(Con(i,j,1)-Cmin))
&-exp(-Csp*(Con(i,j,1)-Cmin))),Vcom*(exp(-Fcom*
&(Con(i,j,1)-Cmin))
&-exp(-Csp*(Con(i,j,1)-Cmin))))
Vsn(i,j,3)=Max(Vmax*(exp(-Fsp*(Con(i,j,2)-Cmin))
&-exp(-Csp*(Con(i,j,2)-Cmin))),Vcom*(exp(-Fcom*
&(Con(i,j,2)-Cmin))
&-exp(-Csp*(Con(i,j,2)-Cmin))))

Else if (Con(i,j,2).le.Tdis) then

Vsn(i,j,2)=Vfrac((ifrac-1)/2)/3600.0

Vsn(i,j,3)=Vfrac((ifrac-1)/2)/3600.0

Else

Vsn(i,j,2)=(0.667*Vfrac((ifrac-1)/2)/3600.0+ 0.333*Vmax*
&(exp(-Fsp*(Con(i,j,1)-Cmin))-exp(-Csp*(Con(i,j,1)-Cmin))))

Vsn(i,j,3)=(0.667*Vfrac((ifrac-1)/2)/3600.0+ 0.333*Vmax*
&(exp(-Fsp*(Con(i,j,2)-Cmin))-exp(-Csp*(Con(i,j,2)-Cmin))))

endif

Con(i,j,ifrac+1)=maski(i,j)*maskk(i,j)*mask(i,j)*((aW(i,j)*
&Con(i,j,ifrac+1)+
&          aS(i,j)*Con(i,j-1,ifrac+1)+
&          aE(i,j)*Con(i+1,j,ifrac+1)+
&          aN(i,j)*Con(i,j+1,ifrac+1))*Wt+
&          (aW(i,j)*Con(i,j,ifrac)+
&          aS(i,j)*Con(i,j-1,ifrac)+
&          aE(i,j)*Con(i+1,j,ifrac)+
&          aN(i,j)*Con(i,j+1,ifrac))*(1.-wt)+
&aPo(i,j)*Con(i,j,ifrac)-Wt*Vsn(i,j,3)*Snb(i,j,2)*maski(i,j-1)
&*maske(i,j-1)*Con(i,j,ifrac+1)*mask(i,j-1)-(1.-Wt)*Vsn(i,j,2)*
&Snb(i,j,2)
&*maski(i,j-1)*maske(i,j-1)*Con(i,j,ifrac)*mask(i,j-1)
&+Wt*Vsn(i,j+1,3)*Snb(i,j+1,2)*Con(i,j+1,ifrac+1)
&+(1.-Wt)*Vsn(i,j+1,2)*Snb(i,j+1,2)*Con(i,j+1,ifrac)
& +(Sfloc(i,j,ifrac+1)+Sflds(i,j,ifrac+1))*Vol(i,j)*Rho(i,j)
&)/aP(i,j)
enddo

j=N

```



```

do i=2,M-1

  If (Con(i,j,2).eq.0.000) then

    Vsn(i,j,2)=0.00

    Vsn(i,j,3)=0.00

  Else If(Con(i,j,2).ge.Thind) then

    Vsn(i,j,2)=Max(Vmax*(exp(-Fsp*(Con(i,j,1)-Cmin))
    &-exp(-Csp*(Con(i,j,1)-Cmin))),Vcom*(exp(-Fcom*
    &(Con(i,j,1)-Cmin))
    &-exp(-Csp*(Con(i,j,1)-Cmin))))
    Vsn(i,j,3)=Max(Vmax*(exp(-Fsp*(Con(i,j,2)-Cmin))
    &-exp(-Csp*(Con(i,j,2)-Cmin))),Vcom*(exp(-Fcom*
    &(Con(i,j,2)-Cmin))
    &-exp(-Csp*(Con(i,j,2)-Cmin))))

  Else if (Con(i,j,2).le.Tdis) then

    Vsn(i,j,2)=Vfrac((ifrac-1)/2)/3600.0

    Vsn(i,j,3)=Vfrac((ifrac-1)/2)/3600.0

  Else

    Vsn(i,j,2)=(0.667*Vfrac((ifrac-1)/2)/3600.0+ 0.333*Vmax*
    &(exp(-Fsp*(Con(i,j,1)-Cmin))-exp(-Csp*(Con(i,j,1)-Cmin))))

    Vsn(i,j,3)=(0.667*Vfrac((ifrac-1)/2)/3600.0+ 0.333*Vmax*
    &(exp(-Fsp*(Con(i,j,2)-Cmin))-exp(-Csp*(Con(i,j,2)-Cmin))))

  endif

  Con(i,j,ifrac+1)=maski(i,j)*maskk(i,j)*mask(i,j)*((aW(i,j)*
  &Con(i-1,j,ifrac+1)+
  &          aS(i,j)*Con(i,j-1,ifrac+1)+
  &          aE(i,j)*Con(i+1,j,ifrac+1)+
  &          aN(i,j)*Con(i,j,ifrac+1))*Wt+
  &          (aW(i,j)*Con(i-1,j,ifrac)+
  &          aS(i,j)*Con(i,j-1,ifrac)+
  &          aE(i,j)*Con(i+1,j,ifrac)+
  &          aN(i,j)*Con(i,j,ifrac))*(1.-wt)+
  &          aPo(i,j)*Con(i,j,ifrac)-Wt*Vsn(i,j,3)*Snb(i,j,2)*
  &Con(i,j,ifrac+1)-(1.-Wt)*Vsn(i,j,2)*Snb(i,j,2)*Con(i,j,ifrac)

```

```

& +(Sfloc(i,j,ifrac+1)+Sflds(i,j,ifrac+1))*Vol(i,j)*Rho(i,j)
&)/aP(i,j)
enddo

do 20 j=2,N-1
do 20 i=2,M-1

If (Con(i,j,2).eq.0.000) then

Vsn(i,j,2)=0.00

Vsn(i,j,3)=0.00

Else If(Con(i,j,2).ge.Thind) then

Vsn(i,j,2)=Max(Vmax*(exp(-Fsp*(Con(i,j,1)-Cmin))
&-exp(-Csp*(Con(i,j,1)-Cmin))),Vcom*(exp(-Fcom*
&(Con(i,j,1)-Cmin))
&-exp(-Csp*(Con(i,j,1)-Cmin))))
Vsn(i,j,3)=Max(Vmax*(exp(-Fsp*(Con(i,j,2)-Cmin))
&-exp(-Csp*(Con(i,j,2)-Cmin))),Vcom*(exp(-Fcom*
&(Con(i,j,2)-Cmin))
&-exp(-Csp*(Con(i,j,2)-Cmin))))

Else if (Con(i,j,2).le.Tdis) then

Vsn(i,j,2)=Vfrac((ifrac-1)/2)/3600.0

Vsn(i,j,3)=Vfrac((ifrac-1)/2)/3600.0

Else

Vsn(i,j,2)=(0.667*Vfrac((ifrac-1)/2)/3600.0+ 0.333*Vmax*
&(exp(-Fsp*(Con(i,j,1)-Cmin))-exp(-Csp*(Con(i,j,1)-Cmin))))

Vsn(i,j,3)=(0.667*Vfrac((ifrac-1)/2)/3600.0+ 0.333*Vmax*
&(exp(-Fsp*(Con(i,j,2)-Cmin))-exp(-Csp*(Con(i,j,2)-Cmin))))

endif

if(Mask(i,j-1). EQ. 0 .AND. Mask(i+1,j). EQ. 0) then
Con(i,j,ifrac+1)=maski(i,j)*maskk(i,j)*mask(i,j)*((aW(i,j)*
&Con(i-1,j,ifrac+1)+
& aS(i,j)*Con(i,j,ifrac+1)+
& (1.0*aE(i,j)*Con(i,j,ifrac+1))+
& aN(i,j)*Con(i,j+1,ifrac+1))*Wt+

```

```

& (aW(i,j)*Con(i-1,j,ifrac)+
& aS(i,j)*Con(i,j,ifrac)+
& (1.0*aE(i,j)*Con(i,j,ifrac))+
& aN(i,j)*Con(i,j+1,ifrac))*(1.-wt)+
& aPo(i,j)*Con(i,j,ifrac)-Wt*Vsn(i,j,3)*Snb(i,j,2)*
&Con(i,j,ifrac+1)*mask(i,j-1)-(1.-Wt)*Vsn(i,j,2)*Snb(i,j,2)*
&Con(i,j,ifrac)*mask(i,j-1)+Wt*Vsn(i,j+1,3)*Snb(i,j+1,2)*
&Con(i,j+1,ifrac+1)
&+(1.-Wt)*Vsn(i,j+1,2)*Snb(i,j+1,2)*Con(i,j+1,ifrac)
& +(Sfloc(i,j,ifrac+1)+Sflds(i,j,ifrac+1))*Vol(i,j)*Rho(i,j)
&)/aP(i,j)

```

else if(Mask(i,j-1).EQ. 0 .AND. Mask(i-1,j-1).EQ. 1) then

```

Con(i,j,ifrac+1)=maski(i,j)*maskk(i,j)*mask(i,j)*((
&(1.0*aW(i,j)*Con(i-1,j,ifrac+1)+0.0*aW(i,j)*Con(i-1,j-1,ifrac+1))+
& aS(i,j)*Con(i,j,ifrac+1)+
& aE(i,j)*Con(i+1,j,ifrac+1)+
& aN(i,j)*Con(i,j+1,ifrac+1))*Wt+
&((1.0*aW(i,j)*Con(i-1,j,ifrac)+0.0*aW(i,j)*Con(i-1,j-1,ifrac))+
& aS(i,j)*Con(i,j,ifrac)+
& aE(i,j)*Con(i+1,j,ifrac)+
& aN(i,j)*Con(i,j+1,ifrac))*(1.-Wt)+
& aPo(i,j)*Con(i,j,ifrac)-Wt*Vsn(i,j,3)*Snb(i,j,2)*
&Con(i,j,ifrac+1)*mask(i,j-1)-(1.-Wt)*Vsn(i,j,2)*Snb(i,j,2)*
&Con(i,j,ifrac)*mask(i,j-1)+Wt*Vsn(i,j+1,3)*Snb(i,j+1,2)*
&Con(i,j+1,ifrac+1)
&+(1.-Wt)*Vsn(i,j+1,2)*Snb(i,j+1,2)*Con(i,j+1,ifrac)
& +(Sfloc(i,j,ifrac+1)+Sflds(i,j,ifrac+1))*Vol(i,j)*Rho(i,j)
&)/aP(i,j)

```

else if(Mask(i,j-1).eq.0) then

```

Con(i,j,ifrac+1)=maski(i,j)*maskk(i,j)*mask(i,j)*((aW(i,j)*
&Con(i-1,j,ifrac+1)+
& aS(i,j)*Con(i,j,ifrac+1)+
& aE(i,j)*Con(i+1,j,ifrac+1)+
& aN(i,j)*Con(i,j+1,ifrac+1))*Wt+
& (aW(i,j)*Con(i-1,j,ifrac)+
& aS(i,j)*Con(i,j,ifrac)+
& aE(i,j)*Con(i+1,j,ifrac)+
& aN(i,j)*Con(i,j+1,ifrac))*(1.-Wt)+
& aPo(i,j)*Con(i,j,ifrac)-Wt*Vsn(i,j,3)*Snb(i,j,2)*
&Con(i,j,ifrac+1)*mask(i,j-1)-(1.-Wt)*Vsn(i,j,2)*Snb(i,j,2)*
&Con(i,j,ifrac)*mask(i,j-1)+Wt*Vsn(i,j+1,3)*Snb(i,j+1,2)*
&Con(i,j+1,ifrac+1)

```

```

&+(1.-Wt)*Vsn(i,j+1,2)*Snb(i,j+1,2)*Con(i,j+1,ifrac)
& +(Sfloc(i,j,ifrac+1)+Sflds(i,j,ifrac+1))*Vol(i,j)*Rho(i,j)
&)/aP(i,j)

    else if(Mask(i,j).EQ. 0 .OR. Maskk(i,j).EQ. 0. OR.
& Maski(i,j).EQ. 0. OR. Maske(i,j).EQ. 0) then

        Con(i,j,ifrac+1)=0.0

    else

        Con(i,j,ifrac+1)=maski(i,j)*maskk(i,j)*mask(i,j)*((aW(i,j)*
&Con(i-1,j,ifrac+1)+
&          aS(i,j)*Con(i,j-1,ifrac+1)+
&          aE(i,j)*Con(i+1,j,ifrac+1)+
&          aN(i,j)*Con(i,j+1,ifrac+1))*Wt+
&          (aW(i,j)*Con(i-1,j,ifrac)+
&          aS(i,j)*Con(i,j-1,ifrac)+
&          aE(i,j)*Con(i+1,j,ifrac)+
&          aN(i,j)*Con(i,j+1,ifrac))*(1.-Wt)+
&          aPo(i,j)*Con(i,j,ifrac)-Wt*Vsn(i,j,3)*Snb(i,j,2)*
&maski(i,j-1)*maske(i,j-1)*Con(i,j,ifrac+1)*mask(i,j-1)
&-(1.-Wt)*Vsn(i,j,2)*Snb(i,j,2)*
&maski(i,j-1)*maske(i,j-1)*Con(i,j,ifrac)*mask(i,j-1)
&+Wt*Vsn(i,j+1,3)*Snb(i,j+1,2)*Con(i,j+1,ifrac+1)
&+(1.-Wt)*Vsn(i,j+1,2)*Snb(i,j+1,2)*Con(i,j+1,ifrac)
& +(Sfloc(i,j,ifrac+1)+Sflds(i,j,ifrac+1))*Vol(i,j)*Rho(i,j)
&)/aP(i,j)
    endif
    Con(i,N+1,ifrac+1)=Con(i,N,ifrac+1)
    Con(M+1,j,ifrac+1)=Con(M,j,ifrac+1)

```

20 continue

```

j=1
do i=2,M-1

```

```

    If (Con(i,j,2).eq.0.000) then

```

```

        Vsn(i,j,2)=0.00

```

```

        Vsn(i,j,3)=0.00

```

```

    Else If(Con(i,j,2).ge.Thind) then

```

```

        Vsn(i,j,2)=Max(Vmax*(exp(-Fsp*(Con(i,j,1)-Cmin))

```

```

&-exp(-Csp*(Con(i,j,1)-Cmin))),Vcom*(exp(-Fcom*
&(Con(i,j,1)-Cmin))
&-exp(-Csp*(Con(i,j,1)-Cmin))))
Vsn(i,j,3)=Max(Vmax*(exp(-Fsp*(Con(i,j,2)-Cmin))
&-exp(-Csp*(Con(i,j,2)-Cmin))),Vcom*(exp(-Fcom*
&(Con(i,j,2)-Cmin))
&-exp(-Csp*(Con(i,j,2)-Cmin))))

Else if (Con(i,j,2).le.Tdis) then

Vsn(i,j,2)=Vfrac((ifrac-1)/2)/3600.0

Vsn(i,j,3)=Vfrac((ifrac-1)/2)/3600.0

Else

Vsn(i,j,2)=(0.667*Vfrac((ifrac-1)/2)/3600.0+ 0.333*Vmax*
&(exp(-Fsp*(Con(i,j,1)-Cmin))-exp(-Csp*(Con(i,j,1)-Cmin))))

Vsn(i,j,3)=(0.667*Vfrac((ifrac-1)/2)/3600.0+ 0.333*Vmax*
&(exp(-Fsp*(Con(i,j,2)-Cmin))-exp(-Csp*(Con(i,j,2)-Cmin))))

endif

Con(i,j,ifrac+1)=maski(i,j)*maskk(i,j)*mask(i,j)*((aW(i,j)*
&Con(i-1,j,ifrac+1)+
& aS(i,j)*Con(i,j,ifrac+1)+
& aE(i,j)*Con(i+1,j,ifrac+1)+
& aN(i,j)*Con(i,j+1,ifrac+1))*Wt+
& (aW(i,j)*Con(i-1,j,ifrac)+
& aS(i,j)*Con(i,j,ifrac)+
& aE(i,j)*Con(i+1,j,ifrac)+
& aN(i,j)*Con(i,j+1,ifrac))*(1.-Wt)+
& aPo(i,j)*Con(i,j,ifrac)+Wt*Vsn(i,j+1,3)*Snb(i,j+1,2)*
& Con(i,j+1,ifrac+1)
& +(1.-Wt)*Vsn(i,j+1,2)*Snb(i,j+1,2)*Con(i,j+1,ifrac)
& +(Sfloc(i,j,ifrac+1)+Sflds(i,j,ifrac+1))*Vol(i,j)*Rho(i,j)
&)/aP(i,j)
enddo

i =M
do j = 2,N-1

If (Con(i,j,2).eq.0.000) then

Vsn(i,j,2)=0.00

```

$$V_{sn}(i,j,3)=0.00$$

Else If(Con(i,j,2).ge.Thind) then

$$\begin{aligned} V_{sn}(i,j,2) &= \text{Max}(V_{\text{max}} * (\exp(-F_{\text{sp}} * (\text{Con}(i,j,1) - C_{\text{min}})) \\ &\& \exp(-C_{\text{sp}} * (\text{Con}(i,j,1) - C_{\text{min}}))), V_{\text{com}} * (\exp(-F_{\text{com}} * \\ &\& (\text{Con}(i,j,1) - C_{\text{min}})) \\ &\& \exp(-C_{\text{sp}} * (\text{Con}(i,j,1) - C_{\text{min}})))) \\ V_{sn}(i,j,3) &= \text{Max}(V_{\text{max}} * (\exp(-F_{\text{sp}} * (\text{Con}(i,j,2) - C_{\text{min}})) \\ &\& \exp(-C_{\text{sp}} * (\text{Con}(i,j,2) - C_{\text{min}}))), V_{\text{com}} * (\exp(-F_{\text{com}} * \\ &\& (\text{Con}(i,j,2) - C_{\text{min}})) \\ &\& \exp(-C_{\text{sp}} * (\text{Con}(i,j,2) - C_{\text{min}})))) \end{aligned}$$

Else if (Con(i,j,2).le.Tdis) then

$$V_{sn}(i,j,2) = V_{\text{frac}}((\text{ifrac}-1)/2)/3600.0$$

$$V_{sn}(i,j,3) = V_{\text{frac}}((\text{ifrac}-1)/2)/3600.0$$

Else

$$V_{sn}(i,j,2) = (0.667 * V_{\text{frac}}((\text{ifrac}-1)/2)/3600.0 + 0.333 * V_{\text{max}} * \& (\exp(-F_{\text{sp}} * (\text{Con}(i,j,1) - C_{\text{min}})) - \exp(-C_{\text{sp}} * (\text{Con}(i,j,1) - C_{\text{min}}))))$$

$$V_{sn}(i,j,3) = (0.667 * V_{\text{frac}}((\text{ifrac}-1)/2)/3600.0 + 0.333 * V_{\text{max}} * \& (\exp(-F_{\text{sp}} * (\text{Con}(i,j,2) - C_{\text{min}})) - \exp(-C_{\text{sp}} * (\text{Con}(i,j,2) - C_{\text{min}}))))$$

endif

$$\begin{aligned} \text{Con}(i,j,\text{ifrac}+1) &= \text{maski}(i,j) * \text{maskk}(i,j) * \text{mask}(i,j) * \text{maske}(i,j) * \\ &\& ((aW(i,j) * \text{Con}(i-1,j,\text{ifrac}+1) + \\ &\& aS(i,j) * \text{Con}(i,j-1,\text{ifrac}+1) + \\ &\& aE(i,j) * \text{Con}(i,j,\text{ifrac}+1) + \\ &\& aN(i,j) * \text{Con}(i,j+1,\text{ifrac}+1)) * Wt + \\ &\& (aW(i,j) * \text{Con}(i-1,j,\text{ifrac}) + \\ &\& aS(i,j) * \text{Con}(i,j-1,\text{ifrac}) + \\ &\& aE(i,j) * \text{Con}(i,j,\text{ifrac}) + \\ &\& aN(i,j) * \text{Con}(i,j+1,\text{ifrac})) * (1.-Wt) + \\ &\& aPo(i,j) * \text{Con}(i,j,\text{ifrac}) - Wt * V_{sn}(i,j,3) * \text{Snb}(i,j,2) * \\ &\& \text{maske}(i,j-1) * \text{Con}(i,j,\text{ifrac}+1) * \text{mask}(i,j-1) - \\ &\& (1.-Wt) * V_{sn}(i,j,2) * \text{Snb}(i,j,2) * \\ &\& \text{maske}(i,j-1) * \text{Con}(i,j,\text{ifrac}) * \text{mask}(i,j-1) \\ &\& + Wt * V_{sn}(i,j+1,3) * \text{Snb}(i,j+1,2) * \text{Con}(i,j+1,\text{ifrac}+1) \\ &\& + (1.-Wt) * V_{sn}(i,j+1,2) * \text{Snb}(i,j+1,2) * \text{Con}(i,j+1,\text{ifrac}) \\ &\& + (Sfloc(i,j,\text{ifrac}+1) + Sflds(i,j,\text{ifrac}+1)) * Vol(i,j) * Rho(i,j) \end{aligned}$$

```

&)/aP(i,j)
enddo

i=M
j=N

If (Con(i,j,2).eq.0.000) then

Vsn(i,j,2)=0.00

Vsn(i,j,3)=0.00

Else If(Con(i,j,2).ge.Thind) then

Vsn(i,j,2)=Max(Vmax*(exp(-Fsp*(Con(i,j,1)-Cmin))
&-exp(-Csp*(Con(i,j,1)-Cmin))),Vcom*(exp(-Fcom*
&(Con(i,j,1)-Cmin))
&-exp(-Csp*(Con(i,j,1)-Cmin))))
Vsn(i,j,3)=Max(Vmax*(exp(-Fsp*(Con(i,j,2)-Cmin))
&-exp(-Csp*(Con(i,j,2)-Cmin))),Vcom*(exp(-Fcom*
&(Con(i,j,2)-Cmin))
&-exp(-Csp*(Con(i,j,2)-Cmin))))

Else if (Con(i,j,2).le.Tdis) then

Vsn(i,j,2)=Vfrac((ifrac-1)/2)/3600.0

Vsn(i,j,3)=Vfrac((ifrac-1)/2)/3600.0

Else

Vsn(i,j,2)=(0.667*Vfrac((ifrac-1)/2)/3600.0+ 0.333*Vmax*
&(exp(-Fsp*(Con(i,j,1)-Cmin))-exp(-Csp*(Con(i,j,1)-Cmin))))

Vsn(i,j,3)=(0.667*Vfrac((ifrac-1)/2)/3600.0+ 0.333*Vmax*
&(exp(-Fsp*(Con(i,j,2)-Cmin))-exp(-Csp*(Con(i,j,2)-Cmin))))

endif

Con(M,N,ifrac+1)=maski(i,j)*maskk(i,j)*mask(j,i)*((aW(M,N)*
&Con(i-1,j,ifrac+1)+
& aS(i,N)*Con(i,j-1,ifrac+1)+
& aE(i,j)*Con(i,N,ifrac+1)+
& aN(i,j)*Con(i,N,ifrac+1))*Wt+
& (aW(M,N)*Con(i-1,j,ifrac) +

```

```

&          aS(i,N)*Con(i,j-1,ifrac)+
&          aE(i,j)*Con(i,N,ifrac)+
&          aN(i,j)*Con(i,N,ifrac))*(1.-Wt)+
&          aPo(i,j)*Con(i,N,ifrac)-Wt*Vsn(i,j,3)*Snb(i,j,2)*
&          Con(i,j,ifrac+1)
&-(1.-Wt)*Vsn(i,j,2)*Snb(i,j,2)*Con(i,j,ifrac)
& +(Sfloc(i,j,ifrac+1)+Sflds(i,j,ifrac+1))*Vol(i,j)*Rho(i,j)
&)/aP(i,j)

```

```

i=M
j=1

```

```

If (Con(i,j,2).eq.0.000) then

```

```

Vsn(i,j,2)=0.00

```

```

Vsn(i,j,3)=0.00

```

```

Else If(Con(i,j,2).ge.Thind) then

```

```

Vsn(i,j,2)=Max(Vmax*(exp(-Fsp*(Con(i,j,1)-Cmin))
&-exp(-Csp*(Con(i,j,1)-Cmin))),Vcom*(exp(-Fcom*
&(Con(i,j,1)-Cmin))
&-exp(-Csp*(Con(i,j,1)-Cmin))))
Vsn(i,j,3)=Max(Vmax*(exp(-Fsp*(Con(i,j,2)-Cmin))
&-exp(-Csp*(Con(i,j,2)-Cmin))),Vcom*(exp(-Fcom*
&(Con(i,j,2)-Cmin))
&-exp(-Csp*(Con(i,j,2)-Cmin))))

```

```

Else if (Con(i,j,2).le.Tdis) then

```

```

Vsn(i,j,2)=Vfrac((ifrac-1)/2)/3600.0

```

```

Vsn(i,j,3)=Vfrac((ifrac-1)/2)/3600.0

```

```

Else

```

```

Vsn(i,j,2)=(0.667*Vfrac((ifrac-1)/2)/3600.0+ 0.333*Vmax*
&(exp(-Fsp*(Con(i,j,1)-Cmin))-exp(-Csp*(Con(i,j,1)-Cmin))))

```

```

Vsn(i,j,3)=(0.667*Vfrac((ifrac-1)/2)/3600.0+ 0.333*Vmax*
&(exp(-Fsp*(Con(i,j,2)-Cmin))-exp(-Csp*(Con(i,j,2)-Cmin))))

```

```

endif

```

```

Con(i,j,ifrac+1)=maski(i,j)*maskk(i,j)*mask(i,j)*((aW(i,j)*

```



```

&Con(i-1,j,ifrac+1)+
&          aS(i,j)*Con(i,j,ifrac+1)+
&          aE(i,j)*Con(i,j,ifrac+1)+
&          aN(i,j)*Con(i,j+1,ifrac+1))*Wt+
&          (aW(i,j)*Con(i-1,j,ifrac)+
&          aS(i,j)*Con(i,j,ifrac)+
&          aE(i,j)*Con(i,j,ifrac)+
&          aN(i,j)*Con(i,j+1,ifrac))*(1.-Wt)+
&          aPo(i,j)*Con(i,j,ifrac)+Wt*Vsn(i,j+1,3)*Snb(i,j+1,2)*
&          Con(i,j+1,ifrac+1)
&+(1.-Wt)*Vsn(i,j+1,2)*Snb(i,j+1,2)*Con(i,j+1,ifrac)
& +(Sfloc(i,j,ifrac+1)+Sflds(i,j,ifrac+1))*Vol(i,j)*Rho(i,j)
&)/aP(i,j)
120 continue

return
end

```

```

c*****
c*****SUBROUTINE: FLOCCU*****
c*****Subroutine to Calculate the Flocculation Parameters*****
c*****
subroutine Floccu(mm)
c
c    Called from Main
c    Calls: none
c    include 'comdeck'

Include 'comdeck3.h'
REAL nu0, nut,LL,mask,maskk,NBl,Inlet,maski,maske
INTEGER IPRINT

c    psi= streamfunction, vort = vorticity
c    u= x velocity, v= y velocity, p = pressure
c    phi=scalar variable, C = Concentration, rho= density
c    Temp(200,100), nut(200,100), Con(200,100)
c    Fnb = face value of advection flux, Dnb=face value of diffusion flux, XX=??
c    rhonb(200,100,nf)= face density of fluid, nf = 1 vert face, nf = 2 horiz face
c    nu0 = kinematic viscosity
c    dyr=Dy/Dr
c    dry=Dr/Dy
c Boundary Conditions

```

c***** G VALUES - CALCULATION *****

```

CoreS=4.
CoreL=CoreS*WidthIn/2.
Do i=1,M
  Do j=1,N

    If (con(i,j,1).LE.1) Then
      Fnut(i,j)=Max((0.000001*Exp(1.386294361*con(i,j,1))),1E-6)
    Else
      Fnut(i,j)=Max((0.0000029*Exp(0.3218875825*con(i,j,1))),1E-6)
    Endif

    CDv(i,j)=Min(1./((2.*Hbl*Abs(Vbl(i,j))*0.01/Fnut(i,j))**(1./3.)),
&1.)

  Enddo
Enddo

If(NCenter.eq.1) then

  do i=1,Icenter-1
  do j=N,(N+1-Ninl),-1

    Gf(i,j)=1.53*((Uw(1,j)**1.5)*(Inlet**0.75)/((Fnut(i,j)**0.5)*
&((Dr/2.+(i-1)*Dr)**1.25)))*Min(1.0,((Dr/2.+(i-1)*Dr)/CoreL))
&+Grad(i,j)

  enddo
enddo

  do i=1,Icenter-1
  do j=(N-Ninl),1,-1

    If (((dr/2.+(i-1)*dr)/5.).GE.(Dy/2.+(N-Ninl-j)*Dy)) Then

      Gf(i,j)=1.53*((Uw(1,N-1)**1.5)*(Inlet**0.75)/((Fnut(i,j)**0.5)*
&((Dr/2.+(i-1)*Dr)**1.25)))*Min(1.0,((Dr/2.+(i-1)*Dr)/CoreL))
&+Grad(i,j)

    Else

      Gf(i,j)=Grad(i,j)

    endif
  enddo
enddo

```

```

enddo

do i=Icenter,M+1
do j=N+1,1,-1

Gf(i,j)=Grad(i,j)

enddo
enddo

VollT=0.0
do i=1,Icenter-1
do j=Jcenter,N,1
VollT=VollT+Vol(i,j)
enddo
enddo

Gavg=SQRT(1.03*Uw(1,N)**2*Q1/(1E-6*2*VollT*2*pi))

VolGL=0.0
VolJT=0.0
do i=1,Icenter-1
do j=Jcenter,N,1

If (((dr/2.+(i-1)*dr)/5.).GE.(Dy/2.+(N-Ninl-j)*Dy)) Then

VolJT=VolJT+Vol(i,j)
VolGL=VolGL+Gf(i,j)*Vol(i,j)

Endif

enddo
enddo

Gjet=Gavg*VollT/VolJT

GLavg=VolGL/VolJT

Gcor=Min((GLavg/Gjet),2.4)

do i=1,Icenter-1
do j=Jcenter,N,1

If (((dr/2.+(i-1)*dr)/5.).GE.(Dy/2.+(N-Ninl-j)*Dy)) Then

Gf(i,j)=Max((Gf(i,j)/Gcor),Gavg)

```

Else

Gf(i,j)=Gavg

endif

enddo

enddo

c***Flocculation por the case without a Center Well and EDI**

Else if(NCenter2.eq.1) then

do i=1,icenter2

do j=N,Min((N+1-Ninl),jcenter2),-1

Gf(i,j)=0.5*1.53*((Uw(1,N)**1.5)*(Inlet**0.75)/((Fnut(i,j)**0.5)*
&((Dr/2.+(i-1)*Dr)**1.25)))*Min(1.0,((Dr/2.+(i-1)*Dr)/CoreL))
&+Grad(i,j)

enddo

enddo

do i=icenter2+1,M

do j=N+1,jcenter2,-1

Gf(i,j)=Grad(i,j)

enddo

enddo

do i=1,M

do j=Min(jcenter2-1,(N-Ninl)),1,-1

If (((dr/2.+(i-1)*dr)/4.).GE.(Dy/2.+(Min(jcenter2-1,(N-Ninl))-j)
&*Dy)) Then

Gf(i,j)=(0.35-.35*i/M)*1.53*((Uw(1,N)**1.5)*(Inlet**0.75)/
&((Fnut(i,j)**0.5)*
&((Dr/2.+(i-1)*Dr)**1.25)))*Min(1.0,((Dr/2.+(i-1)*Dr)/CoreL))
&+Grad(i,j)

Else

Gf(i,j)=Grad(i,j)

endif

enddo

enddo

c***Flocculation por the case without a Center Well**

Else

do i=1,M

do j=N,(N+1-Ninl),-1

Gf(i,j)=(0.35-.35*i/M)*1.53*((Uw(1,j)**1.5)*(Inlet**0.75)/
&((Fnut(i,j)**0.5)*
&((Dr/2.+(i-1)*Dr)**1.25)))*Min(1.0,((Dr/2.+(i-1)*Dr)/CoreL))
&+Grad(i,j)

enddo

enddo

do i=1,M

do j=(N-Ninl),1,-1

If (((dr/2.+(i-1)*dr)/5.).GE.(Dy/2.+(N-Ninl-j)*Dy)) Then

Gf(i,j)=(0.35-.35*i/M)*1.53*((Uw(1,N-1)**1.5)*(Inlet**0.75)/
&((Fnut(i,j)**0.5)*
&((Dr/2.+(i-1)*Dr)**1.25)))*Min(1.0,((Dr/2.+(i-1)*Dr)/CoreL))
&+Grad(i,j)

Else

Gf(i,j)=Grad(i,j)

endif

enddo

enddo

Endif

c**** **Diameter Calculation particle diameter based on discrete settling velocity**

Do i=1,Nfraction

If ((Vfrac(i)/3.6).GE.0.527) then

Dfrac(i)=(Vfrac(i)/3.6-0.35)/(1.77*1000) !Li&Ganczarczyk Relationship

Else

Dfrac(i)=(Vfrac(i)/3.6)/(5.27*1000) !ModifiedLi&Ganczarczyk Relationship

Endif

enddo

c*******Flocculation Source Term Calculation*******

Do i=1,M

Do j=1,N

c***** **Aggregation and Breakup Terms** *****

SFloc(i,j,4)= (Fka*Con(i,j,4)*(Con(i,j,6)+Con(i,j,8))*Gf(i,j)-
&Fkb*Con(i,j,4)*Gf(i,j)**fm)

SFloc(i,j,3)=SFloc(i,j,4)

Sfloc(i,j,6)= (-Fka*Con(i,j,4)*Con(i,j,6)*Gf(i,j) +
&(Frac(2)/(Frac(2)+Frac(3)))*Fkb*Con(i,j,4)*Gf(i,j)**fm)

SFloc(i,j,5)=SFloc(i,j,6)

Sfloc(i,j,8)= (-Fka*Con(i,j,4)*Con(i,j,8)*Gf(i,j) +
&(Frac(3)/(Frac(2)+Frac(3)))*Fkb*Con(i,j,4)*Gf(i,j)**fm)

SFloc(i,j,7)=SFloc(i,j,8)

c***** **Differential Settling Terms** *****

Sflds(i,j,4)= 1.5*Fkds*Con(i,j,4)*(Con(i,j,6)**2)*
&(Vfrac(1)-Vfrac(2))*((1+2*Dfrac(2)/Dfrac(1))**2)/(
&3600.0*Dfrac(1)*(Densr(i,j)*Spegra)**2) +
&1.5*Fkds*Con(i,j,4)*(Con(i,j,8)**2)*
&(Vfrac(1)-Vfrac(3))*((1+2*Dfrac(3)/Dfrac(1))**2)/(
&3600.0*Dfrac(1)*(Densr(i,j)*Spegra)**2)
Sflds(i,j,3)= Sflds(i,j,4)

```

      Sflds(i,j,6)= -1.5*Fkds*Con(i,j,4)*(Con(i,j,6)**2)*
&(Vfrac(1)-Vfrac(2))*((1+2*Dfrac(2)/Dfrac(1))**2)/(
&3600.0*Dfrac(1)*(Densr(i,j)*Spegra)**2)

```

```

      Sflds(i,j,5)= Sflds(i,j,6)

```

```

      Sflds(i,j,8)= -1.5*Fkds*Con(i,j,4)*(Con(i,j,8)**2)*
&(Vfrac(1)-Vfrac(3))*((1+2*Dfrac(3)/Dfrac(1))**2)/(
&3600.0*Dfrac(1)*(Densr(i,j)*Spegra)**2)

```

```

      Sflds(i,j,7)= Sflds(i,j,8)

```

```

      enddo

```

```

      enddo

```

```

      return

```

```

      end

```

```

c*****
c*****SUBROUTINE: DYETRA*****
c*****Subroutine for the transport of dye*****
c*****Subroutine to calculate Dye*****
c*****

```

```

      subroutine dyetra(mm)

```

```

c This subroutine computes the transport of a conservative scalar quality in 2-D and
Concentration.

```

```

c      Called from Main

```

```

c      Calls: none

```

```

c      include 'comdeck'

```

```

      Include 'comdeck3.h'

```

```

      REAL nuo, nut,LL,mask,maskk,NB1,Inlet,maski,maske

```

```

      INTEGER IPRINT

```

```

c      psi= streamfunction, vort = vorticity

```

```

c      u= x velocity, v= y velocity, p = pressure

```

```

c      phi=scalar variable, C = concentration, rho= density

```

```

c      Temp(200,100), nut(200,100), Dye(200,100)

```

```

c      Fnb = face value of advection flux, Dnb=face value of diffusion flux, XX=??

```

```

c      rhonb(200,100,nf)= face density of fluid, nf = 1 vert face, nf = 2 horiz face

```

```

c      nuo = kinematic viscosity

```

```

      do i=1,M

```

```

do j=1,N
Dye(i,j,2)=Dye(i,j,3)
enddo
enddo

do 110 mmm=1,100

i=1
j=N

if(Iswitch.eq.0) then

Vsn(i,j,3)=0

else

Vsn(i,j,3)=Max(Vmax*(exp(-Fsp*(Dye(i,j,2)-Cmin))
&-exp(-Csp*(Dye(i,j,2)-Cmin))),0.0)

endif

Dye(i,j,3)=maski(i,j)*maskk(i,j)*mask(i,j)*((aW(1,N)*Dyeo+
&          aS(i,j)*Dye(i,j-1,3)+
&          aE(i,j)*Dye(i+1,N,3)+
&          aN(i,j)*Dye(1,N,3))*Wt+
&          (aW(1,N)*Dyeo +
&          aS(i,j)*Dye(i,j-1,2)+
&          aE(i,j)*Dye(i+1,N,2)+
&          aN(i,j)*Dye(1,N,2))*(1.-Wt)+
&          aPo(i,j)*Dye(1,N,2)-Vsn(1,N,3)*Snb(i,j,2)*
&          Dye(1,N,3))/aP(i,j)

i=1
do ii=2,Ninl
j=N-(ii-1)

if(Iswitch.eq.0) then

Vsn(i,j,3)=0

else

Vsn(i,j,3)=Max(Vmax*(exp(-Fsp*(Dye(i,j,2)-Cmin))
&-exp(-Csp*(Dye(i,j,2)-Cmin))),0.0)

endif

```



```

Dye(i,j,3)=maski(i,j)*maskk(i,j)*mask(i,j)*((aW(i,j)*Dyeo +
&          aS(i,j)*Dye(i,j-1,3)+
&          aE(i,j)*Dye(i+1,j,3)+
&          aN(i,j)*Dye(i,j+1,3))*Wt+
&          (aW(i,j)*Dyeo +
&          aS(i,j)*Dye(i,j-1,2)+
&          aE(i,j)*Dye(i+1,j,2)+
&          aN(i,j)*Dye(i,j+1,2))*(1.-Wt)+
&          aPo(i,j)*Dye(i,j,2)-Vsn(i,j,3)*Snb(i,j,2)*maski(i,j-1)*
& maske(i,j-1)*Dye(i,j,3)*mask(i,j-1)+Vsn(i,j+1,3)*Snb(i,j+1,2)*
&          Dye(i,j+1,3))/aP(i,j)
enddo

```

```

i=1
j=1
if(Iswitch.eq.0) then
  Vsn(i,j,3)=0
else
  Vsn(i,j,3)=Max(Vmax*(exp(-Fsp*(Dye(i,j,2)-Cmin))
&-exp(-Csp*(Dye(i,j,2)-Cmin))),0.0)

```

```
endif
```

```

Dye(i,j,3)=maski(i,j)*maskk(i,j)*mask(i,j)*((aW(i,j)*Dye(1,1,3)+
&          aS(i,j)*Dye(i,j,3)+
&          aE(i,j)*Dye(i+1,j,3)+
&          aN(i,j)*Dye(i,j+1,3))*Wt+
&          (aW(i,j)*Dye(1,1,2)+
&          aS(i,j)*Dye(i,j,2)+
&          aE(i,j)*Dye(i+1,j,2)+
&          aN(i,j)*Dye(i,j+1,2))*(1.-Wt)+
&          aPo(i,j)*Dye(i,j,2)+Vsn(i,j+1,3)*Snb(i,j+1,2)*
&          Dye(i,j+1,3))/aP(i,j)

```

```

i=1
do j=2,N-Ninl
  if(Iswitch.eq.0) then
    Vsn(i,j,3)=0
  else
    Vsn(i,j,3)=Max(Vmax*(exp(-Fsp*(Dye(i,j,2)-Cmin))
&-exp(-Csp*(Dye(i,j,2)-Cmin))),0.0)
  endif

```

```

Dye(i,j,3)=maski(i,j)*maskk(i,j)*mask(i,j)*((aW(i,j)*Dye(i,j,3)+
&          aS(i,j)*Dye(i,j-1,3)+

```

```

&          aE(i,j)*Dye(i+1,j,3)+
&          aN(i,j)*Dye(i,j+1,3))*Wt+
&      (aW(i,j)*Dye(i,j,2)+
&          aS(i,j)*Dye(i,j-1,2)+
&          aE(i,j)*Dye(i+1,j,2)+
&          aN(i,j)*Dye(i,j+1,2))*(1.-Wt)+
&          aPo(i,j)*Dye(i,j,2)-Vsn(i,j,3)*Snb(i,j,2)*maski(i,j-1)*
&  maske(i,j-1)*Dye(i,j,3)*mask(i,j-1)+Vsn(i,j+1,3)*Snb(i,j+1,2)*
&      Dye(i,j+1,3))/aP(i,j)
enddo

      j=N
      do i=2,M-1
        if(Iswitch.eq.0) then
          Vsn(i,j,3)=0
        else
          Vsn(i,j,3)=Max(Vmax*(exp(-Fsp*(Dye(i,j,2)-Cmin))
&-exp(-Csp*(Dye(i,j,2)-Cmin))),0.0)
        endif

        Dye(i,j,3)=maski(i,j)*maskk(i,j)*mask(i,j)*((aW(i,j)*Dye(i-1,j,3)+
&          aS(i,j)*Dye(i,j-1,3)+
&          aE(i,j)*Dye(i+1,j,3)+
&          aN(i,j)*Dye(i,j,3))*Wt+
&      (aW(i,j)*Dye(i-1,j,2)+
&          aS(i,j)*Dye(i,j-1,2)+
&          aE(i,j)*Dye(i+1,j,2)+
&          aN(i,j)*Dye(i,j,2))*(1.-Wt)+
&          aPo(i,j)*Dye(i,j,2)-Vsn(i,j,3)*Snb(i,j,2)*
&      Dye(i,j,3))/aP(i,j)
        enddo

        do 10 i=2,M-1
          do 10 j=2,N-1
            if(Iswitch.eq.0) then
              Vsn(i,j,3)=0
            else
              Vsn(i,j,3)=Max(Vmax*(exp(-Fsp*(Dye(i,j,2)-Cmin))
&-exp(-Csp*(Dye(i,j,2)-Cmin))),0.0)
            endif

            if(Mask(i,j-1).EQ.0.AND.Mask(i+1,j).EQ.0) then
              Dye(i,j,3)=maski(i,j)*maskk(i,j)*mask(i,j)*((aW(i,j)*Dye(i-1,j,3)+
&          aS(i,j)*Dye(i,j,3)+
&      (1.0*aE(i,j)*Dye(i,j,3))+
&          aN(i,j)*Dye(i,j+1,3))*Wt+

```

```

&          (aW(i,j)*Dye(i-1,j,2)+
&          aS(i,j)*Dye(i,j,2)+
& (1.0*aE(i,j)*Dye(i,j,2))+
&          aN(i,j)*Dye(i,j+1,2))*(1.-Wt)+
&          aPo(i,j)*Dye(i,j,2)-Vsn(i,j,3)*Snb(i,j,2)*
&          Dye(i,j,3)*mask(i,j-1)+Vsn(i,j+1,3)*Snb(i,j+1,2)*
&          Dye(i,j+1,3))/aP(i,j)

```

else if(Mask(i,j-1).EQ. 0 .AND. Mask(i-1,j-1).EQ. 1) then

```

Dye(i,j,3)=maski(i,j)*maskk(i,j)*mask(i,j)*((
& (1.0*aW(i,j)*Dye(i-1,j,3)+0.0*aW(i,j)*Dye(i-1,j-1,3))+
&          aS(i,j)*Dye(i,j,3)+
&          aE(i,j)*Dye(i+1,j,3)+
&          aN(i,j)*Dye(i,j+1,3))*Wt+
& ((1.0*aW(i,j)*Dye(i-1,j,2)+0.0*aW(i,j)*Dye(i-1,j-1,2))+
&          aS(i,j)*Dye(i,j,2)+
&          aE(i,j)*Dye(i+1,j,2)+
&          aN(i,j)*Dye(i,j+1,2))*(1.-Wt)+
&          aPo(i,j)*Dye(i,j,2)-Vsn(i,j,3)*Snb(i,j,2)*
&          Dye(i,j,3)*mask(i,j-1)+Vsn(i,j+1,3)*Snb(i,j+1,2)*
&          Dye(i,j+1,3))/aP(i,j)

```

else if(Mask(i,j-1).eq.0) then

```

Dye(i,j,3)=maski(i,j)*maskk(i,j)*mask(i,j)*((aW(i,j)*Dye(i-1,j,3)+
&          aS(i,j)*Dye(i,j,3)+
&          aE(i,j)*Dye(i+1,j,3)+
&          aN(i,j)*Dye(i,j+1,3))*Wt+
& (aW(i,j)*Dye(i-1,j,2)+
&          aS(i,j)*Dye(i,j,2)+
&          aE(i,j)*Dye(i+1,j,2)+
&          aN(i,j)*Dye(i,j+1,2))*(1.-Wt)+
&          aPo(i,j)*Dye(i,j,2)-Vsn(i,j,3)*Snb(i,j,2)*
&          Dye(i,j,3)*mask(i,j-1)+Vsn(i,j+1,3)*Snb(i,j+1,2)*
&          Dye(i,j+1,3))/aP(i,j)

```

else if(Mask(i,j).EQ. 0 .OR. Maskk(i,j).EQ. 0 .OR.
& Maski(i,j).EQ. 0 .OR. Maske(i,j).EQ. 0) then

Dye(i,j,3)=0.0

else

```

Dye(i,j,3)=maski(i,j)*maskk(i,j)*mask(i,j)*((aW(i,j)*Dye(i-1,j,3)+
&          aS(i,j)*Dye(i,j-1,3)+
&          aE(i,j)*Dye(i+1,j,3)+

```

```

&          aN(i,j)*Dye(i,j+1,3))*Wt+
&          (aW(i,j)*Dye(i-1,j,2)+
&          aS(i,j)*Dye(i,j-1,2)+
&          aE(i,j)*Dye(i+1,j,2)+
&          aN(i,j)*Dye(i,j+1,2))*(1.-Wt)+
&          aPo(i,j)*Dye(i,j,2)-Vsn(i,j,3)*Snb(i,j,2)*maski(i,j-1)*
& maske(i,j-1)*Dye(i,j,3)*mask(i,j-1)+Vsn(i,j+1,3)*Snb(i,j+1,2)*
&          Dye(i,j+1,3))/aP(i,j)
endif
dye(i,N+1,3)=dye(i,N,3)
dye(M+1,j,3)=dye(M,j,3)

```

10 continue

i =M

do j = 2,N-1

if(Iswitch.eq.0) then

Vsn(i,j,3)=0

else

Vsn(i,j,3)=Max(Vmax*(exp(-Fsp*(Dye(i,j,2)-Cmin))

&-exp(-Csp*(Dye(i,j,2)-Cmin))),0.0)

endif

Dye(i,j,3)=maski(i,j)*maskk(i,j)*mask(i,j)*maske(i,j)*

& ((aW(i,j)*Dye(i-1,j,3)+

& aS(i,j)*Dye(i,j-1,3)+

& aE(i,j)*Dye(i,j,3)+

& aN(i,j)*Dye(i,j+1,3))*Wt+

& (aW(i,j)*Dye(i-1,j,2)+

& aS(i,j)*Dye(i,j-1,2)+

& aE(i,j)*Dye(i,j,2)+

& aN(i,j)*Dye(i,j+1,2))*(1.-Wt)+

& aPo(i,j)*Dye(i,j,2)-Vsn(i,j,3)*Snb(i,j,2)*

& maske(i,j-1)*Dye(i,j,3)*mask(i,j-1)+Vsn(i,j+1,3)*Snb(i,j+1,2)*

& Dye(i,j+1,3))/aP(i,j)

enddo

j=1

do i=2,M-1

if(Iswitch.eq.0) then

Vsn(i,j,3)=0

else

Vsn(i,j,3)=Max(Vmax*(exp(-Fsp*(Dye(i,j,2)-Cmin))

&-exp(-Csp*(Dye(i,j,2)-Cmin))),0.0)

endif

Dye(i,j,3)=maski(i,j)*maskk(i,j)*mask(i,j)*((aW(i,j)*Dye(i-1,j,3)+

```

&          aS(i,j)*Dye(i,j,3)+
&          aE(i,j)*Dye(i+1,j,3)+
&          aN(i,j)*Dye(i,j+1,3))*Wt+
&      (aW(i,j)*Dye(i-1,j,2)+
&          aS(i,j)*Dye(i,j,2)+
&          aE(i,j)*Dye(i+1,j,2)+
&          aN(i,j)*Dye(i,j+1,2))*(1.-Wt)+
&          aPo(i,j)*Dye(i,j,2)+Vsn(i,j+1,3)*Snb(i,j+1,2)*
&      Dye(i,j+1,3))/aP(i,j)
enddo

i=M
j=N
if(Iswitch.eq.0) then
  Vsn(i,j,3)=0
else
  Vsn(i,j,3)=Max(Vmax*(exp(-Fsp*(Dye(i,j,2)-Cmin))
&-exp(-Csp*(Dye(i,j,2)-Cmin))),0.0)
endif

Dye(M,N,3)=maski(i,j)*maskk(i,j)*mask(i,j)*((aW(M,N)*Dye(i-1,j,3)+
&          aS(i,N)*Dye(i,j-1,3)+
&          aE(i,j)*Dye(i,N,3)+
&          aN(i,j)*Dye(i,N,3))*Wt+
&      (aW(M,N)*Dye(i-1,j,2) +
&          aS(i,N)*Dye(i,j-1,2)+
&          aE(i,j)*Dye(i,N,2)+
&          aN(i,j)*Dye(i,N,2))*(1.-Wt)+
&          aPo(i,j)*Dye(i,N,2)-Vsn(i,j,3)*Snb(i,j,2)*
&      Dye(i,j,3))/aP(i,j)

i=M
j=1
if(Iswitch.eq.0) then
  Vsn(i,j,3)=0
else
  Vsn(i,j,3)=Max(Vmax*(exp(-Fsp*(Dye(i,j,2)-Cmin))
&-exp(-Csp*(Dye(i,j,2)-Cmin))),0.0)
endif

Dye(i,j,3)=maski(i,j)*maskk(i,j)*mask(i,j)*((aW(i,j)*Dye(i-1,j,3)+
&          aS(i,j)*Dye(i,j,3)+
&          aE(i,j)*Dye(i,j,3)+
&          aN(i,j)*Dye(i,j+1,3))*Wt+
&      (aW(i,j)*Dye(i-1,j,2)+
&          aS(i,j)*Dye(i,j,2)+

```

```

&          aE(i,j)*Dye(i,j,2)+
&          aN(i,j)*Dye(i,j+1,2))*(1.-Wt)+
&          aPo(i,j)*Dye(i,j,2)+Vsn(i,j+1,3)*Snb(i,j+1,2)*
&          Dye(i,j+1,3))/aP(i,j)
110 continue

```

c ***** Calculations in the other direction *****

```

do 120 mmm=1,100

i=1
j=N

if(Iswitch.eq.0) then
  Vsn(i,j,3)=0
else
  Vsn(i,j,3)=Max(Vmax*(exp(-Fsp*(Dye(i,j,2)-Cmin))
&-exp(-Csp*(Dye(i,j,2)-Cmin))),0.0)
endif

Dye(i,j,3)=maski(i,j)*maskk(i,j)*mask(i,j)*((aW(1,N)*Dyeo+
&          aS(i,j)*Dye(i,j-1,3)+
&          aE(i,j)*Dye(i+1,N,3)+
&          aN(i,j)*Dye(1,N,3))*Wt+
&          (aW(1,N)*Dyeo +
&          aS(i,j)*Dye(i,j-1,2)+
&          aE(i,j)*Dye(i+1,N,2)+
&          aN(i,j)*Dye(1,N,2))*(1.-Wt)+
&          aPo(i,j)*Dye(1,N,2)-Vsn(i,j,3)*Snb(i,j,2)*
&          Dye(i,j,3))/aP(i,j)

i=1
do ii=2,Ninl
  j=N-(ii-1)

  if(Iswitch.eq.0) then

    Vsn(i,j,3)=0

  else
    Vsn(i,j,3)=Max(Vmax*(exp(-Fsp*(Dye(i,j,2)-Cmin))
&-exp(-Csp*(Dye(i,j,2)-Cmin))),0.0)

  endif

  Dye(i,j,3)=maski(i,j)*maskk(i,j)*mask(i,j)*((aW(i,j)*Dyeo +

```

```

&          aS(i,j)*Dye(i,j-1,3)+
&          aE(i,j)*Dye(i+1,j,3)+
&          aN(i,j)*Dye(i,j+1,3))*Wt+
&      (aW(i,j)*Dyeo +
&          aS(i,j)*Dye(i,j-1,2)+
&          aE(i,j)*Dye(i+1,j,2)+
&          aN(i,j)*Dye(i,j+1,2))*(1.-Wt)+
&          aPo(i,j)*Dye(i,j,2)-Vsn(i,j,3)*Snb(i,j,2)*maski(i,j-1)*
& maske(i,j-1)*Dye(i,j,3)*mask(i,j-1)+Vsn(i,j+1,3)*Snb(i,j+1,2)*
&      Dye(i,j+1,3))/aP(i,j)

enddo

i=1
j=1
if(Iswitch.eq.0) then
  Vsn(i,j,3)=0
else
  Vsn(i,j,3)=Max(Vmax*(exp(-Fsp*(Dye(i,j,2)-Cmin))
&-exp(-Csp*(Dye(i,j,2)-Cmin))),0.0)
endif

Dye(i,j,3)=maski(i,j)*maskk(i,j)*mask(i,j)*((aW(i,j)*Dye(1,1,3)+
&          aS(i,j)*Dye(i,j,3)+
&          aE(i,j)*Dye(i+1,j,3)+
&          aN(i,j)*Dye(i,j+1,3))*Wt+
&      (aW(i,j)*Dye(1,1,2)+
&          aS(i,j)*Dye(i,j,2)+
&          aE(i,j)*Dye(i+1,j,2)+
&          aN(i,j)*Dye(i,j+1,2))*(1.-Wt)+
&          aPo(i,j)*Dye(i,j,2)+Vsn(i,j+1,3)*Snb(i,j+1,2)*
&      Dye(i,j+1,3))/aP(i,j)

i=1
do j=2,N-Ninl
  if(Iswitch.eq.0) then
    Vsn(i,j,3)=0
  else
    Vsn(i,j,3)=Max(Vmax*(exp(-Fsp*(Dye(i,j,2)-Cmin))
&-exp(-Csp*(Dye(i,j,2)-Cmin))),0.0)
  endif

  Dye(i,j,3)=maski(i,j)*maskk(i,j)*mask(i,j)*((aW(i,j)*Dye(i,j,3)+
&          aS(i,j)*Dye(i,j-1,3)+

```

```

&          aE(i,j)*Dye(i+1,j,3)+
&          aN(i,j)*Dye(i,j+1,3))*Wt+
&      (aW(i,j)*Dye(i,j,2)+
&          aS(i,j)*Dye(i,j-1,2)+
&          aE(i,j)*Dye(i+1,j,2)+
&          aN(i,j)*Dye(i,j+1,2))*(1.-Wt)+
&          aPo(i,j)*Dye(i,j,2)-Vsn(i,j,3)*Snb(i,j,2)*maski(i,j-1)*
&      maske(i,j-1)*Dye(i,j,3)*mask(i,j-1)+Vsn(i,j+1,3)*Snb(i,j+1,2)*
&      Dye(i,j+1,3))/aP(i,j)
enddo

j=N
do i=2,M-1
  if(Iswitch.eq.0) then
    Vsn(i,j,3)=0
  else
    Vsn(i,j,3)=Max(Vmax*(exp(-Fsp*(Dye(i,j,2)-Cmin))
&-exp(-Csp*(Dye(i,j,2)-Cmin))),0.0)
  endif

  Dye(i,j,3)=maski(i,j)*maskk(i,j)*mask(i,j)*((aW(i,j)*Dye(i-1,j,3)+
&          aS(i,j)*Dye(i,j-1,3)+
&          aE(i,j)*Dye(i+1,j,3)+
&          aN(i,j)*Dye(i,j,3))*Wt+
&      (aW(i,j)*Dye(i-1,j,2)+
&          aS(i,j)*Dye(i,j-1,2)+
&          aE(i,j)*Dye(i+1,j,2)+
&          aN(i,j)*Dye(i,j,2))*(1.-Wt)+
&          aPo(i,j)*Dye(i,j,2)-Vsn(i,j,3)*Snb(i,j,2)*
&      Dye(i,j,3))/aP(i,j)
enddo
do 20 j=2,N-1
do 20 i=2,M-1
  if(Iswitch.eq.0) then
    Vsn(i,j,3)=0
  else
    Vsn(i,j,3)=Max(Vmax*(exp(-Fsp*(Dye(i,j,2)-Cmin))
&-exp(-Csp*(Dye(i,j,2)-Cmin))),0.0)
  endif

  if((Mask(i,j-1).EQ.0).AND.Mask(i+1,j).EQ.0) then
    Dye(i,j,3)=maski(i,j)*maskk(i,j)*mask(i,j)*((aW(i,j)*Dye(i-1,j,3)+
&          aS(i,j)*Dye(i,j,3)+
&      (1.0*aE(i,j)*Dye(i,j,3))+
&          aN(i,j)*Dye(i,j+1,3))*Wt+

```



```

&          (aW(i,j)*Dye(i-1,j,2)+
&          aS(i,j)*Dye(i,j,2)+
& (1.0*aE(i,j)*Dye(i,j,2))+
&          aN(i,j)*Dye(i,j+1,2))*(1.-Wt)+
&          aPo(i,j)*Dye(i,j,2)-Vsn(i,j,3)*Snb(i,j,2)*
&          Dye(i,j,3)*mask(i,j-1)+Vsn(i,j+1,3)*Snb(i,j+1,2)*
&          Dye(i,j+1,3))/aP(i,j)

```

else if(Mask(i,j-1).EQ. 0 .AND. Mask(i-1,j-1).EQ. 1) then

```

Dye(i,j,3)=maski(i,j)*maskk(i,j)*mask(i,j)*((
& (1.0*aW(i,j)*Dye(i-1,j,3)+0.0*aW(i,j)*Dye(i-1,j-1,3))+
&          aS(i,j)*Dye(i,j,3)+
&          aE(i,j)*Dye(i+1,j,3)+
&          aN(i,j)*Dye(i,j+1,3))*Wt+
& ((1.0*aW(i,j)*Dye(i-1,j,2)+0.0*aW(i,j)*Dye(i-1,j-1,2))+
&          aS(i,j)*Dye(i,j,2)+
&          aE(i,j)*Dye(i+1,j,2)+
&          aN(i,j)*Dye(i,j+1,2))*(1.-Wt)+
&          aPo(i,j)*Dye(i,j,2)-Vsn(i,j,3)*Snb(i,j,2)*
&          Dye(i,j,3)*mask(i,j-1)+Vsn(i,j+1,3)*Snb(i,j+1,2)*
&          Dye(i,j+1,3))/aP(i,j)
else if(Mask(i,j-1).eq.0) then
Dye(i,j,3)=maski(i,j)*maskk(i,j)*mask(i,j)*((aW(i,j)*Dye(i-1,j,3)+
&          aS(i,j)*Dye(i,j,3)+
&          aE(i,j)*Dye(i+1,j,3)+
&          aN(i,j)*Dye(i,j+1,3))*Wt+
&          (aW(i,j)*Dye(i-1,j,2)+
&          aS(i,j)*Dye(i,j,2)+
&          aE(i,j)*Dye(i+1,j,2)+
&          aN(i,j)*Dye(i,j+1,2))*(1.-Wt)+
&          aPo(i,j)*Dye(i,j,2)-Vsn(i,j,3)*Snb(i,j,2)*
&          Dye(i,j,3)*mask(i,j-1)+Vsn(i,j+1,3)*Snb(i,j+1,2)*
&          Dye(i,j+1,3))/aP(i,j)

```

else if(Mask(i,j).EQ. 0 .OR. Maskk(i,j).EQ. 0. OR.
& Maski(i,j).EQ. 0. OR. Maske(i,j).EQ. 0) then

Dye(i,j,3)=0.0

else

```

Dye(i,j,3)=maski(i,j)*maskk(i,j)*mask(i,j)*((aW(i,j)*Dye(i-1,j,3)+
&          aS(i,j)*Dye(i,j-1,3)+
&          aE(i,j)*Dye(i+1,j,3)+
&          aN(i,j)*Dye(i,j+1,3))*Wt+

```

```

&          (aW(i,j)*Dye(i-1,j,2)+
&          aS(i,j)*Dye(i,j-1,2)+
&          aE(i,j)*Dye(i+1,j,2)+
&          aN(i,j)*Dye(i,j+1,2))*(1.-Wt)+
&          aPo(i,j)*Dye(i,j,2)-Vsn(i,j,3)*Snb(i,j,2)*maski(i,j-1)*
& maske(i,j-1)*Dye(i,j,3)*mask(i,j-1)+Vsn(i,j+1,3)*Snb(i,j+1,2)*
&          Dye(i,j+1,3))/aP(i,j)
endif

```

```

dye(i,N+1,3)=dye(i,N,3)
dye(M+1,j,3)=dye(M,j,3)

```

20 continue

```

j=1
do i=2,M-1
  if(Iswitch.eq.0) then
    Vsn(i,j,3)=0
  else
    Vsn(i,j,3)=Max(Vmax*(exp(-Fsp*(Dye(i,j,2)-Cmin))
&-exp(-Csp*(Dye(i,j,2)-Cmin))),0.0)
  endif

  Dye(i,j,3)=maski(i,j)*maskk(i,j)*mask(i,j)*((aW(i,j)*Dye(i-1,j,3)+
&          aS(i,j)*Dye(i,j,3)+
&          aE(i,j)*Dye(i+1,j,3)+
&          aN(i,j)*Dye(i,j+1,3))*Wt+
&          (aW(i,j)*Dye(i-1,j,2)+
&          aS(i,j)*Dye(i,j,2)+
&          aE(i,j)*Dye(i+1,j,2)+
&          aN(i,j)*Dye(i,j+1,2))*(1.-Wt)+
&          aPo(i,j)*Dye(i,j,2)+Vsn(i,j+1,3)*Snb(i,j+1,2)*
&          Dye(i,j+1,3))/aP(i,j)
enddo

```

```

i =M
do j = 2,N-1
  if(Iswitch.eq.0) then
    Vsn(i,j,3)=0
  else
    Vsn(i,j,3)=Max(Vmax*(exp(-Fsp*(Dye(i,j,2)-Cmin))
&-exp(-Csp*(Dye(i,j,2)-Cmin))),0.0)
  endif

```

```

  Dye(i,j,3)=maski(i,j)*maskk(i,j)*mask(i,j)*maske(i,j)*
&          ((aW(i,j)*Dye(i-1,j,3)+

```

```

&          aS(i,j)*Dye(i,j-1,3)+
&          aE(i,j)*Dye(i,j,3)+
&          aN(i,j)*Dye(i,j+1,3))*Wt+
&      (aW(i,j)*Dye(i-1,j,2)+
&          aS(i,j)*Dye(i,j-1,2)+
&          aE(i,j)*Dye(i,j,2)+
&          aN(i,j)*Dye(i,j+1,2))*(1.-Wt)+
&          aPo(i,j)*Dye(i,j,2)-Vsn(i,j,3)*Snb(i,j,2)*
&  maske(i,j-1)*Dye(i,j,3)*mask(i,j-1)+Vsn(i,j+1,3)*Snb(i,j+1,2)*
&      Dye(i,j+1,3))/aP(i,j)
&  enddo

  i=M
  j=N

  if(Iswitch.eq.0) then
    Vsn(i,j,3)=0
  else
    Vsn(i,j,3)=Max(Vmax*(exp(-Fsp*(Dye(i,j,2)-Cmin))
&-exp(-Csp*(Dye(i,j,2)-Cmin))),0.0)
  endif

  Dye(M,N,3)=maski(i,j)*maskk(i,j)*mask(i,j)*((aW(M,N)*Dye(i-1,j,3)+
&          aS(i,N)*Dye(i,j-1,3)+
&          aE(i,j)*Dye(i,N,3)+
&          aN(i,j)*Dye(i,N,3))*Wt+
&      (aW(M,N)*Dye(i-1,j,2) +
&          aS(i,N)*Dye(i,j-1,2)+
&          aE(i,j)*Dye(i,N,2)+
&          aN(i,j)*Dye(i,N,2))*(1.-Wt)+
&          aPo(i,j)*Dye(i,N,2)-Vsn(i,j,3)*Snb(i,j,2)*
&      Dye(i,j,3))/aP(i,j)

  i=M
  j=1
  if(Iswitch.eq.0) then
    Vsn(i,j,3)=0
  else
    Vsn(i,j,3)=Max(Vmax*(exp(-Fsp*(Dye(i,j,2)-Cmin))
&-exp(-Csp*(Dye(i,j,2)-Cmin))),0.0)
  endif

  Dye(i,j,3)=maski(i,j)*maskk(i,j)*mask(i,j)*((aW(i,j)*Dye(i-1,j,3)+
&          aS(i,j)*Dye(i,j,3)+
&          aE(i,j)*Dye(i,j,3)+
&          aN(i,j)*Dye(i,j+1,3))*Wt+

```

```

&      (aW(i,j)*Dye(i-1,j,2)+
&      aS(i,j)*Dye(i,j,2)+
&      aE(i,j)*Dye(i,j,2)+
&      aN(i,j)*Dye(i,j+1,2))*(1.-Wt)+
&      aPo(i,j)*Dye(i,j,2)+Vsn(i,j+1,3)*Snb(i,j+1,2)*
&      Dye(i,j+1,3))/aP(i,j)
120  continue

      return
      end

```

```

c*****
c*****SUBROUTINE: TEMSUB*****
c*****Subroutine for the transport of temperature*****
c*****

```

```

      subroutine Temsub(mm)
c This subroutine computes the transport of a conservative scalar quality in 2-D and
Concentration.
c      Called from Main
c      Calls: none
c      include 'comdeck'

```

```

      Include 'comdeck3.h'
      REAL nuo, nut,LL,mask,maskk,NBl,Inlet,maski,maske
      INTEGER IPRINT

```

```

c      psi= streamfunction, vort = vorticity
c      u= x velocity, v= y velocity, p = pressure
c      phi=scalar variable, C = concentration, rho= density
c      Temp(200,100), nut(200,100), Dye(200,100)
c      Fnb = face value of advection flux, Dnb=face value of diffusion flux, XX=?
c      rhonb(200,100,nf)= face density of fluid, nf = 1 vert face, nf = 2 horiz face
c      nuo = kinematic viscosity
c      dyr=Dy/Dr
c      dry=Dr/Dy
c      Boundary Conditions

```

```

c*****Calculation of the Isolation and Surface Heat Exchange*****

```

```

c*****Shortwave Radiation (HIs)
      Stime=Stimi+float(mm)*Dt/3600.0

```

```

CosAng=cos((Stime-12)*pi/12.0)

SinSal=Max((Sins+Coss*CosAng),0.0)

HIs=Wbo*SinSal*Clouf

if (SinSal.gt.0.0) then

HIs=HIs*Exp(-Nturb*(0.128-0.054*log10(1./SinSal))*(1./SinSal))

Endif

Sal=asin(SinSal)*180.0/pi

Albe=0.05+0.35*Exp(-0.083*Sal)

HIs=HIs*(1.0-Albe)

```

c***Atmospheric Longwave Radiation (HLWR)**

```

Tair=0.5*(Tama+Timi)+0.5*(Tama-Timi)*Sin((Stime-3)*pi/12.-pi/2.)

HLWR=SteBol*0.97*Ea*(Tair+273.0)**4

```

c***Water Longwave Effective Back Radiation (HWLB), Conduction &
c Convection, Evaporation & Condensation, Total Heat Exchange**

```

j=N

do i=1,M

HWLB(i,N)=0.97*SteBol*(Temp(i,N,2)+273)**4

es(i,N)=4.596*Exp(17.27*Temp(i,N,2)/(237.3+Temp(i,N,2)))

HCoC(i,N)=Bowen*FUw*(Temp(i,N,2)-Tair)

HEvC(i,N)=FUw*(es(i,N)-eair)

Heat(i,N)= HIs+HLWR-HWLB(i,N)-HCoC(i,N)-HEvC(i,N)

enddo

```

c*****Transport Subroutine for Temperature*****

```

      do i=1,M
      do j=1,N
      Temp(i,j,2)=Temp(i,j,3)
      enddo
      enddo

      do 110 mmm=1,50
      i=1
      j=N

      Temp(i,j,3)=maski(i,j)*maskk(i,j)*mask(i,j)*((aW(1,N)*Tempo+
&          aS(i,j)*Temp(i,j-1,3)+
&          aE(i,j)*Temp(i+1,N,3)+
&          aN(i,j)*Temp(1,N,3))*Wt+          !aN(i,j)*Temp(1,N,3))*Wt+
&          (aW(1,N)*Tempo +
&          aS(i,j)*Temp(i,j-1,2)+
&          aE(i,j)*Temp(i+1,N,2)+
&          aN(i,j)*Temp(1,N,2))*(1.-Wt)+
&          0.48458333*Heat(i,N)*(r(i,j)*dr+dr*dr/2.0)/Cp+
&          !aN(i,j)*Temp(1,N,2))*(1.-Wt)+
&          aPo(i,j)*Temp(1,N,2))/aP(i,j)

      i=1
      do ii=2,Ninl
      j=N-(ii-1)

      Temp(i,j,3)=maski(i,j)*maskk(i,j)*mask(i,j)*((aW(i,j)*Tempo +
&          aS(i,j)*Temp(i,j-1,3)+
&          aE(i,j)*Temp(i+1,j,3)+
&          aN(i,j)*Temp(i,j+1,3))*Wt+
&          (aW(i,j)*Tempo +
&          aS(i,j)*Temp(i,j-1,2)+
&          aE(i,j)*Temp(i+1,j,2)+
&          aN(i,j)*Temp(i,j+1,2))*(1.-Wt)+
&          aPo(i,j)*Temp(i,j,2))/aP(i,j)
      enddo

      i=1
      j=1

      Temp(i,j,3)=maski(i,j)*maskk(i,j)*mask(i,j)*((aW(i,j)*Temp(1,1,3)+
&          aS(i,j)*Temp(i,j,3)+
&          aE(i,j)*Temp(i+1,j,3)+

```

```

&          aN(i,j)*Temp(i,j+1,3))*Wt+
&      (aW(i,j)*Temp(1,1,2)+
&          aS(i,j)*Temp(i,j,2)+
&          aE(i,j)*Temp(i+1,j,2)+
&          aN(i,j)*Temp(i,j+1,2))*(1.-Wt)+
&          aPo(i,j)*Temp(i,j,2))/aP(i,j)

      i=1
      do j=2,N-Ninl

        Temp(i,j,3)=maski(i,j)*maskk(i,j)*mask(i,j)*((aW(i,j)*Temp(i,j,3)+
&          aS(i,j)*Temp(i,j-1,3)+
&          aE(i,j)*Temp(i+1,j,3)+
&          aN(i,j)*Temp(i,j+1,3))*Wt+
&      (aW(i,j)*Temp(i,j,2)+
&          aS(i,j)*Temp(i,j-1,2)+
&          aE(i,j)*Temp(i+1,j,2)+
&          aN(i,j)*Temp(i,j+1,2))*(1.-Wt)+
&          aPo(i,j)*Temp(i,j,2))/aP(i,j)
      enddo

      j=N
      do i=2,M-1

        Temp(i,j,3)=maski(i,j)*maskk(i,j)*mask(i,j)*((aW(i,j)*
&          Temp(i-1,j,3)+aS(i,j)*Temp(i,j-1,3)+
&          aE(i,j)*Temp(i+1,j,3)+
&          aN(i,j)*Temp(i,j,3))*Wt+      !aN(i,j)*Temp(i,j,3))*Wt+
&      (aW(i,j)*Temp(i-1,j,2)+
&          aS(i,j)*Temp(i,j-1,2)+
&          aE(i,j)*Temp(i+1,j,2)+
&          aN(i,j)*Temp(i,j,2))*(1.-Wt)+
&      0.484583333*Heat(i,N)*(r(i,j)*dr+dr*dr/2.0)/Cp+      !
&          aN(i,j)*Temp(i,j,2))*(1.-Wt)+
&          aPo(i,j)*Temp(i,j,2))/aP(i,j)
      enddo

      do 10 i=2,M-1
      do 10 j=2,N-1

        if(Mask(i,j-1). EQ. 0 .AND. Mask(i+1,j). EQ. 0) then
          Temp(i,j,3)=maski(i,j)*maskk(i,j)*mask(i,j)*((aW(i,j)*
&      Temp(i-1,j,3)+aS(i,j)*Temp(i,j,3)+
&      (1.0*aE(i,j)*Temp(i,j,3))+
&          aN(i,j)*Temp(i,j+1,3))*Wt+
&          (aW(i,j)*Temp(i-1,j,2)+

```

```

&          aS(i,j)*Temp(i,j,2)+
& (1.0*aE(i,j)*Temp(i,j,2))+
&          aN(i,j)*Temp(i,j+1,2))*(1.-Wt)+
&          aPo(i,j)*Temp(i,j,2))/aP(i,j)

else if(Mask(i,j-1). EQ. 0 .AND. Mask(i-1,j-1). EQ. 1) then

Temp(i,j,3)=maski(i,j)*maskk(i,j)*mask(i,j)*((
& (1.0*aW(i,j)*Temp(i-1,j,3)+0.0*aW(i,j)*Temp(i-1,j-1,3))+
&          aS(i,j)*Temp(i,j,3)+
&          aE(i,j)*Temp(i+1,j,3)+
&          aN(i,j)*Temp(i,j+1,3))*Wt+
& ((1.0*aW(i,j)*Temp(i-1,j,2)+0.0*aW(i,j)*Temp(i-1,j-1,2))+
&          aS(i,j)*Temp(i,j,2)+
&          aE(i,j)*Temp(i+1,j,2)+
&          aN(i,j)*Temp(i,j+1,2))*(1.-Wt)+
&          aPo(i,j)*Temp(i,j,2))/aP(i,j)

      else if(Mask(i,j-1).eq.0) then
Temp(i,j,3)=maski(i,j)*maskk(i,j)*mask(i,j)*((aW(i,j)*
& Temp(i-1,j,3)+aS(i,j)*Temp(i,j,3)+
&          aE(i,j)*Temp(i+1,j,3)+
&          aN(i,j)*Temp(i,j+1,3))*Wt+
& (aW(i,j)*Temp(i-1,j,2)+
&          aS(i,j)*Temp(i,j,2)+
&          aE(i,j)*Temp(i+1,j,2)+
&          aN(i,j)*Temp(i,j+1,2))*(1.-Wt)+
&          aPo(i,j)*Temp(i,j,2))/aP(i,j)

      else if(Mask(i,j). EQ. 0 .OR. Maskk(i,j). EQ. 0. OR.
& Maski(i,j). EQ. 0. OR. Maske(i,j). EQ. 0) then

Temp(i,j,3)=0.0

      else

Temp(i,j,3)=maski(i,j)*maskk(i,j)*mask(i,j)*((aW(i,j)*
& Temp(i-1,j,3)+ aS(i,j)*Temp(i,j-1,3)+
&          aE(i,j)*Temp(i+1,j,3)+
&          aN(i,j)*Temp(i,j+1,3))*Wt+
& (aW(i,j)*Temp(i-1,j,2)+
&          aS(i,j)*Temp(i,j-1,2)+
&          aE(i,j)*Temp(i+1,j,2)+
&          aN(i,j)*Temp(i,j+1,2))*(1.-Wt)+
&          aPo(i,j)*Temp(i,j,2))/aP(i,j)
endif

```



```

Temp(i,N+1,3)=Temp(i,N,3)
Temp(M+1,j,3)=Temp(M,j,3)

10  continue
    i =M
    do j = 2,N-1

        Temp(i,j,3)=maski(i,j)*maskk(i,j)*mask(i,j)*maske(i,j)*
&      ((aW(i,j)*Temp(i-1,j,3)+
&          aS(i,j)*Temp(i,j-1,3)+
&          aE(i,j)*Temp(i,j,3)+
&          aN(i,j)*Temp(i,j+1,3))*Wt+
&      (aW(i,j)*Temp(i-1,j,2)+
&          aS(i,j)*Temp(i,j-1,2)+
&          aE(i,j)*Temp(i,j,2)+
&          aN(i,j)*Temp(i,j+1,2))*(1.-Wt)+
&          aPo(i,j)*Temp(i,j,2))/aP(i,j)
        enddo

        j=1
        do i=2,M-1

            Temp(i,j,3)=maski(i,j)*maskk(i,j)*mask(i,j)*((aW(i,j)*
&      Temp(i-1,j,3)+aS(i,j)*Temp(i,j,3)+
&      aE(i,j)*Temp(i+1,j,3)+
&      aN(i,j)*Temp(i,j+1,3))*Wt+
&      (aW(i,j)*Temp(i-1,j,2)+
&      aS(i,j)*Temp(i,j,2)+
&      aE(i,j)*Temp(i+1,j,2)+
&      aN(i,j)*Temp(i,j+1,2))*(1.-Wt)+
&      aPo(i,j)*Temp(i,j,2))/aP(i,j)
            enddo

            i=M
            j=N

            Temp(M,N,3)=maski(i,j)*maskk(i,j)*mask(i,j)*((aW(M,N)*
&      Temp(i-1,j,3)+aS(i,N)*Temp(i,j-1,3)+
&      aE(i,j)*Temp(i,N,3)+
&      aN(i,j)*Temp(i,N,3))*Wt+
&      (aW(M,N)*Temp(i-1,j,2) +
&      aS(i,N)*Temp(i,j-1,2)+
&      aE(i,j)*Temp(i,N,2)+
&      aN(i,j)*Temp(i,N,2))*(1.-Wt)+
&      0.484583333*Heat(i,N)*(r(i,j)*dr+dr*dr/2.0)/Cp+
&      aPo(i,j)*Temp(i,N,2))/aP(i,j)

```

```

      i=M
      j=1

      Temp(i,j,3)=maski(i,j)*maskk(i,j)*mask(i,j)*((aW(i,j)*
&      Temp(i-1,j,3)+aS(i,j)*Temp(i,j,3)+
&      aE(i,j)*Temp(i,j,3)+
&      aN(i,j)*Temp(i,j+1,3))*Wt+
&      (aW(i,j)*Temp(i-1,j,2)+
&      aS(i,j)*Temp(i,j,2)+
&      aE(i,j)*Temp(i,j,2)+
&      aN(i,j)*Temp(i,j+1,2))*(1.-Wt)+
&      aPo(i,j)*Temp(i,j,2))/aP(i,j)
110 continue

```

c *****Calculations in the other direction *****

```

      do 120 mmm=1,50
      i=1
      j=N

      Temp(i,j,3)=maski(i,j)*maskk(i,j)*mask(i,j)*((aW(1,N)*Tempo+
&      aS(i,j)*Temp(i,j-1,3)+
&      aE(i,j)*Temp(i+1,N,3)+
&      aN(i,j)*Temp(1,N,3))*Wt+      !aN(i,j)*Temp(1,N,3))*Wt+
&      (aW(1,N)*Tempo +
&      aS(i,j)*Temp(i,j-1,2)+
&      aE(i,j)*Temp(i+1,N,2)+
&      aN(i,j)*Temp(1,N,2))*(1.-Wt)+
&      0.484583333*Heat(i,N)*(r(i,j)*dr+dr*dr/2.0)/Cp+
!aN(i,j)*Temp(1,N,2))*(1.-Wt)+
&      aPo(i,j)*Temp(1,N,2))/aP(i,j)

      i=1
      do ii=2,Ninl
      j=N-(ii-1)

      Temp(i,j,3)=maski(i,j)*maskk(i,j)*mask(i,j)*((aW(i,j)*Tempo +
&      aS(i,j)*Temp(i,j-1,3)+
&      aE(i,j)*Temp(i+1,j,3)+
&      aN(i,j)*Temp(i,j+1,3))*Wt+
&      (aW(i,j)*Tempo +
&      aS(i,j)*Temp(i,j-1,2)+
&      aE(i,j)*Temp(i+1,j,2)+
&      aN(i,j)*Temp(i,j+1,2))*(1.-Wt)+
&      aPo(i,j)*Temp(i,j,2))/aP(i,j)

```

```

        enddo

        i=1
        j=1

        Temp(i,j,3)=maski(i,j)*maskk(i,j)*mask(i,j)*((aW(i,j)*Temp(1,1,3)+
&          aS(i,j)*Temp(i,j,3)+
&          aE(i,j)*Temp(i+1,j,3)+
&          aN(i,j)*Temp(i,j+1,3))*Wt+
&          (aW(i,j)*Temp(1,1,2)+
&          aS(i,j)*Temp(i,j,2)+
&          aE(i,j)*Temp(i+1,j,2)+
&          aN(i,j)*Temp(i,j+1,2))*(1.-Wt)+
&          aPo(i,j)*Temp(i,j,2))/aP(i,j)

        i=1
        do j=2,N-Ninl

            Temp(i,j,3)=maski(i,j)*maskk(i,j)*mask(i,j)*((aW(i,j)*Temp(i,j,3)+
&          aS(i,j)*Temp(i,j-1,3)+
&          aE(i,j)*Temp(i+1,j,3)+
&          aN(i,j)*Temp(i,j+1,3))*Wt+
&          (aW(i,j)*Temp(i,j,2)+
&          aS(i,j)*Temp(i,j-1,2)+
&          aE(i,j)*Temp(i+1,j,2)+
&          aN(i,j)*Temp(i,j+1,2))*(1.-Wt)+
&          aPo(i,j)*Temp(i,j,2))/aP(i,j)
            enddo

        j=N
        do i=2,M-1

            Temp(i,j,3)=maski(i,j)*maskk(i,j)*mask(i,j)*((aW(i,j)*
&          Temp(i-1,j,3)+aS(i,j)*Temp(i,j-1,3)+
&          aE(i,j)*Temp(i+1,j,3)+
&          aN(i,j)*Temp(i,j,3))*Wt+      !aN(i,j)*Temp(i,j,3))*Wt+
&          (aW(i,j)*Temp(i-1,j,2)+
&          aS(i,j)*Temp(i,j-1,2)+
&          aE(i,j)*Temp(i+1,j,2)+
&          aN(i,j)*Temp(i,j,2))*(1.-Wt)+
&          0.484583333*Heat(i,N)*(r(i,j)*dr+dr*dr/2.0)/Cp+
&          aPo(i,j)*Temp(i,j,2))/aP(i,j)
            enddo
        do 20 j=2,N-1
        do 20 i=2,M-1

```

```

    if (Mask(i,j-1). EQ. 0 .AND. Mask(i+1,j). EQ. 0) then
      Temp(i,j,3)=maski(i,j)*maskk(i,j)*mask(i,j)*((aW(i,j)*
&      Temp(i-1,j,3)+aS(i,j)*Temp(i,j,3)+
&      (1.0*aE(i,j)*Temp(i,j,3))+
&      aN(i,j)*Temp(i,j+1,3))*Wt+
&      (aW(i,j)*Temp(i-1,j,2)+
&      aS(i,j)*Temp(i,j,2)+
&      (1.0*aE(i,j)*Temp(i,j,2))+
&      aN(i,j)*Temp(i,j+1,2))*(1.-Wt)+
&      aPo(i,j)*Temp(i,j,2))/aP(i,j)

    else if (Mask(i,j-1). EQ. 0 .AND. Mask(i-1,j-1). EQ. 1) then

      Temp(i,j,3)=maski(i,j)*maskk(i,j)*mask(i,j)*((
&      (1.0*aW(i,j)*Temp(i-1,j,3)+0.0*aW(i,j)*Temp(i-1,j-1,3))+
&      aS(i,j)*Temp(i,j,3)+
&      aE(i,j)*Temp(i+1,j,3)+
&      aN(i,j)*Temp(i,j+1,3))*Wt+
&      ((1.0*aW(i,j)*Temp(i-1,j,2)+0.0*aW(i,j)*Temp(i-1,j-1,2))+
&      aS(i,j)*Temp(i,j,2)+
&      aE(i,j)*Temp(i+1,j,2)+
&      aN(i,j)*Temp(i,j+1,2))*(1.-Wt)+
&      aPo(i,j)*Temp(i,j,2))/aP(i,j)

    else if (Mask(i,j-1).eq.0) then
      Temp(i,j,3)=maski(i,j)*maskk(i,j)*mask(i,j)*((aW(i,j)*
&      Temp(i-1,j,3)+aS(i,j)*Temp(i,j,3)+
&      aE(i,j)*Temp(i+1,j,3)+
&      aN(i,j)*Temp(i,j+1,3))*Wt+
&      (aW(i,j)*Temp(i-1,j,2)+
&      aS(i,j)*Temp(i,j,2)+
&      aE(i,j)*Temp(i+1,j,2)+
&      aN(i,j)*Temp(i,j+1,2))*(1.-Wt)+
&      aPo(i,j)*Temp(i,j,2))/aP(i,j)

    else if (Mask(i,j). EQ. 0 .OR. Maskk(i,j). EQ. 0 .OR.
& Maski(i,j). EQ. 0 .OR. Maske(i,j). EQ. 0) then

      Temp(i,j,3)=0.0

    else

      Temp(i,j,3)=maski(i,j)*maskk(i,j)*mask(i,j)*((aW(i,j)*
&      Temp(i-1,j,3)+aS(i,j)*Temp(i,j-1,3)+
&      aE(i,j)*Temp(i+1,j,3)+

```

```

&          aN(i,j)*Temp(i,j+1,3))*Wt+
&          (aW(i,j)*Temp(i-1,j,2)+
&          aS(i,j)*Temp(i,j-1,2)+
&          aE(i,j)*Temp(i+1,j,2)+
&          aN(i,j)*Temp(i,j+1,2))*(1.-Wt)+
&          aPo(i,j)*Temp(i,j,2))/aP(i,j)
endif

Temp(i,N+1,3)=Temp(i,N,3)
Temp(M+1,j,3)=Temp(M,j,3)

20  continue

j=1
do i=2,M-1

Temp(i,j,3)=maski(i,j)*maskk(i,j)*mask(i,j)*((aW(i,j)*
&          Temp(i-1,j,3)+aS(i,j)*Temp(i,j,3)+
&          aE(i,j)*Temp(i+1,j,3)+
&          aN(i,j)*Temp(i,j+1,3))*Wt+
&          (aW(i,j)*Temp(i-1,j,2)+
&          aS(i,j)*Temp(i,j,2)+
&          aE(i,j)*Temp(i+1,j,2)+
&          aN(i,j)*Temp(i,j+1,2))*(1.-Wt)+
&          aPo(i,j)*Temp(i,j,2))/aP(i,j)
enddo

i=M
do j=2,N-1

Temp(i,j,3)=maski(i,j)*maskk(i,j)*mask(i,j)*maske(i,j)*
&          ((aW(i,j)*Temp(i-1,j,3)+
&          aS(i,j)*Temp(i,j-1,3)+
&          aE(i,j)*Temp(i,j,3)+
&          aN(i,j)*Temp(i,j+1,3))*Wt+
&          (aW(i,j)*Temp(i-1,j,2)+
&          aS(i,j)*Temp(i,j-1,2)+
&          aE(i,j)*Temp(i,j,2)+
&          aN(i,j)*Temp(i,j+1,2))*(1.-Wt)+
&          aPo(i,j)*Temp(i,j,2))/aP(i,j)
enddo

i=M
j=N

Temp(M,N,3)=maski(i,j)*maskk(i,j)*mask(i,j)*((aW(M,N)*

```

```

&          Temp(i-1,j,3)+aS(i,N)*Temp(i,j-1,3)+
&          aE(i,j)*Temp(i,N,3)+
&          aN(i,j)*Temp(i,N,3))*Wt+
&      (aW(M,N)*Temp(i-1,j,2) +
&          aS(i,N)*Temp(i,j-1,2)+
&          aE(i,j)*Temp(i,N,2)+
&          aN(i,j)*Temp(i,N,2))*(1.-Wt)+
&      0.484583333*Heat(i,N)*(r(i,j)*dr+dr*dr/2.0)/Cp+
&      aPo(i,j)*Temp(i,N,2))/aP(i,j)

      i=M
      j=1

      Temp(i,j,3)=maski(i,j)*maskk(i,j)*mask(i,j)*((aW(i,j)*
&          Temp(i-1,j,3)+aS(i,j)*Temp(i,j,3)+
&          aE(i,j)*Temp(i,j,3)+
&          aN(i,j)*Temp(i,j+1,3))*Wt+
&      (aW(i,j)*Temp(i-1,j,2)+
&          aS(i,j)*Temp(i,j,2)+
&          aE(i,j)*Temp(i,j,2)+
&          aN(i,j)*Temp(i,j+1,2))*(1.-Wt)+
&      aPo(i,j)*Temp(i,j,2))/aP(i,j)
120  continue

      do i=1,M+1
      do j=1,N+1

      Temp(i,j,2)=Temp(i,j,3)

      enddo
      enddo

      return
      end

```

```

c*****
c*****SUBROUTINE: COEFS*****
cc*****Subroutine to Calculate Coefficient for Transport Equations *****
c*****

```

```

      subroutine coefs(mm)
c This subroutine computes the transport of a conservative scalar quality in 2-D.
c   Called from Main
c   Calls: none
c   include 'comdeck'
c   Include 'comdeck3.h'
c   REAL nu0, nut,LL,mask,maskk,NBl,Inlet,maski,maske
c   INTEGER IPRINT
c   psi= streamfunction, vort = vorticity
c   u= x velocity, v= y velocity, p = pressure
c   phi=scalar variable, C = Concentration, rho= density
c   Temp(200,100), nut(200,100), Con(200,100)
c   Fnb = face value of advection flux, Dnb=face value of diffusion flux, XX=??
c   rhonb(200,100,nf)= face density of fluid, nf = 1 vert face, nf = 2 horiz face
c   nu0 = kinematic viscosity
c   dyr=Dy/Dr
c   dry=Dr/Dy

      i=1
      j=1
      aW(i,j)=max((+Fnb(i,j,1)/2.+Dnb(i,j,1)*0.0*      !Hybrid Differencing
&1.0),0.0,Fnb(i,j,1))                                !Scheme, Fully implicit

      aS(i,j)=max((+Fnb(i,j,2)/2.+1.00*Dnb(i,j,2)*0.0*
&1.0),0.0,Fnb(i,j,2))

      aE(i,j)=max((-Fnb(i+1,j,1)/2.+Dnb(i+1,j,1)*mask(i+1,j)*
&maskk(i+1,j)),0.0,-Fnb(i+1,j,1))

      aN(i,j)=max((-Fnb(i,j+1,2)/2.+1.00*Dnb(i,j+1,2)*mask(i,j+1)*
&maskk(i,j+1)),0.0,-Fnb(i,j+1,2))

      i=1
      do j=2,N
      aW(i,j)=max((+Fnb(i,j,1)/2.+Dnb(i,j,1)*0.0*      !Hybrid Differencing
&1.0),0.0,Fnb(i,j,1))                                !Scheme, Fully implicit

      aS(i,j)=max((+Fnb(i,j,2)/2.+1.*Dnb(i,j,2)*mask(i,j-1)*
&maski(i,j-1)*maskk(i,j-1)),0.0,Fnb(i,j,2))

      aE(i,j)=max((-Fnb(i+1,j,1)/2.+1.*Dnb(i+1,j,1)*mask(i+1,j)*

```

```

&maskk(i+1,j)),0.0,-Fnb(i+1,j,1))

      aN(i,j)=max((-Fnb(i,j+1,2)/2.+1.*Dnb(i,j+1,2)*mask(i,j+1)*
&maski(i,j+1)*maskk(i,j+1)),0.0,-Fnb(i,j+1,2))

      enddo

      j=1
      do i=2,M

          aW(i,j)=max((+Fnb(i,j,1)/2.+1.*Dnb(i,j,1)*mask(i-1,j)*      !Hybrid Differencing
&maskk(i-1,j)),0.0,Fnb(i,j,1))                                     !Scheme, Fully implicit

          aS(i,j)=max((+Fnb(i,j,2)/2.+1.*Dnb(i,j,2)*0.0*
&1.0),0.0,Fnb(i,j,2))

          aE(i,j)=max((-Fnb(i+1,j,1)/2.+1.*Dnb(i+1,j,1)*mask(i+1,j)*
&maskk(i+1,j)),0.0,-Fnb(i+1,j,1))

          aN(i,j)=max((-Fnb(i,j+1,2)/2.+1.*Dnb(i,j+1,2)*mask(i,j+1)*
&maskk(i,j+1)),0.0,-Fnb(i,j+1,2))

          enddo

          do 10 j=2,N
          do 10 i=2,M

              aW(i,j)=max((+Fnb(i,j,1)/2.+1.*Dnb(i,j,1)*mask(i-1,j)*      !Hybrid Differencing
&maske(i-1,j)*maski(i-1,j)*maskk(i-1,j)),0.0,Fnb(i,j,1)) !Scheme, Fully implicit

              aS(i,j)=max((+Fnb(i,j,2)/2.+1.*Dnb(i,j,2)*mask(i,j-1)*
&maske(i,j-1)*maski(i,j-1)*maskk(i,j-1)),0.0,Fnb(i,j,2))

              aE(i,j)=max((-Fnb(i+1,j,1)/2.+1.*Dnb(i+1,j,1)*mask(i+1,j)*
&maske(i+1,j)*maski(i+1,j)*maskk(i+1,j)),0.0,-Fnb(i+1,j,1))

              aN(i,j)=max((-Fnb(i,j+1,2)/2.+1.*Dnb(i,j+1,2)*mask(i,j+1)*
&maske(i,j+1)*maski(i,j+1)*maskk(i,j+1)),0.0,-Fnb(i,j+1,2))
c*****
10    continue

          do 101 j=1,N
          do 101 i=1,M

              DF(i,j)= -Fnb(i,j,1)-Fnb(i,j,2)+Fnb(i+1,j,1)+Fnb(i,j+1,2)
              aPo(i,j)=rho(i,j)*(r(i,j)*Dr+Dr*Dr/2.0)*Dy/Dt

```


$&-(1.-Wt)*((aW(i,j)+aS(i,j)+aE(i,j)+aN(i,j))+DF(i,j))$

$aP(i,j)=rho(i,j)*(r(i,j)*Dr+Dr*Dr/2.0)*Dy/Dt$
 $&+((aW(i,j)+aS(i,j)+aE(i,j)+aN(i,j))+DF(i,j))*Wt$

101 continue
return
end

```
c*****  
c*****END OF FORTRAN CODE*****  
cCOPYRIGHT 2004, ALONSO G. GRIBORIO, JOHN ALEX McCORQUODALE  
c*****ALL RIGHTS RESERVED*****  
c*****
```

APPENDIX K

INPUT FILES FOR RUNNING THE Q3D CLARIFIER MODEL FORTRAN

SOURCE CODE

K.1 Input File for the General Geometry of the Clarifier

```
17.60  !Radius of the Clarifier (including inlet, m)
0.50   !Radius of the inlet (m)
4.3    !Depth of circular tank (m) (at outer wall)
8.33   !Bottom slope (%) Slope (positive sloping towards the center,
negative sloping towards the outer wall)
1.0    !Inlet Height (m) (from the water surface downward)
0.4    !Inlet Width (m) (width of individual ports)
4      !Number of Inlet Ports
0      !Modeling Inlet Deflector (yes=1, no=0)
45     !Deflector Angle at the Inlet (degrees)
1      !Modeling Center Well(yes=1, no=0)'
4.5    !Center Well Radius (m)
2.6    !Center Well Depth (m)
0      !Modeling Vertical - EDI (yes=1, no=0)'
1.5    !EDI Radius (m)
1.8    !EDI Depth (m)
1      !Modeling Scum Baffle (yes=1, no=0)'
17.0   !Scum Baffle Radius (m)
0.5    !Scum Baffle Depth (m)
0      !Modeling Canopy Baffle (yes=1, no=0)'
1.5    !Canopy Baffle Radius (m)
2.5    !Canopy Baffle Depth (m)
0      !Modeling Peripheral or Stamford Baffle (yes=1, no=0)'
0.5    !Peripheral Baffle Depth (m)
1.0    !Peripheral Baffle Length (m)
0      !Modeling Mid-radius or Crosby Baffle (yes=1, no=0)'
10.0   !Mid-radius Baffle Radius (m)
1.5    !Mid-radius Baffle Height (m)
```

K.2 Input File for Type of Outlet Recirculation: Hopper or Suction

```
1      !Type of Outlet Recirculation: Hopper=1, Suction =2
2.0    !Radial Length of Hopper (m), ignore if suction is used
1.5    !Starting Radius of Hopper from the center of the tank (m),
ignore if suction is used
```

K.3 Input File for Type of Outlet

```
2          !Type of Outlet: Inboard=1, Outboard=2
0          !Width of Launder (m), Ignore if Outboard launder is used
0          !End Wall Clearance (m), Ignore if Outboard launder is used
```

K.4 Input File for the Simulation of the Scraper

```
1          !Simulating Scraper. yes=1 no=2
1          !Simulating Rake (1) or Spiral Scraper (2)
0.20       !Height of Blade (m)
0.03333    !Angular Velocity of the blades (rpm)
45         !Angle of the Blade (degrees)
1          !Number of Arms
```

K.5 Input File for Loading with Constant SOR and Constant MLSS (Can also be used for Simulations of Diurnal Variations as a Cosine Function)

```
1.125      !SOR average, based on Effluent Flow Rate (m/h) [ignore if
Time Series Input is used]
1.00       !Peaking factor [ignore if Time Series Input is used]
24.0       !Diurnal period in hours [ignore if Time Series Input is used]
2.80       !Suspended Solids Concentration (g/L)[ignore if Time Series
Input is used]
1.00       !Peaking Factor for MLSS [ignore if Time Series Input is used]
3.00       !Period of sinusoidal diurnal variation of MLSS concentration.
[ignore if Time Series Input is used]
1          !Proportional(1) or Constant(2) Recirculation Flow (Iras)
0.50       !Ratio for Proportional Recirculation Flow Rate
1270.      !Constant Recirculation Flow Rate (m3/h)
```

K.6 Input File for the Simulation of the Surface Heat Exchange

```
1          !Modeling Heat Exchange (Yes=1, No=2)
10.0       !Starting Time of Run (hour of day - 24 h clock)
180        !Julian day
40.0       !Local Latitude (Degrees)
3          !Atmospheric Turbidity Factor of the air, Integer: 2 (clear) to
5 (smoggy)
0.5        !Fraction of the sky obscured by clouds (1 for overcast sky)
25         !Dew Point Temperature, °C
28.        !Maximum Air Temperature, °C
28.        !Minimum Air Temperature, °C
1.2        !Wind Speed (m/s) at a height of 7 m above the water surface
```

K.7 Input File for Settling Properties and Flocculation Constants. Include Fractions and Individual Settling Velocities for Discrete Settling, and Threshold for Hindered and Discrete Settling

```
10.535     !Maximum Settling Velocity (m/h)for zone settling, Vo in
Equation 3.11
0.40       !Floc Settling Parameter ( $\text{m}^3/\text{Kg}$ ) for zone settling,  $K_1$  in
Equation 3.11
10.00      !Colloids Settling Parameter ( $\text{m}^3/\text{Kg}$ ),  $K_2$  in Takacs' equation
0.005      !Concentration of nonsettling floc  $\text{Kg}/\text{m}^3$ ,  $C_{\text{min}}$  in Takacs'
equation. This values is equal to the FSS of the Sample
3.20       !Compression Settling velocity (m/h),  $V_c$  in Equation 3.11
0.184      !Compression Settling Parameter ( $\text{m}^3/\text{Kg}$ ),  $K_c$  in Equation 3.11
1          !Is flocculation submodel used? Yes =1; No = 2
1.5        !Flocculation Constant for Differential Settling
(turbulence),  $K_{ds}$  in Equation 4.18 (dimensionless)
7.4E-5     !Flocculation Constant for Aggregation,  $K_a$  (L/g)
8.0E-9     !Flocculation Constant for Breakup,  $K_b$  (sec)
2.00       !Floc Breakup rate coefficient
1200.0     !Threshold for hindered Settling,  $\text{mg}/\text{L}$  (Threshold = 0 when
running Takacs Model for the complete settling curve)
600.00     !Threshold for discrete particles settling,  $\text{mg}/\text{L}$  (Threshold =
0 when running Takacs Model for the complete settling curve)
3          !Number of fraction for discrete particles, Limitation now =
3 (Make it equal to 1 when running Takacs Model for the complete
settling curve)
0.700      !Fraction in class 1 (good settling --- highly flocculated)
(Make it equal to 1 when running Takacs Model for the complete settling
curve)
10.8       !Settling Velocity for Fraction in class 1 (m/h)
0.256      !Fraction in class 2
3.00       !Settling Velocity for Fraction in class 2 (m/h)
0.044      !Fraction in class 3
0.68       !Settling Velocity for Fraction in class 3 (m/h)
```

K.8 Input File for General Coefficients. Advance Settings

```
0.10      !Diffusion Coefficient in the vertical direction
5.0       !Diffusion Coefficient in the Radial direction
1.0       !Coefficient for the Source Term in Vorticity Transport
Equation
1.45      !Specific Gravity of the Solid Particles
1000.0    !Reference density
0.001     ! 1 mm, roughness coefficient for Turbulence Model
9.81      ! gravity m/s2
0.80      ! Drag coefficient
0.32      !nonNewtonian Exponent for the Rheology Submodel
0.5       !Weight factor for time level (Wt=1 Implicit, Wt=0 Explicit)
0.0       !Salinity Concentration in Kg/m3 , STDS
2880      !Isolation at the outer limit of earth's atmosphere,
cal/(cm2*d)
1700      !Cloud-Base altitude
4182      !Specific heat, j(Kg°C)-1
0.47      !Bowen's Coefficient mm Hg/°C
11.7E-8   !Stefan-Boltzmann Constant, cal/(cm2*d*°K4)
```

K.9 Input File for the Control of the Simulation

```
60        !Number of cells in the radial-X direction (Integer,
default=100; maximum = 200)
20        !Number of cells in vertical-Y direction (Integer, default=50;
maximum = 100)
1.00      !Time Step (seconds)
1         !Run dye (Yes=0, No=1)
1         !Time Series, (Trig. Function=0, Time Series =1)
1         !Modeling Temperature (No=0, Yes=1)
1         !Initial Tank Temperature(User defined=1, Average of Influent
Temp.=2)
26.5      !Value for Initial Water Temperature if it is user defined
21600     !Number of time step in the run (integer)
450       !Every how many time steps would you like to PRINT the
results?
15        !Time Step for reading from the Time Series input file,
Constant (minutes)
```

K.10 Input File for the Time Series of SOR, MLSS and Temperature

Time(min),	SOR(m/h),	MLSS(g/L),	Influent Temp. (°C)
0	1.0	2.80	26.5
15	1.0	2.80	26.5
30	1.0	2.80	26.5
45	1.0	2.80	26.5

60	1.0	2.80	26.5
75	1.0	2.80	26.5
90	1.0	2.80	26.5
105	1.0	2.80	26.5
120	1.0	2.80	26.5
135	1.0	2.80	26.5
150	1.0	2.80	26.5
165	1.0	2.80	26.5
180	1.0	2.80	26.5
195	1.0	2.80	26.5
210	1.0	2.80	26.5
225	1.0	2.80	26.5
240	1.0	2.80	26.5
255	1.0	2.80	26.5
270	1.0	2.80	26.5
285	1.0	2.80	26.5
300	1.0	2.80	26.5
315	1.0	2.80	26.5
330	1.0	2.80	26.5
345	1.0	2.80	26.5
360	1.0	2.80	26.5
375	1.0	2.80	26.5
390	1.0	2.80	26.5
405	1.0	2.80	26.5
420	1.0	2.80	26.5
435	1.0	2.80	26.5
450	1.0	2.80	26.5
465	1.0	2.80	26.5
480	1.0	2.80	26.5
495	1.0	2.80	26.5
510	1.0	2.80	26.5
525	1.0	2.80	26.5
540	1.0	2.80	26.5

VITA

Alonso Gustavo Griborio born in Merida, Venezuela, on July 11, 1972. In 1994, he graduated with honors (Cum Laude) from University Rafael Urdaneta at Maracaibo, Venezuela, obtaining a degree of Bachelor of Science in Civil Engineering. In June 1994, he started at the Municipal Water Company of Maracaibo as a design engineer, working in this company for about two years. After receiving his Bachelor Degree, Mr. Griborio started working as a part time professor at the University Rafael Urdaneta. In October 1995, he obtained a position as a full-time assistant professor at the University of Zulia at Maracaibo, which is the third largest university in Venezuela in terms of degrees awarded and research funding.

In March 2000, Mr. Griborio received a degree as Masters of Science in Environmental Engineering from the University of Zulia, Maracaibo, Venezuela. Mr. Griborio has been involved in research for about six years. At the University of Zulia he was in charge of a major research project that studied the treatability of industrial wastewaters by anaerobic treatment, and previously he had been involved in research in the sanitary field. He received an award as qualify researcher from the University of Zulia in 2003.

In August 2001, he received a research assistantship from the University of New Orleans (UNO), New Orleans, USA, where he started pursuing a Ph.D. in Engineering and Applied Sciences. At UNO he has been working in the development of a hydrodynamic model for clarifiers and also involved in different studies, including research on settling properties and bioflocculation.